Geochronology, Petrogenesis and Crustal Evolution of the Saglek-Hebron Complex (Northern Labrador): Over one billion years of Archean geological history

Benjamin Wasilewski

Supervised by Dr. O'Neil, Jonathan.
Co-supervised by Dr. Rizo, Hanika.
reviewed by :
Prof. Schneider, David. A., (Internal - Ottawa U.)
Dr. Cousens, Brian., (Internal - Carleton U.)
Prof. Davies, Joshua. (Internal - Université du Quebéc à Montréal)
Dr. Hoffmann, J. Elis., (External - Freie Universität Berlin)

A thesis submitted in partial fulfillment of the requirements for the Doctorate in Philosophy degree in Geosciences.

Departement of Earth and Environemental Sciences
University of Ottawa

$\rightarrowtail$ *The picture displayed on the front page has been taken by Dr.* Rizo *Hanika. It shows a panorama of the Pangertok inlet (Kutsugak Siurak: local name) to the east of the basecamp. We can see, in the foreground, a developed sequence of the* $\sim$3750 Ma *Nulliak supracrustal metavolcanic/metasedimentary assemblage (described with more detail in Chapter 1). In the background, behind the Pangertok inlet, the highest peak visible is the Mount Pinguksoak (*$\sim$*1243 m) mainly built of 3800 to* 3300 Ma *quartzofeldspathic igneous rock (e.g. the Uivak gneiss; described in chapter 2) as well as being the highest point of the region.*

Abstract

The Saglek-Hebron Complex (SHC) in Northern Labrador represents one of the oldest terrains on Earth and it is closely related to the Archean Itsaq Gneiss Complex (IGC) in Greenland. The SHC is a typical granite-greenstone terrain that recorded over one billion years of magmatic history between ∼3900 Ma and ∼2700 Ma. Our geochronological and geochemical study shows that the SHC includes five generations of trondhjemite-tonalite-granodiorite suites (TTG): the ∼3870 Ma Iqaluk gneiss, the ∼3750 Ma Uivak I gneiss, the ∼3600 Ma Uivak II gneiss, the newly described ∼3300 Ma Iluilik gneiss, and the ∼3220 Ma Lister gneiss. These granitoid units are mostly consist of trondhjemite and tonalite with only rare granodiorites that appear to define a distinct unit formed at ∼3330 Ma and newly defined as the *Iluilik* gneiss. The Iluilik granodiorite appears to be derived from a Hadean mafic crust as supported by its combined whole-rock geochemical composition, its positive μ^{142}Nd value of +6, and its low ε^{176}Hf = −6 and ε^{143}Nd = −3, at 3300 Ma. SHC granites were emplaced throughout the Archean, from 3800 to 2700 Ma, but are predominant in the Neoarchean. They appear to have been mainly formed from the reworking of the SHC TTG, as supported by their low ε^{176}Hf and ε^{143}Nd initial values of respectively −16 and −11 at 2700 Ma. The granitoids include numerous enclaves of supracrustal rocks from various size, up to a few kilometers in scale, consisting of metavolcanic metasedimentary rocks. Previous work has suggested that they were formed at two different ages, with the younger Upernavik supracrustal unit deposited around 3400 Ma and the older Nulliak supracrustal assemblage deposited at around 3750 Ma. We show that both units are comparatively geochemically homogeneous with no distinction between the mafic and ultramafic rocks from both supracrustal assemblages. They mainly consist of mafic metavolcanic amphibolites with tholeiitic affinities, consistent with more depleted mafic and more enriched compositions produced by magmatic differentiation. Their complementary Eu anomaly

and whole-rock geochemistry suggest that they formed from fractional crystallization of gabbroic assemblage that derived from similar if not the same parental magma. The mafic metavolcanic rocks are also often associated with ultramafic rocks that we divided into two distinct units, respectively referred as the high-Fe and the low-Fe ultramafic rocks, characterized by different FeO contents and Al/Ti ratio. They both represent olivine-rich cumulative rocks derived from distinct parental komatiitic basalt magmas. Our interpretation contrasts with previous work suggesting that the SHC ultramafic rocks were komatiites and slivers of residual lithospheric mantle. Most SHC TTG exhibit a positive ^{142}Nd anomaly, as high as $\mu^{142}\text{Nd} = +15$, suggesting a source formed by differentiation in the Hadean. This ^{142}Nd isotopic composition is similar to the Nulliak supracrustal rocks that exhibit on average a μ^{142}Nd of +10. TTG is generally considered to derive from a mafic precursor. This study therefore shows that mafic crustal source of the SHC Eoarchean TTG, potentially the Nulliak metabasalts, derives from an ancient highly depleted mantle, described as the Saglek mantle, sharing a similar early history as the mantle reservoir involved in the formation of the ancient Itsaq terrane of southwest Greenland. The Saglek depleted mantle is interpreted to have formed at $\sim$4400 Ma, exhibit highly depleted signature with a $^{147}\text{Sm}/^{144}\text{Nd}$ ratio of $0.221 - 0.240$.

Keywords: Saglek-Hebron Complex, Eoarchean crust, Geochemistry, Petrology, Geochronology, Isotope

Aknowlegements

First, I would like to thank my supervisor the Dr. O'Neil Jonathan who helped me to cross the pond over to Ontario and allowed me to study in the field, and in lab, such a wonderful and exciting project as this thesis has been. This Ph.D. thesis would not have been possible with the tremendous help given by Dr. Rizo Hanika all along this adventure. I want to address a special thanks to Mrs. Susan R. Rust and Dr. Colin J. Rust who awarded me the Brian Rust memorial scholarship in 2016. the government of the Nunatsiavut and Park Canada Staff have been a tremendous help to conduct the fieldwork in the safest way possible. I would like to especially thank Janice Goudie (manager of the basecamp), Wayne Broomfield (manager of the basecamp), Tuumasi Itua Annanack (bear guard), Joe (bear guard), Ryan (bear guard), Elie (bear guard), John (bear guard), Jobie (Park Canada Staff), and Lary (Health and safety responsible) for their help and support in the field and at the Torngat Mountains Base Camp. We thank Bruce Ryan from the Department of Natural Resources of Newfoundland for his advice before fieldwork and to have shared a few samples. I thank Dr. Paquette Jean-Louis for its helpful experience in geochronology and his work on zircon and Dr. Zhang Shuangquan for its troubleshooting abilities and experience with mass spectrometry issues. I thank Dr. Arndt Nicolas for his helpful insight and experience on Archean ultramafic rocks from our field of study.

I want to also thank all our Precambrian research team here at the University of Ottawa and Carleton University, more particularly MSc. Rouleau Alexandre, MSc. Stepner Dan, MSc. Flageole Janick, MSc. Landon-Browne Ayesha, MSc. Sole Christian for their insightful conversations. I would also like to thank the administrative staff of the Department of Earth and environmental sciences of the University of Ottawa. Lisa Murphy and Hélène De Gouffe that have been a great moral support and also for their help and support through the insertion and administrative process. I want to thank my family in France and, now, also in Canada, as well as all the friends I found over the Canadian country, for their tremendous moral support available at any time. A special thanks also goes to my best friend Pascal Daoust who was always for her great help, support and few drinks.

Finally, I want to warmly thank my wife and future doctor Moreau Gwenaëlle who has never stopped believing in me and provided the greatest support and love over the oceans and times.

Contribution of authors

This Ph.D. thesis is the result of the collaboration of multiple laboratories and includes one peer-reviewed published paper and two additional papers to be submitted shortly for publication. This present thesis is the result of the fruitful collaboration of many researchers from the University of Ottawa, Carleton University in Canada, the Université Blaise Pascal Clermont II in France and the Université du Québec à Montréal (UQÀM).

I conducted all steps of the research for chapter 1, 2 and 3. I have done the work in the field during two summers in 2014 and 2016 where we have collected 247 samples. I have performed all steps of petrological sample characterization, sample preparation for whole-rock geochemistry, zircon separation and lab work for isotopic analyses. I have conducted the in-situ U-Pb and Hf analyses as well as the Sm-Nd isotope measurements. I was the lead author for all three studies. I was in charge of the interpretation of the data and the redaction of the manuscripts, with input from my supervisors. Most of the collected samples are part of this thesis and additional samples fed many other projects form our department and other international collaborators. Most major and trace element analyses were analysed by commercial labs ACME and Actlab and part of it was handled by the University of Ottawa XRF laboratory and are detailed in Chapters 1 and 2 (Table: 1.1 & 2.1. All imaging and in-situ mineral analysis were performed at the University of Ottawa SEM and microprobe lab with the great help of Dr. Poirier Glenn. The zircon separation and in-situ U-Pb and Lu-Hf analysis available in chapter 2 (Table: B.1) would not have been possible without the tremendous help of Dr. Paquette Jean-Louis, Dr. Gannoun Abdelmouhcine and Dr. Boyet Maud from the Université Blaise Pascal Clermont II. The chemistry protocols for the Nd isotopic data included in Chapter 3 were performed at the University of Ottawa and the measurement was performed at Carleton University and UQÀM with the fruitful collaboration of respectively Dr. Zhang Shuangquan and Dr. Poirier André.

Peer-reviewed article (see the full article in the appendix D)

Wasilewski, B., O'Neil, J., Rizo, H., 2019. Geochemistry and petrogenesis of the early Archean mafic crust from the Saglek-Hebron Complex (Northern Labrador). Precambrian Research, 328, pp. 129-150.

Conferences: poster and oral presentation (see abstractes in appendix D)

Poster: Wasilewski, B., ONeil, J., Rizo, H., **2015**. Petrological and geochemical investigation of the Eoarchean crust from the Saglek-Hebron complex,Northern Labrador. *GAC-MAC*, Montreal, Canada.

Oral: Wasilewski, B., ONeil, J., Rizo, H., **2016**. Geochemical investigation of the Saglek-Hebron Complex Northern Labrador : Implication for the formation of the early crust. *Advances in Earth Science Research Conference*, Carleton university, Ottawa, Canada.

Oral: Wasilewski, B., ONeil, J., Rizo, H., Paquette, J-L., Abdelmouhcine, G., Boyet, M., **2016**. Crustal evolution of the Eoarchean SaglekHebron Complex, Northern Labrador. *American Geophysical Union Fall meeting*, San Francisco, United-States.

Oral:Wasilewski, B., ONeil, J., Rizo, H., Paquette, J-L., Boyet, M., **2017**. Over one billion years of crustal evolution recorded in the Saglek-Hebron Complex (Northern Labrador) *Goldschmidt*, Paris, France.

Oral: Wasilewski, B., ONeil, J., Rizo, H., Paquette, J-L., Abdelmouhcine, G., Boyet, M., **2017**. Évolution crustale du complexe éoarchéen de Saglek-Hebron, au nord du Labrador. *Geotope*, Québec, Canada.

Oral: Wasilewski, B., ONeil, J., Rizo, H., Paquette, J-L., Boyet, M., **2018**. From early juvenile source to late crustal reworking: The evolution of the Saglek-Hebron crust. *European Geosciences Union*, Wien, Austria.

Oral: Wasilewski, B., ONeil, J., Rizo, H., **2019**. Geochronology and crustal evolution of the Eoarchean Saglek-Hebron Complex (Northern Labrador). 6^{th} *Young Natural History Scientists Meeting*, Paris, France.

Awards

- Brian Rust Memorial graduate scholarship in 2016
- Best oral presentation in "Earth and planetary sciences" session at the 6^{th}YNHM (Young Natural History Scientific meeting) in 2019

Contents

List of Figures

List of Tables

Introduction & overview

The biggest challenge in the study of the early Earth is the paucity and sometimes lack of rocks formed within the first billion years of its history. The violent nature of its early forming stages, such as accretion and meteoritic bombardment, and geological processes such as metamorphism and crustal melting, have tremendously erased the geological record from which geologist gather the information they need to interpret the Earth's formation and its early evolution. Bringing forward new data sets and methods is fundamental to understand such ancient history, slowly overwritten by crustal processes such as impacts, delamination, volcanism, alteration, weathering or metamorphism, over the past 4 billion years. The present introductory chapter is meant to contextualize these challenges, the most recent discoveries and the ongoing research about Archean/Hadean geology. In the second part, I present a historical overview of the research made on the area investigated in this thesis: the Saglek-Hebron Complex (SHC). Each one of these three following chapters can stand as individual publications and present new results, on the petrology, geochronology and crustal evolution of the SHC. They introduce and put the SHC in context according to their specific point of interest.

0.1 Advances in Early Earth Studies

Unlike any other terrestrial body that orbits around the Sun, the Earth host complex form of life, large surface water reservoirs, a dense oxidizing atmosphere and unique plate tectonics geodynamic (Wegener, 1915). The other terrestrial bodies in the Solar system have experienced mostly stagnant-lid-style tectonics and exhibit evidences of plume activity, lineament, polygonal terrains, rift, deformed belts and potentially relatively short period of Earth-like plate tectonic regime, allowing some recent planetary resurfacing (Connerney et al., 2005; Smrekar et al., 2018; Waiters, 1992). The Earth, as we observe and experience every day, is not representative of its entire 4568 Ma of history and was in its beginning drastically different from what we see today. The crustal formation, recycling, reworking, and weathering are fundamental processes that impact geochemical cycles and transformed the planetary bodies to how we know them today. Understanding such processes is fundamental to understand how and why planets evolved to their present state. However, if these processes are relatively well understood from the present Earth, they remain unclear if not mostly unknown for the primitive Earth. Therefore the composition of early Earth's reservoirs, the chronology of their formation, the Hadean/Archean pressure/temperature conditions, the ancient heat flow, the early tectonic setting or the onset of the magnetic field, is necessary information to shed light on early Earth geology.

Improving the accessibility to more and more rock samples as well as the development of new methodologies to study them, will greatly broaden our understanding of the past geology and could allow:

1. New insights into early volcanic and sedimentary environments.
2. The improvement of geochemical and isotopical interpretations.
3. A better understanding of the evolution of the crust-mantle system.
4. The study of Earth's early dynamics
5. The possibility of finding evidence of the earliest life habitats
6. A better understanding of Earth's early climate

0.1.1 The Hadean Eon

The two earliest Eras of the geological timescale are called the Hadean (4568 to 4000 Ma) and the Eoarchean (4000 to 3600 Ma) and are represented only by a handful of a few tens to hundreds of km^2 terrains worldwide (Fig. 1). They are the periods for which we have the least geological constraints. Therefore various tantalizing questions regarding major geological events and processes occurring during these early times of our planet are, still today, the subject of large controversy and debates.

The Hadean Eon begins at the formation of the Solar system at 4568.22 ± 0.17 Ma (Bouvier and Wadhwa, 2010) when the Earth and our telluric neighbors quickly accreted from asteroids, condensed gas, and dust from the protoplanetary disk. The Earth then cooled down and differentiated forming the core within the first tens of millions of years (*e.g.* Kleine et al., 2009). This lower limit for the Hadean is not officially

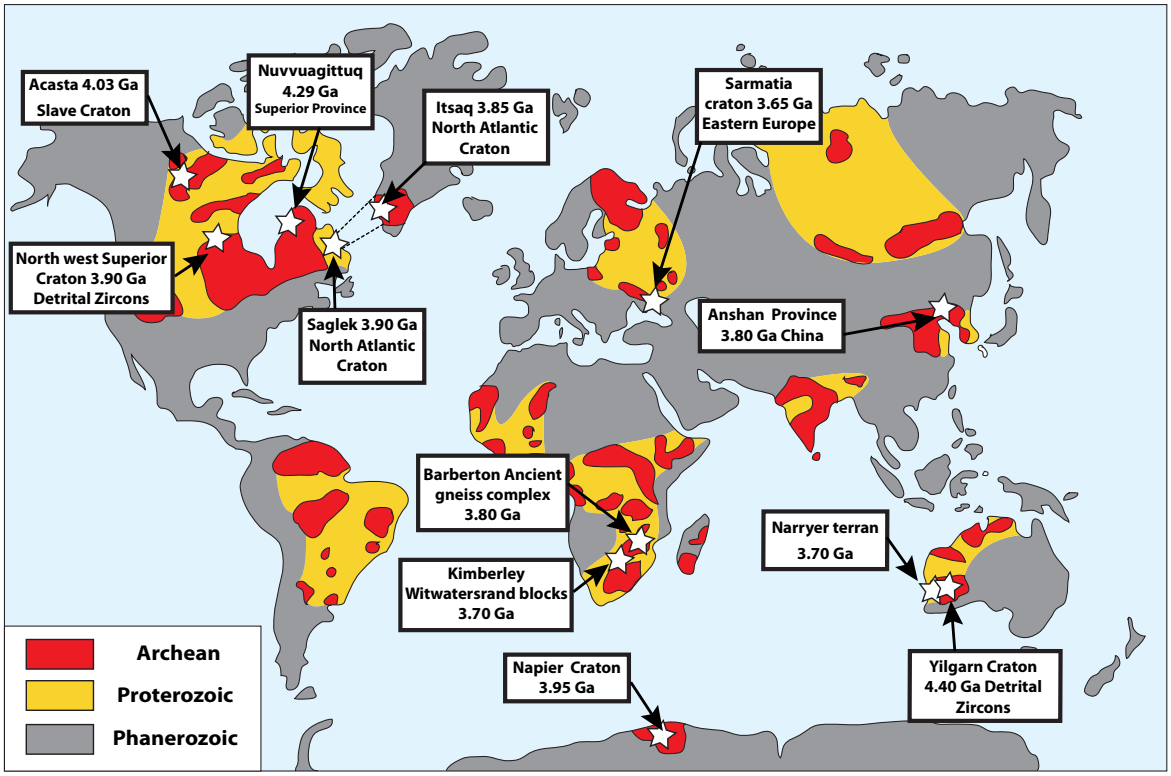

Figure 1

World map of the repartitions of Precambrian cratons on Earth (modified from Martin and Moyen (2002))

defined (Van Kranendonk et al., 2012) but is commonly taken to be at ∼4000 Ma. The Hadean used to be characterized by the absence of geological records mostly due to intense meteoritic bombardment, still visible today on the resurfaced lunar crust. Giant impacts, such as the Moon-forming impact, also had the potential to create magma oceans affecting most of the silicate portion of the planet (*e.g.* Elkins-Tanton, 2012). The early Earth was also affected by the Late Heavy Bombardment (LHB) which is an intense and protracted (∼200 Ma) meteoritic bombardment that occurred in the vicinity of 3900 Ma which has resurfaced most of the terrestrial bodies, including the Earth (Bottke and Norman, 2017). Nonetheless, rare Hadean material has been preserved on Earth such as within the Yilgarn Craton, in southwest Australia, hosting ∼3000 Ma

conglomerates that include detrital zircons as old as 4400 Ma with a main population around ~4100 Ma (Cavosie et al., 2004, 2019; Wilde et al., 2001), known as the Jack Hills zircons. These zircons provided numerous insights on the Hadean geology such as the suggested rapid cooling of the Earth between 4500 and 4400 Ma allowing the presence of surface water on Earth (Cavosie et al., 2005; Mojzsis et al., 2001; Valley et al., 2010; Wilde et al., 2001). Another group of least-altered zircons suggests the existence of long-lived ~4500 Ma early mafic crust over 400 Ma that could involve a stagnant lid tectonic regime (Kemp et al., 2010). During this past decade, extinct isotope systems such as ^{146}Sm-^{142}Nd or ^{182}Hf-^{182}W became extremely useful to study the earliest stages of the Solar system and early Earth's reservoirs (*e.g.* Bennett et al., 2007; Boyet et al., 2003; Boyet and Carlson, 2005; Caro et al., 2003; Kleine et al., 2005; Liu et al., 2016; O'Neil et al., 2008; Rizo et al., 2013, 2016; Willbold et al., 2011). The Nuvvuaguittuq Greenstone Belt from the Superior Province hosts what seems to be the oldest piece of mafic metavolcanic crust on Earth, called the Ujaraaluk unit, dated at ~4300 Ma using an ^{146}Sm-^{142}Nd system isochron (O'Neil et al., 2008, 2012). The Ujaraaluk unit is intruded by large differentiated gabbroic intrusions which yielded a ^{147}Sm-^{143}Nd isochron age of ~4100 Ma (O'Neil et al., 2012). However the rare zircon-bearing felsic rocks intruding the belt were dated by U-Pb at 3768 Ma, thus the exact age of the Nuvvuaguittuq Greenstone belt is still debated (Cates and Mojzsis, 2007, 2009; Darling et al., 2013; Guitreau et al., 2013; O'Neil et al., 2012, 2019). The Acasta gneiss in the Slave Province (western Canadian shield) also includes U-Pb zircon ages of ~4030 Ma (Bowring and Williams, 1999; Reimink et al., 2016).

0.1.2 The Archean Crust

After 4000 Ma, it is the beginning of the Archean, comprising rocks hosted in sev-

eral cratons spread around the world (Fig. 1). This eon ends at ∼2500 Ma and it is divided into 4 sub-periods the Eo-Paleo-Meso- and Neoarchean respectively ending at ∼3600 Ma, ∼3200, ∼2900, and ∼2500 Ma. This may soon be updated for the new Geological time scale in 2020 with more relevant age subdivisions for the Hadean and the Archean Eon (Ogg et al., 2016). Since this Ph.D. thesis is written in 2019 and since the final version of the new geological time scale will be released in 2020, the 2018 official version of the time scale will be used for this work. A number of Eoarchean terrains are found within the Canadian Shield and, by extension, the North Atlantic Craton (Fig. 1). Otherwise, the Eoarchean crust is concentrated in patches around the world. In the southwest of Australia, there is the Narryer terrane, which hosts the Yilgarn Craton, and exhibit rocks of 3730 Ma (Nutman et al., 1991; Wilde and Spaggiari, 2007). The Barberton Ancient crustal rocks from the Africa craton show also rocks as old as 3661 Ma (Compston and Kroner, 1988; Kröner, 2007; Kröner et al., 2014). In northeast China the Anshan Province in China exhibits tonalites as old as ∼3890 Ma (Song et al., 1996; Wu et al., 2008). Another important craton is the Napier Province in Antarctica, which is mostly unknown but shows the presence of remnant ∼3850 Ma (Black et al., 1986; Kusiak et al., 2014). The Eastern Europe craton exhibits rocks from the late Eoarchean in the Sarmatia craton with ages around 3650 Ma old (Bibikova and Baadsgaard, 1986; Bibikova and Williams, 1990). Within the western part of the Canadian shield, The Slave Province hosts the Eoarchean/Hadean Acasta Gneiss Complex which yields U-Pb zircon ages of ∼4030 Ma (Bowring and Williams, 1999; Reimink et al., 2016). The Eoarchean/Hadean Nuvvuagittuq Greenstone Belt of the Superior Province includes 3770-4280 Ma rocks (O'Neil et al., 2019). The North Atlantic Craton, mostly in Greenland, extends over the Labrador Sea onto Labrador's east shore and hosts the Itsaq Gneiss Complex (IGC), which includes the Isua Green-

stone Belt that comprises ∼3850 Ma old mafic and sialic crust (Baadsgaard et al., 1984; Nutman et al., 1996, 2009). The Nain Province of the North Atlantic Craton hosts the Saglek-Hebron Complex including the ∼3900 Ma old Iqaluk gneiss (Komiya et al., 2015, 2017; Shimojo et al., 2016) and potentially older mafic/ultramafic crust (Collerson et al., 1991; Komiya et al., 2017; Shimojo et al., 2016).

Geochemical tools applied to Archean rocks cannot clearly constrain a precise tectonic setting. The results will only provide information on petrogenesis and the environment of the rock formation (Moyen and Laurent, 2018; Wilson, 2007). Therefore the application of the principles of uniformitarianism should be approached with cautions when comparing the compositions of modern and ancient rocks. Many models tend to overlook the context of their interpretation, focusing mainly on the geochemical composition of the studied rocks. However, the field relationship, the nature of the rock, the environment in which the rocks have been preserved and/or adequate geophysical simulations are important features that should be taken into account and can lead to a more comprehensive interpretation framework (Roberts and Spencer, 2014).

Rocks formed in a modern-day geological environment are mostly classified in terms of rock composition (mineralogy and geochemistry) and can often be associated with specific tectonic regimes. The continental crust formation and evolution are formed mostly by arc processes (Scholl and von Huene, 2009) which produce mainly K-rich granitic rocks and calc-alkaline mafic rocks. The oceanic crust is formed as mid oceanic ridge basalt (MORB) tholeiites in oceanic spreading ridges and in a much less extent, the oceanic island basalt (OIB) type of mafic crust are issued from mantle plume activity as flood basalts. Modern mafic rocks exhibit some correlation between their chemistry and Earth's main geodynamic sites (Rollinson, 1993; Wilson, 2007). Archean mafic rocks are often found as enclaves in Archean TTG, forming belts of sometimes several

hundreds of square kilometers, but they are often out of their original geological context, commonly metamorphosed, remelted and deformed. Archean mafic rocks can often be divided into two main types of geochemical affinities: tholeiitic and calc-alkaline, and are regularly associated with komatiites. Mafic Archean rocks, in contrast with their modern analogs, are rarely alkaline in composition and present some geochemical similarities to ocean plateau basalts (Barnes and Arndt, 2019). Moyen and Laurent (2018) used a Th/Yb vs. Nb/Yb plot from Pearce (2008) to highlight that Archean basalts do not show bimodal patterns (arc vs. non-arc composition) as markedly as the Phanerozoic rocks. Most Archean mafic rocks in fact plot in between the mantle array (defined by MORB and OIB) and the arc array, displaced to higher Th/Yb ratios. (Moyen and Laurent, 2018). They exhibit almost systematically less compositional variation relative to the moderns analogue and mostly cluster around the normal MORB (N-MORB) and enriched MORB (E-MORB) source mantle, closer to what would be expected for derivation from the primitive mantle composition (Barnes and Arndt, 2019). This observation may suggest that the dominant source of the Archean mafic rocks remained relatively homogeneous and close to the primitive mantle. However, Lu-Hf and Sm-Nd isotopic data for some Eoarchean mantle-derived and felsic rocks show increasing evidence for an early highly depleted mantle (Bennett et al., 1993; Blichert-Toft and Albarède, 1999; Hoffmann et al., 2011; Nebel-Jacobsen et al., 2010; Rizo et al., 2011). The signature of this early highly depleted source is not apparent in $\sim$<3500 Ma rocks and seems to have been recorded only by Eoarchean mafic rocks and granitoids.

The geochemistry of Archean continental crust shows major differences compared with modern continental crust. Modern granitoids are generally more potassic in composition and are formed after magmatic fractionation of magma derived from a metasomatized mantle or reworked older crust. In contrast, the trondhjemite-tonalites-

granodiorites (TTG) formed during the Archean exhibit a more sodic composition and are generally interpreted to derived from an altered mafic precursor at relatively high-pressure where garnet is at equilibrium in the source (from ∼3.5 kbar) (*e.g.* Moyen and Martin, 2012). To produce Archean TTG, geophysical and thermodynamic modeling suggest that high pressure melting of a basaltic precursor can be achieved in both subduction and stagnant lid tectonic setting (Martin et al., 2014). Attempting to explain the formation and evolution of early crust is not as straight forward as explaining the modern Earth dynamic. Therefore, the tectonic regime in the early Earth has been the subject of debates (Bédard, 2018; Kemp et al., 2010; Laurent et al., 2014; Moyen and Laurent, 2018; Müller et al., 2009; Turner et al., 2014; Valley et al., 2010; Wilde et al., 2001) and presently there is still no scientific consensus on the exact tectonic settings forming the Archean crust.

Combining geochemistry, petrography, isotopic data and in-situ zircon geochronology study supported by existing geophysical modeling will bring further constraints to refine current theories and ideas about early crustal evolution.

0.2 Previous research on the Saglek-Hebron Complex

This thesis will focus on the crust formation and evolution of the Saglek-Hebron Complex (SHC). The SHC is one of the oldest remnants of Eoarchean terrains, recording one of the most protracted geological histories, including over 1600 million years (from 3900 Ma to 2200 Ma) within a 400 km^2 terrain. It is included in the Nain Province (Fig. 2), part of the North Atlantic Craton (NAC), separated from Greenland by the Labrador Sea opening that occurred 61 Ma ago (Storey et al., 1998). The Nain Province

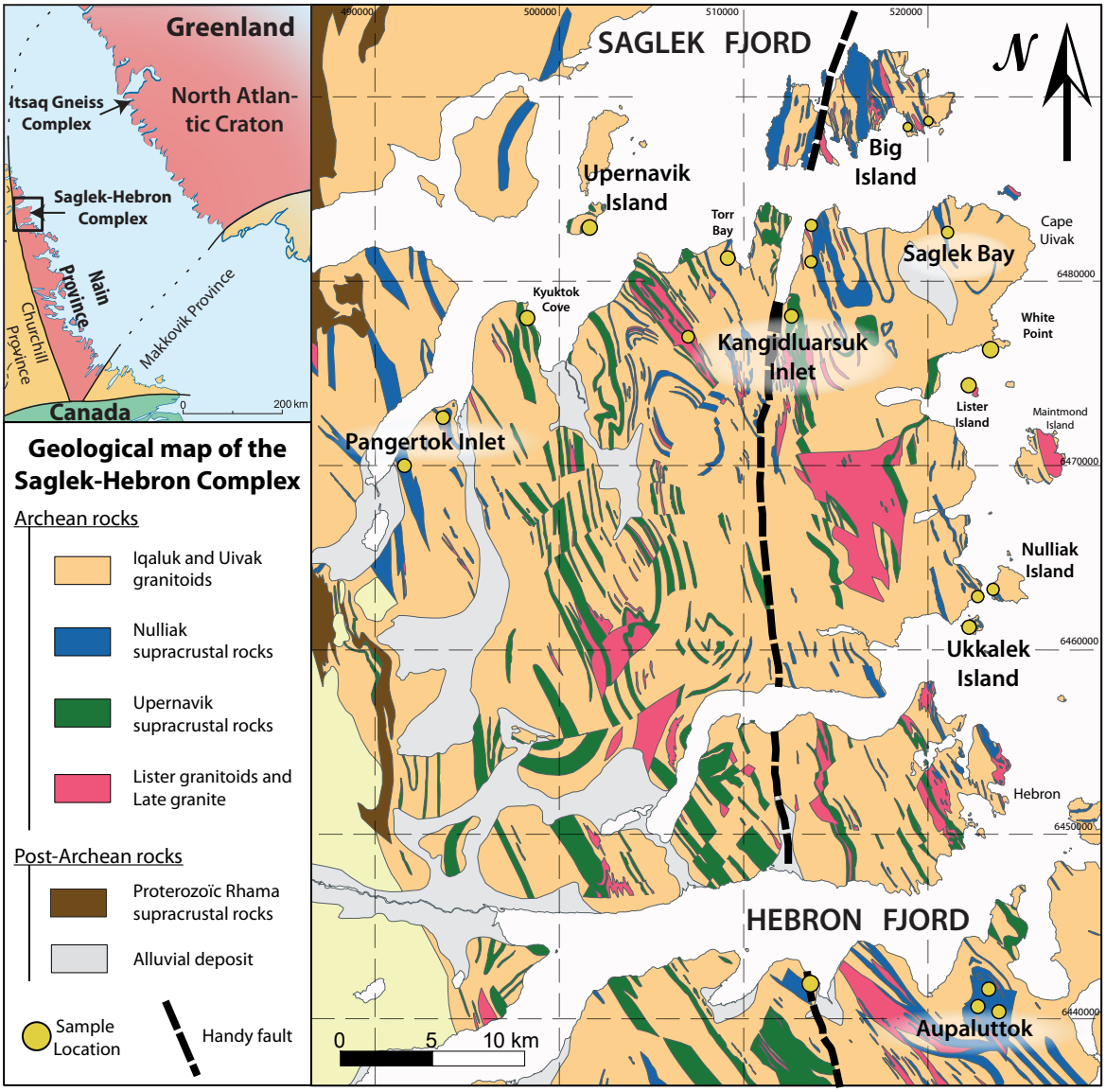

Figure 2

Geological map of the Saglek-Hebron Complex (SHC) modified from Ryan and Martineau (2012) and Komiya et al. (2015). Sample locations (yellow circles) show the main localities where multiple samples were collected for this study. Detailed GPS locations for each sample can be found in Table 1.1 2.1. Coordinates are in UTM NAD 27 zone 20.

spreads over the eastern coast of Labrador and it is separated into two structural blocks, respectively the Saglek block in the north and the Hopedale block in the south (Schiøtte et al., 1989b; Taylor, 1979). The Saglek-Hebron Complex is located within the Saglek

block and bordered between the Saglek Fjord to the north and the Hebron Fjord to the south (Fig. 2). Its western border is marked by the Pinguksoak thrust faults that separate it from the Churchill Province, accreted to the Nain Province during the 1800 Ma Torngat orogen.

Historically, research in Labrador started on the basis of geophysical work on the Canadian and Greenland cratons (Bullard et al., 1965; Le Pichon et al., 1971) associated with the discovery of 3750 Ma old rocks on the western coast of Greenland (Baadsgaard, 1973; Black et al., 1971; Moorbath et al., 1972) of which the geology showed "stunning similarities". Field reports (Morse, 1972, 1973, 1974, 1975, 1976, 1977) show a detailed characterization of most of the Torngat Mountains and the Labrador. The SHC was then intensively studied since the first Rb-Sr isochron age of 3600 Ma obtained within the Uivak gneiss (Barton, 1975; Hurst, 1974; Hurst et al., 1975). From then, most research was focused on field studies, Rb-Sr, K-Ar, Sm-Nd, and zircon U-Pb geochronology, from the early 1970's to the late 1990's since the development of new methods of investigation and the recent progress in Hadean and Archean geology, we see a recent revival for the interest on the SHC (Komiya et al., 2015, 2017; Kusiak et al., 2018; Krogh and Kamo, 2006; Morino et al., 2017, 2018; Sałacińska et al., 2018; Vezinet et al., 2018).

The SHC experienced at least two protracted high grade metamorphic episodes with peaks at 3600 and 2700 Ma respectively (Kusiak et al., 2018; Van Kranendonk, 1990). The Torngat orogen that accreted the NAC with the Churchill Province produced brittle deformation that cut the SHC into two structural blocks separated by a N-S striking fault called the Handy fault. On the eastern side of the fault, the metamorphic grade shows amphibolite facies and grades to granulite facies toward the south. On the western side of the Handy fault, the overall area shows granulite facies conditions.

The oldest unit found in the SHC was described as a 3800 to 4000 Ma grey gneiss (Collerson, 1983a; Nutman et al., 1989; Regelous and Collerson, 1996) originally called the Nanok gneiss, that could be derived from a 4100 to 4300 Ma mantle source (Regelous and Collerson, 1996). It is only recently, that a pre-3900 Ma age was obtained on a granitoid sample dated at 3920±49 Ma and renamed the Iqaluk Gneiss (Komiya et al., 2015, 2017; Shimojo et al., 2016). However, other authors have questioned the exactitude of this 3920 Ma age (Sałacińska et al., 2018; Vezinet et al., 2018; Whitehouse et al., 2019) and rather proposed an age closer to 3850 Ma due to the unrepresentative old ages and the vast minority of >3850 Ma zircon in the studied rock sample.

The dominant TTG unit in the SHC, called the Uivak gneiss, is a younger grey gneiss divided into two distinct units: the Uivak I and Uivak II, respectively 3750 and 3600 Ma. However, until recently, the Uivak II age of 3622 Ma was only supported by Rb-Sr whole rock isochron ages from Hurst (1974), Hurst (1974), and Wanless et al. (1979). Therefore, the geological meaning of this age was highly debated and often attributed to a metamorphic event, until more recent studies confirmed the existence of rocks with crystallization ages around 3600 Ma (Komiya et al., 2017; Krogh and Kamo, 2006; Sałacińska et al., 2018). The exact timing of the formation of the oldest SHC TTG units is still debated. Komiya et al. (2017) suggested that the Uivak unit could represent a single protracted magmatic pulse including 5 stages defined as Uivak-A;-B;-C;-D;-E and spanning between 3890 and 3610 Ma. Nevertheless, Krogh and Kamo (2006) showed, using an isotopic dilution of multi-grain zircons, U-Pb ages for only three dominant crustal production events at 3850-3800 Ma, 3750-3700 Ma, and 3630 Ma. Two different minor Paleoarchean generations of granitoids named the Lister gneisses were originally dated at 3348 and 3200 Ma (Krogh and Kamo, 2006; Schiøtte et al., 1989a). Komiya et al. (2017) suggested that the protolith of the Lister gneiss could

have been emplaced during a protracted event occurring between 3350 and 3200 Ma. During the late Archean, a high-grade thermal event produced large amounts of granites and migmatites in the SHC between 2800 and 2700 Ma (Krogh and Kamo, 2006; Kusiak et al., 2018; Schiøtte et al., 1992, 1989a; Van Kranendonk, 1990). So far, most studies associated a specific rock composition to each of the different generations of felsic rocks: the Iqaluk gneiss is described as trondhjemite, the Uivak I gneiss is also defined as trondhjemite, the Uivak II gneiss is classified as granodiorite and Neoarchean granitoids are described as granite. However, such restricted compositional definition of the distinct granitoid units in the SHC is more nuanced, but no clear geochemical characterization has yet been done on the different generations of granitoids.

The Eoarchean to Paleoarchean granitoids include enclaves of up to several square kilometers of metavolcanic and metasedimentary rocks. Baadsgaard et al. (1979) identified two supracrustal assemblages with debated origins (Bridgwater and Collerson, 1977; Collerson et al., 1991; Glikson, 1977; Komiya et al., 2015; Morino et al., 2017, 2018; Schiøtte et al., 1989b, 1992; Ryan, 1977). Originally, only one supracrustal sequence called the Upernavik unit was described, supposedly formed during the late Mesoarchean. Bridgwater et al. (1975) and Ryan (1977) highlighted the existence of deformed dykes (called the Saglek dykes), exhibiting elongated plagioclase phenocrysts, that are crosscutting the supracrustal rocks as well as the older Uivak I gneiss. This led them to conclude the existence of two different supracrustal units they named the Nuliak supracrustal assemblage and the Upernavik supracrustal assemblage, respectively interpreted to be Eoarchean and Paleoarchean in age. Collerson (1983b) suggested an emplacement age of 3400 to 3060 Ma for the younger Upernavik assemblage. However, this argument was only based on the interpreted field relationship to the Saglek dykes, which age is equally, if not more, unconstrained as that of the Upernavik supracrustal

rocks (Bridgwater et al., 1975, 1978; Komiya et al., 2015; Nutman and Collerson, 1991; Ryan, 1977). Nonetheless, detrital zircon studies confirmed the ancient age of the Nulliak supracrustal assemblage, interpreted to have a maximum age of $\sim 3776 \pm 8$ Ma (Schiøtte et al., 1989b) and associated with 3065 ± 8 Ma zircon overgrowth rims caused by a later thermal event. Collerson et al. (1991) obtained an age of 4017 ± 194 Ma from a Sm-Nd isochron in what they interpreted as a meta-komatiitic suite. Moreover, isotopic studies, mostly on ultramafic rocks from the Nulliak assemblage, showed Sm-Nd and Lu-Hf isochron ages of respectively 3782 ± 93 and 3794 ± 130 Ma (Morino et al., 2017, 2018). The Nulliak rocks also yielded a positive ^{142}Nd anomaly, suggesting derivation from a Hadean mantle source (Morino et al., 2017). In contrast, the younger Upernavik assemblage yielded 3362 ± 100 Ma and 3023 ± 390 Ma Sm-Nd and Lu-Hf isochron ages, without ^{142}Nd anomalies (Morino et al., 2017, 2018), which is consistent with the zircon Lu-Hf chondritic model age produced by Collerson (1983b) suggesting a minimum age for mantle extraction of the Upernavik detrital zircons of 3050 Ma.

The tectonic setting operating during the formation of the SHC has been discussed mostly regarding the Nulliak (Komiya et al., 2015) and Upernavik (Schiøtte et al., 1992) supracrustal assemblages. Komiya et al. (2015) proposed that the Nulliak supracrustal assemblage showed complex duplex structures, as well as a stratigraphy resembling what is observed in modern subducted plates, indicative of emplacement within an accretion prism. Based on these arguments, they discussed the possibility of a subduction-like tectonic regime as early as 3900 Ma. It has also been suggested that the Uivak I gneiss formed at 3750 Ma by shallow melting of the subducted slab beneath the accretion prism, due to anomalously high temperatures caused by the subduction of a spreading ridge (Komiya et al., 2015). Schiøtte et al. (1992) showed that the Upernavik metasedimentary rocks include detrital zircons with a wide range of ages and thus diverse detrital

sources from 3235 to 2840 Ma. They suggested that the contrasted detrital sources for the Saglek block, the Hopedale block, and southwestern Greenland, support continental accretion during the Late Archean, most likely between 2760 and 2690 Ma. However, the age constraint on the Upernavik supracrustal assemblage from the detrital zircons appears inconsistent with the age of 3362 ± 100 Ma for the formation of the Upernavik rocks suggested by Morino et al. (2017) from a Sm-Nd isochron on ultramafic rocks.

Recently, δ^{13}C analysis of metasedimentary rocks reveals the potential evidence of the oldest traces of life in the Saglek area (Tashiro et al., 2017). However, as Whitehouse et al. (2019) mentioned, the pre-3900 Ma age of the metasedimentary rock carrying the potential bio-signatures is based on equivocal field relationships with the Iqaluk grey gneiss and an imprecise age of 3920 ± 49 Ma (Shimojo et al., 2016), from zircon data they would interpret differently. This >3900 Ma age has not yet been reproduced by recent geochronology studies (Komiya et al., 2017; Sałacińska et al., 2018; Vezinet et al., 2018).

0.3 Ph.D. Objectives

Despite the recent renewed interest for the SHC, only a few studies have thoroughly looked at the petrology and whole-rock geochemistry of the Saglek-Hebron Complex. However, to better understand the crustal formation and evolution of these ancient rocks, it is crucial to understand the fundamental petrography and geochemistry to constraint the petrogenesis of these rocks. Without such a result, it can be difficult to interpret the newest isotopic data and build well-constrained geological models, given the complex and prolonged thermal history of the SHC capable of causing element mobility and obscuring the nature of the rocks. More importantly, geological relationships between the different rocks have to be well established to provide new insight into the

Table 1

List of localities sampled during fieldwork seasons. Localities are sorted from west to East and rocks types are cited by quantity sampled in the area. This is representative of the samples studied in this thesis. "#spl" = number of samples.

Locality	**GPS coordinates**		**#spl**	**Sampled lithologies**
	Northing	Easting		
Pangertok Inlet (Kutsugak Siurak)	491531	6470075	32	Mafic rock - Granite
Kyuktok Cove	498186	6478228	2	Mafic rock - Tonalite
Upernavik Island	501822	6483227	7	Mafic rock - Granite
Banana Lake	506896	6477255	2	Granite
Torr Bay (Situjunnait)	509865	6480510	8	Ultramafic rock - Tonalite - Mafic rock
Kangidluasuk (St John's Harbourg)	512541	6478501	32	Ultramafic rock - Trondhjemite - Tonalite - Granite - Mafic rock
Hebron Fjord	513698	6441583	3	Mafic rock - Trondhjemite - Ultramafic rock
Big Island	518901	6488011	7	Tonalite - Trondhjemite - Granite - Mafic rock
Saglek Bay (Itillek)	520740	6483084	11	Ultramafic rock - Mafic rock - Granite
Lister Island	522598	6474064	3	Tonalite - Trondhjemite
Iluilik (the opposit coast of Nulliak)	522697	6463625	7	Ultramafic rock - Mafic rock - Granodiorite - Granite
Ukkalek Island	522612	6461304	22	Ultramafic rock - Tonalite - Trondhjemite - Granite - Mafic rock
White Point (Tikiratsuk)	523239	6476427	4	Trondhjemite - Granite
Aupaluttoq	523364	6440463	29	Ultramafic rock - Mafic rock
Nulliak Island	523727	6462886	13	Mafic rock - Granite - Ultramafic rock
		Total	182	

processes taking place to form the early SHC crust and how it has been preserved.

The main objectives of this thesis were:

1. To provide a detailed petrological and geochemical study of the different magmatic lithologies of the SHC, including the mafic/ultramafic mantle-derived rocks and felsic granitoids, to better constrain their origin and petrogenesis.

2. To study the geochronology of the different generations of granitoids in the SHC,

over one billion years of early crustal history.

3. To constrain the crustal evolution of the SHC using long-lived (^{176}Lu-^{176}Hf, ^{147}Sm-^{143}Nd) and short-lived (^{146}Sm-^{142}Nd) isotopic systems, to investigate the involvement of Hadean reservoirs in the formation of the SHC crust and to decipher its complex and protracted crustal reworking history.

In this optic, two fieldwork seasons have been conducted in the summers of 2014 and 2016. Figure 2 shows the main sampling locations where a total of 247 samples were collected from accessible and extended supracrustal rocks and granitoid exposures in the Saglek-Hebron Complex (Supplementary material B.1 and A.1 show photographs from the field for respectively the granitoids and the mafic/ultramafic rocks). Thin sections were done for all samples. Table 1 presents the subset of 182 samples that were analyzed (whole-rock geochemistry and/or isotopic analyses) for this thesis. Solid care has been taken to sample the least altered outcrops for every lithology. Granitoid samples have been collected according to the description and presumed ages from the literature. A suite of samples has been collected from the same outcrop as that sampled by Shimojo et al. (2016), from which they obtained the oldest age of 3920 Ma reported in the SHC, in order to reproduce and discuss their controversial results (Shimojo et al., 2016; Whitehouse et al., 2019).

This thesis presents a thorough petrological and geochemical (whole-rock major and trace elements) characterization of all generations of mantle-derived rocks (Chapter 1) and granitoids (Chapter 2) from the SHC. It includes an extensive and detailed geochronology study with in-situ U-Pb isotopic analyses of over 1500 zircons from 18 granitoid samples. A subset of 250 zircons was then analyzed for in-situ Lu-Hf isotopic compositions (Chapter 2). Fifteen of these granitoids were analyzed for their isotopic composition of the long-lived ^{147}Sm-^{143}Nd and short-lived ^{146}Sm-^{142}Nd systems, to in-

vestigate the crustal reworking history and study the contribution of Hadean reservoirs (Chapter 3). Finally, a summary and active comparison between the SHC crustal evolution and Southwest Greenland is addressed in general conclusions.

With these three scientific contributions (cf. Chapter 1.2.3), this thesis provides an extensive new dataset that allows for a better comprehension of the SHC magmatic lithologies and their petrogenesis. It also allows addressing petrogenetic and isotopic links with other early terrains (including SW Greenland) and provides a crustal evolution model over the 1600 Ma of magmatic and metamorphic activity of this early giant rock library: The Saglek-Hebron Complex.

References

Baadsgaard, H., 1973. U-Th*Pb dates on zircons from the early Precambrian Amitsoq Gneisses, Godthaab District, West Greenland. Earth and Planetary Science Lettersc 12, 22.

Baadsgaard, H., Collerson, K. D., Bridgwater, D., 1979. The Archean gneiss complex of northern Labrador. 1. Preliminary U-Th-Pb geochronology. Canadian Journal of Earth Sciences, 951–961.

Baadsgaard, H., Cumming, G. L., Woden, J. M., 1984. U-Pb geochronology of minerals from the Midwest uranium deposit, northern Saskatchewan. Canadian Journal of Earth Sciences 21, 642–648.

Barnes, S., Arndt, N., 2019. Distribution and Geochemistry of Komatiites and Basalts Through the Archean. In: Van Kranendonk, M., Bennett, V. C., Hoffmann, J. E. (Eds.), Earth's Oldest Rocks, 2nd Edition. Elsevier, Ch. 6, pp. 103–132.

Barton, J., 1975. Rb-Sr isotopic characteristics and chemistry of the 3.6-B.Y. Hebron gneiss, Labrador. Earth and planetary 27, 427–435.

Bédard, J. H., 2018. Stagnant lids and mantle overturns: Implications for Archaean tectonics, magmagenesis, crustal growth, mantle evolution, and the start of plate tectonics. Geoscience Frontiers 9 (1), 19–49.

Bennett, V. C., Brandon, A. D., Nutman, A. P., 2007. Coupled 142Nd-143Nd isotopic evidence for Hadean mantle dynamics. Science 318 (5858), 1907–1910.
URL http://www.sciencemag.org/cgi/doi/10.1126/science.1145928

Bennett, V. C., Nutman, A. P., McCulloch, M. T., 1993. Nd isotopic evidence for transient, highly depleted mantle reservoirs in the early history of the Earth. Earth and Planetary Science Letters 119 (3), 299–317.

Bibikova, E., Baadsgaard, H., 1986. Sm-Nd isotopic dating of the ancient formations of the Ukrainian shield and Omolon massif. Geochemisrty International 5, 601–618.

Bibikova, E., Williams, I., 1990. Ion microprobe U-Th-Pb isotopic studies of zircons from three early Precambrian areas in the USSR. Precambrian Research 48, 203–221.

Black, L. P., Gale, N., Moorbath, S., Pankurst, R., McGregor, V. R., 1971. Isotopic dating of very early Precambrian amphibolite facies gneisses from Godthaab district, West GReenland. Earth and Planetary Science Letters 12, 245–259.

Black, L. P., Williams, I. S., Compston, W., 1986. Four zircon ages from one rock: the history of a 3930 Ma-old granulite from Mount Sones, Enderby Land, Antarctica. Contributions to Mineralogy and Petrology 94 (4), 427–437.

Blichert-Toft, J., Albarède, F., 1999. Hf isotopic compositions of the Hawaii Scientific Drilling Project Core and the source mineralogy of Hawaiian basalts. Geophysical Research Letters 26 (7), 935–938.

Bottke, W. F., Norman, M. D., 2017. The Late Heavy Bombardment. The Annual Review of Earth and Planetary Sciences is online at earth.annualreviews.org 45, 619–666.

Bouvier, A., Wadhwa, M., 2010. The age of the Solar System redefined by the oldest Pb–Pb age of a meteoritic inclusion. Nature Geoscience 3, 637–641.

Bowring, S. a., Williams, I. S., 1999. Priscoan (4.00-4.03 Ga) orthogneisses from northwestern Canada. Contributions to Mineralogy and Petrology 134 (July 1998), 3–16.

Boyet, M., Blichert-Toft, J., Rosing, M., Storey, M., Télouk, P., Albarède, F., sep 2003. 142Nd evidence for early Earth differentiation. Earth and Planetary Science Letters 214 (3-4), 427–442.
URL https://www-sciencedirect-com.proxy.bib.uottawa.ca/science/article/pii/S0012821X03004230

Boyet, M., Carlson, R. W., 2005. 142Nd evidence for early (>4.53 Ga) global differentiation of the silicate Earth. Science (New York, N.Y.) 309 (5734), 576–81.
URL http://science.sciencemag.org/content/309/5734/576.abstract

Bridgwater, D., Collerson, K., Myers, J. S., 1978. The development of the Archean Gneiss Complex of the North Atlantic Region. In: Evolution of the Earth's crust: academic Press, tarlingm d Edition. Royal Society, pp. 19–69.

Bridgwater, D., Collerson, K. D., 1977. On the origin of Early Archean gneisses: a reply. Contributions to Mineralogy and Petrology 62, 179–191.

Bridgwater, D., Collerson, K. D., Hurst, R. W., Jesseau, C. W., 1975. Field characters of the early precambrian rocks from Saglek, Coast of Labrador. Geological survey of Canada 75 (1), 287–296.

Bullard, E., Everett, J., Smith, A., 1965. The fit of the continents around the Atlantic. Philosophical Transactions of the Royal Society of London 258, 41.

Caro, G., Bourdon, B., Brick, J.-L., Moorbath, S., 2003. 146Sm-142Nd evidence from Isua metamorphosed sediments for early differentiation of the Earth's mantle. Nature 423, 428–432.
URL www.nature.com/nature.

Cates, N., Mojzsis, S., apr 2009. Metamorphic zircon, trace elements and Neoarchean metamorphism in the ca. 3.75Ga Nuvvuagittuq supracrustal belt, Québec (Canada). Chemical Geology 261 (1-2), 99–114.
URL https://www-sciencedirect-com.proxy.bib.uottawa.ca/science/article/pii/S0009254109000576

Cates, N. L., Mojzsis, S. J., 2007. Pre-3750 Ma supracrustal rocks from the Nuvvuagittuq supracrustal belt, northern Québec. Earth and Planetary Science Letters 255 (1-2), 9–21.

Cavosie, A., Valley, J., Wilde, S., 2019. The Oldest Terrestrial Mineral Record: Thirty Years of Research on Hadean Zircon From Jack Hills, Western Australia. In: Van Kranendonk, M., Bennett, V. C., Hoffmann, J. E. (Eds.), Earth's Oldest Rocks, 2nd Edition. Elsevier, Ch. 12, pp. 255–273.

Cavosie, A., Valley, J. W., Wilde, S. A., 2005. Magmatic δ 18 O in 4400-3900 Ma detrital zircons: a record of the alteration and recycling of crust in the Early Archean. Earth and Planetary Science Letters 235, 663–681.

Cavosie, A., Wilde, S., Liu, D., Weiblen, P., Valley, J., dec 2004. Internal zoning and UThPb chemistry of Jack Hills detrital zircons: a mineral record of early Archean to Mesoproterozoic (43481576Ma) magmatism. Precambrian Research 135 (4), 251–279.
URL https://www-sciencedirect-com.proxy.bib.uottawa.ca/science/article/pii/S0301926804002232

Collerson, K., 1983a. Ion Microprobe Zircon Geochrnonology of the Uivak Gneiss: Implication for the evolution of the early terrestrial crust in the north Atlantic craton. Workshop on a Cross Section of Archean Crust. LPI Technical report, 83-03, 28–33.

Collerson, K., 1983b. The Archean gneiss complex of northern Labrador. 2. Mineral ages, secondary isochrons, and diffusion of strontium during polymetamorphism of the Uivak gneisses. Can. J. Earth Sci. 20, 707–718.

Collerson, K. D., Campbell, L. M., Weaver, B. L., Palacz, Z. A., 1991. Evidence for extreme mantle fractionation in early Archean ultramafic rocks from northern Labrador. Nature 349 (6306), 209–214.

Compston, W., Kroner, A., 1988. Multiple zircon growth within early Archean tonalitic gneiss from Ancient Gneiss Complex, Swaziland. Earth and Planetary Science Letters 87, 13–28.

Connerney, J. E. P., Acuña, M. H., Ness, N. F., Kletetschka, G., Mitchell, D. L., Lin, R. P., Reme, H., 2005. Tectonic Implications of Mars Crustal Magnetism. Membrane Meshwork Protein and Cell Survival 102 (42), 14970–14975.

Darling, J. R., Moser, D. E., Heaman, L. M., Davis, W. J., O'Neil, J., Carlson, R., 2013. Eoarchean to neoarchean evolution of the Nuvvuagittuq Supracrustal belt: New insights from U-Pb zircon geochronology. American Journal of Science 313 (9), 844–876.

Elkins-Tanton, L., 2012. Magma Oceans in the Inner Solar System. Annual Review of Earth and Planetary Sciences 40, 113–139.

Glikson, A. Y., 1977. On the Origin of Early Archaean Gneisses. Contributions to Mineralogy and Petrology 62, 171–178.

Guitreau, M., Blichert-Toft, J., Mojzsis, S. J., Roth, A. S. G., Bourdon, B., 2013. A legacy of Hadean silicate differentiation inferred from Hf isotopes in Eoarchean rocks of the Nuvvuagittuq supracrustal belt (Quebec, Canada). Earth and Planetary Science Letters 362, 171–181.

Hoffmann, J. E., Munker, C., Naeraa, T., Rosing, M. T., Herwartz, D., Garbe-Schonberg, D., Svahnberg, H., 2011. Mechanisms of Archean crust formation inferred from high-precision HFSE systematics in TTGs. Geochimica et Cosmochimica Acta 75 (15), 4157–4178.

Hurst, R. W., 1974. The early Archean of coastal Labrador. In: Morse, S. A. (Ed.), The Nain anorthosite project: Field report 1973. U. Mass. Ceol. Dept ., Massachusetts, U.S., pp. 29–32.

Hurst, R. W., Bridgwater, D., Collerson, K. D., Wetherill, G. W., 1975. 3600-m,y, Rb-Sr ages from very early Archean gneisses from Saglek Bay, Labrador. Earth and Planetary Science Letters 27, 393–403.

Kemp, A. I. S., Wilde, S. A., Hawkesworth, C. J., Coath, C. D., Nemchin, A., Pidgeon, R. T., Vervoort, J. D., DuFrane, S. A., 2010. Hadean crustal evolution revisited: New constraints from Pb-Hf isotope systematics of the Jack Hills zircons. Earth and Planetary Science Letters 296 (1-2), 45–56.

Kleine, T., Mezger, K., Palme, H., Scherer, E., Münker, C., dec 2005. Early core formation in asteroids and late accretion of chondrite parent bodies: Evidence from 182Hf-182W in CAIs, metal-rich chondrites, and iron meteorites. Geochimica et Cosmochimica Acta 69 (24), 5805–5818.

Kleine, T., Touboul, M., Bourdon, B., Nimmo, F., Mezger, K., Palme, H., Jacobsen, S. B., Yin, Q.-Z., Halliday, A. N., sep 2009. HfW chronology of the accretion and early evolution of asteroids and terrestrial planets. Geochimica et Cosmochimica Acta 73 (17), 5150–5188.

Komiya, T., Yamamoto, S., Aoki, S., Koshida, K., Shimojo, M., Sawaki, Y., Aoki, K., Sakata, S., Yokoyama, T. D., Maki, K., Ishikawa, A., Hirata, T., Collerson, K. D., 2017. A prolonged granitoid formation in Saglek Block, Labrador: Zonal growth and crustal reworking of continental crust in the Eoarchean. Geoscience Frontiers 8 (2), 355–385.

Komiya, T., Yamamoto, S., Aoki, S., Sawaki, Y., Ishikawa, A., Tashiro, T., Koshida, K., Shimojo, M., Aoki, K., Collerson, K. D., nov 2015. Geology of the Eoarchean, > 3.95 Ga, Nulliak supracrustal rocks in the Saglek Block, northern Labrador, Canada: The oldest geological evidence for plate tectonics. Tectonophysics 662, 40–66.

Krogh, T., Kamo, S., 2006. Precise U-Pb zircon ID-TIMS ages provide an alternative interpretation to the early ion microprobe ages and new insights into Archean crustal processes, northern Labrador. In: Reimold, W., Gibson, R. (Eds.), Processes on the Early Earth. Geological Society of America, pp. 91–103.

Kröner, A., 2007. The Ancient Gneiss Complex of Swaziland and Environs: Record of Early Archean Crustal Evolution in Southern Africa. Earth's Oldest Rocks, 465–480.

Kröner, A., Wan, A., Liu, X., Liu, D., 2014. Dating of zircon from high-grade rocks: which is the most reliable method? Geoscience Frontiers 5, 515–523.

Kusiak, M. A., Dunkley, D. J., Whitehouse, M. J., Wilde, S. A., Sałacińska, A., Konečný, P., Szopa, K., Gawęda, A., Chew, D., 2018. Peak to post-peak thermal history of the Saglek Block of Labrador: A multiphase and multi-instrumental approach to geochronology. Chemical Geology 484 (May), 210–223.

Kusiak, M. A., Whitehouse, M. J., Wilde, S. A., Dunkley, D. J., Menneken, M., Nemchin, A. A., Clark, C., 2014. Changes in zircon chemistry during Archean UHT metamorphism in the Napier Complex, Antarctica. American Journal of Science 313 (9), 933–967.

Laurent, O., Martin, H., Moyen, J. F., Doucelance, R., 2014. The diversity and evolution of late-Archean granitoids: Evidence for the onset of "modern-style" plate tectonics between 3.0 and 2.5 Ga. Lithos 205, 208–235.

Le Pichon, X., Hyndman, R., Pantot, G., 1971. Geophysical study of the opening of the Labrador Sea. Journal of Geophysical Research 76, 4724.

Liu, J., Touboul, M., Ishikawa, A., Walker, R. J., Graham Pearson, D., 2016. Widespread tungsten isotope anomalies and W mobility in crustal and mantle rocks of the Eoarchean Saglek Block, northern Labrador, Canada: Implications for early Earth processes and W recycling. Earth and Planetary Science Letters 448, 13–23.

Martin, H., Moyen, J. F., 2002. Secular changes in tonalite-trondhjemite-granodiorite composition as markers of the progressive cooling of Earth. Geology 30 (4), 319–322.

Martin, H., Moyen, J. F., Guitreau, M., Blichert-Toft, J., Le Pennec, J. L., 2014. Why Archaean TTG cannot be generated by MORB melting in subduction zones. Lithos 198-199 (1), 1–13.

Mojzsis, S. J., Harrison, T. M., Pidgeon, R. T., 2001. Oxygen-isotope evidence from ancient zircons for liquid water at the Earth's surface 4,300 Myr ago. Nature 409, 178–181.

Moorbath, S., O'Nions, R., Pankurst, R., Gale, N., McGregor, V. R., 1972. Further Rubidium-Strontium age determinations on the very early Precambrian Rocks of the Godthaab District, West Greenland. Natural Physics Sciences 240, 78.

Morino, P., Caro, G., Reisberg, L., 2018. Differentiation mechanisms of the early Hadean mantle: Insights from combined176Hf-142,143Nd signatures of Archean rocks from the Saglek Block. Geochimica et Cosmochimica Acta 240, 43–63.

Morino, P., Caro, G., Reisberg, L., Schumacher, A., 2017. Chemical stratification in the post-magma ocean Earth inferred from coupled 146,147Sm142,143Nd systematics in ultramafic rocks of the Saglek block (3.253.9 Ga; northern Labrador, Canada). Earth and Planetary Science Letters 463, 136–150.

Morse, S. A., 1972. The Nain Anorthosite Project, Labrador: Field report 1971. Geology department University of Massachusetts.

Morse, S. A., 1973. The Nain Anorthosite Project, Labrador: Field report 1972. Geology department University of Massachusetts.

Morse, S. A., 1974. The Nain Anorthosite Project, Labrador: Field report 1973. Geology department University of Massachusetts.

Morse, S. A., 1975. The Nain Anorthosite Project, Labrador: Field report 1974. Geology department University of Massachusetts.

Morse, S. A., 1976. The Nain anorthosite project, Labrador: Field report 1975. Geology department University of Massachusetts.

Morse, S. A., 1977. The Nain anorthosite project, Labrador: Field report 1976. Geology department University of Massachusetts, Amherst, Massachusetts.

Moyen, J., Laurent, O., 2018. Archaean tectonic systems: A view from igneous rocks. Lithos 302-303, 99–125.

Moyen, J., Martin, H., 2012. Forty years of TTG research. Lithos 148, 312–336.

Müller, W., Shelley, M., Miller, P., Broude, S., 2009. Initial performance metrics of a new custom-designed ArF excimer LA-ICPMS system coupled to a two-volume laser-ablation cell. Journal of Analytical Atomic Spec 24, 209–214.

Nebel-Jacobsen, Y., Münker, C., Nebel, O., Gerdes, A., Mezger, K., Nelson, D. R., 2010. Reworking of Earth's first crust: Constraints from Hf isotopes in Archean zircons from Mt. Narryer, Australia. Precambrian Research 182, 175–186. URL https://journals-scholarsportal-info.proxy.bib.uottawa.ca/pdf/03019268/v182i0003/175{_}roefccazfmna.xml

Nutman, A. P., Collerson, K. D., 1991. Very early Archean crustal-accretion complexes preserved in the North Atlantic craton. Geology 19, 791–794.

Nutman, A. P., Friend, C. R. L., Paxton, S., 2009. Detrital zircon sedimentary provenance ages for the Eoarchaean Isua supracrustal belt southern West Greenland: Juxtaposition of an imbricated ca. 3700 Ma juvenile arc against an older complex with 3920-3760 Ma components. Precambrian Research 172 (3-4), 212–233.

Nutman, A. P., Fryer, B. J., Bridgwater, D., 1989. The early Archaean Nulliak (supracrustal) assemblage, northern Labrador. Can. J. Earth Sci. 26, 2159–2168.

Nutman, A. P., Kinny, P. D., Compston, W., Williams, I. S., 1991. SHRIMP U-Pb zircon geochronology of the Narryer Gneiss Complex, Western Australia. Precambrian Research 52, 275–300.

Nutman, A. P., McGregor, V. R., Friend, C. R., Bennett, V. C., Kinny, P. D., may 1996. The Itsaq Gneiss Complex of southern West Greenland; the world's most extensive record of early crustal evolution (3900-3600 Ma). Precambrian Research 78 (1-3), 1–39.

Ogg, J., Ogg, G., Gradstein, F., 2016. A Concise Geologic Time Scale, 1st Edition. Elsevier.

O'Neil, J., Carlson, R., Papineau, D., Levine, Y., Francis, D., 2019. The Nuvvuagittuq greenstone belt: A glimpse of Earth's earliest crust. In: Van Kranendonk, M. J., Bennett, V. C., Hoffmann, J. E. (Eds.), Earth's Oldest Rocks, 2nd Edition. Elsevier, Ch. 16, pp. 349–374.

O'Neil, J., Carlson, R. W., Francis, D., Stevenson, R. K., 2008. Neodymium-142 evidence for hadean mafic crust. Science 321 (5897), 1828–1831.

O'Neil, J., Carlson, R. W., Paquette, J. L., Francis, D., 2012. Formation age and metamorphic history of the Nuvvuagittuq Greenstone Belt. Precambrian Research 220-221, 23–44.

Pearce, J. A., jan 2008. Geochemical fingerprinting of oceanic basalts with applications to ophiolite classification and the search for Archean oceanic crust. Lithos 100 (1-4), 14–48.

Regelous, M., Collerson, K. D., 1996. 147Sm-143Nd, 146Sm-142Nd systematics of early Archaean rocks and implications for crust-mantle evolution. Geochimica et Cosmochimica Acta 60 (18), 3513–3520.

Reimink, J. R., Chacko, T., Stern, R. A., Heaman, L. M., aug 2016. The birth of a cratonic nucleus: Lithogeochemical evolution of the 4.02-2.94 Ga Acasta Gneiss Complex. Precambrian Research 281, 453–472.

Rizo, H., Boyet, M., Blichert-Toft, J., Rosing, M., 2011. Combined Nd and Hf isotope evidence for deep-seated source of Isua lavas. Earth and Planetary Science Letters 312 (3-4), 267–279.
URL http://dx.doi.org/10.1016/j.epsl.2011.10.014

Rizo, H., Boyet, M., Blichert-Toft, J., Rosing, M. T., 2013. Early mantle dynamics inferred from 142Nd variations in Archean rocks from southwest Greenland. Earth and Planetary Science Letters 377-378, 324–335.
URL http://dx.doi.org/10.1016/j.epsl.2013.07.012

Rizo, H., Walker, R. J., Carlson, R. W., Touboul, M., Horan, M. F., Puchtel, I. S., Boyet, M., Rosing, M. T., 2016. Early Earth differentiation investigated through 142Nd, 182W, and highly siderophile element abundances in samples from Isua, Greenland. Geochimica et Cosmochimica Acta 175, 319–336.
URL http://dx.doi.org/10.1016/j.gca.2015.12.007

Roberts, N., Spencer, C., 2014. The zircon archive of continent formation through time. Geological Society, London, Special Publications 389, 314.

Rollinson, H., 1993. Using eochemical sata: evaluation, presentation, interpretation. Longman, London.

Ryan, B., Martineau, Y., 2012. Revised and coloured edition of 1992 map showing the Geology of the Saglek Fiord - Hebron Fiord area, Labrador (NTS 14L/2,3,6,7). Scale: 1:100 000. Government of Newfoundland and Labrador, Department of Natural Resources, Geological Survey, Map 2012-15, Open File 14L/0091.

Ryan, B. A., 1977. Progressive structural reworking of the Uivak Gneisses, Jerusalem Harbour, Northern Labrador. Ph.D. thesis, Department of Geology Memorial University of Newfoundland.

Sałacińska, A., Kusiak, M. A., Whitehouse, M. J., Dunkley, D. J., Wilde, S. A., Kielman, R., 2018. Complexity of the early Archean Uivak Gneiss: Insights from Tigigakyuk Inlet, Saglek Block, Labrador, Canada and possible correlations with south West Greenland. Precambrian Research 315 (October 2017), 103–119.

Schiøtte, L., Compston, W., Bridgwater, D., 1989a. Ion probe UThPb zircon dating of polymetamorphic orthogneisses from northern Labrador, Canada. Canadian Journal of Earth Sciences 26 (8), 1533–1556.

Schiøtte, L., Compston, W., Bridgwater, D., 1989b. U-Th-Pb ages of single zircons in Archaean supracrustals from Nain Province, Labrador, Canada. Can. J. Earth Sci. 26, 2636–2644.

Schiøtte, L., Nutman, A. P., Bridgwater, D., 1992. U-Pb ages of single zircons within Upernavik metasedimentary rocks and regional implications for the tectonic evolution of the Archaean Nain Province, Labrador. Can. J. Earth Sci. 29, 260–276.

Scholl, D. W., von Huene, R., 2009. Implications of estimated magmatic additions and recycling losses at the subduction zones of accretionary (non-collisional) and collisional (suturing) orogens. Geological Society, London, Special Publications 318 (1), 105–125.

Shimojo, M., Yamamoto, S., Sakata, S., Yokoyama, T. D., Maki, K., Sawaki, Y., Ishikawa, A., Aoki, K., Aoki, S., Koshida, K., Tashiro, T., Hirata, T., Collerson, K. D., Komiya, T., 2016. Occurrence and geochronology of the Eoarchean, ˜3.9Ga, Iqaluk Gneiss in the Saglek Block, northern Labrador, Canada: Evidence for the oldest supracrustal rocks in the world. Precambrian Research 278, 218–243.

Smrekar, S. E., Davaille, A., Sotin, C., aug 2018. Venus Interior Structure and Dynamics. Space Science Reviews 214 (5), 88.

Song, B., Nutman, A. P., Liu, D., Wu, J., 1996. 3800 to 2500 Ma crustal evolution in the Anshan area of Liaoning Province, northeastern China. Precambrian Research 78 (1-3), 79–94.

Storey, M., Duncan, R. A., Pedersen, A. K., Larsen, L. M., Larsen, H. C., 1998. 40Ar/39Ar geochronology of the Wevanst Greenland Tertiary volcanic province. Earth and Planetary Science Letters 160 (3-4), 569–586.

Tashiro, T., Ishida, A., Hori, M., Igisu, M., Koike, M., Méjean, P., Takahata, N., Sano, Y., Komiya, T., sep 2017. Early trace of life from 3.95 Ga sedimentary rocks in Labrador, Canada. Nature 549 (7673), 516–518.

Taylor, F., 1979. Reconnaissance geology of a part of the precambrian shield, northeastern quebec, northern labrador and northwest territories, 393rd Edition. Geological Survey of Canada, Ottawa.

Turner, S., Rushmer, T., Reagan, M., Moyen, J.-F., feb 2014. Heading down early on? Start of subduction on Earth. Geology 42 (2), 139–142.

Valley, P. M., Fisher, C. M., Hanchar, J. M., Lam, R., Tubrett, M., 2010. Hafnium isotopes in zircon: A tracer of fluid-rock interaction during magnetite-apatite ("Kiruna-type") mineralization. Chemical Geology 275, 208–220.

Van Kranendonk, M., 1990. Late Archean geologic history of the Nain Province, North River-Nutak map area, Labrador, and its tectonic significance. Geoscience Canada 17 (4), 231–237.

Van Kranendonk, M., Altermann, W., Beard, B., Hoffmann, P., Johnson, C., Kasting, J., Melezhik, V., Nutman, A., Papineau, D., Pirajno, F., 2012. A Chronostratigraphic Division of the Precambrian: Possibilities and Challenges. In: The Geologic Time Scale 2012. Elsevier, pp. 299–392.

Vezinet, A., Pearson, D., Thomassot, E., Stern, R., Sarkar, C., Luo, Y., Fisher, C., 2018. Hydrothermally-altered mafic crust as source for early Earth TTG: Pb/Hf/O isotope and trace element evidence in zircon from TTG of the Eoarchean Saglek Block, N. Labrador. Earth and Planetary Science Letters 503, 95–107.

Waiters, T. R., 1992. System of tectonic features common to Earth, Mars, and Venus. Geology 20 (7), 609–612.

Wanless, R., Bridgwater, D., Collerson, K., 1979. Zircon age measurements for Uivak II gneisses from the Saglek area, Labrador. Can. J. Earth Sci. 16, 962–965.

Wegener, A., 1915. Die Entstehung der Kontinente und Ozeane. Dr. WILHELM WESTPHAL.

Whitehouse, M. J., Dunkley, D. J., Kusiak, M. A., Wilde, S. A., 2019. On the true antiquity of Eoarchean chemofossils assessing the claim for Earth's oldest biogenic graphite in the Saglek Block of Labrador. Precambrian Research.

Wilde, S. A., Spaggiari, C., jan 2007. Chapter 3.6 The Narryer Terrane, Western Australia: A Review. In: Earth's Oldest Rocks. Vol. 15. Elsevier, pp. 275–304.

Wilde, S. a., Valley, J. W., Peck, W. H., Graham, C. M., 2001. Evidence from detrital zircons for the existence of continental crust and oceans on the Earth 4.4 Gyr ago. Nature 409 (6817), 175–178.

Willbold, M., Elliott, T., Moorbath, S., 2011. The tungsten isotopic composition of the Earth'e mantle before the terminal bombardment. Nature 477, 195–198.

Wilson, B., 2007. Igneous Petrogenesis A Global Tectonic Approach. Springer.

Wu, F. Y., Zhang, Y. B., Yang, J. H., Xie, L. W., Yang, Y. H., 2008. Zircon U-Pb and Hf isotopic constraints on the Early Archean crustal evolution in Anshan of the North China Craton. Precambrian Research 167 (3-4), 339–362.

Chapter 1

Geochemistry and petrogenesis of the early Archean mafic crust from the Saglek-Hebron Complex (Northern Labrador)

Chapter 1 presents a detailed discussion of the petrography, geochemistry and petrogenesis of the mantle-derived rocks. It provides new insights on the origin and formation of the mafic and ultramafic rocks and establishes the petrogenetical link between these lithologies. This chapter includes the largest and most extensive whole-rock geochemical dataset of the mafic/ultramafic rocks from the Saglek-Hebron Complex.

Keywords: *Saglek-Hebron Complex, Eoarchean crust, Geochemistry, Petrology, Tholeiitic magmas, Komatiitic basalts*

This Chapter is published in Precambrian Geology:

Wasilewski, B., O'Neil, J., Rizo, H., 2019. Geochemistry and petrogenesis of the early Archean mafic crust from the Saglek-Hebron Complex (Northern Labrador). Precambrian Research, 328, pp. 129-150.

1.1 Introduction

The first billion years of Earth's history is poorly represented in the geological record, hindering our ability to understand early crustal formation processes. The oldest minerals preserved on Earth are detrital zircons as old as 4.4 Ga from the Jack Hill's conglomerates of the Yilgarn Craton in Western Australia (Wilde et al., 2001). Despite the fact that these zircons provide invaluable information about the early Earth, the original host rock in which they crystallized no longer exists. Scarce Hadean to Eoarchean terrains thus provide the only rock record to investigate the petrogenesis of the earliest crust, and the processes and tectonic settings in which it was formed. These include the 3.89 Ga Anshan area in China (Song et al., 1996; Wu et al., 2008), the 3.85 Ga Ancient Gneiss complex in Swaziland (Compston and Kroner, 1988; Kröner, 2007), the 3.85 Ga Itsaq Gneiss Complex in Greenland (Baadsgaard et al., 1984; Nutman et al., 1996, 2009), the 3.85 Ga Napier Complex in east Antarctica (Black et al., 1986; Kusiak et al., 2014), the 3.73 Ga Narryer Terrane in Australia (Nutman et al., 1991; Wilde and Spaggiari, 2007), the 4.03 Ga Acasta Gneiss Complex (Bowring and Williams, 1999; Reimink et al., 2016), the 3.77 to 4.28 Ga Nuvvuagittuq greenstone belt (Cates and Mojzsis, 2007; Darling et al., 2013; O'Neil et al., 2008, 2012) and the 3.92 Ga Saglek-Hebron Complex in Canada (Bridgwater et al., 1975; Schiøtte et al., 1989a; Shimojo et al., 2016).

The Saglek-Hebron Complex (SHC) in Northern Labrador is a typical granite-greenstone terrain that includes several enclaves of supracrustal rocks within plutonic felsic rocks. It has been recently proposed that some of the SHC granitoids are as old as 3920 Ma (Shimojo et al., 2016) and intrude the earliest volcano-sedimentary assemblage known as the Nulliak unit, making it one of the oldest known supracrustal suites of rocks on Earth. Understanding the petrogenesis of these early mantle-derived rocks can thus provide key constraints on the processes that formed Earth's primitive crust. Here, we present a petrological and geochemical study focussing on the SHC mantle-derived rocks, including both mafic metavolcanic and ultramafic rocks. This study provides new insights on their origin and petrogenesis, furthering our understanding of the early crustal formation processes of one of the oldest Archean complexes on Earth.

1.2 Geological setting

The Saglek-Hebron Complex is located on the east coast of Northern Labrador (Canada) within the Archean Nain Province of the North Atlantic Craton (Fig. 1.1). It is mainly composed of rocks from the trondjhemite-tonalite-granodiorite (TTG) series known as the Uivak gneiss interpreted to have formed between 3851 ± 46 Ma and 3732 ± 6 Ma (Collerson, 1983; Komiya et al., 2017; Schiøtte et al., 1989a; Shimojo et al., 2016). The Uivak gneiss includes several meters to kilometre-scale enclaves of supracrustal rocks and is intruded by 3240 Ma TTG known as the Lister gneiss (Schiøtte et al., 1989b) and Neoarchean granitic plutons (Fig. 1.1). The oldest felsic component of the SHC consists of banded grey gneisses referred as the Iqaluk gneiss and dated at 3920 ± 49 Ma (Shimojo et al., 2016). Whitehouse et al. (2019) however questioned this >3.9 Ga age, pointing out that a subset of the oldest $^{207}Pb/^{206}Pb$ ages obtained

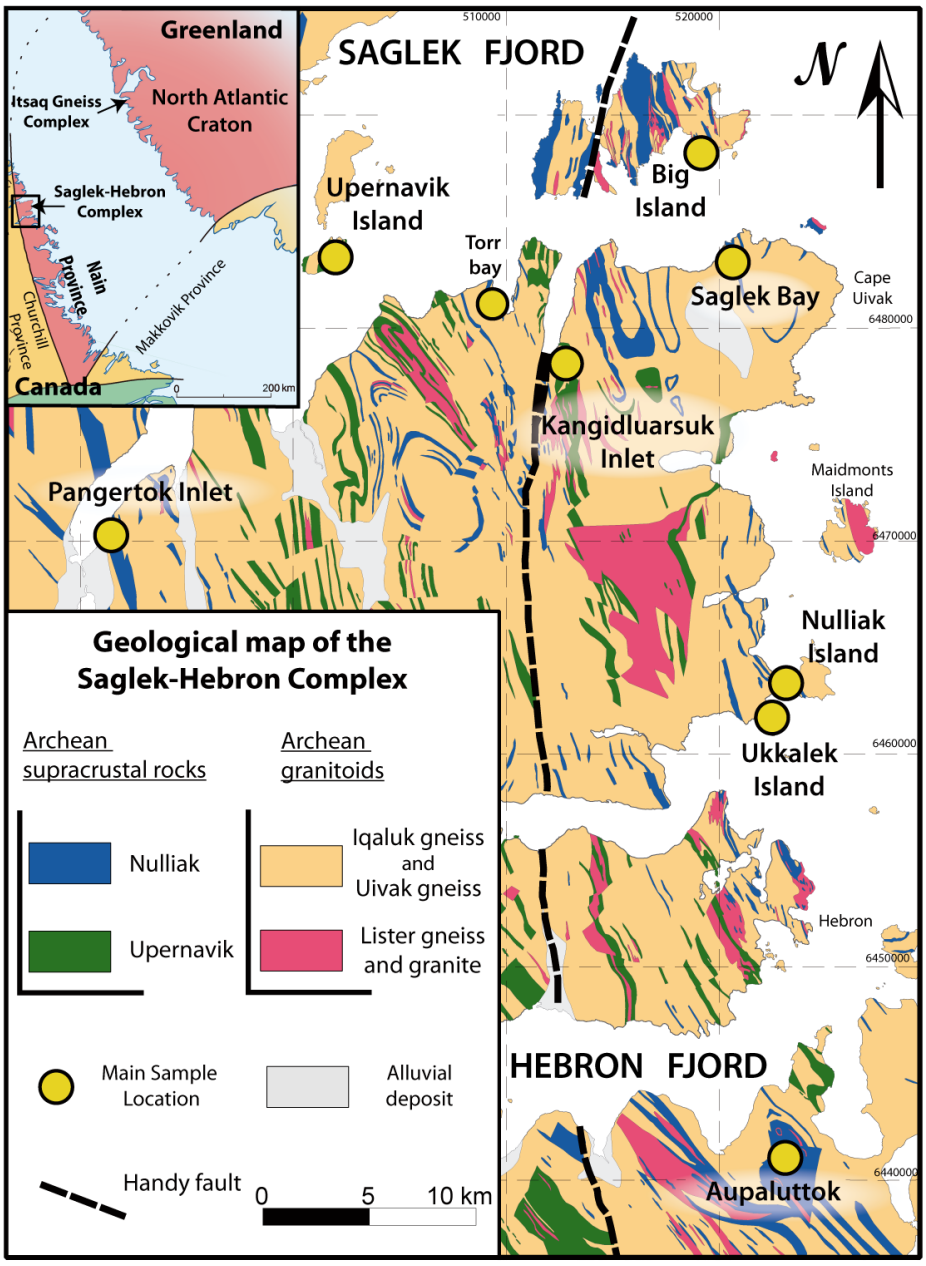

Figure 1.1

Geological map of the Saglek-Hebron Complex (SHC) modified from Ryan and Martineau (2012) and Komiya et al. (2015). Sample locations (yellow circles) show the main localities where multiple samples were collected for this study. Detailed GPS locations for each sample can be found in Table 1.1. The Nulliak and Upernavik Archean supracrustal rocks include mafic metavolcanic rocks, ultramafic and metasedimentary rocks. Coordinates are in UTM NAD 27 zone 20.

by Shimojo et al. (2016) define a statistically significant population with a mean age of 3865 ± 4 Ma. This Iqaluk gneiss unit may be equivalent to felsic rocks previously called the Nanok gneiss dated between 3840 Ma and 3900 Ma (Collerson, 1983; Krogh and Kamo, 2006; Regelous and Collerson, 1996) and found as enclaves within the younger Uivak gneiss. The supracrustal assemblages mainly consist of mafic metavolcanic rocks sometimes interbedded with detrital and chemical metasedimentary rocks (Bridgwater et al., 1975; Bridgwater and Schiøtte, 1991; Nutman et al., 1989).

Baadsgaard et al. (1979) identified two distinct supracrustal assemblages based on the presence or absence of crosscutting porphyritic mafic dykes called the Saglek dykes. The age of the Saglek dykes is poorly constrained, but they were likely emplaced during the Mesoarchean (Bridgwater and Schiøtte, 1991). These dykes seem to intrude only the older Nulliak supracrustal assemblage, while another volcano-sedimentary unit, called the Upernavik assemblage, does not appear to be intruded by the Saglek dykes and thus was interpreted to be younger than the Nulliak unit. Given the high degree of deformation and metamorphic recrystallization of the SHC, it can be difficult to establish clear crosscutting relationships between mafic dykes and mafic metavolcanic rocks, therefore, the occurrence of two distinct supracrustal units in the SHC is still debated (Baadsgaard et al., 1979; Bridgwater and Collerson, 1977; Glikson, 1977; Komiya et al., 2015; Morino et al., 2017; Nutman and Collerson, 1991; Ryan, 1977). The Nulliak unit mainly consists of mafic amphibolites interpreted as basaltic metavolcanic rocks (Nutman et al., 1989) locally interlayered with quartz-biotite-garnet metapelitic schists and horizons of quartzites (Bridgwater and Schiøtte, 1991). Chemical metasedimentary rocks such as banded iron formations (BIF), carbonates and chert-like quartzites occur in some Nulliak rocks (Baadsgaard et al., 1979; Bridgwater et al., 1975; Komiya et al., 2015; Nutman and Collerson, 1991). The Nulliak supracrustal unit is interpreted to be the

oldest lithology of the SHC, and one of the oldest supracrustal assemblages preserved on Earth, but its exact age remains unclear. A maximum age of 3776 ± 8 Ma has been proposed by Schiøtte et al. (1989a) based detrital zircons from quartzites interbedded within Nulliak metavolcanic rocks. However, Shimojo et al. (2016) interpret the oldest 3920 ± 49 Ma felsic gneiss as intruding the Nulliak supracrustal rocks, which would constrain a minimum age of 3.9 Ga on the Nulliak metavolcanic rocks. This age constraint, however, relies on field relationships that have been recently questioned (Sałacińska et al., 2018; Whitehouse et al., 2019). Morino et al. (2017) and Morino et al. (2018) have analysed a series of mafic and ultramafic rocks they interpret as being from the Nulliak unit, producing Sm-Nd and Lu-Hf isochrons yielding ages of 3782 ± 93 Ma and 3794 ± 130 Ma, respectively.

Mafic metavolcanic rocks with interbedded detrital metasediments also dominate the Upernavik unit, but as opposed to the Nulliak, the Upernavik assemblage does not appear to include chemical sediments such as BIF (Bridgwater and Collerson, 1977; Komiya et al., 2015; Nutman and Collerson, 1991). Samarium-Nd and Lu-Hf isochrons obtained on ultramafic and mafic rocks interpreted to be from the Upernavik unit yielded ages of respectively 3362 ± 100 Ma and 3023 ± 390 Ma (Morino et al., 2017, 2018). Detrital zircons in the Upernavik metasediments suggest that the SHC is an accreted terrane formed from multiples blocks that have sampled variable detrital sources between 3235 to 2840 Ma (Schiøtte et al., 1992), and most likely accreted during the peak of metamorphism around 2700 Ma (Bridgwater et al., 1975; Nutman and Collerson, 1991; Schiøtte et al., 1986; Van Kranendonk, 1990).

Finally, the SHC also contains ultramafic rocks, sometimes associated with the supracrustal assemblages, but more commonly occurring as ultramafic bodies within the Uivak TTG. Based on field relationships and geochemical characteristics, it has

been suggested that the ultramafic rocks associated with supracrustal units represent metakomatiites, whereas ultramafic rocks within the TTG constitute slivers of lithospheric mantle (Bridgwater et al., 1975; Bridgwater and Schiøtte, 1991; Collerson et al., 1991). Samarium-Nd isochron ages of 4017 ± 194 Ma and 3815 ± 194 Ma were obtained, respectively, on the proposed metakomatiite and lithospheric mantle suites (Collerson et al., 1991). Ishikawa et al. (2017), however, obtained younger Re-Os isochron ages of 3612 ± 130 Ma and 3096 ± 170 Ma for the same lithologies.

The SHC recorded multiple thermal episodes, including a Paleoarchean metamorphic event (Bridgwater and Collerson, 1976; Hurst et al., 1975; Schiøtte et al., 1986) and a protracted high-grade Neoarchean metamorphic event accompanied by migmatization and plutonic activity between 2800 and 2600 Ma, producing late granitic intrusions (Bridgwater et al., 1975; Kusiak et al., 2018; Nutman and Collerson, 1991; Schiøtte et al., 1986; Van Kranendonk, 1990). The SHC was later affected by brittle deformation during the Proterozoic Torngat Orogeny that caused a major north-south trending fault, known as the Handy fault (Fig. 1.1). This fault divides the SHC into two blocks that appear to have been subjected to different metamorphic conditions with amphibolite-facies to the east and granulite-facies to the west (Bridgwater et al., 1975).

1.3 Sampling and Analytical procedures

A total of 117 mafic metavolcanic and ultramafic rock samples were collected and prepared for polished petrographic thin sections and for whole-rock major and trace element geochemical analyses. Figure 1.1 shows the main sample locations and GPS coordinates for each of the samples can be found in Table 1.1. Two main suites of rocks

from the Nulliak unit were sampled from continuous exposures south of the Pangertok inlet and on the Aupaluttok mount south of the Hebron fjord. Rocks from the Upernavik unit were also sampled in two main well-exposed areas, on the Upernavik Island and in the Kangidluarsuk inlet. Ultramafic rocks were sampled when found in association with metavolcanic rocks on the Aupaluttok mount, but also to the west of Cape Uivak, on Ukkalek Island and in the Torr Bay, where they are mainly found as large enclaves of several tens to hundreds of meters, with only subordinate mafic rocks, surrounded by granitoids.

For all samples, weathered surfaces and secondary veins, if present, were carefully removed prior to crushing. Rock samples were then crushed to subcentimetre size chips using a steel jaw crusher and reduced to powder using an alumina shatter box. All samples were analysed for major element compositions and selected samples were further analysed for trace element concentrations. Major elements were analyzed either by inductively coupled plasma mass spectrometer (ICP-MS) or by X-ray fluorescence (XRF). ICP-MS analyses were performed by Activation Laboratories using a Perkin Elmer Sciex ELAN 9000 ICP-MS high-speed quadrupole. For these analyses, samples were fused using a lithium metaborate flux ($LiBO_2$), using a sample/flux ratio of 1:5. Three blanks and five international standards (three before sample analysis and two after) were analyzed per group of samples. Duplicates were analysed every 15 samples and the instrument was recalibrated every 40 samples. A subset of samples was selected for trace element composition analysis performed by ICP-MS at the same laboratories. Seven samples were selected for blind duplicates (see Table A.1). Full analytical techniques and detection limits (code: research 4B2) are available on the Activation Laboratories website at http://www.actlabs.com/page.aspx?page=555& app=226& cat1=549& tp=12& lk=no& menu=64. Major element analyses by XRF

were performed either by ACME Analytical Laboratories or at the University of Ottawa X-ray Core Facility. Analyses performed by ACME Laboratories were conducted using an AxiosFast X-ray spectrometer. Barium and Cr_2O_3 were also analysed by XRF for these samples (code: LF700). Powdered samples were fused using commercial $LiBO_2$and a sample/flux ratio of 1:5 to produce the glass disks to be analysed. Three blanks, two different standards (OREAS72B and SY-4(D)) as well as three duplicates were run during each analytical session. Details of the analytical procedures can be found on the ACME website at http://acmelab.com/pdfs/FeeSchedule-2015.pdf. XRF analyses performed at the University of Ottawa X-ray Core Facility were done on a Rigaku Supermini200 WDXRF Spectrometer. Powdered samples were fused using a flux made in-house (79/21 $Li_2B_4O_7/LiBO_2$) to produce glass disks (sample/flux ratio of 1:7) with addition of 6080 mg of LiBr. Reference materials used for mafic and ultramafic sample calibration curves were UB-N, UM-2, MRG-1, PM-s, BCR-2, WS-E, SY-3 BHVO-2, BM, AN-G, BCR-032 and PC-1016. Two samples were analyzed for their major element compositions by both ICP-MS and XRF techniques to evaluate the reproducibility between the different methods (see Table A.1: SG-049 & SG-057). No significant differences were observed between ICP-MS and XRF methods.

Major element compositions in olivine single grains were determined using a JEOL-JXA 8230 electron microprobe at the Advanced Research Center of the University of Ottawa. Operating conditions were 40 degrees takeoff angle and a beam energy of 20 keV. The beam diameter was 5 microns with a 40 nA current. Counting time was 20 seconds with an off peak counting time of 20 seconds for all elements. Elements were acquired using analyzing crystals LIF for Mn Kα, Fe Kα, LIFL for Ti Kα, Ni Kα, PETJ for Cr Kα, Ca Kα, K Kα, and TAP for Al Kα, Si Kα, Na Kα, Mg Kα, F Kα. The standards were Albite for Na Kα , Diopside #1 for Ca Kα, Mg Kα, Sanidine for

Al Kα, Si Kα, K Kα, Hematite for Fe Kα, Rutile for Ti Kα, Tephroite for Mn Kα, Fluorite for F Kα, Pentlandite for Ni Kα, and Chromite for Cr Kα. Unknown and standard intensities were corrected for dead time. Standard intensities were corrected for standard drift over time. Results are the average of 2 points and detection limits were 0.006 wt.% for Al Kα, 0.006 wt.% for Mg Kα, 0.011 wt.% for Ni Kα, 0.014 wt.% for Fe Kα and 0.139 wt.% for F Kα. Analytical sensitivity (at the 99% confidence level) was 0.164 % relative for Si Kα, 0.327 % relative for Mg Kα, 1.500 % relative for Na Kα, 3.819 % relative for Ti Kα, and 73.586 % relative for F Kα. Oxygen was calculated by cation stoichiometry and included in the matrix correction. Oxygen equivalent from halogens (F/Cl/Br/I) was not subtracted in the matrix correction.

1.4 Results

The mafic and ultramafic samples studied here were collected over multiple supracrustal enclaves and a wide extent of the SHC (Fig. 1.1). Determination of the Nulliak or Upernavik units in the field was done according to the latest regional scale mapping available (Ryan and Martineau (2012); Fig. 1.1). Collected samples include mafic amphibolites from both the Nulliak and Upernavik islands, the type localities for both supracrustal units. Major and trace element compositions of the SHC mafic and ultramafic rocks are presented in Table 1.1. Major element compositions were normalized to 100% and recalculated to anhydrous compositions for intercomparisons.

1.4.1 Petrography and geochemistry of mafic metavolcanic rocks

The mafic metavolcanic rocks from both the Nulliak and the Upernavik units exhibit comparable mineralogy consisting of medium to coarse-grained plagioclase + horn-

blende ± clinopyroxene ± orthopyroxene ± phlogopite ± garnet ± illmenite (Fig. 1.2a and Fig. 1.2b) with only slight variations in the proportion of clinopyroxene and orthopyroxene. Mineralogical assemblages, mineral proportions and grain sizes can vary between the metavolcanic rocks from each side of the Handy fault, likely due to different metamorphic conditions. Metavolcanic rocks east of the fault correspond to amphibolite facies, and are usually finer in grain size, with ferromagnesian minerals dominated by hornblende and subordinate pyroxene (Fig. 1.2a). Metavolcanic rocks found west of the fault correspond to granulite facies, and are generally coarser, with pyroxene as the dominant mafic mineral and hornblende mainly occurring as rims around pyroxene grains (Fig. 1.2b). Garnets are also more prominent in rocks west of the fault and can be found as large porphyroblasts but are more commonly found as fine grains following the main fabric observed at the outcrop scale. Deformed pillow structures have been observed within amphibolites from both the Nulliak and Upernavik units from Pangertok inlet and Upernavik Island locations (Fig. 1.2c).

Major element concentrations in the Nulliak and Upernavik units are similar and both exhibit relatively uniform compositions. With the exception of a few basaltic andesites, the mafic rocks from both units are basaltic in composition (Fig. 1.3) with SiO_2 contents ranging from 46.8 to 53.5 wt.% and MgO contents ranging from 5.9 to 14.9 wt.%. The TiO_2 content of the mafic samples reflects evolved ($TiO_2 > 0.5$ wt.%) and more depleted ($TiO_2 < 0.5$ wt.%) compositions, both found in the Nulliak and Upernavik units. Titanium and rare earth element (REE) concentrations correlate well with differentiation indices such as MgO or Mg#, with the more evolved metabasalts exhibiting higher REE contents and Mg# between 45 and 65, whereas the less evolved metabasalts display Mg# >65 and lower REE concentrations (Fig. 1.4a and b). Some metabasalts have relatively high Ca contents, with a number of samples having between

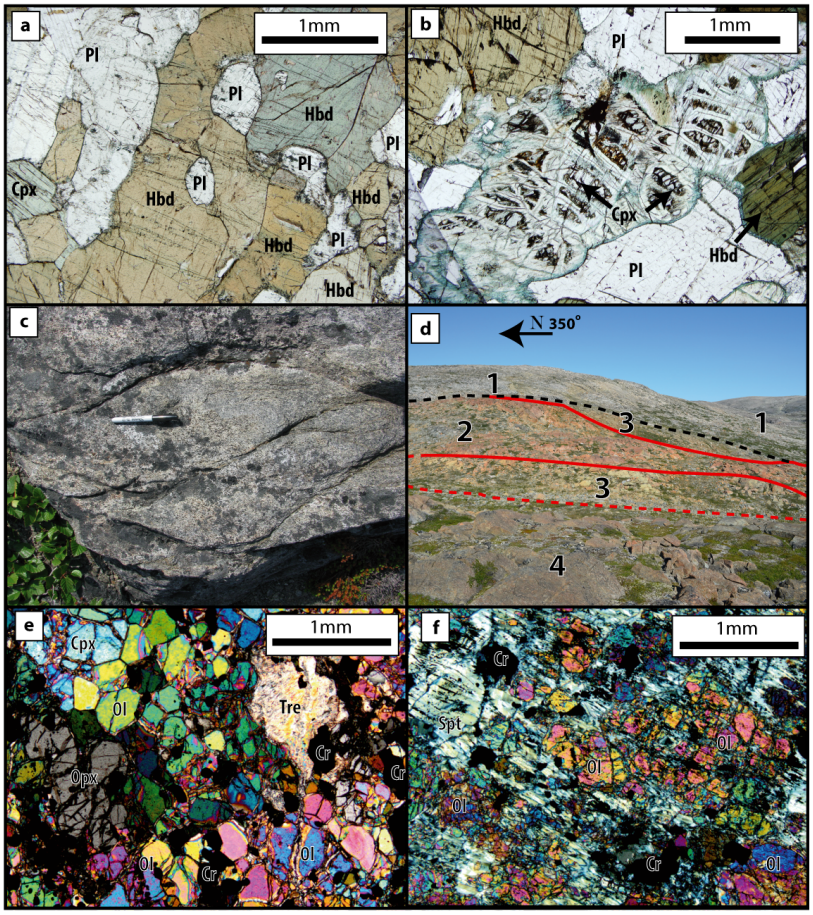

Figure 1.2

a) Photomicrograph in plane-polarized light of a typical mafic hornblende-plagioclase metavolcanic rock (SG-109B) from the amphibolite facies (Aupaluttok locality). b) Photomicrograph in plane-polarized light of a mafic metavolcanic rock (SG-043) from the granulite facies (Pangertok Inlet locality) showing clinopyroxene cores with rims of amphibole. c) Field photograph of deformed pillow lavas in Nulliak metavolcanic rocks from Pangertok Inlet. d) Field photograph of a large ultramafic layered body within the Uivak gneiss of the Saglek Bay area showing the different colours of the weathered surfaces of the different lithologies; 1 Uivak gneiss; 2 peridotite/harzburgite; 3 dunite; 4 mafic amphibolite. e) Photomicrograph in cross-polarized light of a typical ultramafic sample (SG-138) exhibiting olivine with 120-degree angle grain boundaries, chromite, orthopyroxene and tremolite. f) Photomicrograph in cross-polarized light of a serpentinized ultramafic sample (SG-137B) exhibiting serpentine and tremolite around embayed olivine and pyroxene grains. Cpx= clinopyroxene; Pl= plagioclase; Opx= orthopyroxene; Ol= olivine; Hbd= hornblende; Tre= tremolite; Spt= serpentine; Cr= chromite. -More pictures and photomicrographs are available in Supplmentary material Annex A.1 and A.2-

13 and 16 wt.% CaO (Fig. 1.4c). All mafic samples follow a tholeiitic trend, with Fe and Ti enrichments with decreasing MgO (Fig. 1.4d). Most immobile incompatible trace elements, such as Zr and Nb, are well correlated and increase in concentration with increasing TiO_2 content (Fig. 1.4e), whereas compatible elements, such as Cr and Ni, generally decrease with increasing TiO_2. The mafic rocks show variable Cr/Ni ratios following two distinct Cr *vs.* Ni trends (Fig. 1.4f), both found together within the same exposures of metavolcanic rocks (cf. Pangertok and Aupaluttok locations, Table 1.1). The SHC mafic metavolcanic rocks from both the Nulliak and Upernavik units display similar REE compositions with relatively flat profiles, with only a few samples displaying slight light-REE (LREE) enrichments or depletions (Fig. 1.5a). All mafic rocks have similar REE patterns, however, the less evolved metabasalts have lower REE concentrations (Fig. 1.4b) and commonly show slight positive Eu anomalies (Eu/Eu* up to 1.4; Fig. 1.5b). Therefore, these rocks will be referred as the "depleted metabasalts". In contrast, the more evolved rocks have higher REE concentrations and either no Eu anomalies or slight complementary negative ones (Fig. 1.4b, Fig. 1.5a and Fig. 1.5b), and will be thus referred as "enriched metabasalts". A slight LREE enrichment is observed in some samples, which does not appear to correlate with differentiation, and both the depleted and enriched metabasalts exhibit the same range in $(La/Sm)_N$ ratios (normalized to chondrite from McDonough and Sun (1995), Fig. 1.5c).

1.4.2 Petrography and geochemistry of ultramafic rocks

No significant petrological difference was found between the ultramafic rocks found as enclaves in the Uivak gneiss or within the supracrustal units (Nulliak or Upernavik). In the field, the ultramafic rocks display a typical brown weathered surface (Fig. 1.2d). Mineralogical proportions can vary within the large ultramafic bodies,

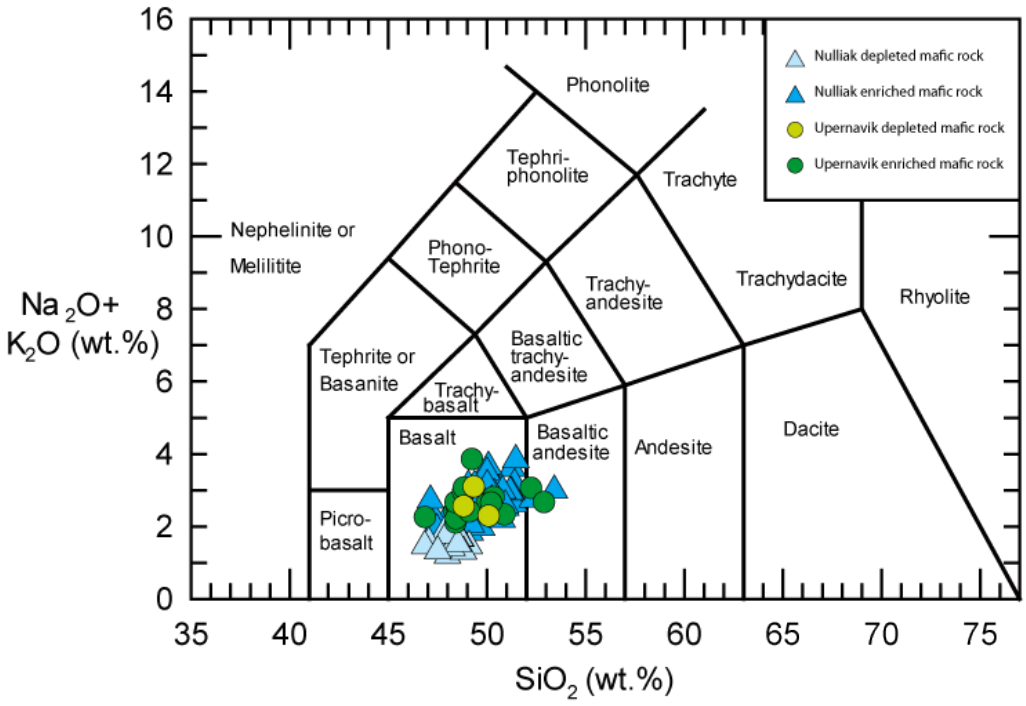

Figure 1.3

Total Alkali Silica (TAS) diagram for the SHC mafic metavolcanic rocks.

but they are mainly composed of olivine + orthopyroxene + clinopyroxene + spinel (chromite-magnetite) ± serpentine ± tremolite ± phlogopite (Fig. 1.2e and Fig. 1.2f). The ultramafic rocks show variable degrees of alteration and are commonly serpentinized with variable amounts of tremolite (Fig. 1.2f). A number of ultramafic samples show relatively fresh olivine grains, but these are characterized by metamorphic textures with 120 degrees grain boundary angles (Fig. 1.2e). Olivine compositions range from forsterite content Fo_{79} to Fo_{96} (Table A.2) and variations can be found within the same samples, with one sample containing olivine grains with compositions of Fo_{82} and Fo_{87} on the same thin section. In terms of calculated CIPW-normative mineralogy, the ultramafic rocks range from 10% to almost 100% normative olivine, which decreases with increasing normative pyroxene and plagioclase contents. Most ultramafic samples can be characterized as dunites, harzburgites or lherzolites with a few samples having

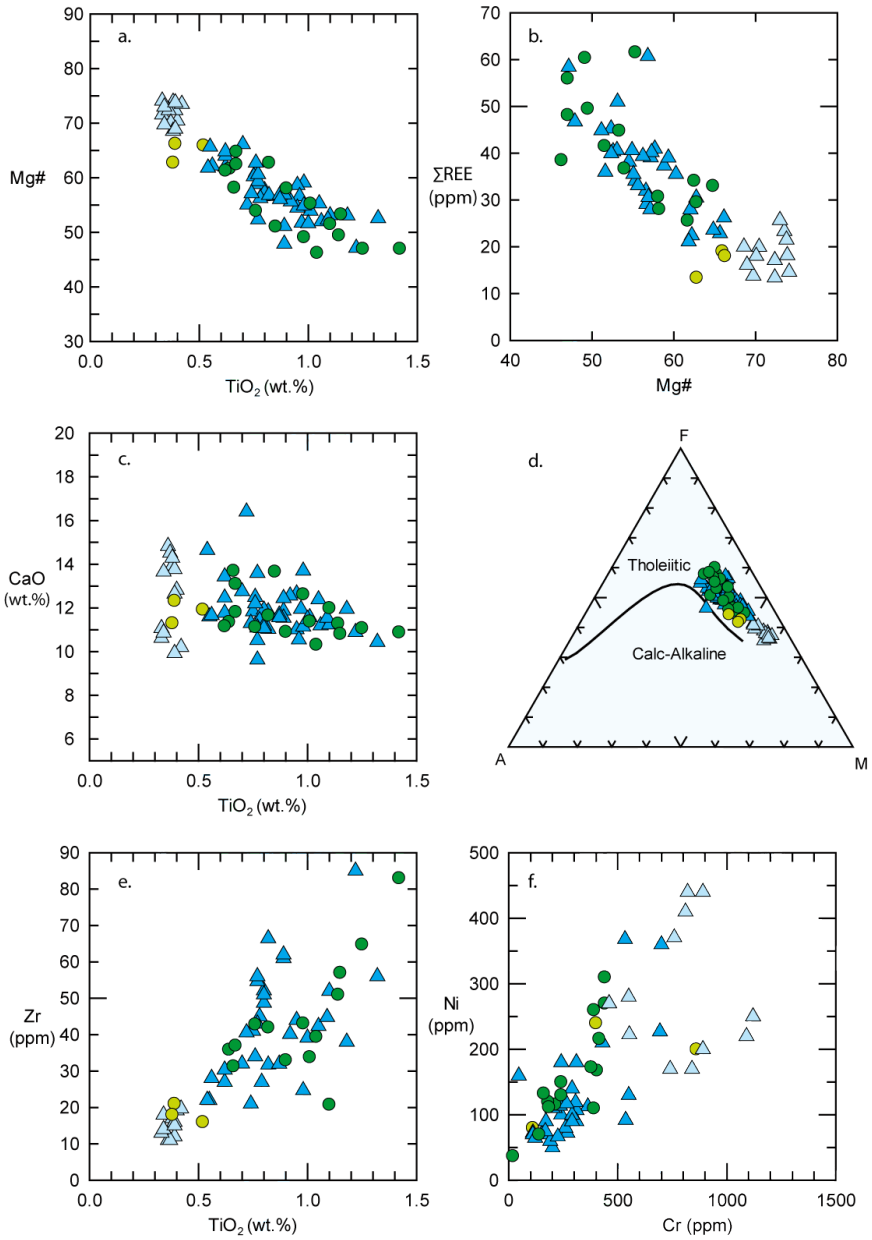

Figure 1.4

Major and trace element compositions for the SHC mafic metavolcanic rocks. a) c) and e) Selected major and trace element concentrations *vs.* TiO_2. b) REE *vs.* Mg# diagram for the mafic metavolcanic rocks. d) AFM ternary diagram after Irvine and Baragar (1971) for the Upernavik and Nulliak mafic samples. A: Na_2O+K_2O F: FeO^T M: MgO. f) Ni *vs.* Cr diagram for the SHC mafic rocks. Mg# = 100*Mg/(Mg+Fe). Same symbols as in figure 1.3.

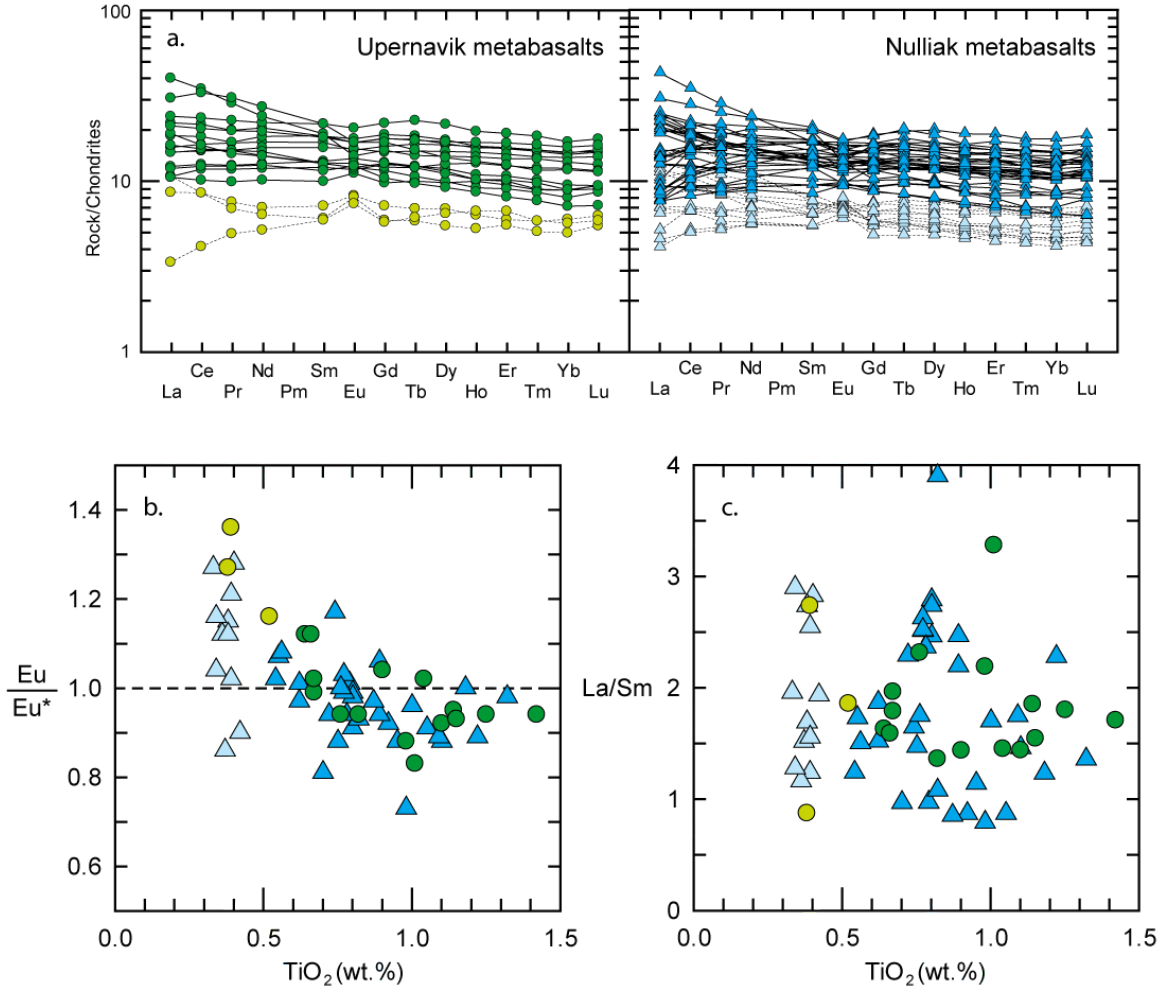

Figure 1.5

Major and trace element compositions for the SHC mafic metavolcanic rocks. a) Chondrite-normalized REE profiles for the Upernavik and Nulliak mafic rocks. b) and c) Selected trace element ratios *vs.* TiO_2. Chondritic normalizing values are from McDonough and Sun (1995). Same symbols as in figure 1.3.

less normative olivine, falling in the olivine-pyroxenite field (Fig. 1.6a). Mineralogical variations are also observed at the outcrop scale of the large ultramafic bodies that commonly exhibit "layers" or "zones" of different rock types (Fig. 1.2d).

Ultramafic rocks from the SHC show SiO_2 concentrations ranging from 40.6 to 51.5 wt.% and MgO contents between 20.3 to 49.9 wt.%. As for the mafic units, there is

no significant difference in major element compositions between ultramafic rocks associated with the Nulliak or the Upernavik units. Altogether, the ultramafic rocks can be divided in two different groups based on their Fe contents. The ultramafic samples that have mainly dunitic to harzburgitic CIPW normative compositions have lower Fe contents ranging from 7 to 11 wt%, whereas the lherzolitic samples have high Fe contents > 11 wt.% (Fig. 1.6b). The Mg# for the high-Fe ultramafic rocks is therefore generally low compared to the low-Fe ultramafic rock group (Fig. 1.6c). This is also somewhat reflected in the measured Fo contents of the olivine with the low-Fe samples containing olivine ranging in composition from Fo_{84} to Fo_{96}, whereas the olivine from the high-Fe rocks seems to be more Fe-rich, ranging from Fo_{79} to Fo_{87}. The high-Fe ultramafic samples generally have higher contents of normative clinopyroxene and CaO concentrations. These also have higher and more scattered Al_2O_3/TiO_2 ratios mainly between 20 and 40, compared to the low-Fe ultramafic rocks, which have homogeneous Al_2O_3/TiO_2 ratios ranging from 5 to 10 (Fig. 1.6d). The two groups of ultramafic rocks also show different trace element compositions. Chromium concentrations are significantly higher for the low-Fe ultramafic rocks than for to the high-Fe rocks (Fig. 1.1c). Compared to the low-Fe ultramafic rocks, the high-Fe rocks generally have higher concentrations in REE (Fig. 1.6e) and most other incompatible trace elements. Both ultramafic groups display different REE profiles, with the high-Fe samples exhibiting relatively flat to slightly enriched profiles, whereas the low-Fe rocks appear compositionally more heterogeneous, with most rocks having LREE enriched profiles and higher HREE concentrations relative to MREE (Gb/Yb_N <1, Fig. 1.6e).

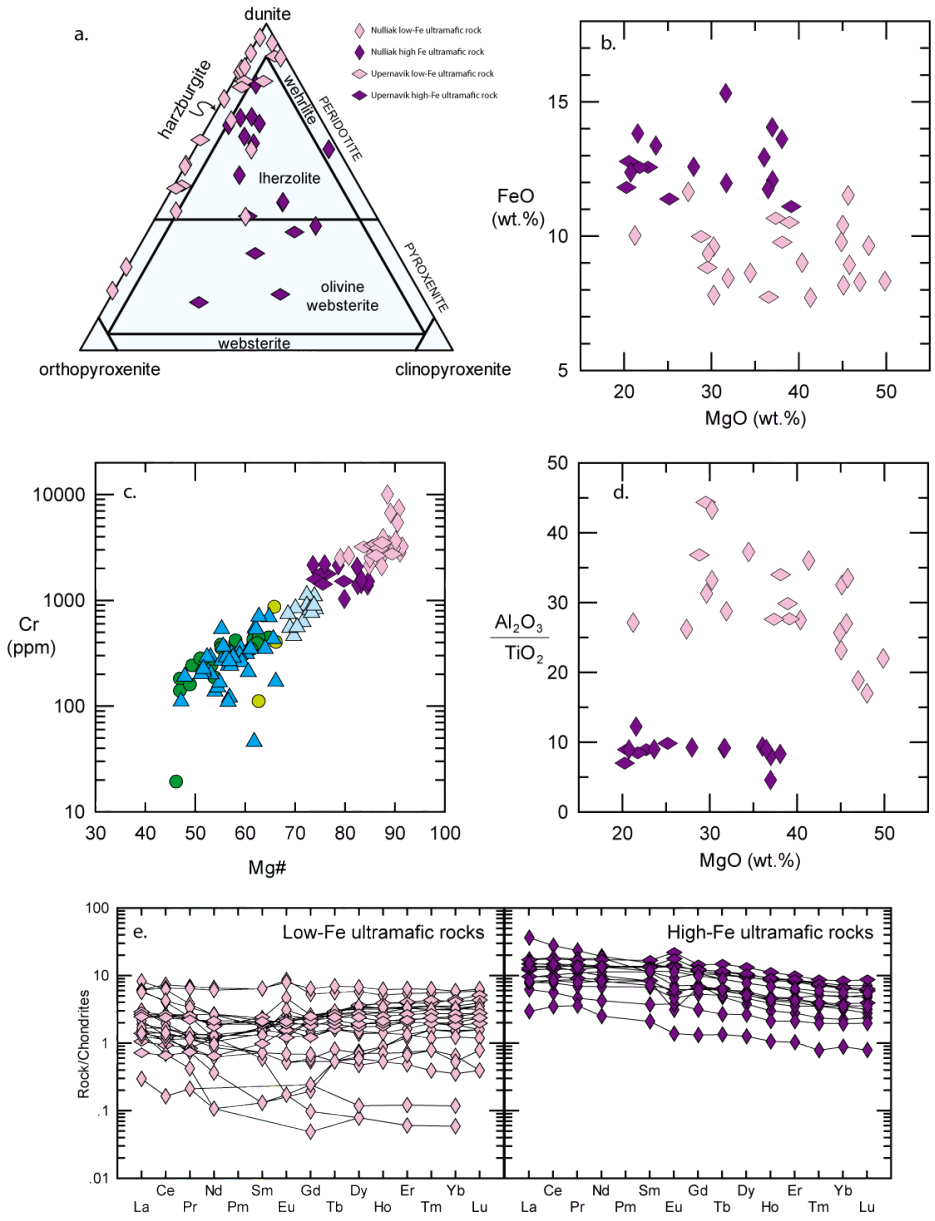

Figure 1.6

Major and trace element compositions for the SHC mafic and ultramafic rocks. a) Rock classification diagram after Le Maître (2002) using the calculated CIPW normative mineralogy for the SHC ultramafic rocks. b) FeO_t *vs.* MgO diagram for the SHC ultramafic rocks. c) Cr *vs.* Mg# diagram for the SHC ultramafic and mafic rocks. Mg# = 100*Mg/(Mg+Fe) d) Al_2O_3/TiO_2 *vs.* MgO diagram for the ultramafic rocks. e) Chondrite-normalized REE profiles for the SHC ultramafic rocks. Chondritic normalizing values are from McDonough and Sun (1995). Symbols for mafic rocks are as in figure 1.3.

1.5 Discussion

1.5.1 Assessment of element mobility

Several studies have shown that the SHC has been subjected to a protracted and complex thermal history with high-grade metamorphism up to granulite facies in some areas, and possible post-emplacement chemical alteration processes (Bridgwater et al., 1975; Komiya et al., 2017; Kusiak et al., 2018; Van Kranendonk, 1990). It is therefore crucial to establish the potential mobility of the different elements before using the geochemical compositions of the SHC rocks to constrain their nature and the petrogenesis of their protoliths.

The most immobile trace elements such as Ti, Zr, Nb, Y, Ta, V, Hf and REE define well-correlated trends for the mafic and ultramafic rocks (*e.g.* Fig. 1.4b and Fig. 1.4e), suggesting their relatively immobile behaviour during magmatic processes and supporting limited post-magmatic remobilization. The high Ca content (up to 16 wt.% CaO) of some mafic rocks could suggest secondary carbonatization, but the fact that the high-Ca rocks are not associated with high LOI values (Fig. 1.7a) or high Sr concentrations, as expected if they contained significant amounts of carbonates, argues against post-magmatic Ca-enrichment through carbonatization. Therefore, the high Ca content of the SHC metavolcanic rocks appears to be a primary compositional feature. Most SHC mafic rocks display relatively flat REE profiles, with a few samples exhibiting slight LREE enrichments (Fig. 1.5a). Correlations between La/Sm ratios and K2O contents, combined with the lack of clear correlations with other incompatible immobile elements such as Ti (Fig. 1.7b and Fig. 1.7c), suggest that the LREE enrichment of some mafic

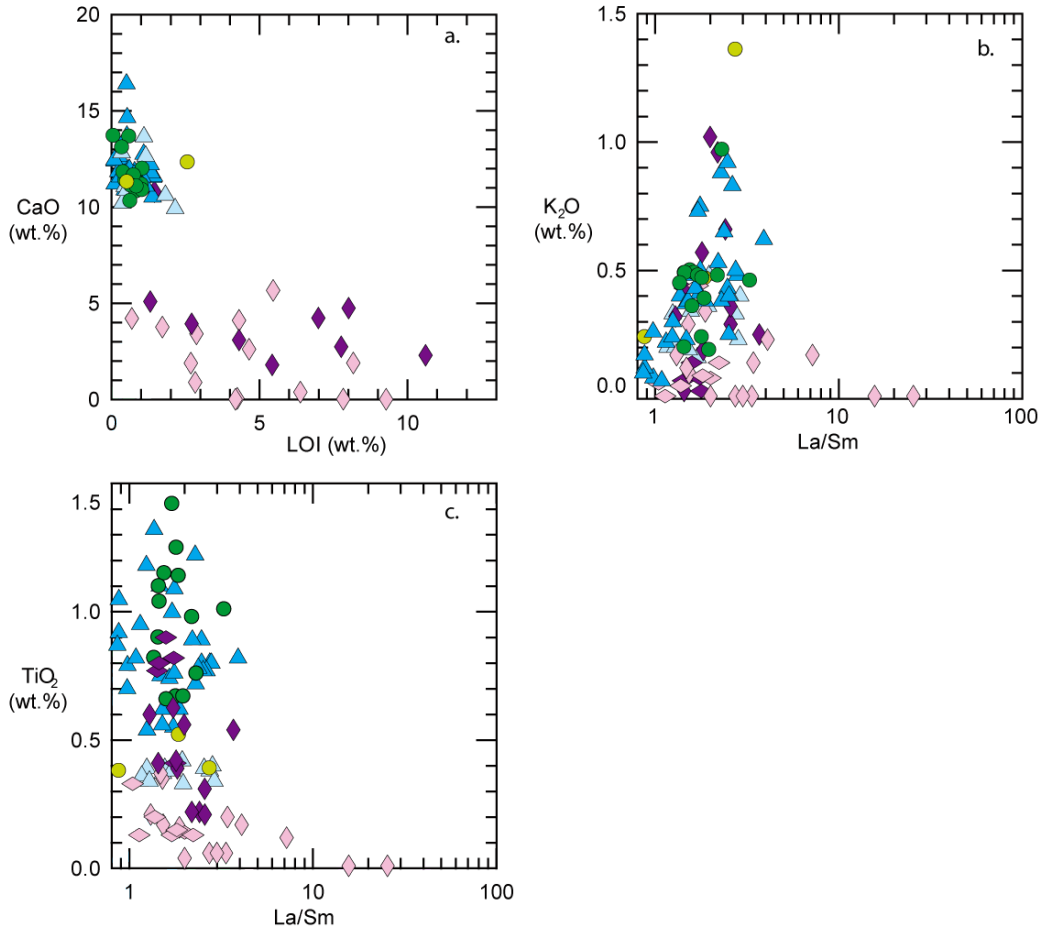

Figure 1.7

a) CaO *vs.* loss on ignition (LOI) diagram for the mafic and ultramafic rocks. b) and c) K_2O and TiO_2 *vs.* La/Sm for the mafic and ultramafic rocks. Symbols are as in figure 1.3 and figure 1.6.

samples is to some extent associated with post-magmatic potassic fluids, instead of being the result of magmatic differentiation. The La/Sm ratios for mafic rocks from both sides of the Handy fault are comparable, suggesting that if the LREE enrichment of the metavolcanic rocks is partly due to post-magmatic processes, both the granulite and amphibolite facies terrains from the SHC have been affected to a similar extent. The SHC ultramafic rocks can have very low trace element concentrations, especially the samples from the low-Fe suite, and perhaps more prone to post-magmatic enrichments.

A number of low-Fe ultramafic rocks exhibit enriched LREE profiles with relatively high La/Sm ratios (Fig. 1.6e). This is unusual for ultramafic rocks, whose primary mineralogy was likely composed of olivine and pyroxene, commonly LREE-depleted. Weak correlations can be observed between La/Sm ratios and mobile elements such as K, Ba or Rb for the ultramafic samples (Fig. 1.7b). This is perhaps more noticeable for the low-Fe samples, but because the concentrations for these elements are below the analytical detection limits for most low-Fe rocks, it is difficult to establish if the ultramafic samples with high La/Sm ratios are generally associated with higher concentrations of mobile elements. However, if the high La/Sm was the result of magmatic differentiation, one would expect a correlation with other immobile element such as Zr, Y, Ti, Al or Mg#. The ultramafic samples exhibiting the strongest LREE-enrichments, however, have the lowest Zr and Ti contents (Fig. 1.7c) which suggests that the higher LREE contents for some ultramafic rocks may not be primary compositional features but resulting from post-magmatic enrichments of the more mobile elements. A number of low-Fe ultramafic samples with enriched LREE compositions exhibit lower MREE contents compared to HREE profiles (Gd/Yb_N <1) (Fig. 1.6e), which is also consistent with LREE re-enrichments of previously depleted ultramafic rocks. The REE compositions for the SHC ultramafic rocks, and particularly for the samples from the low-Fe suite, should therefore be used with caution in order to investigate their petrogenesis.

1.5.2 Origin of the Saglek-Hebron Complex mantle-derived rocks

Early work suggested that the SHC includes two different supracrustal assemblages, the Nulliak and the Upernavik units, interpreted to be respectively Eoarchean and Mesoarchean in age. The interpretation for two separate supracrustal packages was

based on the field observation that some enclaves of supracrustal rocks do not appear to be crosscut by the Mesoarchean Saglek dykes, and thus would be part of a younger Upernavik unit, unrelated from the older Nulliak unit (Baadsgaard et al., 1979; Bridgwater et al., 1975; Ryan, 1977). The occurrence of these two distinct packages of metavolcanic rocks is however still debated (Baadsgaard et al., 1979; Bridgwater and Collerson, 1977; Glikson, 1977; Komiya et al., 2015; Nutman and Collerson, 1991; Ryan, 1977; Schiøtte et al., 1992) and previous authors have recognized that field relationships to distinguish between potentially distinct supracrustal packages can be uncertain (*e.g.* Sałacińska et al., 2018; Whitehouse et al., 2019). Recent Sm-Nd isotopic work by Morino et al. (2017) supports the occurrence of two separate suites of mafic and ultramafic rocks of different ages. They have obtained ^{147}Sm-^{143}Nd isochron ages of 3782 ± 93 Ma and 3362 ± 100 Ma for series of ultramafic and mafic samples they interpreted to be respectively from the Nulliak and Upernavik units. The two suites also showed distinct ^{142}Nd isotopic compositions. Samples defining the Eoarchean isochron yielded higher ^{142}Nd/^{144}Nd ratios than the Nd terrestrial standard, whereas samples interpreted to be Mesoarchean showed no resolvable ^{142}Nd anomalies. Because variability in ^{142}Nd/^{144}Nd ratios can only be produced by Sm/Nd fractionation in the Hadean, ^{142}Nd results suggest that the two rock suites were sourced from distinct mantle reservoirs formed at different times, *i.e.* prior to 4 Ga for the Eoarchean Nulliak suite and after 4 Ga for the Mesoarchean Upernavik suite. The Sm-Nd isochron ages contrast, however, with the Re-Os age obtained by Ishikawa et al. (2017) of 3612 ± 130 Ma for ultramafic rocks they interpret as metakomatiites associated with the Nulliak assemblage. The Sm-Nd and Re-Os age discrepancy may reflect open system behaviour of the different isotopic systems. For example, mostly ultramafic rocks have been studied for Sm-Nd and Re-Os systematics, and as shown in section 1.5.1., some of these samples exhibit unusually

LREE-enriched compositions for olivine-pyroxene-rich rocks (Fig. 1.6f). Ishikawa et al. (2017) argued that the Sm-Nd age of ∼3.4 Ga obtained by Morino et al. (2017),which lead them to interpret these rocks as being from the Mesoarchean Upernavik unit, rather represents the timing of a metasomatic event. Altogether, these results highlight the challenge of obtaining conclusive geochronological evidence using long-lived isotopic system isochron ages to support the occurrence of non-contemporaneous distinct suites of metavolcanic rocks in the SHC.

Petrogenesis of the Saglek-Hebron Complex mafic rocks

Most Archean cratons are dominated by TTG and granites, which are not directly derived from the mantle but are often interpreted to represent melts of an earlier crustal precursors. Eoarchean mantle-derived mafic volcanic rocks are scarce, and constraints on the composition of the early primitive crust come from rare preserved pre-3.6 Ga supracrustal belts such as the Nuvvuagittuq greenstone belt in Northern Canada and the Isua supracrustal belt in Southwest Greenland (*e.g.* Nutman and Friend, 2009; O'Neil et al., 2019). The mafic metavolcanic rocks from the SHC, with possibly distinct Eoarchean and Mesoarchean supracrustal assemblages, thus represent a unique opportunity to further our understanding of the petrogenesis of Earths primitive crust.

The SHC supracrustal rocks mostly occur as discrete enclaves, usually tens of meters wide to up to a few kilometres long (Fig. 1.1), and are dominated by mafic amphibolites interpreted to be basaltic metavolcanic rocks. It is difficult to observe continuous stratigraphy within the supracrustal rocks due to the fact that the deformed enclaves are dispersed within the Uivak TTG. Nonetheless, local occurrence of deformed but preserved pillow lava structures, notably in the Pangertok Inlet and Upernavik Island areas (Fig. 1.2c), as well as the presence of chemical sediments, are consistent with sub-

marine volcanic eruptions. The volcanic rocks are commonly interbedded with clastic sediments (*e.g.* Pangertok Inlet and Aupaluttok areas) and usually occur as relatively thin sequences of a few meters to tens of meters, alternating with meter-scale metasedimentary units, suggesting episodic volcanic activity. The geochemical composition of the mafic amphibolites is generally relatively homogeneous with no noticeable petrological or geochemical differences between rocks from the Nulliak and the Upernavik assemblages (Fig. 1.3, 1.4, 1.5 and 1.6). Compositional variations in major elements follow igneous differentiation trends (*e.g.* Fig. 1.4) suggesting that most metabasalts are formed under similar conditions. The flat REE patterns (Fig. 1.5a) and tholeiitic composition trends with Fe enrichments (Fig. 1.4d) and increasing Ti contents (Fig. 1.4e) suggest the SHC mafic rocks were derived from a relatively undepleted mantle source, and fractionation occurred under relatively dry and low-pressure conditions.

The relative trace element concentrations and the slight complementary Eu-anomalies observed in depleted and enriched mafic rocks (Fig. 1.5a) could be consistent with fractional crystallization within the metabasaltic flows. While Eu anomalies could result from the alteration of plagioclase in these rocks, Eu concentrations and Eu anomalies correlate well with immobile element such as Ti, Zr or Nd, and suggest therefore plagioclase crystallization, as opposed to Eu mobilisation during alteration. The SHC mafic amphibolites thus could represent a series of flows that differentiated to various extents before eruption and/or within the flows, leading to the formation of enriched and depleted metabasalts, representing residual liquids and pyroxene-rich cumulate-liquid mixtures, respectively.

Figure 1.8 shows fractional crystallization models of a gabbroic assemblage (composed of 5% olivine, 10% orthopyroxene, 35% clinopyroxene and 50% plagioclase) using the composition of samples SG-090 and SG-043 as starting compositions. These samples

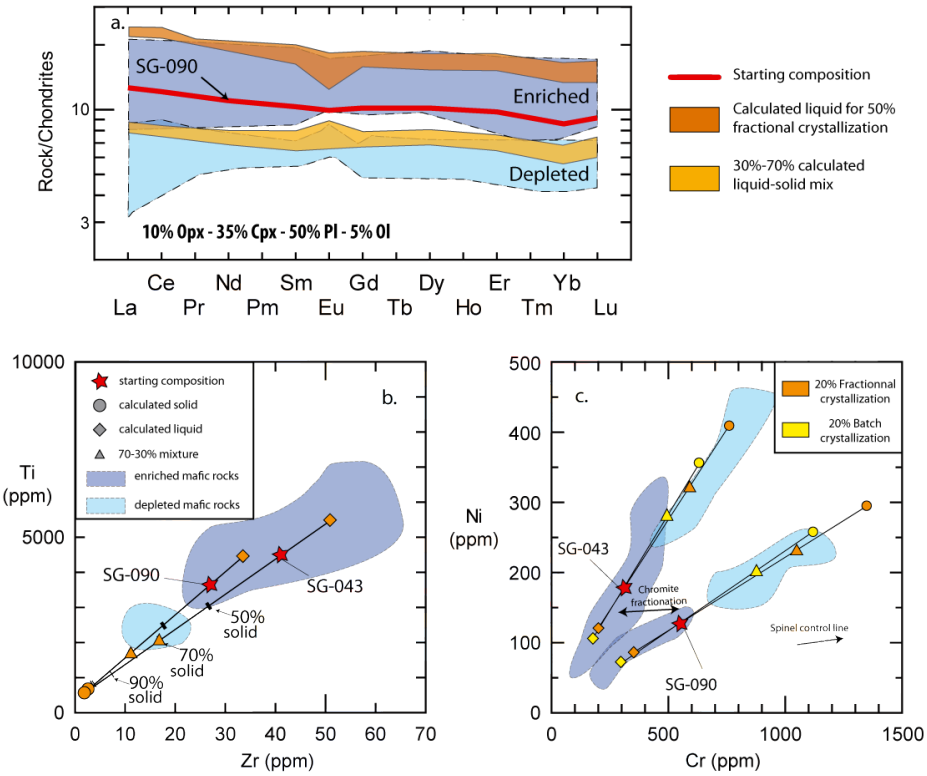

Figure 1.8

Crystallization models for the SHC mafic metavolcanic rocks. Blue fields represent the compositional range for the enriched (dark) and depleted (light) mafic rocks. A gabbroic crystallizing assemblage of 50% plagioclase, 10% orthopyroxene 35% clinopyroxene and 5% olivine was used for the models. a) Normalized REE concentrations obtained for fractional crystallization model using sample SG-090 as starting composition. Dark orange field: REE composition for the calculated residual liquid after 50% fractional crystallization. Light orange field: REE composition for a mixture of 30% liquid and 70% solid. Composition ranges reflect the different partition coefficients used for each element in the models (Table A.3; display at the end of this chapter). b) Fractional crystallization model for Zr and Ti concentrations. Calculated liquids (orange diamonds) and solids (orange circles) are for 20% of crystallization. Black lines show mixing between the solids and liquids. c) Crystallization models for Cr and Ni concentrations for 20% of crystallization of starting compositions SG-090 and SG-043. Starting compositions are represented by red stars. Calculated liquids (diamonds) and solids (circles) in orange symbols are for fractional crystallization and in yellow symbols are for equilibrium crystallization. Black lines show mixing between the solids and liquids. The triangles represent a mixture of 70% solid 30% liquid. Chondrite normalizing values are from McDonough and Sun (1995). Partition coefficient values for the REE are from a compilation by Laurent et al. (2013) from multiple sources within the GERM database. Partition coefficient values for Ti, Zr, Ni and Cr are from Bougault and Hekinian (1974) and Ewart et al. (1973).

have relatively primary compositions within the metavolcanic rock group representing liquids, with flat REE profiles and higher Mg# (6062). The range of REE (Fig. 1.8a), Zr-Ti (Fig. 1.8b) and Cr-Ni (Fig. 1.8c) concentrations of the SHC metavolcanic rocks are well reproduced by the fractional crystallization models with the compositions of the evolved amphibolites consistent with residual liquids, while the more depleted amphibolites would represent cumulates consisting of a mixture of ∼30% liquid and ∼70% solid (Fig. 1.8). At least 50% crystallization would, however, be required to explain the full range of REE concentrations of the metabasalts (Fig. 1.8a). Such high degrees of fractional crystallisation is unlikely to take place within thin flows and would produce liquids with a more intermediate composition rather than basaltic magma, unless most of the differentiation occurs in recharged magma chambers feeding the flows.

Mafic metavolcanic rock samples from the two distinct Cr/Ni groups are found within the same supracrustal enclaves (*e.g.* Pangertok inlet), and could reflect crystallization of variable amounts of chromite and pyroxene from a primary magma. The two Cr-Ni trends, however, do not intersect at the most primary magma compositions (Fig 1.8c) which suggests that fractionation of chromite and/or clinopyroxene prior to eruption may have produced basaltic magmas with variable Cr/Ni ratios, which could then differentiate to produce evolved liquids and more depleted cumulates displaying the distinct Cr-Ni trends (Fig. 1.8c). The two different Cr-Ni arrays are observed in the Nulliak and Upernavik metavolvanic rocks (Fig. 1.4f) suggesting that, regardless of the exact petrological process responsible for these trends, it occurred for both supracrustal units. If the SHC includes two metavolcanic assemblages (the Nulliak and the Upernavik), their identical geochemical composition would imply that despite being formed > 400 Ma apart, comparable petrogenetic processes were involved in the formation and evolution of both Mesoarchean and Eoarchean volcanic units. Given the age inconsis-

tency between Sm-Nd and Re-Os isotope systems (Ishikawa et al., 2017; Morino et al., 2017, 2018),together with the difficulty in the field to identify cross-cutting relationships with Mesoarchean Saglek dykes, it could also be possible that the SHC comprises a single suite of mafic metavolcanic rocks rather than two supracrustal units.

Origin of the ultramafic rocks

The ultramafic rocks in the SHC most commonly occur as meter scale discontinuous outcrops in Uivak gneiss with subordinate mafic rocks, but occasionally also appear to be associated with the more extensive mafic metavolcanic sequences. The origin of these ultramafic rocks is ambiguous and they have been interpreted as metakomatiites, lithospheric residual mantle enclaves and cumulative rocks from basaltic magmas or cumulate facies from hypabyssal intrusions (Bridgwater et al., 1975; Collerson et al., 1991; Ishikawa et al., 2017; Komiya et al., 2015; Nutman et al., 1989; Morino et al., 2017). Here we have used major and trace element compositions of the SHC ultramafic rocks, including new data for 40 samples, to evaluate their origin.

The SHC ultramafic rocks are clearly divided into two geochemically distinct groups. The low and high Fe groups exhibit distinct Al/Ti ratios and contrasting concentrations in most trace elements (Fig. 1.6b, Fig. 1.6d and Fig. 1.6f). The whole-rock major element composition for both ultramafic rock groups is strongly controlled by olivine fractionation (Fig. 1.9a). A number of ultramafic samples exhibit relatively fresh olivine, but these grains are characterized by variable forsterite contents. The low-Fe ultramafic samples contain olivine ranging in composition from Fo_{84} to Fo_{96}, whereas the olivine from the high-Fe rocks ranges from Fo_{79} to Fo_{87}. The olivine composition can also be relatively heterogeneous between grains within the same sample.

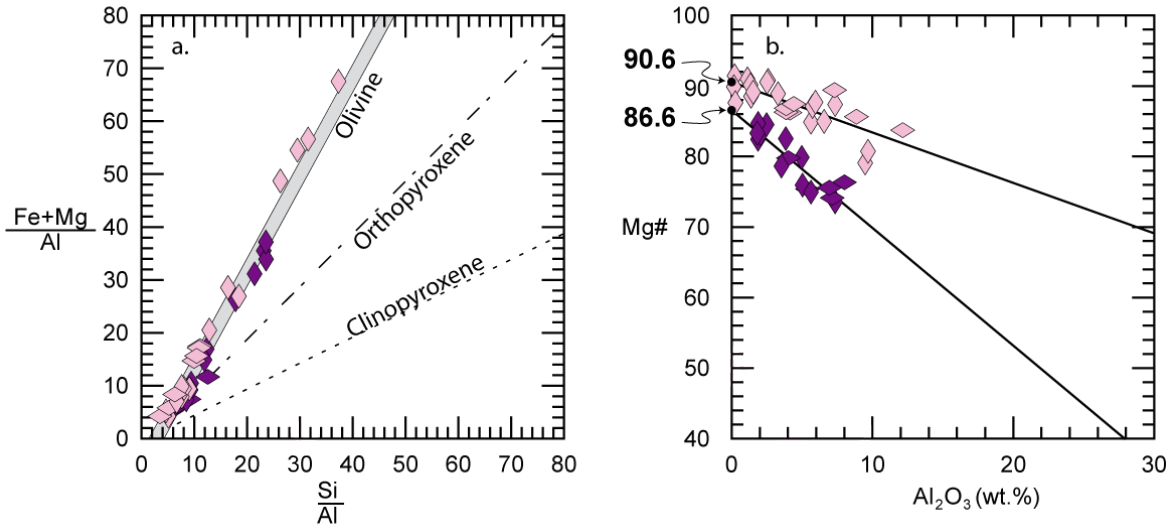

Figure 1.9

a) Pearce-type plot of (Mg+Fe)/Al *vs.* Si/Al for the SHC ultramafic rocks. b) Mg# *vs.* Al_2O_3 diagram for the low-Fe and high-Fe ultramafic rocks showing olivine fractionation trends for both groups. The best-fit lines through the low-Fe and high-Fe ultramafic samples define olivine control lines that are projected on the Mg# axis to define the composition of the accumulated olivine of Fo91-90 for the low-Fe ultramafic rocks and Fo87-86 for the high-Fe ultramafic rocks. Symbols are as in figure 1.6.

Such variability in olivine compositions, including Mg content as high as Fo_{96}, is unlikely to represent the primary olivine compositions but is rather consistent with recrystallization of serpentine with talc during high-grade metamorphism of the SHC ultramafic rocks, similar to what has been observed in other metamorphosed ultramafic complexes (e.g. Arai, 1975; Collerson et al., 1976; Nozaka, 2003). Therefore, it is unlikely that any of the olivine compositions are primary compositions. Assuming that elements such as Al, Ti, Ca, Zr, Hf, Yb and Y are perfectly incompatible in olivine, we can use intercepts of olivine fractionation lines to approximate the composition of the crystallizing olivine controlling the whole-rock major element composition of the ultramafic rocks.Despite some compositional variability of the ultramafic rocks, these olivine fractionation lines define the average composition of the crystallizing olivine, which plots at the intercept

with the y-axis in diagrams of Mg# *vs.* incompatible elements (Fig. 1.8b and Fig. A.3). The average Mg# of the fractionating olivine obtained from fractionation lines using multiple incompatible elements are 86.4 ± 0.6 (2σ) and 90.8 ± 0.6 (2σ) for the high-Fe and the low-Fe ultramafic rocks respectively (Fig. 1.9b and Fig. A.3). The olivine in the high-Fe ultramafic rocks appears to be consistent with the relative lower measured Fo contents, despite the compositional heterogeneity. The two distinct olivine compositions for the low-Fe and the high-Fe ultramafic rocks suggest that both groups are derived from different parental magmas and perhaps formed through different processes.

Collerson et al. (1991)has also suggested that the SHC comprises two distinct ultramafic rock suites of different nature, with tectonically emplaced enclaves of residual lithospheric mantle and metakomatiites associated with the Nulliak supracrustal rocks. They distinguished both series using Mg/Si and Al/Si ratios, where they suggest that the lithospheric mantle suite follows a mantle fractionation trend displaying higher Mg/Si and lower Al/Si ratios compared to the komatiitic samples (Fig. 1.10a). The group we defined as the high-Fe ultramafic rocks appears to correspond to the komatiitic suite defined by Collerson et al. (1991), whereas the low-Fe ultramafic rocks could correspond to the samples they identified as the residual mantle suite. Most low-Fe ultramafic samples analysed here exhibit CIPW normative mineralogy consistent with dunitic and harzbugitic compositions (Fig. 1.6a) and could potentially represent residual mantle enclaves. The low-Fe samples studied here, however, extend to relatively high Al contents and much higher Al/Si and lower Mg/Si ratios compared to the estimates for the primitive upper mantle (Al/Si = 0.10 to 0.12; Mg/Si = 1.0 to 1.1; Hart and Zindler (1986); Jagoutz et al. (1979); McDonough and Sun (1995)).The whole low- Fe ultramafic suite also extends to much higher Al/Si and lower Mg/Si ratios

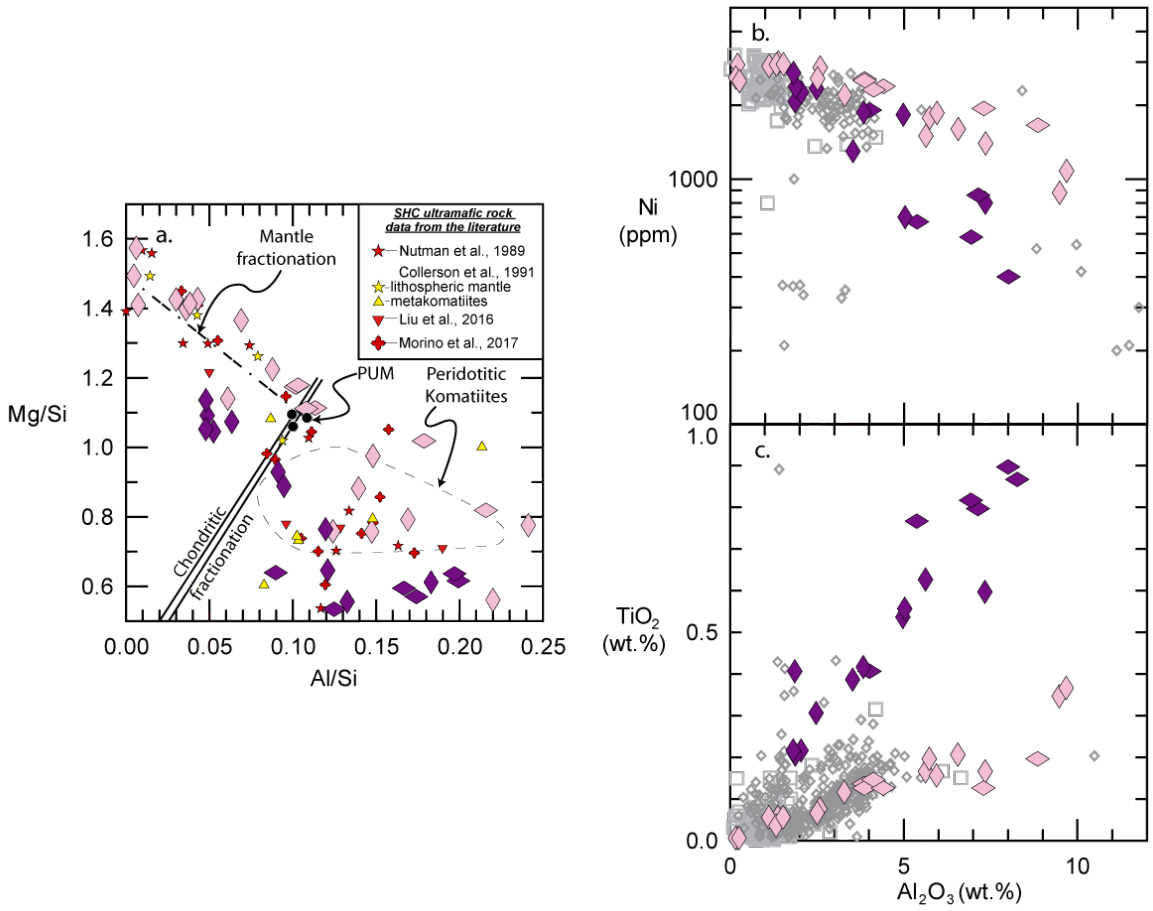

Figure 1.10

a) Mg/Si *vs.* Al/Si diagram (in wt.%) for the SHC ultramafic rocks. Primitive upper mantle (PUM) compositions are from Hart and Zindler (1986), Jagoutz et al. (1979) and McDonough and Sun (1995). Compositional field for the peridotitic komatiites is from Arndt et al. (1977). Other SHC ultramafic data are from Nutman et al. (1989), Collerson et al. (1991), Liu et al. (2016) and Morino et al. (2017). b) and c) Ni and TiO_2 *vs.* Al_2O_3 diagrams for the SHC ultramafic rocks and mantle xenoliths. Lherzolite xenolith compositions (grey diamond) and harzburgite xenolith compositions (grey square) are from the PetDb database (To Earthchem.org). Symbols for ultramafic samples from this study are as in figure 1.6.

compared to what was observed by Collerson et al. (1991) for the suite of ultramafic rocks interpreted to be residual mantle (Fig. 1.10a), inconsistent with their origin as residues from mantle fractionation. Figure 1.10b and 1.10c show that despite some high-Fe and low-Fe ultramafic samples having geochemical compositions overlapping

harburgitic and lherzolitic mantle xenoliths, both suites extend to higher Al and Ti contents compared to lithospheric mantle. The Fo content of 90.8 ± 0.6 obtained from the olivine fractionation lines of the low-Fe ultramafic samples is also inconsistent with refractory mantle olivine and slightly lower than typical Mg# for cratonic upper mantle of 92 to 93 (Bernstein et al., 2007). Herzberg (2004) modeled the composition of residual mantle after fractional melting of fertile mantle peridotite under various pressure conditions. Figure 1.11 shows that only a few low-Fe ultramafic samples could have FeO^T and Al_2O_3 compositions similar to modeled mantle residues but most ultramafic rocks from the SHC are compositionally inconsistent with the sub-cratonic mantle xenolith or what is predicted by mantle fractional melting models. Therefore, whole-rock compositions, together with estimated olivine compositions crystallizing for the high-Fe and low-Fe ultramafic rocks, seem to be inconsistent with the presence of enclaves of residual lithospheric mantle in the SHC.

Some of the SHC ultramafic rocks have also been interpreted by several authors as metakomatiites (*e.g.* Collerson et al., 1991; Ishikawa et al., 2017; Morino et al., 2017). This hypothesis is difficult to evaluate since there are no primary textures preserved, such as spinifex textures, to confirm the extrusive nature of the SHC ultramafic rocks. Coarse grain bladed olivine crystals have been locally observed, but are interpreted to be metamorphic in origin (Bridgwater et al., 1975; Collerson et al., 1976; Komiya et al., 2015). With the absence of primary textural features, the interpretation of the SHC ultramafic rocks as komatiites mainly relies on their geochemical composition. Morino et al. (2017) compare the SHC ultramafic rocks to the Barberton and Abitibi komatiites based on similar Al/Ti and Gd/Yb ratios and suggest that the SHC ultramafic rocks include Al-depleted (ADK), Al-undepleted (AUK) and Al-enriched (AEK) komatiitic

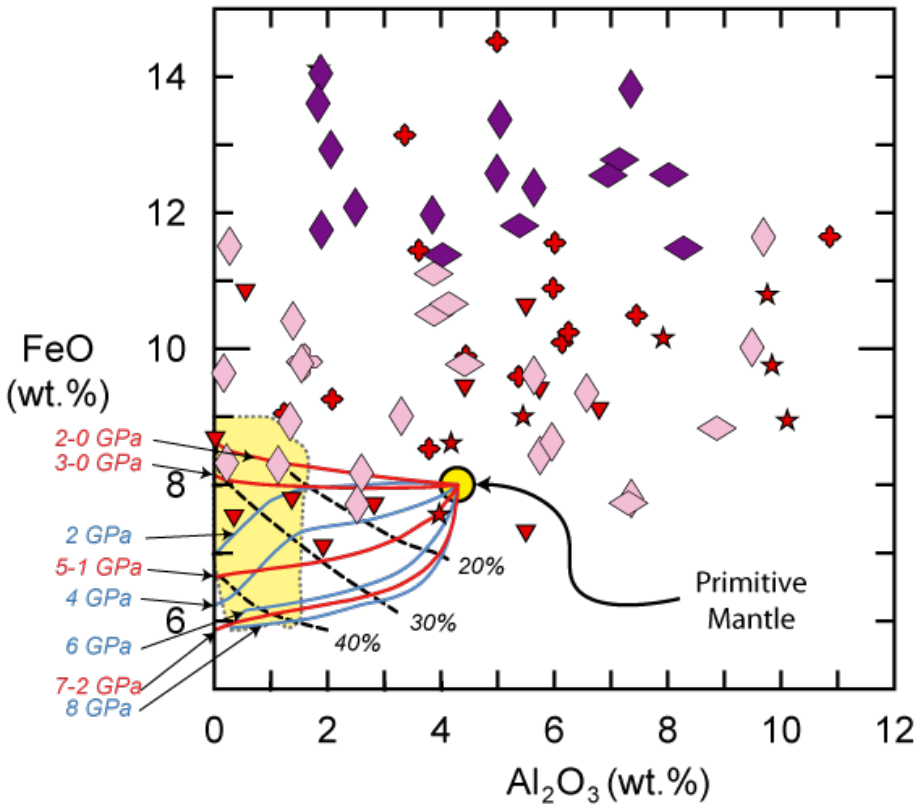

Figure 1.11

FeO_t *vs.* Al_2O_3 diagram for the SHC ultramafic rocks along with mantle melting models after Herzberg (2004). The black dash lines represent the degrees of melting of primitive mantle (yellow circle). The solid lines represent the different pressures for equilibrium melting (blue) and fractional melting (red). The yellow field represents the composition range of cratonic mantle xenolith compiled from the GEOROC databese (http://georoc.mpch-mainz.gwdg.de). Symbols for ultramafic sample from this study are as in figure 6. Symbols for other SHC ultramafic rocks are as in figure 10 and data are from Nutman et al. (1989), Liu et al. (2016) and Morino et al. (2017).

rocks. They define an Eoarchean suite and a Mesoarchean suite of ultramafic rocks based on Sm-Nd isotopic compositions. The younger Mesoarchean suite of ultramafic rocks appears to comprise both ADK and AUK, whereas the suite they interpret to be Eoarchean includes all ADK, AUK and AEK types. The Eoarchean and Mesoarchean komatiitic rocks would also have a distinct mantle source since only the ultramafic rocks interpreted to be Eoarchean yield ^{142}Nd anomalies compared to Nd terrestrial

standards. Ishikawa et al. (2017) on the other hand ascribe AEK affinities to all ultramafic samples they interpret as metakomatiites, which yielded a Re-Os isochron age of 3612 ± 130 Ma and a Re depletion model age of 3.4 to 3.6 Ga. Although ADK and AUK can occur within the same greenstone belts (*e.g.* Dostal and Mueller, 2013) komatiites older than 3.4 Ga are generally dominated by ADK (*e.g.* Arndt et al., 2008; Barnes and Arndt, 2019). If indeed the SHC ultramafic rocks are komatiites, it would suggest, according to the interpretation of Morino et al. (2017), the formation in the SHC of contemporaneous ADK, AUK and AEK at ∼3.8 Ga and of both ADK and AUK at ∼3.4 Ga. The conventional interpretation for the different Al/Ti and Gd/Yb ratios of the different types of komatiites is related to variable depths of melting in the mantle. The ADK magmas would be formed with the presence of residual garnet (or majorite) in the mantle source at higher pressure, whereas the AUK magmas would equilibrate with a garnet-free source at lower pressure relative to ADK, and the AEK would be produced at lower pressure (*e.g.* Arndt et al., 2008; Barnes and Arndt, 2019). This would imply that the coeval ultramafic rock groups were sourced from mantle reservoirs at various depths or from different portion of the same mantle plume (*e.g.* Dostal and Mueller, 2013) at ∼3.8 Ga and again at ∼3.4 Ga. Regardless of the exact age or mantle source(s), the two well defined Al_2O_3 *vs.* TiO_2 trends of the distinct ultramafic suites argue for the presence of only two geochemical groups of ultramafic rocks within the SHC. The high-Fe and low-Fe ultramafic rocks have distinct Al/Ti ratios which could indeed be reminiscent of ADK (or Barberton-type) and AUK (or Munro-type) komatiites, but the Al_2O_3/TiO_2 ratio of ∼33 for the low-Fe ultramafic rocks is higher than the Al_2O_3/TiO_2 ratio of 20 for typical AUK (Fig. 1.12). A few low-Fe ultramafic samples have higher Al/Ti and lower Gd/Yb ratios which could suggest they are similar in composition to AEK and perhaps represent a third group. These samples

exhibit a different normative mineralogy, with harzburgitic compositions as opposed to the low-Fe ultramafic samples with lower Al/Ti being mainly dunitic in composition (Fig. 1.6a). Variation in mineral fractionation could therefore explain the lower Gb/Yb ratios of those low-Fe samples. Orthopyroxene-rich rocks would however generally have higher Gd/Yb with overall higher REE concentrations compared to more olivine-rich cumulates, and this is thus inconsistent with what is observed in the low-Fe suite. Most low-Fe ultramafic rocks have very low REE concentrations and the low-Fe ultramafic samples with the lowest Gd/Yb are generally showing the strongest evidence of post-magmatic LREE-enrichment. These low Gd/Yb low-Fe ultramafic samples actually follow the same trends as the rest of the low-Fe ultramafic suite on most co-variation plots with the same lower FeO and higher Cr concentrations, characteristic of the low-Fe ultramafic samples compared to the high-Fe ultramafic rocks. Their composition is also controlled by fractionation of olivine of the same composition (Fo_{90-91}) as the low-Fe ultramafic suite, consistent with them being petrogenetically linked rather than representing a distinct ultramafic group.

The distinct compositions of the high-Fe and low-Fe ultramafic rocks suggest a different origin for the parental magmas for both suites. Considering the estimated primary olivine compositions of Fo_{90} and Fo_{86} (Fig. 1.9b and Fig. A.3), we can use the Fe/Mg ratio partition coefficient between olivine and liquid to constrain the composition of the parental magma for the low-Fe and high-Fe ultramafic suites. Using a Fe/Mg K_D of 0.32 and Fe^{+2}/FeO_T of 0.9, the primary magmas for the low-Fe and high-Fe ultramafic groups would have Mg# values of 74 and 66 respectively. These Mg# values are lower than all ultramafic samples analysed here from their respective groups, suggesting that none of the ultramafic samples for both the low-Fe and high-Fe ultramafic groups

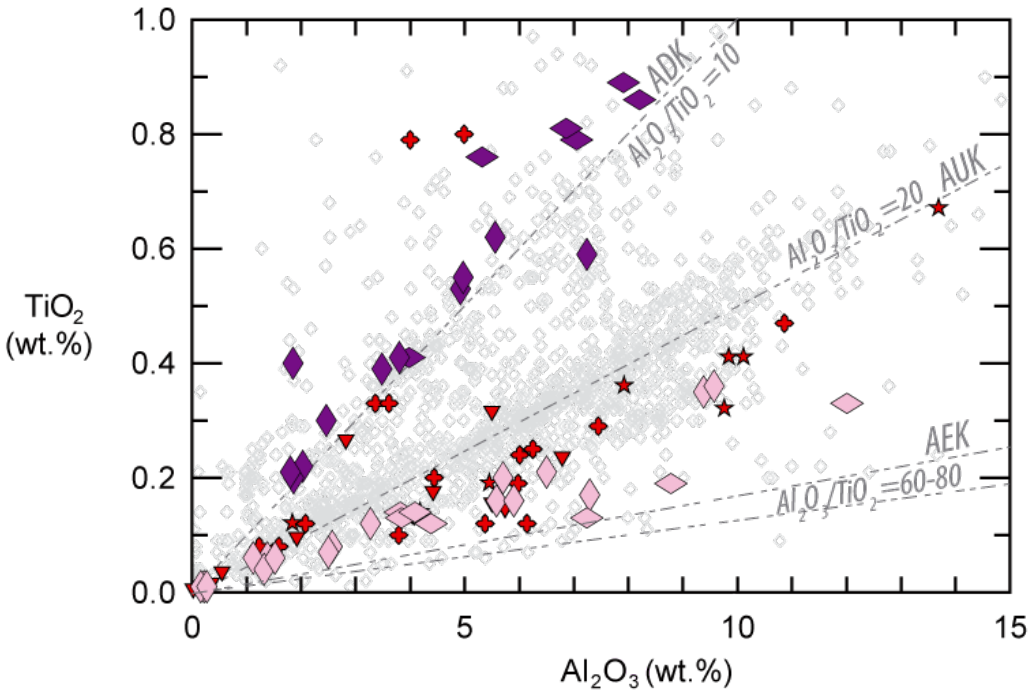

Figure 1.12

TiO_2 *vs.* Al_2O_3 diagram for the SHC ultramafic rocks and komatiites from the literature. Symbols for ultramafic sample from this study are as in figure. 6. Other SHC ultramafic data are from Nutman et al. (1989), Collerson et al. (1991), Liu et al. (2016) and Morino et al. (2017) and symbols as in figure 10. Komatiite compositions (grey diamonds) are compiled from the GEOROC database. Al_2O_3/TiO_2 values for ADK, AUK and AEK are from Arndt et al. (2008).

represent parental magma compositions, but are rather ultramafic cumulates produced by some degrees of fractional crystallization. Since FeO^T contents for the low-Fe and high-Fe ultramafic rocks do not significantly vary with MgO concentration (Fig. 1.6d), we can therefore estimate MgO contents for the parental liquids for both ultramafic groups. Assuming a FeO^T concentration of 10 wt.% for the low-Fe ultramafic rocks (with $Fe^{+2}/FeO_T = 0.9$ and $K_D = 0.32$), the parental liquid crystallizing olivine Fo_{90} would have a MgO content of ∼15 wt.%. Assuming a higher Fe content of FeO_T = 12.5 wt.% for the high-Fe ultramafic rocks which composition is controlled by the fractionation of olivine Fo_{86}, the primary magma would have a lower MgO content of ∼12

wt.%. The parental magmas for the SHC ultramafic rocks are therefore consistent with komatiitic basalts or picritic compositions rather than komatiites *sensu stricto* (MgO >18 wt.%). The Fe/Mg olivine-liquid partition coefficient can vary with temperature and pressure (*e.g.* Toplis, 2005) but assuming a lower K_D such as the commonly used value of 0.3 (Roeder and Emsile, 1970) would decrease the estimated MgO content of the parental magma. Given the fact that MgO is relatively well correlated with Al_2O_3 and TiO_2 for both ultramafic groups, it is also possible to estimate the Al_2O_3 and TiO_2 contents of the parental magmas for the low-Fe and high-Fe ultramafic suites (at MgO contents of respectively 15 wt.% and 12 wt.%). Figure 1.13 shows the composition of the high-Fe and low-Fe ultramafic samples with their respective estimated parental liquids, along with the mafic metavolcanic rocks. Fractionation of the low-Fe ultramafic cumulates from a parental liquid with a komatiitic basalt composition may have produced a mafic magma that would be consistent with the composition of the primary magma for the Nulliak metavolcanic basalts (*i.e.* SG-090 and SG-043). Subsequent gabbroic differentiation would then produce the enriched basaltic liquids and depleted pyroxene-rich cumulates. This could imply a petrogenetic link between the low-Fe ultramafic rocks and the SHC metabasalts. Except for a few enriched metabasalts, no mafic samples appear to have been derived from fractionation of the high-Fe ultramafic cumulates from their parental magma (Fig.1.13), perhaps suggesting no petrogenetic relationship between the high-Fe ultramafic rocks and the SHC mafic metavolcanic rocks.

With the absence of primary textures, it is challenging to constraint the origin of the highly metamorphosed SHC ultramafic rocks and their exact nature remains equivocal. The major and trace element compositional range of the low-Fe and high-Fe ultramafic suites extends to compositions inconsistent with mantle residues. If both groups are

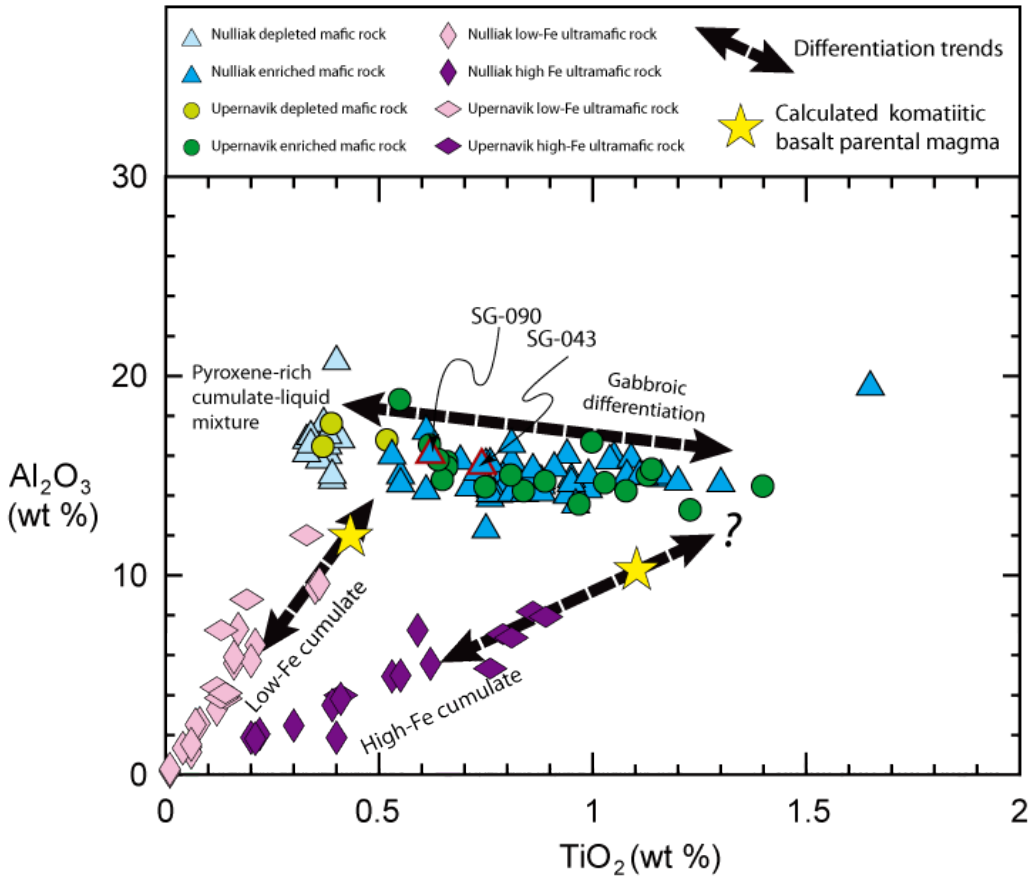

Figure 1.13

Al_2O_3 *vs.* TiO_2 diagram for the SHC mafic and ultramafic rocks. The yellow stars represent the composition of the calculated parental magmas in equilibrium with the low-Fe and high-Fe ultramafic cumulative rocks, crystallizing respectively olivine Fo86 and Fo90. Symbols are as in figure 1.3 and figure 1.6.

interpreted as ADK and AUK, it would imply the presence of both komatiitic types in the SHC, perhaps in the Eoarchean as well as in the Mesoarchean. Nevertheless, none of the SHC ultramafic rocks seems to represent primary liquids but both groups appear to be produced by differentiation of komatiitic basalt parental magmas rather than being komatiites *sensu stricto*. The geochemical composition of the low-Fe ultramafic rocks could, however, be more consistent with ultramafic cumulates that fractionated to produce the primary basaltic magmas forming the SHC metavolcanic rocks. The possible intrusive nature of the low-Fe ultramafic rocks rather than ultramafic flows,

could explain why they mostly occur as large discrete pods within TTG compared to the high-Fe ultramafic rocks more commonly associated with the supracrustal rocks. Despite the fact that the parental magma for the high-Fe ultramafic rocks is relatively MgO-poor compared to komatiites, they share some geochemically affinities with Al-depleted komatiites. The high-Fe ultramafic rocks are, however, more difficult to petrogenetically link with the SHC metabasalts and may not be co-genetic with the metavolcanic Nulliak rocks despite their common association in the field.

1.5.3 Tectonic setting of the Saglek-Hebron Complex and comparison with the Isua and Nuvvuagittuq greenstone belts

The exact tectonic setting operating on the Earth during the Archean has been the subject of a long-lasting debate that is still unresolved (*e.g.* Bédard, 2018; Davies, 1992; Furnes et al., 2009; Moyen and Laurent, 2018; Stern, 2007; Van Hunen et al., 2008; Van Kranendonk, 2010; Wiemer et al., 2018). Several authors have argued that the formation of TTG similar to the SHC Eoarchean gneisses involve subduction-like tectonic settings (*e.g.* Nair and Chacko, 2008; Polat, 2012; Martin et al., 2014) but alternative models not requiring subduction have also been proposed (*e.g.* Bédard et al., 2012; Smithies and Champion, 2000; Johnson et al., 2017). The boninitic-like geochemical composition of mafic mantle-derived rocks from other early (>3.7 Ga) metavolcanic belts, such as the Isua supracrustal belt in Southwest Greenland and the Nuvvuagittuq greenstone belt in Northeastern Canada, have also been used to suggest that settings similar to modern-day plate tectonics may have operated on the early Earth (*e.g.* Furnes et al., 2015; Polat et al., 2002, 2011) at least short-lived intermittent subduction initiation events (O'Neil et al., 2016; Turner et al., 2014). Based on field and structural observations, Komiya et al. (2015) suggested that the SHC rocks provide evidence of

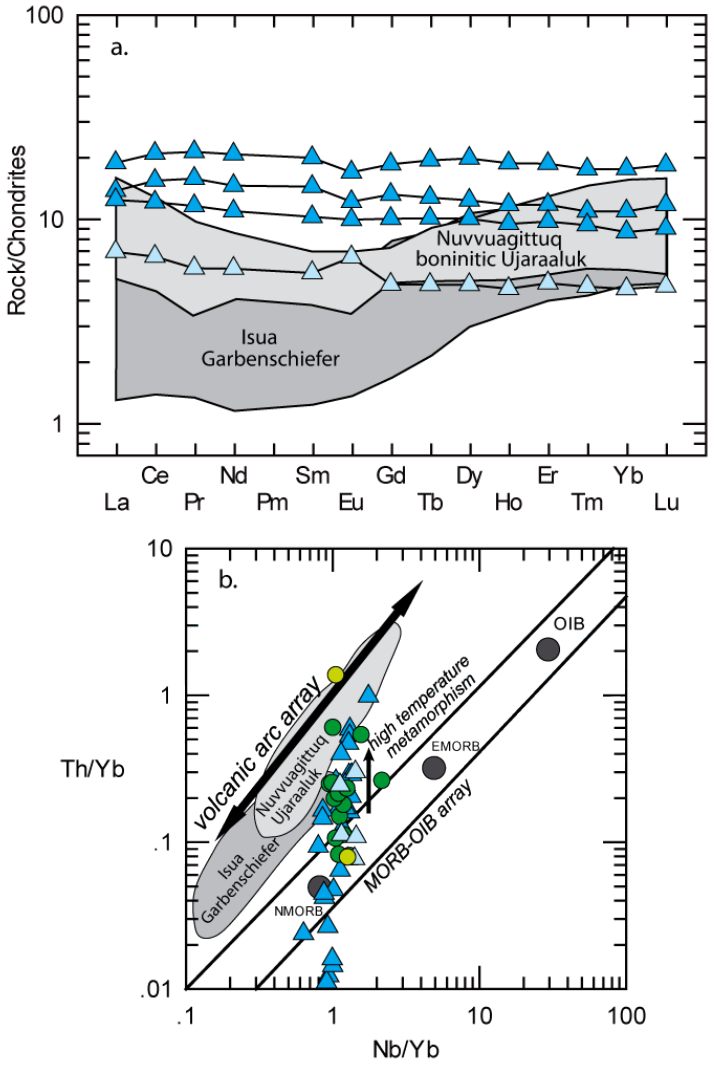

Figure 1.14

a) Chondrite-normalized REE diagram for selected SHC metavolcanic rocks compared to the Isua Garbenschiefer amphibolites and the Nuvvuagittuq Ujaraaluk boninitic rocks. Only a limited number of SHC samples are plotted for clarity, but they include representative depleted and enriched mafic samples showing the full compositional range of the mafic metavolcanic rocks. b) Th/Yb *vs.* Nb/Yb diagram after Pearce (2008) for the SHC mafic metavolcanic rocks. Isua Garbenschiefer data is from O'Neil et al. (2016), Nutman et al. (2013), Polat et al. (2002) and Furnes et al. (2009). Nuvvuagittuq Ujaraaluk data is from O'Neil et al. (2007, 2011). Chondrite normalizing values are from McDonough and Sun (1995). Symbols are as in figure 1.3.

plate tectonics on Earth in the Eoarchean. The SHC Eoarchean metabasaltic rocks can thus be closely examined to establish if their geochemical compositions recorded

evidence of supra-subduction-like settings. As opposed to the Isua and Nuvvuagittuq belts including metavolcanic rocks displaying a U-shape REE profiles reminiscent of boninites formed in supra-subduction settings, the SHC metavolcanic rocks have uniform tholeiitic compositions, with relatively flat trace element profiles (Fig. 1.14a) and with only slight to no Nb-depletions. Furthermore, the increasing Ti content with differentiation of the mafic rocks is consistent with fractionation under relatively dry conditions. When plotted on a Nb/Yb vs. Th/Yb diagram after Pearce (2008),the SHC metavolcanic rocks overlap with the mantle array closer to the N-MORB composition and extend towards higher Th/Yb ratios(Fig. 1.14b), consistent with high temperature mobilization of Th (Pearce, 2008). This contrasts with the volcanic arc rocks generally following a parallel trend above the MORB-OIB array (Pearce, 2008), such as what is observed for the Isua and Nuvvuagittuq boninite-like rocks (Fig. 1.14b). While rocks with supra-subduction setting signatures are absent in the SHC, their geochemical compositions could still be consistent with the involvement of a ridge subduction and the magmatic accretion of basaltic rocks with geochemical affinities closer to mid-ocean-ridge basalts (MORB), as proposed by Komiya et al. (2015). In such case, volcanic rocks with boninitic or calc-alkaline affinities may not be expected. If indeed a tectonic setting resembling modern-day subduction was operating during the formation of the SHC, the mantlederived metavolcanic rocks, Nulliak or Upernavik, do not appear to have been produced by fluid-induced melting or fractionation under hydrous conditions, such as for typical subduction-related rocks. Alternatively, some authors have suggested that Archean tholeiites similar to the SHC metabasaltic rocks may have been formed within Archean oceanic plateaus (Abouchami et al., 1990; Kimura et al., 1993; Arndt et al., 1997; Barnes et al., 2012).

1.6 Conclusion

Archean cratons are often dominated by felsic rocks from the TTG series that cannot be directly produced by melting of peridotitic mantle, but instead must have been derived from the melting of older mafic crust. The Saglek-Hebron Complex includes some of the oldest occurrences of basaltic crust on Earth that can help further our understanding of the formation of Earths most primitive crust. The Saglek-Hebron mafic rocks are interpreted as basaltic metavolcanic rocks. If these metavolcanic rocks represent two distinct supracrustal assemblages formed at different times, as previously suggested, their indistinguishable compositions are consistent with them being produced from similar petrological processes. The compositional range observed in the mafic rocks from the Saglek-Hebron Complex appears to have been the result of gabbroic differentiation producing incompatible trace element enriched evolved Ti-rich residual liquids and depleted pyroxene-rich cumulate-liquid mixtures. Two distinct suites of ultramafic rocks can be found in the Saglek-Hebron Complex, both of which represent cumulates derived from parental magmas with a komatiitic basalt composition rather than truly komatiites or fragments of lithospheric mantle. As opposed to some other early mafic belts such as the Isua and Nuvvuagittuq belts, the Saglek-Hebron Complex does not comprise metavolcanic rocks with geochemical signatures that can be associated with supra-subduction environments. Therefore, if settings resembling modern-day plate tectonics were operating on Earth at the time of formation of the Saglek-Hebron rocks, it was not recorded in the geochemical composition of the Saglek-Hebron mafic volcanic rocks.

Supplementary material: Appendix A

Figure B.1 : Fieldwork photographs of the mafic and ultramafic rocks.

Figure B.2 : Thin section photomicrographs of the mafic and ultramafic rocks.

Figure A.3: Mg# *vs.* selected major and incompatible trace element diagrams for the low-Fe (pink symbols) and high-Fe (purple symbols) ultramafic rocks. The best fit lines though the low-Fe and high-Fe ultramafic samples define olivine control lines that are projected on the Mg# axis to define the composition of the accumulated olivine. Average Mg# values are 86.4 ± 0.6 (2σ) and 90.8 ± 0.6 (2σ) for the low-Fe and high-Fe ultramafic groups respectively.

Table A.1: Major (wt.%) and trace (ppm) element data for duplicate samples (hydrous compositions).

Table A.2: Electron microprobe major element compositions for single olivine grains from ultramafic samples.

Table A.3: Partition coefficients used for crystallization models shown in Figure 1.8.

Table

Table 1.1

Major (wt.%) and trace (ppm) element data for the SHC mafic metavolcanic and ultramafic rocks. Major element data in the table are recalculated to anhydrous compositions. All figures plot anhydrous major element compositions. Coordinates are in UTM NAD 27 Zone 20.

	Enriched Nulliak mafic rocks							
Sample	SG-002	SG-011	SG-028A	SG-029A	SG-029B	SG-029D	SG-035	SG-038A
Easting	513390	522810	491366	491355	491353	491348	491247	491409
Northing	6441404	6461353	6470216	6470197	6470210	6470215	6470184	6470276
SiO_2	50.25	47.14	47.47	50.66	50.77	50.93	50.02	49.38
Al_2O_3	14.48	14.31	15.76	14.23	14.19	14.99	16.20	14.81
FeO_t	11.88	11.55	11.36	11.45	11.48	11.41	10.03	12.72
MnO	0.22	0.16	0.18	0.18	0.21	0.17	0.20	0.21
MgO	7.79	9.35	9.98	8.37	9.13	8.35	6.74	7.91
CaO	11.56	13.69	12.49	11.71	11.01	10.54	12.65	10.43
Na_2O	2.30	2.04	1.48	2.47	2.08	2.50	2.92	2.72
K_2O	0.42	0.68	0.44	0.08	0.10	0.08	0.22	0.40
TiO_2	1.01	0.98	0.76	0.79	0.95	0.96	0.95	1.32
P_2O_5	0.07	0.05	0.03	0.05	0.06	0.05	0.07	0.08
Cr_2O_3	0.02	0.05	0.05	0.00	0.01	0.02	0.00	0.03
LOI	1.04	0.52	0.30	0.00	0.00	0.00	0.25	0.00
Sc	39.6	45.4	-	52.0	-	-	47.0	-
V	289	270	-	319	-	-	288	318
Cr	137	351	347	240	-	-	150	210
Co	51	53	-	52	-	-	39	51
Ni	93	155	-	100	-	-	70	110
Rb	3	5	-	0	-	-	0	2
Sr	176	278	-	211	-	-	209	227
Y	16.2	19.5	-	18.9	-	-	20.7	24.1
Zr	23	37	-	27	-	-	44	56
Nb	3.7	1.5	-	1.8	-	-	2.0	2.1
Ba	67	27	-	15	-	-	37	79
La	4.70	2.71	-	2.05	-	-	2.97	3.49
Ce	11.52	7.08	-	6.88	-	-	9.31	9.81
Pr	1.66	1.09	-	1.18	-	-	1.48	1.57
Nd	7.62	5.77	-	6.35	-	-	7.44	7.66
Sm	2.18	1.99	-	2.10	-	-	2.59	2.56
Eu	0.809	0.715	-	0.806	-	-	0.829	0.941
Gd	2.55	2.64	-	2.82	-	-	3.17	3.32
Tb	0.46	0.49	-	0.49	-	-	0.57	0.62
Dy	2.95	3.26	-	3.51	-	-	3.76	4.02
Ho	0.63	0.71	-	0.74	-	-	0.81	0.82
Er	1.72	2.02	-	2.23	-	-	2.36	2.44
Tm	0.244	0.311	-	0.312	-	-	0.339	0.362
Yb	1.56	2.06	-	2.14	-	-	2.17	2.39
Lu	0.229	0.302	-	0.338	-	-	0.357	0.392
Hf	0.8	1.3	-	1.1	-	-	1.3	1.6
Ta	0.29	0.17	-	0.05	-	-	0.09	0.14
Pb	3	4	-	0	-	-	0	
Th	0.77	0.30	-	0.00	-	-	0.00	0.10
U	0.18	0.20	-	0.00	-	-	0.02	0.05

Continued on next page

	Enriched Nulliak mafic rocks (continued)							
Sample	SG-038B	SG-039	SG-041	SG-043	SG-044	SG-051	SG-053	SG-081
Easting	491401	491380	491327	491217	491234	491726	491734	522696
Northing	6470265	6470263	6470270	6470291	6470293	6469933	6469701	6440464
SiO_2	49.05	48.23	50.38	49.57	47.78	47.26	48.07	51.18
Al_2O_3	16.12	15.94	15.87	15.68	16.06	15.58	15.05	14.68
FeO_t	11.91	11.72	10.38	10.44	13.12	12.38	13.17	10.72
MnO	0.18	0.19	0.17	0.17	0.23	0.24	0.25	0.18
MgO	7.24	8.13	7.60	8.88	8.34	8.70	8.35	8.20
CaO	11.19	12.38	11.83	11.83	11.23	12.55	11.94	11.18
Na_2O	2.89	2.10	2.82	2.38	1.67	2.13	1.65	2.47
K_2O	0.24	0.12	0.07	0.23	0.37	0.17	0.24	0.48
TiO_2	1.06	1.05	0.82	0.75	1.10	0.92	1.18	0.80
P_2O_5	0.07	0.06	0.05	0.05	0.09	0.01	0.08	0.06
Cr_2O_3	0.03	0.07	0.01	0.00	0.00	0.05	0.04	0.04
LOI	0.11	0.11	0.23	0.78	0.00		0.57	1.08
Sc	-	50.3	50.6	34.0	47.0	47.2	-	41.1
V	-	320	297	235	339	326	340	251
Cr	208	536	110	310	200	362	290	288
Co	-	47	48	50	53	51	54	47
Ni	-	92	73	180	110	113	140	96
Rb	-	1	0	0	3	2	-	6
Sr	-	176	248	107	220	105	114	116
Y	-	21.9	17.7	17.3	25.7	24.7	24.5	18.0
Zr	-	42	32	41	52	40	38	52
Nb	-	2.1	1.8	1.8	2.4	2.3	1.6	2.4
Ba	-	25	22	28	70	22	43	172
La	-	2.07	2.07	3.28	4.50	1.96	3.22	5.94
Ce	-	7.11	6.80	9.51	12.90	6.26	9.35	12.14
Pr	-	1.27	1.12	1.51	2.04	1.10	1.49	1.60
Nd	-	6.79	5.73	6.85	9.76	5.87	7.95	7.26
Sm	-	2.36	1.91	2.22	3.07	2.24	2.60	2.12
Eu	-	0.809	0.648	0.709	0.986	0.809	0.983	0.760
Gd	-	3.10	2.34	2.73	3.84	3.19	3.42	2.60
Tb	-	0.56	0.45	0.48	0.73	0.63	0.67	0.47
Dy	-	3.90	3.03	3.16	5.06	4.27	4.27	3.10
Ho	-	0.84	0.65	0.67	1.07	0.93	0.90	0.67
Er	-	2.33	1.90	1.96	3.11	2.60	2.51	1.89
Tm	-	0.356	0.285	0.278	0.453	0.386	0.387	0.292
Yb	-	2.25	1.89	1.87	3.01	2.51	2.53	1.84
Lu	-	0.338	0.290	0.296	0.471	0.369	0.392	0.271
Hf	-	1.4	1.1	1.2	1.6	1.3	1.3	1.5
Ta	-	0.12	0.11	0.08	0.10	0.15	0.09	0.19
Pb	-	1	1	0	0	1		12
Th	-	0.03	0.05	0.00	0.28	0.03	0.06	0.37
U	-	0.01	0.00	0.03	0.03	0.01	0.03	0.16

Continued on next page

	Enriched Nulliak mafic rocks (continued)							
Sample	SG-082	SG-083	SG-088A	SG-090	SG-091	SG-092	SG-093	SG-095
Easting	522634	522668	522461	522486	522541	522628	522668	522733
Northing	6440464	6440383	6463953	6439978	6440119	6440162	6440197	6440261
SiO_2	50.01	50.79	47.49	49.73	51.38	52.30	49.20	53.42
Al_2O_3	15.19	15.06	14.83	16.19	15.76	14.47	14.53	14.01
FeO_t	11.37	10.37	13.97	9.29	10.37	10.50	9.91	10.42
MnO	0.20	0.21	0.24	0.19	0.17	0.18	0.27	0.17
MgO	7.00	7.76	8.40	8.51	8.31	7.89	6.81	8.52
CaO	11.54	11.91	11.94	13.43	10.52	11.06	16.40	9.62
Na_2O	2.74	2.55	1.40	1.58	2.37	2.24	1.67	2.16
K_2O	0.75	0.43	0.66	0.38	0.25	0.50	0.38	0.83
TiO_2	1.09	0.80	0.97	0.62	0.77	0.80	0.72	0.77
P_2O_5	0.08	0.06	0.06	0.07	0.06	0.05	0.07	0.07
Cr_2O_3	0.03	0.04	0.03	0.00	0.04	0.00	0.04	0.00
LOI	1.41	1.06	0.61	1.61	1.39	1.44	0.51	2.40
Sc	45.6	41.4	-	45.0	38.5	43.0	36.2	41.0
V	300	253	-	248	237	280	219	264
Cr	234	311	-	550	306	310	269	260
Co	47	49	-	41	47	44	44	43
Ni	114	107	-	130	119	90	72	80
Rb	11	5	-	5	8	6	7	26
Sr	112	142	-	75	83	123	131	103
Y	24.0	18.5	-	13.8	17.3	17.3	17.4	15.6
Zr	45	49	-	27	55	51	41	56
Nb	3.1	2.4	-	1.5	2.3	2.4	2.0	2.3
Ba	146	79	-	66	31	82	393	215
La	4.64	4.94	-	2.96	4.80	5.57	4.51	5.24
Ce	11.88	11.34	-	7.45	10.88	12.00	10.06	11.40
Pr	1.80	1.55	-	1.11	1.51	1.59	1.40	1.60
Nd	8.71	7.21	-	5.14	6.85	7.31	6.42	7.34
Sm	2.65	2.00	-	1.58	1.91	2.03	1.96	1.99
Eu	0.881	0.741	-	0.575	0.713	0.691	0.676	0.737
Gd	3.42	2.68	-	2.08	2.54	2.63	2.43	2.60
Tb	0.62	0.47	-	0.38	0.44	0.47	0.44	0.45
Dy	4.03	3.13	-	2.57	2.95	3.03	2.95	2.99
Ho	0.88	0.69	-	0.54	0.64	0.64	0.64	0.63
Er	2.52	1.95	-	1.62	1.80	1.85	1.74	1.81
Tm	0.381	0.294	-	0.236	0.262	0.278	0.276	0.270
Yb	2.49	1.82	-	1.48	1.77	1.84	1.77	1.71
Lu	0.360	0.272	-	0.231	0.263	0.284	0.266	0.279
Hf	1.5	1.5	-	0.8	1.6	1.3	1.3	1.5
Ta	0.21	0.19	-	0.07	0.19	0.18	0.17	0.16
Pb	12	9	-	12	7	9	30	5
Th	0.19	0.52	-	0.07	1.04	0.97	0.34	0.49
U	0.08	0.20	-	0.08	0.29	0.31	0.10	0.20

Continued on next page

	Enriched Nulliak mafic rocks (continued)							
Sample	SG-096	SG-097	SG-102	SG-104	SG-105	SG-106	SG-108	SG-109B
Easting	522750	522832	522984	523782	523670	523633	523570	523517
Northing	6440281	6440377	6440506	6440921	6440857	6440819	6440382	6440334
SiO_2	51.26	51.40	50.58	48.27	49.01	47.98	48.71	49.14
Al_2O_3	14.45	14.22	15.22	15.18	17.38	14.40	14.29	15.89
FeO_t	10.35	10.90	11.51	10.65	8.99	11.30	12.08	9.26
MnO	0.21	0.19	0.22	0.19	0.16	0.21	0.21	0.21
MgO	6.38	7.85	6.89	11.42	8.96	11.68	10.43	10.14
CaO	13.59	11.42	11.48	11.60	12.46	11.77	11.09	12.75
Na_2O	2.54	2.52	2.28	1.63	1.94	1.44	1.89	1.57
K_2O	0.40	0.65	0.73	0.41	0.41	0.48	0.44	0.26
TiO_2	0.77	0.78	1.00	0.55	0.62	0.62	0.77	0.70
P_2O_5	0.05	0.06	0.07	0.03	0.03	0.03	0.06	0.05
Cr_2O_3	0.00	0.00	0.03	0.06	0.05	0.10	0.03	0.02
LOI	0.46	0.97	0.76	1.43	1.21	1.35	1.16	1.09
Sc	40.0	43.0	49.2	-	-	42.2	-	-
V	266	277	300	214	-	212	-	260
Cr	290	290	225	430	348	693	210	170
Co	44	45	44	61	-	65	-	44
Ni	100	90	67	210	-	227	-	90
Rb	5	12	12	5	-	9	-	7
Sr	121	120	91	85	-	94	-	96
Y	16.5	17.2	20.6	12.1	-	14.4	-	18.2
Zr	43	45	39	22	-	30	-	32
Nb	2.3	2.1	2.4	1.2	-	1.2	-	1.7
Ba	159	124	76	49	-	41	-	22
La	5.33	4.79	3.61	2.24	-	2.21	-	1.80
Ce	11.70	11.30	9.08	5.51	-	5.61	-	5.75
Pr	1.60	1.63	1.38	0.81	-	0.86	-	0.90
Nd	7.30	7.38	6.59	4.14	-	4.33	-	4.89
Sm	2.11	2.02	2.11	1.29	-	1.45	-	1.85
Eu	0.800	0.729	0.758	0.546	-	0.553	-	0.564
Gd	2.68	2.75	2.71	1.89	-	1.91	-	2.46
Tb	0.47	0.48	0.52	0.36	-	0.36	-	0.44
Dy	3.06	3.15	3.51	2.39	-	2.42	-	2.94
Ho	0.65	0.68	0.76	0.49	-	0.52	-	0.60
Er	1.90	2.01	2.21	1.36	-	1.51	-	1.72
Tm	0.271	0.298	0.327	0.205	-	0.221	-	0.259
Yb	1.79	1.87	2.13	1.40	-	1.45	-	1.80
Lu	0.294	0.298	0.319	0.227	-	0.211	-	0.280
Hf	1.4	1.3	1.2	0.7	-	0.9	-	1.1
Ta	0.13	0.11	0.17	0.12	-	0.09	-	0.24
Pb	11	0	9	0	-	9	-	5
Th	0.84	0.12	0.36	0.23	-	0.21	-	0.00
U	0.30	0.09	0.28	0.10	-	0.11	-	0.02

Continued on next page

	Enriched Nulliak mafic rocks (continued)							
Sample	SG-111	SG-112	SG-113	SG-117	SG-139	SG-141	SG-230	SG-234
Easting	523711	523717	523732	523709	520631	520597	523663	523803
Northing	6440136	6440091	6440000	6439939	6483204	6482931	6462834	6462909
SiO_2	48.11	49.70	49.39	49.19	49.98	51.28	50.08	51.47
Al_2O_3	14.77	15.36	16.15	12.43	14.67	14.91	14.87	16.73
FeO_t	11.62	11.20	8.94	11.77	11.82	11.57	12.65	9.12
MnO	0.21	0.20	0.21	0.22	0.24	0.19	0.23	0.18
MgO	10.73	8.37	8.12	11.12	6.94	5.97	6.33	6.72
CaO	11.66	11.30	14.64	12.20	11.86	11.54	10.88	11.03
Na_2O	1.84	2.64	1.69	1.65	2.62	3.06	2.77	3.21
K_2O	0.38	0.43	0.30	0.50	0.92	0.53	0.88	0.62
TiO_2	0.56	0.74	0.54	0.76	0.89	0.89	1.22	0.82
P_2O_5	0.03	0.04	0.03	0.05	0.06	0.06	0.09	0.10
Cr_2O_3	0.08	0.03	0.00	0.10	0.00	0.00	0.00	0.00
LOI	0.76	0.73	0.53	1.32	0.92	1.19	0.45	0.62
Sc	30.9	-	40.2	-	48.0	47.0	-	28.4
V	166	216	200	226	308	296	319	204
Cr	533	240	46	700	200	190	110	265
Co	65	52	44	68	53	56	44	47
Ni	368	180	159	360	50	60	70	117
Rb	4	6	2	7	19	11	14	13
Sr	136	130	167	113	142	146	88	195
Y	10.9	12.6	11.1	14.4	19.8	19.6	27.7	18.7
Zr	28	21	22	34	61	62	85	66
Nb	1.3	1.4	1.1	1.8	2.5	2.3	3.1	3.3
Ba	48	130	80	81	192	85	77	95
La	2.19	2.99	1.81	3.32	5.69	5.90	7.22	10.16
Ce	5.69	7.58	5.01	8.50	13.20	13.60	17.10	21.27
Pr	0.89	1.11	0.82	1.17	1.85	1.97	2.38	2.69
Nd	4.58	5.37	4.32	6.00	8.27	8.34	11.00	11.19
Sm	1.45	1.81	1.45	1.89	2.30	2.68	3.16	2.60
Eu	0.571	0.752	0.540	0.694	0.904	0.923	1.010	0.871
Gd	1.80	2.11	1.78	2.38	2.95	3.32	3.76	3.10
Tb	0.31	0.40	0.31	0.40	0.54	0.58	0.75	0.51
Dy	1.99	2.50	2.02	2.45	3.57	3.72	4.74	3.27
Ho	0.41	0.48	0.43	0.48	0.73	0.74	0.93	0.70
Er	1.16	1.31	1.19	1.40	2.17	2.14	2.83	1.96
Tm	0.167	0.183	0.178	0.217	0.311	0.327	0.417	0.284
Yb	1.09	1.20	1.09	1.38	2.05	2.19	2.72	1.87
Lu	0.158	0.199	0.160	0.203	0.337	0.328	0.422	0.274
Hf	0.9	0.7	0.7	1.0	1.3	1.4	2.2	1.9
Ta	0.11	0.11	0.11	0.29	0.16	0.18	0.19	0.23
Pb	3	17	4	0	0	10	6	5
Th	0.27	0.15	0.02	0.22	0.35	0.57	1.08	1.84
U	0.07	0.05	0.01	0.11	0.08	0.14	0.33	0.30

Continued on next page

	Enriched Nulliak mafic rocks				Enriched Upernavik mafic rocks			
Sample	SG-281	SG-282	SG-283	SG-284	SG-070	SG-071	SG-072	SG-076A
Easting	491356	491353	491347	491343	512475	512451	512444	512944
Northing	6470215	6470212	6470217	6470216	6478536	6478457	6478360	6478114
SiO_2	49.69	50.97	50.47	50.24	49.17	50.27	48.87	48.45
Al_2O_3	13.71	15.09	14.31	15.47	14.40	15.18	15.49	15.95
FeO_t	13.02	10.72	10.77	10.78	12.93	12.38	12.37	10.85
MnO	0.19	0.18	0.15	0.15	0.23	0.20	0.20	0.20
MgO	8.88	7.94	7.99	7.71	7.71	6.80	7.92	9.80
CaO	11.13	11.68	12.44	11.56	11.99	11.28	10.81	11.35
Na_2O	2.24	2.42	2.79	3.07	1.90	2.25	2.55	2.16
K_2O	0.11	0.10	0.08	0.09	0.49	0.39	0.50	0.49
TiO_2	0.98	0.87	0.89	0.87	1.10	1.14	1.15	0.64
P_2O_5	0.06	0.05	0.11	0.06	0.07	0.09	0.09	0.04
Cr_2O_3	0.00	0.00	0.00	0.00	0.03	0.03	0.03	0.06
LOI	0.00	0.00	0.10	0.29	1.05	0.92	0.84	0.84
Sc	60.0	53.6	-	-	45.0	-	-	39.0
V	360	322	-	-	329	342	350	218
Cr	167	121	-	-	212	240	240	404
Co	55	49	-	-	54	49	52	57
Ni	75	65	-	-	116	130	150	168
Rb	0	1	-	-	12	7	8	11
Sr	169	241	-	-	111	111	93	105
Y	22.0	19.6	-	-	24.5	23.7	24.0	14.9
Zr	25	32	-	-	21	51	57	36
Nb	2.2	1.8	-	-	2.7	3.0	2.8	1.5
Ba	17	17	-	-	43	42	50	163
La	2.39	1.82	-	-	3.75	5.22	4.39	2.51
Ce	9.33	6.50	-	-	10.08	13.20	11.20	6.22
Pr	1.76	1.18	-	-	1.60	1.89	1.61	0.95
Nd	9.48	6.37	-	-	7.93	9.59	8.55	4.76
Sm	3.00	2.12	-	-	2.59	2.81	2.83	1.53
Eu	0.763	0.759	-	-	0.883	1.030	0.982	0.648
Gd	3.34	2.65	-	-	3.30	3.86	3.65	2.02
Tb	0.60	0.49	-	-	0.62	0.69	0.66	0.38
Dy	3.90	3.30	-	-	4.15	4.44	4.22	2.50
Ho	0.84	0.72	-	-	0.90	0.91	0.89	0.57
Er	2.35	2.08	-	-	2.57	2.61	2.59	1.58
Tm	0.340	0.313	-	-	0.382	0.391	0.392	0.228
Yb	2.22	2.01	-	-	2.44	2.52	2.49	1.52
Lu	0.323	0.307	-	-	0.376	0.379	0.394	0.229
Hf	1.0	1.1	-	-	1.1	1.7	1.7	1.0
Ta	0.11	0.09	-	-	0.19	0.28	0.27	0.11
Pb	1	2	-	-	6	0	0	5
Th	0.04	0.09	-	-	0.20	0.28	0.37	0.37
U	0.01	0.01	-	-	0.06	0.16	0.14	0.13

Continued on next page

	Enriched Upernavik mafic rocks (continued)							
Sample	SG-076B	SG-078A	SG-078B	SG-079	SG-085	SG-126	SG-128	SG-129
Easting	512944	513147	513147	513114	512532	502460	501508	501503
Northing	6478114	6477975	6477975	6478006	6478877	6484045	6482743	6482792
SiO_2	48.83	52.27	50.04	52.93	50.38	46.90	48.46	48.76
Al_2O_3	16.68	14.80	14.37	14.83	14.64	16.88	15.84	15.15
FeO_t	10.32	12.31	11.46	9.84	13.04	12.54	10.30	10.62
MnO	0.19	0.20	0.23	0.20	0.21	0.23	0.16	0.18
MgO	9.17	5.94	6.72	7.64	6.49	8.70	10.63	10.04
CaO	11.16	10.31	13.66	10.90	10.88	11.38	11.81	11.65
Na_2O	2.42	2.55	2.20	2.45	2.31	1.78	1.85	2.26
K_2O	0.52	0.49	0.40	0.20	0.48	0.46	0.24	0.45
TiO_2	0.62	1.04	0.85	0.90	1.42	1.01	0.67	0.82
P_2O_5	0.04	0.07	0.04	0.05	0.11	0.07	0.05	0.05
Cr_2O_3	0.05	0.00	0.04	0.05	0.03	0.05	0.00	0.00
LOI	1.02	0.64	0.60	0.88	1.04	0.47	0.40	0.76
Sc	-	50.8	-	-	-	41.4	29.0	33.0
V	-	323	-	320	388	281	198	267
Cr	343	19	274	390	180	378	440	440
Co	-	46	-	51	47	59	55	55
Ni	-	37	-	110	120	173	310	270
Rb	-	11	-	5	15	2	1	3
Sr	-	116	-	125	106	66	93	86
Y	-	22.8	-	14.1	31.8	21.2	13.1	15.5
Zr	-	39	-	33	83	34	37	42
Nb	-	2.3	-	1.8	3.0	2.2	1.8	1.7
Ba	-	89	-	43	40	41	24	43
La	-	3.52	-	2.90	5.69	9.53	3.50	2.53
Ce	-	9.22	-	7.70	14.40	21.26	9.32	7.21
Pr	-	1.45	-	1.18	2.16	2.73	1.44	1.12
Nd	-	7.36	-	5.92	10.30	11.21	6.98	5.57
Sm	-	2.41	-	2.01	3.32	2.90	1.95	1.85
Eu	-	0.903	-	0.789	1.190	0.818	0.701	0.676
Gd	-	3.05	-	2.65	4.50	3.13	2.38	2.58
Tb	-	0.56	-	0.46	0.85	0.53	0.40	0.46
Dy	-	3.80	-	2.91	5.49	3.57	2.54	3.02
Ho	-	0.84	-	0.58	1.11	0.79	0.52	0.62
Er	-	2.39	-	1.66	3.16	2.25	1.50	1.78
Tm	-	0.355	-	0.231	0.473	0.346	0.223	0.260
Yb	-	2.35	-	1.51	2.90	2.20	1.37	1.62
Lu	-	0.354	-	0.236	0.452	0.318	0.219	0.244
Hf	-	1.4	-	1.2	2.2	1.2	1.2	1.3
Ta	-	0.17	-	0.17	0.19	0.15	0.08	0.06
Pb	-	2	-	0	-	3	0	0
Th	-	0.59	-	0.27	0.57	1.32	0.11	0.00
U	-	0.19	-	0.09	0.25	0.27	0.03	0.03

Continued on next page

	Enriched Upernavik mafic rocks (continued)					Depleted Nulliak mafic rocks		
Sample	SG-130	SG-238	SG-244	SG-287	SG-288	SG-031	SG-033A	SG-033B
Easting	501490	509835	509802	498025	498025	491342	491317	491318
Northing	6482839	6480369	6480600	6477836	6477836	6470185	6470175	6470157
SiO_2	48.48	49.29	50.93	48.39	48.50	48.22	47.96	48.54
Al_2O_3	15.57	14.60	13.44	14.94	13.74	20.88	16.15	16.91
FeO_t	10.21	12.13	13.79	11.03	13.82	6.86	7.61	8.86
MnO	0.18	0.20	0.24	0.20	0.25	0.11	0.13	0.17
MgO	9.54	7.97	6.86	8.61	7.49	9.17	12.06	12.50
CaO	13.10	11.12	11.07	13.70	12.62	12.82	13.93	11.06
Na_2O	2.01	2.87	1.84	2.05	2.06	1.17	1.59	1.27
K_2O	0.19	0.97	0.47	0.36	0.48	0.23	0.16	0.25
TiO_2	0.67	0.76	1.25	0.66	0.98	0.40	0.38	0.33
P_2O_5	0.06	0.09	0.10	0.05	0.06	0.04	0.02	0.02
Cr_2O_3	0.00	0.00	0.00	0.00	0.00	0.08	0.00	0.09
LOI	0.36	0.66	0.85	0.07	0.00	0.34	0.75	0.45
Sc	31.0	45.8	51.1	33.7	35.3	21.5	41.0	-
V	215	285	384	204	259	133	193	-
Cr	390	184	139	415	160	553	1090	623
Co	51	52	55	54	57	47	47	-
Ni	260	112	70	216	133	223	220	-
Rb	2	7	19	9	6	2	1	-
Sr	126	84	113	134	112	136	91	-
Y	14.8	19.4	26.8	13.0	20.0	7.4	7.2	-
Zr	37	43	65	31	43	19	17	-
Nb	1.6	2.2	3.4	1.9	4.3	0.9	0.8	-
Ba	38	50	119	44	46	43	11	1300
La	3.86	4.52	5.01	2.82	7.28	2.80	1.85	-
Ce	9.50	9.99	12.48	7.50	20.18	6.44	5.52	-
Pr	1.44	1.38	1.88	1.17	2.93	0.86	0.78	-
Nd	6.61	6.58	9.14	5.81	12.75	3.70	3.65	-
Sm	1.96	1.95	2.77	1.77	3.32	0.99	1.09	-
Eu	0.742	0.699	0.980	0.715	0.983	0.444	0.429	-
Gd	2.49	2.62	3.67	2.16	3.48	1.13	1.18	-
Tb	0.45	0.45	0.65	0.36	0.57	0.20	0.21	-
Dy	2.82	3.21	4.33	2.34	3.50	1.32	1.35	-
Ho	0.58	0.72	0.96	0.49	0.74	0.28	0.29	-
Er	1.69	2.04	2.78	1.35	2.07	0.79	0.82	-
Tm	0.248	0.306	0.418	0.197	0.296	0.117	0.124	-
Yb	1.52	2.03	2.70	1.22	1.99	0.76	0.79	-
Lu	0.237	0.293	0.413	0.184	0.289	0.114	0.118	-
Hf	1.1	1.4	1.9	1.0	1.4	0.6	0.6	-
Ta	0.06	0.15	0.21	0.15	0.31	0.11	0.02	-
Pb	0	5	4	2	4	4	0	-
Th	0.16	0.43	0.62	0.65	0.52	0.19	0.00	-
U	0.06	0.09	0.15	0.36	0.31	0.05	0.01	-

Continued on next page

	Depleted Nulliak mafic rocks (continued)							
Sample	SG-034	SG-042	SG-046	SG-047	SG-055	SG-056	SG-057	SG-060
Easting	491276	491303	491285	491099	491536	491620	491647	491648
Northing	6470174	6470233	6470345	6470302	6469574	6469562	6469672	6469972
SiO_2	47.51	48.82	48.68	48.64	47.06	48.00	46.84	48.17
Al_2O_3	14.90	15.90	17.75	16.63	16.26	16.97	17.11	15.17
FeO_t	8.89	7.56	7.30	8.19	9.16	8.97	9.22	9.43
MnO	0.19	0.14	0.14	0.18	0.19	0.16	0.17	0.19
MgO	13.04	11.08	9.58	10.02	14.71	13.96	13.97	14.89
CaO	13.76	14.82	14.51	14.28	10.61	10.20	10.86	9.92
Na_2O	0.99	1.10	1.47	1.34	1.07	0.83	1.06	1.27
K_2O	0.33	0.20	0.19	0.33	0.48	0.36	0.40	0.40
TiO_2	0.39	0.36	0.37	0.38	0.33	0.42	0.34	0.39
P_2O_5	0.00	0.02	0.01	0.02	0.02	0.02	0.02	0.02
Cr_2O_3	0.00	0.00	0.00	0.00	0.11	0.10	0.00	0.13
LOI	1.13	0.84	0.57	0.45	1.82	0.36	0.51	2.15
Sc	48.0	40.0	39.0	41.0	-	24.2	26.0	-
V	196	184	189	191	143	149	136	143
Cr	1120	890	840	740	820	759	810	890
Co	53	44	41	44	69	65	67	66
Ni	250	200	170	170	440	371	410	440
Rb	4	3	1	8	7	10	4	7
Sr	70	88	90	150	82	89	84	91
Y	10.8	7.7	10.6	9.1	7.2	10.1	7.1	8.0
Zr	12	11	11	15	13	20	18	16
Nb	0.5	0.6	3.9	0.8	1.1	1.2	1.0	1.2
Ba	32	16	17	91	43	78	42	48
La	1.22	0.97	1.66	2.66	1.65	2.48	3.37	2.99
Ce	4.27	3.17	4.35	5.94	4.04	6.99	9.64	7.13
Pr	0.63	0.51	0.65	0.79	0.55	1.03	1.28	0.92
Nd	3.31	2.59	3.03	3.25	2.69	4.66	5.17	3.83
Sm	0.98	0.83	1.09	0.97	0.84	1.28	1.16	1.17
Eu	0.387	0.354	0.366	0.416	0.381	0.411	0.406	0.393
Gd	1.37	1.12	1.53	1.33	0.99	1.51	1.21	1.18
Tb	0.26	0.21	0.29	0.24	0.18	0.27	0.21	0.22
Dy	1.74	1.41	1.91	1.64	1.22	1.80	1.33	1.47
Ho	0.38	0.31	0.41	0.36	0.26	0.37	0.27	0.30
Er	1.16	0.89	1.21	1.07	0.81	1.12	0.73	0.83
Tm	0.171	0.133	0.183	0.163	0.121	0.162	0.112	0.125
Yb	1.10	0.82	1.17	1.03	0.78	1.09	0.70	0.83
Lu	0.170	0.132	0.182	0.161	0.116	0.159	0.105	0.128
Hf	0.5	0.5	0.5	0.5	0.4	0.7	0.5	0.6
Ta	0.00	0.00	0.68	0.01	0.13	0.16	0.07	0.12
Pb	0	0	0	0	0	2	0	0
Th	0.00	0.00	0.00	0.00	0.06	0.12	0.21	0.09
U	0.00	0.00	0.02	0.01	0.04	0.05	0.05	0.02

Continued on next page

	(continued)		Depleted Upernavik mafic rocks			High-Fe Nulliak ultramafic rocks		
Sample	SG-109A	SG-110	SG-075	SG-123	SG-131	SG-004	SG-012	SG-013
Easting	523520	523611	512637	502469	501528	513719	522827	522811
Northing	6440344	6440181	6478211	6483981	6482865	6441236	6461190	6461191
SiO_2	49.11	47.88	50.13	48.86	49.38	43.67	47.19	44.45
Al_2O_3	16.69	17.16	16.90	17.74	16.60	1.88	4.99	2.06
FeO_t	8.08	8.83	8.60	8.54	9.82	14.05	12.58	12.93
MnO	0.15	0.15	0.17	0.17	0.16	0.19	0.22	0.22
MgO	10.43	10.99	9.33	9.40	9.29	36.96	27.97	36.03
CaO	13.65	12.64	11.92	12.32	11.30	2.30	5.09	3.09
Na_2O	1.26	1.53	1.80	1.18	2.84	0.10	0.97	0.12
K_2O	0.20	0.34	0.47	1.36	0.24	0.03	0.25	0.66
TiO_2	0.34	0.39	0.52	0.39	0.38	0.41	0.54	0.22
P_2O_5	0.02	0.02	0.03	0.03	0.00	0.06	0.05	0.00
Cr_2O_3	0.07	0.08	0.12	0.00	0.00	0.35	0.16	0.22
LOI	1.10	1.16	1.63	2.58	0.53	10.61	1.31	4.31
Sc	-	-	-	26.0	51.0	-	-	-
V	119	136	200	153	194	82	106	54
Cr	460	550	860	400	110	2070	1030	1430
Co	53	56	52	53	44	144	108	121
Ni	270	280	200	240	80	2070	1830	2260
Rb	5	4	15	25	1		2	32
Sr	86	96	126	97	58	8	118	39
Y	8.4	8.8	9.3	7.9	9.1	8.3	10.2	5.0
Zr	14	15	16	21	18	24	33	10
Nb	0.9	1.0	1.3	0.9	0.6	0.6	0.5	1.2
Ba	11	37	110	149	26		46	280
La	1.08	1.53	2.05	2.55	0.80	1.81	8.59	4.10
Ce	3.05	4.08	5.25	5.25	2.55	5.21	16.90	11.20
Pr	0.49	0.61	0.72	0.66	0.47	0.82	2.22	1.67
Nd	2.62	2.78	3.29	2.99	2.43	3.70	8.97	8.45
Sm	0.84	0.98	1.10	0.93	0.91	1.26	2.33	1.70
Eu	0.381	0.459	0.484	0.474	0.433	0.179	0.715	0.412
Gd	1.20	1.37	1.48	1.22	1.19	1.38	2.20	1.47
Tb	0.23	0.25	0.26	0.22	0.23	0.23	0.33	0.18
Dy	1.51	1.60	1.76	1.40	1.65	1.48	1.96	0.96
Ho	0.31	0.32	0.36	0.30	0.38	0.27	0.39	0.17
Er	0.91	0.93	0.99	0.92	1.11	0.77	0.97	0.46
Tm	0.135	0.140	0.151	0.133	0.152	0.134	0.128	0.061
Yb	0.91	0.95	1.02	0.85	0.97	0.84	0.82	0.38
Lu	0.142	0.153	0.155	0.135	0.149	0.122	0.126	0.058
Hf	0.4	0.5	0.6	0.6	0.6	0.6	0.8	0.3
Ta	0.09	0.09	0.13	0.04	0.01	0.04	0.05	0.23
Pb	33	0	0	0	0	-	7	0
Th	0.00	0.00	0.08	1.16	0.00	0.23	0.78	0.20
U	0.00	0.00	0.03	0.62	0.03	0.30	0.43	0.11

Continued on next page

	High-Fe Nulliak ultramafic rocks (continued)							
Sample	SG-014	SG-015	SG-023	SG-099	SG-100	SG-205	SG-206	SG-235
Easting	522809	522807	522601	522931	522937	522755	522619	523851
Northing	6461189	6461187	6461303	6440466	6440458	6463676	6463797	6462989
SiO_2	44.45	44.73	45.47	43.94	47.19	46.03	48.16	43.22
Al_2O_3	2.49	1.89	7.35	3.54	5.04	3.85	5.64	1.83
FeO_t	12.08	11.75	13.82	15.32	13.37	11.97	12.37	13.61
MnO	0.14	0.20	0.25	0.19	0.17	0.20	0.21	0.25
MgO	36.99	36.49	21.56	31.64	23.64	31.71	20.75	38.06
CaO	2.74	3.93	9.46	4.23	8.24	4.75	10.80	1.80
Na_2O	0.26	0.19	1.12	0.21	0.40	0.47	0.91	0.04
K_2O	0.29	0.36	0.32	0.19	1.02	0.57	0.48	0.96
TiO_2	0.31	0.21	0.60	0.39	0.56	0.42	0.63	0.22
P_2O_5	0.02	0.02	0.04	0.02	0.03	0.04	0.05	0.01
Cr_2O_3	0.23	0.24	0.00	0.33	0.34	0.00	0.00	0.00
LOI	7.76	2.71	1.01	6.99	3.65	8.01	1.45	5.43
Sc	-	-	29.0	-	-	-	22.9	-
V	69	55	179	101	153	83	160	48
Cr	1380	1510	2150	2140	2190	1400	1587	1560
Co	106	125	97	132	74	101	90	129
Ni	2340	2380	800	1300	700	1870	1000	2710
Rb	8	18	4	4	65	39	5	80
Sr	25	15	76	13	15	8	61	¡ 2
Y	6.6	3.5	12.5	6.2	10.9	7.0	12.4	1.8
Zr	17	11	34	22	27	23	43	16
Nb	0.3		0.9	1.3	1.6	0.3	1.7	0.7
Ba	38	36	9	43	131	23	35	38
La	3.27	1.47	2.23	1.88	3.54	1.96	3.51	0.70
Ce	8.25	3.42	6.24	4.75	8.99	5.16	8.73	2.13
Pr	1.10	0.44	1.03	0.66	1.27	0.75	1.30	0.34
Nd	4.63	1.98	5.27	3.19	6.26	3.86	6.33	1.17
Sm	1.27	0.57	1.73	1.03	1.78	1.09	2.03	0.32
Eu	0.332	0.224	0.533	0.268	0.657	0.363	0.792	0.080
Gd	1.35	0.64	2.20	1.09	2.03	1.27	2.43	0.27
Tb	0.22	0.10	0.38	0.19	0.33	0.23	0.41	0.05
Dy	1.32	0.67	2.36	1.16	1.95	1.29	2.45	0.32
Ho	0.24	0.12	0.49	0.22	0.39	0.25	0.50	0.06
Er	0.66	0.35	1.42	0.58	1.06	0.70	1.32	0.17
Tm	0.091	0.047	0.199	0.087	0.148	0.096	0.174	0.023
Yb	0.54	0.33	1.21	0.59	0.95	0.60	1.11	0.15
Lu	0.074	0.051	0.176	0.083	0.144	0.085	0.147	0.023
Hf	0.4	0.3	0.8	0.6	0.9	0.5	1.2	0.4
Ta	0.05	0.01	0.07	0.24	0.24	0.03	0.08	0.15
Pb	-	-	0	6	0	-	5	-
Th	0.13	0.63	0.20	0.29	0.52	0.38	0.43	0.07
U	0.13	0.08	0.12	0.13	0.29	0.18	0.25	0.03

Continued on next page

	High-Fe Upernavik ultramafic rocks					Low-Fe Nulliak ultramafic rocks		
Sample	SG-061	SG-063	SG-067	SG-068	SG-069	SG-005	SG-006	SG-008
Easting	512642	512629	512554	512546	512551	522693	522662	522718
Northing	6478669	6478655	6478561	6478561	6478553	6461573	6461603	6461515
SiO_2	50.82	46.10	48.92	46.48	47.21	51.46	50.48	46.67
Al_2O_3	4.03	8.02	5.39	7.15	6.95	5.64	6.57	5.75
FeO_t	11.38	12.56	11.81	12.78	12.55	9.61	9.35	8.43
MnO	0.13	0.19	0.20	0.25	0.18	0.20	0.17	0.14
MgO	25.18	22.73	20.26	20.55	21.76	30.25	29.64	31.91
CaO	7.65	8.58	12.08	11.03	9.93	1.89	2.61	5.67
Na_2O	0.09	0.41	0.18	0.21	0.22	0.33	0.40	0.71
K_2O	0.03	0.14	0.07	0.43	0.08	0.10	0.17	0.14
TiO_2	0.41	0.90	0.77	0.80	0.82	0.17	0.21	0.20
P_2O_5	0.02	0.06	0.05	0.05	0.06	0.02	0.00	0.00
Cr_2O_3	0.25	0.30	0.27	0.25	0.23	0.33	0.40	0.38
LOI	4.88	4.64	3.88	4.08	3.97	2.68	4.65	5.46
Sc	-	-	-	-	-	-	-	-
V	107	211	177	187	190	93	110	103
Cr	1510	1780	1810	1580	1420	2140	2520	2450
Co	100	52	70	67	62	86	83	96
Ni	1910	400	670	860	580	1500	1600	1780
Rb		2	1	15	2	3	4	1
Sr	82	99	75	138	82	7	17	22
Y	7.7	16.7	13.4	14.4	14.2	5.7	5.2	4.7
Zr	20	53	41	43	45	5	5	5
Nb	0.3	1.2	1.9	1.0	1.0	-	-	-
Ba	4	21	5	123	16	-	6	4
La	2.28	4.05	2.85	3.05	3.51	0.55	0.34	0.72
Ce	5.89	10.80	7.71	8.27	8.99	1.62	0.69	1.19
Pr	0.86	1.61	1.15	1.31	1.37	0.25	0.11	0.12
Nd	4.10	8.00	6.24	6.35	6.50	1.25	0.54	0.49
Sm	1.28	2.56	2.01	2.10	2.01	0.36	0.26	0.21
Eu	0.322	1.270	0.825	1.030	0.775	0.269	0.147	0.182
Gd	1.40	2.96	2.40	2.54	2.49	0.53	0.47	0.48
Tb	0.24	0.55	0.39	0.42	0.43	0.11	0.11	0.10
Dy	1.38	3.35	2.40	2.59	2.67	0.84	0.81	0.75
Ho	0.26	0.63	0.48	0.52	0.51	0.19	0.18	0.16
Er	0.75	1.64	1.33	1.37	1.44	0.57	0.54	0.54
Tm	0.103	0.223	0.180	0.192	0.187	0.088	0.087	0.083
Yb	0.65	1.42	1.10	1.10	1.13	0.60	0.56	0.52
Lu	0.099	0.219	0.153	0.154	0.162	0.098	0.094	0.086
Hf	0.4	1.3	1.3	1.0	1.1	0.1	0.2	0.1
Ta	0.05	0.11	0.28	0.13	0.11			0.06
Pb	-	-	-	-	-	-	-	-
Th	0.22	0.46	0.32	0.45	0.43	0.08	0.06	0.14
U	0.06	0.14	0.12	0.13	0.15	0.24	0.12	0.10

Continued on next page

	Low-Fe Nulliak ultramafic rocks (continued)							
Sample	SG-009	SG-010	SG-018	SG-020	SG-022	SG-133	SG-135	SG-136
Easting	522717	522714	522495	522602	522635	520818	520811	520778
Northing	6461519	6461519	6461247	6461120	6461145	6483157	6483087	6483104
SiO_2	48.83	45.47	42.53	42.61	46.77	45.57	41.10	42.53
Al_2O_3	9.49	9.69	3.30	2.60	2.52	5.96	1.39	1.13
FeO_t	10.02	11.64	9.01	8.17	7.71	8.63	10.41	8.29
MnO	0.15	0.17	0.17	0.16	0.18	0.17	0.18	0.15
MgO	21.23	27.35	40.38	45.12	41.34	34.45	45.03	46.99
CaO	7.94	4.21	3.41	0.02	0.06	3.76	0.26	0.38
Na_2O	1.31	0.56	0.42	0.01	0.01	0.52	0.01	0.01
K_2O	0.29	0.12	0.17	0.05	0.47	0.34	0.01	0.01
TiO_2	0.35	0.37	0.12	0.08	0.07	0.16	0.06	0.06
P_2O_5	0.00	0.02	0.00	0.00	0.00	0.03	0.01	0.00
Cr_2O_3	0.39	0.41	0.49	1.18	0.86	0.41	1.54	0.45
LOI	1.32	0.69	2.87	4.16	4.25	1.72	2.29	6.38
Sc	-	-	-	-	-	20.0	9.0	7.0
V	142	150	78	57	44	100	44	26
Cr	2490	2630	3300	7310	5410	2740	10000	2830
Co	82	102	131	116	106	103	149	106
Ni	880	1080	2200	2850	2570	1860	2990	2890
Rb	4	1	4	2	26	28	0	0
Sr	69	62	8	-	-	20	0	3
Y	9.0	10.6	2.7	1.7	1.5	4.1	0.8	0.9
Zr	15	16	5	1	6	11	8	6
Nb	-	-	0.4	-	-	0.4	0.0	0.2
Ba	8	7	6	-	9	4	0	0
La	1.47	1.45	1.94	0.07		0.45	0.30	0.37
Ce	4.47	4.00	3.80	0.10	0.10	1.00	0.69	0.83
Pr	0.65	0.61	0.36	0.02	0.02	0.12	0.08	0.11
Nd	3.07	2.83	1.21	-	0.05	0.55	0.29	0.40
Sm	0.97	0.98	0.27	-	0.02	0.24	0.11	0.11
Eu	0.496	0.455	0.103	-	-	0.077	0.025	0.033
Gd	1.09	1.31	0.30	0.05	0.04	0.44	0.11	0.12
Tb	0.21	0.26	0.06	0.02	0.02	0.09	0.02	0.03
Dy	1.47	1.71	0.35	0.19	0.16	0.68	0.12	0.18
Ho	0.29	0.35	0.08	0.05	0.05	0.16	0.03	0.04
Er	0.90	1.05	0.27	0.22	0.20	0.47	0.08	0.12
Tm	0.142	0.160	0.048	0.036	0.036	0.078	0.010	0.017
Yb	0.97	1.00	0.32	0.25	0.26	0.53	0.06	0.11
Lu	0.150	0.155	0.043	0.035	0.044	0.088	0.010	0.013
Hf	0.4	0.5	0.1	-	0.1	0.2	0.1	0.1
Ta	0.02	0.04	0.20	-	-	0.04	0.02	0.03
Pb	-	-	-	-	-	-	-	-
Th	0.15	0.24	0.23	-	0.10	0.00	0.00	0.00
U	0.19	0.12	0.18	0.06	0.06	0.12	0.04	0.01

Continued on next page

	Low-Fe Nulliak ultramafic rocks (continued)						
Sample	SG-137A	SG-137B	SG-138	SG-140	SG-142	SG-201	SG-221
Easting	520722	520734	520703	520618	520638	522492	513991
Northing	6483176	6483179	6483221	6482953	6482898	6463514	6481276
SiO_2	40.87	41.45	41.77	42.25	40.57	49.30	46.32
Al_2O_3	0.22	0.17	0.27	1.34	1.54	7.36	7.31
FeO_t	8.32	9.64	11.51	8.93	9.78	7.80	7.73
MnO	0.19	0.18	0.11	0.18	0.17	0.14	0.14
MgO	49.87	48.01	45.65	45.79	44.88	30.27	36.57
CaO	0.01	0.02	0.01	0.89	1.90	4.11	1.68
Na_2O	0.01	0.01	0.01	0.01	0.01	0.59	0.10
K_2O	0.01	0.01	0.01	0.01	0.01	0.23	0.01
TiO_2	0.01	0.01	0.01	0.04	0.06	0.17	0.13
P_2O_5	0.00	0.00	0.00	0.01	0.00	0.02	0.02
Cr_2O_3	0.49	0.50	0.64	0.55	1.08	0.00	0.00
LOI	4.19	7.83	9.28	2.83	8.17	4.31	9.59
Sc	7.0	4.0	4.0	8.0	7.0	-	-
V	13	15	18	32	40	105	95
Cr	3210	3100	3870	3650	6680	2100	2730
Co	153	145	126	147	137	77	92
Ni	2920	2590	2510	2930	2940	1400	1940
Rb	0	0	0	0	0	10	
Sr	0	0	0	0	35	7	5
Y	0.0	0.0	0.0	1.8	0.9	4.8	3.5
Zr	3	2	4	4	4	7	5
Nb	0.0	0.0	0.0	0.0	0.0	-	-
Ba	0	0	0	0	0	12	-
La	0.33	0.51	1.41	0.40	0.33	1.35	0.17
Ce	0.42	0.78	2.49	1.01	0.87	2.59	0.40
Pr	0.04	0.07	0.23	0.13	0.11	0.32	0.07
Nd	0.05	0.17	0.56	0.60	0.45	1.23	0.30
Sm	0.00	0.02	0.09	0.20	0.11	0.33	0.15
Eu	0.000	0.008	0.012	0.066	0.039	0.124	0.088
Gd	0.01	0.02	0.05	0.27	0.14	0.48	0.25
Tb	0.00	0.00	0.00	0.06	0.02	0.11	0.06
Dy	0.02	0.02	0.03	0.38	0.15	0.89	0.48
Ho	0.00	0.00	0.00	0.08	0.03	0.19	0.12
Er	0.01	0.01	0.02	0.22	0.11	0.55	0.37
Tm	0.000	0.000	0.000	0.033	0.015	0.083	0.059
Yb	0.00	0.01	0.02	0.21	0.09	0.55	0.42
Lu	0.000	0.000	0.003	0.032	0.015	0.082	0.069
Hf	0.0	0.0	0.0	0.0	0.0	0.2	0.2
Ta	0.01	0.00	0.02	0.02	0.00	-	-
Pb	-	11	27	0	0	-	-
Th	0.00	0.00	0.00	0.00	0.06	0.25	-
U	0.01	0.03	0.02	0.00	0.00	0.16	0.03

Continued on next page

	Low-Fe Upernavik ultramafic rocks					
Sample	SG-064	SG-066	SG-239	SG-240	SG-241	SG-243
Easting	512690	512559	509838	509842	509852	509859
Northing	6478633	6478682	6480371	6480373	6480394	6480435
SiO_2	43.02	46.52	43.00	42.58	44.15	43.36
Al_2O_3	12.15	8.87	3.87	3.88	4.42	4.14
FeO_t	9.98	8.83	11.10	10.51	9.77	10.66
MnO	0.13	0.12	0.19	0.18	0.16	0.17
MgO	28.81	29.53	39.13	38.92	38.11	37.37
CaO	4.81	5.13	2.18	3.16	2.35	3.55
Na_2O	0.20	0.19	0.30	0.49	0.43	0.50
K_2O	0.06	0.05	0.08	0.14	0.44	0.09
TiO_2	0.33	0.20	0.14	0.13	0.13	0.15
P_2O_5	0.02	0.01	0.01	0.01	0.03	0.02
Cr_2O_3	0.50	0.56	0.00	0.00	0.00	0.00
LOI	8.47	7.92	0.11	0.87	1.71	1.58
Sc	-	-	-	-	-	-
V	194	120	65	70	83	70
Cr	3190	3320	3400	3090	3500	2640
Co	82	95	130	123	115	123
Ni	830	1660	2560	2520	2390	2310
Rb	2	1	2	3	22	1
Sr	16	16	9	10	14	9
Y	6.7	6.7	3.0	3.0	4.6	3.7
Zr	17	8	5	5	6	6
Nb	0.4	-	-	-	-	-
Ba	0	5	7	8	108	5
La	0.25	0.33	0.58	0.69	0.63	0.58
Ce	0.57	0.73	1.54	1.60	1.60	1.46
Pr	0.08	0.13	0.22	0.22	0.24	0.21
Nd	0.56	0.62	0.89	0.92	0.82	1.00
Sm	0.24	0.24	0.29	0.31	0.37	0.32
Eu	0.127	0.118	0.106	0.119	0.065	0.117
Gd	0.51	0.48	0.40	0.37	0.44	0.51
Tb	0.11	0.11	0.07	0.08	0.10	0.09
Dy	0.90	0.92	0.44	0.49	0.69	0.61
Ho	0.22	0.22	0.10	0.11	0.14	0.12
Er	0.65	0.67	0.34	0.34	0.44	0.36
Tm	0.104	0.106	0.052	0.049	0.065	0.056
Yb	0.75	0.70	0.34	0.31	0.46	0.39
Lu	0.134	0.106	0.055	0.048	0.072	0.064
Hf	0.5	0.2	0.2	0.2	0.2	0.2
Ta	0.18	-	-	-	-	-
Pb	0	-	-	-	-	-
Th	0.00	-	0.07	0.13	0.19	0.11
U	0.05	-	0.05	0.08	0.09	0.09

Continued on next page

References

Abouchami, W., Boher, M., Michard, A., Albarède, F., 1990. A major 2.1 Ga old event of mafic magmatism in West Africa. Journal of Geophysical Research: Solid Earth: Solid Earth 95, 17605–17629.

Arai, S., 1975. Contact metamorphosed dunite-harzburgite complex in the Chugoku district, western Japan. Contributions to Mineralogy and Petrology 52 (1), 1–16.

Arndt, N., Albarède, F., Nisbet, E., 1997. Mafic and ultramafic magmatism. In: Wit, M., Ashwal, L. (Eds.), Greenstone Belts. Oxford Science Publications, Oxford, pp. 233–254.

Arndt, N., Lesher, C., Barnes, S., 2008. Komatiite, cambridge Edition. Cambridge University Press.

Arndt, N. T., Naldrett, A. J., Pyke, D. R., may 1977. Komatiitic and Iron-rich Tholeiitic Lavas of Munro Township, Northeast Ontario. Journal of Petrology 18 (2), 319–369.

Baadsgaard, H., Collerson, K. D., Bridgwater, D., 1979. The Archean gneiss complex of northern Labrador. 1. Preliminary U-Th-Pb geochronology. Canadian Journal of Earth Sciences, 951–961.

Baadsgaard, H., Cumming, G. L., Woden, J. M., 1984. U-Pb geochronology of minerals from the Midwest uranium deposit, northern Saskatchewan. Canadian Journal of Earth Sciences 21, 642–648.

Barnes, S., Arndt, N., 2019. Distribution and Geochemistry of Komatiites and Basalts Through the Archean. In: Van Kranendonk, M., Bennett, V. C., Hoffmann, J. E. (Eds.), Earth's Oldest Rocks, 2nd Edition. Elsevier, Ch. 6, pp. 103–132.

Barnes, S., Van Kranendonk, M., Sonntag, I., 2012. Geochemistry and tectonic setting of basalts from the eastern Goldfields Superterrane. Australian Journal of Earth Sciences 59, 707–735.

Bédard, J., Naslund, H., Nabelek, P., Winpenny, A., Hryciuk, M., MacDonald, W., Hayes, B., Steigerwaldt, K., Hadlari, T., Rainbird, R., Dewing, K., Girard, É., 2012. Fault-mediated melt ascent in a Neoproterozoic continental flood basalt province, the Franklin sills, Victoria Island, Canada. Bulletin of the Geological Society of America 124, 723–736.

Bédard, J. H., 2018. Stagnant lids and mantle overturns: Implications for Archaean tectonics, magmagenesis, crustal growth, mantle evolution, and the start of plate tectonics. Geoscience Frontiers 9 (1), 19–49.

Bernstein, S., Kelemen, P. B., Hanghøj, K., 2007. Consistent olivine Mg# in cratonic mantle reflects Archean mantle melting to the exhaustion of orthopyroxene. Geology 35 (5), 459–462.

Black, L. P., Williams, I. S., Compston, W., 1986. Four zircon ages from one rock: the history of a 3930 Ma-old granulite from Mount Sones, Enderby Land, Antarctica. Contributions to Mineralogy and Petrology 94 (4), 427–437.

Bougault, H., Hekinian, R., dec 1974. Rift Valley in the Atlantic Ocean near 3650N: petrology and geochemistry of basaltic rocks. Earth and Planetary Science Letters 24 (2), 249–261.

Bowring, S. a., Williams, I. S., 1999. Priscoan (4.00-4.03 Ga) orthogneisses from northwestern Canada. Contributions to Mineralogy and Petrology 134 (July 1998), 3–16.

Bridgwater, D., Collerson, K. D., 1976. The major petrological and geochemical characters of the 3,600 m.y. Uivak gneisses from Labrador. Contributions to Mineralogy and Petrology 54 (1), 43–59.

Bridgwater, D., Collerson, K. D., 1977. On the origin of Early Archean gneisses: a reply. Contributions to Mineralogy and Petrology 62, 179–191.

Bridgwater, D., Collerson, K. D., Hurst, R. W., Jesseau, C. W., 1975. Field characters of the early precambrian rocks from Saglek, Coast of Labrador. Geological survey of Canada 75 (1), 287–296.

Bridgwater, D., Schiøtte, L., 1991. The Archean gneiss complex of northern Labrador. A review of current results, ideas and problems. Bulletin of the Geological Society of Denmark 39 (3-4), 153–166.

Cates, N. L., Mojzsis, S. J., 2007. Pre-3750 Ma supracrustal rocks from the Nuvvuagittuq supracrustal belt, northern Québec. Earth and Planetary Science Letters 255 (1-2), 9–21.

Collerson, K., 1983. The Archean gneiss complex of northern Labrador. 2. Mineral ages, secondary isochrons, and diffusion of strontium during polymetamorphism of the Uivak gneisses. Can. J. Earth Sci. 20, 707–718.

Collerson, K. D., Campbell, L. M., Weaver, B. L., Palacz, Z. A., 1991. Evidence for extreme mantle fractionation in early Archean ultramafic rocks from northern Labrador. Nature 349 (6306), 209–214.

Collerson, K. D., Jesseau, C. W., Bridgwater, D., 1976. Contrasting types of bladed olivine in ultramafic rocks from Archean of Labrador. Canadian Journal of Earth Sciences 13 (3), 442–450.

Compston, W., Kroner, A., 1988. Multiple zircon growth within early Archean tonalitic gneiss from Ancient Gneiss Complex, Swaziland. Earth and Planetary Science Letters 87, 13–28.

Darling, J. R., Moser, D. E., Heaman, L. M., Davis, W. J., O'Neil, J., Carlson, R., 2013. Eoarchean to neoarchean evolution of the Nuvvuagittuq Supracrustal belt: New insights from U-Pb zircon geochronology. American Journal of Science 313 (9), 844–876.

Davies, G. F., 1992. On the emergence of plate tectonics. Geology 21 (6), 576.

Dostal, J., Mueller, W. U., 2013. Deciphering an Archean mantle plume: Abitibi greenstone belt, Canada. Gondwana Research 23 (2), 493–505.

Ewart, A., Bryan, W., Gill, J., 1973. Mineralogy and Geochemistry of the Younger Volcanic Island of Tonga S.W. Pacific. Journal of Petrology 14 (3F), 429–465.

Furnes, H., Dilek, Y., de Wit, M., feb 2015. Precambrian greenstone sequences represent different ophiolite types. Gondwana Research 27 (2), 649–685.

Furnes, H., Rosing, M., Dilek, Y., de Wit, M., 2009. Isua supracrustal belt (Greenland)-A vestige of a 3.8 Ga suprasubduction zone ophiolite, and the implications for Archean geology. Lithos 113 (1-2), 115–132.

Glikson, A. Y., 1977. On the Origin of Early Archaean Gneisses. Contributions to Mineralogy and Petrology 62, 171–178.

Hart, S. R., Zindler, A., 1986. In search of a bulk-Earth composition. Chemical Geology 57 (3-4), 247–267.

Herzberg, C. T., aug 2004. Geodynamic Information in Peridotite Petrology. Journal of Petrology 45 (12), 2507–2530.

Hurst, R. W., Bridgwater, D., Collerson, K. D., Wetherill, G. W., 1975. 3600-m,y, Rb-Sr ages from very early Archean gneisses from Saglek Bay, Labrador. Earth and Planetary Science Letters 27, 393–403.

Ishikawa, A., Suzuki, K., Collerson, K. D., Liu, J., Pearson, D. G., Komiya, T., 2017. Rhenium-osmium isotopes and highly siderophile elements in ultramafic rocks from the Eoarchean Saglek Block, northern Labrador, Canada: implications for Archean mantle evolution. Geochimica et Cosmochimica Acta 216, 286–311.

Jagoutz, E., Palme, H., Badenhausen, H., Blum, K., Cendales, M., Dreibus, G., Spettel, G., Lorenz, V., Wanke, H., 1979. Thje abundances of major, minor and trace elements in the Earth's mantle as derived from primitive ultramafic nodules. In: 10th Lunar Planet, Sci. Conf. pp. 2031–2050.

Johnson, T., Brown, M., Gardiner, N., Kirkland, C., Smithies, R., 2017. Earth's first stable continents did not form by subduction. Nature 543, 239–242.

Kimura, G., Ludden, J., Desrochers, J.-P., Hori, R., 1993. A model of ocean-crust accretion for the Superior Province, Canada. Lithos 30, 337–355.

Komiya, T., Yamamoto, S., Aoki, S., Koshida, K., Shimojo, M., Sawaki, Y., Aoki, K., Sakata, S., Yokoyama, T. D., Maki, K., Ishikawa, A., Hirata, T., Collerson, K. D., 2017. A prolonged granitoid formation in Saglek Block, Labrador: Zonal growth and crustal reworking of continental crust in the Eoarchean. Geoscience Frontiers 8 (2), 355–385.

Komiya, T., Yamamoto, S., Aoki, S., Sawaki, Y., Ishikawa, A., Tashiro, T., Koshida, K., Shimojo, M., Aoki, K., Collerson, K. D., nov 2015. Geology of the Eoarchean, > 3.95 Ga, Nulliak supracrustal rocks in the Saglek Block, northern Labrador, Canada: The oldest geological evidence for plate tectonics. Tectonophysics 662, 40–66.

Krogh, T., Kamo, S., 2006. Precise U-Pb zircon ID-TIMS ages provide an alternative interpretation to the early ion microprobe ages and new insights into Archean crustal processes, northern Labrador. In: Reimold, W., Gibson, R. (Eds.), Processes on the Early Earth. Geological Society of America, pp. 91–103.

Kröner, A., 2007. The Ancient Gneiss Complex of Swaziland and Environs: Record of Early Archean Crustal Evolution in Southern Africa. Earth's Oldest Rocks, 465–480.

Kusiak, M. A., Dunkley, D. J., Whitehouse, M. J., Wilde, S. A., Sałacińska, A., Konečný, P., Szopa, K., Gawęda, A., Chew, D., 2018. Peak to post-peak thermal history of the Saglek Block of Labrador: A multiphase and multi-instrumental approach to geochronology. Chemical Geology 484 (May), 210–223.

Kusiak, M. A., Whitehouse, M. J., Wilde, S. A., Dunkley, D. J., Menneken, M., Nemchin, A. A., Clark, C., 2014. Changes in zircon chemistry during Archean UHT metamorphism in the Napier Complex, Antarctica. American Journal of Science 313 (9), 933–967.

Laurent, O., Doucelance, R., Martin, H., Moyen, J. F., 2013. Differentiation of the late-Archaean sanukitoid series and some implications for crustal growth: Insights from geochemical modelling on the Bulai pluton, Central Limpopo Belt, South Africa. Precambrian Research 227, 186–203.

Le Maître, R. W., 2002. Igneous Rocks: A Classification and Glossary of Terms, 2nd Edition. New York: Cambridge University Press.

Liu, J., Touboul, M., Ishikawa, A., Walker, R. J., Graham Pearson, D., 2016. Widespread tungsten isotope anomalies and W mobility in crustal and mantle rocks

of the Eoarchean Saglek Block, northern Labrador, Canada: Implications for early Earth processes and W recycling. Earth and Planetary Science Letters 448, 13–23.

Martin, H., Moyen, J. F., Guitreau, M., Blichert-Toft, J., Le Pennec, J. L., 2014. Why Archaean TTG cannot be generated by MORB melting in subduction zones. Lithos 198-199 (1), 1–13.

McDonough, W. F., Sun, S. S., 1995. The composition of the Earth. Chemical Geology 120, 223–253.

Morino, P., Caro, G., Reisberg, L., 2018. Differentiation mechanisms of the early Hadean mantle: Insights from combined176Hf-142,143Nd signatures of Archean rocks from the Saglek Block. Geochimica et Cosmochimica Acta 240, 43–63.

Morino, P., Caro, G., Reisberg, L., Schumacher, A., 2017. Chemical stratification in the post-magma ocean Earth inferred from coupled 146,147Sm142,143Nd systematics in ultramafic rocks of the Saglek block (3.253.9 Ga; northern Labrador, Canada). Earth and Planetary Science Letters 463, 136–150.

Moyen, J., Laurent, O., 2018. Archaean tectonic systems: A view from igneous rocks. Lithos 302-303, 99–125.

Nair, R., Chacko, T., 2008. Role of oceanic plateaus in the initiation of subduction and origin of continental crust. Geology 36 (7), 583–586.

Nozaka, T., 2003. Compositional heterogeneity of olivine in thermally metamorphosed serpentinite from Southwest Japan. American Mineralogist 88 (8-9), 1377–1384.

Nutman, A. P., Bennett, V. C., Friend, C. R. L., Hidaka, H., Yi, K., Lee, S. R., Kamiichi, T., 2013. The Itsaq Gneiss Complex of Greenland: Episodic 3900 to 3660 Ma juvenile crust formation and recycling in the 3660 to 3600 Ma Isukasian orogeny. American Journal of Science 313 (9), 877–911.

Nutman, A. P., Collerson, K. D., 1991. Very early Archean crustal-accretion complexes preserved in the North Atlantic craton. Geology 19, 791–794.

Nutman, A. P., Friend, C. R. L., 2009. New 1:20,000 scale geological maps, synthesis and history of investigation of the Isua supracrustal belt and adjacent orthogneisses, southern West Greenland: A glimpse of Eoarchaean crust formation and orogeny. Precambrian Research 172 (3-4), 189–211.

Nutman, A. P., Friend, C. R. L., Paxton, S., 2009. Detrital zircon sedimentary provenance ages for the Eoarchaean Isua supracrustal belt southern West Greenland: Juxtaposition of an imbricated ca. 3700 Ma juvenile arc against an older complex with 3920-3760 Ma components. Precambrian Research 172 (3-4), 212–233.

Nutman, A. P., Fryer, B. J., Bridgwater, D., 1989. The early Archaean Nulliak (supracrustal) assemblage, northern Labrador. Can. J. Earth Sci. 26, 2159–2168.

Nutman, A. P., Kinny, P. D., Compston, W., Williams, I. S., 1991. SHRIMP U-Pb zircon geochronology of the Narryer Gneiss Complex, Western Australia. Precambrian Research 52, 275–300.

Nutman, A. P., McGregor, V. R., Friend, C. R., Bennett, V. C., Kinny, P. D., may 1996. The Itsaq Gneiss Complex of southern West Greenland; the world's most extensive record of early crustal evolution (3900-3600 Ma). Precambrian Research 78 (1-3), 1–39.

O'Neil, J., Carlson, R., Papineau, D., Levine, Y., Francis, D., 2019. The Nuvvuagittuq greenstone belt: A glimpse of Earth's earliest crust. In: Van Kranendonk, M. J., Bennett, V. C., Hoffmann, J. E. (Eds.), Earth's Oldest Rocks, 2nd Edition. Elsevier, Ch. 16, pp. 349–374.

O'Neil, J., Carlson, R. W., Francis, D., Stevenson, R. K., 2008. Neodymium-142 evidence for hadean mafic crust. Science 321 (5897), 1828–1831.

O'Neil, J., Carlson, R. W., Paquette, J. L., Francis, D., 2012. Formation age and metamorphic history of the Nuvvuagittuq Greenstone Belt. Precambrian Research 220-221, 23–44.

O'Neil, J., Francis, D., Carlson, R. W., 2011. Implications of the Nuvvuagittuq Greenstone Belt for the Formation of Earth's Early Crust. Journal of Petrology 52 (5), 985–1009.

O'Neil, J., Maurice, C., Stevenson, R. K., Larocque, J., Cloquet, C., David, J., Francis, D., 2007. Chapter 3.4 The Geology of the 3.8 Ga Nuvvuagittuq (Porpoise Cove) Greenstone Belt, Northeastern Superior Province, Canada. Developments in Precambrian Geology 15 (07), 219–250.

O'Neil, J., Rizo, H., Boyet, M., Carlson, R. W., Rosing, M. T., 2016. Geochemistry and Nd isotopic characteristics of Earth's Hadean mantle and primitive crust. Earth and Planetary Science Letters 442, 194–205.

Pearce, J. A., jan 2008. Geochemical fingerprinting of oceanic basalts with applications to ophiolite classification and the search for Archean oceanic crust. Lithos 100 (1-4), 14–48.

Polat, A., 2012. Growth of Archean continental crust in island arcs. Geology 40 (4), 383–384.

Polat, A., Appel, P. W. U., Fryer, B. J., 2011. An overview of the geochemistry of Eoarchean to Mesoarchean ultramafic to mafic volcanic rocks, SW Greenland: Implications for mantle depletion and petrogenetic processes at subduction zones in the early Earth. Gondwana Research 20 (2-3), 255–283.

Polat, A., Hofmann, A. W., Rosing, M. T., 2002. Boninite-like volcanic rocks in the 3.7-3.8 Ga isua greenstone belt, West Greenland: Geochemical evidence for intra-oceanic subduction zone processes in the early earth. Chemical Geology 184 (3-4), 231–254.

Regelous, M., Collerson, K. D., 1996. 147Sm-143Nd, 146Sm-142Nd systematics of early Archaean rocks and implications for crust-mantle evolution. Geochimica et Cosmochimica Acta 60 (18), 3513–3520.

Reimink, J. R., Chacko, T., Stern, R. A., Heaman, L. M., aug 2016. The birth of a cratonic nucleus: Lithogeochemical evolution of the 4.02-2.94 Ga Acasta Gneiss Complex. Precambrian Research 281, 453–472.

Roeder, P. L., Emsile, R. F., 1970. Olivine-liquid equilibrium. Contrib. Mineral. Petrol. 29, 275–289.

Ryan, B., Martineau, Y., 2012. Revised and coloured edition of 1992 map showing the Geology of the Saglek Fiord - Hebron Fiord area, Labrador (NTS 14L/2,3,6,7). Scale: 1:100 000. Government of Newfoundland and Labrador, Department of Natural Resources, Geological Survey, Map 2012-15, Open File 14L/0091.

Ryan, B. A., 1977. Progressive structural reworking of the Uivak Gneisses, Jerusalem Harbour, Northern Labrador. Ph.D. thesis, Department of Geology Memorial University of Newfoundland.

Sałacińska, A., Kusiak, M. A., Whitehouse, M. J., Dunkley, D. J., Wilde, S. A., Kielman, R., 2018. Complexity of the early Archean Uivak Gneiss: Insights from Tigigakyuk Inlet, Saglek Block, Labrador, Canada and possible correlations with south West Greenland. Precambrian Research 315 (October 2017), 103–119.

Schiøtte, L., Bridgwater, D., Collerson, K. D., Nutman, A. P., Ryan, A. B., 1986. Chemical and isotopic effects of Late Archean high-grade metamorphism and granite injection on early Archean gneisses, Saglek-Hebron, northern Labrador. In: J.B. Dawson, D.A. Carswell, J. Hale, K. W. (Ed.), The nature of the lower continental cruste. Geol. Soc. Lond. Spec. Publ., pp. 261–273.

Schiøtte, L., Compston, W., Bridgwater, D., 1989a. Ion probe UThPb zircon dating of polymetamorphic orthogneisses from northern Labrador, Canada. Canadian Journal of Earth Sciences 26 (8), 1533–1556.

Schiøtte, L., Compston, W., Bridgwater, D., 1989b. U-Th-Pb ages of single zircons in Archaean supracrustals from Nain Province, Labrador, Canada. Can. J. Earth Sci. 26, 2636–2644.

Schiøtte, L., Nutman, A. P., Bridgwater, D., 1992. U-Pb ages of single zircons within Upernavik metasedimentary rocks and regional implications for the tectonic evolution of the Archaean Nain Province, Labrador. Can. J. Earth Sci. 29, 260–276.

Shimojo, M., Yamamoto, S., Sakata, S., Yokoyama, T. D., Maki, K., Sawaki, Y., Ishikawa, A., Aoki, K., Aoki, S., Koshida, K., Tashiro, T., Hirata, T., Collerson, K. D., Komiya, T., 2016. Occurrence and geochronology of the Eoarchean, ˜3.9Ga, Iqaluk Gneiss in the Saglek Block, northern Labrador, Canada: Evidence for the oldest supracrustal rocks in the world. Precambrian Research 278, 218–243.

Smithies, R. H., Champion, D. C., 2000. The Archaean High-Mg Diorite Suite: Links to TonaliteTrondhjemiteGranodiorite Magmatism and Implications for Early Archaean Crustal Growth. Journal of Petrology 41 (12), 1653–1671.

Song, B., Nutman, A. P., Liu, D., Wu, J., 1996. 3800 to 2500 Ma crustal evolution in the Anshan area of Liaoning Province, northeastern China. Precambrian Research 78 (1-3), 79–94.

Stern, R. J., 2007. When and how did plate tectonics begin? Theoretical and empirical considerations. Chinese Science Bulletin 52 (5), 578–591.

Toplis, M. J., 2005. The thermodynamics of iron and magnesium partitioning between olivine and liquid: Criteria for assessing and predicting equilibrium in natural and experimental systems. Contributions to Mineralogy and Petrology 149 (1), 22–39.

Turner, S., Rushmer, T., Reagan, M., Moyen, J.-F., feb 2014. Heading down early on? Start of subduction on Earth. Geology 42 (2), 139–142.

Van Hunen, J., Van Keken, P. E., Hynes, A., Davies, G. F., 2008. Tectonics of early Earth: Some geodynamic considerations. In: Special Paper 440: When Did Plate Tectonics Begin on Planet Earth? Geological Society of America, pp. 157–171.

Van Kranendonk, M., 1990. Late Archean geologic history of the Nain Province, North River-Nutak map area, Labrador, and its tectonic significance. Geoscience Canada 17 (4), 231–237.

Van Kranendonk, M. J., dec 2010. Two types of Archean continental crust: Plume and plate tectonics on early Earth. American Journal of Science 310 (10), 1187–1209.

Whitehouse, M. J., Dunkley, D. J., Kusiak, M. A., Wilde, S. A., 2019. On the true antiquity of Eoarchean chemofossils assessing the claim for Earth's oldest biogenic graphite in the Saglek Block of Labrador. Precambrian Research.

Wiemer, D., Schrank, C. E., Murphy, D. T., Wenham, L., Allen, C. M., 2018. Earth's oldest stable crust in the Pilbara Craton formed by cyclic gravitational overturns. Nature Geoscience 11 (5), 357–361.

Wilde, S. A., Spaggiari, C., jan 2007. Chapter 3.6 The Narryer Terrane, Western Australia: A Review. In: Earth's Oldest Rocks. Vol. 15. Elsevier, pp. 275–304.

Wilde, S. a., Valley, J. W., Peck, W. H., Graham, C. M., 2001. Evidence from detrital zircons for the existence of continental crust and oceans on the Earth 4.4 Gyr ago. Nature 409 (6817), 175–178.

Wu, F. Y., Zhang, Y. B., Yang, J. H., Xie, L. W., Yang, Y. H., 2008. Zircon U-Pb and Hf isotopic constraints on the Early Archean crustal evolution in Anshan of the North China Craton. Precambrian Research 167 (3-4), 339–362.

Chapter 2

Petrogeochemistry, Geochronology and crustal evolution of the Saglek-Hebron Complex (Northern Labrador)

Chapter 2 presents a detailed study of the petrology and geochemistry of the felsic rocks in the SHC, which constitutes most of the complex. It comprises an extensive geochronology study to constrain the timing of formation of the different intrusions over the whole complex, including a large dataset of in-situ U-Pb geochronology on zircon. In light of the geochemical compositions and geochronology of the various granitoid units, this chapter also provides new insights on the SHC crustal evolution with in-situ Hf isotopic compositions of granitoids over 1 billion years of early Earth's history.

Keywords: *Saglek-Hebron Complex, Petrogeochemistry, Zircon U-Pb geochronolgy, Lu-Hf isotopes, Archean, subcretion*

2.1 Introduction

The oldest preserved terrestrial materials on Earth are the Jack Hills detrital zircons, as old as 4380 Ma, found in Western Australia (Wilde et al., 2001). The trace element compositions in these Hadean zircons have been used to suggest that they crystallized in evolved melts and that their host rocks were likely metaluminous granitoids (*e.g.* Burnham and Berry, 2017; Trail et al., 2017). Although the extent of the early felsic crust is debated, Archean cratons are mostly composed of silica-rich rocks from the tonalite-trondhjemite-granodiorite (TTG) suites, which abundance appears to significantly decrease after 2500 Ma (Moyen and Martin, 2012; Moyen and Laurent, 2018; Laurent et al., 2014). The geochemical composition of TTG differs from that of the modern continental crust, suggesting they might have formed through distinct processes (*e.g.* Moyen and Martin, 2012).The study of ancient terranes containing TTG, therefore, is crucial to our understanding of how continents formed and stabilized.

The Saglek-Hebron Complex (SHC), located in Northern Labrador, Canada, is a polymetamorphic terrain dominated by TTGs as old as 3900 Ma, and encompassing more than a billion years of geological record (*e.g.* Komiya et al., 2017). With such a protracted geological history, the SHC is one of the best candidates to decipher ancient crustal processes. Previous studies highlighted the existence, in the SHC, of multiple generations of granitoids that exhibit a large variation of chemical compositions and zircon ages (Komiya et al., 2017; Krogh and Kamo, 2006; Sałacińska et al., 2018; Schiøtte et al., 1989b,a; Shimojo et al., 2016; Vezinet et al., 2018).This contribution presents a detailed study of the petrology and geochemistry of the SHC granitoids, along with combined in-situ U-Pb and Lu-Hf isotopic compositions of their zircons. The U-Pb geochronology of zircons is used here to unravel the complex felsic magmatic and metamorphic history of the SHC, while the in-situ zircon Hf isotopic compositions,

combined with the whole-rock geochemical composition of the host rocks, can help to constrain the evolution of the crustal sources involved. Together, these different tools allow us to better understand the timing, the formation and the long-term evolution of the SHC and the Archean sialic crust.

2.2 Geological context

The Saglek-Hebron Complex, located on the east coast of Northern Labrador in Canada, is part of the Archean Nain Province of the North Atlantic Craton. It is dominated by granitoids from the TTG series along with granitic rocks and includes meter to kilometer scale supracrustal enclaves (Fig. 2.1). Supracrustal rocks mainly include mantle-derived rocks (mafic metavolcanic and ultramafic rocks), and chemical or detrital metasediments (Baadsgaard et al., 1979; Bridgwater et al., 1975; Komiya et al., 2015; Nutman and Collerson, 1991). The metavolcanic rocks are divided into two distinct units, the Upernavik supracrustal assemblage interpreted to be Mesoarchean and the Nulliak assemblage interpreted to be Eoarchean (Bridgwater and Schiøtte, 1991; Morino et al., 2017, 2018; Nutman et al., 1989; Schiøtte et al., 1992). Both units, however, are compositionally similar and interpreted as a series of tholeiitic basaltic flows displaying some extent of differentiation (Wasilewski et al., 2019). The Saglek-Hebron granitoids are divided into four main units including the Nanok/Iqaluk grey gneisses, the Uivak gneisses, the Lister gneisses, and late granitic intrusions.

The oldest TTG unit in the SHC is the Nanok/Iqaluk grey gneisses dated at ~3900 Ma (Collerson, 1983b; Komiya et al., 2017; Regelous and Collerson, 1996; Shimojo et al., 2016). The Uivak gneisses are the predominant lithology in the SHC, and were originally subdivided into two units based on their age and mineralogical

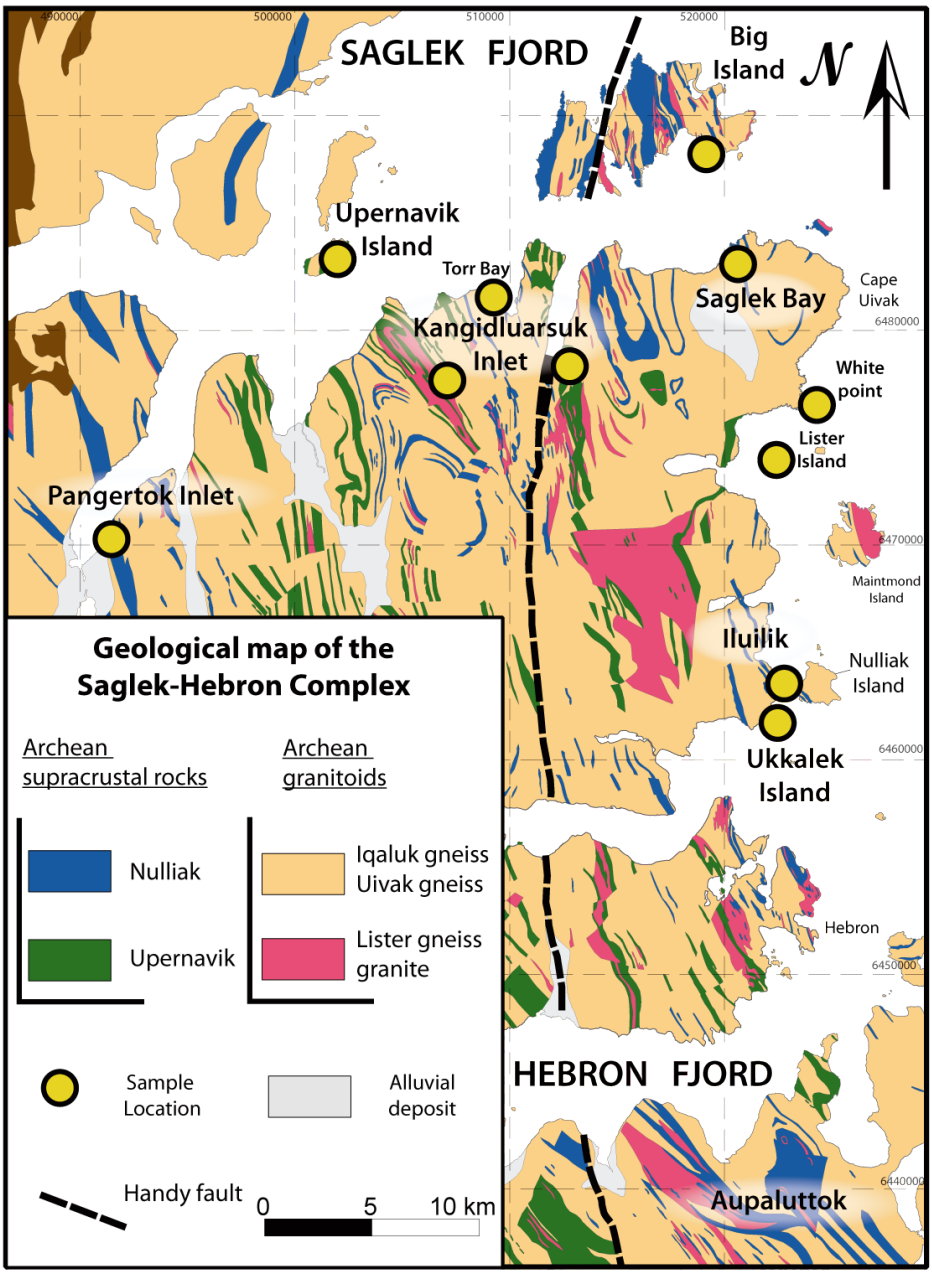

Figure 2.1

Simplified geological map of the Saglek-Hebron Complex (SHC) modified from Ryan and Martineau (2012) and Komiya et al. (2015). Sample locations (yellow circles) show the main localities where multiple samples were collected for this study. Coordinates are in UTM NAD 27 zone 20.

compositions, with the older tonalitic Uivak I dated at 3863 to 3732 Ma (Sałacińska et al., 2018; Schiøtte et al., 1989a; Vezinet et al., 2018) and the younger granodioritic Uivak II interpreted to be 3600 Ma (Hurst et al., 1975; Komiya et al., 2017; Sałacińska et al., 2018). A recent geochronology study, however, argued that the Uivak gneisses rather include five units produced throughout the Eoarchean, from 3890 to 3610 Ma, and thus from almost continuous protracted magmatism, occurring over more than 250 million years (Komiya et al., 2017). Based on structural and stratigraphic observations, Komiya et al. (2015) suggested that the Uivak and the Nanok/Iqaluk gneisses were formed within a subduction-like tectonic setting in the Eoarchean. The younger granitoids include Paleoarchean TTG called the Lister gneisses consisting of granodioritic intrusions emplaced between 3240 and 3350 Ma (Komiya et al., 2017; Schiøtte et al., 1989a) and Neoarchean granitic rocks intruding the SHC with a magmatic peak at ∼2766 Ma (Collerson, 1983a,b; Schiøtte et al., 1989a).

The SHC recorded at least two major protracted thermal episodes leading to some extent of crustal reworking around ∼3620 Ma and high-grade metamorphism up to granulite facies around ∼2760-2600 Ma (Bridgwater and Collerson, 1976; Hurst et al., 1975; Kusiak et al., 2018; Nutman and Collerson, 1991; Sałacińska et al., 2018; Schiøtte et al., 1992, 1986; Van Kranendonk, 1990) Based on detrital zircons, it has also been suggested that the Neoarchean thermal event could have been caused by a massive collision and terrain accretion after the emplacement of the ∼3300 Ma Upernavik metasedimentary assemblage (Schiøtte et al., 1992). Recent thermochronology studies on monazite and apatites suggest two other thermal closure ages at 2500 and 2200 Ma, interpreted either as cooling ages, or as two separate successive thermal events reaching upper amphibolite and greenschist facies metamorphic conditions (Kusiak et al., 2018).

Table 2.1

Major (wt. %) and trace (ppm) element analysis for the SHC granitoids (anhydrous composition). GPS coordinates are in UTM NAD 27 zone 20. Major element compositions are recalculated as anhydrous compositions.

	Trondhjemite							
Sample	SG-003	SG-019	SG-024	SG-025	SG-122	SG-247	SG-266	SG-267
Easting	513393	522590	522423	522390	513518	518854	522596	522648
Northing	6440860	6461143	6460895	6460922	6482946	6488100	6474066	6474107
SiO_2	71.35	76.76	67.26	74.13	70.94	65.23	68.68	70.87
Al_2O_3	16.20	14.45	18.75	15.25	16.83	17.99	17.09	16.04
FeO_t	1.86	0.19	1.41	1.01	1.17	2.57	2.54	2.21
MnO	0.03	0.01	0.02	0.01	0.02	0.04	0.03	0.04
MgO	0.95	0.20	0.51	0.34	0.59	1.76	1.20	0.86
CaO	3.52	3.48	3.16	3.08	3.22	1.98	3.67	3.08
Na_2O	5.01	4.18	5.00	4.73	5.21	5.37	5.02	5.20
K_2O	0.76	0.73	3.58	1.30	1.84	4.48	1.46	1.44
TiO_2	0.23	0.01	0.28	0.12	0.13	0.50	0.30	0.26
P_2O_5	0.09	-	0.03	0.02	0.05	0.09	0.03	-
LOI	0.55	0.37	0.91	0.70	0.70	0.78	1.02	0.78
Sc	2	-	-	-	1	-	-	-
V	26	-	17	11	10	28	29	27
Cr	30	-	20	-	-	-	-	-
Co	6	-	4	2	2	7	7	6
Ni	30	-	-	-	-	-	-	-
Zn	40	-	-	30	40	50	40	50
Ga	20	15	24	18	22	20	20	20
Ge	0.8	0.8	0.8	0.9	1.0	0.8	0.8	0.9
Rb	17	9	92	33	67	151	95	107
Sr	514	366	676	400	390	461	387	308
Y	1.6	-	0.6	0.8	1.2	4.1	2.5	3.8
Zr	124	128	173	59	58	191	107	89
Nb	0.3	-	2.3	0.8	2.8	1.0	2.0	2.7
Ba	247	157	1065	319	304	348	397	400
La	20.90	4.97	17.00	9.82	7.92	22.00	18.80	19.10
Ce	33.00	6.67	26.20	15.90	12.80	44.30	33.30	32.20
Pr	3.17	0.56	2.35	1.47	1.41	4.81	3.49	3.49
Nd	11.10	1.49	6.83	4.67	5.03	16.80	12.10	11.30
Sm	1.38	0.15	0.65	0.59	0.85	2.60	1.80	1.87
Eu	0.73	0.74	0.94	0.77	0.39	0.77	0.53	0.46
Gd	0.80	0.09	0.32	0.36	0.58	1.38	1.06	1.26
Tb	0.08	-	0.03	0.04	0.06	0.16	0.11	0.17
Dy	0.32	0.04	0.12	0.14	0.24	0.85	0.51	0.80
Ho	0.05	0.01	0.02	0.02	0.04	0.14	0.08	0.13
Er	0.15	0.04	0.07	0.07	0.09	0.38	0.23	0.30
Tm	0.02	0.01	0.01	0.01	0.01	0.05	0.03	0.04
Yb	0.14	0.07	0.08	0.06	0.08	0.36	0.17	0.20
Lu	0.03	0.02	0.02	0.01	0.01	0.05	0.02	0.03
Hf	2.80	3.10	5.00	1.30	1.60	4.10	2.70	2.00
Ta	0.04	0.03	0.05	0.06	0.31	0.06	0.16	0.48
Pb	7.0	11.0	17.0	13.0	20.0	13.0	10.0	15.0
Th	0.12	0.07	0.74	0.14	3.78	2.20	2.94	5.77
U	0.10	0.70	0.24	0.10	0.57	0.32	0.32	0.29

Continued on next page

	Trondhjemite		Mg-tonalite					
Sample	SG-272	SG-273	SG-016	SG-026	SG-027	SG-210C	SG-245	SG-252
Easting	523306	523165	522798	522479	522296	512166	509971	518849
Northing	6476392	6476456	6461208	6461234	6461349	6478307	6480682	6487972
SiO_2	68.60	72.13	63.92	66.98	59.76	67.94	64.18	61.35
Al_2O_3	16.45	13.85	16.76	15.54	17.12	16.29	16.47	17.54
FeO_t	3.01	4.10	5.46	3.73	4.90	3.97	4.42	6.26
MnO	0.06	0.06	0.22	0.07	0.09	0.07	0.09	0.06
MgO	1.25	0.76	1.69	2.53	3.99	1.45	2.92	2.18
CaO	3.60	2.31	5.16	4.04	6.60	3.48	5.02	4.06
Na_2O	5.16	4.31	4.23	4.29	4.76	4.50	4.88	4.53
K_2O	1.49	1.86	1.55	2.17	2.04	1.71	1.44	2.48
TiO_2	0.35	0.56	0.76	0.47	0.58	0.50	0.46	1.12
P_2O_5	0.02	0.06	0.25	0.18	0.15	0.08	0.12	0.43
LOI	0.57	0.68	0.67	0.65	0.74	1.63	0.79	1.26
Sc	-	-	13	8	11	-	-	-
V	42	19	121	62	99	47	91	77
Cr	30	-	190	90	100	-	60	30
Co	7	6	9	13	18	9	15	19
Ni	-	-	40	60	80	-	40	-
Zn	60	60	50	80	110	50	70	80
Ga	23	23	23	20	22	24	21	23
Ge	0.9	1.5	0.8	1.0	1.0	1.0	0.8	0.8
Rb	88	99	78	93	80	105	33	123
Sr	424	188	427	508	381	252	695	584
Y	8.2	10.1	14.4	8.7	10.6	7.3	8.4	9.9
Zr	119	250	174	168	104	156	130	299
Nb	1.8	7.0	3.3	2.0	2.8	4.5	1.8	4.5
Ba	226	409	398	569	269	213	423	827
La	5.97	11.60	36.00	32.70	18.70	17.80	30.80	100.00
Ce	22.00	49.00	79.40	65.90	41.30	41.60	59.80	199.00
Pr	2.04	3.08	10.10	7.81	5.52	4.33	6.90	21.90
Nd	8.67	11.10	41.00	30.30	23.00	15.90	25.30	74.40
Sm	2.19	2.48	8.00	5.33	4.64	3.02	4.13	9.70
Eu	0.74	0.70	1.97	1.24	1.08	0.65	1.07	1.64
Gd	1.83	1.87	5.18	3.32	3.39	2.21	2.43	4.91
Tb	0.28	0.34	0.65	0.40	0.42	0.30	0.31	0.51
Dy	1.58	1.99	3.24	1.97	2.26	1.55	1.56	2.11
Ho	0.28	0.36	0.53	0.33	0.40	0.27	0.27	0.35
Er	0.77	0.99	1.40	0.80	1.15	0.72	0.69	0.83
Tm	0.11	0.14	0.18	0.10	0.16	0.09	0.09	0.10
Yb	0.66	0.88	1.16	0.63	0.93	0.54	0.53	0.54
Lu	0.10	0.12	0.19	0.10	0.16	0.08	0.08	0.07
Hf	3.10	6.70	3.90	3.50	2.80	4.30	3.10	5.60
Ta	0.15	0.59	0.24	0.10	0.13	0.31	0.05	0.20
Pb	11.0	20.0	13.0	11.0	9.0	16.0	8.0	6.0
Th	2.07	10.80	5.55	3.93	0.78	3.82	1.37	7.13
U	0.23	0.61	0.93	0.10	0.15	0.47	0.09	0.66

Continued on next page

	Mg-tonalite		Granodiorite		Granite			
Sample	SG-265	SG-290	SG-203	SG-204	SG-007	SG-017	SG-037	SG-080
Easting	522500	498263	522581	522609	522731	-	491059	513607
Northing	6474060	6478780	6463604	6463614	6461538	-	6470294	6477781
SiO_2	60.58	62.46	68.91	69.53	73.04	73.30	74.44	76.16
Al_2O_3	18.90	15.34	13.79	13.89	15.19	14.81	14.02	13.56
FeO_t	5.07	6.43	5.33	5.34	0.89	1.03	1.43	0.69
MnO	0.06	0.11	0.09	0.07	0.01	0.01	0.02	0.01
MgO	2.25	3.86	1.11	1.14	0.68	0.78	0.34	0.19
CaO	5.87	6.04	2.94	2.42	1.17	1.26	1.51	1.23
Na_2O	5.13	3.98	3.31	3.72	3.07	3.00	3.27	3.28
K_2O	1.42	1.26	3.60	2.95	5.79	5.62	4.76	4.77
TiO_2	0.63	0.41	0.77	0.80	0.16	0.18	0.15	0.10
P_2O_5	0.09	0.10	0.14	0.14	0.01	0.01	0.05	0.01
LOI	1.82	0.44	1.10	0.58	0.55	0.52	0.52	0.76
Sc	-	-	-	-	-	-	3	-
V	82	91	48	42	9	10	13	6
Cr	30	210	30	-	-	-	30	-
Co	15	25	9	9	3	3	3	-
Ni	-	110	-	-	-	20	-	-
Zn	70	80	110	70	-	-	40	40
Ga	22	20	20	21	13	13	20	16
Ge	0.7	1.2	2.3	1.9	0.6	0.6	1.6	1.1
Rb	75	21	117	173	125	124	230	162
Sr	493	258	262	195	633	621	128	188
Y	7.4	13.2	33.2	25.2	-	-	5.2	0.9
Zr	159	80	324	385	15	17	114	114
Nb	2.7	2.5	6.4	7.9	-	-	3.9	0.7
Ba	314	361	1010	796	3594	3439	659	571
La	7.60	12.30	69.30	41.10	1.46	1.63	23.70	21.10
Ce	18.30	28.80	145.00	113.00	1.53	1.82	46.60	36.20
Pr	2.54	3.84	16.40	11.10	0.13	0.13	4.46	3.60
Nd	11.10	16.70	57.80	43.00	0.21	0.37	14.90	11.30
Sm	2.63	3.98	9.85	7.94	0.03	0.04	2.37	1.51
Eu	0.80	1.02	1.51	1.27	0.51	0.50	0.49	0.53
Gd	2.03	3.15	6.89	5.68	0.02	0.02	1.53	0.70
Tb	0.29	0.44	1.03	0.86	-	-	0.22	0.07
Dy	1.50	2.46	5.83	4.78	0.03	0.03	1.07	0.26
Ho	0.25	0.46	1.09	0.89	-	-	0.19	0.04
Er	0.64	1.28	3.00	2.47	0.04	0.03	0.50	0.11
Tm	0.09	0.18	0.42	0.34	0.01	-	0.07	0.02
Yb	0.50	1.18	2.67	2.07	0.06	0.02	0.41	0.09
Lu	0.07	0.16	0.39	0.30	0.01	-	0.07	0.01
Hf	3.40	2.10	6.80	9.20	0.30	0.40	3.70	2.90
Ta	0.21	0.09	0.66	0.65	0.03	0.04	0.03	0.05
Pb	8.0	5.0	19.0	14.0	26.0	26.0	25.0	24.0
Th	0.98	0.26	7.63	8.84	-	-	11.50	9.01
U	0.65	0.10	0.86	0.65	0.05	0.08	0.66	0.52

Continued on next page

	Granite							
Sample	SG-084	SG-086	SG-087	SG-119	SG-114	SG-127	SG-134	SG-143
Easting	512529	512514	512263	511800	523711	502065	520849	506844
Northing	6478890	6479020	6478863	6479810	6439920	6483594	6483172	6477239
SiO_2	75.08	74.26	73.24	74.46	76.14	75.09	73.67	74.12
Al_2O_3	14.12	14.23	14.66	14.65	13.65	13.81	14.87	14.31
FeO_t	0.99	1.25	1.57	0.37	1.42	1.13	1.33	1.35
MnO	0.02	0.02	0.02	-	0.03	0.03	0.02	0.02
MgO	0.47	0.69	0.55	0.14	0.51	0.17	0.48	0.29
CaO	1.17	1.39	1.48	1.23	4.45	1.43	1.77	1.74
Na_2O	3.67	3.84	3.80	3.57	3.38	3.66	3.95	3.76
K_2O	4.36	4.17	4.33	5.54	0.28	4.57	3.65	4.14
TiO_2	0.10	0.14	0.27	0.02	0.14	0.07	0.21	0.16
P_2O_5	0.02	0.01	0.08	0.01	-	0.02	0.06	0.09
LOI	0.62	0.55	0.64	0.23	0.45	0.62	0.45	0.33
Sc	2	1	2	-	-	2	2	2
V	-	7	18	-	30	6	14	11
Cr	-	-	-	-	40	20	-	-
Co	1	-	2	-	4	1	3	2
Ni	-	-	-	-	-	-	-	-
Zn	40	40	40	-	30	30	40	50
Ga	20	20	22	-	14	21	20	20
Ge	0.9	1.0	1.1	-	0.8	1.3	1.0	1.2
Rb	155	162	156	-	6	163	122	169
Sr	202	201	359	-	208	120	388	181
Y	4.5	2.7	3.5	-	2.2	5.0	1.7	6.2
Zr	65	96	199	-	6	74	105	134
Nb	2.8	3.3	3.6	-	0.7	3.1	1.3	2.8
Ba	383	340	1632	-	165	595	402	811
La	12.60	20.40	89.60	-	4.10	22.80	21.40	27.30
Ce	22.00	37.10	165.00	-	7.08	41.50	52.10	51.50
Pr	2.34	3.85	15.70	-	0.75	4.39	3.55	5.60
Nd	8.14	12.90	47.50	-	2.87	14.90	11.80	19.30
Sm	1.39	2.23	5.00	-	0.60	2.50	1.61	3.17
Eu	0.40	0.48	0.91	-	0.60	0.40	0.59	0.67
Gd	1.07	1.23	1.96	-	0.60	1.85	0.95	2.30
Tb	0.14	0.13	0.20	-	0.08	0.21	0.09	0.29
Dy	0.78	0.57	0.87	-	0.45	0.98	0.40	1.30
Ho	0.14	0.10	0.13	-	0.08	0.18	0.06	0.24
Er	0.41	0.24	0.29	-	0.19	0.52	0.15	0.60
Tm	0.06	0.03	0.03	-	0.02	0.07	0.02	0.08
Yb	0.42	0.19	0.20	-	0.12	0.44	0.12	0.44
Lu	0.08	0.03	0.03	-	0.01	0.07	0.02	0.07
Hf	2.00	2.60	4.30	-	0.20	2.90	2.50	3.50
Ta	0.11	0.38	0.13	-	0.20	0.08	0.09	0.14
Pb	32.0	31.0	26.0	-	10.0	31.0	26.0	22.0
Th	4.08	4.83	18.40	-	0.18	18.90	7.78	9.43
U	0.69	0.79	0.69	-	0.07	1.86	1.73	0.55

Continued on next page

	Granite								
Sample	SG-144	SG-208	SG-209	SG-227	SG-233	SG-259	SG-260	SG-270	SG-271
Easting	509672	522737	522857	523506	523768	520487	520533	523284	523296
Northing	6477557	6463758	6463475	6462811	6462848	6488574	6488593	6476383	6476389
SiO_2	76.01	75.00	74.04	71.06	77.53	72.76	74.22	72.40	72.60
Al_2O_3	13.82	13.03	13.22	12.85	11.80	15.03	14.25	14.33	14.43
FeO_t	0.88	2.02	2.59	3.40	1.60	1.83	1.09	2.37	2.35
MnO	0.01	0.03	0.04	0.10	0.02	0.03	0.02	0.02	0.02
MgO	0.32	0.44	0.63	1.83	0.50	0.54	0.33	0.43	0.47
CaO	2.06	0.93	1.19	2.28	0.51	1.63	1.22	0.97	0.80
Na_2O	3.62	3.02	3.47	2.47	2.59	4.37	3.82	3.14	3.06
K_2O	3.15	5.28	4.47	5.64	5.29	3.55	4.91	6.10	6.03
TiO_2	0.12	0.24	0.35	0.35	0.17	0.26	0.14	0.24	0.24
P_2O_5	0.02	-	-	-	-	-	-	-	-
LOI	0.56	0.69	0.61	0.68	0.40	0.62	0.88	0.64	0.48
Sc	-	-	-	-	-	-	-	-	-
V	8	11	17	46	-	17	6	9	11
Cr	-	-	-	40	-	-	-	-	-
Co	2	3	4	10	2	3	2	3	3
Ni	-	-	-	20	-	-	-	-	-
Zn	30	-	40	90	-	40	-	40	40
Ga	15	19	19	17	18	25	22	19	19
Ge	1.0	2.2	1.9	1.5	2.0	1.1	1.0	1.0	1.0
Rb	64	269	199	377	194	119	120	184	193
Sr	318	94	115	40	86	335	322	201	214
Y	-	20.4	14.9	18.5	8.5	11.4	6.1	4.6	4.8
Zr	112	153	218	136	152	124	79	259	255
Nb	0.5	4.5	4.8	3.9	4.2	3.8	2.0	1.9	1.7
Ba	980	437	545	386	304	308	397	1330	1480
La	19.80	63.20	64.00	42.40	26.60	58.10	19.30	152.00	170.00
Ce	30.10	125.00	128.00	81.90	70.90	73.70	44.50	273.00	298.00
Pr	2.95	12.60	13.60	8.64	5.97	13.80	5.21	25.20	27.70
Nd	9.11	39.80	45.60	28.60	19.40	50.70	19.50	73.50	79.40
Sm	0.99	5.74	6.83	4.54	3.32	8.31	3.80	7.69	8.23
Eu	0.66	0.57	0.78	0.73	0.47	1.37	0.92	0.96	1.03
Gd	0.36	3.60	3.92	3.22	2.31	5.19	2.33	2.97	3.17
Tb	0.02	0.56	0.56	0.51	0.32	0.62	0.29	0.27	0.27
Dy	0.07	3.18	2.80	3.01	1.74	2.74	1.34	1.12	1.17
Ho	0.02	0.65	0.49	0.59	0.31	0.40	0.21	0.17	0.18
Er	0.05	1.94	1.38	1.75	0.81	0.96	0.50	0.41	0.43
Tm	0.01	0.30	0.20	0.26	0.11	0.12	0.06	0.06	0.06
Yb	0.05	1.92	1.20	1.80	0.72	0.64	0.33	0.39	0.40
Lu	0.01	0.27	0.17	0.26	0.12	0.09	0.05	0.06	0.07
Hf	2.90	4.70	6.00	4.20	5.60	3.80	2.60	6.40	6.50
Ta	0.06	0.67	0.65	0.57	0.39	0.39	0.29	0.02	0.02
Pb	14.0	22.0	20.0	31.0	24.0	15.0	16.0	26.0	26.0
Th	3.14	18.70	13.60	9.12	19.60	8.07	5.61	34.20	38.00
U	0.23	0.97	0.93	0.89	0.89	0.49	0.46	0.51	0.55

Continued on next page

2.3 Methods

2.3.1 Whole-rock major and trace element geochemistry

A total of 47 granitoids were sampled from all felsic units described in the literature, including type localities for the Nanok/Iqaluk gneiss described by Shimojo et al. (2016) in the Kangidluarsuk inlet (St John's Harbour), the Uivak II gneiss described by (Bridgwater et al., 1975) on the opposite coast of Nulliak Island and White Point and the Lister gneiss found on Lister Island. Figure 2.1 shows the main sample locations, and GPS coordinates for each of the samples can be found in table 2.1 (Field potographs are available in the supplementaary material annex B.1).

Polished petrographic thin sections (See supplementary material annex B.2) and whole-rock major and trace element analyses were performed for all samples. Weathered surfaces and any secondary veins present were carefully removed prior to crushing. Rock samples were firstly crushed to sub-centimeter size chips with a steel jaw crusher and then reduced to powder using an alumina shatter box. Major elements were analyzed either by inductively coupled plasma mass spectrometer (ICP-MS) by Activation Laboratories or by X-ray fluorescence (XRF) by ACME Analytical Laboratories and at the University of Ottawa X-ray Core Facility. ICP-MS analyses were performed on a Perkin Elmer Sciex ELAN 9000 ICP-MS high-speed quadrupole. Prior to the analysis, samples were fused into a glass disk using a sample: lithium metaborate flux ($LiBO_2$) ratio of 1:5. Three blanks and four georeference materials (two before sample analysis and two after) were analyzed per group of samples. Duplicates were analysed every 15 samples and the instrument was recalibrated every 40 samples. Major element analyses done by XRF by ACME Laboratories were conducted using an AxiosFast X-ray spectrometer. Barium and Cr_2O_3 were also analysed by XRF for these samples (Code: LF700). Samples were

fused using commercial $LiBO_2$ and a sample: flux ratio of 1:5 to produce the glass disks to be analysed. Three blanks, two different standards (OREAS72B and SY-4(D)) as well as three duplicates were run during each analytical session. Details of the analytical procedures can be found on the ACME website at http://acmelab.com/pdfs/FeeSchedule-2015.pdf. XRF analyses performed at the University of Ottawa X-ray Core Facility were done on a Rigaku Supermini200 WDXRF Spectrometer. The glass disks were produced using a flux made in-house (79/21 $Li_2B_4O_7/LiBO_2$) and a sample: flux ratio of 1:7, with the addition of 60-80 mg of LiBr. Reference materials used for felsic sample calibration curves were AMH-1, GSP-2, GS-N, AN-G, SY-3, MA-N, OU-3, BCR-032, PC-1016, GPO-16, GPO-17, and GPO-18. Trace element composition analyses were performed by ICP-MS at the Activation Laboratories. Full analytical techniques and detection limits (Code: research 4B2) are available on the Activation Laboratories website at: http://www.actlabs.com/page.aspx?page=555& app=226& cat1=549& tp=12& lk=no& menu=64.

2.3.2 In-situ U-Pb geochronology and Hf isotopes

A selection of 18 samples was analysed for in-situ U-Pb geochronology and Hf isotopes on zircons. Rock samples were crushed using a steel jaw crusher and disk mill and then sieved to collect grain sizes between 250-106 μm. Heavy minerals, such as zircons and metallic oxides, were separated using a water shaking table and methylene iodide heavy liquid. The heavy mineral fractions were then passed through a magnetic Frantz separator to remove the magnetic minerals. Between 100 and 120 zircons were then handpicked and mounted on an epoxy resin that was then polished.

Cathodoluminescence (CL) images of the polished zircons were taken using the JEOL 6610LV scanning electron microscope (SEM), at the University of Ottawa, to

identify the different zones of the zircons and guide the laser ablation work. Both U-Th-Pb and Hf isotope analyses were performed at the Laboratoire Magmas et Volcans (LMV) in Clermont-Ferrand, France. U-Th-Pb isotope analyses were performed on a Thermo Scientific Element XR inductively coupled plasma mass spectrometer (ICP-MS), and Hf isotope analyses were conducted on a Thermo Scientific Neptune Plus multicollector ICP-MS, both instruments were coupled with a Resonetics M50E 193 nm excimer laser ablation (LA) system. The full analytical method for isotope dating by LA-ICP-MS is described in Paquette and Tiepolo (2007), Hurai et al. (2010) and Paquette et al. (2014) and more details on analytic conditions are available in the Supplementary Item table B.1 (Appendix B). primary and secondary refeference standards have been measured to enshur the quality of the data over the different analytic session and are displayed in the Supplementary material annexes B.2 and B.4. The ablated zircon zones were carefully chosen in order to avoid any mixed zones and Hf isotopic measurements were performed on the same spots than those chosen for the U-Pb analyses. Initial $^{176}Hf/^{177}Hf$ ratios were calculated using the $\lambda^{176}Lu$ decay constant of 1.867×10^{-11} yr^{-1} of Söderlund et al. (2004) and the CHUR parameters of $^{176}Hf/^{177}Hf = 0.282785$ and $^{176}Lu/^{177}Hf = 0.0336$ (Bouvier et al., 2008) were used for calculation of $\varepsilon^{176}Hf$ values. A ratio of $^{176}Lu/^{177}Hf = 0.03915$ was used for the long-term evolution of the depleted mantle, starting with a chondritic $^{176}Hf/^{177}Hf$ composition at 4568 Ma. Detailed results and standard analyses are available in the supplementary material, table B.4 in the Appendix B.

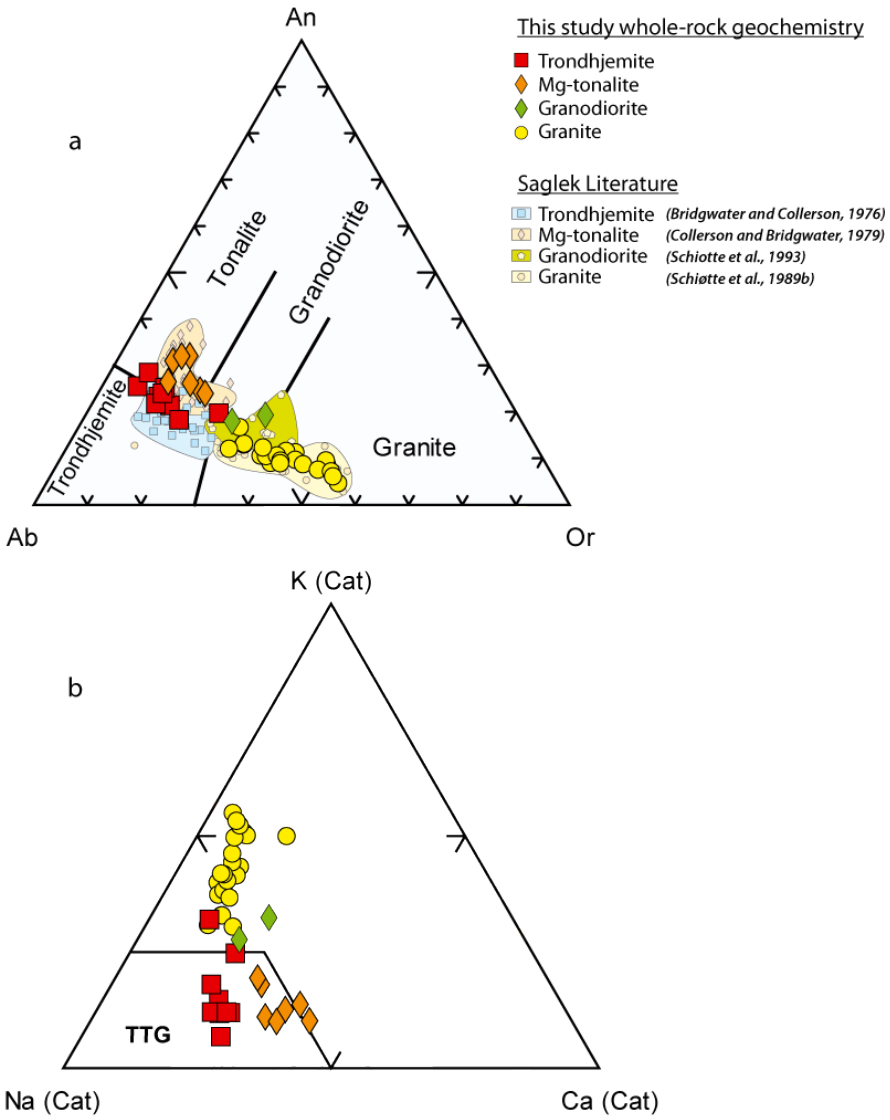

Figure 2.2

a) Ab-An-Or ternary diagram (Barker, 1979) for the SHC granitoids. Shaded fields represent SHC granitoids compositions from the literature (Bridgwater and Collerson, 1976; Collerson and Bridgwater, 1979; Schiøtte et al., 1993, 1989b). b) K-Na-Ca ternary diagram comparing the different TTG to the granites of the SHC. Archean TTG field from Martin et al. (2005).

2.4 Results

2.4.1 Petrography & Geochemistry

Based on observed mineralogy and CIPW normative compositions, the SHC granitoids can be divided into four distinct groups, including trondhjemites, tonalites and granodiorites (grouped as the TTG, *s.l.*) and granites (Fig. 2.2). Only a few samples of granodiorites have been collected for this study, but they are compositionally similar (Fig. 2.2) to other SHC granodiorites previously described (Schiøtte et al., 1993). The TTG, are commonly medium grained and exhibit variable degrees of deformation with local evidence of migmatization. Pegmatitic and porphyritic textures can also occasionally be observed. Trondhjemite samples consist of typical grey gneisses composed of quartz + oligoclase + biotite + titanite ± zircon ± apatite. Compared to the trondhjemites, rocks that exhibit tonalitic to granodioritic compositions are commonly darker and can be described as melanocratic grey gneisses containing higher amounts of titanite and ferromagnesian minerals such as clinopyroxene or biotite. The granodiorites and tonalites locally exhibit augen textures at the outcrop scale (*e.g.* Iluilik & White Point), which is not observed in the trondhjemitic grey gneisses. Granite samples are leucocratic units typically composed of quartz + orthoclase + oligoclase ± biotite ± zircon ± apatite ± garnet. They often occur as migmatitic veins but also as larger plutonic bodies. Grain size in these rocks can vary from coarse grained (which can be pegmatitic within migmatitic veins) to medium-fine grained, more common for the plutonic bodies. Granites usually show little fabric and minor deformation compared to the TTG.

The TTG display a wide range of silica content (56.6 wt. % to 77.4 wt. % SiO_2),

with most samples having below 72 wt. % SiO_2. Except for one sample, the granites show high and uniform silica contents ranging from 73.0 to 76.1 wt. % SiO_2 (Fig. 2.3a). The tonalites have the lowest SiO_2 contents among the TTG and display high Mg concentrations relative to the other SHC granitoids (Fig. 2.3a), and therefore are here referred to as Mg-rich tonalites. The FeOt content correlates with TiO_2 concentration for all granitoids (Fig. 2.3b) and both the Mg-rich tonalites and the granodiorites display relatively high FeOt and TiO_2 contents compared to the granites and the trondhjemites (Fig. 2.3a-b).Compared to all TTG, the granites exhibit higher concentrations in K_2O (from 3 to 6 wt.%; Fig. 2.3c), Rb and lower CaO concentrations (<2 wt. %; Fig. 2.3e).The tonalites and trondhjemites exhibit higher Na2O, CaO, and Al_2O_3 but lower K_2O compared to the granites and granodiorites (Fig. 2.3c-d-e). The Mg-rich tonalites, however, exhibit lower A/CNK ratios relative to the trondhjemites, with the granite showing the highest A/CNK ratios (Fig. 2.3f).

Normalized to the primitive mantle composition, all granitoids exhibit pronounced Nb-Ta negative anomalies (Fig. 2.4a) along with strong depletion in heavy rare earth elements (HREE) compared to light rare earth elements (LREE), typical of Archean granitoids. Mg-rich tonalites and granodiorites exhibit similar rare earth element (REE) profiles (Fig. 2.4b) and are generally characterized by lower $(La/Yb)_N$ ratios than most trondhjemites and granites (Fig. 2.5). The granodiorites exhibit the highest HREE concentrations among all TTG in the SHC and have slight negative Eu anomalies. Contrastingly, the trondhjemites exhibit higher $(La/Yb)_N$ ratios (up to 150) and most samples display positive Eu anomalies (Fig. 2.4a-b; Fig. 2.5). The trondhjemite samples SG-272 and SG-273 collected on White Point, however, display higher HREE contents and thus lower $(La/Yb)_N$ ratios compared to other trondhjemites. Their REE

profiles are more similar to Mg-rich tonalites, although their overall major element composition is more consistent with the trondhjemites (Fig. 2.4). Trondhjemite sample the SG-019 collected on Ukkalek Island exhibits extremely low trace element and REE concentrations and mostly plots outside of the compositional field comprising the other trondhjemite samples (Fig. 2.4). The Lister gneiss (SG-265) is compositionally similar to the Mg-rich tonalites but exhibits the lowest REE concentrations (Fig. 2.4b). Granitic samples exhibit high Rb and Pb with lower Sr concentrations, relative to all other TTG. In general, granites are more enriched in LREE compared to the trondhjemitic rocks with large variability in $(La/Yb)_N$ ratios ranging from 0-300 (Fig. 2.5). The granites also commonly display small positive or negative Eu anomalies (Fig. 2.4b). Granite samples SG-007 and SG-017 exhibit very low REE concentrations with pronounced positive Eu anomalies (Eu_N/Eu^* ~60).

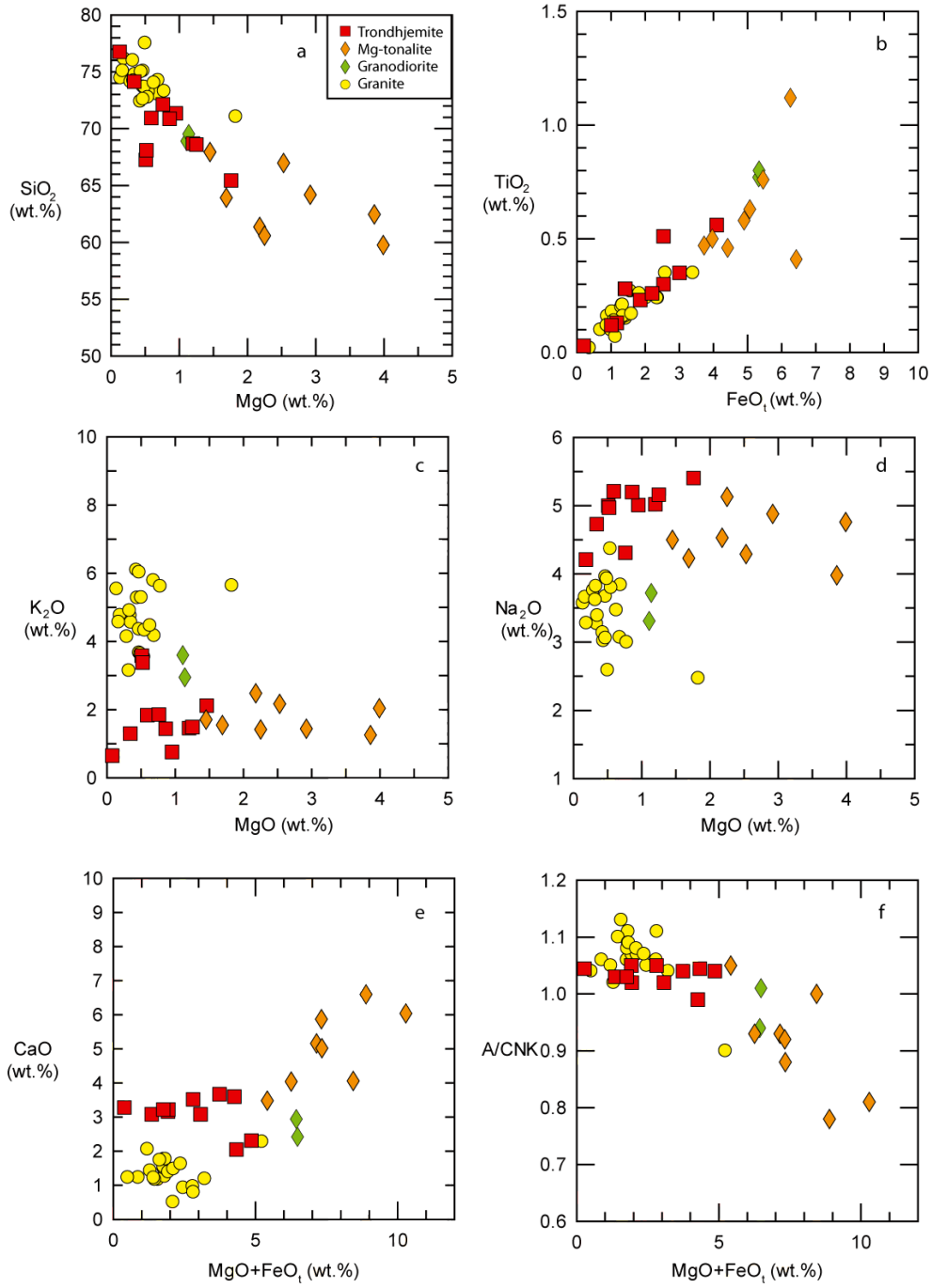

Figure 2.3

Selected major element compositions of the SHC granitoids. a), c) and d) selected elements respectively *vs.* MgO b) TiO_2 *vs.* FeOt e) and f) have MgO + FeOt on their absciss that show covariations with CaO (wt. %) and A/CNK (Relative aluminium concentration in molar unit calculated as followed A/CNK = Al/(2Ca + Na + K). Symbols are as in figure 2.2.

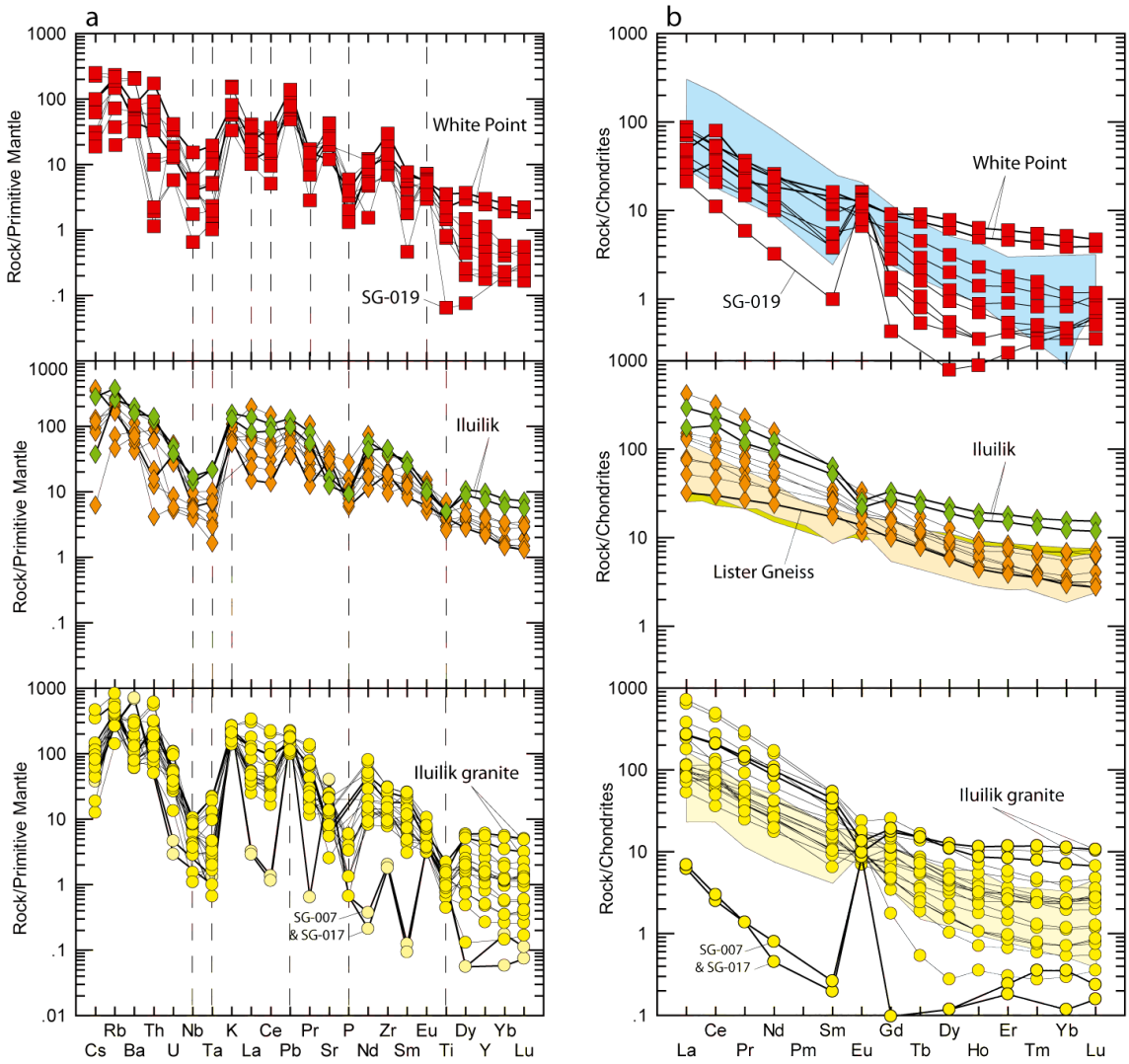

Figure 2.4

a) Trace element spider diagrams normalized to the primitive mantle (Lyubetskaya and Korenaga, 2007), b) Rare earth element compositions normalized to chondrites (McDonough and Sun, 1995).The shaded fields show the data for SHC granitoids from the literature (Bridgwater and Collerson, 1976; Collerson and Bridgwater, 1979; Schiøtte et al., 1993, 1989b). Symbols and colors for fields are as in figure 2.2.

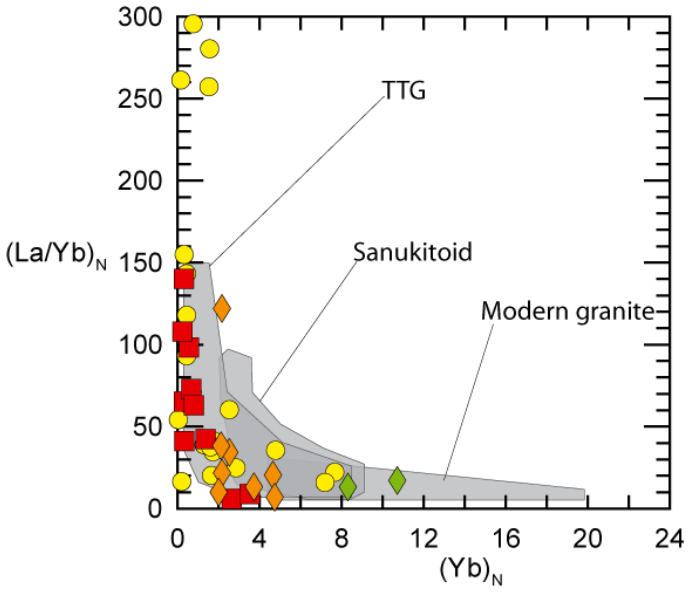

Figure 2.5

$(La/Yb)_N$ *vs.* Yb_N diagram reflecting LREE/HREE ratios of all SHC TTG and granites compared to typical TTG, sanukitoids and modern granites from the literature (Moyen and Martin (2012) and references therein). Normalization values are after Masuda et al. (1973). Symbols are as in figure 2.2.

Table 2.2

Summary of geochronological data and initial Hf isotopic composition in the SHC zircons. Age type = method used to calculate the age. N= number of zircons used in age calculation. Age= interpreted crystallization, inherited or metamorphic age. $\varepsilon^{176}Hf_{(i)}$ are the average initial values of $\varepsilon^{176}Hf$ of all zircons calculated at the crystallization age. Full dataset can be found in the Supplementary Tables B.3: and B.4 in the Appendix B.

Sample #	Lithology	Age type	N	Age ($\pm 2\sigma$ Ma)	Magmatic event	$\varepsilon Hf_{(i)} \pm 2\sigma$
		Crystallization age				
SG-019	Trondhjemite	Weighted mean $^{207}Pb/^{206}Pb$	12	2732 ± 25	Late granites	-11.3 ± 0.2
SG-024	Trondhjemite	Mean concordia age	2	3869 ± 10	Iqaluk	2.4 ± 0.3
SG-025	Trondhjemite	Oldest concordant zircon	1	3838 ± 10	Iqaluk	2.5 ± 0.3
SG-122	Trondhjemite	Oldest concordant zircon	1	3781 ± 12	Uivak I	1.7 ± 0.2
SG-026	Mg-rich tonalite	Upper intercept	103	3820 ± 20	Iqaluk	3.7 ± 0.2
SG-027	Mg-rich tonalite	2 oldest concordant zircons	2	3632 ± 9	Uivak II	-1.1 ± 0.3
SG-210c	Mg-rich tonalite	Mean concordia age	34	3869 ± 6	Iqaluk	1.8 ± 0.2
SG-265	Mg-rich tonalite	Mean concordia age	13	3224 ± 7	Lister	1.0 ± 0.3
SG-203	Granodiorite	Upper intercept	103	3330 ± 15	Iluilik	-6.3 ± 0.2
SG-007	Leuco-granite	Oldest concordant zircon	1	3883 ± 10	Iqaluk	2.0 ± 0.3
SG-017	Leuco-granite	Weighted mean $^{207}Pb/^{206}Pb$	13	2802 ± 13	Late granites	-4.6 ± 0.3
SG-037	Granite	Weighted mean $^{207}Pb/^{206}Pb$	44	2744 ± 8	Late granites	-14.6 ± 0.2
SG-080	Granite	Weighted mean $^{207}Pb/^{206}Pb$	3	3612 ± 9	Uivak II	-1.2 ± 0.2
SG-084	Granite	Weighted mean $^{207}Pb/^{206}Pb$	10	3710 ± 24	Uivak I	-0.1 ± 0.3
SG-087	Granite	Weighted mean $^{207}Pb/^{206}Pb$	8	2996 ± 42	Late granites	-2.6 ± 0.2
SG-127	Granite	Weighted mean $^{207}Pb/^{206}Pb$	18	2789 ± 12	Late granites	-12.2 ± 0.2
SG-143	Granite	Weighted mean $^{207}Pb/^{206}Pb$	42	2780 ± 8	Late granites	-11.2 ± 0.2
SG-208	Granite	Mean concordia age	18	3330 ± 7	Iluilik	-6 ± 0.2

Continued on next page

Table 2.2 – *Continued from previous page*

Sample #	Lithology	Age type	N	Age ($\pm 2\sigma$ Ma)	Magmatic event	$\varepsilon Hf_{(i)} \pm 2\sigma$
		Inherited age				
SG-019	Trondhjemite	Concordia age	1	3553 ± 15	Uivak II	-1.8 ± 0.9
SG-017	Leuco-granite	Concordia age	1	3576 ± 14	Uivak II	-4.8 ± 0.5
SG-037	Granite	Discordant $^{207}Pb/^{206}Pb$	1	3303 ± 48	Iluilik	-8.0 ± 0.7
SG-080	Granite	Concordia age	1	3805 ± 15	Iqaluk	0.4 ± 1.3
SG-087	Granite	Mean concordia age	4	3745 ± 17	Uivak I	1.3 ± 0.4
SG-127	Granite	Discordant $^{207}Pb/^{206}Pb$	1	3661 ± 48	Uivak II ?	-2.0 ± 1
SG-143	Granite	Concordia age	1	3655 ± 12	Uivak II ?	-0.4 ± 0.5
		Metamorphic age				
SG-019	Trondhjemite	Weighted mean $^{207}Pb/^{206}Pb$	14	2574 ± 14	Late granites	
SG-024	Trondhjemite	Weighted mean $^{207}Pb/^{206}Pb$	23	2769 ± 19	Late granites	
SG-025	Trondhjemite	Weighted mean $^{207}Pb/^{206}Pb$	91	2747 ± 5	Late granites	
SG-122	Trondhjemite	Weighted mean $^{207}Pb/^{206}Pb$	28	2804 ± 9	Late granites	
SG-026	Mg-rich tonalite	Lower intercept	103	2514 ± 71	Late Granites	
SG-027	Mg-rich tonalite	Weighted mean $^{207}Pb/^{206}Pb$	46	2785 ± 7	Late granites	
SG-028	Mg-rich tonalite	Weighted mean $^{207}Pb/^{206}Pb$	6	2595 ± 20	Late granites	
SG-210c	Mg-rich tonalite	Weighted mean $^{207}Pb/^{206}Pb$	19	3558 ± 11	Uivak II	
SG-210c	Mg-rich tonalite	Weighted mean $^{207}Pb/^{206}Pb$	1	2720 ± 16	Late granites	
SG-265	Mg-rich tonalite	Lower intercept	70	887 ± 110	Proterozoic ?	
SG-203	Granodiorite	Weighted mean $^{207}Pb/^{206}Pb$	9	2975 ± 17	Mesoarchean ?	
SG-203	Granodiorite	Weighted mean $^{207}Pb/^{206}Pb$	3	2703 ± 30	Late granites	
SG-007	Leuco-granite	Weighted mean $^{207}Pb/^{206}Pb$	13	2769 ± 22	Late granites	
SG-017	Leuco-granite	Weighted mean $^{207}Pb/^{206}Pb$	4	2712 ± 13	Late granites	
SG-037	Granite	Scattered zirons	-	2700 to 2200	Late granites	

Continued on next page

Table 2.2 – *Continued from previous page*

Sample #	**Lithology**	**Age type**	**N**	**Age ($\pm 2\sigma$ Ma)**	**Magmatic event**	**$\varepsilon Hf_{(i)} \pm 2\sigma$**
SG-080	Granite	Mean concordia age	2	2752 ± 9	Uivak II	
SG-087	Granite	Weighted mean $^{207}Pb/^{206}Pb$	15	2755 ± 13	Late granites	
SG-087	Granite	Weighted mean $^{207}Pb/^{206}Pb$	14	2584 ± 14	Late granites	
SG-127	Granite	Weighted mean $^{207}Pb/^{206}Pb$	8	2662 ± 18	Late granites	
SG-143	Granite	Weighted mean $^{207}Pb/^{206}Pb$	7	2706 ± 19	Late granites	
SG-208	Granite	Weighted mean $^{207}Pb/^{206}Pb$	23	3241 ± 11	Lister	
		Secondary sector zoned population				
SG-024	Trondhjemite	Weighted mean $^{207}Pb/^{206}Pb$	42	2721 ± 8	Late granites	
SG-025	Trondhjemite	Weighted mean $^{207}Pb/^{206}Pb$	91	2747 ± 5	Late granites	

2.4.2 U-Pb Geochronology

Zircons from 18 granitoid samples have been analyzed by LA-ICP-MS for U-Pb geochronology. For each sample, a set of 100 to 120 zircons have been analyzed. Data for all individual zircons are available in supplementary data table S2. Samples were selected to cover all granitoid groups. Figure 2.6 shows cathodoluminescence (CL) images for representative zircons for 6 samples and the Concordia plots for each sample are displayed in figure 2.7. Table 2.2 presents a summary of the crystallization ages, inherited ages and metamorphic ages obtained for each sample analysed. Reported ages were determined from one of the Concordia age for samples with populations of concordant zircons, or upper intercept ages for populations with mostly discordant zircons, and weighted mean $^{207}Pb/^{206}Pb$ ages -for more scattered populations-. For samples with populations showing concordant results over a wide range of ages, indicative of ancient Pb-loss, the oldest concordant zircons were considered as the most representative of their crystallization age.

Trondhjemites

The four trondhjemite samples SG-019, SG-024, SG-025, and SG-122 have been analysed for U-Pb on zircons.

Zircons from sample SG-019 are dominated by metamict rounded zircon grains. A total of 33 analyses were performed (Fig. 2.7a). The main population of zircons yields a weighted mean $^{207}Pb/^{206}Pb$ age of 2732 ± 25 Ma (MSWD=2.2; N=12) is taken as the crystallization age. These zircons consisting of relatively low U (mostly <700 ppm; average ~470 ppm), black core to oscillatory zoned grains. A resolvable second population of zircons (U concentrations from 600 to 2860 ppm; average ~1629 ppm) mostly consists of metamict grains and yields a weighted mean $^{207}Pb/^{206}Pb$ age of 2574 ± 14 Ma

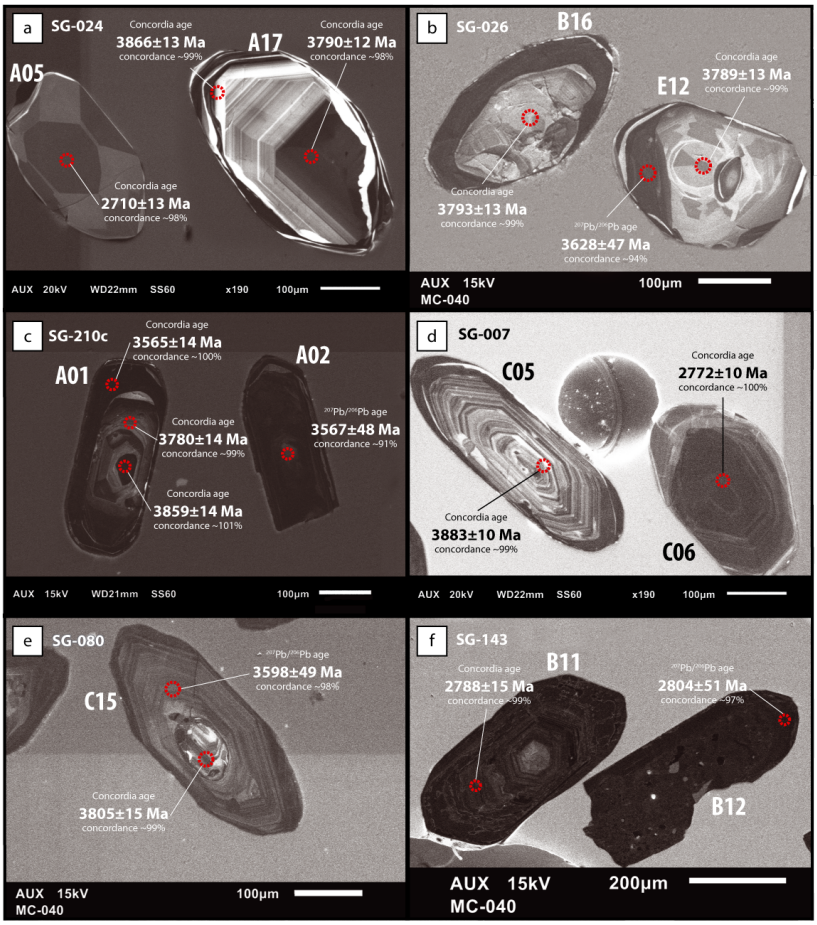

Figure 2.6

Cathodoluminecsence images of representative zircons used to interpret the texture sof the different grain populations and guide laser ablation work. a) Trondhjemite sample SG-0024: grain #A05 shows typical sector zoning of zircons that crystallized during the 2700-2800 thermal events. Zircon #A17 exhibiting igneous sector zonation and a younger core age relative to the rim. b) Mg-rich tonalite sample SG-026 from Ukkalek Island: grains #B16 and #E12 how oscillatory zoned cores and discordant black coloured rims. c) Mg-rich tonalite sample SG-210c from the Kangidluarsuk fjord: grain #A01exhibits multiple ages decreasing from the core to the rim, suggesting the spread of zircon ages observed on the concordia diagram can be explained by ancient Pb-loss. Zircon #A02 is a discordant metamict U-rich grain. d) Granite sample SG-007 from Ukkalek Island: grain #C05 yields an Eoarchean magmatic age and grain #C06 from the same sample is a black U-rich metamict zircon. e) Granite sample SG-080 from the Kangidluarsuk fjord: grain #C15 is a good example of an Eoarchean inherited zircon within an early-Paleoarchean oscillatory zoned crystal. f) Granite sample SG-143: U-rich zircon #B11 shows oscillatory zoning and zircon B12is a metamict crystal typically found in Neoarchean rocks.

(MSWD= 0.46; N=14). Two inherited zircon cores yield Concordia ages at 3477±18 Ma and 3553 ± 15 Ma.

A total of 128 U-Pb analyses have been conducted on sample SG-024 (Fig. 7b). Zircons are dominated by two main populations that exhibit relatively low U concentrations (<1000 ppm) associated with a wide range of Th/U ratios (< 3). A number of zircons from SG-024 are subeuhedral to euhedral and exhibit well defined oscillatory zoning (*e.g.* zircon #A17: Fig. 2.6a). The few Concordant analyses spread between 3800 and 3870 Ma, but zircons from this population are mostly discordant and spread along a poorly defined discordia line (Fig. 2.7b). The two oldest concordant cores yield a Concordia mean age of 3869 ± 10 Ma (MSWD=3.6; N=2) considered as the crystallization age for this sample. A population of Neoarchean zircons is dominated by subeuhedral to rounded zircons that show clear sector zoning with higher Th/U ratios (*e.g.* zircon #A05: Fig. 2.6a) which altogether yield an age of 2721 ± 8 Ma (MSWD= 0.89; N=42). A few Neoarchean oscillatory zoned rims and cores with lower Th/U ratios (<0.2) are also present. However, these Neoarchean zircons exhibit much more scattered ages and yield a weighted mean $^{207}Pb/^{206}Pb$ age of 2769 ± 19 Ma (MSWD= 4; N=28).

Zircons from sample SG-025 are dominated by oscillatory and sector zoned grains to black in CL images. A total of 125 U-Pb analyses have been done on sample SG-025 (Fig. 2.7c) with all oscillatory zoned zircons spreading along the Concordia curve from 3838 to 3000 Ma. The older zircons from this population are characterised by high Th/U ratios, whereas the younger ones yield lower Th/U and more consistent with the evidence of ancient Pb-loss. The crystallization age for this sample is, therefore, best represented by the oldest concordant zircon with a Concordia age of 3838 ± 10 Ma. Sample SG-025 also includes a population of sector zoned and black zircons with high

Th/U (>0.2) and yielding Neoarchean ages. These clusters around a weighted mean $^{207}Pb/^{206}Pb$ age of 2747 ± 5 Ma (MSWD =0.54; N=91).

A total of 105 U-Pb analyses were conducted on sample SG-122 (Fig. 2.7d). Zircons from this trondhjemite sample are dominated by rounded grains with oscillatory zoned textures to black in CL images. The main population scatters along a discordia line with an upper intercept age at 3752 ± 33 Ma (MSWD=13; N= 62). Moreover, a number of concordant zircons from this population spread along the concordia curve between ∼3790 and ∼3700 Ma, indicative of a certain extent of ancient Pb-loss. The oldest concordant zircon from this scattered population gives an age of 3781 ± 12 Ma, representing the crystallization age for this sample. This euhedral zircon grain shows a clear oscillatory zoned texture and exhibits a relatively high Th/U ratio (∼0.2). A subordinate population of U-rich zircons yields a younger weighted mean $^{207}Pb/^{206}Pb$ age of 2804 ± 9 Ma (MSWD= 0.81; N=28).

Mg-rich tonalites

Four Mg-rich tonalite samples have been analysed for U-Pb on zircons, including sample SG-026, SG-027, SG-210c, and SG-265.

Zircons from sample SG-026 are dominated by oscillatory zoned to sector zoned subeuhedral grains (*e.g.* zircon #B16 & #E12; Fig. 2.6b) that exhibit low U concentrations (20 to 1000 ppm) and relatively highTh/U ratios (>0.6) compared to zircons from other samples. A total of 115 U-Pb analyses were performed on sample SG-026 including a single population of zircons defining a discordia line with an upper intercept at 3820 ± 20 Ma, interpreted as the crystallization age, and a lower intercept at 2514 ± 71 Ma (MSWD=1.12; N=103)(Fig. 2.7e).

A total of 138 analyses were done for sample SG-027 which includes three main

zircon populations (Fig. 2.7f). Zircons from the oldest population exhibit oscillatory zoned textures and igneous Th/U ratios from 0.2 to 0.5. A number of zircons from this population are concordant, spreading on the Concordia curve between ~3600 and ~3500 Ma, which may reflect ancient Pb-loss. Therefore, the average of the two oldest concordant zircons was taken as the crystallization age, at 3632 ± 9 Ma (MSWD =3.6; N=2). The two other populations are Neoarchean zircons, which include two groups characterized by metamict textures and black CL images, often occurring as rims around older cores. One Neoarchean population exhibits lower Th/U ratio and yields a weighted mean $^{207}Pb/^{206}Pb$ age of 2785 ± 7 Ma (MSWD= 1.3: N=46), while a secondary smaller population with higher Th/U ratios (>0.4) yields a weighted mean $^{207}Pb/^{206}Pb$ age of 2592 ± 20 Ma (MSWD= 0.93; N=6).

Sample SG-210c was collected from the same outcrop and lithology as the sample previously dated at 3920 ± 49 Ma (Shimojo et al., 2016). A total of 120 U-Pb analyses were obtained from this sample. A number of zircons scatter along the Concordia curve from ~3900 to ~3500 Ma in two defined populations (Fig. 2.7g). The oldest concordant zircons display a relatively homogenous population exhibiting oscillatory zoning (*e.g.* zircon #A01; Fig. 2.6c), with high Th/U ratios (> 0.3) and a mean Concordia age of 3869±6 Ma (MSWD= 0.50; N=34) interpreted as the crystallization age. The younger zircons show a fair amount of scattering and a progressive decrease of Th/U ratios (to <0.1) as ages decrease. This population consists of U-rich recrystallized zircons that are black on CL images (*e.g.* zircon #A02; Fig. 2.6c) and displays a weighted mean $^{207}Pb/^{206}Pb$ age of 3558±11 Ma (MSWD=0.49; N=19). A single zircon yields a Concordia age of 2720±16 Ma.

A total of 86 U-Pb analyses were performed on sample SG-265 that was collected on Lister Island. All zircons from this sample show clear and well-defined oscillatory

zoning as well as relatively high Th/U ratios, between 0.3 and 0.5. Zircons from a single population defining a discordia line with an upper intercept age of 3229 ± 8 Ma (MSWD= 1.3; N=70)(Fig. 2.7h). The most concordant zircons yield a Concordia mean age of 3224 ± 7 Ma (MSWD= 0.27; N= 13) and considered as the crystallization age.

Granodiorites

One sample of granodiorite SG-203 has been analysed for U-Pb with a total of 121 in-situ analyses (Fig. 2.7i). The main population of zircons exhibits oscillatory zoning and high Th/U ratios ranging between 0.3 and 0.5. They define an upper intercept age of 3330 ± 15 Ma (MSWD=1.2; N=103) interpreted to be the crystallization age. Two additional minor populations of zircons with lower Th/U ratios (<0.1) yield younger weighted mean $^{207}Pb/^{206}Pb$ ages of 2975±17 Ma (MSWD= 1.02; N=9) and 2703±30 Ma (MSWD=0.69; N=3).

Granites

Nine granite samples have been analysed for U-Pb on zircons, including sample SG-007, SG-017, SG-037, SG-080, SG-084, SG-087,SG-127,SG-143, and SG-208.

Sample SG-007 is a granite for which 114 U-Pb analyses have been obtained (Fig. 2.7j). Zircons are dominantly elongated subeuhedral grains with oscillatory zoning or with metamict textures. Most zircons with oscillatory zoned cores show thin recrystallized rims. This sample displays zircons with variable ages and multiple heterogeneous populations. Concordant zircons display a wide range of ages from 3883 to 3300 Ma which correlates with a decrease of Th/U ratios (from 0.7 to <0.1). The three oldest concordant grains consist of oscillatory zoned low U cores that exhibit ages spreading on the Concordia line from 3883 ± 10 Ma (cf. zircon #C5; Fig. 2.6d) to 3853 ± 12 Ma

$^{207}Pb/^{206}Pb$ weighted mean age = 3869±26 Ma MSWD=0.41; N=3).Therefore, only the oldest concordant zircon has been used to define the crystallization age of the rock.The younger concordant ages mostly correspond to rims around oscillatory zoned older cores. On a Kernel density estimation (KDE) diagram (Fig. 2.7j), two high-density peaks of apparent ages yield weighted mean $^{207}Pb/^{206}Pb$ ages at 3521 ± 19 Ma (MSWD = 5.4; N=35) and 3815 ± 22 Ma (MSWD= 3.14; N= 15) indicative of ancient Pb-loss around 3800 and 3500 Ma. A younger concordant population consisting of recrystallized rims to completely metamict grains (*e.g.* zircon #C6; Fig. 6d) with relatively high concentrations in U (up to 2599 ppm) and a low Th/U ratio (<0.1), yields a weighted mean $^{207}Pb/^{206}Pb$ age of 2769 ± 22 Ma. A third population of U-rich metamict zircon rims (up to 5790 ppm) yields a weighted mean $^{207}Pb/^{206}Pb$ age of 2649 ± 17 Ma (MSWD =1.7; N=9).

A total of 22 U-Pb analyses were conducted on granite sample SG-017 (Fig. 2.7k). Zircons from this sample are dominated by rounded to elongated metamict grains. Two populations of zircons with low Th/U ratios (<0.1) yield weighted mean $^{207}Pb/^{206}Pb$ ages of 2802 ± 13 Ma (MSWD= 1.2; N=13) and 2712 ± 13 Ma (MSWD= 1.2; N=4). A single zircon, perhaps inherited, yielded a Concordia age of 3576 ± 14 Ma. Because zircons from this sample are metamict with low Th/U ratios, a clear crystallization age is difficult to establish and ages found likely represent metamorphic ages.

A total of 99 U-Pb analyses were obtained on sample SG-037 (Fig. 2.7l). Most zircons from this granite are black on CL images and display metamict cores or rare zoned cores with high Th/U ratios (>0.2). The main population yields a weighted mean $^{207}Pb/^{206}Pb$ age of 2744 ± 8 Ma (MSWD=0.6; N=44). Younger grains spread along the Concordia curve from 2744 to 2200 Ma and mostly consist of metamict grains with relatively high U concentrations (700-3800 ppm) and low Th/U ratios (<0.3).

Two older discordant inherited zircons are also present, with the oldest zircon yielding a $^{207}Pb/^{206}Pb$ age of 3303 ± 48 Ma.

A total of 38 U-Pb analyses were conducted on granitic sample SG-080 (Fig. 2.7m). The dominant population of zircons is characterized by high Th/U ratios and oscillatory zoned grains yielding a weighted mean $^{207}Pb/^{206}Pb$ age of 3612 ± 9 Ma (MSWD=0.71; N=26), interpreted as the crystallization age. Three inherited cores appear to exhibit older ages with one concordant zircon(*e.g.* zircon #C15; Fig. 2.6e) which yielded a Concordia age of 3805 ± 15 Ma. Two low Th/U younger zircons yield mean Concordia ages of 2752 ± 9 Ma (MSWD =2.4: N=2).

Zircons from sample SG-084 are dominated by metamict grains frequently including a large amount of inclusions. A total of 19 analyses were performed but only 10 oscillatory zoned cores yield a poorly defined population with a weighted mean $^{207}Pb/^{206}Pb$ age of 3710 ± 24 Ma (MSWD= 1.9; N=10)(Fig. 2.7n).

A total of 57 analyses were obtained on sample SG-087(Fig. 2.7o). Zircons from this granite sample are dominated by sector and oscillatory zoned grains that exhibit variable Th/U ratios. Sector zoned grains are grouped in three major clusters with weighted mean $^{207}Pb/^{206}Pb$ ages of 2996 ± 42 Ma (MSWD=3.8; N=8), 2755 ± 13 Ma (MSWD=1.2; N=15) and 2584 ± 14 Ma (MSWD=1.5; N=14). The age of 2996 ± 42 Ma is possibly the age of crystallization. Few oscillatory zoned inherited older zircon cores spread along the Concordia curve with a mean Concordia age of 3745 ± 17 Ma (MSWD= 3.3; N=4).

A total of 50 U-Pb analyses were conducted on granite sample SG-127 (Fig. 2.7p). Zircons with high Th/U ratios (>0.2) showing oscillatory zoned cores with few metamict U-rich grains, yield a weighted mean $^{207}Pb/^{206}Pb$ age of 2789 ± 12 Ma (MSWD=0.83; N=18) interpreted as the crystallization age. A younger population with lower Th/U ra-

tios yields a weighted mean $^{207}Pb/^{206}Pb$ age of 2662 ± 18 Ma (MSWD=0.68; N=8).One inherited zircon with clear oscillatory zoning yields a discordant (∼4%) $^{207}Pb/^{206}Pb$ age of 3661 ± 48 Ma. All other analyzed zircons were low Th/U ratio metamict grains with$^{207}Pb/^{206}Pb$ ages ranging from 2600 to 2200 Ma.

A total of 53 U-Pb analyses were done for sample SG-143 (Fig. 2.7q). Zircons from this granite are dominated by metamict zircons with subordinate euhedral oscillatory zoned grains (*e.g.* zircon#B11 and#B12; Fig. 2.6f). These zircons exhibit a wide range of Th/U ratios (from 0.02 to 0.7) with the main population yielding a weighted mean $^{207}Pb/^{206}Pb$ age of 2780 ± 8 Ma (MSWD=0.78; N=42) that corresponds to the crystallization age. A smaller population of U-rich metamict grains yields a slightly younger weighted mean $^{207}Pb/^{206}Pb$ age of 2706 ± 19 Ma (MSWD=1.7; N=7). Three inherited cores yield older $^{207}Pb/^{206}Pb$ ages with only one concordant inherited core, which exhibits a Concordia age of 3655 ± 12 Ma.

A total of 77 U-Pb analyses were obtained on sample SG-208 (Fig 2.7r). Zircons from this granitic sample mostly consist of oscillatory zoned grains with low U concentrations (31-400 ppm) and relatively high Th/U ratios ranging between 0.2 and 0.6. Concordant zircons yield two different populations. The first population gives a Concordia mean age of 3330 ± 7 Ma (MSWD=0.033; N=18) and is considered as the crystallization age. The second slightly younger population yields a weighted mean $^{207}Pb/^{206}Pb$ age of 3241 ± 11 Ma (MSWD=0.68; N=23), possibly reflecting age resetting. Four zircons also exhibit a younger weighted mean $^{207}Pb/^{206}Pb$ age around 2946 ± 8 Ma (MSWD= 0.33; N=4).

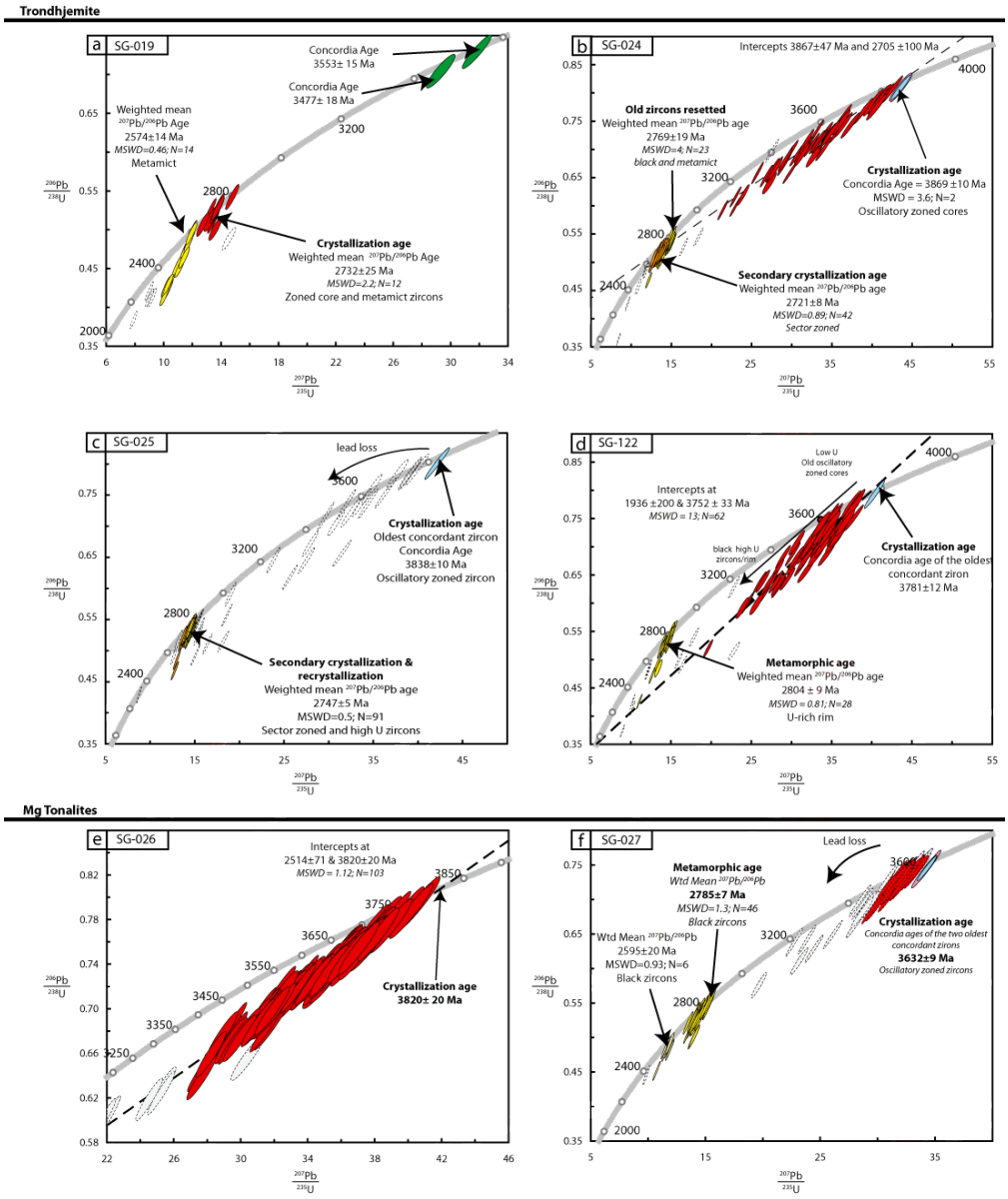

Figure 2.7

Concordia diagrams of trondhjemites (a-b-c-d), Mg-rich tonalites (e-f-g-h), granodiorites (i) and granites (j-k-l-m-n-o-p-q-r) from the SHC. All the diagrams show interpreted crystallisation ages, inherited grains and metamorphic secondary populations. Colors of the ellipses reflect the different age populations which are classified from the criteria described in the results (*cf.* section 2.4); green: inherited zircons; red: primary igneous zircons; orange: secondary igneous zircons; yellow: metamorphic recrystallized zircons; pink: zircons used for Concordia mean ages; light blue: Concordia ages. The dashed empty symbols are used for zircons too discordant and chemically altered to either be grouped in a consistent population or used in any sorts of relevant age calculation.

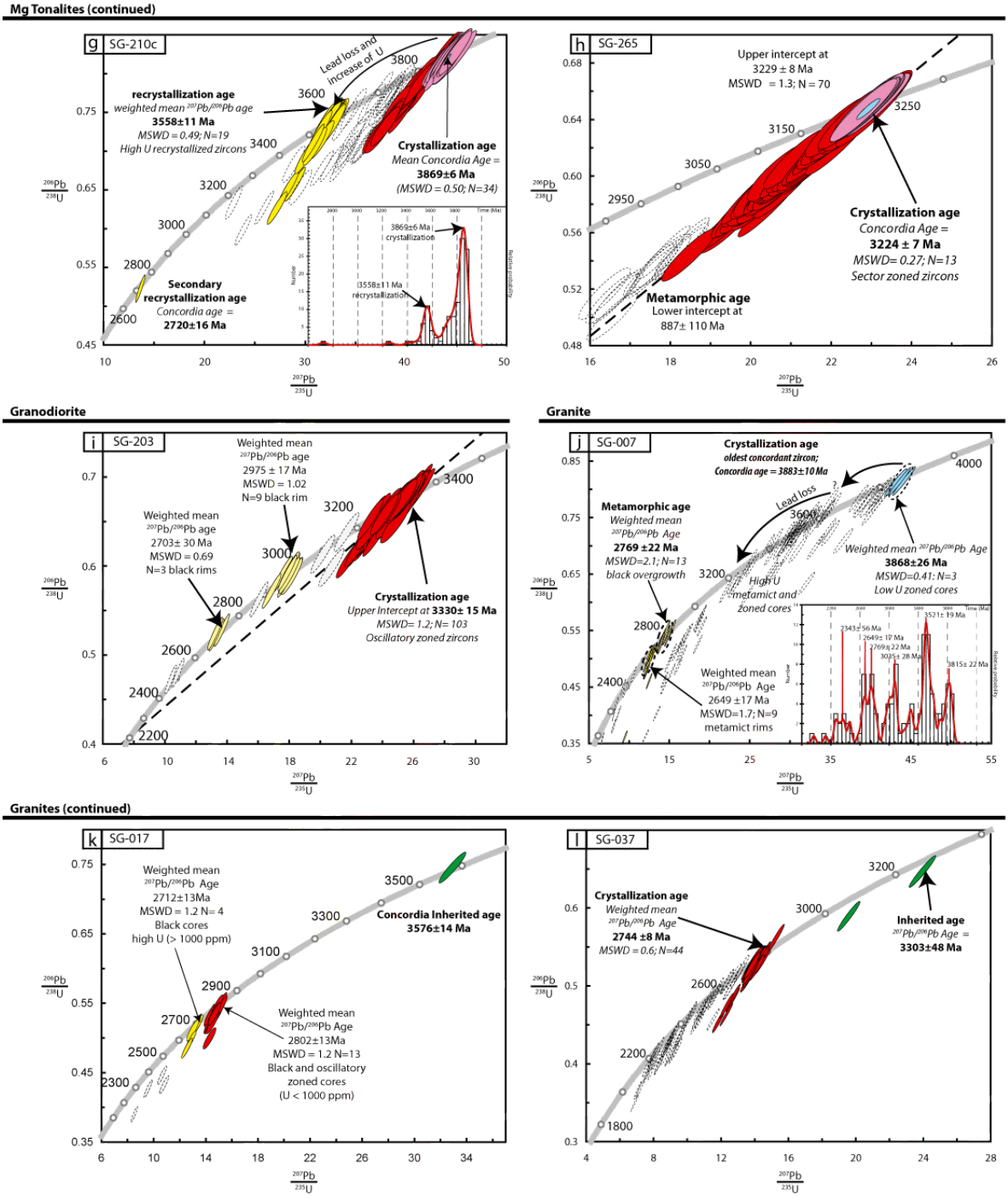

Continued from figure 2.7

Granites (continued)

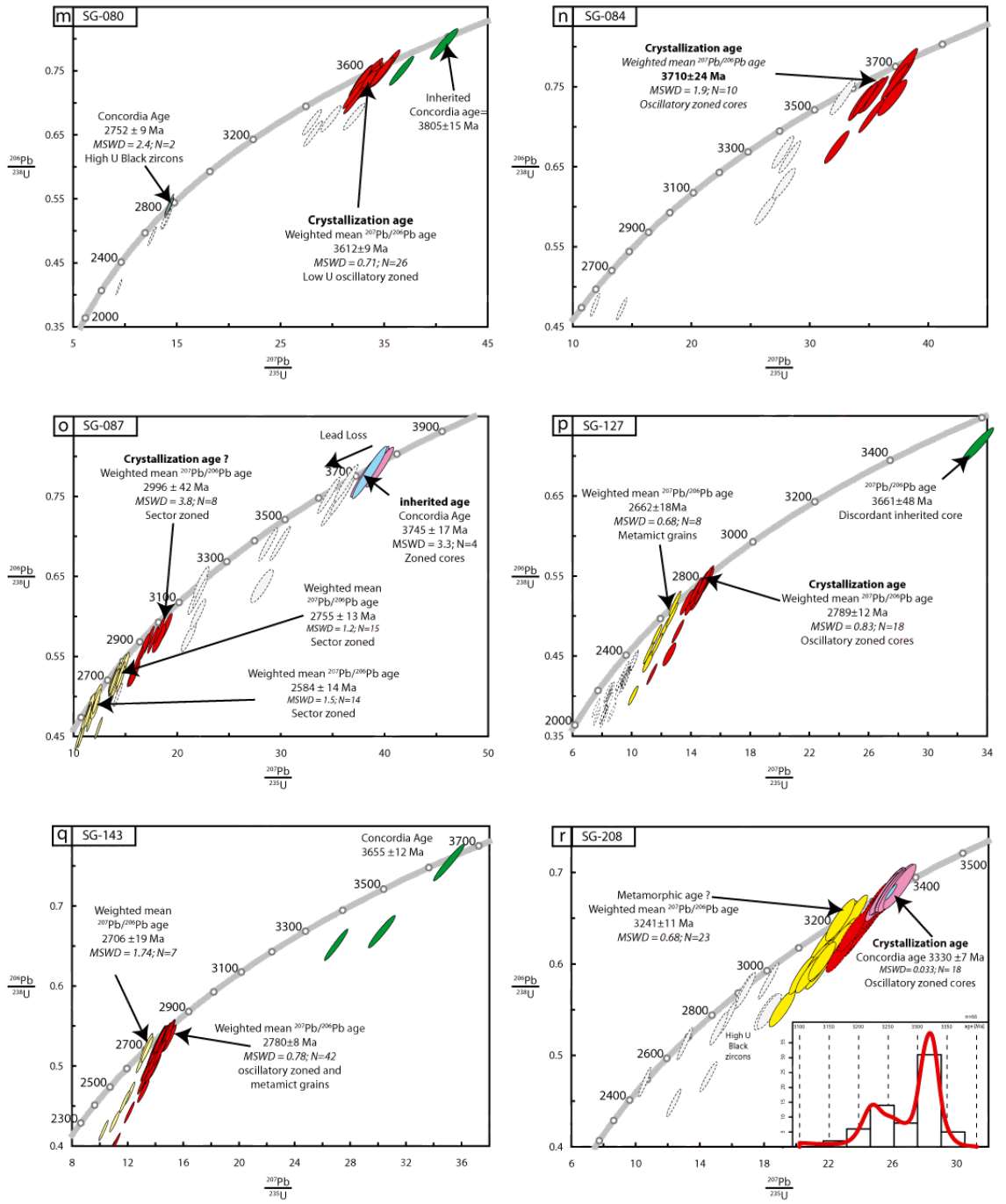

Continued from figure 2.7

2.4.3 Zircon Lu-Hf isotopic compositions

For each rock sample, a subset of 10 to 30 representative concordant zircons (±2 % concordance) has been analyzed for in-situ Hf isotopes (Supplementary Table B.4 in appendix B). Measurements were acquired on the same spot used for the U-Pb analyses. Figure 2.8 shows the initial ε^{176}Hf values for each zircon, calculated at their respective measured ^{207}Pb/^{206}Pb age. However, given that the studied samples are granitoid rocks with a single crystallization age, the initial Hf isotopic composition for all of the zircons from a single sample should be at the same crystallization age. Therefore, initial Hf isotope compositions of each zircon from the same sample were also calculated at the age of crystallization reported in Table 2.2 and the average (± 2SE) are also shown on Figure 2.8. This is performed in order to avoid calculating an initial Hf composition at an over or underestimated ^{207}Pb/^{206}Pb age for zircons that would have suffered ancient Pb-loss but remained on the Concordia curve (Kemp et al., 2010; Fisher et al., 2014b,a) as illustrated in figure 2.9. Figure 2.8 shows that Eoarchean samples (3883 to 3781 Ma) display initial Hf isotope compositions that are slightly suprachondritic, with initial ε^{176}Hf values ranging between +3.7 to +1.7. The Mg-rich tonalite sample SG-026 contains zircons exhibiting the most radiogenic Hf isotopic composition with an average initial ε^{176}Hf value of $+3.7 \pm 0.2$ at 3820 Ma, falling on the depleted mantle evolution line. Most samples with positive ε^{176}Hf initial values are tonalitic or trondhjemitic in composition, except for granitic sample SG-007 with initial ^{176}Hf/^{177}Hf ratios between 0.28027 and 0.28042 and an average ε^{176}Hf initial value of +2.0 at 3883 Ma. This sample, however, shows a complex zircon population (Fig. 2.7j). Five granitoid samples with Paleoarchean ages from 3632 to 3330 Ma display subchondritic initial ^{176}Hf/^{177}Hf ratios corresponding to average ε^{176}Hf initial values from -1.0 to -6.3. The low ε^{176}Hf initial value of -4.6 at 3576 Ma for sample SG-017, however, is from a zircon that is inherited

and the main Neoarchean zircon population for this sample shows an average ε^{176}Hf of -12.7 ± 0.3 at 2802 Ma. Sample SG-203 is the only granodiorite analysed, but displays the same 3330 Ma age and Hf isotopic composition as the associated granitic sample SG-208, with initial ε^{176}Hf values of around -6. Sample SG-208 includes a single zircon exhibiting a significantly higher ^{176}Hf/^{177}Hf initial ratio of 0.28063 corresponding to an initial value of $\varepsilon^{176}\text{Hf} = +0.2$, but this zircon contains numerous inclusions that may have affected the measured Hf isotopic composition. The later ∼3200 Ma Paleoarchean Mg-rich tonalite from the Lister Island, SG-265 is characterized by a radiogenic initial Hf isotopic composition and does not appear to follow the general ε^{176}Hf trend *vs.* time that most other granitoids display on figure 2.8. This sample has a slightly suprachondritic initial ε^{176}Hf value of $+1.0 \pm 0.3$ at 3224 Ma .The late Mezoarchean granitic sample SG-087 is characterized by an initial ε^{176}Hf of -2.6 ± 0.2 at 2996 Ma. This sample, however, has multiple and complex zircon generations (Fig. 2.7o) and geochronology results should be taken with caution. Sample SG-087 also includes few inherited older zircon cores with initial $\varepsilon^{176}\text{Hf} = +1.5 \pm 0.4$ at 3745 Ma.

Four Neoarchean samples have been analysed for zircon Hf isotopic composition, including three granite samples and one trondhjemitic sample. They all display low initial ^{176}Hf/^{177}Hf ratios corresponding to average ε^{176}Hf initial values of -11.2 to -14.3, between 2732 and 2789 Ma. The trondhjemitic sample SG-019 included two inherited zircon cores with ages of 3477 and 3553 Ma that respectively yielded initial ε^{176}Hf values of -3.3 and +7.0. Although the initial ε^{176}Hf value of -3.3 for the younger inherited zircon cores would be consistent with the main array defined by the other granitoids, an initial value of $\varepsilon^{176}\text{Hf} = +7$ at 3553 Ma would be much more radiogenic than the depleted mantle. This unlikely initial ε^{176}Hf value could result from the ablation of a mixed zone on this complex zircon rather than reflect the Hf isotopic composition of its

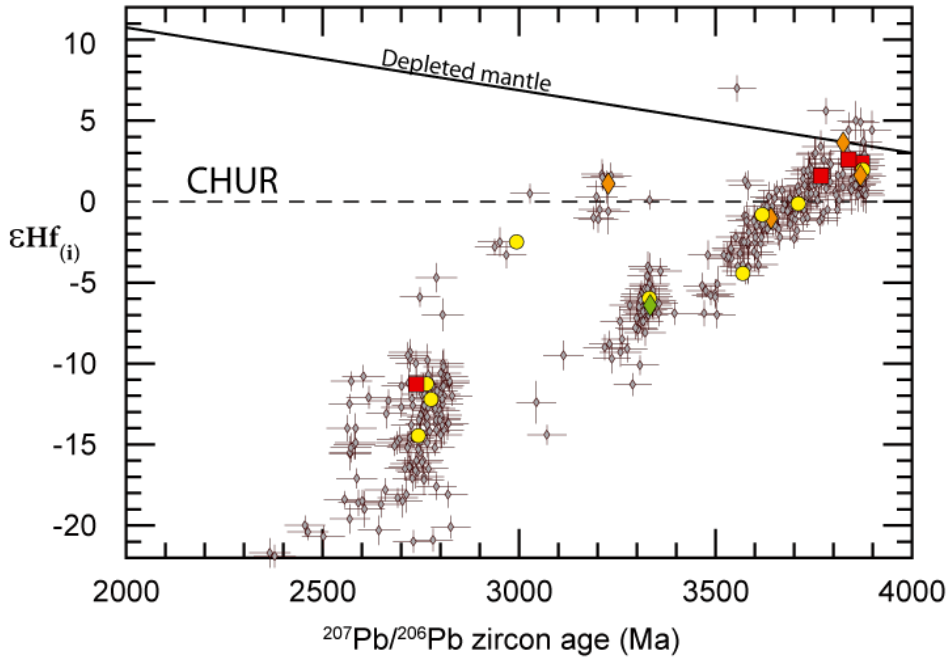

Figure 2.8

Initial ε^{176}Hf values *vs.* ^{207}Pb/^{206}Pb ages for zircons analyzed here. Grey diamonds represent single grains, and the coloured symbols show average initial ε^{176}Hf values calculated at the interpreted crystallisation age of the rocks. Symbols are as in figure 2.2. Note that average ε^{176}Hf values only include relevant analysis for the defined population, such that metamorphic and inherited zircons are not included in the average epsilon calculation.

source. The other Neoarchean granites also include a few inherited older grains which ε^{176}Hf values fall within the main time *vs.* initial ε^{176}Hf array with two ∼3660 Ma cores with intial ε^{176}Hf = -0.2 to -1.7 and one 3303 Ma core with initial ε^{176}Hf = -7.8. A few Eoarchean to Paleoarchean granitoids display Neoarchean zircon rims (sample SG-024, SG-025, and SG-027) with variable initial ε^{176}Hf values ranging from ∼-15 to ∼-22. These zircons, however, show variable and often low Th/U ratios, which could be indicative of metamorphic recrystallization. Therefore, the initial ε^{176}Hf values calculated at these ages may not be reflective of their crustal source.

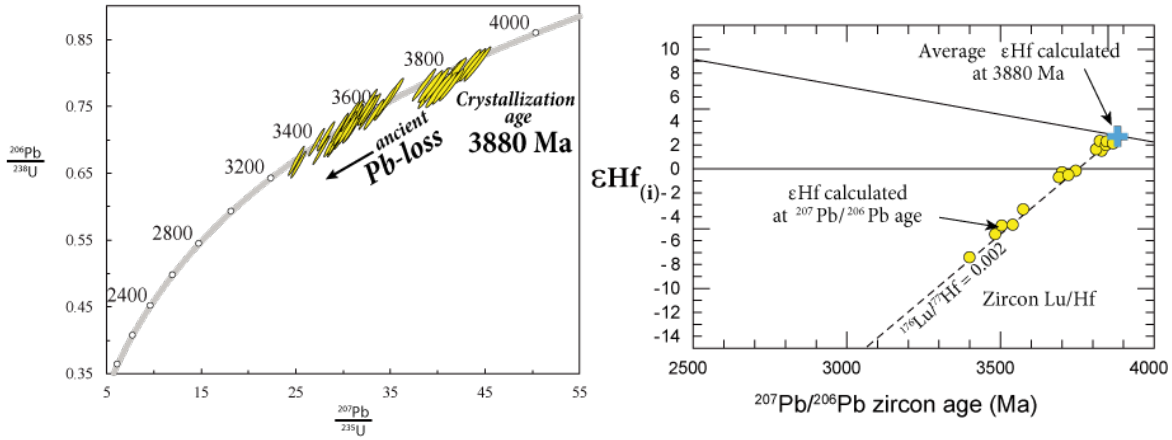

Figure 2.9

Cartoon showing how average initial ε^{176}Hf values are calculated in figure 8, from the interpreted age of crystallization of the rocks, in order to avoid apparent ε^{176}Hf *vs.* ^{207}Pb/^{206}Pb trends caused by ancient Pb-loss. Panel a) shows an example of a sample with a crystallization age of 3880 Ma, which was affected by ancient Pb-loss and for which most zircon analyses are still relatively concordant. Panel b) illustrates that if initial ε^{176}Hf values are calculated for individual zircons at their respective concordant ages (yellow circles), it produced a steep array on the ε^{176}Hf *vs.* ^{207}Pb/^{206}Pb age diagram that is consistent with the low Lu/Hf of zircons, rather than representative of the evolution of a crustal source. The blue cross symbol shows the average ε^{176}Hf value for all zircon analyses calculated at the 3880 Ma crystallization age.

2.5 Discussion

2.5.1 Composition and petrogenesis of the SHC felsic crust

The geochemical composition of Archean felsic rocks has been widely used to constrain the nature of their sources and the various processes leading to the formation of the Archean crust (*e.g.* Laurent et al., 2014; Moyen and Martin, 2012; Moyen et al., 2001; Whalen et al., 2002; Hoffmann et al., 2019). Rocks from the tonalite-trondhjemite-granodiorite series make up the major part of the Archean cratonic nucleus forming our stable continents. Various petrogenetic models have been proposed to explain the origin of TTG, and several lines of evidence point to an incompatible element enriched mafic source as the precursor of Archean TTG (*e.g.* Hoffmann et al., 2011; Jayananda et al.,

2015; Moyen, 2011; Smithies et al., 2009; Moyen and Martin, 2012; Hoffmann et al., 2019). In comparison, granites require a K-rich source and are generally thought to derive from the melting of older felsic lithologies (*e.g.* Moyen, 2011; Moyen and Laurent, 2018; Laurent et al., 2014). Melting at medium to high-pressures, with the involvement of garnet in the source, is the mechanism dominantly proposed to account for the TTG's typical HREE depletions, correlated with high Sr/Y ratios (Moyen, 2011; Nagel et al., 2012).

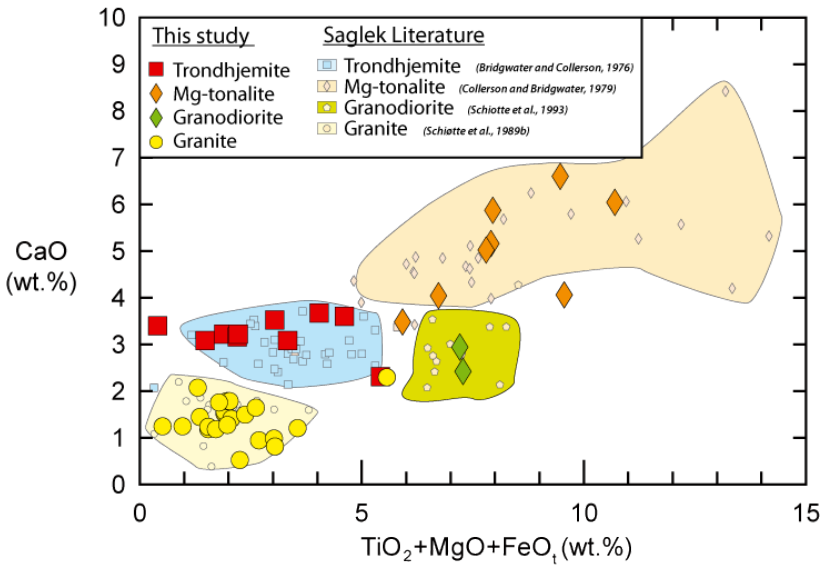

Figure 2.10

Proposed major element composition discrimination diagram for all granitoids from the SHC. Symbols and coloured fields are as in figure 2.2.

Granitoids from the SHC comprise felsic rocks with various geochemical compositions. Based on our sampling and data from the literature, the SHC granitoids are divided into four main rock types including trondhjemites, Mg-rich tonalites, granodiorites, and granites. Table 2.3 presents the main compositional characteristics of each type. Key geochemical features can be used to discriminate these 4 granitoid groups,

Table 2.3

Key characteristics discriminating the four compositional types of granitoids from the SHC, based on this study and compositions from the literature (Bridgwater and Collerson, 1976; Collerson and Bridgwater, 1979; Schiøtte et al., 1993, 1989a).

-	**Trondhjemite**	**Mg-Tonalite**	**Granodiorite**	**Granite**
K_2O	0.9 - 3.0 wt. %	0.8 - 3.0 wt. %	1.0 - 3.8 wt. %	3.0 - 8.0 wt. %
Na_2O	4.0 - 6.5 wt. %	4.0 - 5.0 wt. %	3.0 - 4.5 wt. %	2.5 - 4.6 wt. %
MgO+FeO_t	1.0 - 4.0 wt. %	5.4 - 11.8 wt. %	4.0 - 7.0 wt. %	0.5 - 3.0 wt. %
TiO_2	0.1 - 0.6 wt. %	0.4 - 1.1 wt. %	0.3 - 0.8 wt. %	0.0 - 0.5 wt. %
La/Yb	90 - 220	10 - 70	10 - 80	10 - 500
CaO	2.8 - 3.9 wt. %	3.5 - 7 wt. %	2.5 - 3.2 wt. %	0.5 - 2.2 wt. %

such as MgO, FeO_t, TiO_2, CaO, K_2O and REE contents. Figure 2.10 shows major element compositions for the rocks studied here, as well as data from the literature (Bridgwater and Collerson, 1976; Schiøtte et al., 1993, 1989a), which are consistent with our findings. Granites display the lowest CaO and MgO+FeO_t+TiO_2 contents, whereas the Mg-rich tonalites show characteristic high contents for all of these major elements. The trondhjemites and granodiorites display similar CaO contents, in between the tonalites and granites, but can be discriminated from each other by their MgO+FeO_t+TiO_2 contents. While there is no systematic relationship between the age of the SCH granitoids and their whole-rock geochemical compositions, there appears to be a general temporal evolution of the SHC felsic rocks composition. The tonalites, trondhjemites, and granodiorites are more commonly found in the Eoarchean and the Paleoarchean, whereas most granites are commonly Neoarchean (Table 2.2). This broad compositional secular evolution is observed in most Archean cratons (Laurent et al., 2014).

In general, the SHC granitoids exhibit a wide range of HREE depletion with most rocks exhibiting high $(La/Yb)_N$ ratios typical of Archean TTG (La/Yb_N >15; Fig. 2.4 and 2.5). The HREE depletion in TTG is generally attributed to the presence of residual garnet in the source, which seems to be mainly controlled by the pressure of melting (*e.g.* Moyen, 2011; Nagel et al., 2012). Most SHC trondhjemites exhibit a more pronounced HREE depletion compared to the Mg-rich tonalites and granodiorites (Fig. 2.4 and 2.5), which would suggest that they were produced from melting at higher pressures. Based on Sr/Y and La/Yb ratios, Moyen (2011) divided the Archean TTG into high-pressure, medium-pressure and low-pressure felsic magmas (Fig. 2.11a). According to this plot, most SHC TTG seem to be produced at medium to high-pressures. Trondhjemites have the highest Sr/Y ratios from 150 up to 1100 (Fig. 2.11a), suggesting these magmas were produced at the highest pressures among the SHC TTG. Compared to trondhjemites, Mg-rich tonalites have trace element compositions consistent with formation at medium-pressure (Fig. 2.11a), and the only low-pressure granitoids would be the granodiorites and some granites. These geochemical compositions further suggest that the SHC trondhjemites and Mg-rich tonalites were produced at pressures between ~10-20 kbar (Moyen, 2011; Nagel et al., 2012).Using structural and field observations, Komiya et al. (2015), however, proposed that the oldest 3920 Ma Nanok/Iqaluk gneiss protolith was formed by the melting of an accretion prism at low-pressures during the subduction of an oceanic ridge. Sample SG-210c, collected from the same Iqaluk outcrop as the sample dated at 3920 Ma by Shimojo et al. (2016), is a Mg-rich tonalite exhibiting HREE depletion and geochemical compositions rather consistent with melting at medium to high-pressure (Fig. 2.4 and 2.11a). The geochemical compositions of SHC TTG, therefore, contrast with the model of shallow melting previously proposed

for the oldest granitoids. The only SHC TTG with geochemical signatures suggestive of low-pressure shallow melting is the 3330 Ma granodiorites from the Iluilik locality, which appear to be only a minor component of the SHC.

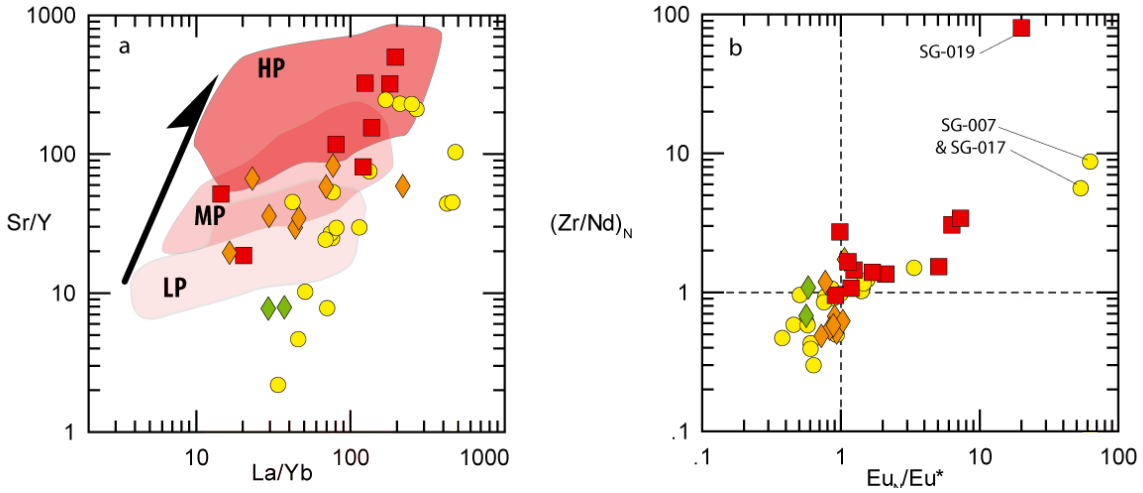

Figure 2.11

a) Sr/Y *vs.* La/Yb diagram of the SHC granitoids with field for TTG produced by variable melting pressures (Moyen and Martin, 2012). b) Zr/Nd_N *vs.* $Eu_N/Eu*$ diagram showing the correlation between the Eu anomalies and incompatible trace element ratio (Nd and Zr). Eu is normalized to chondrite, Zr and Nd are normalized to primitive mantle. Normalization values are from McDonough and Sun (1995). Symbols are as in figure 2.2.

A number of trondhjemite samples exhibit pronounced positive Eu anomalies that appear to correlate with La/Yb and Zr/Nd ratios (Fig. 2.11b). Different petrogenetic processes have been proposed to explain positive Eu anomalies in Archean granitoids such as accumulation of feldspars, fractionation of small amounts of allanite, or residual rocks from partial melting (Condie et al., 1985; Martin, 1987; Rudnick, 1992). Given the complex reworking history displayed by some SHC granitoids, supported by the high discordance of some Eoarchean zircons (Fig. 2.7a-b-c-d & supplementary tables B.3 in appendix B) and the relative abundance of secondary sector zoned zircons in the trondhjemites, it is possible that the trondhjemites which exhibit positive Eu anomalies

represent residual rocks after some extent of partial melting. In fact, all trondhjemitic samples analysed here for U-Pb include at least a small proportion of Neoarchean sector zoned igneous zircons, despite their Eoarchean crystallization ages. Fieldwork observation supports the relatively high migmatitisation of the Saglek-Hebron Complex crust, which exhibits important, if not systematic, leucocratic veins of granitic melt (see supplementary material B.1. Sample SG-019, displaying the largest Eu anomaly, mostly includes Neoarchean zircons with a few older cores (Fig. 2.7a). It is therefore likely that the SHC trondhjemites were subjected to remelting processes. Contrastingly, the Mg-rich tonalites and granodiorites do not exhibit such Eu anomalies or secondary sector zoned zircon populations, suggesting that they have not been as extensively reworked as the trondhjemitic rocks. The SHC granodiorites have a REE composition similar to modern granites as opposed to the high La/Yb ratios typically displayed by TTG (Fig. 2.5). They also exhibit lower Sr/Y ratios, more similar to low-pressure granitoids (Fig. 2.11a), and consistent with formation through shallower processes at <10 kbar (Moyen, 2011), without the presence of garnet.

The SHC granitic rocks show a wide range of HREE compositions (Fig. 2.4) and La/Yb ratios similar to, or much higher than, the TTG (Fig. 2.5). They also display variable Sr/Y ratios with compositions overlapping the high, medium and low-pressure TTG (Fig. 2.11a). Since the most likely crustal source of K-rich granitoids is a felsic precursor (Laurent et al., 2014), the wide compositional range of the SHC granitic rocks is consistent with re-melting of the older SHC trondhjemites, Mg-rich tonalites or granodiorites. Most granitic samples exhibit negative to slightly positive Eu anomalies (Fig. 2.11b) consistent with the suggested petrogenesis. The leucogranites SG-007 and SG-017 are the two exceptions that exhibit an extremely pronounced positive Eu anomaly and very low REE concentrations (Fig. 2.4 and 2.11b). These leucogranite samples,

with such pronounced positive Eu anomalies, most likely represent restites from the melting of an older crust. This is also consistent with their zircon populations. SG-017 includes mainly low Th/U Neoarchean zircons with a single inherited Paleoarchean zircon (Fig. 2.7k), whereas sample SG-007 displays a complex zircon population with a number of Eoarchean zircons that show evidence of important Pb-loss between 3800 and 3500 Ma and abundant Neoarchean re-crystallized zircons (Fig. 2.7j). This is indicative of a complex protracted crustal reworking history consistent with the restitic compositions of the leucogranite samples.

Figure 2.12 shows ternary diagrams that can be used to determine the potential source for felsic melts and therefore, the precursors of Archean granitoids. The diagram presented in Figure 2.12a was proposed by Laurent et al. (2014), which based on multiple experimental studies, discriminates granitoids as a function of the composition of their crustal precursors. Using this discrimination diagram, the SHC TTG appear to result from the melting of a mafic source characterized by variable K contents. The SHC granodiorites would be TTG derived from the most K-rich mafic precursor, whereas Mg-rich tonalites and trondhjemites would derive from low-K precursors. The SHC granitic rocks, on the other hand, are more consistent with a felsic crustal source. This would explain the relatively wide Sr/Y composition range, most likely reflecting inherited pressures of melting since there represent reworked crusts (Fig. 2.11a). Given the fact that most granites in the SHC are younger than the TTG (Table 2.2), the older Eoarchean and Paleoarchean tonalites and trondhjemites would be a likely crustal precursor to the Neoarchean granitic rocks. This is supported by the wide range of REE compositions of the granites with La/Yb ratios similar to both the Mg-rich tonalites and the trondhjemites, consistent with chemically heterogeneous sources. A number

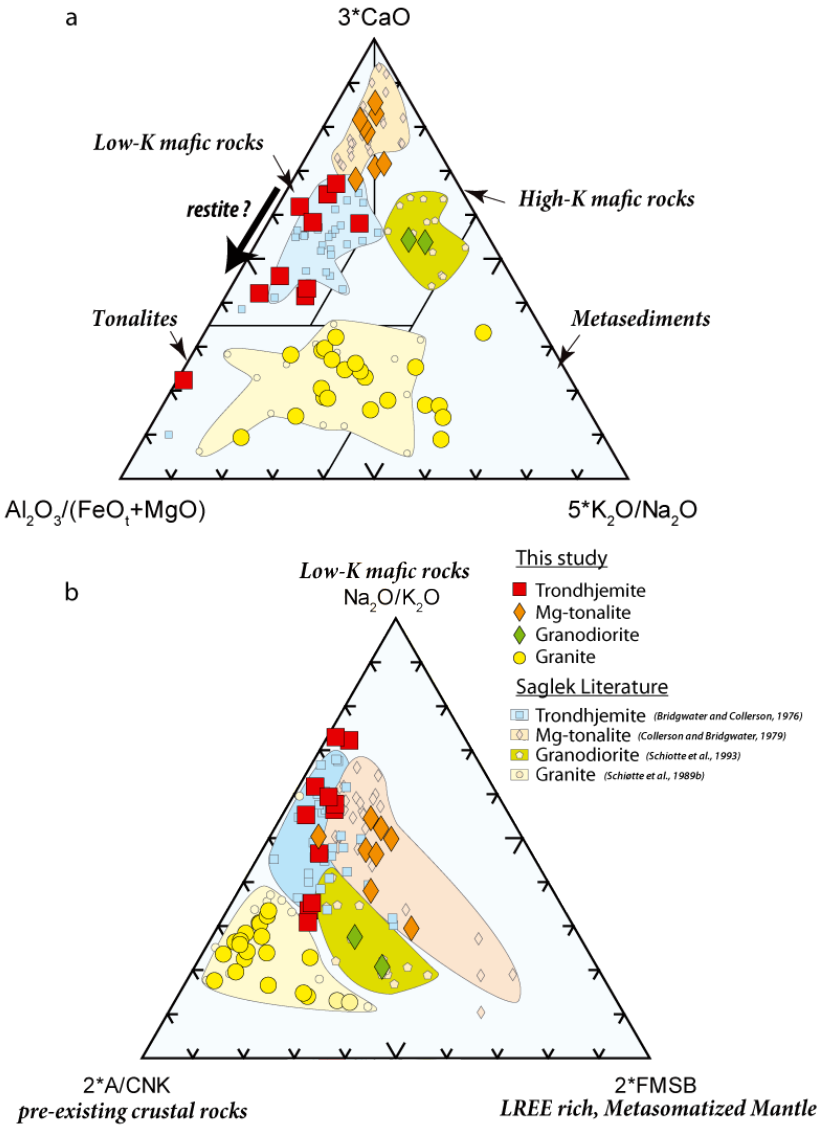

Figure 2.12

Discrimination ternary diagrams for granitoids proposed by Laurent et al. (2014). a) Major element ternary diagram showing the possible crustal source(s) for the granitoids. b) Ternary diagram showing the petrogenetic processes involved in the formation of Archean granitoids. Contribution of mantle component in the melt is highlighted by the FMSB value =[(FeO_t + MgO)wt.% x (Sr + Ba)wt.%]. Symbols and coloured fields are as in figure 2.2.

of granite samples exhibit negative Eu anomalies which could be complementary with the positive anomalies found in the trondhjemitic (perhaps restitic) rocks. The ternary diagram shown in figure 2.12b was proposed by Laurent et al. (2014) to highlight the

relative end-member petrogenetic processes involved in the formation of Archean granitoids. A high Na_2O/K_2O ratio indicates the melting of mafic rocks producing K-poor granitoids, a high A/CNK ratio is consistent with an Al-rich source such as metasediments, and the FMSB value is indicative of the interaction with a metasomatized mantle. Applied to the SHC granitoids, this diagram further supports the fact that the likely source of the tonalites and trondhjemites is a mafic crust,whereas the granites are more consistent with derivation from the melting of Al-rich felsic crust. Some Mg-rich tonalites and granodiorites plot towards the FMSB end member, suggesting that they may have interacted with, or included, a mantle component. Similar geochemical characteristics are observed in Archean sanukitoids (Laurent et al., 2014) originally defined as diorite to granodiorite with high Mg# (>0.6), Ni (>100 ppm) and Cr contents (200-500 ppm), with variable TiO_2 contents and relatively high K, Sr, Zr and Nb concentrations (Shirey and Hanson, 1984). Despite the geochemical signature that could be supportive of interaction with the mantle and the relatively high abundance of Cr-Ni displayed by the SHC Mg-rich tonalites, they still do not reach the typical enrichment in Ni-Cr-Sr found in typical sanukitoids (Heilimo et al., 2010; Martin and Moyen, 2005; Martin et al., 2009). The SHC tonalites, nevertheless, exhibit high Mg, Fe, Cr, Ti and V concentrations relative to the trondhjemites, but perhaps not quite comparable to typical Neoarchean sanukitoids.

2.5.2 Geochronology of the SHC granitoids

Early work on the SHC granitoids associated the main episodes of felsic magmatism with defined rock compositions. For example, the Uivak I gneiss was described as ∼3700-3800 Ma tonalites, whereas the Uivak II gneiss was defined as ∼3600 Ma granodi-

orites (Baadsgaard et al., 1979; Bridgwater and Schiøtte, 1991; Nutman and Collerson, 1991). It has become clear with the more recent work, however, that specific granitoid geochemical compositions are not associated with a specific age (*e.g.* Komiya et al., 2017; Kusiak et al., 2018; Vezinet et al., 2018). This is also evident from the new dataset we present in this study, that Paleo- to Eoarchean granitoids in the SHC includes trondhjemitic, tonalitic, granodioritic and granitic rocks, while Mesoarchean and Neoarchean felsic rocks comprise a majority of granites with subordinate trondhjemites (Table 2.2, Fig. 2.10-2.12). Therefore, we propose here that the terminology for the different SHC granitoid units (*e.g.* "Iqaluk" or "Uivak I", etc...) refers to distinct temporal magmatic events, regardless of geochemical compositions. Therefore, we will use names such as: "Uivak I Mg-rich tonalites", "Uivak I trondhjemites" or "Iqaluk Mg-rich tonalites", in order to refer to both, the age and respective geochemical composition.

In order to get a statistical overview of the age distribution of the felsic magmatism in the SHC, we have used Kernel density estimation diagrams (KDE; Fig. 2.13a-b) to highlight the probability of a zircon to be either metamorphic or magmatic, based on the textural and chemical characteristics of each zircons, at a given time. Probabilities from KDE, however, do not define precise timing of magmatic events or rock formation ages, which rather occur over several tens to hundreds of millions of years. Instead, KDE can provide an overview of maximum magmatic production, thermal recrystallization, relative timing between different maximums and can show whether magmatic production is punctual (sharp Gaussian peak) or diffused in time (asymmetrical peak or large wavelength Gaussian distribution). It should also be noted that sample bias or missing data can be a caveat for interpretation of these KDE.

Magmatic history

The SHC is one of the rare geological terrains on Earth preserving Eoarchean rocks. Precise and accurate age determination of Earth's oldest rocks has important implications, as it imposes timing constraints on various geological processes in order to understand the early Earth (*e.g.* Whitehouse et al., 2019). Shimojo et al. (2016) proposed an age of 3920±49 Ma for a banded grey gneiss sample (LAA995) they interpreted as from the Iqaluk gneiss. This would represent the second oldest occurrence of felsic crust on Earth, after the Acasta gneiss (Bowring and Williams, 1999; Reimink et al., 2016). Over 300 spots from 231 zircons were analysed by LA-ICP-MS for this sample, however, and only the 6 oldest zircons were used to defined this age, of which 5 yield over-concordant ages. Whitehouse et al. (2019) recently questioned the exactitude of this age and pointed out that a larger subset of analyses from this granitoid sample yields a statistically significant population with a mean $^{207}Pb/^{206}Pb$ age of 3865±4 Ma. Sample SG-210c (this study) is the same banded grey gneiss, collected on the same outcrop as sample LAA995 (Supplementary material figure B.3 in appendix B). The weighted mean Concordia age we obtained for the 34 oldest concordant zircons from sample SG-210c is 3869±6 Ma. When we apply the same data filtering method used for SG-210c to select a subset of analyses from sample LAA995 (±2% concordance; Th/U >0.3; $^{207}Pb/^{206}Pb$ age older than 3800 Ma), it defines a consistent concordant population with a well-defined Gaussian distribution around a weighted mean Concordia age of 3869±5 Ma (MSWD=1.1 N=181). Although it still represents one of the oldest rocks on Earth, the oldest Iqaluk granitoids unit is thus more consistent with a <3900 Ma age, an age displayed by other older granitoids samples over the SHC, such as 3860 ± 10 Ma (Vezinet et al., 2018); 3851 ± 46 Ma, 3829 ± 27 Ma, 3869 ± 31 Ma, 3895 ± 33 Ma and 3897 ± 33 Ma (Komiya et al., 2017); 3849 ± 260 Ma (Collerson and Bridgwater, 1979); 3863 ± 12 Ma (Schiøtte et al., 1989b).

Most granitoids from the SHC display multiple zircon populations and commonly

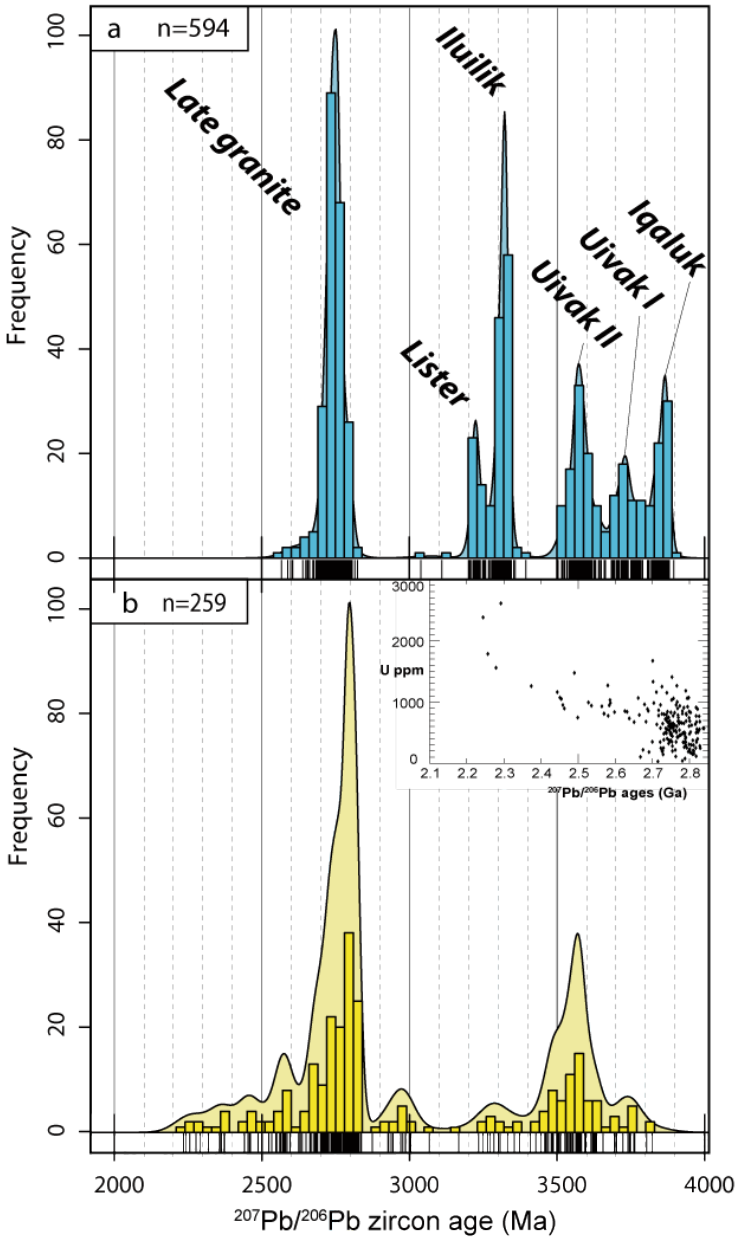

Figure 2.13

Kernel density estimate (KDE) and frequency diagrams for a) igneous zircons and b) metamorphic zircons. Top right inset on figure 2.13b shows a U (ppm) *vs.* ^{207}Pb/^{206}Pb age diagram for the Neoarchean zircons that illustrates the increase of the U concentrations in younger zircons.

exhibit signs of ancient Pb-loss, suggesting that they have been affected by complex crustal reworking history. Some trondhjemitic samples display geochemical compositions suggestive of a restitic nature, but this would not necessarily affect the U-Pb isotopic composition of the zircons crystals unless the U concentration is high (Lee et al., 1997). Figure 2.13 present KDE diagrams coupled with frequency histograms for Concordia ages of the different zircon populations for all granitoids samples analysed here. Figure 2.13a displays the probability density for concordant zircons (±2%) that exhibit Th/U ratios >0.3 and igneous textures (sector/oscillatory zoned), interpreted to represent the probability of crystallization ages. The limit of 0.3 for Th/U ratios was set based on the correlation between the rock crystallization age and the zircon's Th/U ratio. Within our dataset, the zircon grains that are closer in age to the interpreted crystallization age of their host rocks, exhibit higher Th/U ratios that are generally above 0.3. The Concordia age deconvolution analysis shows that three distinct probability peaks of zircon production are recorded during the Eoarchean and early Paleoarchean, at 3857 Ma, 3744 Ma and 3575 Ma (relative misfit of 0.131). These three oldest major magmatic events in the SHC would correspond to the units previously defined as the Iqaluk gneiss, the Uivak I gneiss and the Uivak II gneiss. In contrast to the proposed protracted and continuous magmatic activity proposed by Komiya et al. (2017), we suggest that the magmatic activity is most likely represented by three discrete magmatic pulses during the Eoarchean.

Between 3400 and 3200 Ma, two distinct generations of granitoids intruded the SHC. This is supported by the mean Concordia age of 3224 ± 7 Ma for sample SG-265 collected on Lister Island, consistent with the age for the Lister gneiss previously determined (Schiøtte et al., 1989b), and the identical ages of 3330 ± 15 Ma and 3330 ± 7 Ma, obtained respectively from samples SG-203 and SG-208. These late Paleoarchean ages

were also obtained on some SHC granitoids by Komiya et al. (2017), but these samples were all interpreted to be included in the Lister gneiss unit. The 3224 and 3330 Ma samples, however, have distinct initial ε^{176}Hf values of +1 and -6, and thus these felsic magmas derived from distinct sources and from two separate magmatic events. We therefore define the Lister gneiss unit as being emplaced at ∼3220 Ma and propose a distinct ∼3330 Ma magmatic event, referred to as the *"Iluilik"*, the local *Inuit* name for the area described as the *"opposite coast of Nulliak Island"* by Komiya et al. (2015, 2017), where samples SG-203, SG-204, SG-208, and SG-209 were collected. The Iluilik locality appears to host granitoids with a composition and age that have only previously been found in Maidmonts Island (*e.g.*Sałacińska et al. (2019); Fig. 2.1). Despite our extensive sampling, we collected only 2 samples corresponding to this granodioritic rock type (Fig. 2.4, 2.10, 2.12). Rocks described in the literature as granodiorite gneiss with an augen texture are only found in the Iluilik locality and Nulliak Island (Collerson, 1979; Schiøtte et al., 1993). This suggests that although recognizably distinct, this Iluilik magmatic event appears to be a minor component of the SHC.

A prominent Neoarchean event is dominated by granitic intrusions and defines a single magmatic peak with an age of 2750 Ma (Fig. 2.13a). This suggests that the Neoarchean thermal event generally associated with peak metamorphism in the SHC (*e.g.* Kusiak et al., 2018; Komiya et al., 2017; Van Kranendonk, 1990; Nutman et al., 1991; Schiøtte et al., 1989b), was also accompanied by an important magmatic activity.

Metamorphic history

The SHC has been subjected to a complex thermal history with prevalent metamorphism between 2700-2800 Ma, but later high-temperature events have also been

recognized (Kusiak et al., 2018; Sałacińska et al., 2018, 2019; Van Kranendonk, 1990; Schiøtte et al., 1992; Komiya et al., 2017). Figure 2.13b shows the KDE diagram of the probability density ages for recrystallized zircons and zircons exhibiting evidence of age resetting. Since it is clear that the SHC has undergone multiple metamorphic episodes, only zircons yielding concordant (±2%) ages, and thus fully reset ages, are included on figure 2.13b. A second filter has been used to only include zircons that exhibit low Th/U ratios, since all zircon ages interpreted as metamorphic recrystallization in the SHC yield Th/U ratios lower than 0.3. Eoarchean zircons consistent with a metamorphic recrystallization exhibit only one major probability peak that appears to be contemporaneous, if not slightly later, to the ∼3600 Ma Uivak II magmatic event. This would be consistent with a thermal event described in previous work (*e.g.* Sałacińska et al., 2018; Van Kranendonk, 1990; Bridgwater et al., 1975; Collerson, 1983a). These concurrent igneous and metamorphic events are supported by the presence of 3600 Ma metamorphic recrystallization rims surrounding pristine igneous oscillatory zoned 3860 Ma old zircon cores (*e.g.* SG-210c; Fig. 2.6c & 2.7g; Supplementary Table B.3 in appendix B), as well as the presence of inherited 3805 Ma igneous cores surrounded by a Uivak II oscillatory zoned crystallization (*e.g.* SG-080; Fig 2.6e & Fig 2.7m; Supplementary Material Table B.3 in appendix B). An older subordinate Eoarchean population of metamorphic recrystallized zircons is seen at ∼3750 Ma, but we suggest that these zircons could result from ancient Pb-loss in Iqaluk gneisses rather than reflecting a distinct metamorphic event. A minor metamorphic peak is also coeval with the Lister/Iluilik magmatic event (∼3200-3300 Ma) and can be observed on the KDE diagram including zircons more consistent with a metamorphic origin (Fig. 2.13b). These zircons, however, mainly come from only two samples (granite samples SG-007 and SG-208). While sample SG-007 contains zircons exhibiting strong evidence

of ancient Pb-loss (Fig. 2.7j), zircons from sample SG-208 exhibits clear metamorphic characteristics which define a much tighter population, compared to SG-007 zircons, with ages succeeding the main igneous event at 3250 Ma (Fig. 2.7r). A slight metamorphic event appears to be associated with the 3220 Ma Lister magmatic event, However, this 3250 Ma metamorphic event remains equivocal due to the lack of resolution of the KDE diagram. Similarly, the single Iluilik granodiorite sample SG-203 exhibits a tight zircon population that yields a mean $^{207}Pb/^{206}Pb$ age at 2975 ± 17 Ma, which could indicate a ∼3000 Ma thermal event. Considering the relative rarity of these populations and the total absence of magmatic or metamorphic records for this age, this interpretation remains highly speculative and this may simply reflect ancient Pb-loss produced by an Eoarchean metamorphic event.

The highest probability peak of recrystallization occurs during the Neoarchean (Fig. 2.13b), which is consistent with the extensive metamorphic event previously suggested at 2700 Ma (*e.g.* Kusiak et al., 2018; Schiøtte et al., 1989b). However, our maximum of recrystallized zircon ages appears to occur closer to 2800 Ma, perhaps shortly before the 2750 Ma Neoarchean peak defined by igneous zircons (Fig. 2.13a). This may suggest a slight delay (∼50 Ma) between the maximum intensity of the thermal event and the maximum probability of granitic magmatism. The overall distribution of the Neoarchean recrystallized zircons shows an asymmetric peak shape that reaches its maximum at 2800 Ma, before gradually decreasing to lower probabilities until 2200 Ma, after which no zircon is produced in the SHC. This could be an artefact from our selection criteria used to build the KDE diagram combined with the analytical precision, that would comprised a minor amount of zircon that experienced incomplete lead loss. However, we cannot disregard the possibility that it suggests protracted granulite facies metamorphism occurring over at least 80 Ma, before gradually decreasing until 2400-

2200 Ma. This would be consistent with what was suggested by Kusiak et al. (2018), evidenced by the zircon ages they obtained between 2700 and 2200 Ma, that correlate with U concentrations (Fig. 2.13b top right inset). The high U concentrations in some zircons could have increased the susceptibility of the U-Pb system to be reopened (Lee et al., 1997). Therefore, in such a scenario, a protracted thermal event that gradually decreased in intensity would keep the U-rich zircons in isotopically open conditions longer than those with lower U contents. The latter would then record older ages compared to the more U-rich zircons. This protracted thermal event is also in agreement with what was suggested by Kusiak et al. (2018) based on younger ages obtained on monazite and apatite in the SHC that yielded respectively at 2600-2500 and 2200 Ma.

2.5.3 Crustal sources and reworking history

Combined U-Pb and Hf isotopes in zircons have been widely used to study the crustal evolution of early gneissic complexes (*e.g.* Iizuka et al., 2009; Reimink et al., 2016; Guitreau et al., 2014; Næraa et al., 2012; O'Neil et al., 2013; Vezinet et al., 2018) and the Earth's oldest detrital zircons from the Jack Hills conglomerate (*e.g.* Amelin et al., 1999; Harrison, 2005; Harrison et al., 2008; Blichert-Toft and Albarède, 2008; Kemp et al., 2010). Even though the U-Pb-Hf isotopic composition of the Eoarchean and Hadean Jack Hills detrital zircons provided invaluable information about the early crust, the fact that their host granitoid rocks have been eroded away limits the constraints we can put on the earliest crustal history. It can also be difficult to clearly establish the crystallization age of detrital zircons because of possible ancient Pb-loss, which would result in younger apparent $^{207}Pb/^{206}Pb$ ages and consequently bias the calculated initial Hf isotopic composition (*e.g.* Vervoort and Kemp, 2016). The SHC zircons studied here are all from rock samples with a single interpreted crystallization

age. To avoid the possible calculation of the Hf isotopic compositions at an incorrect apparent Pb-Pb age, we have calculated the initial Hf isotopic composition of all magmatic zircons to the crystallization age of their respective host rock and considered the average zircon initial ε^{176}Hf value for each granitoid (Table 2.2, Figure 2.9 & 2.14a). The composition of the crustal precursor from which the felsic zircon-bearing host granitoid was derived often needs to be assumed in order to interpret variations in initial ε^{176}Hf values in zircons through time and to study the evolution of crustal sources. If we compare a felsic and a mafic crustal precursor formed at the same time and from the same source, the felsic precursor will evolve with a lower Lu/Hf ratio, and to lower ^{176}Hf/^{177}Hf ratios, compared to the mafic precursor (Fig. 2.14b). Although we still need to assume a Lu/Hf ratio for the crustal precursor(s) from which the SHC granitoids were derived, we use here the geochemical composition of each of the host rock samples to better constraint the composition of their crustal sources and evolution. As discussed previously, the geochemical compositions of SHC TTG suggest they derive from the melting of a mafic precursor, while the granitic rocks are consistent with the melting of a felsic crustal source (Fig. 2.12a).

The Eoarchean Iqaluk and Uivak I gneisses exhibit positive initial ε^{176}Hf values from +1.7 to +3.7, between 3700 and 3900 Ma (Fig. 2.14a), suggesting that the precursor source of these granitoids had a suprachondritic Hf isotopic composition in the Eoarchean. This contrasts with zircons from most other Eoarchean TTG, generally displaying chondritic or subchondritic initial ε^{176}Hf values (*e.g.* Iizuka et al., 2009; Reimink et al., 2016; Guitreau et al., 2014; Næraa et al., 2012; O'Neil et al., 2013), leading some authors to suggest that widespread depletion of the mantle, at least in terms of Lu-Hf, did not take place prior to ∼3800 Ma (*e.g.* Vervoort and Kemp, 2016). Vezinet et al.

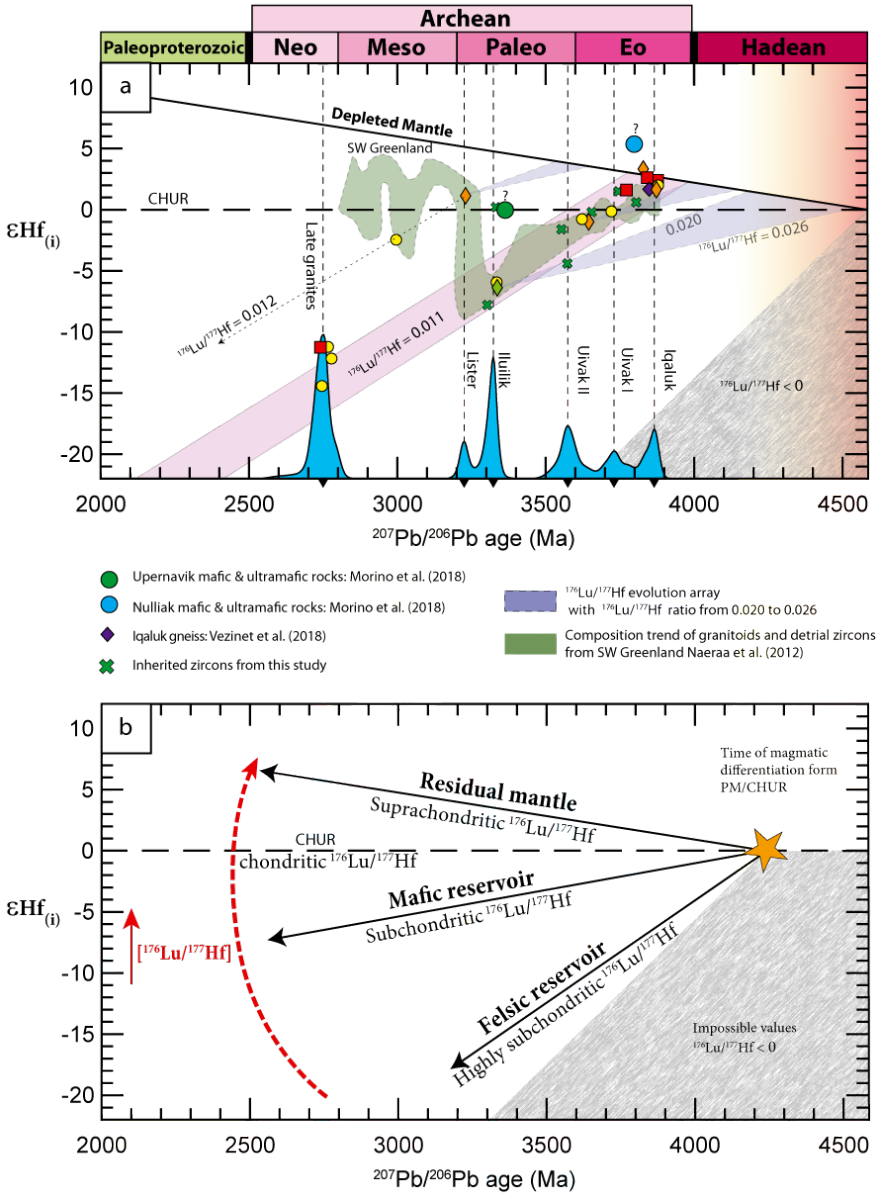

Figure 2.14

a) Initial Hf values *vs.* $^{207}Pb/^{206}Pb$ age diagram for the SHC rocks. Green field shows data for the SW Greenland TTG and detrital zircons from Næraa et al. (2012). Zircon data from Vezinet et al. (2018) were recalculated at the crystallization age of the host TTG. Data from Morino et al. (2018) is from whole-rock Lu-Hf isochrons for mafic and ultramafic rocks. Blue field is the KDE from figure 2.13 for igneous zircons. -b) Schematic diagram showing the relative evolutions for reservoirs with different $^{176}Lu/^{177}Hf$ ratios.

(2018) recently analyzed the Hf isotopic composition of zircons from a single SHC TTG sample dated at 3860 Ma and concluded that it displayed chondritic initial ε^{176}Hf values within uncertainty. However, when the ε^{176}Hf values for each analyzed zircons from this sample are all calculated at the crystallization age of the host rock of 3860 Ma, it yields an average initial ε^{176}Hf value of $+1.6 \pm 0.2$ (2 S.E.), consistent with the slight suprachondritic Hf isotopic compositions we have obtained for all SHC Eoarchean granitoids analyzed here (Fig. 2.14a). We, therefore, argue that the oldest granitoids from the SHC were sourced from a depleted reservoir characterized by a suprachondritic Lu/Hf ratio. The Iqaluk sample SG-026 yields the highest initial ^{176}Hf/^{177}Hf with corresponding to an initial ε^{176}Hf value of +3.2 at 3820 Ma. In order to evolve to such positive ε^{176}Hf values, a reservoir formed at 4568 Ma with chondritic ^{176}Hf/^{177}Hf would need a ^{176}Lu/^{177}Hf ratio of 0.0435, which is higher than most estimation for the present-day depleted mantle (*e.g.* Blichert-Toft and Puchtel, 2010). The age of 3820 Ma for SG-026 was however determined from the upper intercept of the discordia line (Fig. 2.7e) and one could argue that this age may have been overestimated, leading to a higher calculated initial ε^{176}Hf value. The zircon population for this sample, however, is homogeneous with the oldest concordant zircon yielding a ^{207}Pb/^{206}Pb age of 3793 Ma, which would only lower its average ε^{176}Hf initial value to $+2.6 \pm 0.2$. Furthermore, the other SHC Eoarchean granitoids also have suprachondritic initial ε^{176}Hf values corresponding time-integrated ^{176}Lu/^{177}Hf ratios for their source ranging from 0.0393 to 0.0412. This would suggest that the crustal precursor source of the SHC Eoarchean granitoids was derived from a mantle with a comparable degree of depletion as the present-day depleted mantle with ^{176}Lu/^{177}Hf = 0.03933, (Blichert-Toft and Puchtel, 2010).

The 3883 Ma sample SG-007 exhibits a granitic composition contrasting with the majority of the Iqaluk samples that mostly exhibit trondhjemitic or Mg-rich tonalites

compositions. As discussed previously, granites are likely produced from crustal reworking of a felsic precursor. The lack of evidence for an older felsic source to SG-007 could suggest that its granitic composition is more consistent with later reworking, perhaps during the Neoarchean, which may have affected the whole-rock geochemical composition while preserving Eoarchean zircons and the Lu-Hf signature.

The Uivak gneiss has previously been interpreted to result from the melting of the Nulliak mafic supracrustal rocks (Komiya et al., 2015, 2017; Nutman and Collerson, 1991; Shimojo et al., 2016; Morino et al., 2018). A Lu-Hf isochron, mainly including ultramafic rocks interpreted to be from the Nulliak assemblage, yielded an initial ε^{176}Hf value of +5.1 at 3794 Ma (Morino et al., 2018) with $\varepsilon^{176}\mathrm{Hf}_{(3770Ma)}$ for individual samples as high +12.8. No zircons from SHC granitoids have however yielded such high initial ε^{176}Hf values (This study; Vezinet et al., 2018). The highly positive ε^{176}Hf values of the Nulliak rocks may in part be due to some extent of disturbance of the Lu-Hf isotopic system, as suggested by the high MSWD value of 142 of the Lu-Hf isochron (Morino et al., 2018). It nevertheless suggests that the SHC includes Eoarchean mafic/ultramafic crust with suprachondritic Hf isotopic compositions, which would be a possible crustal source for the Iqaluk and Uivak I TTG. Since the Iqaluk granitoids are older than any age previously obtained from the Nulliak mafic rocks, it could be argued that the Nulliak metabasalts cannot represent the precursor source of the oldest SHC granitoids. However, all long-lived isotopic systems used to constrain the age of the Nulliak mafic rocks, such as Sm-Nd, Lu-Hf or Re-Os (Morino et al., 2017, 2018; Collerson et al., 1991; Ishikawa et al., 2017), show evidence of some degree of disturbance with large errors on isochron ages (hundreds of Ma), therefore, we cannot rule out the Nulliak mafic rocks as the possible source of the Iqaluk gneiss.

Although trondhjemites and Mg-rich tonalites are more dominant within the Eoarchean

Iqaluk and Uivak I gneisses, tonalitic samples also occur within the ~3600 Ma Uivak II and ~3200 Ma Lister gneisses. The Uivak II tonalitic sample has a slight subchondritic initial ε^{176}Hf value of -1.1 at 3632 Ma. While reworking of Eoarchean felsic crust evolving with a low ^{176}Lu/^{177}Hf ratio of ~0.010 could explain the Hf isotopic composition of the zircons from this Uivak II tonalite (Fig. 2.14a), its whole-rock geochemical composition is inconsistent with remelting of a felsic precursor, but rather suggests derivation from a mafic crustal source (Fig. 2.12a). Assuming a ^{176}Lu/^{177}Hf ratio between 0.020 and 0.026 for this mafic precursor crust (Kemp et al., 2010; Blichert-Toft and Albarède, 2008), it would suggest a Hadean age between ~4000 and ~4200 Ma for the mafic crustal source of the Uivak II tonalite, if this mafic crust was derived from a long-term depleted mantle-like reservoir (Fig. 2.14a, 2.15). This mafic precursor crust could be younger, between 3700 and 3900 Ma, if it was sourced from a reservoir with chondritic Hf compositions, but there is no evidence for the occurrence of an Eoarchean mafic reservoir with chondritic Hf isotopic compositions in the SHC. As mentioned previously, the Lu-Hf isotopic data from the few Eoarchean Nulliak mafic samples that have been analysed by Morino et al. (2018) rather point toward slightly suprachondritic compositions (Fig. 2.14a).

The 3224 Ma Lister tonalitic gneiss is the only post-Eoarchean granitoid in the SHC with zircons displaying slightly suprachondritic initial ^{176}Hf/^{177}Hf ratios (Fig. 2.14a), corresponding to a positive initial ε^{176}Hf value of +1.0. This value contrasts with the lower initial ε^{176}Hf value of ~-6 for the 3330 Ma Iluilik granitoids, suggesting that although these granitoid units were produced only ~100 Ma apart, they were derived from sources with distinct early histories. If we consider a mafic composition for the crustal precursor of the Lister tonalitic gneiss (Fig. 2.12a), it would suggest that the tonalite was derived from the melting of ~3500 Ma to ~3700 Ma mafic crust (Fig. 2.14a).

Morino et al. (2017, 2018) proposed the occurrence of a Paleoarchean suite of mafic rocks in the SHC, but these have chondritic $^{176}Hf/^{177}Hf$ compositions at ~3400 Ma, and thus not a suitable precursor source for the Lister gneiss. Other mafic rocks in the SHC that could be potential sources for the ~3200 Ma Lister tonalites would include the ~3800 Ma Nulliak mafic supracrustal rocks or perhaps the Paleoarchean Saglek dikes.

The ~3300 Ma Iluilik granitoids analysed here include a granite and a granodiorite samples with comparable initial $\varepsilon^{176}Hf$ values of ~-6. While the granitic sample can be produced by reworking of the older SHC Eoarchean felsic crust (Fig. 2.14a), the whole-rock geochemical composition of the granodiorite would be more consistent with a mafic crustal source (Fig 2.12a). In order for a mafic reservoir with a $^{176}Lu/^{177}Hf$ between 0.020 and 0.026 to evolve to an initial $\varepsilon^{176}Hf$ value of -6 at 3300 Ma, it would need to be ~4200 to ~4500 Ma and thus Hadean in age (Fig. 2.14a, 2.15).The Iluilik granodiorites have, however, higher K contents compared to the trondhjemites and Mg-rich tonalites. They have intermediate compositions, for most major elements, between the granites and the tonalites (Fig. 2.3) and their REE compositions are more similar to low-pressure TTG (Moyen, 2011), contrasting with the HREE depletion observed in other SHC TTG (Fig. 2.4, 2.11) and perhaps suggesting a distinct petrogenetic process for their formation. The relatively high K content of the Iluilik TTG would be consistent, if they are derived from a mafic source, with a more enriched, potassic mafic crust (Fig. 2.12a-b). No evidence of Hadean mafic crust has been observed in the SHC, but the existence of Hadean hydrothermally altered enriched mafic crust has been proposed as the source of the Jack Hills detrital zircons (Kemp et al., 2010) and the Nuvvuagittuq TTG (O'Neil et al., 2013; O'Neil and Carlson, 2017).

Except for sample SG-087, all SHC granites define a initial $\varepsilon^{176}Hf$ *vs.* time trend

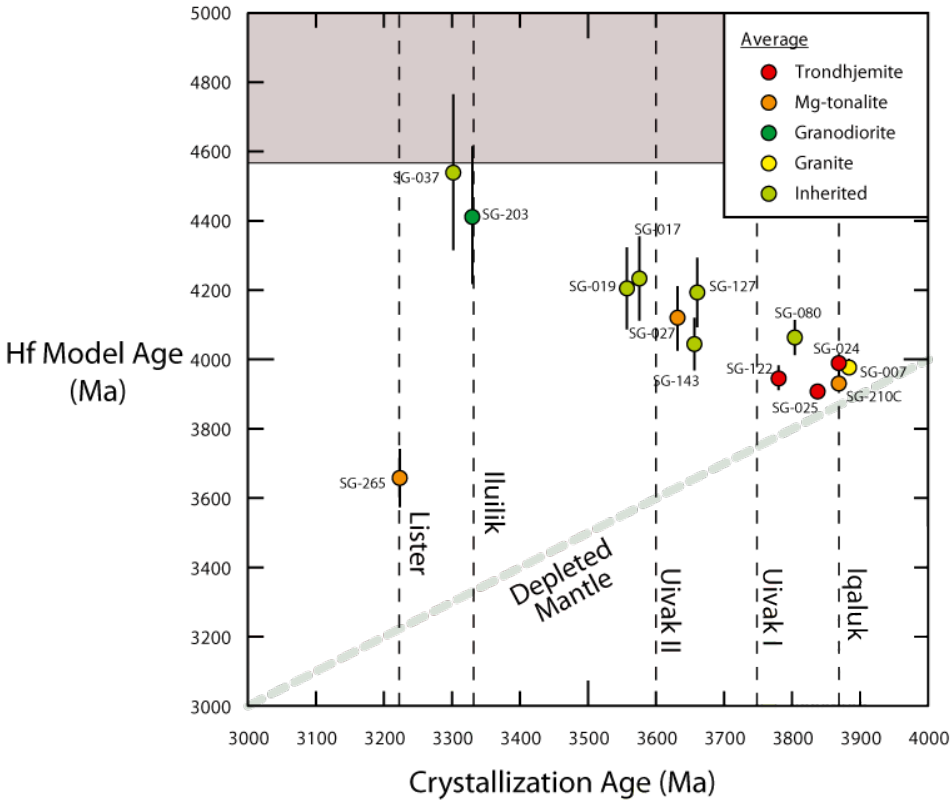

Figure 2.15

Hf model ages *vs.* crystallization ages diagram for the SHC TTG, including inherited zircons.. The vertical bars for each sample represent the variation of model ages using $^{176}Lu/^{177}Hf$ ratios of 0.020 and 0.026, with the symbols plotted as the average.

consistent with reworking of an Eoarchean felsic reservoir evolving with a $^{176}Lu/^{177}Hf$ of ∼0.010 that originates from the Iqualuk/Uivak I gneisses (Fig. 2.14a). Most inherited zircons are found in granitic samples and follow the same felsic reservoir trend (Fig. 2.14a), which further supports the fact that the granites are produced from the melting of the Eoarchean felsic crust. The combined whole-rock geochemical and Hf isotopic compositions of the granitic rocks of Iqaluk, Uivak I, Uivak II, Iluilik and Neoarchean ages, therefore suggest that they were produced from the remelting of the SHC Eoarchean tonalites/trondhjemites over ∼1 billion years. The ∼3000 Ma granitic sample SG-087, however, would be consistent with the reworking of the ∼3200 Ma Lis-

ter gneiss rather than the Eoarchean TTG. Except for one trondhjemite sample, all Neoarchean granitoids analysed here are granitic in composition, containing zircons with low initial $^{176}Hf/^{177}Hf$ ratios. This suggests that the ~2750 Ma felsic magmatism is dominated by remelting older felsic crust, with little to no input from a more juvenile source. The major Neoarchean high-grade metamorphic event that affected the SHC, therefore, appears to also have been accompanied by important crustal reworking and anataxis.

Given that the SHC is part of the North Atlantic Craton, it is often compared to the Itsaq Gneiss Complex of Southwest Greenland, also comprising Eoarchean TTG and supracrustal rocks. Figure 2.14a shows the evolution of Hf isotopic compositions for detrital and igneous zircons from southwest Greenland (Næraa et al., 2012) compared to the SHC igneous zircons. The Eoarchean zircons from Greenland overall display lower initial $\varepsilon^{176}Hf$ values, with mostly chondritic to slightly subchondritic compositions, compared to the SHC where the 3700-3900 Ma zircons generally display positive initial $\varepsilon^{176}Hf$ values (Fig. 2.14a). The Hf isotopic compositions of zircons from both SW Greenland and the SHC are consistent with reworking of Eoarchean crust until the late-Paleoarchean when it abruptly shifts from low initial $\varepsilon^{176}Hf$ values around 3300 Ma to suprachondritic compositions at ~3200 Ma (Næraa et al., 2012; Hoffmann et al., 2011, Fig. 2.14a). Neoarchean zircons from both complexes, however, display contrasting Hf compositions. The SW Greenland zircons recorded important input of juvenile crust with mostly positive initial $\varepsilon^{176}Hf$ values between 2800 and 2500 Ma (Næraa et al., 2012, 2014), while the Neoarchean granitoids from the SHC have zircons displaying very negative $\varepsilon^{176}Hf$ values, consistent with the continued reworking of older felsic crust and without the involvement of newly formed mantle-derived rocks. Therefore, even if the SHC and SW Greenland appear to share a similar early crustal

evolution, their Neoarchean histories diverge. The striking shift to more juvenile initial Hf isotopic compositions after 3200 Ma in SW Greenland was interpreted by Næraa et al. (2012) to represent a change of geodynamic setting that involved juvenile crust generation by plate tectonic processes. Although this shift to more juvenile compositions seems to have been also recorded in the SHC, the reworking of older continental crust appears as the dominant process forming the Neoarchean rocks in the SHC.

2.5.4 Tectonic context of the SHC

One of the most highly debated subjects about the early Earth concerns the tectonic setting operating and responsible for the formation of the Archean cratons. The geochemical and isotopic compositions of rocks from early terrains have been widely used to constrain the tectonic environments in which they formed, but there is still no consensus on Earth's early geodynamics. Previous work has also proposed possible geodynamic contexts for the formation of the SHC. Although the compositions of the SHC metavolcanic rocks do not exhibit geochemical signatures typically found in suprasubduction environments (Wasilewski et al., 2019), Komiya et al. (2015) suggested evidence of Eoarchean subduction settings in the SHC. Based on field and structural observations, they describe the stratigraphy of the Nulliak supracrustal assemblage as an analogue to the duplex structures observed in the Japanese trench, interpreted as large accretion prisms. In this model, the Uivak I granitoids would be produced from the melting of basaltic crust within an accretionary complex at shallow depths. However, Uivak I and Iqaluk TTG exhibit strong HREE depletions (Fig. 2.4) consistent with the melting of a garnet-bearing precursor at relatively high-pressures (Fig. 2.11), which is at odds with shallow-level melting of a tholeiitic possibly komatiitic crust.

Although U-Pb and Hf isotopes cannot directly be linked to tectonic settings, these

data can help to constrain the type of crustal precursor and its reworking history, to better establish the architecture of the reworked crustal sources and evaluate which tectonic context would be more likely. Figure 2.15 shows the crystallization age *vs.* Hf model age for the zircons from the SHG TTG with compositions consistent with derivation from a mafic crustal precursor. Model ages are obtained using the zircon average initial $^{176}Hf/^{177}Hf$ ratios for each of the samples, back calculated to the depleted mantle evolution line, and assuming a $^{176}Lu/^{177}Hf$ between 0.020 and 0.026 for a mafic crustal reservoir (Blichert-Toft and Albarède, 2008; Kemp et al., 2010). Figure 2.15 also includes inherited zircons from granitic samples, which likely crystallized within their tonalitic/trondhjemitic precursor. The zircons from Eoarchean granitoids are the only samples with relatively juvenile compositions, consistent with the remelting of almost contemporaneous mafic crust, potentially the Nulliak basaltic crust. The younger Uivak II and Iluilik granitoids appear to be derived from the melting of pre-Nulliak Hadean mafic crust. In the case of the 3330 Ma Iluilik TTG, its mafic precursor source with a Hf model age of ∼4200-4400 Ma, seems to have survived ∼1 billion years before it was reworked. The presence of such a long-lived Hadean mafic crustal source was also recorded in the Northeastern Superior Province (O'Neil and Carlson, 2017). Except for the Lister gneiss (SG-265), the SHC granitoids derived from the melting of mafic crust show a negative correlation between their crystallization age and their Hf model age, suggesting that the latest granitoids were produced from the melting of the oldest crustal source. In a modern-style subduction setting, it would be unlikely that: −1) the subducting mafic crustal reservoir displayed such a wide age range (from ∼3900 to ∼4400 Ma) and −2) the oldest portions of the subducting mafic crust melted the latest. While one could suggest that a thick mafic crust, similar to an oceanic plateau, could include mafic crust with the range of ages suggested by the Hf model ages from

Figure 2.15, it would be expected that the base of this thickened mafic crust, *i.e.* the oldest portions, melts before the younger overlying portions. This is inconsistent with the negative trend observed in Figure 2.15. As an alternative for both uniformitarian and non-uniformitarian models, some authors have proposed a subcretion model (Barr et al., 1999; Ducea et al., 2009; Grove et al., 2003; Hacker et al., 2015; Taramon et al., 2015). Tectonic models involving sequential stacking or tectonic imbrication have been suggested as a mechanism for early Archean crustal growth (*e.g.* de Wit, 1986; Smithies and Champion, 2000) and for the formation of the Eoarchean Itsaq Gneiss Complex of Southwest Greenland (Nutman et al., 2007; Nutman and Bennett, 2019).This tectonic regime has the potential to imbricate or stack portions of the mafic crust of variable ages in a configuration where older crust could overlie younger crust and perhaps melt later, in a thickened oceanic crust. Reworking of such an imbricated mafic crustal source could explain the crystallization age *vs.* Hf model age trend was seen for the SHC TTG. It could also be consistent with the fact the late Paleoarchean Iluilik TTG, derived from the oldest (>4200 Ma) crustal source, shows geochemical compositions similar to low-pressure TTG, suggesting that the older portions of the crustal precursor were perhaps at shallower levels.

2.6 Conclusion

The SHC granitoids recorded over more than 1 billion years of complex crustal history, including several episodes of felsic magmatism. The different generations of gneisses in the SHC were previously associated with certain geochemical characteristics, but they appear to be more geochemically and petrologically diverse. We, therefore, suggest that the different gneissic units should refer to distinct temporal magmatic

events regardless of their exact composition. Six major distinct felsic magmatic events can be identified in the SHC: the oldest 3850 Ma Iqaluk gneiss, the 3750 Ma Uivak I gneiss, the 3600 Ma Uivak II gneiss, the 3330 Ma Iluilik gneiss, the 3230 Ma Lister gneiss, and the 2700-2800 Ma Neoarchean granites. The Eoarchean gneisses are dominated by high-Mg tonalites and trondhjemites, whereas the Neoarchean felsic intrusions are mostly granitic in composition. The slightly suprachondritic Hf isotopic composition of the Eoarchean zircons from the SHC granitoids denote the existence of a long-term depleted source, contrasting with the chondritic to subchondritic Hf compositions that most Eoarchean zircons from other early terrains exhibit. Most of the juvenile continental crust in the SHC appears to have been formed during the Eoarchean, after which the magmatic activity is dominated by crustal reworking of the earlier TTG. Considering the whole-rock geochemical composition of the SHC granitoids to constraint the nature of their crustal precursor, the Hf isotopic compositions of the different generations of TTG suggest the remelting of Eoarchean to Hadean mafic crust. The juvenile Iqaluk and Uivak I TTG are consistent with remelting of ∼3800-3900 Ma mafic crust at relatively high-pressures, potentially the Nulliak basaltic rocks, while the younger Uivak II and Iluilik TTG would suggest melting of increasingly older (up to ∼4400 Ma) mafic sources at medium and low-pressures. Such long-lived Hadean mafic crust may have been formed by subcretion tectonics, which could explain the later reworking of the oldest mafic crustal source. Similar to what is observed in Southwest Greenland, the zircon Hf isotopic compositions of the SHC granitoids show a marked transition between ∼3300 and 3200 Ma from relatively unradiogenic compositions to more juvenile compositions. The Neoarchean felsic magmatism in the SHC, however, appears to be dominated by reworking of the Eoarchean TTG, without the contribution of juvenile material.

Supplementary material: Appendix B

Figure B.1 : Fieldwork photographs of the mafic and ultramafic rocks.

Figure B.2 : Thin section photomicrographs of the mafic and ultramafic rocks.

Figure B.3: Schematic of the outrcrop from Shimojo et al. (2016), where the Iqaluk gneiss has been described and dated at 3920 Ma. The precise location of sample SG-210c (this study) and the sample LAA995 (Shimojo et al., 2016) of Iqaluk gneiss are shown respectively in black and green boxes.

Figure B.4: SConcordia plot of the GJ-1 and 91500 for both analytical session.

Table B.1: Analytical methods for isotope analysis for U-Pb, Lu-Hf and LA-ICP-MS.

Table B.2: Full Standard measurement table.

Table B.3: Full geochronological data of the 18 granitoids.

Table B.4: Full data set of the in-situ Lu-Hf composition analysis.

References

Amelin, Y., Lee, D.-C., Halliday, A. N., Pidgeon, R. T., 1999. Nature of the Earth's earliest crust from hafnium isotopes in single detrital zircons. Nature 399, 252–255.

Baadsgaard, H., Collerson, K. D., Bridgwater, D., 1979. The Archean gneiss complex of northern Labrador. 1. Preliminary U-Th-Pb geochronology. Canadian Journal of Earth Sciences, 951–961.

Barker, F., 1979. Trondhjemites: definition, environment and hypotheses of origin. In: Trondhjemites, Dacites and Related Rocks,, barker,f. Edition. Elsevier, Amsterdam, pp. 1–12.

Barr, S. R., Temperley, S., Tarney, J., 1999. Lateral growth of the continental crust through deep level subduction-accretion: a re-evaluation of central Greek Rhodope. Lithos 46, 69–94.

Blichert-Toft, J., Albarède, F., jan 2008. Hafnium isotopes in Jack Hills zircons and the formation of the Hadean crust. Earth and Planetary Science Letters 265 (3-4), 686–702.

Blichert-Toft, J., Puchtel, I. S., 2010. Depleted mantle sources through time: evidence from Lu-Hf and Sm-Nd isotope systematics of Archean komatiites. Earth and Planetary Science Letters 297, 598–606.

Bouvier, A., Vervoort, J. D., Patchett, P. J., 2008. The LuHf and SmNd isotopic composition of CHUR: Constraints from unequilibrated chondrites and implications for the bulk composition of terrestrial planets. Earth and Planetary Science Letters 273 (12), 48–57.

Bowring, S. a., Williams, I. S., 1999. Priscoan (4.00-4.03 Ga) orthogneisses from northwestern Canada. Contributions to Mineralogy and Petrology 134 (July 1998), 3–16.

Bridgwater, D., Collerson, K. D., 1976. The major petrological and geochemical characters of the 3,600 m.y. Uivak gneisses from Labrador. Contributions to Mineralogy and Petrology 54 (1), 43–59.

Bridgwater, D., Collerson, K. D., Hurst, R. W., Jesseau, C. W., 1975. Field characters of the early precambrian rocks from Saglek, Coast of Labrador. Geological survey of Canada 75 (1), 287–296.

Bridgwater, D., Schiøtte, L., 1991. The Archean gneiss complex of northern Labrador. A review of current results, ideas and problems. Bulletin of the Geological Society of Denmark 39 (3-4), 153–166.

Burnham, A. D., Berry, A. J., 2017. Formation of Hadean granites by melting of igneous crust. Nature Geoscience 10 (6).

Collerson, K., 1979. Early Archean Crustal Relationships in the Saglek-Hebron Area - Northern Labrador. LPI Contributions 371, 19–21.

Collerson, K., 1983a. Ion Microprobe Zircon Geochrnonology of the Uivak Gneiss: Implication for the evolution of the early terrestrial crust in the north Atlantic craton. Workshop on a Cross Section of Archean Crust. LPI Technical report, 83-03, 28–33.

Collerson, K., 1983b. The Archean gneiss complex of northern Labrador. 2. Mineral ages, secondary isochrons, and diffusion of strontium during polymetamorphism of the Uivak gneisses. Can. J. Earth Sci. 20, 707–718.

Collerson, K. D., Bridgwater, D., 1979. Metamorphic development of early archean tonalitic and trondhjemitic gneisses: Saglek area, Labrador. In: Barker, F. (Ed.), Trondhjemites, Dacites, and related rocks. Vol. 6. U.S. Geological Survey, Denver, Colorado, Ch. 7, pp. 205–273.

Collerson, K. D., Campbell, L. M., Weaver, B. L., Palacz, Z. A., 1991. Evidence for extreme mantle fractionation in early Archean ultramafic rocks from northern Labrador. Nature 349 (6306), 209–214.

Condie, K., Bowling, G., Allen, P., 1985. Missing Eu anomaly and Archean high-grade granites. Geology 13, 633–636.

de Wit, M., 1986. What the oldest rocks say. In: Ashwal, L., Burke, K., de Wit, M., Wells, G. (Eds.), The Earth as a Planet. Lunar and Planetary Institute, Houston, Texas. Lunar and Planetary Institute Technical Report 86-08.

Ducea, M. N., Kidder, S., Chesley, J. T., Saleeby, J. B., 2009. International Geology Review Tectonic underplating of trench sediments beneath magmatic arcs: the central California example.
URL http://www.tandfonline.com/action/journalInformation?journalCode=tigr20

Fisher, C. M., Vervoort, J. D., Dufrane, S. A., 2014a. Accurate Hf isotope determinations of complex zircons using the laser ablation split stream " method. Geochemistry Geophysics Geosystems 15 (1), 121–139.

Fisher, C. M., Vervoort, J. D., Hanchar, J. M., 2014b. Guidelines for reporting zircon Hf isotopic data by LA-MC-ICPMS and potential pitfalls in the interpretation of these data. Chemical Geology 363, 125–133.
URL http://dx.doi.org/10.1016/j.chemgeo.2013.10.019

Grove, M., Jacobson, C. E., Barth, A. P., Vucic, A., 2003. Temporal and spatial trends of Late Cretaceous-early Tertiary underplating Pelona and related schist beneath southern California and southwestern Arizona. In: Special Paper 374: Tectonic evolution of northwestern Mexico and the Southwestern USA. Geological Society of America, pp. 381–406.

Guitreau, M., Blichert-Toft, J., Mojzsis, S., Roth, A., Bourdon, B., Cates, N., Bleeker, W., jun 2014. LuHf isotope systematics of the HadeanEoarchean Acasta Gneiss Complex (Northwest Territories, Canada). Geochimica et Cosmochimica Acta 135, 251–269.
URL https://www-sciencedirect-com.proxy.bib.uottawa.ca/science/article/pii/S001670371400218X

Hacker, B. R., Kelemen, P. B., Behn, M. D., 2015. Continental Lower Crust. Annual Review of Earth and Planetary Sciences 43 (1), 167–205.

Harrison, T. M., dec 2005. Heterogeneous Hadean Hafnium: Evidence of Continental Crust at 4.4 to 4.5 Ga. Science 310 (5756), 1947–1950.
URL http://www.sciencemag.org/cgi/doi/10.1126/science.1117926

Harrison, T. M., Schmitt, A. K., McCulloch, M. T., Lovera, O. M., apr 2008. Early (4.5 Ga) formation of terrestrial crust: LuHf, δ18O, and Ti thermometry results for Hadean zircons. Earth and Planetary Science Letters 268 (3-4), 476–486.
URL http://linkinghub.elsevier.com/retrieve/pii/S0012821X08000897

Heilimo, E., Halla, J., Heltte, P., 2010. Discrimination and origin of the sanukitoid series: Geochemical constraints from the Neoarchean western Karelian Province (Finland). Lithos 115 (1-4), 27–39.
URL http://dx.doi.org/10.1016/j.lithos.2009.11.001

Hoffmann, J., Zhang, C., Moyen, J.-F., Nagel, T., 2019. The Formaton of Tonalite-Trondjhemite-Granodiorites in Early Continental Crust. In: Earth's Oldest Rockss, 2nd Edition. Elsevier, Ch. 7, pp. 133–168.

Hoffmann, J. E., Munker, C., Naeraa, T., Rosing, M. T., Herwartz, D., Garbe-Schonberg, D., Svahnberg, H., 2011. Mechanisms of Archean crust formation inferred from high-precision HFSE systematics in TTGs. Geochimica et Cosmochimica Acta 75 (15), 4157–4178.

Hurai, V., Paquette, J. L., Huraiová, M., Konečný, P., 2010. Age of deep crustal magmatic chambers in the intra-Carpathian back-arc basin inferred from LA-ICPMS U-Th-Pb dating of zircon and monazite from igneous xenoliths in alkali basalts. J. Volcanol. Geotherm. Res. 198, 275–287.

Hurst, R. W., Bridgwater, D., Collerson, K. D., Wetherill, G. W., 1975. 3600-m,y, Rb-Sr ages from very early Archean gneisses from Saglek Bay, Labrador. Earth and Planetary Science Letters 27, 393–403.

Iizuka, T., Komiya, T., Johnson, S., Kon, Y., Maruyama, T., feb 2009. Reworking of Hadean crust in the Acasta gneisses, northwestern Canada: Evidence from in-situ LuHf isotope analysis of zircon. Chemical Geology 259 (3-4), 230–239.
URL https://www-sciencedirect-com.proxy.bib.uottawa.ca/science/article/pii/S0009254108005202

Ishikawa, A., Suzuki, K., Collerson, K. D., Liu, J., Pearson, D. G., Komiya, T., 2017. Rhenium-osmium isotopes and highly siderophile elements in ultramafic rocks from the Eoarchean Saglek Block, northern Labrador, Canada: implications for Archean mantle evolution. Geochimica et Cosmochimica Acta 216, 286–311.

Jayananda, M., Chardon, D., Peucat, J. J., Tushipokla, Fanning, C. M., 2015. Paleo- to Mesoarchean TTG accretion and continental growth in the western Dharwar craton, Southern India: Constraints from SHRIMP U-Pb zircon geochronology, whole-rock geochemistry and Nd-Sr isotopes. Precambrian Research 268.

Kemp, A. I. S., Wilde, S. A., Hawkesworth, C. J., Coath, C. D., Nemchin, A., Pidgeon, R. T., Vervoort, J. D., DuFrane, S. A., 2010. Hadean crustal evolution revisited: New constraints from Pb-Hf isotope systematics of the Jack Hills zircons. Earth and Planetary Science Letters 296 (1-2), 45–56.

Komiya, T., Yamamoto, S., Aoki, S., Koshida, K., Shimojo, M., Sawaki, Y., Aoki, K., Sakata, S., Yokoyama, T. D., Maki, K., Ishikawa, A., Hirata, T., Collerson, K. D., 2017. A prolonged granitoid formation in Saglek Block, Labrador: Zonal growth and crustal reworking of continental crust in the Eoarchean. Geoscience Frontiers 8 (2), 355–385.

Komiya, T., Yamamoto, S., Aoki, S., Sawaki, Y., Ishikawa, A., Tashiro, T., Koshida, K., Shimojo, M., Aoki, K., Collerson, K. D., nov 2015. Geology of the Eoarchean, > 3.95 Ga, Nulliak supracrustal rocks in the Saglek Block, northern Labrador, Canada: The oldest geological evidence for plate tectonics. Tectonophysics 662, 40–66.

Krogh, T., Kamo, S., 2006. Precise U-Pb zircon ID-TIMS ages provide an alternative interpretation to the early ion microprobe ages and new insights into Archean crustal processes, northern Labrador. In: Reimold, W., Gibson, R. (Eds.), Processes on the Early Earth. Geological Society of America, pp. 91–103.

Kusiak, M. A., Dunkley, D. J., Whitehouse, M. J., Wilde, S. A., Sałacińska, A., Konečný, P., Szopa, K., Gawęda, A., Chew, D., 2018. Peak to post-peak thermal history of the Saglek Block of Labrador: A multiphase and multi-instrumental approach to geochronology. Chemical Geology 484 (May), 210–223.

Laurent, O., Martin, H., Moyen, J. F., Doucelance, R., 2014. The diversity and evolution of late-Archean granitoids: Evidence for the onset of "modern-style" plate tectonics between 3.0 and 2.5 Ga. Lithos 205, 208–235.

Lee, J. K. W., Williams, I. S., Ellis, D. J., nov 1997. Pb, U and Th diffusion in natural zircon. Nature 390 (6656), 159–162.

Lyubetskaya, T., Korenaga, J., 2007. Chemical composition of Earth's primitive mantle and its variance: 1. Method and results. Journal of Geophysical Research: Solid Earth.

Martin, H., Moyen, J.-F., 2005. The Archaean-Proterozoic transition: sanukitoid and Closepet-type magmatism. Mineralogical Society of Poland Special Papers 26, 57–68.

Martin, H., Moyen, J.-F., Rapp, R., 2009. The sanukitoid series: magmatism at the ArchaeanProterozoic transition. Earth and Environmental Science Transactions of the Royal Society of Edinburgh 100 (1-2), 15–33.

Martin, H., Smithies, R. H., Rapp, R., Moyen, J. F., Champion, D., 2005. An overview of adakite, tonalite-trondhjemiten-granodiorite (TTG), and sanukitoid: Relationships and some implications for crustal evolution. Lithos 79 (1-2 SPEC. ISS.), 1–24.

Martin, H. N., 1987. Petrogenesis of Archean Trondhjemites, Tonalites, and Granodiorites from eastern Finland: Major and Trace Element Geochemistry. Journal of Petrology 28 (5), 921–953.

Masuda, A., Nakamura, N., Tanaka, T., 1973. Fine structures of mutually normalized rare-earth patterns of chondrites. Geochimica Et Cosmochimica Acta 37, 239–244.

McDonough, W. F., Sun, S. S., 1995. The composition of the Earth. Chemical Geology 120, 223–253.

Morino, P., Caro, G., Reisberg, L., 2018. Differentiation mechanisms of the early Hadean mantle: Insights from combined176Hf-142,143Nd signatures of Archean rocks from the Saglek Block. Geochimica et Cosmochimica Acta 240, 43–63.

Morino, P., Caro, G., Reisberg, L., Schumacher, A., 2017. Chemical stratification in the post-magma ocean Earth inferred from coupled 146,147Sm142,143Nd systematics in ultramafic rocks of the Saglek block (3.253.9 Ga; northern Labrador, Canada). Earth and Planetary Science Letters 463, 136–150.

Moyen, J., Laurent, O., 2018. Archaean tectonic systems: A view from igneous rocks. Lithos 302-303, 99–125.

Moyen, J., Martin, H., 2012. Forty years of TTG research. Lithos 148, 312–336.

Moyen, J.-F., 2011. The composite Archaean grey gneisses: Petrological significance, and evidence for a non-unique tectonic setting for Archaean crustal growth. Lithos 123 (1-4), 21–36.
URL http://dx.doi.org/10.1016/j.lithos.2010.09.015

Moyen, J. F., Martin, H., Jayananda, M., 2001. Multi-element geochemical modelling of crust-mantle interactions during late-Archaean crustal growth: The closepet granite (South India). Precambrian Research 112 (1-2), 87–105.

Næraa, T., Kemp, A. I., Scherstén, A., Rehnström, E. F., Rosing, M. T., Whitehouse, M. J., 2014. A lower crustal mafic source for the ca. 2550Ma Qôrqut Granite Complex in southern West Greenland. Lithos 192-195, 291–304.
URL http://dx.doi.org/10.1016/j.lithos.2014.02.013

Næraa, T., Scherstén, A., Rosing, M. T., Kemp, a. I. S., Hoffmann, J. E., Kokfelt, T. F., Whitehouse, M. J., 2012. Hafnium isotope evidence for a transition in the dynamics of continental growth 3.2 Gyr ago. Nature 485 (7400), 627–630.

Nagel, T., Hoffmann, J., Münker, C., 2012. Melting of Eoarchean TTGs from thickened mafic arc crust. Geology 40, 375–378.

Nutman, A., Bennett, V. C., 2019. The 3.9-3.6 Ga Itsaq Gneiss Complex of Greenland. In: Earth's Oldest Rocks, 2nd Edition. Elsevier, Ch. 17, pp. 375–399.

Nutman, A., Bennett, V. C., Friend, C. R. L., Horie, K., Hidaka, H., 2007. ˜3,850 Ma tonalites in the Nuuk region, Greenland: geochemistry and their reworking within an Eoarchaean gneiss complex. Contrib Mineral Petrol 154, 385–408.
URL https://journals-scholarsportal-info.proxy.bib.uottawa.ca/pdf/00107999/v154i0004/385{_}titnrgrwaegc.xml

Nutman, A. P., Collerson, K. D., 1991. Very early Archean crustal-accretion complexes preserved in the North Atlantic craton. Geology 19, 791–794.

Nutman, A. P., Fryer, B. J., Bridgwater, D., 1989. The early Archaean Nulliak (supracrustal) assemblage, northern Labrador. Can. J. Earth Sci. 26, 2159–2168.

Nutman, A. P., Kinny, P. D., Compston, W., Williams, I. S., 1991. SHRIMP U-Pb zircon geochronology of the Narryer Gneiss Complex, Western Australia. Precambrian Research 52, 275–300.

O'Neil, J., Boyet, M., Carlson, R. W., Paquette, J. L., 2013. Half a billion years of reworking of Hadean mafic crust to produce the Nuvvuagittuq Eoarchean felsic crust. Earth and Planetary Science Letters 379, 13–25.

O'Neil, J., Carlson, R. W., 2017. Building Archean cratons from Hadean mafic crust. Science 355 (6330).

Paquette, J., Tiepolo, M., jun 2007. High resolution (5 μm) UThPb isotope dating of monazite with excimer laser ablation (ELA)-ICPMS. Chemical Geology 240 (3-4), 222–237.

Paquette, J.-L., Piro, J.-L., Devidal, J.-L., Bosse, V., Didier, A., Sannac, S., Abdelnour, Y., 2014. Sensitivity Enhancement in LA-ICP-MS by N2 Addition to Carrier Gas: Application to Radiometric Dating of U-Th-Bearing Minerals. Agilent ICP-MS Journal 58, 4–5.

Regelous, M., Collerson, K. D., 1996. 147Sm-143Nd, 146Sm-142Nd systematics of early Archaean rocks and implications for crust-mantle evolution. Geochimica et Cosmochimica Acta 60 (18), 3513–3520.

Reimink, J. R., Chacko, T., Stern, R. A., Heaman, L. M., aug 2016. The birth of a cratonic nucleus: Lithogeochemical evolution of the 4.02-2.94 Ga Acasta Gneiss Complex. Precambrian Research 281, 453–472.

Rudnick, R. L., 1992. Restites, Eu anomalies and the lower continental crust. Geochimica & Cosmochimica Acta 56, 963–970.

Ryan, B., Martineau, Y., 2012. Revised and coloured edition of 1992 map showing the Geology of the Saglek Fiord - Hebron Fiord area, Labrador (NTS 14L/2,3,6,7). Scale: 1:100 000. Government of Newfoundland and Labrador, Department of Natural Resources, Geological Survey, Map 2012-15, Open File 14L/0091.

Sałacińska, A., Kusiak, M. A., Whitehouse, M. J., Dunkley, D. J., Wilde, S. A., Kielman, R., 2018. Complexity of the early Archean Uivak Gneiss: Insights from Tigigakyuk Inlet, Saglek Block, Labrador, Canada and possible correlations with south West Greenland. Precambrian Research 315 (October 2017), 103–119.

Sałacińska, A., Kusiak, M. A., Whitehouse, M. J., Dunkley, D. J., Wilde, S. A., Kielman, R., Król, P., 2019. Gneiss-forming events in the Saglek Block, Labrador; a reappraisal of the Uivak gneiss. International Journal of Earth Sciences 108 (3), 753–778.

Schiøtte, L., Bridgwater, D., Collerson, K. D., Nutman, A. P., Ryan, A. B., 1986. Chemical and isotopic effects of Late Archean high-grade metamorphism and granite injection on early Archean gneisses, Saglek-Hebron, northern Labrador. In: J.B. Dawson, D.A. Carswell, J. Hale, K. W. (Ed.), The nature of the lower continental cruste. Geol. Soc. Lond. Spec. Publ., pp. 261–273.

Schiøtte, L., Compston, W., Bridgwater, D., 1989a. Ion probe UThPb zircon dating of polymetamorphic orthogneisses from northern Labrador, Canada. Canadian Journal of Earth Sciences 26 (8), 1533–1556.

Schiøtte, L., Compston, W., Bridgwater, D., 1989b. U-Th-Pb ages of single zircons in Archaean supracrustals from Nain Province, Labrador, Canada. Can. J. Earth Sci. 26, 2636–2644.

Schiøtte, L., Hansen, B. T., Shirey, S. B., Bridgwater, D., 1993. Petrological and whole rock isotopic characteristics of tectonically juxtaposed Archaean gneisses in the Okak area of the Nain Province, Labrador: relevance for terrane models. Precambrian Research 63, 293–323.

Schiøtte, L., Nutman, A. P., Bridgwater, D., 1992. U-Pb ages of single zircons within Upernavik metasedimentary rocks and regional implications for the tectonic evolution of the Archaean Nain Province, Labrador. Can. J. Earth Sci. 29, 260–276.

Shimojo, M., Yamamoto, S., Sakata, S., Yokoyama, T. D., Maki, K., Sawaki, Y., Ishikawa, A., Aoki, K., Aoki, S., Koshida, K., Tashiro, T., Hirata, T., Collerson, K. D., Komiya, T., 2016. Occurrence and geochronology of the Eoarchean, ˜3.9Ga, Iqaluk Gneiss in the Saglek Block, northern Labrador, Canada: Evidence for the oldest supracrustal rocks in the world. Precambrian Research 278, 218–243.

Shirey, S. B., Hanson, G. N., jul 1984. Mantle-derived Archaean monozodiorites and trachyandesites. Nature 310 (5974), 222–224.

Smithies, R. H., Champion, D. C., 2000. The Archaean High-Mg Diorite Suite: Links to TonaliteTrondhjemiteGranodiorite Magmatism and Implications for Early Archaean Crustal Growth. Journal of Petrology 41 (12), 1653–1671.

Smithies, R. H., Champion, D. C., Van Kranendonk, M. J., 2009. Formation of Paleoarchean continental crust through infracrustal melting of enriched basalt. Earth and Planetary Science Letters 281 (3-4), 298–306.

Söderlund, U., Patchett, P., Vervoort, J. D., Isachsen, C. E., mar 2004. The 176Lu decay constant determined by LuHf and UPb isotope systematics of Precambrian mafic intrusions. Earth and Planetary Science Letters 219 (3-4), 311–324.
URL https://www.sciencedirect.com/science/article/pii/S0012821X04000123

Taramon, J., Rodriguez-Gonzalez, J., Negredo, A., Billen, M., 2015. Influence of cratonic lithosphere on the formation and evolution of flat slabs: Insights from 3-D time-dependent modeling. Geochemistry Geophysics Geosystems 16, 2933–2948.

Trail, D., Tailby, N., Wang, Y., Mark Harrison, T., Boehnke, P., apr 2017. Aluminum in zircon as evidence for peraluminous and metaluminous melts from the Hadean to present. Geochemistry, Geophysics, Geosystems 18 (4), 1580–1593.
URL http://doi.wiley.com/10.1002/2016GC006794

Van Kranendonk, M., 1990. Late Archean geologic history of the Nain Province, North River-Nutak map area, Labrador, and its tectonic significance. Geoscience Canada 17 (4), 231–237.

Vervoort, J. D., Kemp, A. I., 2016. Clarifying the zircon Hf isotope record of crust-mantle evolution. Chemical Geology 425, 65–75.
URL http://dx.doi.org/10.1016/j.chemgeo.2016.01.023

Vezinet, A., Pearson, D., Thomassot, E., Stern, R., Sarkar, C., Luo, Y., Fisher, C., 2018. Hydrothermally-altered mafic crust as source for early Earth TTG: Pb/Hf/O isotope and trace element evidence in zircon from TTG of the Eoarchean Saglek Block, N. Labrador. Earth and Planetary Science Letters 503, 95–107.

Wasilewski, B., O'Neil, J., Rizo, H., 2019. Geochemistry and petrogneesis of the early Archean mafic crust from the Saglek-Hebron Complex (Northren labrador). Precambrian geology 328, 129–150.

Whalen, J. B., Percival, J. A., Mcnicoll, V. J., Longstaffe, F. J., 2002. A Mainly Crustal Origin for Tonalitic Granitoid Rocks, Superior Province, Canada: Implications for Late Archean Tectonomagmatic Processes. Journal of Petrology 43 (8), 1551–1570.

Whitehouse, M. J., Dunkley, D. J., Kusiak, M. A., Wilde, S. A., 2019. On the true antiquity of Eoarchean chemofossils assessing the claim for Earth's oldest biogenic graphite in the Saglek Block of Labrador. Precambrian Research.

Wilde, S. a., Valley, J. W., Peck, W. H., Graham, C. M., 2001. Evidence from detrital zircons for the existence of continental crust and oceans on the Earth 4.4 Gyr ago. Nature 409 (6817), 175–178.

Chapter 3

Combined long- and short-lived Sm-Nd systematics of the Saglek-Hebron Complex felsic crust and implications for its early evolution

Chapter 3 combines the long-lived ^{147}Sm-^{143}Nd and short-lived ^{146}Sm-^{142}Nd isotopic systems to study the crustal evolution of the SHC. Both isotopic systems together allow investigating the source reservoirs involved in the formation of the SHC crust, and to better understand the complex protracted crustal reworking history of the SHC.

Keywords: *Saglek-Hebron Complex, Eoarchean crust, Granitoids,* ^{142}*Nd, Extinct isotopes, Hadean*

3.1 Introduction

Hadean rocks are rare, if not absent from the geological record. Besides the Nuvvuagittuq greenstone belt, which 4300 Ma age remains debated (see O'Neil et al., 2019, for review), the oldest remnant of crust preserved on Earth is the 4030 Ma Acasta gneiss (*e.g.* Bowring and Williams, 1999; Reimink et al., 2016). This gap of nearly 600 Ma in the earliest geological rock record hinders our ability to study and understand the early crustal processes that formed Archean cratons. Moreover, the oldest parts of these Archean cratons are generally felsic granitoids, likely not sourced directly from the mantle, but from an older crustal precursor that appears to be missing from the geological records. It can be challenging to decipher the earliest crustal evolution of the most ancient Archean terrains because long-lived isotopic systems can be affected by the complex post-magmatic history that these cratons commonly witnessed. Recent analytical developments allowed the measurement of short-lived isotopic systems, which now provide powerful new tools to help us understand Earth's early crustal history. The ^{146}Sm-^{142}Nd system is becoming the ideal isotopic tracer to study the Hadean Earth. Because ^{146}Sm decays in ^{142}Nd with a half-life of 103 Ma (Meissner et al., 1987; Marks et al., 2014), variability in the ^{142}Nd/^{144}Nd of rocks implies Sm/Nd fractionation while the ^{146}Sm was still extant, *i.e.* before 4000 Ma. This short-lived isotope system has been applied to rocks from most of the oldest terrains (*e.g.* Boyet and Carlson, 2006; Caro et al., 2006; Bennett et al., 2007; Rizo et al., 2011, 2012, 2013; O'Neil et al., 2008, 2012, 2016; O'Neil and Carlson, 2017; Roth et al., 2013, 2014; Reimink et al., 2018; Debaille et al., 2013; Puchtel et al., 2016; Garçon et al., 2018), however, the granitoids from the Saglek-Hebron complex remain uncharacterized.

Eoarchean mafic and ultramafic rocks from the Saglek-Hebron Complex (SHC) in Northern Labrador yielded excesses in ^{142}Nd compared to the modern terrestrial stan-

dard, suggesting these rocks derived from a mantle source that differentiated 160 Ma after solar system formation (Morino et al., 2017). The SHC recorded multiple episodes of felsic magmatism, from ∼3900 to ∼2700 Ma, including granitoids of various compositions (Chapter 2). The Hf isotopic compositions of the zircons from these granitoids suggest they were produced from the reworking of the Eoarchean SHC mantle-derived rocks, with possible involvement of a much older Hadean mafic crust (Chapter 2). The short-lived ^{146}Sm -^{142}Nd system, therefore, represents the ideal isotopic tool to unravel the SHC earliest crustal evolution. In this study, we present new coupled $^{147-146}$Sm -$^{143-142}$Nd data for granitoids from the Saglek Hebron Complex (SHC), ranging in age from ∼3900 to ∼2700 Ma. These new results bring important constraints on the involvement of Hadean reservoirs in the SHC to help better understanding its early crustal evolution.

3.2 Geological context

The SHC is an Archean granite-greenstone terrain exposed on the east coast of Northern Labrador (Canada) within the Nain Province of the North Atlantic Craton (Fig. 3.1). It is mainly composed of rocks from the trondhjemite-tonalite-granodiorite (TTG) series including several meters to kilometre-scale enclaves of supracrustal rocks (Bridgwater et al., 1975; Bridgwater and Schiøtte, 1991; Nutman et al., 1989). Baadsgaard et al. (1979) identified two distinct supracrustal assemblages based on the presence or absence of crosscutting porphyritic mafic dykes called the Saglek dykes, which age has recently been constrained with a Sm-Nd isochron at 3565 ± 120 Ma (Flageole, 2019). The Nulliak unit mainly consists of mafic amphibolites interpreted as differentiated tholeiitic basaltic metavolcanic rocks (Nutman et al., 1989) with Sm-Nd and

Lu-Hf isochron ages of 3782±93 Ma and 3794±130 Ma respectively (Morino et al., 2017, 2018). Younger ages of 3362 ± 100 Ma and 3023 ± 390 Ma have been obtained from Sm-Nd and Lu-Hf isochrons including mafic and ultramafic rocks from the Upernavik unit (Morino et al., 2017, 2018), although Flageole (2019) concluded that $^{147}Sm/^{144}Nd$ isotopic compositions of the Nulliak and Upernavik rocks were partially disturbed for the long-lived Sm-Nd system. A number of mafic and ultramafic rocks from the Nulliak unit have yielded high $^{142}Nd/^{144}Nd$ ratios compared to modern terrestrial standards, attesting to the involvement of a Hadean reservoir in the formation of the SHC rocks (Morino et al., 2017).

The SHC recorded multiple thermal episodes, including a Paleoarchean metamorphic event (Bridgwater and Collerson, 1976; Hurst et al., 1975; Schiøtte et al., 1986). A detail study on the petrology, geochemistry and geochronology of the SHG TTG is shown in the Chapter 2 (Wasilewski et *al.*, in prep). The TTG in the SHC are Mg-rich tonalites, trondhjemites, granodiorites and granites in composition, with the granitic component being mostly present in younger lithologies. Extensive U-Pb geochronology on zircons allowed recognizing different magmatic episodes, with the oldest Iqaluk gneiss emplaced at ∼3850 Ma, followed by the ∼3730 Ma Uivak I gneiss and the ∼3630 Ma Uivak II gneiss (Chapter 2; Collerson, 1983; Komiya et al., 2015; Krogh and Kamo, 2006; Schiøtte et al., 1989; Shimojo et al., 2016; Whitehouse et al., 2019). The SHC includes younger Mesoarchean granitoids with the ∼3300 Ma Iluilik gneiss and the ∼3240Ma Lister gneiss (Chapter 2, Schiøtte et al., 1989; Krogh and Kamo, 2006; Komiya et al., 2017) with also Neoarchean granites formed contemporaneously with high-grade metamorphism (Bridgwater et al., 1975; Kusiak et al., 2018; Nutman and Collerson, 1991; Schiøtte et al., 1986; Van Kranendonk, 1990), between 2800 and 2600 Ma.

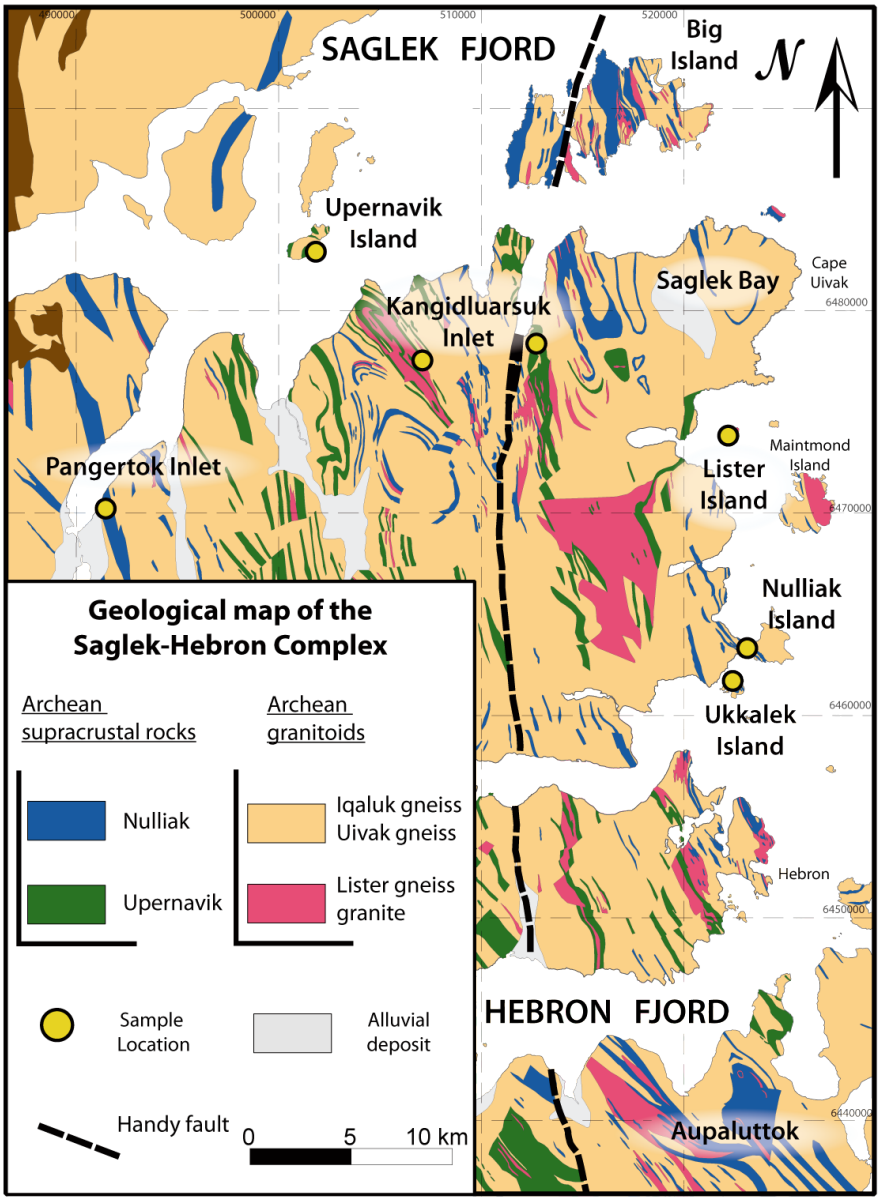

Figure 3.1

Geological map of the Saglek-Hebron Complex (SHC) modified from Ryan and Martineau (2012)and Komiya et al. (2015). Sample locations (yellow circles) show the main localities where multiple samples were collected for this study. Detailed GPS locations for each sample can be found in Table 3.1. The Nulliak and Upernavik Archean supracrustal rocks include mafic metavolcanic rocks, ultramafic and metasedimentary rocks. Coordinates are in UTM NAD 27 zone 20.

The Eoarchean Iqaluk and Uivak and the Paleoarchean Lister gneisses mostly consist of clinopyroxene or hornblende bearing trondhjemites and Mg-rich tonalites with geochemical compositions consistent with derivation from the melting of a mafic source (Chapter 2). The Hf isotopic compositions of the Eoarchean TTG suggests a slightly suprachondritic precursor source, perhaps as depleted as the depleted mantle source of mid-ocean ridge basalts (Vezinet et al., 2018, ; Chapter 2). Most SHC granitic rocks have whole-rock geochemical and zircon-Hf isotopic compositions consistent with the reworking of the Eoarchean TTG (Chapter 2). Some Paleoarchean granitoids, however, have tonalitic-granodioritic whole-rock geochemical compositions more consistent with melting of a mafic crustal source and the Hf isotopic compositions of their zircons suggest a possible Hadean mafic source involved in their petrogenesis (Chapter 2).

3.3 Methods

A total of 15 granitoid samples have been analysed for coupled $^{147-146}$Sm -$^{143-142}$Nd isotopic compositions. The geochemical and petrographic composition of these granitoids are detailed in Chapter 2 (Wasilewski et *al.*, in prep) and summarized in Table C.1 in the appendix C. Except for sample SG-267, U-Pb ages for all samples studied here were previously been obtained and detailed in Chapter 2, Table 2.2. Prior to crushing, all secondary veins or weathered surfaces were removed with a diamond bladed saw. Samples were then crushed with a steel jaw crusher and powdered using a ceramic grinder.

3.3.1 Digestion and Sm-Nd chemical separation

Sample digestion and chemical separation of Sm and Nd were performed at the clean laboratories of the Advanced Research Complex (ARC) of the University of Ottawa.

Between 30 and 300 mg of powdered rock samples were dissolved in a 5:1 concentrated HF-HNO_3 mixture and using high-pressure steel jacketed Teflon Parr bombs at 140 °C for 5 days. Samples were then dried down and re-dissolved in 6N HCl in the same Teflonbombs at 140 °C for 1 day. A few drops of boric acid were added before evaporation of the HCl to prevent the formation of fluorides. An aliquot for an equivalent of ∼300 ng of Nd was taken from each dissolved sample and spiked with a ^{149}Sm-^{150}Nd tracer, for determination of Sm and Nd concentrations by isotopic dilution. The light rare earth elements (LREE) were extracted from the spiked aliquots using columns filled with 200-400 mesh AG50W-X8 cation-exchange resin. Nd and Sm were then separated from the LREE fractions using columns filled with 50-100 μm Eichrom Ln resin. Neodymium was extracted from the unspiked sample fractions for high-precision isotopic analyses of ^{142}Nd. Chemical separation and purification of Nd were achieved following the protocols of Garçon et al. (2018) and Li et al. (2015), and only the main steps are summarized here. The LREE were separated from the whole-rock matrix using 200-400 mesh AG50W-X8 cation-exchange resin. The LREE fractions were then dissolved in HNO_3 with $NaBrO_3$ in order to oxidize Ce to its +4 form and passed through columns filled with 100-150 μm Eichrom Ln resin which fixes the oxidized Ce^{+4} but lets the other $LREE^{+3}$ pass through. The collected $LREE^{+3}$ are dried and passed through the same Ce-removal procedure a second time. The fractions were then passed through AG50W-X8 cation-exchange resin again, to mainly remove the Na and Br added during the Ce-removal step. The Nd is finally purified from Sm and any remaining Ce using 0.4 cm × 12 cm columns filled with 20-50 μm Eichrom Ln resin. Total chemistry Nd yields were 95%.

3.3.2 Mass spectrometry

All technical characteristics are summarized in Table C.2, C.3 (in supplementary appendix C).

Sm-Nd isotopie dilution

The Sm and Nd isotopic compositions of the spiked aliquots were measured at the GEOTOP laboratories of the Université du Québec à Montréal (UQÀM) and at the Isotope Geochemistry and Geochronology Research Centre (IGGRC) of Carleton University in Ottawa. Analyses were performed on a Thermo-Fisher Triton thermal-ionisation mass spectrometer (TIMS) using double Re filaments.

Isotope ratios were measured using one acquisition step, monitoring ^{147}Sm for isobaric interference corrections on Nd isotopes, and monitoring ^{146}Nd and ^{155}Gd for isobaric interference corrections on Sm isotopes. Neodymium runs are the average of measurements of 140 ratios, while Sm runs represent averages of 100 ratios, every ratio determined with 8.39 seconds integration time. The instrumental mass bias fractionation was corrected using the exponential law and a ^{147}Sm/^{152}Sm = 0.56081 for Sm and ^{146}Nd/^{144}Nd = 0.7219 for Nd. The JNdi-1 terrestrial standard yielded an average ^{143}Nd/^{144}Nd ratio of 0.512096 ± 0.000006 (2, n=4) for analyses done at GEOTOP and 0.512104 ± 0.000003 (2, n=4) for analyses done at the IGGRC. These values are slightly below the accepted value of 0.512115 ± 0.000007 from Tanaka et al. (2000), therefore, ^{143}Nd/^{144}Nd ratios for each sample were corrected to the accepted JNdi-1 value.

High-precision ^{142}Nd isotope measurements

High-precision Nd isotopic measurements of the unspiked fractions were performed on a Thermo-Fisher Triton TIMS at the IGGRC during three separate analytical ses-

sions. Between 1000 and 800 ng of Nd from each sample was loaded onto pre-outgassed zone refined Re filaments. Neodymium isotopes were measured using a 2-step dynamic routine, that provides static measurements of all Nd isotope ratios and dynamic measurements of the $^{142}Nd/^{144}Nd$ ratio. Masses 140 and 147 were measured for Ce and Sm mass interference corrections. Measurements consist of 600 ratios measured in 24 blocks of 25 cycles each, with an integration time of 8.39 seconds per step and a background measurement performed between each block. Data were corrected for instrumental mass fractionation using the exponential law to $^{146}Nd/^{144}Nd = 0.7219$. Samples with enough Nd were measured multiple times using the same filament and were combined into a single run of up to 1200 ratios. The JNdi-1 standard was analysed multiple times during each analytical session and yielded an average for all sessions of $^{142}Nd/^{144}Nd = 1.141836 \pm 0.000003$ (2, n=14), in perfect agreement with the results reported by other high-precision Nd isotope studies (*e.g.* Garçon et al., 2018). The $\mu^{142}Nd$ values for the samples were calculated following:

$$\mu^{142}Nd = \left(\frac{\left(\frac{^{142}Nd}{^{144}Nd}\right)^{Sample}}{\left(\frac{^{142}Nd}{^{144}Nd}\right)^{JNdi-1}} - 1 \right) \times 10^6 \tag{3.1}$$

And using the average $^{142}Nd/^{144}Nd$ of the JNdi-1 standard analysed during the same analytical session: session-1 $^{142}Nd/^{144}Nd = 1.141838 \pm 0.000005$ (2, n=4); session-2 $^{142}Nd/^{144}Nd = 1.141834 \pm 0.000004$ (2σ, n=5); session-3 $^{142}Nd/^{144}Nd = 1.141837 \pm 0.000003$ (2, n=5). This corresponds to a 2σ reproducibility of 4.3, 3.7 and 2.5 ppm for each session and a long-term reproducibility of 4.6 ppm for all analytical session combined. The total Nd blank was 84 pg.

3.4 Results

Table 3.1 presents the long-lived ^{147}Sm-^{143}Nd and short-lived ^{146}Sm-^{142}Nd isotopic data, along with rock types and crystallization ages discussed in Chapter 2. The granitoids analysed for their Sm-Nd isotopic compositions include all different rock types found in the SHC with 4 trondhjemite samples, 4 Mg-rich tonalite samples, 1 granodiorite sample and 6 granite samples. Samples are also from all magmatic events defined in Chapter 2, from the oldest Iqaluk gneiss to the Neoarchean granitoids (Table 3.1). All granitoid samples are LREE-enriched (Chapter 2) with ^{147}Sm/^{144}Nd ranging from 0.1336 to 0.0615 and ^{143}Nd/^{144}Nd between 0.509530 and 0.511311 (Table 3.1). Initial ε^{143}Nd were calculated using the respective U-Pb zircon ages for the rocks. Eoarchean granitoids generally have suprachondritic initial ε^{143}Nd values between 0 and +10, whereas the younger Neoarchean granitoids have lower initial ε^{143}Nd values between -6 and -10. Depleted mantle model ages (TDM) for most SHC granitoids samples are Eoarchean, ranging from 3800 to 3300 Ma, independently of their crystallization ages.

All 15 granitoid samples were analyzed for their ^{142}Nd isotopic compositions, and the results are shown in Table 3.1 and Figure 3.2 (the details of all measured isotopic ratios are found in Table C.4). From these, twelve samples yield positive μ^{142}Nd values compared to the JNdi-1 standard ranging between +5.9 to +14.9. These mainly comprise the Eoarchean granitoids, along with both ~3300 Ma Iluilik samples and 2 of the 3 Neoarchean granitic samples analyzed. The only granodiorite sample analysed, the Iluilik sample SG-203, is the sample with the lowest resolvable positive ^{142}Nd anomaly of $+5.9 \pm 2.8$. Both 3200 Ma Lister gneiss samples (SG-267 and SG-265) and one Neoarchean granite sample (SG-037) show no deviation of ^{142}Nd/^{144}Nd compared to the JNdi-1 terrestrial standard, yielding μ^{142}Nd values of +1.8, +2.3 and +1.6, re-

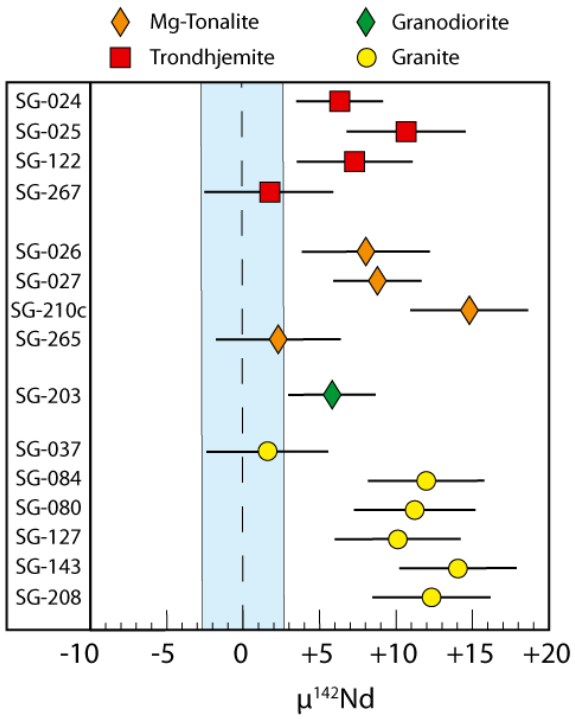

Figure 3.2

Summary of the μ^{142}Nd values for the granitoids from the SHC relative to the terrestrial standard JNdi-1. The blue field represents the 2S uncertainty on the μ^{142}Nd value.

spectively.

3.5 Discussion

The Sm-Nd isotopic system is commonly used to study the evolution of the Archean crust and constrain the composition of its source. Both Sm and Nd are relatively immobile elements and the ^{147}Sm-^{143}Nd system is relatively resistant to isotopic resetting generally up to upper amphibolite facies (Vance and O'Nions, 1990; Hensen and Zhou, 1995; Jung and Mezger, 2001). Long-lived isotopic systems, however, can be affected by post-magmatic processes. Changes in the parent-daughter ratio in a rock will lead to variations in its isotopic composition with time. This can be particularly concerning

in the SHC that has recorded multiple thermal events over one billion years (Chapter 1 : Wasilewski et al., 2019; Van Kranendonk, 1990; Kusiak et al., 2018; Bridgwater and Schiøtte, 1991; Schiøtte et al., 1992, 1989). The short-lived isotopic systems, however, are much more robust to post-magmatic disturbance. In the case of the ^{146}Sm-^{142}Nd system, variations in the ^{142}Nd/^{144}Nd ratio can only be produced while ^{146}Sm was extant. Given the half-life of ^{146}Sm of 103 Ma, any deviations in ^{142}Nd/^{144}Nd compared to the terrestrial mantle implies an event that fractionated Sm from Nd in the Hadean (prior to 4000 Ma). After the extinction of ^{146}Sm, any process that changes the Sm/Nd ratio of a rock or a reservoir, will not affect its ^{142}Nd/^{144}Nd ratio. Coupling long-lived and short-lived isotopic systems is therefore a powerful way to investigate the crustal evolution of the oldest Archean crust and that of its precursor source(s).

Table 3.1

^{142}Nd data averages and ^{143}Nd/^{144}Nd as well as a recap of U-Pb geochronology data from the Chapter 2 for the rocks of this study. For calculation of initial ratios and ε^{143}Nd, CHUR values from Bouvier et al. (2008) of ^{147}Sm/^{144}Nd = 0.1960 and present-day ^{143}Nd/^{144}Nd = 0.512630, with the decay constant of ^{147}Sm λ= 6.54 x10^{-12}, were used. The depleted mantle (DM) curve was obtained using present-day ^{143}Nd/^{144}Nd = 0.5132 and ^{147}Sm/^{144}Nd = 0.2152. The STD refer to the terrestrial standard JNdi-1 ^{142}Nd/^{144}Nd measured ratio of 1.141840 ± 0.000005 on average. All uncertainty values are quoted at (2σ). All data are summarized in Figure 3.2. The values of ^{143}Nd/^{144}Nd measured are from non-spiked fractions from the same dissolution that the fraction used for the ^{147}Sm/^{144}Nd ratio analysis. This value is also normalized to the accepted values for the ^{143}Nd/^{144}Nd ratio from Tanaka et al. (2000) 0.512115 ± 0.000007.

Sample	**Age** ±2σ	**Nd** (ppm)	**Sm** (ppm)	$\frac{^{147}Sm}{^{144}Nd}$	$\frac{^{143}Nd}{^{144}Nd}$ ±2σ	$\frac{^{143}Nd}{^{144}Nd_{(i)}}$ ±2σ	$\varepsilon^{143}Nd_{(i)}$ ±2σ	$\frac{^{142}Nd}{^{144}Nd}$ ±2σ	$\mu^{142}Nd$ ±2σ
	Trondjhemite								
SG-024	3869 ± 10	4.42	0.45	0.0615	0.509521 ± 3	0.507945 ± 3	6.65 ± 0.06	1.141845 ± 3	6.4 ± 2.8
SG-025	3838 ± 10	4.54	0.57	0.0754	0.510055 ± 4	0.508137 ± 4	9.63 ± 0.08	1.141846 ± 4	10.7 ± 3.8
SG-122	3781 ± 12	4.83	0.79	0.0994	0.510516 ± 4	0.508027 ± 4	5.99 ± 0.08	1.141846 ± 4	7.4 ± 3.7
SG-267	3229 ± 8	11.92	1.97	0.1001	0.510656 ± 5	0.508520 ± 5	1.44 ± 0.10	1.141839 ± 5	1.8 ± 4.1
	Mg-tonalite								
SG-026	3820 ± 20	29.98	5.09	0.1027	0.510424 ± 5	0.507825 ± 5	3.02 ± 0.10	1.141843 ± 5	8.1 ± 4.1
SG-027	3632 ± 9	23.51	4.71	0.1211	0.510867 ± 3	0.507956 ± 3	0.73 ± 0.06	1.141848 ± 3	8.8 ± 2.8
SG-210C	3869 ± 6	15.91	2.86	0.1088	0.510602 ± 5	0.507812 ± 5	4.04 ± 0.10	1.141855 ± 4	14.9 ± 3.8
SG-265	3229 ± 8	11.46	2.53	0.1336	0.511316 ± 5	0.508465 ± 5	0.35 ± 0.10	1.141840 ± 5	2.3 ± 4.0
	Granodiorite								
SG-203	3330 ± 15	57.36	9.40	0.0991	0.510416 ± 3	0.508235 ± 3	-1.58 ± 0.06	1.141844 ± 3	5.9 ± 2.8
	Granite								
SG-037	2744 ± 8	12.93	2.05	0.0958	0.510300 ± 5	0.508565 ± 5	-10.13 ± 0.10	1.141835 ± 4	1.6 ± 3.9
SG-080	3612 ± 9	11.27	1.47	0.0788	0.510072 ± 5	0.508188 ± 5	4.78 ± 0.10	1.141851 ± 4	11.3 ± 3.9
SG-084	3710 ± 24	8.04	1.49	0.1117	0.510569 ± 4	0.507826 ± 4	0.20 ± 0.08	1.141847 ± 4	12.0 ± 3.7
SG-127	2789 ± 12	15.01	2.52	0.1016	0.510563 ± 5	0.508694 ± 5	-6.45 ± 0.10	1.141845 ± 5	10.1 ± 4.0
SG-143	2780 ± 8	18.91	3.15	0.1008	0.510501 ± 4	0.508653 ± 4	-7.49 ± 0.08	1.141854 ± 4	14.1 ± 3.8
SG-208	3330 ± 7	40.03	5.55	0.0839	0.510095 ± 5	0.508249 ± 5	-1.30 ± 0.10	1.141848 ± 4	12.4 ± 3.8

3.5.1 Nd isotopic composition of the SHC granitoids and implications for an early depleted source

The Saglek-Hebron Complex experienced multiple and protracted thermal events and was metamorphosed up granulite facies (Van Kranendonk, 1990; Bridgwater and Schiøtte, 1991; Schiøtte et al., 1989, 1992; Kusiak et al., 2018). Major and trace element compositions of mafic and ultramafic rocks from the SHC show limited mobility of the REE, except perhaps for the low-Fe ultramafic rocks, showing LREE enrichment suggestive of post-emplacement remobilization (Wasilewski et al., 2019, : Chapter 1). Nevertheless, disagreement between ages from the Re-Os, Rb-Sr, Sm-Nd and Lu-Hf systems (Ishikawa et al., 2017; Hurst et al., 1975; Morino et al., 2017, 2018) suggests disturbance, at least to some extent, of some long-lived isotopic systems. It is therefore important to closely examine the Nd isotopic composition of the SHC granitoids to establish if it is representative of their source or if post-magmatic processes may have affected their isotopic compositions, before interpreting its geological meaning.

The SHC Eoarchean granitoid samples from the Iqaluk and Uivak I gneisses exhibit variable positive initial ε^{143}Nd values, from +4 to +10 (Table 3.1), significantly higher than the Depleted Mantle composition in the Eoarchean (Boyet and Carlson, 2005; Carlson et al., 2007). Such high ε^{143}Nd values between 3900 and 3700 Ma suggest the SHC derive from a highly incompatible element depleted source, more depleted than the DM. It has been suggested that Eoarchean gneisses with high ε^{143}Nd values from southwest Greenland, also part of the North Atlantic Craton, were evidence of a highly depleted mantle reservoir (*e.g.* Bennett et al., 1993; Bennett, 2003). The initial ε^{143}Nd values up to ∼+4 for these rocks from Greenland, however, are significantly lower than the value of +10 for the SHC granitoids (Fig. 3.3). An ε^{143}Nd value of +9.8 at 3838 Ma as mea-

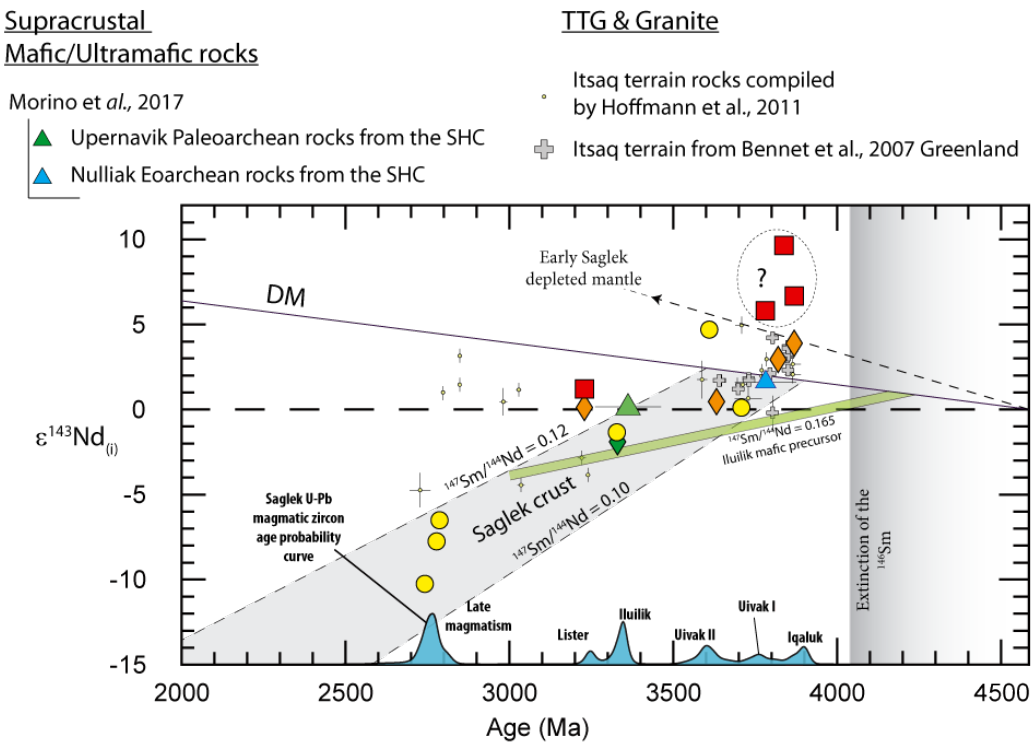

Figure 3.3

Age (Ma) *vs.* initial ε^{143}Nd of samples from the SHC the DM is calculated using a ^{147}Sm/^{144}Nd ratio of 0.2152. Chondritic normalisation values are from Bouvier et al. (2008) with ^{147}Sm/^{144}Nd = 0.196 and ^{143}Nd/^{144}Nd = 0.51263. Data from Southwest Greenland (Bennett et al., 2007; Hoffmann et al., 2011; O'Neil et al., 2016). The SHC supracrustal data come from (Morino et al., 2017). Symbols are as in Figure 3.2.

sured in the trondhjemite sample SG-025, would require a source formed at 4568 Ma to evolve with a ^{147}Sm/^{144}Nd of 0.305. While an extreme LREE-depleted mantle has previously been suggested for the source of the Saglek lavas (Collerson et al., 1991; Bennett et al., 1993), a differentiation event causing this degree of depletion would have also been recorded in the ^{142}Nd isotopic composition of these rocks. Morino et al. (2017) have suggested a differentiation of the mantle source occurring at 4400 Ma to account for the excess in ^{142}Nd in the SHC ultramafic rocks. A similar age of 4470 Ma was proposed for the mantle source of the Eoarchean Isua mantle-derived rocks with high ^{142}Nd/^{144}Nd ratios (Rizo et al., 2011; O'Neil et al., 2016). A differentiation occurring at

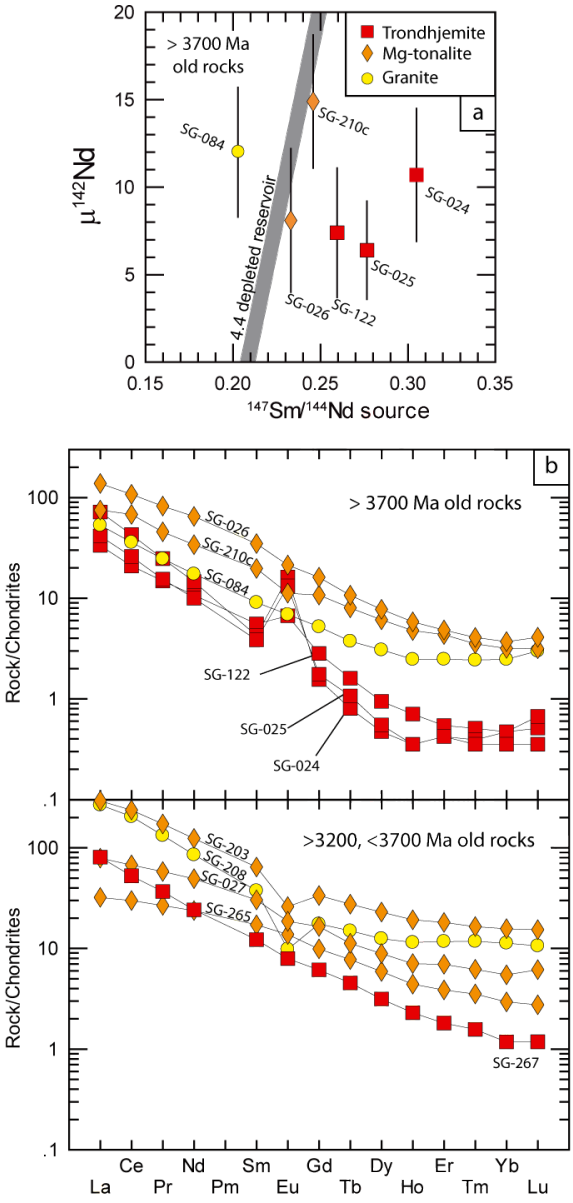

Figure 3.4

a) $^{147}Sm/^{144}Nd$ ratio of the source *vs.* $\mu^{142}Nd$ value for the granitoids from this study which exhibits an age of over 3700 Ma. The thick grey line refers to a hypothetical reservoir formed at 4400 Ma. b) Two REE diagram normalized to chondrite (Sun and McDonough, 1989) that show on the top the REE profile of the granitoids older than 3700 Ma and at the bottom the profile of the granitoids encompassed between 3200 and 3700 Ma. Symbols are as in Figure 3.2.

4400 Ma forming a mantle reservoir with a minimum $^{147}Sm/^{144}Nd$ ratio of 0.305, as suggested by the $\varepsilon^{143}Nd$ value of +10, would produce $\mu^{142}Nd$ values of $\sim +50$, much higher than the $\mu^{142}Nd$ values measured in all Saglek rocks analyzed. Figure 3.4a shows time integrated $^{147}Sm/^{144}Nd$ source ratios for the SHC Eoarchean rocks *vs.* their measured $\mu^{142}Nd$ values. Hadean sources of similar ages but with higher time integrated Sm/Nd ratios should produce Eoarchean rocks with higher $\mu^{142}Nd$ values, therefore, a correlation would be expected on Figure 3.4a. The lack of correlation and the similar $\mu^{142}Nd$ values for all Eoarchean granitoids could indicate that the initial $\varepsilon^{143}Nd$ observed in some SHC granitoid may not be representative of their source. The grey bar on Figure 3.4a shows the $^{147}Sm/^{144}Nd$ ratio of a source with the corresponding $\mu^{142}Nd$ values of a mantle reservoir formed at 4400 Ma. All Eoarchean trondhjemite samples are falling to the right of this 4400 Ma mantle reservoir, indicating that their Sm/Nd source is higher than what expected given their $\mu^{142}Nd$ values. If a geological process increased the Sm/Nd ratio of these trondhjemites after the extinction of ^{146}Sm, it would affect their calculated initial $\varepsilon^{143}Nd$ (and thus Sm/Nd source), without affecting their $^{142}Nd/^{144}Nd$. The strong depletion in HREE of the SHC Eoarchean trondhjemites, with their pronounced positive Eu anomalies (Fig. 3.4b), has led to suggest that they likely represent residual rocks after crustal melting (Chapter 2). One could argue that residue from partial melting should exhibit higher Sm/Nd values and thus a lower back calculated $\varepsilon^{143}Nd$. Lower Sm/Nd ratios are however commonly observed in high-grade granulite, perhaps restitic, felsic rocks, consistent with the presence of some accessory phases such as allanite, apatite and titanite (**?**Martin, 1987; Rudnick, 1992). If the Eoarchean trondhjemites were subjected to partial melting during any post-Eoarchean thermal event affecting the SHC, it could lower their Sm/Nd ratio without affecting the crystallization U-Pb age obtained from their zircons, nor their $\mu^{142}Nd$ value. Back-calculation

of ε^{143}Nd at the crystallization age, using a Sm/Nd ratio lower than that measured of the original rock will lead to overestimation of the initial ε^{143}Nd values, as illustrated in Figure 3.5a. Partial melting of the SHC Eoarchean felsic crust could have occurred during high-grade thermal events around 3500 or 2700 Ma (Chapter 2; Sałacińska et al., 2018; Van Kranendonk, 1990). The later the event lowering the Sm/Nd ratio of the whole rock is after the crystallization of the zircons, the larger the effect will be on the calculated initial ε^{143}Nd (Fig. 3.5a). Samples SG-024 and SG-025 exhibit the highest initial ε^{143}Nd values, respectively +9.8 and +6.8 at 3870 to 3840 Ma. Most zircons from both samples are highly metamict associated with secondary sector zoned zircons, with only a few scarce old clean and not inherited zircons (Chapter 2). These trondhjemite samples show the lowest Sm/Nd ratios measured here in the SHC granitoids, with ^{147}Sm/^{144}Nd of 0.0615 and 0.0754. The third trondhjemite sample SG-122 with a ε^{143}Nd = +6.0 at 3780 Ma exhibit a strong zircon discordance and a slight positive Eu anomaly which could suggest as well a restitic composition. Its ^{147}Sm/^{144}Nd source of 0.26 would also lead to a μ^{142}Nd of +25 for a mantle reservoir formed at 4400 Ma, which is higher than any ^{142}Nd/^{144}Nd measured in the SHC rocks. Therefore for these three samples, we suggest that these disturbance perhaps leads to an overestimation of their initial ε^{143}Nd value.

Disturbance of the parent-daughter ratio in the long-lived systems could also explain the apparent decoupling of Sm-Nd and Lu-Hf systematic observed for some SHC rocks (Fig. 3.5b). The behaviour of the Sm-Nd isotopic system is generally coupled with that of the Lu-Hf isotopic system since both the parents are less incompatible than the daughters. The Eoarchean trondhjemites samples exhibit higher initial ε^{143}Nd values than what would be expected if they were coupled with the ε^{176}Hf values measured in their zircons (Fig. 3.5b). Similarly to the U-Pb ages, the Hf isotopic compositions

obtained from the zircons may not have been affected by a potential thermal event causing partial melting at the whole-rock scale.

The Eoarchean Mg-tonalite samples SG-210c and SG-026 are most likely to represent the best estimation of the Nd isotopic composition for the source of the SHC Eoarchean granitoids. With a ε^{143}Nd value of +4.0 and +3.1 between 3870 and 3820 Ma, it corresponds to ^{147}Sm/^{144}Nd source between 0.246 and 0.233. A mantle reservoir formed at 4400 Ma with a ^{147}Sm/^{144}Nd of 0.246 to 0.233 would evolved to μ^{142}Nd value between +18 and +12, similar to the value of $+14.9 \pm 3.8$ and 8.1 ± 4.1 measured in SG-210c and SG-026. This ε^{143}Nd value of $\sim$+4 at 3850 Ma is also similar to the initial ε^{143}Nd values of the SW Greenland Eoarchean rocks (Bennett et al., 1993, 2007, Fig. 3.3), consistent with a possible common early evolution between the SHC and SW Greenland, as it was proposed in Chapter 2. These ε^{143}Nd values suggest the involvement of a source more depleted than the current terrestrial model mantle, consistent with the existence of an early depleted mantle reservoir in the Hadean and Eoarchean (Bennett et al., 1993; Caro et al., 2003; Wang et al., 2015). Because fractionation events affecting the Sm/Nd ratio after $\sim$4000 Ma would not affect the ^{142}Nd/^{144}Nd isotopic ratio, the μ^{142}Nd values of the restitic trondhjemite samples are also representative of their Hadean precursor source. Except for the Mesoarchean Lister gneiss and one Neoarchean granite, all other SHC granitoids yielded positive μ^{142}Nd values with an average value of $+10.2 \pm 5.9$ similar to the value of $+8.6 \pm 3.3$ obtained by Morino et al. (2017) on mafic and ultramafic rocks from the SHC. This therefore strongly confirms the involvement of a Hadean depleted source into the formation of the SHC crust. Tonalitic rocks from the Anshan Province in northeastern China also show this early depleted source with positive ^{142}Nd anomalies (Li et al., 2017), suggesting that this early depleted mantle source may have not been restricted to the North Atlantic Craton.

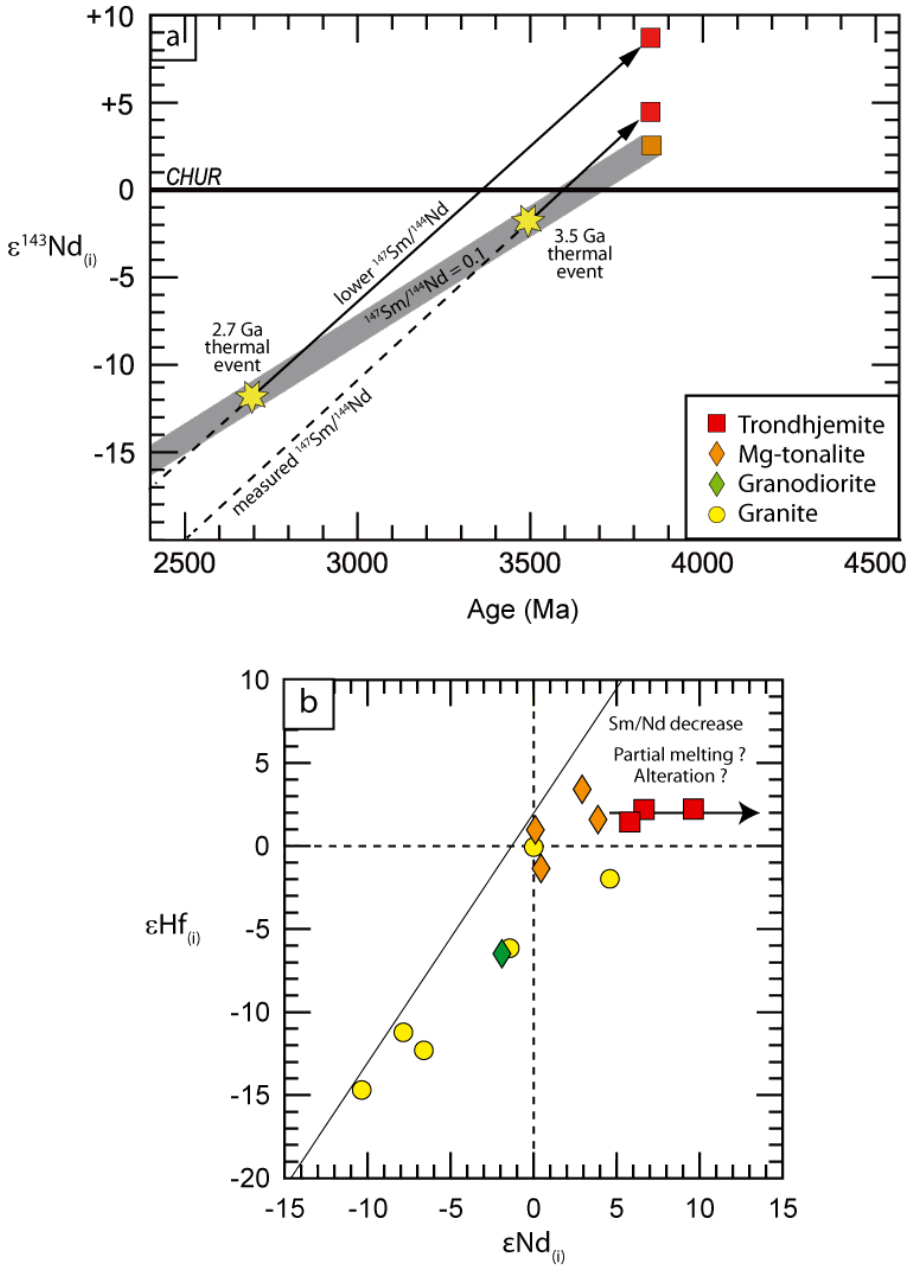

Figure 3.5

a) $\varepsilon^{143}Nd_{(i)}$ *vs.* time (Ma) diagram showing the effect of a thermal event on the interpretation of the $\varepsilon^{143}Nd_{(i)}$ of the granitoids that exhibit restitic characteristic. b) $\varepsilon^{143}Nd_{(i)}$ *vs.* $\varepsilon^{176}Hf_{(i)}$ initial composition that shows the decoupling of the $^{143}Nd/^{144}Nd$ isotopic composition due to post-magmatic processes.

3.5.2 Crustal evolution of the SHC

Crustal evolution in the Eoarchean

The whole-rock geochemical compositions of the SHC granitoids along with the Hf isotopic composition of their zircons were discussed in Chapter 2 to suggest that the SHC TTG were likely sourced from the melting of older mafic crustal precursors, possibly of variable ages, while the granitic rocks were more consistent with reworking of felsic crust within processes such as crustal anatexis. It was previously suggested that the Nulliak supracrustal rocks were the crustal precursor of the SHC Eoarchean felsic crust (Bridgwater and Schiøtte, 1991; Komiya et al., 2015; Morino et al., 2017; Nutman and Collerson, 1991). Because the SHC Eoarchean tonalites and trondhjemites may derive from the partial melting of the Nulliak or pre-Nulliak mafic assemblage after the extinction of ^{146}Sm, the SHC TTG would inherit the ^{142}Nd/^{144}Nd ratios of these mafic precursors. While this is consistent with our ^{142}Nd/^{144}Nd results, the oldest 3870 Ma SHC granitoids (Chapter 2; Shimojo et al., 2016; Vezinet et al., 2018) are significantly older than the age estimates of 3780 Ma obtained from the Nulliak rocks (Morino et al., 2017, 2018). The TTG have slightly higher initial ε^{143}Nd values compared to the Nulliak mantle-derived rocks (Fig. 3.3). This could therefore put back to question whether the Iqaluk and Uivak I gneisses were produced from the melting of the Nulliak supracrustal assemblage. Mafic rocks older than the 3870 Ma Iqaluk gneiss have not been identified in the SHC. Nonetheless, the large uncertainties on Sm-Nd and Lu-Hf isochron ages of 3782 ± 93 Ma and 3794 ± 130 Ma and initial ε^{143}Nd values do not allow eliminating the Nulliak rocks as the crustal precursor of the SHC Eoarchean felsic rocks. Regardless of the exact crustal source of the SHC oldest felsic rocks, the positive μ^{142}Nd values recorded in both the SHC granitoids and mafic/ultramafic rocks indicate that a Hadean reservoir with a Sm/Nd ratio higher than the *"normal"* depleted mantle

was involved in their formation. Figure 3.6 shows that the depleted reservoir extracted from the normal depleted mantle at 4400 Ma suggested by Morino et al. (2017), would produce the ^{142}Nd excesses measured in the SHC granitoids (μ^{142}Nd from ~+6 to +15) with a ^{147}Sm/^{144}Nd ranging between 0.221 and 0.240. Any mafic reservoir derived from such early depleted mantle after or shortly before the extinction of ^{146}Sm, could be the crustal precursor source(s) of the SHC Eoarchean TTG.

Crustal evolution in the Paleoarchean

The Hf isotopic composition of the SHC zircons discussed in Chapter 2 showed an abrupt change in isotopic signatures at the end of the Paleoarchean. The ~3300 Ma Iluilik granitoids displayed low ε^{176}Hf values while the ~3200 Ma Lister gneiss showed a more radiogenic suprachondritic composition. A similar shift could have been recorded by the ^{147}Sm-^{144}Nd system with both Iluilik samples displaying slight subchondritic ε^{143}Nd values, lower than the Lister gneiss samples with ε^{143}Nd values of +0.3 and +1.4 (Fig. 3.3).

The 3300 Ma Iluilik intrusions include granodiorites, which are uncommon for the SHC and characterized by a less pronounced HREE depletion compared to the more dominant granitoids (Chapter 2). The granodiorite sample SG-203 is the SHC granitoids that yielded the smallest ^{142}Nd anomaly with a μ^{142}Nd value of $+5.9 \pm 2.8$. This value still overlaps with those of the Eoarchean tonalites and trondhjemites and the Iluilik granodiorites could be explained by reworking of the Iqaluk and Uivak gneisses. Morino et al. (2017) have proposed the existence of 3360 Ma mafic/ultramafic rocks they interpreted as from the Upernavik unit, which yielded no ^{142}Nd anomaly and derived from a distinct mantle source. The lower μ^{142}Nd value of the 3330 Ma Iluilik granodiorite could therefore result from the interaction between a melt from the Eoarchean

granitoids and the Upernavik rocks or source. This should however also affect the Hf isotopic composition, but such mixing is not consistent with the ε^{176}Hf-zircon of the Iluilik zircons (Chapter 2). It was proposed in Chapter 2 that the geochemical compositions of these granodiorites are more consistent with remelting of a mafic precursor rather than a felsic source. Based on the Hf isotopic composition of the Iluilik granodiorite zircons, a ∼4200-4300 Ma enriched mafic crustal reservoir was suggested as their precursorcrustal source (Chapter 2). Figure 3.6 shows that a 4200 Ma enriched mafic crust with a ^{147}Sm/^{144}Nd of 0.165, derived from an early Saglek depleted mantle source, would evolved to a μ^{142}Nd value of ∼+6, as measured in granodiorite sample SG-203. Therefore, similarly to the ε^{176}Hf-zircon and whole-rock geochemical composition, the lower ^{142}Nd/^{144}Nd of the Iluilik granodiorite could be explained by remelting of Hadean mafic crust. The sample SG-208 is also from the Iluilik age, however, is a granite that yields a μ^{142}Nd value of $+12.4 \pm 3.8$, similar to Eoarchean tonalites and trondhjemites that could be consistent with the crustal reworking of the SHC felsic crust.

Both samples from the 3200 Ma Lister gneiss yield μ^{142}Nd values unresolved from the Nd terrestrial standard (Fig. 3.6). Along with a single Neoarchean granite sample, the Lister gneiss is the only granitoid unit in the SHC showing no ^{142}Nd anomaly. The Lister gneiss also exhibits more radiogenic initial ε^{143}Nd values between +0.1 and +1.2 at 3230Ma, compared to the 3330 Ma Iluilik gneiss. The Hf isotopic composition of the Lister gneiss also showed the contribution of more juvenile material with suprachondritic ε^{176}Hf values of its zircons (Chapter 2). This near-chondritic composition for the Lister gneiss could suggest a common source with the Upernavik unit, which appears to be chondritic in both Nd and Hf isotopic compositions, with no ^{142}Nd anomaly (Morino et al., 2017, 2018). The Lister gneiss, however, shows slightly more radiogenic ε^{143}Nd

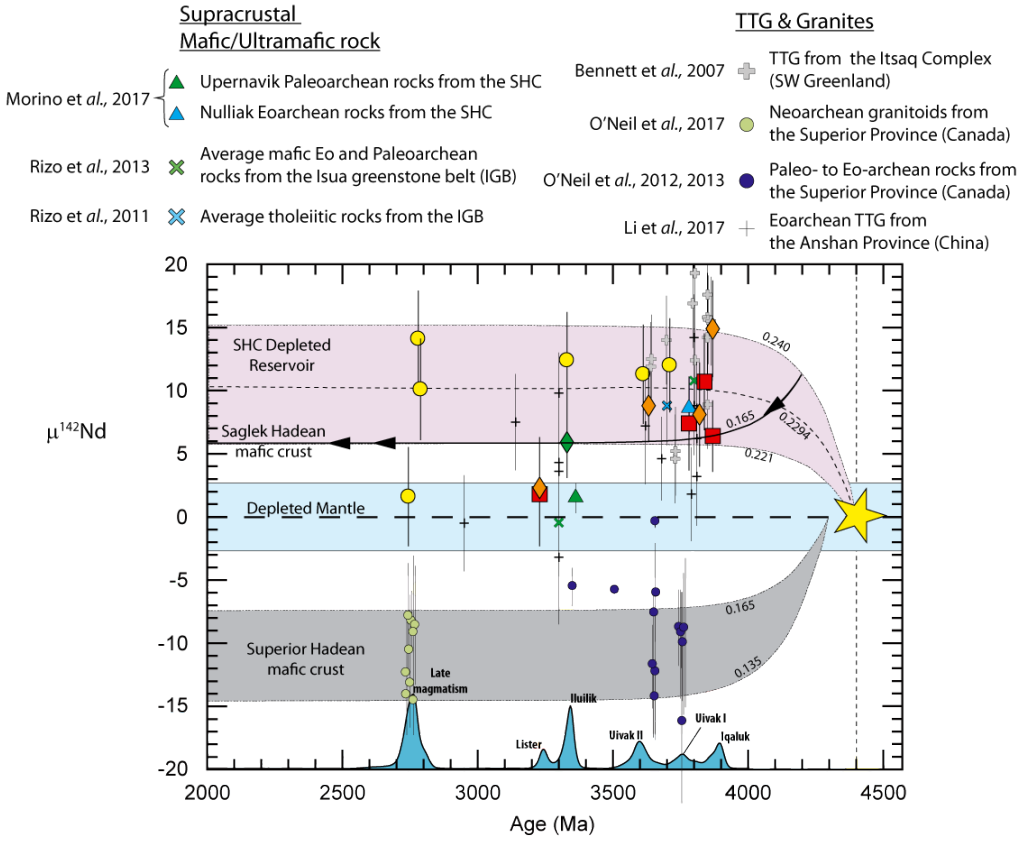

Figure 3.6

$^{207}Pb/^{206}Pb$ age (Ma) *vs.* $\mu^{142}Nd$ that shows the evolution of the $^{142}Nd/^{144}Nd$ isotopic ratio over the first 1500 Ma of the SHC history. Salgek's data are from Morino et al. (2017), SW Greenland data are from Bennett et al. (2007); Rizo et al. (2011, 2013), and Nuvvuagittuq data are from O'Neil et al. (2012); O'Neil and Carlson (2017). At 4200 Ma we modeled the extraction of a mafic crust;, with a $^{147}Sm/^{144}Nd$ ratio of 0.165, which represents the hypothetical precursors of the Iluilik tonalites. All other mafic precursors have been differentiated after or to close to the extinction of the ^{146}Nd, therefore, xhibit $\sim$+10 $\mu^{142}Nd$ anomaly. The symbols from our study are as in Figure 3.2.

and $\varepsilon^{176}Hf$ compared to the composition of the Upernavik unit obtained by Morino et al. (2017, 2018). If the $\sim$3400 Ma Upernavik rock exhibits a subchondritic Sm/Nd and Lu/Hf ratios and this unit is the crustal precursor source of the younger Lister unit, one would expect the Lister gneisses to exhibit a higher $\varepsilon^{143}Nd$ and $\varepsilon^{176}Hf$ initial values. Another possible crustal source for the Lister gneiss could be the 3560 Ma mafic Saglek dikes that yielded an initial $\varepsilon^{143}Nd$ value of +1.7 (Flageole, 2019). The uncer-

tainties on initial ε^{143}Nd and ε^{176}Hf values may not allow the identification of an exact crustal source of the Lister gneiss, but increasing evidence points to the existence in the SHC of a near-chondritic reservoir (ε^{143}Nd, ε^{176}Hf) without ^{142}Nd anomaly in the Late Paleoarchean. This supposed source appears however not to have been involved during the Neoarchean magmatism.

Crustal evolution in the Neoarchean

The SHC Neoarchean granitoids are dominated by granites. The Hf isotopic composition of the zircons from the Neoarchean granitoid showed that they were mainly produced by crustal reworking of the Eoarchean Iqaluk and Uivak gneisses (Chapter 2). All Neoarchean samples analysed here have low initial ^{143}Nd/^{144}Nd ratios that would be consistent with reworking an old crustal felsic source (Fig. 3.3). Out of the three Neoarchean granite samples analysed, two show positive μ^{142}Nd values comparable to the Eoarchean TTG, suggesting that remelting of the Iqaluk and Uivak gneisses was the likely process forming the SHC Neoarchean crust. One granite sample (SG-037), however, has no ^{142}Nd anomaly and therefore cannot be derived from the Eoarchean TTG. If we assume, based on its granitic composition, that the precursor source of SG-037 was a felsic tonalitic-trondhjemitic reservoir, and with no ^{142}Nd anomaly, the only known candidate in the SHC would be the 3200 Ma Lister gneiss. It would however require a ^{147}Sm/^{144}Nd ratio of 0.03 to evolved from ε^{143}Nd =+0.3 (Lister gneiss SG-265) to ε^{143}Nd =-10.1 (observed in SG-037), between 3230 and 2740 Ma. Such a low ^{147}Sm/^{144}Nd ratio is unrealistic for a typical tonalite-trondhjemite, especially given the ^{147}Sm/^{144}Nd of 0.100 to 0.133 measured in the Lister gneiss samples (Table 3.1). The granite sample SG-037 contains inherited zircon with ^{207}Pb/^{206}Pb age of 3300 Ma, which could be consistent with the 3300 Ma Iluilik gneiss as its crustal precursor. The

Iluilik granodiorite exhibit a lower initial ε^{143}Nd values associated with a slight positive ^{142}Nd anomaly (μ^{142}Nd = +5.9). Strictly according to the μ^{142}Nd value, the Iluilik granodiorite as the source of the granite SG-037 (μ^{142}Nd = +1.6) could be inconsistent. However, given the typical resolution of ∼3-4 ppm error on the ^{142}Nd/^{144}Nd ratio of each sample analysed, this scenario cannot be discarded. The exact crustal source of the Neoarchean granite with no ^{142}Nd remains unclear but this hints to the existence of a crustal reservoir with lower ^{142}Nd/^{144}Nd than the Eoarchean TTG dominating the SHC, which was also reworked in the Neoarchean.

3.6 Conclusion

The combined $^{147-146}$Sm-$^{143-142}$Nd isotopes are a powerful tool to understand and constraint early crustal processes. Here, we have studied these systematics in well characterized granitoids from the SHC. The Saglek-Hebron Complex felsic crust formed 3870 Ma ago and recorded crustal growth over ∼600 Ma. While the long-lived Sm-Nd system suggests this felsic crust derived from a Hadean mafic precursor, ^{142}Nd results indicate the presence of at least two different reservoirs from which the crust has been extracted. Most Archean granitoids exhibit similar ^{142}Nd positive anomaly as the Nuliak supracrustal mafic and ultramafic rocks with μ^{142}Nd values up to +15. Therefore, the positive μ^{142}Nd of ∼+15 of the Eoarchean TTG might have been inherited from the mafic metavolcanic rocks. Combined $^{147-146}$Sm-$^{143-142}$Nd results suggest that the mantle source of the Saglek rocks was depleted in incompatible elements and that it differentiated early on Earth's history evolving with a ^{147}Sm/^{144}Nd ratio of 0.246. The Paleoarchean Lister gneiss does not exhibit ^{142}Nd anomalies and is characterized by a chondritic ε^{143}Nd initial value, suggesting its source is more juvenile. In comparison,

the Iluilik granodiorites that have similar ages to the Lister gneiss, exhibit a μ^{142}Nd anomaly of +6 associated with a low ε^{143}Nd initial suggesting these rocks have a different source, more consistent with their derivation from a Hadean mafic crust. The Neoarchean magmatism in Saglek is dominated by the crustal reworking processes with rocks exhibiting either positive or no anomalies in ^{142}Nd and very low ε^{143}Nd initial values down to -11. The SHC geological history seems to be associated with the Itsaq gneiss complex in SW Greenland. Similar μ^{142}Nd anomalies have been measured in Eoarchean ultramafic, mafic and granitoid rocks (*e.g.* Rizo et al., 2011, 2013; Bennett et al., 2007) as well as very similar initial ε^{143}Nd and ε^{176}Hf (Chapter 2; Rizo et al., 2011, 2013; Bennett et al., 2007; O'Neil and Carlson, 2017; Hoffmann et al., 2011) suggesting a common evolution. Furthermore, the Paleoarchean geological history seems to have recorded similar events leading to the production of juvenile crust in both terrains. However, while the Itsaq terrain recorded a maintained production of juvenile TTG (Næraa et al., 2012), the SHC experienced a short juvenile magmatic activity followed by a large scale thermal event that reworked most of the Saglek's felsic crust (Kusiak et al., 2018; Schiøtte et al., 1992; Van Kranendonk, 1990).

Supplementary material appendix C

Table C.1: Summary of the major (wt. %; anhydrous composition) and trace (ppm) element composition associated with the respective age and epsilon Hf initial values for the SHC granitoids used in this study. Data are from chapter 2. Coordinates are in UTM NAD 27 Zone 20

Table C.2: Detail summary of the analytic conditions for the Nd isotopic analyses

Table C.3: Cup configurations used for both Sm-Nd and ^{142}Nd analysis

Table C.4: Full results of the dynamic analysis of ^{142}Nd/^{144}Nd isotopic composition for each analytic session. Label *"a"*, *"b"* refer to duplicate runs of the sample filament for a single samples. The compilation of both a and b duplicate analysis is label as *"tot"*

References

Baadsgaard, H., Collerson, K. D., Bridgwater, D., 1979. The Archean gneiss complex of northern Labrador. 1. Preliminary U-Th-Pb geochronology. Canadian Journal of Earth Sciences, 951–961.

Bennett, V., 2003. Compositional evolution of the mantle. In: Carlson, R. (Ed.), Treatise on geochemistry, volume 2: The mantle. New York, pp. 493–519.

Bennett, V. C., Brandon, A. D., Nutman, A. P., 2007. Coupled 142Nd-143Nd isotopic evidence for Hadean mantle dynamics. Science 318 (5858), 1907–1910.
URL http://www.sciencemag.org/cgi/doi/10.1126/science.1145928

Bennett, V. C., Nutman, A. P., McCulloch, M. T., 1993. Nd isotopic evidence for transient, highly depleted mantle reservoirs in the early history of the Earth. Earth and Planetary Science Letters 119 (3), 299–317.

Bouvier, A., Vervoort, J. D., Patchett, P. J., 2008. The LuHf and SmNd isotopic composition of CHUR: Constraints from unequilibrated chondrites and implications for the bulk composition of terrestrial planets. Earth and Planetary Science Letters 273 (12), 48–57.

Bowring, S. a., Williams, I. S., 1999. Priscoan (4.00-4.03 Ga) orthogneisses from northwestern Canada. Contributions to Mineralogy and Petrology 134 (July 1998), 3–16.

Boyet, M., Carlson, R. W., 2005. 142Nd evidence for early (>4.53 Ga) global differentiation of the silicate Earth. Science (New York, N.Y.) 309 (5734), 576–81.
URL http://science.sciencemag.org/content/309/5734/576.abstract

Boyet, M., Carlson, R. W., 2006. A new geochemical model for the Earth's mantle inferred from 146Sm142Nd systematics. Earth and Planetary Science Letters 250 (12), 254–268.

Bridgwater, D., Collerson, K. D., 1976. The major petrological and geochemical characters of the 3,600 m.y. Uivak gneisses from Labrador. Contributions to Mineralogy and Petrology 54 (1), 43–59.

Bridgwater, D., Collerson, K. D., Hurst, R. W., Jesseau, C. W., 1975. Field characters of the early precambrian rocks from Saglek, Coast of Labrador. Geological survey of Canada 75 (1), 287–296.

Bridgwater, D., Schiøtte, L., 1991. The Archean gneiss complex of northern Labrador. A review of current results, ideas and problems. Bulletin of the Geological Society of Denmark 39 (3-4), 153–166.

Carlson, R. W., Lucia, A., Araujo, N., Junqueira-Brod, T. C., Carlos Gaspar, J., Affonso Brod, J., Petrinovic, I. A., Helena, M., Hollanda, B. M., Pimentel, M. M., Sichel, S., 2007. Chemical and isotopic relationships between peridotite xenoliths and mafic-ultrapotassic rocks from Southern Brazil. Chemical Geology 242, 415–434. URL www.elsevier.com/locate/chemgeoCorrespondingauthor.Fax: +12024878821.

Caro, G., Bourdon, B., Birck, J. L., Moorbath, S., 2006. High-precision 142Nd/144Nd measurements in terrestrial rocks: Constraints on the early differentiation of the Earth's mantle. Geochimica et Cosmochimica Acta 70, 164–191.

Caro, G., Bourdon, B., Brick, J.-L., Moorbath, S., 2003. 146Sm-142Nd evidence from Isua metamorphosed sediments for early differentiation of the Earth's mantle. Nature 423, 428–432.
URL www.nature.com/nature.

Collerson, K., 1983. Ion Microprobe Zircon Geochrnonology of the Uivak Gneiss: Implication for the evolution of the early terrestrial crust in the north Atlantic craton. Workshop on a Cross Section of Archean Crust. LPI Technical report, 83-03, 28–33.

Collerson, K. D., Campbell, L. M., Weaver, B. L., Palacz, Z. A., 1991. Evidence for extreme mantle fractionation in early Archean ultramafic rocks from northern Labrador. Nature 349 (6306), 209–214.

Debaille, V., O'neill, C., Brandon, A. D., Haenecour, P., Yin, Q.-Z., Mattielli, N., Treiman, A. H., 2013. Stagnant-lid tectonics in early Earth revealed by 142 Nd variations in late Archean rocks. Earth and Planetary Science Letters 373, 83–92.
URL http://dx.doi.org/10.1016/j.epsl.2013.04.016

Flageole, J., 2019. Sm-Nd Isotopic Composition of Mantle-Derived Rocks from the Saglek-Hebron Gneiss Complex, Northern Labrador. Msc, University of Ottawa.

Garçon, M., Boyet, M., Carlson, R., Horan, M., Auclaire, D., Mock, T., jan 2018. Factors influencing the precision and accuracy of Nd isotope measurements by thermal ionization mass spectrometry. Chemical Geology 476, 493–514.
URL https://www-sciencedirect-com.proxy.bib.uottawa.ca/science/article/pii/S0009254117306769

Hensen, B., Zhou, B., 1995. Retention of isotopic memory in garnets partially broken down during an overprinting granulite-facies metamorphism: implications for the Sm-Nd closure temperature. Geology 23 (3), 225–228.
URL https://pubs.geoscienceworld.org/gsa/geology/article-pdf/23/3/225/3515608/i0091-7613-23-3-225.pdf

Hoffmann, J. E., Munker, C., Naeraa, T., Rosing, M. T., Herwartz, D., Garbe-Schonberg, D., Svahnberg, H., 2011. Mechanisms of Archean crust formation inferred from high-precision HFSE systematics in TTGs. Geochimica et Cosmochimica Acta 75 (15), 4157–4178.

Hurst, R. W., Bridgwater, D., Collerson, K. D., Wetherill, G. W., 1975. 3600-m,y, Rb-Sr ages from very early Archean gneisses from Saglek Bay, Labrador. Earth and Planetary Science Letters 27, 393–403.

Ishikawa, A., Suzuki, K., Collerson, K. D., Liu, J., Pearson, D. G., Komiya, T., 2017. Rhenium-osmium isotopes and highly siderophile elements in ultramafic rocks from the Eoarchean Saglek Block, northern Labrador, Canada: implications for Archean mantle evolution. Geochimica et Cosmochimica Acta 216, 286–311.

Jung, S., Mezger, K., 2001. Geochronology in migmatites - a Sm-Nd, U-Pb and Rb-Sr study from the Proterozoic Damara belt (Namibia): Implications for polyphase development of migmatites in high-grade terranes. Journal of Metamorphic Geology 19 (1), 77–97.

Komiya, T., Yamamoto, S., Aoki, S., Koshida, K., Shimojo, M., Sawaki, Y., Aoki, K., Sakata, S., Yokoyama, T. D., Maki, K., Ishikawa, A., Hirata, T., Collerson, K. D., 2017. A prolonged granitoid formation in Saglek Block, Labrador: Zonal growth and crustal reworking of continental crust in the Eoarchean. Geoscience Frontiers 8 (2), 355–385.

Komiya, T., Yamamoto, S., Aoki, S., Sawaki, Y., Ishikawa, A., Tashiro, T., Koshida, K., Shimojo, M., Aoki, K., Collerson, K. D., nov 2015. Geology of the Eoarchean, > 3.95 Ga, Nulliak supracrustal rocks in the Saglek Block, northern Labrador, Canada: The oldest geological evidence for plate tectonics. Tectonophysics 662, 40–66.

Krogh, T., Kamo, S., 2006. Precise U-Pb zircon ID-TIMS ages provide an alternative interpretation to the early ion microprobe ages and new insights into Archean crustal processes, northern Labrador. In: Reimold, W., Gibson, R. (Eds.), Processes on the Early Earth. Geological Society of America, pp. 91–103.

Kusiak, M. A., Dunkley, D. J., Whitehouse, M. J., Wilde, S. A., Sałacińska, A., Konečný, P., Szopa, K., Gawęda, A., Chew, D., 2018. Peak to post-peak thermal history of the Saglek Block of Labrador: A multiphase and multi-instrumental approach to geochronology. Chemical Geology 484 (May), 210–223.

Li, C. F., Wang, X. C., Li, Y. L., Chu, Z. Y., Guo, J. H., Li, X. H., 2015. Ce-Nd separation by solid-phase micro-extraction and its application to high-precision 142Nd/144Nd measurements using TIMS in geological materials. Journal of Analytical Atomic Spectrometry 30 (4), 895–902.

Li, C. F., Wang, X. C., Wilde, S. A., Li, X. H., Wang, Y. F., Li, Z., 2017. Differentiation of the early silicate Earth as recorded by 142Nd-143Nd in 3.83.0 Ga rocks from the Anshan Complex, North China Craton. Precambrian Research 301, 86–101. URL http://dx.doi.org/10.1016/j.precamres.2017.09.001

Marks, N. E., Borg, L. E., Hutcheon, I. D., Jacobsen, B., Clayton, R. N., 2014. Samarium-neodymiumchronology and rubidium-strontium systematics of an Allende calcium-aluminum-rich inclusion with implications for 146Sm half-life. Earth and Planetary Science Letters 405, 15–24.

Martin, H. N., 1987. Petrogenesis of Archean Trondhjemites, Tonalites, and Granodiorites from eastern Finland: Major and Trace Element Geochemistry. Journal of Petrology 28 (5), 921–953.

Meissner, F., Schmidt-Ott, W. D., Ziegeler, L., jun 1987. Half-life and α-ray energy of146Sm. Zeitschrift for Physik and Atomic Nuclei 327 (2), 171–174.

Morino, P., Caro, G., Reisberg, L., 2018. Differentiation mechanisms of the early Hadean mantle: Insights from combined176Hf-142,143Nd signatures of Archean rocks from the Saglek Block. Geochimica et Cosmochimica Acta 240, 43–63.

Morino, P., Caro, G., Reisberg, L., Schumacher, A., 2017. Chemical stratification in the post-magma ocean Earth inferred from coupled 146,147Sm142,143Nd systematics in ultramafic rocks of the Saglek block (3.253.9 Ga; northern Labrador, Canada). Earth and Planetary Science Letters 463, 136–150.

Næraa, T., Scherstén, A., Rosing, M. T., Kemp, a. I. S., Hoffmann, J. E., Kokfelt, T. F., Whitehouse, M. J., 2012. Hafnium isotope evidence for a transition in the dynamics of continental growth 3.2 Gyr ago. Nature 485 (7400), 627–630.

Nutman, A. P., Collerson, K. D., 1991. Very early Archean crustal-accretion complexes preserved in the North Atlantic craton. Geology 19, 791–794.

Nutman, A. P., Fryer, B. J., Bridgwater, D., 1989. The early Archaean Nulliak (supracrustal) assemblage, northern Labrador. Can. J. Earth Sci. 26, 2159–2168.

O'Neil, J., Carlson, R., Papineau, D., Levine, Y., Francis, D., 2019. The Nuvvuagittuq greenstone belt: A glimpse of Earth's earliest crust. In: Van Kranendonk, M. J., Bennett, V. C., Hoffmann, J. E. (Eds.), Earth's Oldest Rocks, 2nd Edition. Elsevier, Ch. 16, pp. 349–374.

O'Neil, J., Carlson, R. W., 2017. Building Archean cratons from Hadean mafic crust. Science 355 (6330).

O'Neil, J., Carlson, R. W., Francis, D., Stevenson, R. K., 2008. Neodymium-142 evidence for hadean mafic crust. Science 321 (5897), 1828–1831.

O'Neil, J., Carlson, R. W., Paquette, J. L., Francis, D., 2012. Formation age and metamorphic history of the Nuvvuagittuq Greenstone Belt. Precambrian Research 220-221, 23–44.

O'Neil, J., Rizo, H., Boyet, M., Carlson, R. W., Rosing, M. T., 2016. Geochemistry and Nd isotopic characteristics of Earth's Hadean mantle and primitive crust. Earth and Planetary Science Letters 442, 194–205.

Puchtel, I. S., Blichert-Toft, J., Touboul, M., Horan, M. F., Walker, R. J., jun 2016. The coupled 182 W- 142 Nd record of early terrestrial mantle differentiation. Geochemistry, Geophysics, Geosystems 17 (6), 2168–2193.
URL http://doi.wiley.com/10.1002/2016GC006324

Reimink, J. R., Chacko, T., Carlson, R. W., Shirey, S. B., Liu, J., Stern, R. A., Bauer, A. M., Pearson, D. G., Heaman, L. M., 2018. Petrogenesis and tectonics of the Acasta Gneiss Complex derived from integrated petrology and 142 Nd and 182 W extinct nuclide-geochemistry. Earth and Planetary Science Letters 494, 12–22.
URL www.elsevier.com/locate/epsl

Reimink, J. R., Chacko, T., Stern, R. A., Heaman, L. M., aug 2016. The birth of a cratonic nucleus: Lithogeochemical evolution of the 4.02-2.94 Ga Acasta Gneiss Complex. Precambrian Research 281, 453–472.

Rizo, H., Boyet, M., Blichert-toft, J., Neil, J. O., Rosing, M. T., Paquette, J.-l., 2012. The elusive Hadean enriched reservoir revealed by 142Nd deficits in Isua Archaean rocks. Nature 490 (7422), 96–100.

Rizo, H., Boyet, M., Blichert-Toft, J., Rosing, M., 2011. Combined Nd and Hf isotope evidence for deep-seated source of Isua lavas. Earth and Planetary Science Letters 312 (3-4), 267–279.
URL http://dx.doi.org/10.1016/j.epsl.2011.10.014

Rizo, H., Boyet, M., Blichert-Toft, J., Rosing, M. T., 2013. Early mantle dynamics inferred from 142Nd variations in Archean rocks from southwest Greenland. Earth and Planetary Science Letters 377-378, 324–335.
URL http://dx.doi.org/10.1016/j.epsl.2013.07.012

Roth, A. S., Bourdon, B., Mojzsis, S. J., Touboul, M., Sprung, P., Guitreau, M., Blichert-Toft, J., jan 2013. Inherited 142Nd anomalies in Eoarchean protoliths. Earth and Planetary Science Letters 361, 50–57.
URL https://www.sciencedirect.com/science/article/pii/S0012821X12006413

Roth, A. S. G., Bourdon, B., Mojzsis, S. J., Rudge, J. F., Guitreau, M., Blichert-Toft, J., jun 2014. Combined 147,146 Sm- 143,142 Nd constraints on the longevity

and residence time of early terrestrial crust. Geochemistry, Geophysics, Geosystems 15 (6), 2329–2345.
URL http://doi.wiley.com/10.1002/2014GC005313

Rudnick, R. L., 1992. Restites, Eu anomalies and the lower continental crust. Geochimica & Cosmochimica Acta 56, 963–970.

Ryan, B., Martineau, Y., 2012. Revised and coloured edition of 1992 map showing the Geology of the Saglek Fiord - Hebron Fiord area, Labrador (NTS 14L/2,3,6,7). Scale: 1:100 000. Government of Newfoundland and Labrador, Department of Natural Resources, Geological Survey, Map 2012-15, Open File 14L/0091.

Sałacińska, A., Kusiak, M. A., Whitehouse, M. J., Dunkley, D. J., Wilde, S. A., Kielman, R., 2018. Complexity of the early Archean Uivak Gneiss: Insights from Tigigakyuk Inlet, Saglek Block, Labrador, Canada and possible correlations with south West Greenland. Precambrian Research 315 (October 2017), 103–119.

Schiøtte, L., Bridgwater, D., Collerson, K. D., Nutman, A. P., Ryan, A. B., 1986. Chemical and isotopic effects of Late Archean high-grade metamorphism and granite injection on early Archean gneisses, Saglek-Hebron, northern Labrador. In: J.B. Dawson, D.A. Carswell, J. Hale, K. W. (Ed.), The nature of the lower continental cruste. Geol. Soc. Lond. Spec. Publ., pp. 261–273.

Schiøtte, L., Compston, W., Bridgwater, D., 1989. U-Th-Pb ages of single zircons in Archaean supracrustals from Nain Province, Labrador, Canada. Can. J. Earth Sci. 26, 2636–2644.

Schiøtte, L., Nutman, A. P., Bridgwater, D., 1992. U-Pb ages of single zircons within Upernavik metasedimentary rocks and regional implications for the tectonic evolution of the Archaean Nain Province, Labrador. Can. J. Earth Sci. 29, 260–276.

Shimojo, M., Yamamoto, S., Sakata, S., Yokoyama, T. D., Maki, K., Sawaki, Y., Ishikawa, A., Aoki, K., Aoki, S., Koshida, K., Tashiro, T., Hirata, T., Collerson, K. D., Komiya, T., 2016. Occurrence and geochronology of the Eoarchean, ˜3.9Ga, Iqaluk Gneiss in the Saglek Block, northern Labrador, Canada: Evidence for the oldest supracrustal rocks in the world. Precambrian Research 278, 218–243.

Sun, S., McDonough, W., 1989. Chemical and isotopic systematics of oceanic basalts: implications for manlte composition and processes and processes. In: Suanders, A., Norry, M. (Eds.), Magmatism in the Ocean Basins, vol. 42 Edition. The geological society, pp. 313–345.

Tanaka, T., Togashi, S., Kamioka, H., Amakawa, H., Kagami, H., Hamamoto, T., Yuhara, M., Orihashi, Y., Yoneda, S., Shimizu, H., Kunimaru, T., Takahashi, K.,

Yanagi, T., Nakano, T., Fujimaki, H., Shinjo, R., Asahara, Y., Tanimizu, M., Dragusanu, C., aug 2000. JNdi-1: a neodymium isotopic reference in consistency with LaJolla neodymium. Chemical Geology 168 (3-4), 279–281.
URL https://linkinghub.elsevier.com/retrieve/pii/S0009254100001984

Van Kranendonk, M., 1990. Late Archean geologic history of the Nain Province, North River-Nutak map area, Labrador, and its tectonic significance. Geoscience Canada 17 (4), 231–237.

Vance, D., O'Nions, R., mar 1990. Isotopic chronometry of zoned garnets: growth kinetics and metamorphic histories. Earth and Planetary Science Letters 97 (3-4), 227–240.
URL https://www-sciencedirect-com.proxy.bib.uottawa.ca/science/article/pii/0012821X9090044X?via{%}3Dihub

Vezinet, A., Pearson, D., Thomassot, E., Stern, R., Sarkar, C., Luo, Y., Fisher, C., 2018. Hydrothermally-altered mafic crust as source for early Earth TTG: Pb/Hf/O isotope and trace element evidence in zircon from TTG of the Eoarchean Saglek Block, N. Labrador. Earth and Planetary Science Letters 503, 95–107.

Wang, Y. F., Li, X. H., Jin, W., Zhang, J. H., 2015. Eoarchean ultra-depleted mantle domains inferred from ca. 3.81Ga Anshan trondhjemitic gneisses, North China Craton. Precambrian Research 263, 88–107.
URL http://dx.doi.org/10.1016/j.precamres.2015.03.005

Wasilewski, B., O'Neil, J., Rizo, H., 2019. Geochemistry and petrogneesis of the early Archean mafic crust from the Saglek-Hebron Complex (Northren labrador). Precambrian geology 328, 129–150.

Whitehouse, M. J., Dunkley, D. J., Kusiak, M. A., Wilde, S. A., 2019. On the true antiquity of Eoarchean chemofossils assessing the claim for Earth's oldest biogenic graphite in the Saglek Block of Labrador. Precambrian Research.

Chapter 4

Conclusion

This Ph.D. thesis has contributed to new insights on the origin and evolution of the Archean Saglek-Hebron Complex of Northern Labrador, Canada. A detailed petrological, geochemical and geochronological study of mafic, ultramafic and granitoid rocks from this complex allowed a better understanding of the timing and petrogenesis of one of the oldest terranes on Earth. Over the course of this study, we have performed 248 geochemical major and trace element analysis, 1500 single zircon U-Pb in situ analysis, 285 Lu-Hf in situ analysis of zircons, and 15 whole-rock $^{147-146}$Sm-$^{143-142}$Nd studies. Results from these analyses led to several hypotheses, including the following:

1. The petrogenesis of the mafic rocks from Saglek reflects fractional crystallization processes of primary mafic magmas forming pyroxene-rich cumulates and more evolved basaltic liquids. Two groups of ultramafic rocks have been defined that are interpreted as olivine-rich cumulates derived from komatiitic basalt parental magmas with different Fe concentrations. Contrary to previous interpretations, we suggest that none of these ultramafic rocks are truly komatiites or residual lithospheric mantle.

2. Granitoids of the SHC consist of rocks from the TTG series (trondhjemites, Mg-rich tonalites, and granodiorites) and granites. All TTG seem to derive from mafic precursors and the trondhjemites show geochemical evidence of restitic composition. The granites derive from the crustal reworking of TTG.

3. Zircon U-Pb geochronology allowed refining the age for the granitoids of the SHC. Contrary to previous studies, we have found that specific geochemical compositions of granitoids are not restricted to defined ages but rather occur at different times during the geological history of the SHC. The oldest rocks in the SHC are the Iqaluk gneiss, that yield an U-Pb age of ∼3870 Ma instead of the previously defined age of ∼3920 Ma (Shimojo et al., 2016), but consistent with results

from other publications (Whitehouse et al., 2019; Vezinet et al., 2018). Later felsic magmatism includes a the Uivak I & II suites of TTG respectively intruded ∼3750 and ∼3600 Ma, the newly recognized Paleoarchean unit, called the Iluilik gneiss emplaced at 3330 Ma, the Lister gneiss emplaced ∼3220 Ma ago, and late granites emplaced at ∼2700 Ma

4. The Hf isotopes on zircons, combined with U-Pb geochronology, show that Eoarchean TTG are mostly juvenile and derived from a slightly suprachondritic mantle. Combined U-Pb-Hf with whole-rock geochemical compositions suggests that some SHC TTG may be derived from the melting of Hadean mafic crust. A shift in Hf isotopic composition occurred in the Paleoarchean that produced briefly more juvenile crust at 3200 Ma (Lister gneiss).

5. The combined long- and short-lived Sm-Nd isotope study of these well characterized granitoids show that a Hadean mantle source is involved in the majority of the SHC magmas. Crustal reworking between 3800 Ma and 2700 Ma appears to be an important process in the evolution of the SHC, but the ∼3200 Ma Lister gneiss shows a different Nd isotopic composition to most other granitoids, suggesting that more than a single crustal reservoir is involved in the crustal formation of the SHC.

Since the early 70's the SHC has been considered related to the Eoarchean Itsaq Gneiss Complex (IGC) of SW Greenland. This thesis showed that the different lithologies from both complexes share some similarities but also distinctions, such as the absence of boninite-like rocks in the SHC. The early crustal history of both complexes is also comparable with the involvement of an early depleted mantle reservoir and the abrupt shift in isotopic composition at the end of the Paleoarchean, but the Neoarchean

crustal processes appear to diverge. Further geochemical and isotopic work would be required to better establish the link between these two important pieces of Earth's earliest crust.

Most research on the SHC originally took place during the last century. It produced important foremost papers that built the fundamental descriptions of the SHC and uncovered the existence of some of the oldest rocks in the world. Almost 20 years later and after the tremendous technological advances made the past decades, I and multiple other teams worldwide, were committed to pursuing research, add a brick to what we already know about the SHC and make progress and advances in early Earth research. This thesis is the accomplishment of almost five years of fieldwork, meticulous lab work, data computing, and interpretation. Nonetheless, there are still numerous questions pending to be answered. Therefore, the Saglek-Hebron Complex does show a considerable potential to uncover the past tectonics, the nature of early crust and perhaps the oldest traces of life.

References

Shimojo, M., Yamamoto, S., Sakata, S., Yokoyama, T. D., Maki, K., Sawaki, Y., Ishikawa, A., Aoki, K., Aoki, S., Koshida, K., Tashiro, T., Hirata, T., Collerson, K. D., Komiya, T., 2016. Occurrence and geochronology of the Eoarchean, ˜3.9Ga, Iqaluk Gneiss in the Saglek Block, northern Labrador, Canada: Evidence for the oldest supracrustal rocks in the world. Precambrian Research 278, 218–243.

Vezinet, A., Pearson, D., Thomassot, E., Stern, R., Sarkar, C., Luo, Y., Fisher, C., 2018. Hydrothermally-altered mafic crust as source for early Earth TTG: Pb/Hf/O isotope and trace element evidence in zircon from TTG of the Eoarchean Saglek Block, N. Labrador. Earth and Planetary Science Letters 503, 95–107.

Whitehouse, M. J., Dunkley, D. J., Kusiak, M. A., Wilde, S. A., 2019. On the true antiquity of Eoarchean chemofossils assessing the claim for Earth's oldest biogenic graphite in the Saglek Block of Labrador. Precambrian Research.

Appendix A

Supplementary materials for the "Chapter 1"

This appendix contains all Supplementary Figures and Tables referenced in Chapter 1: "Geochemisrty and petrogenesis of the early Archean mafic crust from the Saglek-Hebron Complex (Northern Labrador)".

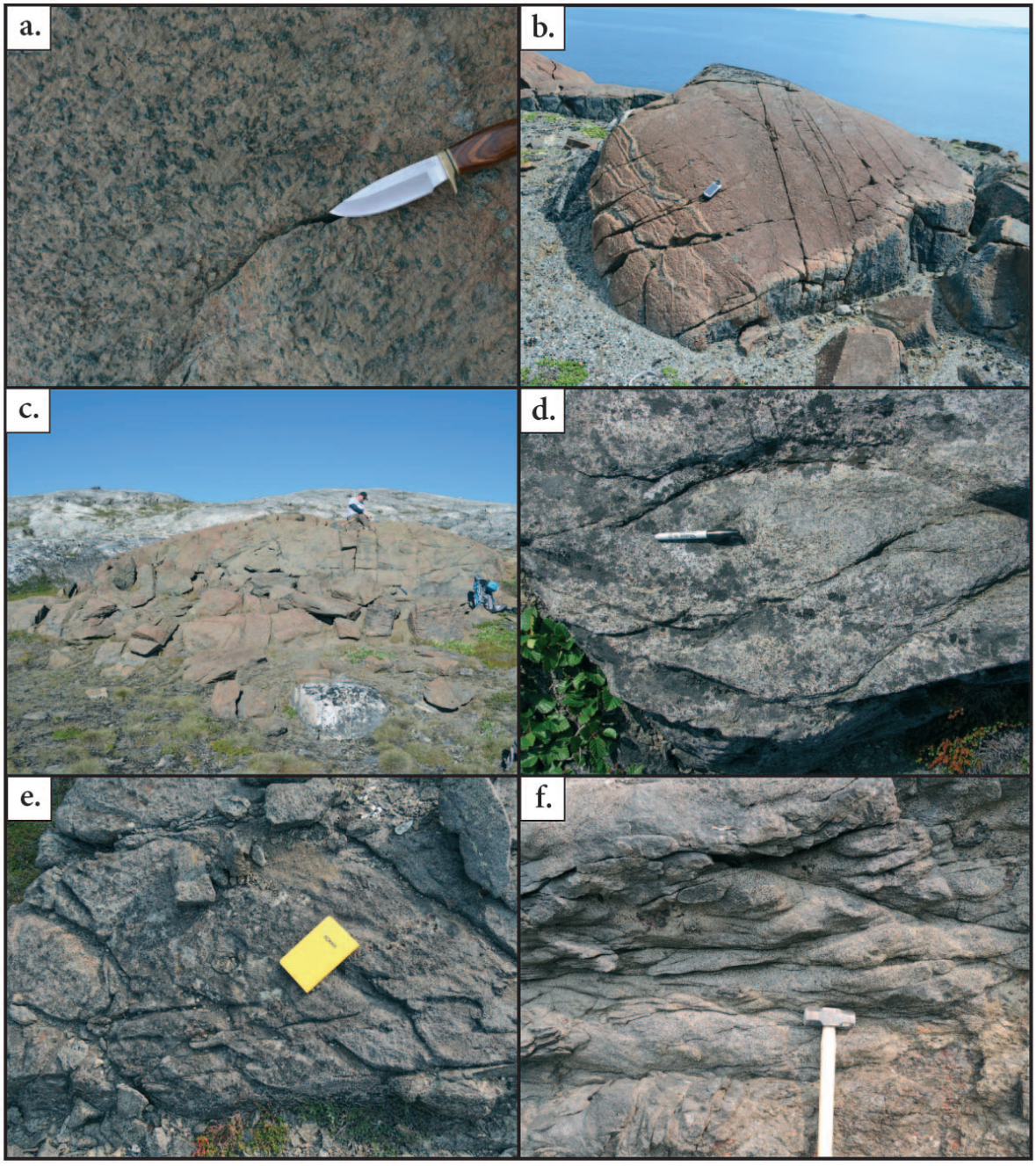

Figure A.1

Fieldwork photographs of the mafic and ultramafic rocks. Full descriptions at the end of the figure.

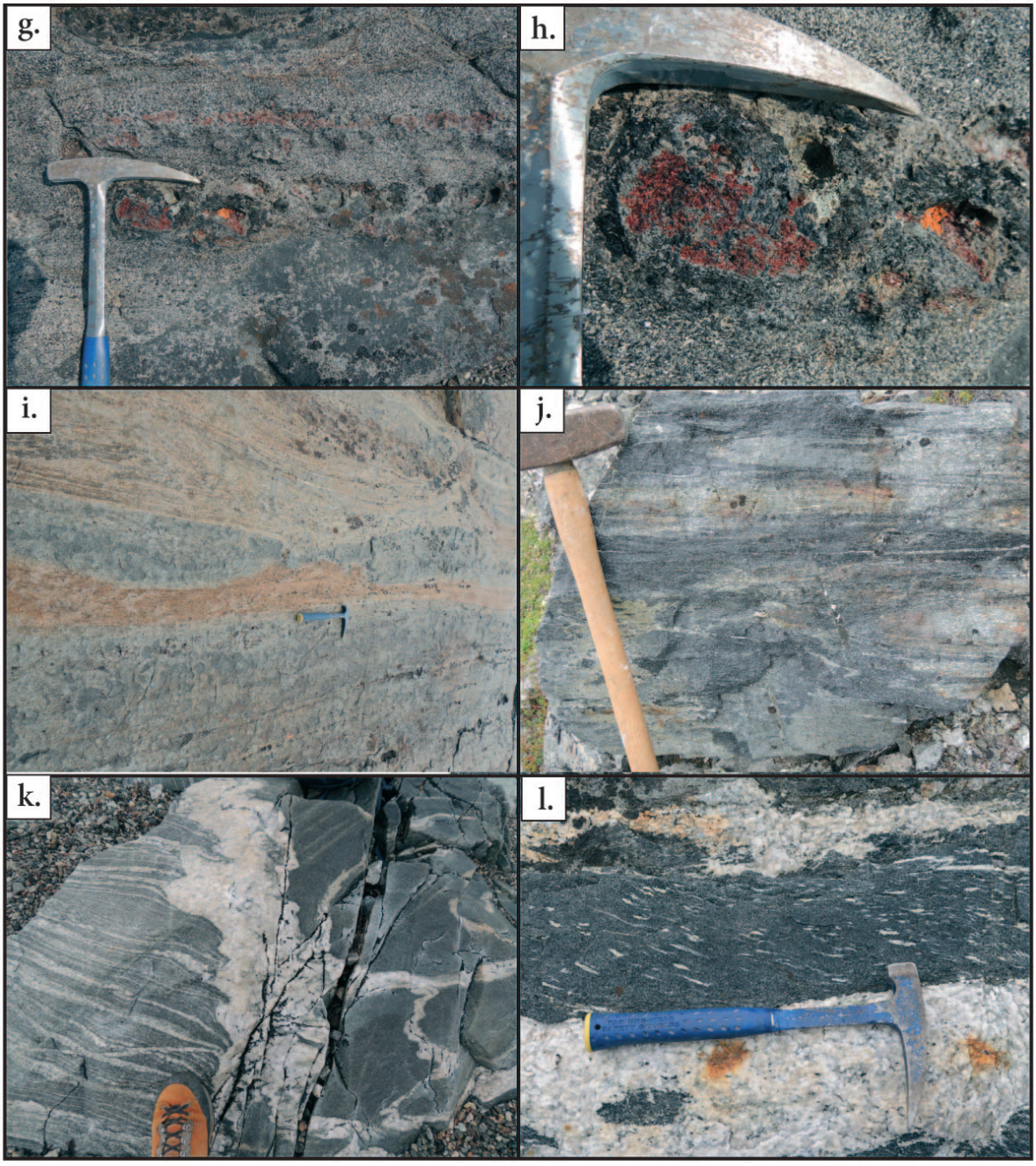
g.
h.
i.
j.
k.
l.

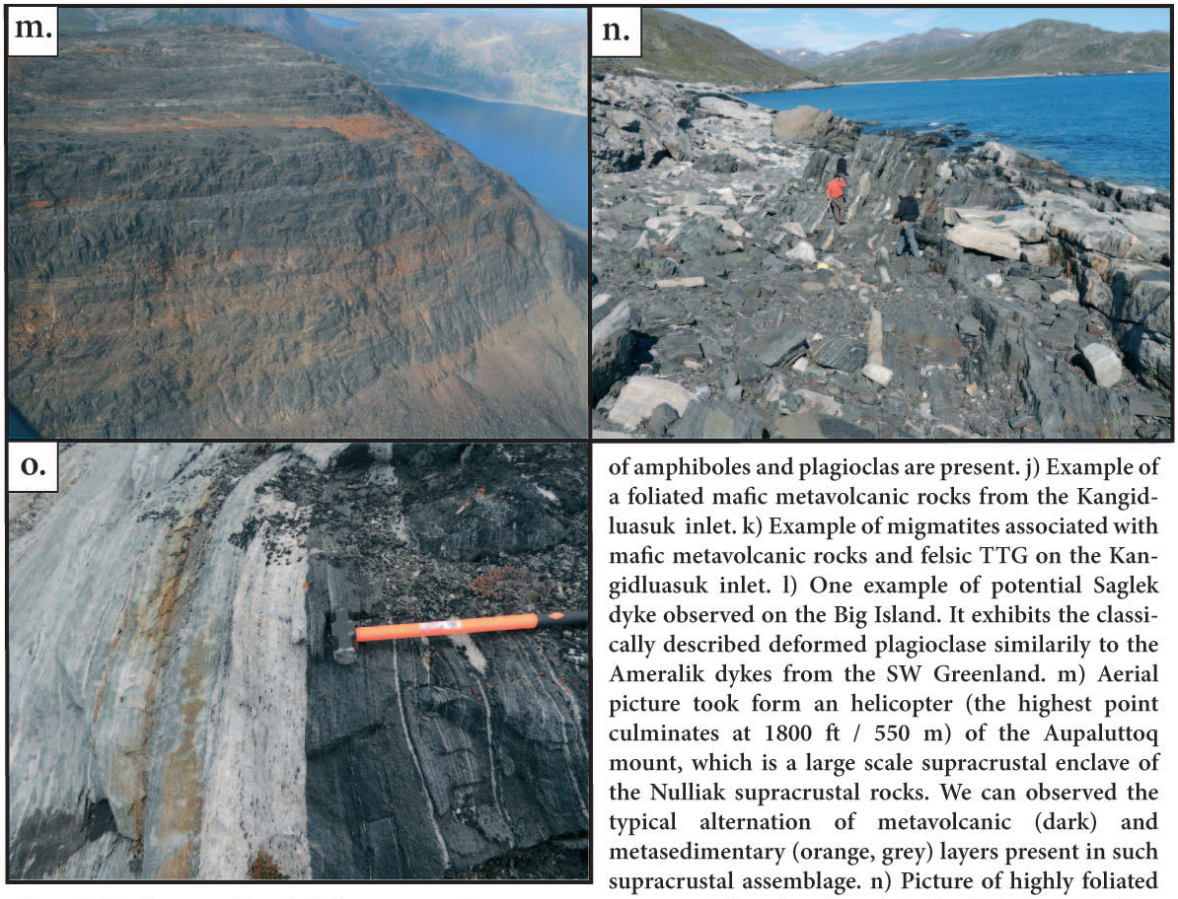

Set of 15 photographs of differents complementary field observations made in the Saglek-Hebron Complex. a) Picture of a pyroxenite took on the Ukkalek Island, very large green CPX can be observed on the alteration patina b) Ultramafic pod of dunite/peridotite observed on the Ukkalek Island, on its left side, a few layers of serpentinites a present. c) Example of an isolated ultramafic pod found on the Nulliak Island. d- e- f) Represent few of the best examples of potential pillow lava structure found in the Pangertok inlet Nulliak assemblage enclave. g- h) picture of a garnet bearing amphibolite associated to a close up view found in the Pangertok inlet. Corronas of amphiboles and plagioclas are present. j) Example of a foliated mafic metavolcanic rocks from the Kangidluasuk inlet. k) Example of migmatites associated with mafic metavolcanic rocks and felsic TTG on the Kangidluasuk inlet. l) One example of potential Saglek dyke observed on the Big Island. It exhibits the classically described deformed plagioclase similarily to the Ameralik dykes from the SW Greenland. m) Aerial picture took form an helicopter (the highest point culminates at 1800 ft / 550 m) of the Aupaluttoq mount, which is a large scale supracrustal enclave of the Nulliak supracrustal rocks. We can observed the typical alternation of metavolcanic (dark) and metasedimentary (orange, grey) layers present in such supracrustal assemblage. n) Picture of highly foliated supracrustal enclave found in the Iluilik gneiss (see chapter 2). o) Close up of the contact between the deformed metavolcanic rocks and the Iluilik gneiss, it systematically is filled with migmatitic melt.

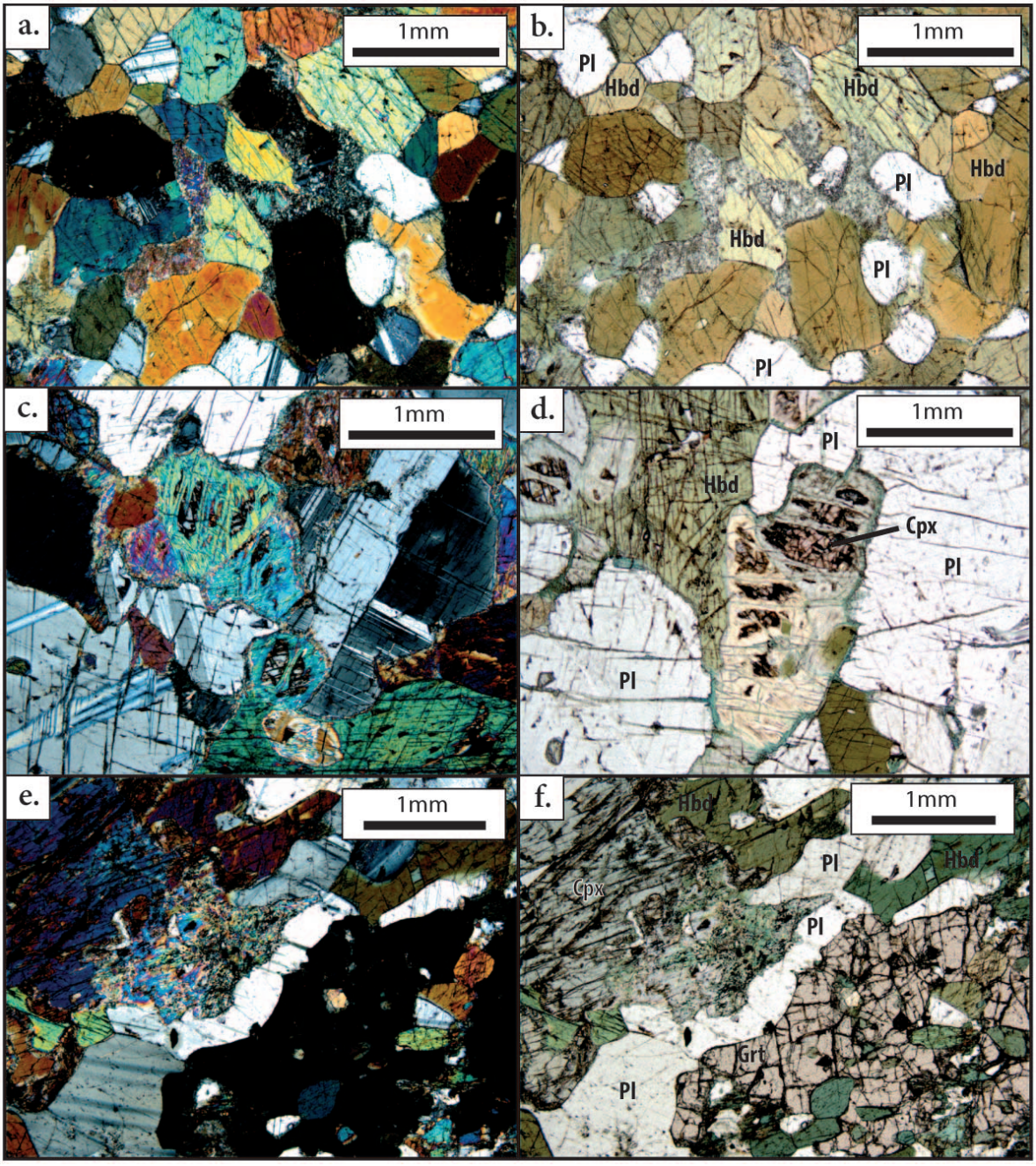

Figure A.2

Thin section photomicrogarphs of the mafic and ultramafic rocks. Full descriptions at the end of the figure.

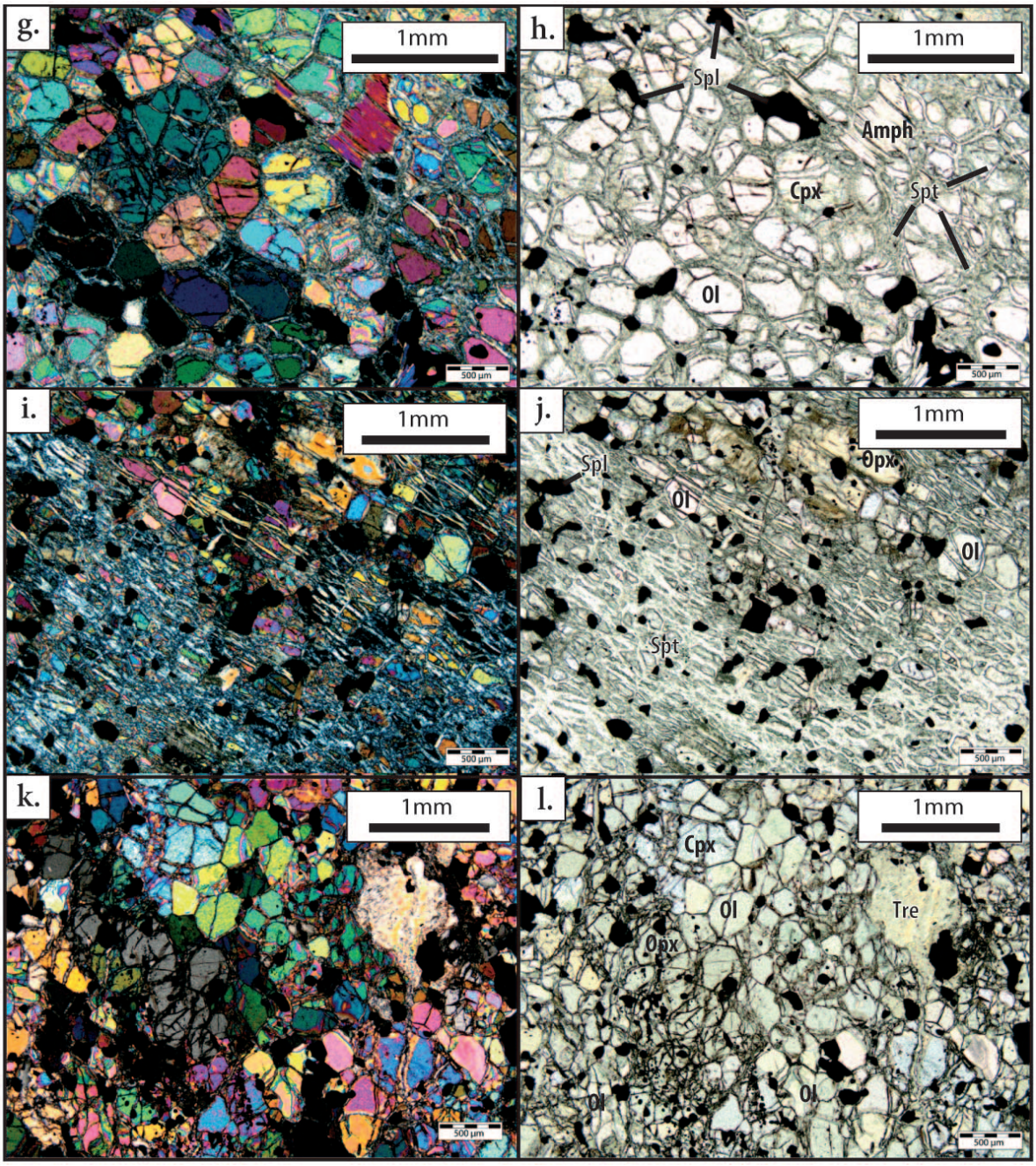
g.
1mm
500 µm
h.
1mm
Spl
Amph
Cpx
Spt
Ol
500 µm
i.
1mm
500 µm
j.
1mm
Spl
Opx
Ol
Ol
Spt
500 µm
k.
1mm
500 µm
l.
1mm
Cpx
Ol
Tre
Opx
Ol
Ol
500 µm

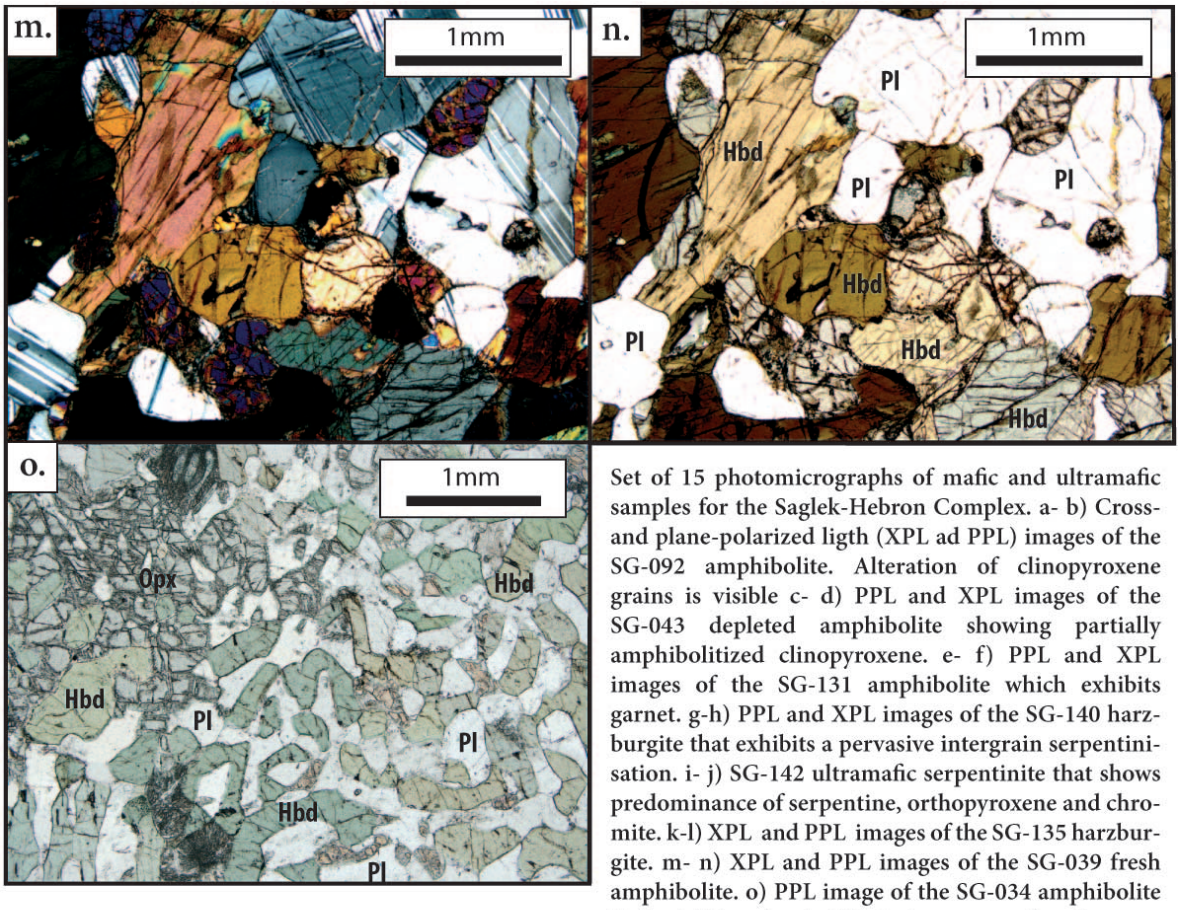

Set of 15 photomicrographs of mafic and ultramafic samples for the Saglek-Hebron Complex. a- b) Cross- and plane-polarized ligth (XPL ad PPL) images of the SG-092 amphibolite. Alteration of clinopyroxene grains is visible c- d) PPL and XPL images of the SG-043 depleted amphibolite showing partially amphibolitized clinopyroxene. e- f) PPL and XPL images of the SG-131 amphibolite which exhibits garnet. g-h) PPL and XPL images of the SG-140 harzburgite that exhibits a pervasive intergrain serpentinisation. i- j) SG-142 ultramafic serpentinite that shows predominance of serpentine, orthopyroxene and chromite. k-l) XPL and PPL images of the SG-135 harzburgite. m- n) XPL and PPL images of the SG-039 fresh amphibolite. o) PPL image of the SG-034 amphibolite that exhibites simplectitic texture suggesting the presence of a garnet precursor

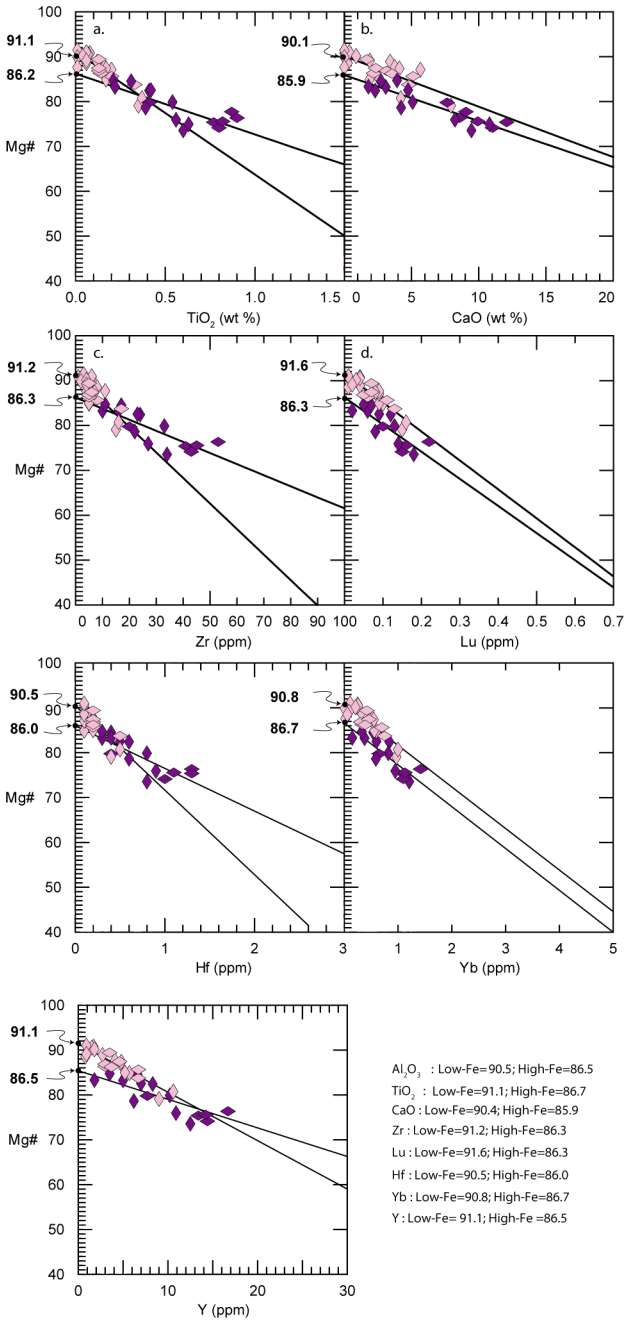

Figure A.3

Additionnal plot supporting the Figure 1.9-b

Table A.1

Major (wt.%) and trace (ppm) element data for duplicate samples. (hydrous composition)

Sample	SG-034	SG-034-db1	SG-039	SG-039-db1	SG-057	SG-057-db1	SG-092	SG-092-db1
Method	FUS-ICP Actlabs	FUS-ICP Actlabs	XRF ACME	XRF ACME	XRF ACME	FUS-ICP Actlabs	FUS-ICP Actlabs	FUS-ICP Actlabs
SiO_2	46.58	46.4	47.29	47.42	46.81	46.34	50.82	50.99
Al_2O_3	14.61	14.32	15.63	15.7	16.29	16.93	14.06	14.03
Fe_2O_3	9.69	6.97	12.77	12.77	10	10.14	11.34	11.28
MnO	0.185	0.188	0.19	0.18	0.16	0.168	0.173	0.173
MgO	12.79	12.7	7.97	7.98	14.14	13.82	7.67	7.68
CaO	13.49	14	12.14	12.16	10.52	10.75	10.75	10.79
Na_2O	0.97	0.92	2.06	2.06	1.04	1.05	2.18	2.19
K_2O	0.32	0.3	0.12	0.12	0.41	0.4	0.49	0.48
TiO_2	0.386	0.387	1.03	1.04	0.35	0.341	0.775	0.772
P_2O_5	0	0	0.06	0.06	0.02	0.02	0.05	0.06
Cr_2O_3	-	-	0.07	0.07	0.12	-	-	-
Method	FUS-ICP/Actlabs	FUS-ICP/Actlabs	N.A.	N.A.	N.A.	FUS-ICP/Actlabs	FUS-ICP/Actlabs	FUS-ICP/Actlabs
Sc	48	45	-	-	-	26	43	43
V	196	191	-	-	-	136	280	280
Cr	1120	1100	-	-	-	810	310	310
Co	53	53	-	-	-	67	44	44
Ni	250	250	-	-	-	410	90	90
Rb	4	5	-	-	-	4	6	6
Sr	70	66	-	-	-	84	123	123
Y	10.8	10.4	-	-	-	7.1	17.3	17.2
Zr	12	12	-	-	-	18	51	49
Nb	0.5	0.5	-	-	-	1.0	2.4	2.3
Ba	32	31	-	-	-	42	82	82
La	1.22	1.19	-	-	-	3.37	5.57	5.63
Ce	4.27	4.36	-	-	-	9.64	12.00	12.10
Pr	0.63	0.63	-	-	-	1.28	1.59	1.59
Nd	3.31	3.63	-	-	-	5.17	7.31	7.21
Sm	0.98	1.06	-	-	-	1.16	2.03	2.05
Eu	0.39	0.34	-	-	-	0.41	0.69	0.69
Gd	1.37	1.38	-	-	-	1.21	2.63	2.68
Tb	0.26	0.26	-	-	-	0.21	0.47	0.47
Dy	1.74	1.73	-	-	-	1.33	3.03	3.07
Ho	0.38	0.38	-	-	-	0.27	0.64	0.65
Er	1.16	1.13	-	-	-	0.73	1.85	1.82
Tm	0.17	0.17	-	-	-	0.11	0.28	0.27
Yb	1.10	1.08	-	-	-	0.70	1.84	1.82
Lu	0.17	0.17	-	-	-	0.11	0.28	0.28
Hf	0.5	0.3	-	-	-	0.5	1.3	1.2
Ta	0.00	0.00	-	-	-	0.07	0.18	0.19
Pb	0	0	-	-	-	0	9	9
Th	0.00	0.00	-	-	-	0.21	0.97	0.96
U	0.00	0.00	-	-	-	0.05	0.31	0.32

Continued on next page

Sample	SG-100	SG-100-db1	SG-109A	SG-109A-db1	SG-109A-db2	SG-117	SG-117-db1
Method	XRF/ACME	XRF/ACME	XRF/ACME	N.A.	N.A.	XRF/ACME	N.A.
SiO_2	44.75	44.76	48.4	-	-	47.9	-
Al_2O_3	4.78	4.76	16.45	-	-	12.1	-
Fe_2O_3	14.09	14.11	8.85	-	-	12.74	-
MnO	0.16	0.16	0.15	-	-	0.21	-
MgO	22.42	22.41	10.28	-	-	10.83	-
CaO	7.81	7.8	13.45	-	-	11.88	-
Na_2O	0.38	0.37	1.24	-	-	1.61	-
K_2O	0.97	0.98	0.2	-	-	0.49	-
TiO_2	0.53	0.53	0.34	-	-	0.74	-
P_2O_5	0.03	0.03	0.02	-	-	0.05	-
Cr_2O_3	-	0.32	-	-	-	0.1	-
Method	FUS-ICP/Actlabs	N.A.	FUS-ICP/Actlabs	FUS-ICP/Actlabs	FUS-ICP/Actlabs	N.A.	FUS-ICP/Actlabs
Sc	-	-	-	-	-	-	-
V	153	-	119	118	120	-	224
Cr	2190	-	460	460	460	-	690
Co	74	-	53	52	53	-	68
Ni	700	-	270	270	280	-	370
Rb	65	-	5	5	5	-	7
Sr	15	-	86	85	87	-	112
Y	10.9	-	8.4	8.2	8.6	-	14.2
Zr	27	-	14	14	14	-	32
Nb	1.6	-	0.9	0.9	0.9	-	1.6
Ba	131	-	11	11	10	-	80
La	3.54	-	1.08	1.09	1.07	-	3.27
Ce	8.99	-	3.05	3.02	3.07	-	8.56
Pr	1.27	-	0.49	0.50	0.48	-	1.16
Nd	6.26	-	2.62	2.58	2.65	-	6.06
Sm	1.78	-	0.84	0.85	0.83	-	1.81
Eu	0.66	-	0.38	0.36	0.41	-	0.69
Gd	2.03	-	1.20	1.19	1.20	-	2.41
Tb	0.33	-	0.23	0.24	0.23	-	0.39
Dy	1.95	-	1.51	1.53	1.50	-	2.41
Ho	0.39	-	0.31	0.31	0.32	-	0.47
Er	1.06	-	0.91	0.88	0.94	-	1.37
Tm	0.15	-	0.14	0.13	0.14	-	0.21
Yb	0.95	-	0.91	0.91	0.91	-	1.34
Lu	0.14	-	0.14	0.14	0.14	-	0.20
Hf	0.9	-	0.4	0.4	0.4	-	1.0
Ta	0.24	-	0.09	0.10	0.09	-	0.29
Pb	0	-	33	37	28	-	0
Th	0.52	-	0.00	0.00	0.00	-	0.21
U	0.29	-	0.00	0.01	0.00	-	0.10

Continued on next page

Sample	SG-126	SG-126-db1	SG-142	SG-142-db1	SG-142-db2
Method	XRF/ACME	XRF/ACME	FUS-ICP/Actlabs	FUS-ICP/Actlabs	FUS-ICP/Actlabs
SiO_2	45.82	45.76	36.67	36.59	36.74
Al_2O_3	16.49	16.5	1.39	1.4	1.38
Fe_2O_3	13.62	13.6	9.82	9.8	9.85
MnO	0.22	0.22	0.152	0.152	0.152
MgO	8.5	8.5	40.56	40.2	40.92
CaO	11.12	11.11	1.72	1.72	1.73
Na_2O	1.74	1.73	0	0	0
K_2O	0.45	0.45	0	0	0
TiO_2	0.99	0.99	0.058	0.058	0.058
P_2O_5	0.07	0.07	0	0	0
Cr_2O_3	0.05	0.05	-	-	-
Method	N.A.	N.A.	FUS-ICP/Actlabs	FUS-ICP/Actlabs	FUS-ICP/Actlabs
Sc	-	-	7	7	7
V	-	-	40	39	41
Cr	-	-	6680	6790	6570
Co	-	-	137	139	134
Ni	-	-	2940	2980	2890
Rb	-	-	0	0	0
Sr	-	-	35	35	36
Y	-	-	0.9	0.9	0.9
Zr	-	-	4	4	4
Nb	-	-	0.0	0.0	0.0
Ba	-	-	0	-	-
La	-	-	0.33	0.35	0.32
Ce	-	-	0.87	0.92	0.81
Pr	-	-	0.11	0.12	0.11
Nd	-	-	0.45	0.49	0.42
Sm	-	-	0.11	0.11	0.11
Eu	-	-	0.04	0.04	0.04
Gd	-	-	0.14	0.14	0.14
Tb	-	-	0.02	0.02	0.02
Dy	-	-	0.15	0.15	0.15
Ho	-	-	0.03	0.03	0.03
Er	-	-	0.11	0.11	0.10
Tm	-	-	0.02	0.02	0.02
Yb	-	-	0.09	0.10	0.09
Lu	-	-	0.02	0.02	0.02
Hf	-	-	0.0	0.0	0.0
Ta	-	-	0.00	0.01	0.00
Pb	-	-	0	12	0
Th	-	-	0.06	0.06	0.06
U	-	-	0.00	0.00	0.00

Continued on next page

Table A.2

Electron microprobe major element compositions for single olivine grains from ultramafic samples

	SG-010					
grain #	349-003	350-003	351-003	370-008	371-008	372-008
CaO	0.00	0.01	0.05	0.01	0.00	0.01
Cr_2O_3	-	-	0.01	0.01	0.00	-
Al_2O_3	-	-	-	-	-	-
FeO	15.54	15.79	15.31	15.82	15.87	15.50
MnO	0.21	0.23	0.20	0.19	0.20	0.21
TiO_2	0.01	0.00	0.10	-	0.02	0.02
NiO	0.32	0.33	0.34	0.32	0.31	0.31
SiO_2	39.99	39.87	39.94	39.81	39.88	39.85
MgO	44.78	44.76	44.58	44.29	44.29	44.49
Na_2O	0.01	0.01	0.09	0.00	-	-
Total	100.87	101.01	100.64	100.45	100.57	100.38
Mg#	83.7	83.5	83.8	83.3	83.3	83.6

	SG-012							
grain #	377-010	378-010	379-010	380-010	381-010	392-014	393-014	394-014
CaO	0.00	0.01	0.01	0.01	0.01	0.01	0.00	0.01
Cr_2O_3	-	-	-	-	0.00	0.01	-	-
Al_2O_3	-	-	-	-	0.36	-	-	-
FeO	18.56	20.06	18.57	18.73	20.24	18.84	20.62	19.13
MnO	0.28	0.59	0.27	0.29	0.59	0.33	0.57	0.27
TiO_2	-	0.02	0.01	-	0.03	0.01	-	0.00
NiO	0.45	0.25	0.41	0.44	0.18	0.43	0.28	0.46
SiO_2	39.02	38.91	39.47	39.27	39.14	39.22	39.12	39.08
MgO	41.31	40.15	41.68	41.71	39.90	41.36	39.74	40.79
Na_2O	-	0.01	-	-	-	0.00	0.00	-
Total	99.62	100.00	100.43	100.44	100.44	100.20	100.34	99.74
Mg#	79.9	78.1	80.0	79.9	77.8	79.6	77.5	79.2

SG-133

grain #	poi1 ol1	poi1 ol2	poi2 ol1	poi2 ol2
CaO	0.00	0.01	0.00	0.01
Cr_2O_3	0.01	0.00	0.00	0.00
Al_2O_3	0.00	0.00	0.00	0.00
FeO	11.95	12.04	11.59	11.57
MnO	0.17	0.19	0.20	0.15
TiO_2	0.00	0.00	0.01	0.00
NiO	0.40	0.37	0.38	0.38
SiO_2	39.44	39.54	39.27	39.34
MgO	47.84	48.07	48.41	48.40
Na_2O	0.01	0.00	0.00	0.00
Total	99.83	100.22	99.88	99.86
Mg#	87.7	87.7	88.2	88.2

SG-135

grain #	poi1 ol1	poi1 ol2	poi3 ol1	poi3 ol2	poi3 ol3	poi4 ol2
CaO	0.00	0.00	0.00	0.00	0.00	0.01
Cr_2O_3	0.00	0.00	0.00	0.00	0.03	0.00
Al_2O_3	0.00	0.00	0.01	0.00	0.00	0.00
FeO	3.29	3.30	3.51	3.35	3.36	3.53
MnO	0.12	0.11	0.12	0.11	0.12	0.13
TiO_2	0.00	0.01	0.00	0.00	0.01	0.00
NiO	0.37	0.35	0.37	0.37	0.36	0.34
SiO_2	41.64	41.62	41.74	41.49	41.53	41.41
MgO	55.48	55.98	55.78	55.46	55.34	55.31
Total	100.91	101.40	101.56	100.82	100.82	100.74
Mg#	96.8	96.8	96.6	96.7	96.7	96.5

SG-137A

grain #	poi1 ol1	poi1 ol2	poi1 ol3	poi2 ol2	poi3 ol1	poi3 ol2	poi3 ol3	poi4 ol2
CaO	0.01	0.00	0.01	0.01	0.00	0.00	0.00	0.01
Cr_2O_3	0.00	0.00	0.00	0.00	0.01	0.00	0.00	0.03
Al_2O_3	0.00	0.00	0.00	0.00	0.01	0.00	0.00	0.00
FeO	5.12	5.09	5.15	4.91	5.08	5.11	5.19	5.07
MnO	0.13	0.17	0.17	0.14	0.15	0.12	0.15	0.14
TiO_2	0.00	0.00	0.00	0.00	0.00	0.00	0.01	0.00
NiO	0.38	0.42	0.42	0.40	0.40	0.42	0.43	0.45
SiO_2	40.67	40.87	40.88	40.71	40.55	40.80	40.72	40.74
MgO	54.15	54.25	53.70	54.19	53.70	54.22	54.14	54.42
Total	100.53	100.84	100.36	100.37	99.93	100.81	100.70	100.94
Mg#	95.0	95.0	94.9	95.2	95.0	95.0	94.9	95.0

SG-140

grain #	poi1 ol1	poi1 ol2	poi1 ol3	poi1 ol4	poi1 ol4.2	poi1 ol5	poi2 ol1.1	poi2 ol1.2	poi2 ol2	poi2 ol4
CaO	0.01	0.01	0.00	0.00	0.00	0.00	0.02	0.01	0.01	0.02
Cr_2O_3	0.00	0.02	0.03	0.00	0.03	0.00	0.02	0.01	0.00	0.00
Al_2O_3	0.00	0.00	0.00	0.00	0.00	0.00	0.00	0.00	0.00	0.00
FeO	11.50	11.63	11.63	11.75	11.69	11.73	11.66	11.58	11.68	11.53
MnO	0.14	0.19	0.18	0.18	0.15	0.17	0.18	0.21	0.19	0.18
TiO_2	0.00	0.00	0.00	0.00	0.00	0.02	0.00	0.00	0.01	0.00
NiO	0.39	0.38	0.36	0.41	0.39	0.38	0.38	0.36	0.40	0.40
SiO_2	39.26	38.86	39.05	39.13	38.90	39.17	38.89	39.25	39.22	39.12
MgO	48.07	47.82	47.69	48.22	48.02	48.26	47.72	48.19	47.96	47.95
Total	99.42	98.91	98.94	99.69	99.25	99.72	98.88	99.61	99.47	99.20
Mg#	88.2	88.0	88.0	88.0	88.0	88.0	87.9	88.1	88.0	88.1

SG-142

grain #	poi1 ol1	poi1 ol2	poi1 ol3	poi1 ol4	poi2 t2 ol	poi2 t3 ol	poi2 t4 ol	poi2 t5 ol	poi2 t6 ol	poi2 ol2.1	poi2 ol2.2
CaO	0.00	0.01	0.00	0.00	0.00	0.00	0.00	0.00	0.00	0.00	0.00
Cr_2O_3	0.00	0.00	0.01	0.00	0.00	0.02	0.00	0.00	0.00	0.03	0.02
Al_2O_3	0.00	0.00	0.00	0.00	0.00	0.00	0.00	0.00	0.00	0.00	0.00
FeO	5.01	5.00	5.16	5.20	5.26	5.34	5.33	5.29	5.30	5.01	1.72
MnO	0.15	0.14	0.15	0.16	0.15	0.16	0.13	0.15	0.12	0.14	0.21
TiO_2	0.00	0.00	0.00	0.00	0.01	0.00	0.01	0.01	0.01	0.01	0.00
NiO	0.40	0.41	0.40	0.41	0.42	0.40	0.40	0.38	0.41	0.39	0.29
SiO_2	40.32	40.49	40.29	40.41	40.55	40.28	40.31	40.33	40.26	40.14	41.33
MgO	54.11	54.56	54.46	54.54	54.66	54.26	54.09	54.13	53.98	54.00	57.38
Total	99.99	100.61	100.49	100.76	101.11	100.47	100.32	100.34	100.09	99.73	101.08
Mg#	95.1	95.1	95.0	94.9	94.9	94.8	94.8	94.8	94.8	95.1	98.3

	SG-243												
grain #	421-023	422-023	423-023	431-026	432-026	440-029	441-029	449-033	450-033	451-033	452-033	453-033	454-033
CaO	0.01	0.01	-	0.00	-	0.00	0.01	0.01	-	0.01	0.00	0.01	-
Cr_2O_3	-	-	-	0.00	-	-	0.02	0.00	-	-	-	-	-
Al_2O_3	0.00	-	-	-	-	-	-	-	-	-	-	-	-
FeO	12.07	11.49	11.51	11.24	11.57	11.26	11.29	11.42	11.40	11.60	11.36	11.45	11.50
MnO	0.20	0.19	0.19	0.16	0.17	0.17	0.18	0.18	0.18	0.17	0.18	0.18	0.21
TiO_2	-	0.01	-	-	0.03	-	0.02	0.01	0.02	-	0.01	0.00	0.02
NiO	0.43	0.41	0.42	0.42	0.42	0.42	0.45	0.46	0.43	0.42	0.42	0.44	0.41
SiO_2	40.38	40.51	40.57	40.24	40.40	40.57	40.56	40.56	40.51	40.49	40.38	40.41	40.43
MgO	47.45	47.53	47.64	47.17	47.43	47.24	47.17	47.01	47.18	47.35	47.28	47.47	47.27
Na_2O	-	0.00	-	-	-	-	-	-	-	-	0.00	-	-
Total	100.54	100.14	100.33	99.24	100.02	99.66	99.69	99.65	99.72	100.04	99.64	99.96	99.84
Mg#	87.5	88.1	88.1	88.2	88.0	88.2	88.2	88.0	88.1	87.9	88.1	88.1	88.0

Table A.3

Partition coefficients (Kd) used for trace element modeling shown in Figure 1.8

.

Element	Clinopyroxene		Orthopyroxene		Plagioclase		Olivine
(ppm)	Min	Max	Min	Max	Min	Max	-
La	0.02	0.2	0.002	0.015	0.075 0.25	0.012	-
Ce	0.03	0.25	0.001	0.025	0.025	0.175	0.009
Nd	0.1 0.5	0.003	0.03	0.02	0.14	0.004	-
Sm	0.1	0.8	0.01	0.11	0.015	0.11	0.003
Eu	0.25	0.75	0.01	0.1	0.05	0.8	0.003
Gd	0.3	0.9	0.02	0.15	0.025	0.07	0.004
Dy	0.4 1	0.025	0.3	0.015	0.055	0	-
Y	0.2	1.2	0.1	0.5	0.01 0.04	0.013	-
Er	0.3 0.9	0.025	0.25	0.005	0.05	0.008	-
Yb	0.2	0.9	0.05	0.5	0.002	0.045	0.013
Lu	0.3	1	0.075	0.75	0.005	0.05	0.018
Ti	0.37	-	0.024	-	0.083	-	0.006
Zr	0.123	-	0.02	-	0.0127	-	0.025
Cr	9.7	-	3.7	-	0.02	-	1.1
Ni	5.6	-	7.3	-	0.06	-	12.2

Appendix B

Supplementary materials for the "Chapter 2"

This appendix contains all Supplementary Figures and Tables referenced in Chapter 2: "Petrogeochemistry, Geochronology and crustal evolution of the Saglek-Hebron Complex (Northern Labrador)".

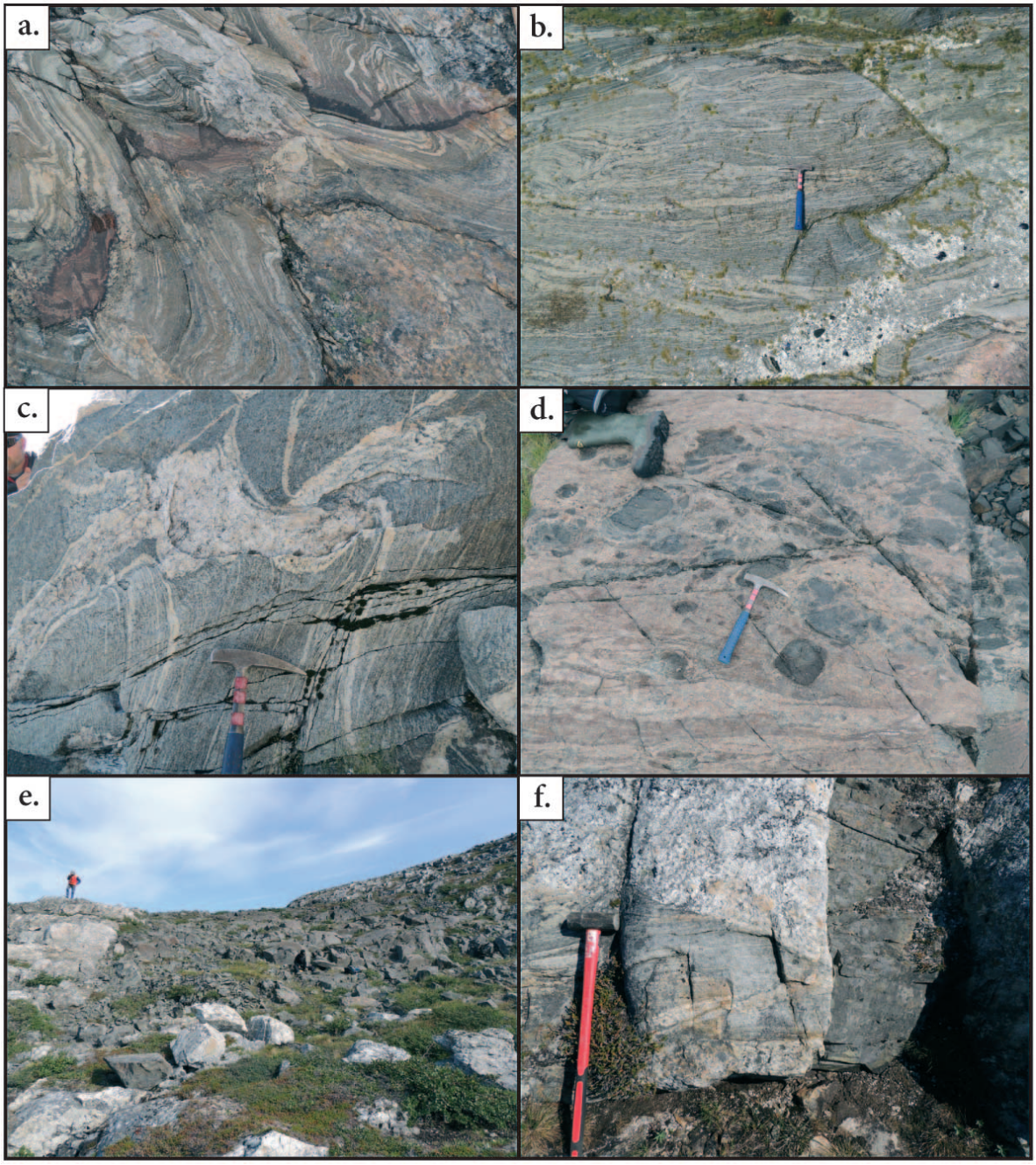

Figure B.1

Fieldwork photographs of the granitoids. Full descriptions at the end of the figure.

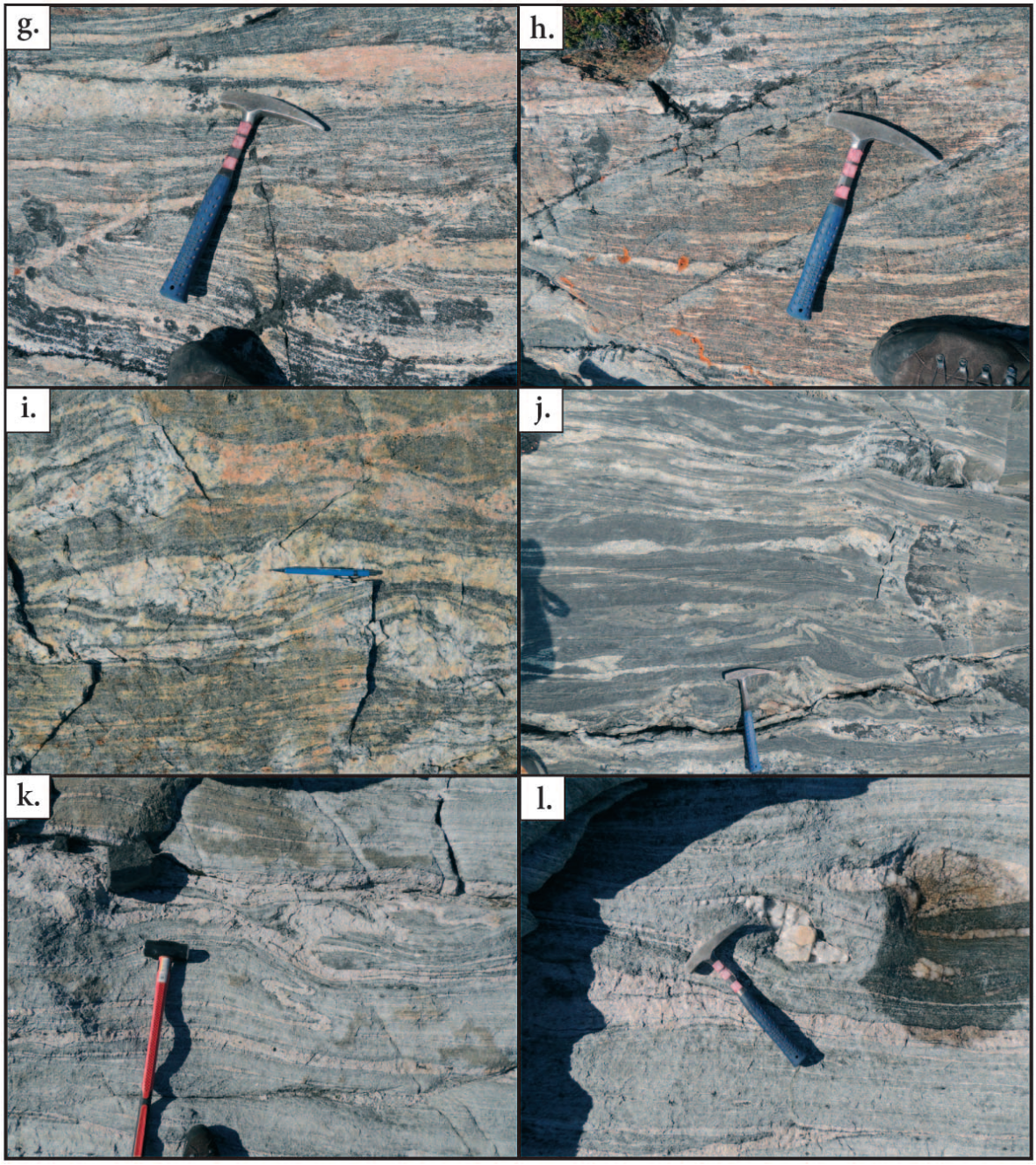
g.
h.
i.
j.
k.
l.

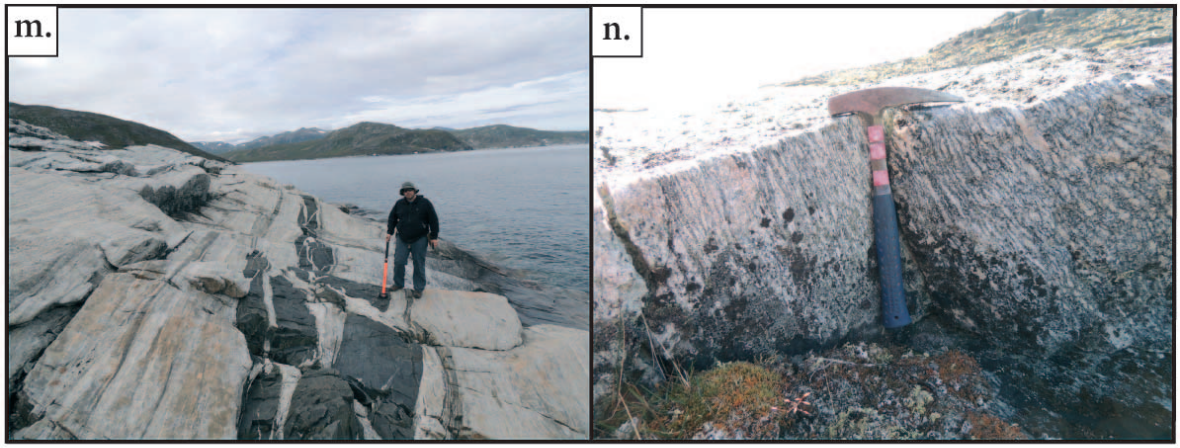

Fieldwork photographs of different rock localities and points of interest. a) Picture of the sampling location of the SG-210c used to reproduce the results from Shimojo et al., (2016). b) Banded grey gneiss from the Nulliak Island. c) Banded grey gneiss dated at 3200 Ma from the Lister Island crosscut by granitic migmatite. d) Tonalites from the kyuktok cove location. e) 3800 Ma old trondhjemite crosscut by a Neoarchean dyke in the Kangidluasuk inlet. f) Crosscutting relationship observed at the White Point location showing banded grey gneiss supposedley Lister in age crosscut by migmatite melt both crosscut by neoarchean dyke. g) Banded grey gneiss observed in Big Island infiltrated by migmatites (SG-260). h) Similar grey gneiss to that shown in "g", with higher content of Fe andmagnetic material (SG-258). i) Migmatitized trondhjemite SG-024 found on the Ukkalek Island. j) Migmatitized Mg-rich tonalite (SG-026) found on the Ukkalek Island. k)- l Iluilik banded granodiorite that exhibits sheared plagioclase and migmatitic veins. m) Typical meter scale enclaves of supracrustal rocks in the Iluilik gneiss which could be interpreted as dykes. n) Typical Iluilik augen granodiorite as described in the litterature as the Uivak II (Hurst et *al.*, 1975; Bridgwater and Collerson, 1991).

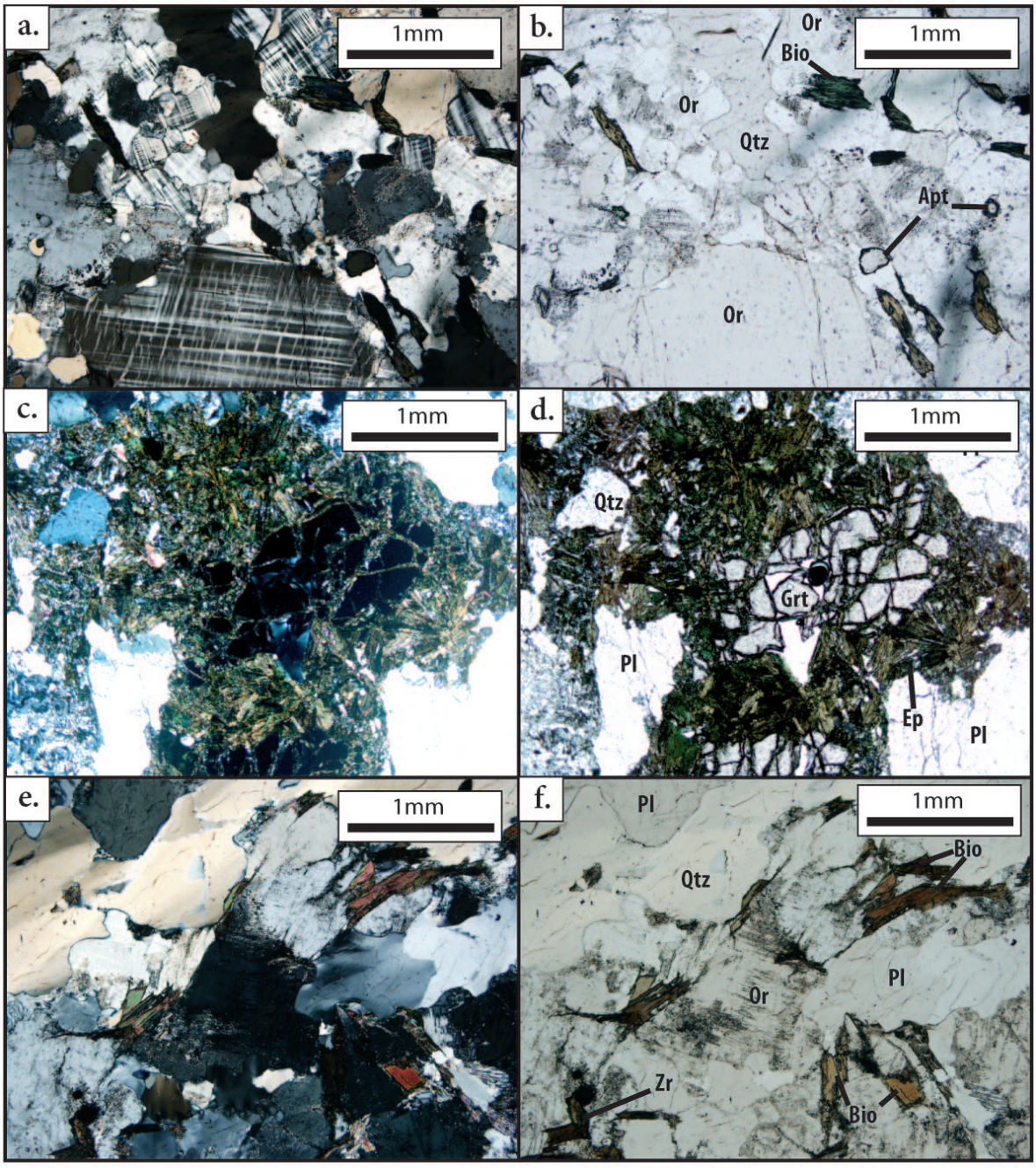

Figure B.2

Thin section photomicrogarphs of the granitoids. Full descriptions at the end of the figure.

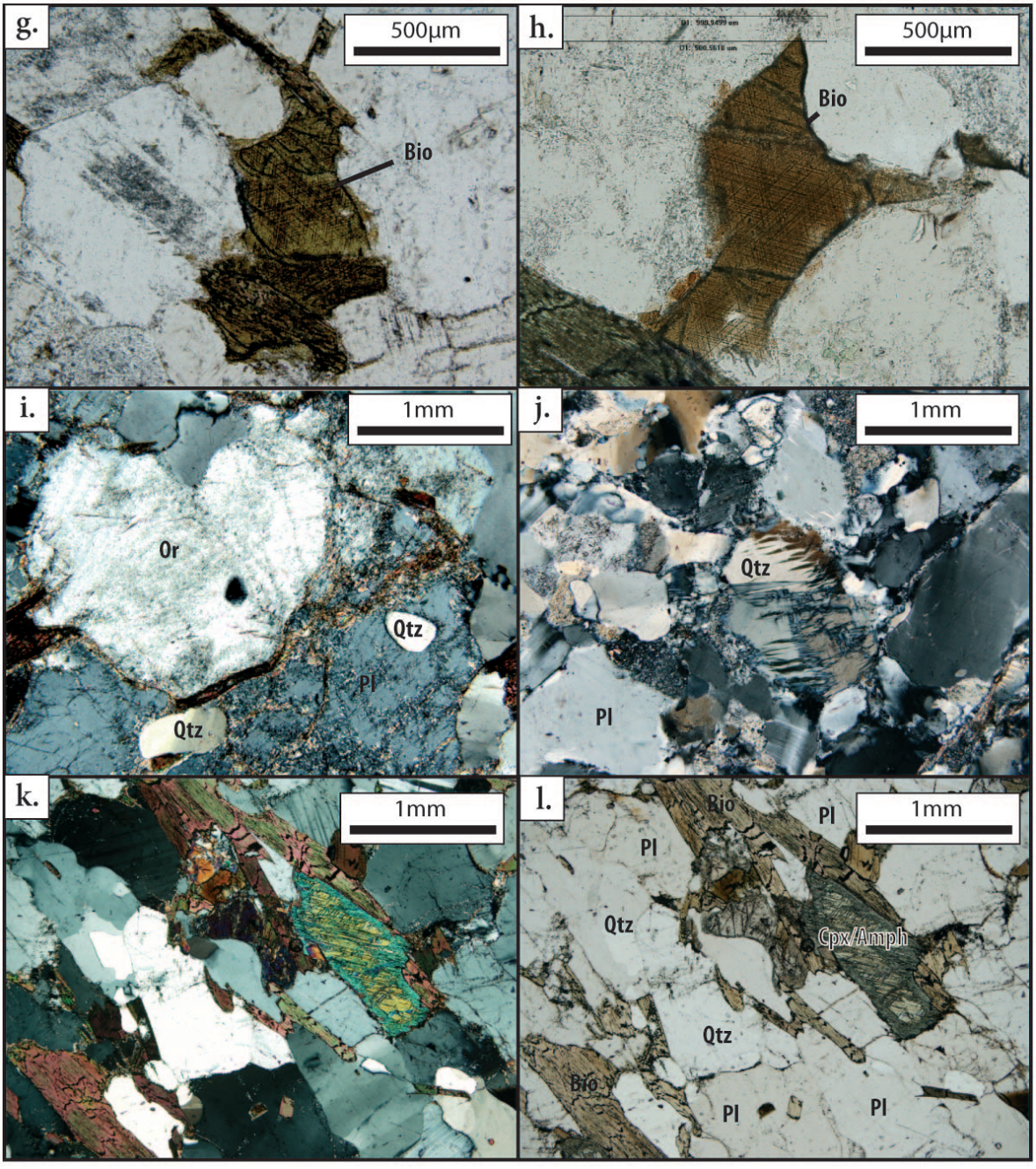
g.
500µm
Bio
h.
500µm
Bio
i.
1mm
Or
Qtz
Pl
Qtz
j.
1mm
Qtz
Pl
k.
1mm
l.
1mm
Bio
Pl
Pl
Qtz
Cpx/Amph
Qtz
Bio
Pl
Pl

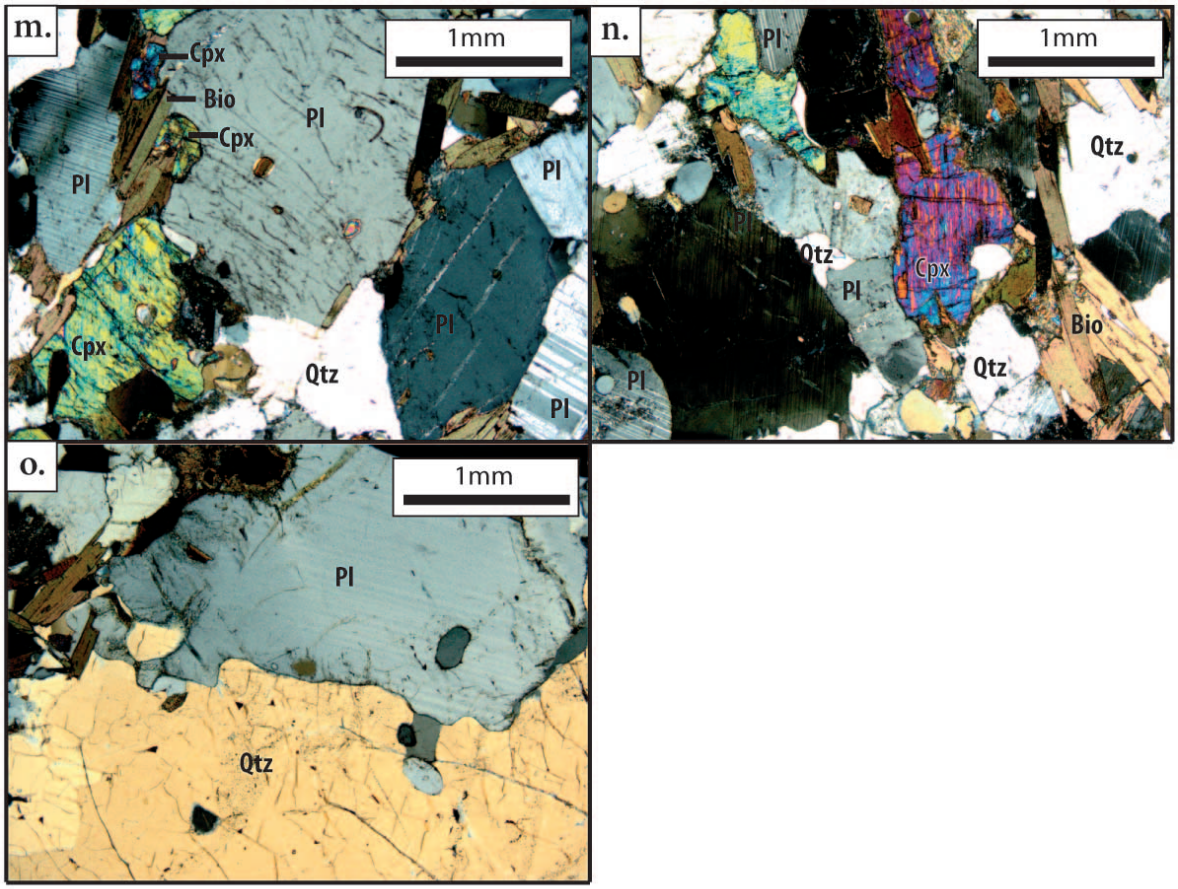

Set of 15 photomicrographs of granitoids. a- b) SG-134 granite. c- d) SG-127 granite e- f) SG-122 trondhjemite. g- h) SG-024 Good example of sagenitic texture in biotite formed by secondary exsolution of titanium oxides in the crystal lattices. i) SG-024 indicator of alteration and high deformation in the quartz and feldspar. j) SG-080 highly deformed quartz and feldspar in granites from the Kangidluasuk inlet. k- l) SG-026 shows the presence of clinopyroxene. m- n) SG-027 tonalite similarily shows the presence of clinopyroxene. o) SG-027 shows subgrain formation in plagioclase.

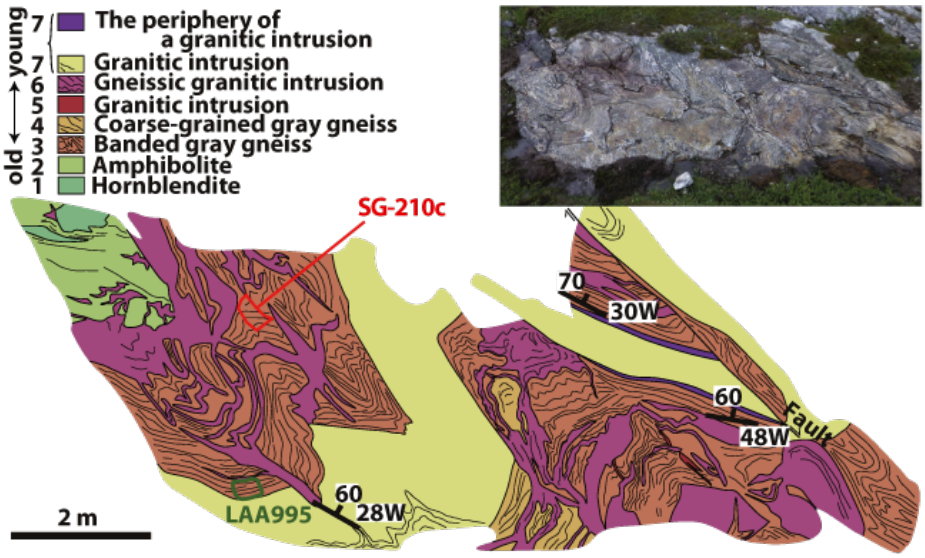

Figure B.3

Schematic of the outcrop from Shimojo et *al.*, (2016) where the Iqaluk gneiss has been described and dated at 3920 Ma. The precise location of sample SG-210c (this study) and the Sample LAA995 (Shimojo et *al.*, 2016) of Iqaluk gneiss are showned respectively in black and green.

Data Reduction Lu-Hf isotope

Our Lu-Hf data set was reduced in the following order. The average signal intensity of the gas background (20 s) was subtracted from the signal acquired during the ablation of the sample. Only these corrected intensities were used further for the data reduction. The mass bias factor βYb was determined using the ^{173}Yb/^{171}Yb measured during each zircon analysis and the ref ^{173}Yb/^{171}Yb of 1.132685 (Chu et *al.*, 2002; Fisher et *al.*, 2011), following the equation :

$$\beta Yb = \frac{ln\left(\frac{(^{173}Yb/^{171}Yb)_{ref}}{(^{173}Yb/^{171}Yb)_{meas}}\right)}{ln\left(\frac{M173}{M171}\right)} \tag{B.1}$$

Using a ^{176}Yb/^{173}Yb of 0.79618 we determined the ^{176}Yb isobaric interference on ^{176}Hf. Then, the ^{176}Lu isobaric interference on ^{176}Hf was determined assuming that Lu = Yb and using the measured interference-free ^{17}5Lu mass. We used a reference ^{176}Lu/^{175}Lu value of 0.02655 from Vervoort et *al.*, (2004).

$$^{176}Yb_{calculated} = ^{173}\,Yb_{meas} \times \left(\frac{^{176}Yb}{^{173}Yb}\right)_{ref} \times \left(\frac{M173}{M176}\right)^{\beta Yb} \tag{B.2}$$

$$^{176}Lu_{calculated} = ^{175}\,Lu_{meas} \times \left(\frac{^{176}Lu}{^{175}Lu}\right)_{ref} \times \left(\frac{M175}{M176}\right)^{\beta Yb} \tag{B.3}$$

Both ^{176}Lu and ^{176}Yb signals were subtracted from the total signal intensity on the mass 176. Form there the Calculated ^{176}Hf signal was used in the determination of the Hf mass bias. We also used the true ^{179}Hf/^{177}Hf ratio of 0.7325 (Patchett and Tatsumoto, 1980), following this equation :

$$\beta Hf = \frac{ln\left(\frac{(^{179}Hf/^{177}Hf)_{ref}}{(^{179}Hf/^{177}Hf)_{meas}}\right)}{ln\left(\frac{M179}{M177}\right)} \tag{B.4}$$

The final interference corrected ^{176}Hf/^{177}Hf ratio was then defined using the following equation:

$$\left(\frac{^{176}Hf}{^{177}Hf}\right)_{corrected} = \left(\frac{^{176}(Hf + Yb + Lu)_{meas} - ^{176}Yb_{calc} - ^{176}Lu_{calc}}{^{177}Hf_{meas}}\right) \times \left(\frac{M176}{M177}\right)^{\beta Hf} \tag{B.5}$$

For all samples the ^{176}Lu/^{177}Hf was corrected for mass bias using β Hf. Outlier rejection of the Hf isotopic ratio for each analysis were performed using a two-standard deviation criterion.

References

Chu, N-C., Taylor, R., Nesbitt, R., Boella M.R., Milton, A.J., German, C., Bayon, G., Burton, K., (2002). Hf Isotope Ratio Analysis Using Multi-collector Inductively Coupled Plasma Mass Spectrometry: An Evaluation of Isobaric Interference Corrections. Journal of Analytical Atomic Spectrometry - J ANAL ATOM SPECTROM. 17. 1567-1574. 10.1039/b206707b.

Fisher, C.M., Hanchar, J.M., Samson, S.D., Dhuime, B., Blichert-Toft, J., Vervoort, J.D., Lam, R., 2011. Synthetic zircon doped with hafnium and rare earth elements: A reference material for in situ hafnium isotope analysis. Chem. Geol. 286, 3247. https://doi.org/10.1016/j.chemgeo.2011.04.013

Patchett, P.J., Tatsumoto, M., 1981. A routine high-precision method for Lu-Hf isotope geochemistry and chronology. Contrib. to Mineral. Petrol. 75, 263267. https://doi.org/10.1007/BF01166766

Vervoort, J., Patchett, J.P., Söderlund, U., Baker, M.E., (2004). Isotopic composition of Yb and the determination of Lu concentrations and Lu/Hf ratios by isotope dilution using MC-ICPMS. Geochemistry, Geophysics, Geosystems. 5 (11). 10.1029/2004GC000721.

Table B.1

Detail summary of the analytic procedure and conditions for the in-situ U-Pb geochronological analyses and the in-situ Lu-Hf isotopic analyses

.

Analytical Procedure: Part 1	
Laboratory and Sample Preparation	
Laboratory name	Laboratoire Magmas & Volcans, Clermont-Ferrand, France
Sample type/mineral	Magmatic zircons
Sample preparation	Conventional mineral separation: Wilfley Table, heavy liquids, Frantz magnetic separator, handpicking under binocular microscope 1 inch Epotek resin mount, 0.25μm polish to finish
Imaging	JEOL 6610LV SEM for Back scattered electron imaging Gatan MINI-Cl cathodoluminescence detector
Laser ablation system for U-Pb geochronology	
Make, Model & type	Resonetics/M-50E 193nm, Excimer
Ablation cell & volume	Laurin Cell two volumes cell, Laurin Technic Ltd., volume ca. 1cm^3
Laser wavelength	193 nm
Pulse width	< 4 ns
Laser Fluence	2.5 J.cm^{-2}
Repetition rate	3 Hz
Spot size	20μm
Sampling mode / pattern	Single spot
Carrier gas	100% He, Ar make-up gas and N^2 combined using the Squid® device from Resolution Instruments.
Background collection	30 s
Ablation duration	60 s
Wash-out delay	30 s
Cell carrier gas flow	0.70 l/min He
ICP-MS Instrument for U-Pb geochronology	
Make, Model & type	Element XR SF-ICP-MS
Sample introduction	Via conventional tubing
RF power	1200 W
Make-up gas flow	0.98 l/min Ar
Detection system	Single collector secondary electron multiplier (Faraday cup)
Masses measured	204, 206, 207, 208, 232, 238
Integration time per peak	20 ms
Sensitivity /Efficiency	150 000 cps/ppm ^{238}U (47 μm, 10 Hz, 3.5 J/cm^2)
Dead time	6 ns

Analytical Procedure: Part 2	
Data Processing	
Gas blank	30 second on-peak
Calibration strategy	GJ-1 used as primary reference material, 91500 and Plesovice used as secondary reference material (Quality Control)
Reference material info	91500 (Wiedenbeck et al., 1995) Plesovice (Slama et al., 2008) GJ1 (Jackson et al., 2004)
Data processing package used / Correction for LIEF	GLITTER ® (van Achterbergh et al., 2001)
Mass discrimination	Standard-sample bracketing with $^{207}Pb/^{206}Pb$ and $^{206}Pb/^{238}U$ normalized to reference material GJ-1
Common-Pb correction	No common-Pb correction.
Uncertainty level & propagation	Ages are quoted at 2σ absolute, propagation is by quadratic addition according to Horstwood et al. (2003). Reproducibility and age uncertainty of reference material are propagated.
Quality control / Validation	91500: Concordia age = 1064.2 ± 2.7 (2SD, MSWD = 0.79, N = 72) Plesovice: Wtd ave $^{206}Pb/^{238}U$ age = 339 ± 2 (2SD, MSWD = 0.9, N = 24)
Other information	For detailed method description see Hurai et al. (2010). For detailed laser technical description see Müller et al. (2009).
Laser ablation system for Lu-Hf isotopic ratios measurement	
Make, Model & type	Resonetics/M-50E 193nm, Excimer
Ablation cell & volume	Laurin Cell two volumes cell, Laurin Technic Ltd., volume ca. $1cm^3$
Laser wavelength	193 nm
Pulse width	< 4 ns
Laser Fluence	3.6 $J.cm^{-2}$
Repetition rate	6 Hz
Spot size	40-47 μm
Sampling mode / pattern	Single spot
Carrier gas	100% He, Ar make-up gas and N^2 combined using the Squid® device from Resolution Instruments.
Ablation duration	60 s
Wash-out delay	30 s
Hellium gas flow rate	0.67-0.70 l/min
Nitrogen gas flow rate	0.0045 L/min

Analytical Procedure: Part 3	
ICP-MS Instrument for Lu-Hf analysis	
Make, Model & type	Thermo Neptune Plus HRMC-ICP-MS
RF power	1200 W
Sample introduction	Via conventional tubing
Cool gas flow	14 L/min
Auxiliary gas	0.66 L/min
Sample gas	0.86 L/min
Scan mode	Static
Detection system	Multi-collector secondary electron multiplier (Faraday cup)
Scaned Masses (L4 to H3)	171 [$L4$], 173 [$L3$], 174 [$L2$], 175 [$L1$], 176 [C], 177 [$H1$], 178 [$H2$], 179 [$H3$]
Mass resolution	300
Number of scans	70
background	20 s
Integration time	1.05 s
Data Processing	
Gas blank	30 second on-peak
Calibration strategy	GJ-1 used as primary reference material, 91500 and Plesovice used as secondary reference material (Quality Control)
Reference material info	91500 (Wiedenbeck et al., 1995) Plesovice (Slama et al., 2008) GJ1 (Jackson et al., 2004)
Yb Mass bias correction	$^{173}Yb/^{171}Yb = 1.132685$
Yb interference correction	$^{176}Yb/^{173}Yb = 0.796218$

Primary and secondary Standard for U-Pb measurement

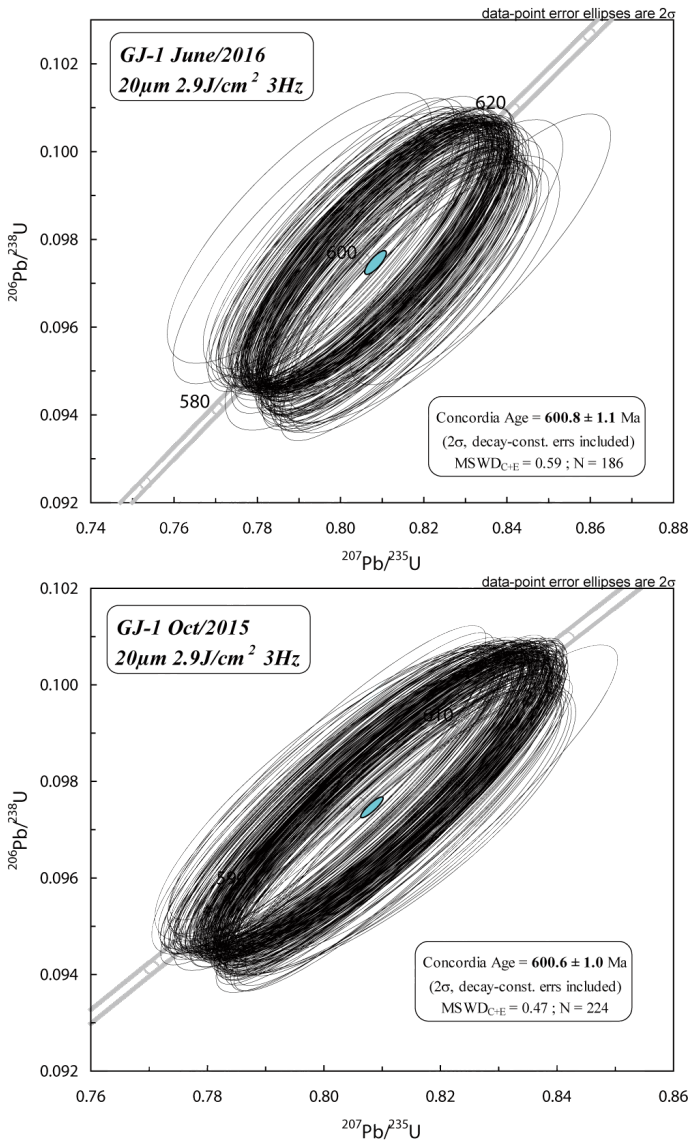

Figure B.4

Primary and Secondary standard reproducibility of U-Pb analysis. The primary standard is the GJ-1 and the secondary is the 91500

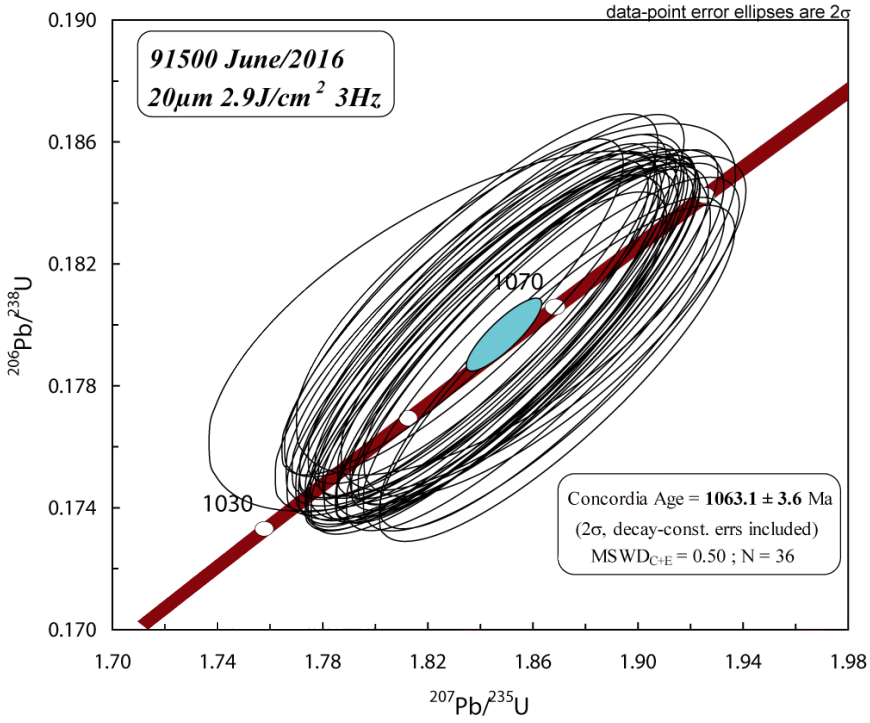
data-point error ellipses are 2σ
91500 June/2016
20µm 2.9J/cm² 3Hz
1070
1030
Concordia Age = 1063.1 ± 3.6 Ma
(2σ, decay-const. errs included)
MSWD C+E = 0.50 ; N = 36
206Pb/238U
207Pb/235U
0.190
0.186
0.182
0.178
0.174
0.170
1.70
1.74
1.78
1.82
1.86
1.90
1.94
1.98

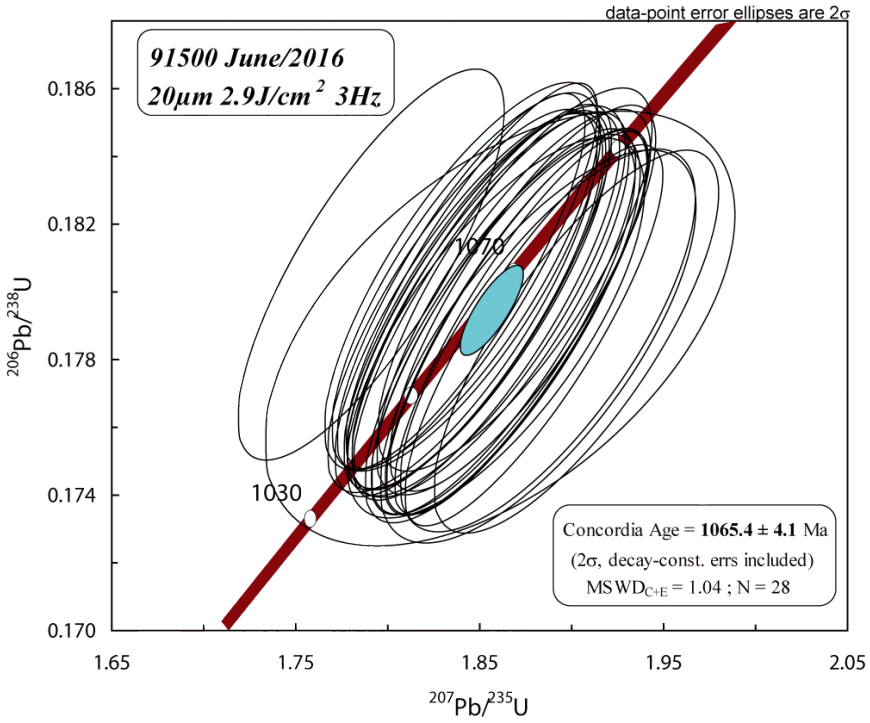
data-point error ellipses are 2σ
91500 June/2016
20µm 2.9J/cm² 3Hz
1070
1030
Concordia Age = 1065.4 ± 4.1 Ma
(2σ, decay-const. errs included)
MSWD C+E = 1.04 ; N = 28
206Pb/238U
207Pb/235U
0.186
0.182
0.178
0.174
0.170
1.65
1.75
1.85
1.95
2.05

Table B.2

Full set of U-Pb analysis on standard zircon primary standard GJ-1 and secondary standard 91500. ρ is the error correlation coefficient.

Spot #	^{207}**Pb**/^{235}**U** $\pm 2\sigma$	^{206}**Pb**/^{238}**U** $\pm 2\sigma$	ρ
	GJ-1 session of October 2015		
Zr4 261015a	0.8007 ± 0.0242	0.09769 ± 0.00246	0.83
Zr15	0.8094 ± 0.0222	0.09780 ± 0.00246	0.92
Zr16	0.8122 ± 0.0243	0.09697 ± 0.00243	0.84
Zr23	0.8031 ± 0.0244	0.09775 ± 0.00246	0.83
Zr24	0.8093 ± 0.0224	0.09750 ± 0.00243	0.90
Zr33	0.8085 ± 0.0223	0.09757 ± 0.00243	0.90
Zr34	0.8110 ± 0.0224	0.09723 ± 0.00243	0.90
Zr43	0.8109 ± 0.0245	0.09695 ± 0.00243	0.83
Zr44	0.8113 ± 0.0227	0.09742 ± 0.00243	0.89
Zr53	0.8046 ± 0.0226	0.09750 ± 0.00243	0.89
Zr54	0.8079 ± 0.0227	0.09771 ± 0.00243	0.89
Zr63	0.8096 ± 0.0227	0.09725 ± 0.00243	0.89
Zr64	0.8086 ± 0.0228	0.09756 ± 0.00243	0.88
Zr73	0.8072 ± 0.0231	0.09752 ± 0.00243	0.87
Zr74	0.8121 ± 0.0233	0.09772 ± 0.00243	0.87
Zr75	0.8014 ± 0.0231	0.09780 ± 0.00246	0.87
Zr76	0.8121 ± 0.0234	0.09724 ± 0.00243	0.87
Zr1 261015b	0.8072 ± 0.0217	0.09743 ± 0.00240	0.92
Zr2	0.8052 ± 0.0216	0.09748 ± 0.00240	0.92
Zr3	0.8087 ± 0.0216	0.09773 ± 0.00240	0.92
Zr4	0.8117 ± 0.0218	0.09742 ± 0.00240	0.92
Zr13	0.8078 ± 0.0216	0.09751 ± 0.00240	0.92
Zr14	0.8091 ± 0.0233	0.09770 ± 0.00243	0.86
Zr23	0.8006 ± 0.0215	0.09764 ± 0.00240	0.92
Zr24	0.8120 ± 0.0219	0.09758 ± 0.00240	0.91
Zr33	0.8072 ± 0.0220	0.09756 ± 0.00240	0.90
Zr34	0.8120 ± 0.0221	0.09776 ± 0.00240	0.90
Zr43	0.8121 ± 0.0219	0.09762 ± 0.00240	0.91
Zr44	0.8077 ± 0.0215	0.09771 ± 0.00240	0.92
Zr53	0.8103 ± 0.0216	0.09693 ± 0.00240	0.93
Zr54	0.8093 ± 0.0217	0.09695 ± 0.00240	0.92
Zr63	0.8027 ± 0.0247	0.09728 ± 0.00243	0.81

Continued on next page

Table B.2 – *Continued from previous page*

Spot #	^{207}**Pb**/^{235}**U** $\pm 2\sigma$	^{206}**Pb**/^{238}**U** $\pm 2\sigma$	ρ
Zr64	0.8086 ± 0.0220	0.09719 ± 0.00240	0.91
Zr73	0.8058 ± 0.0219	0.09749 ± 0.00240	0.90
Zr74	0.8125 ± 0.0221	0.09763 ± 0.00240	0.90
Zr83	0.8094 ± 0.0219	0.09747 ± 0.00240	0.91
Zr84	0.8144 ± 0.0221	0.09764 ± 0.00240	0.91
Zr93	0.8089 ± 0.0221	0.09751 ± 0.00240	0.90
Zr94	0.8053 ± 0.0222	0.09761 ± 0.00240	0.89
Zr104	0.8050 ± 0.0222	0.09752 ± 0.00240	0.89
Zr105	0.8097 ± 0.0222	0.09773 ± 0.00240	0.89
Zr110	0.8139 ± 0.0223	0.09691 ± 0.00240	0.90
Zr111	0.8088 ± 0.0224	0.09770 ± 0.00243	0.90
Zr112	0.8018 ± 0.0219	0.09777 ± 0.00243	0.91
Zr113	0.8071 ± 0.0221	0.09766 ± 0.00240	0.90
Zr1 271015a	0.8030 ± 0.0235	0.09758 ± 0.00255	0.89
Zr2	0.8051 ± 0.0234	0.09756 ± 0.00255	0.90
Zr3	0.8210 ± 0.0240	0.09767 ± 0.00258	0.90
Zr4	0.8070 ± 0.0231	0.09758 ± 0.00255	0.91
Zr13	0.8069 ± 0.0240	0.09741 ± 0.00258	0.89
Zr14	0.8107 ± 0.0239	0.09745 ± 0.00258	0.90
Zr23	0.8060 ± 0.0231	0.09749 ± 0.00258	0.92
Zr24	0.8103 ± 0.0234	0.09734 ± 0.00258	0.92
Zr33	0.8108 ± 0.0232	0.09748 ± 0.00258	0.93
Zr34	0.8082 ± 0.0233	0.09765 ± 0.00258	0.91
Zr43	0.8072 ± 0.0236	0.09744 ± 0.00258	0.91
Zr44	0.8099 ± 0.0236	0.09747 ± 0.00258	0.91
Zr53	0.8069 ± 0.0232	0.09746 ± 0.00258	0.92
Zr54	0.8096 ± 0.0238	0.09743 ± 0.00258	0.90
Zr63	0.8058 ± 0.0234	0.09732 ± 0.00258	0.91
Zr64	0.8090 ± 0.0234	0.09757 ± 0.00258	0.92
Zr73	0.8058 ± 0.0236	0.09731 ± 0.00258	0.91
Zr74	0.8088 ± 0.0238	0.09750 ± 0.00261	0.91
Zr83	0.8091 ± 0.0239	0.09750 ± 0.00261	0.91
Zr84	0.8092 ± 0.0238	0.09753 ± 0.00261	0.91
Zr93	0.8088 ± 0.0245	0.09748 ± 0.00261	0.88
Zr94	0.8006 ± 0.0246	0.09761 ± 0.00261	0.87

Continued on next page

Table B.2 – *Continued from previous page*

Spot #	^{207}**Pb**/^{235}**U** $\pm 2\sigma$	^{206}**Pb**/^{238}**U** $\pm 2\sigma$	ρ
Zr97	0.8115 ± 0.0242	0.09771 ± 0.00261	0.89
Zr98	0.8123 ± 0.0242	0.09752 ± 0.00261	0.90
Zr1 271015b	0.8094 ± 0.0235	0.09730 ± 0.00264	0.94
Zr2	0.8117 ± 0.0235	0.09757 ± 0.00264	0.93
Zr3	0.8075 ± 0.0233	0.09763 ± 0.00264	0.94
Zr4	0.8011 ± 0.0233	0.09766 ± 0.00264	0.93
Zr13	0.8039 ± 0.0234	0.09767 ± 0.00264	0.93
Zr14	0.8047 ± 0.0233	0.09770 ± 0.00264	0.94
Zr23	0.8112 ± 0.0235	0.09770 ± 0.00264	0.93
Zr24	0.8094 ± 0.0236	0.09780 ± 0.00264	0.93
Zr33	0.8118 ± 0.0236	0.09711 ± 0.00264	0.94
Zr34	0.8069 ± 0.0237	0.09768 ± 0.00264	0.92
Zr43	0.8121 ± 0.0237	0.09701 ± 0.00264	0.93
Zr44	0.8107 ± 0.0237	0.09703 ± 0.00264	0.93
Zr53	0.8067 ± 0.0239	0.09762 ± 0.00264	0.91
Zr54	0.8106 ± 0.0240	0.09757 ± 0.00264	0.91
Zr64	0.8108 ± 0.0237	0.09774 ± 0.00264	0.92
Zr65	0.8111 ± 0.0236	0.09711 ± 0.00264	0.93
Zr73	0.8136 ± 0.0237	0.09690 ± 0.00264	0.93
Zr74	0.8088 ± 0.0238	0.09756 ± 0.00264	0.92
Zr83	0.8051 ± 0.0237	0.09765 ± 0.00264	0.92
Zr84	0.8124 ± 0.0240	0.09764 ± 0.00264	0.92
Zr93	0.8121 ± 0.0239	0.09740 ± 0.00264	0.92
Zr94	0.8075 ± 0.0238	0.09770 ± 0.00264	0.92
Zr103	0.8111 ± 0.0241	0.09743 ± 0.00264	0.91
Zr104	0.8007 ± 0.0235	0.09743 ± 0.00264	0.92
Zr113	0.8026 ± 0.0238	0.09759 ± 0.00264	0.91
Zr114	0.8092 ± 0.0241	0.09763 ± 0.00267	0.92
Zr123	0.8035 ± 0.0239	0.09766 ± 0.00267	0.92
Zr124	0.8117 ± 0.0242	0.09770 ± 0.00267	0.92
Zr125	0.8114 ± 0.0241	0.09730 ± 0.00264	0.91
Zr126	0.8073 ± 0.0241	0.09765 ± 0.00267	0.92
Zr1 281015a	0.8097 ± 0.0233	0.09710 ± 0.00258	0.92
Zr2	0.8103 ± 0.0233	0.09736 ± 0.00258	0.92
Zr3	0.8103 ± 0.0232	0.09705 ± 0.00258	0.93

Continued on next page

Table B.2 – *Continued from previous page*

Spot #	^{207}**Pb**/^{235}**U** $\pm 2\sigma$	^{206}**Pb**/^{238}**U** $\pm 2\sigma$	ρ
Zr4	0.8061 ± 0.0232	0.09767 ± 0.00258	0.92
Zr13	0.8129 ± 0.0230	0.09776 ± 0.00258	0.93
Zr14	0.8104 ± 0.0230	0.09781 ± 0.00258	0.93
Zr23	0.8092 ± 0.0228	0.09782 ± 0.00258	0.93
Zr24	0.8032 ± 0.0228	0.09761 ± 0.00255	0.92
Zr33	0.8111 ± 0.0229	0.09727 ± 0.00255	0.93
Zr34	0.8106 ± 0.0229	0.09765 ± 0.00255	0.93
Zr43	0.8014 ± 0.0227	0.09796 ± 0.00255	0.92
Zr44	0.8100 ± 0.0228	0.09707 ± 0.00252	0.92
Zr53	0.7996 ± 0.0226	0.09762 ± 0.00252	0.91
Zr54	0.8080 ± 0.0228	0.09746 ± 0.00252	0.92
Zr63	0.8087 ± 0.0226	0.09752 ± 0.00252	0.93
Zr64	0.8021 ± 0.0226	0.09765 ± 0.00252	0.92
Zr73	0.8096 ± 0.0230	0.09746 ± 0.00249	0.90
Zr74	0.8095 ± 0.0227	0.09756 ± 0.00249	0.91
Zr83	0.8098 ± 0.0226	0.09707 ± 0.00249	0.92
Zr84	0.8093 ± 0.0227	0.09700 ± 0.00249	0.92
Zr93	0.8112 ± 0.0231	0.09780 ± 0.00249	0.89
Zr94	0.8107 ± 0.0228	0.09744 ± 0.00249	0.91
Zr97	0.8090 ± 0.0228	0.09760 ± 0.00249	0.91
Zr98	0.8103 ± 0.0226	0.09774 ± 0.00249	0.91
Zr1 281015b	0.8070 ± 0.0236	0.09757 ± 0.00249	0.87
Zr2	0.8018 ± 0.0222	0.09758 ± 0.00249	0.92
Zr3	0.8115 ± 0.0223	0.09749 ± 0.00246	0.92
Zr4	0.8084 ± 0.0224	0.09771 ± 0.00249	0.92
Zr13	0.8004 ± 0.0236	0.09757 ± 0.00249	0.87
Zr14	0.8061 ± 0.0227	0.09759 ± 0.00249	0.91
Zr23	0.8116 ± 0.0223	0.09761 ± 0.00246	0.92
Zr24	0.8128 ± 0.0224	0.09725 ± 0.00246	0.92
Zr33	0.8126 ± 0.0224	0.09678 ± 0.00246	0.92
Zr34	0.8118 ± 0.0224	0.09720 ± 0.00246	0.92
Zr43	0.8007 ± 0.0222	0.09818 ± 0.00249	0.92
Zr44	0.8109 ± 0.0224	0.09750 ± 0.00246	0.91
Zr53	0.8117 ± 0.0225	0.09761 ± 0.00246	0.91
Zr54	0.8081 ± 0.0223	0.09763 ± 0.00246	0.91

Continued on next page

Table B.2 – *Continued from previous page*

Spot #	^{207}**Pb**/^{235}**U** $\pm 2\sigma$	^{206}**Pb**/^{238}**U** $\pm 2\sigma$	ρ
Zr63	0.8124 ± 0.0227	0.09749 ± 0.00246	0.90
Zr64	0.8066 ± 0.0223	0.09764 ± 0.00246	0.91
Zr73	0.8112 ± 0.0256	0.09702 ± 0.00246	0.80
Zr74	0.8096 ± 0.0226	0.09752 ± 0.00246	0.90
Zr83	0.8101 ± 0.0224	0.09752 ± 0.00246	0.91
Zr84	0.8007 ± 0.0221	0.09755 ± 0.00246	0.91
Zr93	0.8111 ± 0.0225	0.09739 ± 0.00246	0.91
Zr94	0.8109 ± 0.0226	0.09693 ± 0.00243	0.90
Zr103	0.8098 ± 0.0233	0.09754 ± 0.00246	0.88
Zr104	0.8120 ± 0.0255	0.09701 ± 0.00246	0.81
Zr113	0.8075 ± 0.0227	0.09766 ± 0.00246	0.90
Zr114	0.8071 ± 0.0229	0.09779 ± 0.00246	0.89
Zr115	0.8068 ± 0.0225	0.09759 ± 0.00246	0.90
Zr116	0.8074 ± 0.0228	0.09760 ± 0.00246	0.89
Zr1 291015a	0.8023 ± 0.0237	0.09754 ± 0.00264	0.92
Zr2	0.8101 ± 0.0237	0.09724 ± 0.00264	0.93
Zr3	0.8080 ± 0.0235	0.09761 ± 0.00264	0.93
Zr4	0.8082 ± 0.0241	0.09752 ± 0.00264	0.91
Zr13	0.8120 ± 0.0236	0.09720 ± 0.00264	0.93
Zr14	0.8111 ± 0.0236	0.09768 ± 0.00264	0.93
Zr23	0.8115 ± 0.0236	0.09733 ± 0.00261	0.92
Zr24	0.8109 ± 0.0238	0.09749 ± 0.00264	0.92
Zr33	0.8082 ± 0.0235	0.09762 ± 0.00261	0.92
Zr34	0.8027 ± 0.0233	0.09761 ± 0.00261	0.92
Zr43	0.8108 ± 0.0233	0.09745 ± 0.00261	0.93
Zr44	0.8092 ± 0.0233	0.09762 ± 0.00261	0.93
Zr54	0.8106 ± 0.0235	0.09738 ± 0.00261	0.92
Zr55	0.8090 ± 0.0235	0.09756 ± 0.00261	0.92
Zr63	0.8090 ± 0.0235	0.09767 ± 0.00261	0.92
Zr64	0.8011 ± 0.0238	0.09763 ± 0.00261	0.90
Zr73	0.8107 ± 0.0233	0.09730 ± 0.00258	0.92
Zr74	0.8082 ± 0.0235	0.09750 ± 0.00261	0.92
Zr83	0.8025 ± 0.0233	0.09761 ± 0.00258	0.91
Zr84	0.8097 ± 0.0236	0.09766 ± 0.00258	0.91
Zr93	0.8100 ± 0.0235	0.09751 ± 0.00258	0.91

Continued on next page

Table B.2 – *Continued from previous page*

Spot #	^{207}**Pb**/^{235}**U** $\pm 2\sigma$	^{206}**Pb**/^{238}**U** $\pm 2\sigma$	ρ
Zr94	0.8083 ± 0.0235	0.09766 ± 0.00258	0.91
Zr103	0.8038 ± 0.0233	0.09762 ± 0.00258	0.91
Zr104	0.8019 ± 0.0234	0.09765 ± 0.00258	0.91
Zr113	0.8118 ± 0.0242	0.09743 ± 0.00258	0.89
Zr114	0.8114 ± 0.0237	0.09719 ± 0.00255	0.90
Zr123	0.8075 ± 0.0239	0.09749 ± 0.00258	0.89
Zr124	0.8123 ± 0.0238	0.09739 ± 0.00255	0.90
Zr125	0.8106 ± 0.0241	0.09761 ± 0.00258	0.89
Zr126	0.8104 ± 0.0236	0.09730 ± 0.00255	0.90
Zr1 291015b	0.8059 ± 0.0227	0.09743 ± 0.00252	0.92
Zr2	0.8101 ± 0.0226	0.09763 ± 0.00252	0.92
Zr3	0.8066 ± 0.0229	0.09776 ± 0.00255	0.92
Zr4	0.8031 ± 0.0231	0.09770 ± 0.00255	0.91
Zr13	0.8136 ± 0.0230	0.09770 ± 0.00255	0.92
Zr14	0.8102 ± 0.0230	0.09769 ± 0.00255	0.92
Zr23	0.8111 ± 0.0230	0.09729 ± 0.00252	0.92
Zr24	0.8081 ± 0.0229	0.09754 ± 0.00255	0.92
Zr33	0.8048 ± 0.0228	0.09764 ± 0.00255	0.92
Zr34	0.8108 ± 0.0229	0.09715 ± 0.00252	0.92
Zr43	0.8124 ± 0.0232	0.09674 ± 0.00252	0.91
Zr54	0.8073 ± 0.0231	0.09734 ± 0.00255	0.91
Zr55	0.8091 ± 0.0236	0.09742 ± 0.00255	0.90
Zr63	0.8046 ± 0.0231	0.09751 ± 0.00255	0.91
Zr64	0.8081 ± 0.0232	0.09747 ± 0.00255	0.91
Zr73	0.8099 ± 0.0231	0.09759 ± 0.00255	0.92
Zr74	0.8055 ± 0.0233	0.09755 ± 0.00255	0.91
Zr83	0.8099 ± 0.0236	0.09747 ± 0.00255	0.90
Zr84	0.8068 ± 0.0239	0.09762 ± 0.00255	0.88
Zr93	0.8111 ± 0.0244	0.09721 ± 0.00255	0.87
Zr94	0.8103 ± 0.0239	0.09763 ± 0.00255	0.89
Zr103	0.8111 ± 0.0237	0.09755 ± 0.00255	0.90
Zr104	0.8082 ± 0.0255	0.09750 ± 0.00258	0.84
Zr105	0.8082 ± 0.0239	0.09761 ± 0.00255	0.88
Zr106	0.8052 ± 0.0236	0.09776 ± 0.00258	0.90
Zr1 301015a	0.8107 ± 0.0249	0.09741 ± 0.00270	0.90

Continued on next page

Table B.2 – *Continued from previous page*

Spot #	^{207}**Pb**/^{235}**U** $\pm 2\sigma$	^{206}**Pb**/^{238}**U** $\pm 2\sigma$	ρ
Zr2	0.8047 ± 0.0248	0.09739 ± 0.00270	0.90
Zr3	0.8083 ± 0.0248	0.09757 ± 0.00270	0.90
Zr4	0.8114 ± 0.0249	0.09739 ± 0.00270	0.90
Zr13	0.8085 ± 0.0243	0.09760 ± 0.00270	0.92
Zr14	0.8113 ± 0.0243	0.09753 ± 0.00270	0.92
Zr23	0.8109 ± 0.0244	0.09755 ± 0.00267	0.91
Zr24	0.8062 ± 0.0244	0.09761 ± 0.00267	0.90
Zr33	0.8020 ± 0.0240	0.09771 ± 0.00267	0.91
Zr34	0.8050 ± 0.0244	0.09772 ± 0.00267	0.90
Zr43	0.8108 ± 0.0243	0.09738 ± 0.00264	0.90
Zr44	0.8115 ± 0.0245	0.09686 ± 0.00264	0.90
Zr53	0.8052 ± 0.0243	0.09752 ± 0.00264	0.90
Zr54	0.8094 ± 0.0245	0.09754 ± 0.00264	0.89
Zr61	0.8096 ± 0.0248	0.09763 ± 0.00264	0.88
Zr62	0.8112 ± 0.0244	0.09758 ± 0.00261	0.89
Zr63	0.8120 ± 0.0247	0.09724 ± 0.00261	0.88
Zr64	0.8048 ± 0.0243	0.09768 ± 0.00261	0.89
	91500 session of October 2015		
Zr5 261015a	1.8320 ± 0.0783	0.1798 ± 0.0048	0.63
Zr6	1.8533 ± 0.0686	0.1808 ± 0.0047	0.70
Zr71	1.8682 ± 0.0595	0.1800 ± 0.0046	0.80
Zr72	1.8585 ± 0.0559	0.1797 ± 0.0045	0.84
Zr5 261015b	1.8673 ± 0.0537	0.1787 ± 0.0044	0.86
Zr6	1.8436 ± 0.0524	0.1795 ± 0.0044	0.87
Zr108	1.8292 ± 0.0532	0.1806 ± 0.0045	0.86
Zr109	1.8597 ± 0.0596	0.1802 ± 0.0046	0.79
Zr5 271015a	1.8526 ± 0.0557	0.1793 ± 0.0047	0.88
Zr6	1.8387 ± 0.0557	0.1801 ± 0.0048	0.88
Zr95	1.8604 ± 0.0572	0.1798 ± 0.0048	0.87
Zr96	1.8407 ± 0.0573	0.1803 ± 0.0049	0.87
Zr5 271015b	1.8430 ± 0.0563	0.1793 ± 0.0049	0.89
Zr6	1.8533 ± 0.0560	0.1796 ± 0.0049	0.90
Zr121	1.8608 ± 0.0589	0.1793 ± 0.0049	0.87
Zr122	1.8485 ± 0.0603	0.1797 ± 0.0050	0.84
Zr5 281015a	1.8363 ± 0.0581	0.1810 ± 0.0049	0.85

Continued on next page

Table B.2 – *Continued from previous page*

Spot #	^{207}**Pb**/^{235}**U** $\pm 2\sigma$	^{206}**Pb**/^{238}**U** $\pm 2\sigma$	ρ
Zr6	1.8442 ± 0.0582	0.1795 ± 0.0048	0.85
Zr95	1.8397 ± 0.0575	0.1793 ± 0.0046	0.82
Zr96	1.8537 ± 0.0559	0.1799 ± 0.0046	0.85
Zr5 281015b	1.8430 ± 0.0554	0.1787 ± 0.0046	0.85
Zr6	1.8581 ± 0.0531	0.1797 ± 0.0046	0.89
Zr111	1.8691 ± 0.0555	0.1784 ± 0.0045	0.85
Zr112	1.8359 ± 0.0557	0.1799 ± 0.0046	0.84
Zr5 291015a	1.8417 ± 0.0621	0.1802 ± 0.0050	0.82
Zr6	1.8459 ± 0.0586	0.1808 ± 0.0050	0.86
Zr121	1.8428 ± 0.0591	0.1793 ± 0.0048	0.83
Zr122	1.8352 ± 0.0603	0.1797 ± 0.0048	0.81
Zr5 291015b	1.8461 ± 0.0558	0.1801 ± 0.0047	0.86
Zr6	1.8465 ± 0.0572	0.1802 ± 0.0047	0.85
Zr101	1.8544 ± 0.0567	0.1795 ± 0.0047	0.86
Zr102	1.8669 ± 0.0586	0.1790 ± 0.0047	0.84
Zr5 301015a	1.8463 ± 0.0594	0.1794 ± 0.0050	0.87
Zr6	1.8453 ± 0.0591	0.1794 ± 0.0050	0.87
Zr59	1.8366 ± 0.0578	0.1797 ± 0.0049	0.86
Zr60	1.8519 ± 0.0585	0.1795 ± 0.0049	0.86
	GJ-1 session of June 2016		
Zr1 300516a	0.8116 ± 0.0242	0.09743 ± 0.00249	0.86
Zr2	0.8108 ± 0.0242	0.09756 ± 0.00249	0.85
Zr3	0.8090 ± 0.0236	0.09775 ± 0.00249	0.88
Zr4	0.8116 ± 0.0239	0.09724 ± 0.00249	0.87
Zr13	0.8112 ± 0.0236	0.09747 ± 0.00249	0.88
Zr14	0.8107 ± 0.0234	0.09747 ± 0.00249	0.89
Zr23	0.8130 ± 0.0237	0.09687 ± 0.00249	0.88
Zr24	0.8113 ± 0.0237	0.09706 ± 0.00249	0.88
Zr33	0.8038 ± 0.0234	0.09776 ± 0.00249	0.87
Zr34	0.8120 ± 0.0237	0.09717 ± 0.00249	0.88
Zr43	0.8065 ± 0.0233	0.09777 ± 0.00249	0.88
Zr44	0.8058 ± 0.0237	0.09783 ± 0.00252	0.88
Zr53	0.8008 ± 0.0233	0.09791 ± 0.00252	0.89
Zr54	0.8091 ± 0.0237	0.09776 ± 0.00252	0.88
Zr63	0.8107 ± 0.0239	0.09746 ± 0.00249	0.87

Continued on next page

Table B.2 – *Continued from previous page*

Spot #	^{207}**Pb**/^{235}**U** $\pm 2\sigma$	^{206}**Pb**/^{238}**U** $\pm 2\sigma$	ρ
Zr64	0.7979 ± 0.0241	0.09814 ± 0.00252	0.85
Zr73	0.8102 ± 0.0240	0.09704 ± 0.00249	0.87
Zr74	0.8023 ± 0.0237	0.09795 ± 0.00252	0.87
Zr83	0.8062 ± 0.0239	0.09758 ± 0.00252	0.87
Zr84	0.8098 ± 0.0242	0.09724 ± 0.00249	0.86
Zr93	0.8067 ± 0.0242	0.09765 ± 0.00252	0.86
Zr94	0.7992 ± 0.0238	0.09794 ± 0.00252	0.86
Zr103	0.8073 ± 0.0247	0.09778 ± 0.00252	0.84
Zr104	0.8155 ± 0.0244	0.09646 ± 0.00249	0.86
Zr113	0.8094 ± 0.0242	0.09705 ± 0.00249	0.86
Zr114	0.8102 ± 0.0243	0.09743 ± 0.00252	0.86
Zr123	0.8037 ± 0.0242	0.09767 ± 0.00252	0.86
Zr124	0.8091 ± 0.0242	0.09749 ± 0.00252	0.86
Zr133	0.8101 ± 0.0247	0.09765 ± 0.00252	0.85
Zr134	0.8104 ± 0.0244	0.09769 ± 0.00252	0.86
Zr143	0.8114 ± 0.0246	0.09670 ± 0.00249	0.85
Zr144	0.8110 ± 0.0250	0.09717 ± 0.00252	0.84
Zr153	0.8109 ± 0.0248	0.09795 ± 0.00252	0.84
Zr155	0.8110 ± 0.0245	0.09770 ± 0.00252	0.86
Zr156	0.8091 ± 0.0246	0.09760 ± 0.00252	0.85
Zr1 310516a	0.8029 ± 0.0242	0.09758 ± 0.00249	0.85
Zr2	0.8111 ± 0.0240	0.09772 ± 0.00249	0.86
Zr3	0.8125 ± 0.0238	0.09701 ± 0.00249	0.88
Zr4	0.8062 ± 0.0236	0.09775 ± 0.00249	0.87
Zr13	0.8114 ± 0.0237	0.09761 ± 0.00249	0.87
Zr14	0.8065 ± 0.0236	0.09774 ± 0.00249	0.87
Zr23	0.8108 ± 0.0238	0.09755 ± 0.00249	0.87
Zr24	0.8012 ± 0.0233	0.09793 ± 0.00249	0.87
Zr33	0.8132 ± 0.0239	0.09698 ± 0.00249	0.87
Zr34	0.8155 ± 0.0240	0.09675 ± 0.00246	0.86
Zr43	0.8106 ± 0.0245	0.09762 ± 0.00249	0.85
Zr44	0.8004 ± 0.0239	0.09772 ± 0.00249	0.85
Zr53	0.8064 ± 0.0238	0.09766 ± 0.00249	0.86
Zr54	0.8117 ± 0.0238	0.09758 ± 0.00249	0.87
Zr63	0.8039 ± 0.0238	0.09758 ± 0.00249	0.86

Continued on next page

Table B.2 – *Continued from previous page*

Spot #	^{207}**Pb**/^{235}**U** $\pm 2\sigma$	^{206}**Pb**/^{238}**U** $\pm 2\sigma$	ρ
Zr64	0.8118 ± 0.0242	0.09764 ± 0.00249	0.86
Zr73	0.8113 ± 0.0248	0.09678 ± 0.00249	0.84
Zr74	0.8040 ± 0.0239	0.09768 ± 0.00249	0.86
Zr83	0.8152 ± 0.0244	0.09661 ± 0.00246	0.85
Zr84	0.8084 ± 0.0244	0.09763 ± 0.00249	0.84
Zr93	0.8003 ± 0.0242	0.09811 ± 0.00252	0.85
Zr94	0.8105 ± 0.0247	0.09762 ± 0.00249	0.84
Zr103	0.8035 ± 0.0242	0.09760 ± 0.00249	0.85
Zr104	0.8126 ± 0.0246	0.09701 ± 0.00249	0.85
Zr113	0.8103 ± 0.0247	0.09754 ± 0.00249	0.84
Zr114	0.8059 ± 0.0243	0.09764 ± 0.00249	0.84
Zr117	0.8116 ± 0.0250	0.09756 ± 0.00249	0.83
Zr118	0.8099 ± 0.0249	0.09773 ± 0.00252	0.84
Zr1 310516b	0.8115 ± 0.0245	0.09753 ± 0.00249	0.85
Zr2	0.8072 ± 0.0240	0.09756 ± 0.00249	0.86
Zr3	0.8070 ± 0.0239	0.09752 ± 0.00249	0.86
Zr4	0.8076 ± 0.0236	0.09766 ± 0.00249	0.87
Zr13	0.8065 ± 0.0239	0.09765 ± 0.00249	0.86
Zr14	0.8134 ± 0.0247	0.09688 ± 0.00249	0.85
Zr23	0.8051 ± 0.0239	0.09767 ± 0.00252	0.87
Zr24	0.8143 ± 0.0246	0.09667 ± 0.00249	0.85
Zr33	0.8093 ± 0.0242	0.09757 ± 0.00252	0.86
Zr34	0.8114 ± 0.0243	0.09763 ± 0.00252	0.86
Zr43	0.8068 ± 0.0243	0.09758 ± 0.00252	0.86
Zr44	0.8118 ± 0.0244	0.09771 ± 0.00252	0.86
Zr54	0.8060 ± 0.0246	0.09758 ± 0.00252	0.85
Zr63	0.8063 ± 0.0249	0.09766 ± 0.00252	0.84
Zr64	0.8129 ± 0.0252	0.09709 ± 0.00252	0.84
Zr73	0.8061 ± 0.0252	0.09764 ± 0.00252	0.83
Zr74	0.8117 ± 0.0245	0.09705 ± 0.00249	0.85
Zr83	0.8062 ± 0.0248	0.09773 ± 0.00252	0.84
Zr84	0.8191 ± 0.0253	0.09664 ± 0.00249	0.83
Zr93	0.8179 ± 0.0251	0.09718 ± 0.00252	0.84
Zr94	0.8073 ± 0.0252	0.09775 ± 0.00252	0.82
Zr103	0.8075 ± 0.0253	0.09783 ± 0.00255	0.83

Continued on next page

Table B.2 – *Continued from previous page*

Spot #	^{207}**Pb**/^{235}**U** $\pm 2\sigma$	^{206}**Pb**/^{238}**U** $\pm 2\sigma$	ρ
Zr104	0.8038 ± 0.0251	0.09814 ± 0.00255	0.83
Zr113	0.8135 ± 0.0258	0.09723 ± 0.00252	0.82
Zr114	0.8147 ± 0.0258	0.09673 ± 0.00252	0.82
Zr115	0.8015 ± 0.0251	0.09776 ± 0.00255	0.83
Zr116	0.8021 ± 0.0254	0.09776 ± 0.00255	0.82
Zr1 010616a	0.8115 ± 0.0297	0.09752 ± 0.00255	0.71
Zr2	0.8081 ± 0.0256	0.09751 ± 0.00252	0.82
Zr3	0.8044 ± 0.0257	0.09742 ± 0.00252	0.81
Zr4	0.7994 ± 0.0258	0.09770 ± 0.00252	0.80
Zr13	0.8112 ± 0.0246	0.09736 ± 0.00249	0.84
Zr14	0.8134 ± 0.0242	0.09687 ± 0.00246	0.85
Zr23	0.8094 ± 0.0242	0.09767 ± 0.00249	0.85
Zr24	0.8066 ± 0.0241	0.09772 ± 0.00249	0.85
Zr33	0.8102 ± 0.0241	0.09761 ± 0.00249	0.86
Zr34	0.8099 ± 0.0241	0.09772 ± 0.00249	0.86
Zr43	0.8035 ± 0.0237	0.09756 ± 0.00249	0.86
Zr44	0.8114 ± 0.0244	0.09801 ± 0.00249	0.84
Zr53	0.8083 ± 0.0308	0.09752 ± 0.00255	0.69
Zr54	0.8110 ± 0.0241	0.09734 ± 0.00246	0.85
Zr63	0.8111 ± 0.0241	0.09710 ± 0.00246	0.85
Zr64	0.8106 ± 0.0242	0.09766 ± 0.00246	0.84
Zr73	0.8083 ± 0.0240	0.09753 ± 0.00246	0.85
Zr74	0.8134 ± 0.0277	0.09679 ± 0.00249	0.76
Zr83	0.7998 ± 0.0238	0.09786 ± 0.00246	0.84
Zr84	0.8051 ± 0.0244	0.09757 ± 0.00246	0.83
Zr93	0.8080 ± 0.0248	0.09747 ± 0.00246	0.82
Zr94	0.8085 ± 0.0243	0.09754 ± 0.00246	0.84
Zr103	0.8100 ± 0.0247	0.09733 ± 0.00246	0.83
Zr104	0.8103 ± 0.0245	0.09686 ± 0.00243	0.83
Zr113	0.8087 ± 0.0245	0.09762 ± 0.00246	0.83
Zr114	0.8124 ± 0.0249	0.09763 ± 0.00246	0.82
Zr115	0.8077 ± 0.0247	0.09765 ± 0.00246	0.82
Zr116	0.8065 ± 0.0249	0.09765 ± 0.00246	0.81
Zr1 010616b	0.8075 ± 0.0240	0.09744 ± 0.00243	0.84
Zr2	0.8089 ± 0.0243	0.09747 ± 0.00243	0.83

Continued on next page

Table B.2 – *Continued from previous page*

Spot #	^{207}**Pb**/^{235}**U** $\pm 2\sigma$	^{206}**Pb**/^{238}**U** $\pm 2\sigma$	ρ
Zr3	0.8107 ± 0.0240	0.09748 ± 0.00243	0.84
Zr4	0.8085 ± 0.0240	0.09775 ± 0.00243	0.84
Zr13	0.8070 ± 0.0241	0.09763 ± 0.00243	0.83
Zr14	0.8129 ± 0.0239	0.09762 ± 0.00243	0.85
Zr23	0.8041 ± 0.0248	0.09751 ± 0.00246	0.82
Zr24	0.8112 ± 0.0240	0.09767 ± 0.00246	0.85
Zr33	0.7976 ± 0.0240	0.09754 ± 0.00246	0.84
Zr34	0.8164 ± 0.0244	0.09677 ± 0.00243	0.84
Zr43	0.8058 ± 0.0244	0.09751 ± 0.00246	0.83
Zr44	0.8096 ± 0.0245	0.09721 ± 0.00246	0.84
Zr53	0.8033 ± 0.0272	0.09751 ± 0.00249	0.76
Zr54	0.8079 ± 0.0251	0.09763 ± 0.00246	0.81
Zr63	0.8025 ± 0.0252	0.09763 ± 0.00246	0.80
Zr64	0.8112 ± 0.0258	0.09762 ± 0.00249	0.80
Zr73	0.8118 ± 0.0257	0.09703 ± 0.00246	0.80
Zr74	0.8213 ± 0.0262	0.09768 ± 0.00249	0.80
Zr75	0.8000 ± 0.0254	0.09769 ± 0.00249	0.80
Zr76	0.8094 ± 0.0263	0.09776 ± 0.00249	0.78
Zr2 020616a	0.8037 ± 0.0244	0.09712 ± 0.00252	0.85
Zr3	0.8051 ± 0.0249	0.09724 ± 0.00252	0.84
Zr4	0.8069 ± 0.0250	0.09768 ± 0.00252	0.83
Zr13	0.8099 ± 0.0246	0.09702 ± 0.00249	0.84
Zr14	0.8110 ± 0.0254	0.09716 ± 0.00252	0.83
Zr23	0.8081 ± 0.0247	0.09789 ± 0.00252	0.84
Zr24	0.8053 ± 0.0245	0.09793 ± 0.00252	0.85
Zr33	0.8130 ± 0.0252	0.09758 ± 0.00252	0.83
Zr43	0.8336 ± 0.0256	0.09777 ± 0.00252	0.84
Zr44	0.8082 ± 0.0251	0.09790 ± 0.00252	0.83
Zr53	0.8070 ± 0.0247	0.09790 ± 0.00252	0.84
Zr54	0.8143 ± 0.0249	0.09702 ± 0.00249	0.84
Zr64	0.8115 ± 0.0249	0.09791 ± 0.00252	0.84
Zr65	0.8071 ± 0.0245	0.09793 ± 0.00252	0.85
Zr73	0.8038 ± 0.0247	0.09784 ± 0.00252	0.84
Zr74	0.8140 ± 0.0256	0.09759 ± 0.00252	0.82
Zr83	0.8126 ± 0.0257	0.09738 ± 0.00249	0.81

Continued on next page

Table B.2 – *Continued from previous page*

Spot #	^{207}**Pb**/^{235}**U** $\pm 2\sigma$	^{206}**Pb**/^{238}**U** $\pm 2\sigma$	ρ
Zr84	0.8126 ± 0.0258	0.09711 ± 0.00249	0.81
Zr93	0.8127 ± 0.0260	0.09702 ± 0.00249	0.80
Zr94	0.8131 ± 0.0257	0.09756 ± 0.00249	0.81
Zr103	0.8150 ± 0.0264	0.09674 ± 0.00249	0.79
Zr104	0.8040 ± 0.0259	0.09670 ± 0.00249	0.80
Zr113	0.8088 ± 0.0263	0.09753 ± 0.00249	0.78
Zr114	0.7901 ± 0.0259	0.09826 ± 0.00252	0.78
Zr115	0.8109 ± 0.0263	0.09735 ± 0.00249	0.79
Zr116	0.8050 ± 0.0261	0.09777 ± 0.00252	0.79
Zr1 020616b	0.8133 ± 0.0254	0.09717 ± 0.00249	0.82
Zr2	0.8096 ± 0.0253	0.09722 ± 0.00249	0.82
Zr3	0.8117 ± 0.0251	0.09765 ± 0.00249	0.82
Zr4	0.8073 ± 0.0251	0.09760 ± 0.00249	0.82
Zr13	0.8108 ± 0.0252	0.09780 ± 0.00249	0.82
Zr14	0.7899 ± 0.0247	0.09776 ± 0.00249	0.82
Zr23	0.8080 ± 0.0251	0.09778 ± 0.00249	0.82
Zr24	0.8066 ± 0.0248	0.09761 ± 0.00249	0.83
Zr33	0.8078 ± 0.0246	0.09764 ± 0.00246	0.83
Zr34	0.8117 ± 0.0256	0.09779 ± 0.00249	0.81
Zr43	0.8185 ± 0.0279	0.09686 ± 0.00249	0.75
Zr44	0.8119 ± 0.0254	0.09700 ± 0.00246	0.81
Zr63	0.8167 ± 0.0258	0.09683 ± 0.00246	0.80
Zr64	0.8043 ± 0.0250	0.09763 ± 0.00246	0.81
Zr73	0.8090 ± 0.0253	0.09759 ± 0.00246	0.81
Zr74	0.8111 ± 0.0257	0.09732 ± 0.00246	0.80
Zr83	0.8112 ± 0.0256	0.09730 ± 0.00246	0.80
Zr84	0.8073 ± 0.0256	0.09743 ± 0.00246	0.80
Zr93	0.8077 ± 0.0269	0.09766 ± 0.00246	0.76
Zr94	0.8093 ± 0.0258	0.09762 ± 0.00246	0.79
Zr95	0.8085 ± 0.0264	0.09767 ± 0.00246	0.77
Zr96	0.7993 ± 0.0264	0.09790 ± 0.00246	0.76
	91500 session of June 2016		
Zr5 300516a	1.8509 ± 0.0578	0.1798 ± 0.0047	0.83
Zr6	1.8725 ± 0.0566	0.1791 ± 0.0046	0.85
Zr151	1.8702 ± 0.0580	0.1791 ± 0.0047	0.84

Continued on next page

Table B.2 – *Continued from previous page*

Spot #	^{207}**Pb**/^{235}**U** $\pm 2\sigma$	^{206}**Pb**/^{238}**U** $\pm 2\sigma$	ρ
Zr152	1.8623 ± 0.0611	0.1789 ± 0.0047	0.80
Zr5 310516a	1.8456 ± 0.0559	0.1805 ± 0.0047	0.85
Zr6	1.8793 ± 0.0575	0.1787 ± 0.0046	0.84
Zr115	1.8402 ± 0.0611	0.1805 ± 0.0047	0.78
Zr116	1.8684 ± 0.0610	0.1797 ± 0.0047	0.79
Zr5 310516b	1.8733 ± 0.0591	0.1798 ± 0.0047	0.82
Zr6	1.8697 ± 0.0583	0.1791 ± 0.0047	0.83
Zr111	1.8536 ± 0.0594	0.1796 ± 0.0047	0.81
Zr112	1.8533 ± 0.0620	0.1797 ± 0.0047	0.78
Zr5 010616a	1.8819 ± 0.0703	0.1784 ± 0.0047	0.71
Zr6	1.8608 ± 0.1047	0.1789 ± 0.0053	0.52
Zr111	1.8492 ± 0.0582	0.1798 ± 0.0046	0.81
Zr112	1.8472 ± 0.0584	0.1797 ± 0.0046	0.80
Zr5 010616b	1.8398 ± 0.0552	0.1803 ± 0.0045	0.84
Zr6	1.8629 ± 0.0587	0.1790 ± 0.0045	0.80
Zr71	1.8870 ± 0.0657	0.1786 ± 0.0046	0.74
Zr72	1.8691 ± 0.0609	0.1804 ± 0.0046	0.79
Zr5 020616a	1.8628 ± 0.0590	0.1791 ± 0.0047	0.82
Zr6	1.7909 ± 0.0592	0.1808 ± 0.0047	0.79
Zr111	1.9025 ± 0.0635	0.1785 ± 0.0046	0.78
Zr112	1.8558 ± 0.0617	0.1796 ± 0.0047	0.78
Zr5 020616b	1.8403 ± 0.0599	0.1797 ± 0.00462	0.79
Zr6	1.8440 ± 0.0594	0.1796 ± 0.00462	0.80
Zr91	1.8426 ± 0.0596	0.1803 ± 0.00456	0.78
Zr92	1.8588 ± 0.0662	0.1789 ± 0.00459	0.72

Table B.3

Full set of U-Pb analysis on zircon from the 18 samples presented in Chapter 2. Abbreviations: Osci.= Oscilatory; Inh= Inherited; Ext.= External; Int.= Internal; Meta.= Metamict; Z.= Zoned; Conc = concordance. In the internal structure column when the rim or core is not precised the mentioned characteristic describe the whole grain. ρ is the error correlation coefficient.

Spot #	Internal Structure	Pb (ppm)	Th (ppm)	U (ppm)	Th/U	$^{207}Pb/^{235}U$ $\pm 2\sigma$	$^{206}Pb/^{238}U$ $\pm 2\sigma$	ρ	$\frac{^{207}Pb}{^{206}Pb}$	Ages (Ma) $\frac{^{206}Pb}{^{238}U}$	Ages (Ma) $\frac{^{207}Pb}{^{206}Pb}$	Conc %
SG-007 granite												
A5-C	Osci. zoned core	183	97	178	0.55	39.1428 ± 1.0865	0.7731 ± 0.0209	0.97	0.367	3692 ± 76	3780 ± 46	98
A8-C	Osci. zoned core	214	138	205	0.67	39.7857 ± 1.1059	0.7829 ± 0.0212	0.97	0.368	3728 ± 77	3785 ± 46	98
A10-R	Osci. zoned rim	105	28	106	0.27	41.0910 ± 1.1453	0.7930 ± 0.0215	0.97	0.376	3764 ± 77	3815 ± 46	99
A13	White zoned core	100	72	94	0.76	41.5322 ± 1.1608	0.7966 ± 0.0216	0.97	0.378	3777 ± 78	3824 ± 46	99
A14	Osci. zoned core	181	135	174	0.78	40.0175 ± 1.1245	0.7746 ± 0.0211	0.97	0.375	3698 ± 77	3810 ± 47	97
C5	Osci. zoned core	162	104	142	0.73	44.1255 ± 1.1701	0.8139 ± 0.0212	0.98	0.393	3839 ± 75	3883 ± 46	99
D14-C	Osci. zoned core	140	40	145	0.28	39.1258 ± 1.0298	0.7804 ± 0.0200	0.97	0.364	3719 ± 72	3765 ± 46	99
E1-C	Osci. zoned core	230	141	248	0.57	36.5566 ± 0.9630	0.7062 ± 0.0180	0.97	0.375	3444 ± 68	3813 ± 46	90
E10-C	Osci. zoned core	409	118	399	0.30	43.1143 ± 1.1309	0.8108 ± 0.0206	0.97	0.386	3828 ± 73	3854 ± 46	99
E15-C	Osci. zoned core	361	289	309	0.93	43.5835 ± 1.1180	0.8128 ± 0.0205	0.98	0.389	3835 ± 73	3867 ± 46	99
F9	Osci. zoned rim	204	95	205	0.47	40.1331 ± 1.0325	0.7588 ± 0.0192	0.98	0.384	3640 ± 70	3846 ± 46	95
F13-C1	Osci. zoned core	245	40	255	0.16	38.4560 ± 0.9877	0.7826 ± 0.0197	0.98	0.356	3727 ± 71	3734 ± 46	100
H7-C	Osci. zoned core	168	125	199	0.63	31.9519 ± 0.8276	0.6310 ± 0.0159	0.97	0.367	3153 ± 63	3780 ± 46	83
H9-C	Osci. zoned core	173	104	165	0.63	41.3605 ± 1.0649	0.7822 ± 0.0197	0.98	0.383	3725 ± 71	3845 ± 46	97
H11	Osci. zoned core	125	68	121	0.57	40.6353 ± 1.0478	0.7774 ± 0.0196	0.98	0.379	3708 ± 71	3828 ± 46	97
H13	Osci. zoned core	67	22	75	0.30	34.9560 ± 0.9041	0.7208 ± 0.0182	0.98	0.352	3499 ± 68	3714 ± 47	94
A9-C	Black rim	478	5	852	0.01	14.4727 ± 0.4021	0.5393 ± 0.0146	0.97	0.195	2781 ± 61	2781 ± 50	100
A11-R	Black rim	438	11	766	0.01	15.1218 ± 0.4205	0.5483 ± 0.0149	0.98	0.200	2818 ± 62	2826 ± 50	100
C6	Black core	375	122	647	0.19	14.3371 ± 0.3794	0.5375 ± 0.0140	0.98	0.193	2773 ± 59	2772 ± 50	100
C17	Metamict	858	44	2599	0.02	8.6830 ± 0.2287	0.3159 ± 0.0082	0.99	0.199	1770 ± 40	2821 ± 50	63
D1	Black rim	582	5	1032	0.01	14.4369 ± 0.3810	0.5478 ± 0.0141	0.98	0.191	2816 ± 59	2752 ± 50	102
D5-R	Black rim	671	6	1250	0.00	13.5758 ± 0.3575	0.5233 ± 0.0134	0.97	0.188	2713 ± 57	2726 ± 50	100
E2	Metamict	346	4	640	0.01	13.7199 ± 0.3603	0.5207 ± 0.0133	0.97	0.191	2702 ± 56	2751 ± 50	98
E3	Metamict	763	145	2030	0.07	9.2391 ± 0.2426	0.3569 ± 0.0091	0.97	0.188	1968 ± 43	2722 ± 50	72
E14-C	Metamict	506	15	910	0.02	14.6884 ± 0.3765	0.5351 ± 0.0135	0.98	0.199	2763 ± 57	2818 ± 49	98

Continued on next page

Table B.3 – *Continued from previous page*

Spot #	Internal Structure	Pb (ppm)	Th (ppm)	U (ppm)	Th/U	$^{207}Pb/^{235}U$ $\pm 2\sigma$	$^{206}Pb/^{238}U$ $\pm 2\sigma$	ρ	$\frac{^{207}Pb}{^{206}Pb}$ ^{206}Pb	Ages (Ma)$\pm 2\sigma$ $\frac{^{206}Pb}{^{238}U}$	Ages (Ma)$\pm 2\sigma$ $\frac{^{207}Pb}{^{206}Pb}$	Conc %
F8-C	Metamict core	806	126	1678	0.08	12.2720 ± 0.3143	0.4564 ± 0.0115	0.98	0.195	2424 ± 51	2785 ± 50	87
F11	Black	403	56	720	0.08	13.9087 ± 0.3566	0.5333 ± 0.0134	0.98	0.189	2756 ± 56	2735 ± 50	101
H2-R	Black rim	437	69	791	0.09	13.8165 ± 0.3544	0.5286 ± 0.0133	0.98	0.190	2735 ± 56	2738 ± 50	100
H3-R	Black rim	440	47	785	0.06	14.3319 ± 0.3677	0.5382 ± 0.0135	0.98	0.193	2776 ± 57	2769 ± 50	100
A12-R	Black rim	513	187	959	0.19	12.7489 ± 0.3560	0.5055 ± 0.0137	0.97	0.183	2637 ± 59	2679 ± 51	98
B10-R	Black rim	340	89	675	0.13	11.9930 ± 0.3202	0.4751 ± 0.0125	0.99	0.183	2506 ± 55	2681 ± 50	93
C1	Metamict	632	63	1261	0.05	11.9601 ± 0.3175	0.4878 ± 0.0127	0.98	0.178	2561 ± 55	2632 ± 50	97
C4-R	Metamict rim	440	55	850	0.06	12.1943 ± 0.3229	0.4994 ± 0.0130	0.98	0.177	2611 ± 56	2626 ± 50	99
E11	Metamict	1849	227	5790	0.04	7.6057 ± 0.1994	0.3078 ± 0.0078	0.97	0.179	1730 ± 38	2645 ± 51	65
F2	Metamict	354	50	671	0.08	12.5760 ± 0.3225	0.5073 ± 0.0128	0.98	0.180	2645 ± 55	2651 ± 50	100
F6	Metamict	791	182	2380	0.08	7.6278 ± 0.1958	0.3216 ± 0.0081	0.98	0.172	1798 ± 40	2577 ± 51	70
F8-R	Metamict rim	363	87	728	0.12	11.9491 ± 0.3077	0.4756 ± 0.0120	0.98	0.182	2508 ± 52	2673 ± 50	94
H15	Metamict	645	20	1273	0.02	12.4153 ± 0.3196	0.4942 ± 0.0124	0.97	0.182	2589 ± 53	2673 ± 50	97
A1	Osci. zoned core	142	16	171	0.09	30.6753 ± 0.8512	0.7208 ± 0.0195	0.97	0.309	3499 ± 73	3514 ± 47	100
A2	Osci. zoned core	698	22	879	0.03	29.2249 ± 0.8090	0.6983 ± 0.0189	0.98	0.303	3414 ± 72	3488 ± 47	98
A4	Osci. zoned core	782	79	1046	0.08	24.9461 ± 0.6905	0.6692 ± 0.0181	0.98	0.270	3303 ± 70	3308 ± 48	100
A5-R	Osci. zoned rim	676	107	1778	0.06	7.8449 ± 0.2180	0.3754 ± 0.0102	0.98	0.152	2055 ± 48	2364 ± 52	87
A7	Metamict	889	4	1280	0.00	23.2897 ± 0.6463	0.6331 ± 0.0171	0.97	0.267	3162 ± 68	3287 ± 48	96
A11-C	Metamict core	1043	401	1761	0.23	16.5384 ± 0.4594	0.5380 ± 0.0146	0.98	0.223	2775 ± 61	3002 ± 49	92
A12-C	Metamict core	718	44	1319	0.03	15.9190 ± 0.4434	0.5100 ± 0.0138	0.97	0.226	2657 ± 59	3026 ± 49	88
A15-C	Metamict core	908	30	1154	0.03	28.8124 ± 0.8030	0.6980 ± 0.0189	0.97	0.299	3413 ± 72	3467 ± 47	98
A16-C	Osci. zoned core	368	51	456	0.11	30.8827 ± 0.8633	0.6912 ± 0.0188	0.97	0.324	3387 ± 71	3589 ± 47	94
A17	Convo. zoned core	204	73	227	0.32	34.5333 ± 0.9255	0.7236 ± 0.0191	0.98	0.346	3509 ± 71	3690 ± 46	95
B3-R	Metamict	1398	132	2939	0.04	13.8612 ± 0.3708	0.4473 ± 0.0118	0.99	0.225	2383 ± 53	3015 ± 49	79
B6-C	Metamict	1007	165	1726	0.10	16.8991 ± 0.4515	0.5424 ± 0.0143	0.99	0.226	2794 ± 60	3023 ± 48	92
B7-C	Metamict core	397	35	465	0.07	32.5945 ± 0.8709	0.7388 ± 0.0195	0.99	0.320	3566 ± 72	3570 ± 47	100
B7-R	Metamict rim	1191	157	2351	0.07	14.7773 ± 0.3947	0.4735 ± 0.0125	0.99	0.226	2499 ± 55	3026 ± 48	83
B9-R	Metamict	491	232	1194	0.19	7.8922 ± 0.2106	0.3982 ± 0.0105	0.99	0.144	2161 ± 48	2273 ± 52	95
B10-C	Metamict core	1214	358	3826	0.09	6.3327 ± 0.1687	0.3105 ± 0.0082	0.99	0.148	1743 ± 40	2322 ± 52	75
B11	Metamict core	834	25	1398	0.02	18.6128 ± 0.4953	0.5546 ± 0.0146	0.99	0.243	2844 ± 60	3142 ± 48	91

Continued on next page

Table B.3 – *Continued from previous page*

Spot #	Internal Structure	Pb (ppm)	Th (ppm)	U (ppm)	Th/U	$^{207}Pb/^{235}U$ $\pm 2\sigma$	$^{206}Pb/^{238}U$ $\pm 2\sigma$	ρ	$\frac{^{207}Pb}{^{206}Pb}$ ^{206}Pb	Ages (Ma)$\pm 2\sigma$ $\frac{^{206}Pb}{^{238}U}$	Ages (Ma)$\pm 2\sigma$ $\frac{^{207}Pb}{^{206}Pb}$	Conc %
B12	Metamict core	799	96	2075	0.05	11.5020 ± 0.3066	0.3594 ± 0.0094	0.98	0.232	1979 ± 45	3067 ± 48	65
B13	Convo. metamict	801	31	1449	0.02	15.8946 ± 0.4232	0.5235 ± 0.0137	0.98	0.220	2714 ± 58	2982 ± 49	91
B15	Metamict	745	24	1208	0.02	18.6297 ± 0.4954	0.5754 ± 0.0151	0.99	0.235	2930 ± 62	3085 ± 48	95
B16-C	Osci. zoned core	133	75	147	0.51	33.1151 ± 0.8858	0.6971 ± 0.0183	0.98	0.345	3410 ± 70	3683 ± 46	93
B17-C2	Black core	474	8	607	0.01	29.6904 ± 0.7890	0.6848 ± 0.0179	0.98	0.314	3363 ± 68	3543 ± 47	95
C2	Metamict	1125	57	2080	0.03	16.1682 ± 0.4285	0.5057 ± 0.0132	0.98	0.232	2638 ± 56	3065 ± 48	86
C3	Metamict	627	29	1562	0.02	8.4473 ± 0.2242	0.3999 ± 0.0104	0.98	0.153	2169 ± 48	2382 ± 52	91
C7-C2	Metamict core	1400	875	2253	0.39	18.0873 ± 0.4782	0.5230 ± 0.0136	0.98	0.251	2712 ± 57	3190 ± 48	85
C8	Black core	742	168	972	0.17	27.5338 ± 0.7289	0.6477 ± 0.0168	0.98	0.308	3219 ± 66	3512 ± 47	92
C9	Metamict core	686	23	892	0.03	27.6034 ± 0.7295	0.6845 ± 0.0178	0.98	0.293	3362 ± 68	3431 ± 47	98
C10	Black core	909	220	1834	0.12	13.8783 ± 0.3671	0.4590 ± 0.0119	0.98	0.219	2435 ± 53	2975 ± 49	82
C11	Metamict	516	16	648	0.02	29.2497 ± 0.7727	0.7004 ± 0.0182	0.98	0.303	3422 ± 69	3485 ± 47	98
C12	Metamict	696	24	1622	0.01	12.9107 ± 0.3405	0.3998 ± 0.0104	0.99	0.234	2168 ± 48	3081 ± 48	70
C14-C	Black core	656	14	790	0.02	31.0173 ± 0.8180	0.7300 ± 0.0189	0.98	0.308	3534 ± 70	3512 ± 47	101
C14-R	Black rim	877	58	1044	0.06	31.1120 ± 0.8199	0.7383 ± 0.0191	0.98	0.306	3564 ± 71	3499 ± 47	102
C16	Metamict	693	46	1029	0.04	21.7635 ± 0.5735	0.6154 ± 0.0159	0.98	0.256	3092 ± 63	3225 ± 48	96
D2	Black core	483	21	563	0.04	32.8215 ± 0.8648	0.7464 ± 0.0192	0.98	0.319	3594 ± 71	3564 ± 47	101
D3	Osci. zoned core	217	20	246	0.08	34.2909 ± 0.9035	0.7534 ± 0.0194	0.98	0.330	3620 ± 71	3617 ± 47	100
D4-R	Metamict	1131	93	1855	0.05	18.1733 ± 0.4780	0.5641 ± 0.0145	0.98	0.234	2884 ± 60	3077 ± 49	94
D4-C	Metamict	797	21	1007	0.02	28.0842 ± 0.7386	0.7060 ± 0.0182	0.98	0.288	3443 ± 69	3409 ± 47	101
D5-C	Metamict	1369	77	5379	0.01	5.0263 ± 0.1322	0.2543 ± 0.0065	0.97	0.143	1461 ± 34	2268 ± 52	64
D7	Metamict	871	72	1956	0.04	9.0688 ± 0.2385	0.4459 ± 0.0115	0.98	0.147	2377 ± 51	2317 ± 52	103
D8	Metamict	899	35	1666	0.02	15.3899 ± 0.4048	0.5103 ± 0.0131	0.98	0.219	2658 ± 56	2971 ± 49	89
D9-R	Metamict	1077	159	2062	0.08	14.4295 ± 0.3791	0.4896 ± 0.0125	0.97	0.214	2569 ± 54	2934 ± 49	88
D9-C	Metamict	882	77	1672	0.05	15.6321 ± 0.4106	0.4841 ± 0.0124	0.98	0.234	2545 ± 54	3081 ± 49	83
D11-C	Metamict	1066	77	3442	0.02	6.6410 ± 0.1744	0.3028 ± 0.0078	0.98	0.159	1705 ± 38	2445 ± 52	70
D13	Metamict	1089	221	3624	0.06	6.4695 ± 0.1699	0.2912 ± 0.0074	0.97	0.161	1648 ± 37	2467 ± 52	67
D14-R	Black rim	579	16	710	0.02	30.1894 ± 0.7925	0.7215 ± 0.0185	0.98	0.303	3502 ± 69	3488 ± 47	100
D15-C	Osci. zoned core	286	19	320	0.06	35.1387 ± 0.9232	0.7684 ± 0.0197	0.98	0.331	3675 ± 72	3624 ± 47	101
D15-R	Metamict rim	452	52	950	0.05	10.3296 ± 0.2712	0.4671 ± 0.0119	0.97	0.160	2471 ± 52	2459 ± 52	100

Continued on next page

Table B.3 – *Continued from previous page*

Spot #	Internal Structure	Pb (ppm)	Th (ppm)	U (ppm)	Th/U	$^{207}Pb/^{235}U$ $\pm 2\sigma$	$^{206}Pb/^{238}U$ $\pm 2\sigma$	ρ	$\frac{^{207}Pb}{^{206}Pb}$ ^{206}Pb	Ages (Ma)$\pm 2\sigma$ $\frac{^{206}Pb}{^{238}U}$	Ages (Ma)$\pm 2\sigma$ $\frac{^{207}Pb}{^{206}Pb}$	Conc %
D16	Metamict core	785	115	1117	0.10	22.7222 ± 0.5961	0.6304 ± 0.0161	0.97	0.261	3151 ± 64	3255 ± 48	97
D17	Metamict core	485	40	580	0.07	30.9913 ± 0.8134	0.7209 ± 0.0184	0.97	0.312	3500 ± 69	3530 ± 47	99
E1-R	Osci. zoned rim	836	27	1025	0.03	30.3494 ± 0.7964	0.7164 ± 0.0182	0.97	0.307	3482 ± 69	3507 ± 47	99
E5	Black rim	758	26	922	0.03	30.4173 ± 0.7979	0.7215 ± 0.0183	0.97	0.306	3502 ± 69	3499 ± 47	100
E6	Metamict	648	24	798	0.03	29.8219 ± 0.7826	0.7131 ± 0.0181	0.97	0.303	3470 ± 68	3487 ± 47	100
E7	Metamict	558	13	1258	0.01	9.2827 ± 0.2435	0.4415 ± 0.0112	0.97	0.152	2357 ± 50	2374 ± 52	99
E10-R	Metamict rim	905	39	1321	0.03	22.9027 ± 0.6005	0.6240 ± 0.0158	0.97	0.266	3126 ± 63	3283 ± 48	95
E12-C	Black rim	1165	24	1940	0.01	18.2999 ± 0.4692	0.5603 ± 0.0142	0.99	0.237	2868 ± 58	3099 ± 48	93
E13	Metamict	880	62	1051	0.06	30.6434 ± 0.7849	0.7356 ± 0.0186	0.99	0.302	3554 ± 69	3481 ± 47	102
E16-C	Black core	918	42	1489	0.03	18.5906 ± 0.4766	0.5742 ± 0.0145	0.99	0.235	2925 ± 59	3085 ± 48	95
F1	Osci. zoned rim	487	28	562	0.05	32.5087 ± 0.8338	0.7533 ± 0.0190	0.98	0.313	3620 ± 70	3536 ± 47	102
F3	Metamict	985	22	2827	0.01	6.4630 ± 0.1658	0.3545 ± 0.0089	0.98	0.132	1956 ± 43	2127 ± 53	92
F4-C2	Metamict	444	31	584	0.05	27.4885 ± 0.7049	0.6533 ± 0.0165	0.98	0.305	3241 ± 64	3496 ± 47	93
F5	Metamict	637	41	782	0.05	29.5270 ± 0.7562	0.7190 ± 0.0181	0.98	0.298	3492 ± 68	3459 ± 47	101
F7	Metamict	590	16	703	0.02	31.7332 ± 0.8127	0.7354 ± 0.0185	0.98	0.313	3553 ± 69	3535 ± 47	101
F10-R	Black rim	349	40	457	0.09	28.2241 ± 0.7235	0.6537 ± 0.0165	0.98	0.313	3242 ± 64	3536 ± 47	92
F12	Metamict	897	155	3400	0.05	4.4192 ± 0.1132	0.2658 ± 0.0067	0.98	0.121	1520 ± 34	1965 ± 54	77
F13-C2	Sector zoned	299	17	338	0.05	34.4304 ± 0.8828	0.7575 ± 0.0191	0.98	0.330	3635 ± 70	3615 ± 46	101
F15	Black core	851	81	1027	0.08	30.8054 ± 0.7898	0.7170 ± 0.0180	0.98	0.312	3485 ± 68	3529 ± 47	99
H1	Osci. zoned core	901	770	915	0.84	32.5361 ± 0.8336	0.7447 ± 0.0187	0.98	0.317	3588 ± 69	3554 ± 47	101
H2-C	Metamict core	743	67	942	0.07	27.0956 ± 0.6943	0.6970 ± 0.0175	0.98	0.282	3409 ± 67	3373 ± 47	101
H3-C	Black core	739	22	1084	0.02	24.4725 ± 0.6279	0.6084 ± 0.0153	0.98	0.292	3063 ± 61	3427 ± 47	89
H4	Metamict	962	115	1785	0.06	14.9399 ± 0.3830	0.5082 ± 0.0128	0.98	0.213	2649 ± 55	2930 ± 49	90
H7-R	Metamict rim	697	54	972	0.06	24.0870 ± 0.6179	0.6478 ± 0.0163	0.98	0.270	3220 ± 64	3304 ± 48	97
H8-C	Osci. zoned core	167	52	199	0.26	29.9141 ± 0.7693	0.7077 ± 0.0178	0.98	0.307	3450 ± 67	3504 ± 47	98
H8-R	Metamict rim	748	190	1783	0.11	8.1515 ± 0.2092	0.4150 ± 0.0104	0.98	0.142	2238 ± 47	2257 ± 52	99
H9-R	Metamict rim	765	7	1047	0.01	25.1532 ± 0.6455	0.6633 ± 0.0167	0.98	0.275	3280 ± 65	3335 ± 48	98
H10-C2	Metamict	378	10	421	0.02	34.8642 ± 0.8958	0.7778 ± 0.0195	0.98	0.325	3709 ± 71	3594 ± 47	103
H12	Metamict	143	6	165	0.04	33.1189 ± 0.8528	0.7382 ± 0.0185	0.97	0.325	3564 ± 69	3595 ± 47	99

Continued on next page

Table B.3 – *Continued from previous page*

Spot #	Internal Structure	Pb (ppm)	Th (ppm)	U (ppm)	Th/U	$^{207}Pb/^{235}U$ $\pm 2\sigma$	$^{206}Pb/^{238}U$ $\pm 2\sigma$	ρ	$\frac{^{207}Pb}{^{206}Pb}$ ^{206}Pb	Ages (Ma)$\pm 2\sigma$ $\frac{^{206}Pb}{^{238}U}$	Ages (Ma)$\pm 2\sigma$ $\frac{^{207}Pb}{^{206}Pb}$	Conc %
SG-017 granite												
A7	Black core	596	29	1168	0.03	12.8257 ± 0.3380	0.4964 ± 0.0123	0.94	0.187	2598 ± 53	2719 ± 52	96
A11	Osci. zoned core	499	15	899	0.02	14.7589 ± 0.3861	0.5341 ± 0.0132	0.94	0.200	2759 ± 56	2830 ± 51	97
A15	Black core	624	53	726	0.07	32.9596 ± 0.8619	0.7445 ± 0.0184	0.95	0.321	3587 ± 68	3575 ± 48	100
A17	Metamict	59	44	97	0.46	14.1062 ± 0.3827	0.5214 ± 0.0131	0.93	0.196	2705 ± 55	2795 ± 53	97
B2	Black core	582	32	1158	0.03	12.5708 ± 0.3307	0.4862 ± 0.0120	0.94	0.187	2554 ± 52	2720 ± 52	94
B7	Metamict	746	64	1886	0.03	8.5029 ± 0.2243	0.3899 ± 0.0096	0.93	0.158	2122 ± 45	2436 ± 53	87
B10	Osci. zoned core	728	50	1676	0.03	9.5819 ± 0.2519	0.4266 ± 0.0105	0.94	0.163	2291 ± 48	2486 ± 53	92
B13	Metamict	623	23	1365	0.02	10.6486 ± 0.2804	0.4461 ± 0.0110	0.94	0.173	2378 ± 49	2588 ± 52	92
C16	Black core	354	3	621	0.01	14.9271 ± 0.3972	0.5481 ± 0.0136	0.93	0.198	2817 ± 56	2806 ± 52	100
C9	Black core	273	16	490	0.03	14.1713 ± 0.3768	0.5259 ± 0.0130	0.93	0.195	2724 ± 55	2788 ± 52	98
C2	White core	18	25	29	0.87	13.0145 ± 0.3787	0.5111 ± 0.0130	0.87	0.185	2661 ± 55	2695 ± 56	99
D2	Black core	526	24	969	0.02	14.2050 ± 0.3792	0.5205 ± 0.0128	0.92	0.198	2701 ± 54	2809 ± 52	96
D3	Osci. zoned core	449	14	809	0.02	14.4167 ± 0.3979	0.5340 ± 0.0131	0.89	0.196	2758 ± 55	2791 ± 54	99
D9	Grey core	77	2	145	0.02	14.0839 ± 0.4052	0.4981 ± 0.0126	0.88	0.205	2606 ± 54	2867 ± 55	91
D11	Osci. zoned core	344	43	606	0.07	14.4749 ± 0.4002	0.5335 ± 0.0131	0.89	0.197	2756 ± 55	2799 ± 54	98
E7	Black core	556	83	1228	0.07	10.8140 ± 0.2911	0.4324 ± 0.0107	0.92	0.181	2317 ± 48	2665 ± 53	87
E6-C	Black core	505	21	883	0.02	14.9635 ± 0.4031	0.5439 ± 0.0134	0.91	0.199	2800 ± 56	2822 ± 52	99
F3	Metamict	526	39	951	0.04	14.1203 ± 0.3819	0.5319 ± 0.0131	0.91	0.193	2750 ± 55	2764 ± 53	99
F4	Metamict	513	24	922	0.03	14.4333 ± 0.3912	0.5333 ± 0.0131	0.91	0.196	2756 ± 55	2795 ± 53	99
F6	Black	512	20	906	0.02	14.6647 ± 0.3983	0.5453 ± 0.0134	0.90	0.195	2806 ± 56	2785 ± 53	101
F7	Grey core	84	2	156	0.01	14.3165 ± 0.3971	0.5209 ± 0.0129	0.89	0.199	2703 ± 55	2820 ± 54	96
F11	Black	620	31	1160	0.03	13.3162 ± 0.3667	0.5179 ± 0.0128	0.90	0.186	2690 ± 54	2711 ± 54	99
SG-019 trondhjemite												
A2	Metamict	542	44	1269	0.03	8.8629 ± 0.2286	0.4175 ± 0.0103	0.96	0.154	2249 ± 47	2391 ± 53	94
A7-R	Convoluted rim	122	30	219	0.14	13.1355 ± 0.3413	0.5223 ± 0.0129	0.95	0.182	2709 ± 55	2675 ± 52	101
A8	Black cracked core	270	51	541	0.09	11.1965 ± 0.2888	0.4736 ± 0.0117	0.96	0.171	2499 ± 51	2572 ± 52	97
B4	Metamict core	629	32	1191	0.03	13.3574 ± 0.3459	0.5082 ± 0.0125	0.95	0.191	2649 ± 54	2748 ± 51	96
B7-C	Metamict core	521	17	951	0.02	13.6899 ± 0.3541	0.5291 ± 0.0130	0.95	0.188	2738 ± 55	2722 ± 51	101
B7-R	Black rim	141	61	248	0.25	13.5013 ± 0.3520	0.5217 ± 0.0129	0.95	0.188	2706 ± 54	2723 ± 51	99

Continued on next page

Table B.3 – *Continued from previous page*

Spot #	Internal Structure	Pb (ppm)	Th (ppm)	U (ppm)	Th/U	$^{207}Pb/^{235}U$ $\pm 2\sigma$	$^{206}Pb/^{238}U$ $\pm 2\sigma$	ρ	$\frac{^{207}Pb}{^{206}Pb}$ ^{206}Pb	Ages (Ma)$\pm 2\sigma$ $\frac{^{206}Pb}{^{238}U}$	Ages (Ma)$\pm 2\sigma$ $\frac{^{207}Pb}{^{206}Pb}$	Conc %
C1	Black	373	45	691	0.06	13.5220 ± 0.3516	0.5172 ± 0.0127	0.94	0.190	2687 ± 54	2739 ± 51	98
C2	Metamict	900	65	2071	0.03	10.0615 ± 0.2617	0.4217 ± 0.0104	0.95	0.173	2268 ± 47	2588 ± 52	88
C7-R	Black rim	265	8	490	0.02	13.6950 ± 0.3596	0.5243 ± 0.0129	0.94	0.190	2717 ± 55	2738 ± 52	99
C9	Metamict	862	53	1943	0.03	10.2545 ± 0.2678	0.4335 ± 0.0107	0.95	0.172	2321 ± 48	2573 ± 52	90
C10	Metamict rim	889	45	1935	0.02	10.5981 ± 0.2770	0.4492 ± 0.0110	0.94	0.171	2392 ± 49	2569 ± 52	93
C11	Metamict	969	60	2248	0.03	9.8311 ± 0.2573	0.4237 ± 0.0104	0.94	0.168	2277 ± 47	2541 ± 53	90
C17	Metamict rim	817	79	2167	0.04	7.7609 ± 0.2041	0.3805 ± 0.0094	0.94	0.148	2079 ± 44	2322 ± 54	90
D2-C	Inherited core	16	2	29	0.06	13.1847 ± 0.4037	0.5116 ± 0.0133	0.85	0.187	2663 ± 57	2715 ± 58	98
D2-R	Black rim	726	130	859	0.15	31.8440 ± 0.8370	0.7289 ± 0.0179	0.93	0.317	3529 ± 67	3555 ± 48	99
D3-C	Inherited core	53	54	54	1.00	29.3061 ± 0.8184	0.7037 ± 0.0179	0.91	0.302	3435 ± 68	3481 ± 51	99
D8	Metamict	283	9	508	0.02	14.6901 ± 0.3900	0.5403 ± 0.0133	0.93	0.197	2785 ± 56	2803 ± 52	99
D9	Black	387	99	774	0.13	11.5083 ± 0.3051	0.4841 ± 0.0119	0.93	0.172	2545 ± 52	2581 ± 53	99
D10	Oscillatory zoned	109	32	199	0.16	13.5476 ± 0.3636	0.5217 ± 0.0129	0.92	0.188	2706 ± 55	2728 ± 53	99
D11	Black	477	136	945	0.14	11.4859 ± 0.3052	0.4824 ± 0.0119	0.93	0.173	2538 ± 52	2584 ± 53	98
D13	Black rim	415	109	805	0.14	11.6977 ± 0.3114	0.4954 ± 0.0122	0.93	0.171	2594 ± 53	2570 ± 53	101
D14	Convoluted core	317	66	606	0.11	14.4571 ± 0.3891	0.4860 ± 0.0120	0.92	0.216	2553 ± 52	2949 ± 52	87
D15	Sector zoned	140	46	249	0.18	13.6667 ± 0.3668	0.5256 ± 0.0130	0.92	0.189	2723 ± 55	2730 ± 53	100
D18	Metamict	822	54	1990	0.03	8.8896 ± 0.2387	0.4090 ± 0.0101	0.92	0.158	2210 ± 46	2431 ± 54	91
D19	Black	414	73	812	0.09	11.6600 ± 0.3139	0.4937 ± 0.0122	0.92	0.171	2587 ± 53	2570 ± 54	101
E7	Metamict	639	43	1521	0.03	9.7738 ± 0.2650	0.4123 ± 0.0102	0.91	0.172	2225 ± 46	2577 ± 54	86
E13	Metamict core	701	47	1697	0.03	9.0493 ± 0.2446	0.4094 ± 0.0101	0.91	0.160	2212 ± 46	2459 ± 54	90
E14-C	Convoluted core	55	6	103	0.06	12.6333 ± 0.3575	0.5044 ± 0.0126	0.88	0.182	2633 ± 54	2668 ± 55	99
F6	Metamict	705	30	1533	0.02	10.8427 ± 0.2957	0.4499 ± 0.0111	0.90	0.175	2395 ± 49	2604 ± 54	92
F7	Metamict	1134	87	2397	0.04	11.1364 ± 0.3039	0.4620 ± 0.0114	0.90	0.175	2448 ± 50	2604 ± 54	94
F9	Black rim	1009	72	2438	0.03	9.9099 ± 0.2717	0.4253 ± 0.0105	0.90	0.169	2284 ± 47	2548 ± 54	90
F10	Metamict	1193	74	2858	0.03	10.0233 ± 0.2750	0.4278 ± 0.0105	0.89	0.170	2296 ± 48	2557 ± 54	90
F17	Black rim	457	31	905	0.03	13.4883 ± 0.3758	0.4988 ± 0.0123	0.89	0.196	2609 ± 53	2794 ± 54	93
SG-024 trondhjemite												
A1-C	Osci. zoned core	72	55	125	0.44	13.5561 ± 0.3525	0.5018 ± 0.0125	0.96	0.196	2622 ± 54	2792 ± 51	94
A1-R	Osci. zoned rim	78	52	146	0.36	11.6675 ± 0.3032	0.4825 ± 0.0121	0.97	0.175	2538 ± 52	2610 ± 51	97

Continued on next page

Table B.3 – *Continued from previous page*

Spot #	**Internal Structure**	**Pb (ppm)**	**Th (ppm)**	**U (ppm)**	**Th/U**	^{207}**Pb**/^{235}**U** $\pm 2\sigma$	^{206}**Pb**/^{238}**U** $\pm 2\sigma$	ρ	$\frac{^{207}Pb}{^{206}Pb}$ ^{206}Pb	**Ages (Ma)**$\pm 2\sigma$ $\frac{^{206}Pb}{^{238}U}$	$\frac{^{207}Pb}{^{206}Pb}$	**Conc** %
A2-C	Black core	151	68	262	0.26	14.2435 ± 0.3687	0.5292 ± 0.0132	0.96	0.195	2738 ± 56	2786 ± 50	98
A2-R	Osci. zoned rim	59	91	90	1.01	13.5479 ± 0.3542	0.5173 ± 0.0129	0.95	0.190	2688 ± 55	2741 ± 51	98
A3-C	Osci. zoned core	243	41	438	0.09	14.2412 ± 0.3695	0.5235 ± 0.0131	0.96	0.197	2714 ± 55	2804 ± 50	97
A3-R	Sector zoned rim	50	111	71	1.57	13.4478 ± 0.3524	0.5144 ± 0.0129	0.96	0.190	2676 ± 55	2738 ± 51	98
A4	Sector zoned	65	142	91	1.56	13.3599 ± 0.3490	0.5159 ± 0.0129	0.96	0.188	2682 ± 55	2723 ± 51	98
A5	Sector zoned	65	175	85	2.06	13.1471 ± 0.3442	0.5109 ± 0.0128	0.96	0.187	2661 ± 55	2712 ± 51	98
A6	Sector zoned	47	117	63	1.84	13.2486 ± 0.3483	0.5127 ± 0.0128	0.95	0.187	2668 ± 55	2719 ± 51	98
A7	Convoluted core	54	42	93	0.45	13.3105 ± 0.3482	0.5156 ± 0.0129	0.96	0.187	2681 ± 55	2718 ± 51	99
A8	Black core	185	105	323	0.32	13.5917 ± 0.3523	0.5154 ± 0.0128	0.96	0.191	2680 ± 55	2753 ± 51	97
A9	Sector zoned	37	66	56	1.18	13.2431 ± 0.3497	0.5068 ± 0.0127	0.95	0.190	2643 ± 54	2738 ± 51	97
A10	Sector zoned	50	122	68	1.79	13.1451 ± 0.3459	0.5125 ± 0.0128	0.95	0.186	2667 ± 55	2707 ± 51	99
A11-C	Black core	97	62	170	0.36	13.5336 ± 0.3523	0.5083 ± 0.0127	0.96	0.193	2649 ± 54	2768 ± 51	96
A12	Sector zoned	46	82	69	1.19	13.3006 ± 0.3501	0.5121 ± 0.0128	0.95	0.188	2665 ± 55	2728 ± 51	98
A14	Sector zoned	68	173	89	1.94	13.3944 ± 0.3516	0.5145 ± 0.0129	0.96	0.189	2676 ± 55	2732 ± 51	98
A15	Sector zoned	46	92	67	1.38	13.2546 ± 0.3494	0.5131 ± 0.0128	0.95	0.187	2670 ± 55	2719 ± 51	98
A16	Sector zoned	41	152	54	2.83	12.5048 ± 0.3297	0.4956 ± 0.0124	0.95	0.183	2595 ± 53	2680 ± 52	97
A17-C	Osci. zoned core	139	127	131	0.97	39.9623 ± 1.0396	0.7831 ± 0.0195	0.96	0.370	3728 ± 71	3792 ± 47	98
A17-R	Osci. zoned rim	37	21	35	0.59	43.4547 ± 1.1429	0.8102 ± 0.0203	0.95	0.389	3826 ± 72	3867 ± 47	99
B1	Sector zoned	35	94	49	1.90	13.2483 ± 0.3562	0.5198 ± 0.0131	0.94	0.185	2698 ± 55	2697 ± 52	100
B2	Sector zoned	34	90	47	1.90	13.5563 ± 0.3595	0.5229 ± 0.0131	0.94	0.188	2712 ± 55	2725 ± 52	100
B3	Sector zoned	32	87	44	1.97	13.6049 ± 0.3616	0.5248 ± 0.0131	0.94	0.188	2720 ± 56	2725 ± 52	100
B4	Sector zoned	54	176	70	2.54	13.3299 ± 0.3518	0.5191 ± 0.0130	0.95	0.186	2695 ± 55	2709 ± 52	99
B5	Sector zoned	30	45	50	0.90	12.9648 ± 0.3445	0.5092 ± 0.0128	0.95	0.185	2653 ± 54	2695 ± 52	98
B6	Sector zoned	25	37	37	1.00	14.1093 ± 0.3787	0.5262 ± 0.0132	0.93	0.194	2725 ± 56	2780 ± 52	98
B7	Sector zoned	69	176	93	1.90	12.9605 ± 0.3424	0.5100 ± 0.0128	0.95	0.184	2657 ± 54	2692 ± 52	99
B8	Sector zoned	57	140	76	1.85	13.2491 ± 0.3511	0.5139 ± 0.0128	0.94	0.187	2673 ± 55	2716 ± 52	98
B9	Sector zoned	46	98	65	1.52	13.2983 ± 0.3534	0.5152 ± 0.0129	0.94	0.187	2679 ± 55	2717 ± 52	99
B10	Sector zoned	42	91	60	1.53	13.4560 ± 0.3629	0.5224 ± 0.0131	0.93	0.187	2709 ± 56	2714 ± 52	100
B11	Sector zoned	44	90	63	1.44	13.2595 ± 0.3533	0.5151 ± 0.0129	0.94	0.187	2678 ± 55	2713 ± 52	99
B12	Sector zoned core	41	38	69	0.56	13.4377 ± 0.3578	0.5187 ± 0.0130	0.94	0.188	2694 ± 55	2724 ± 52	99

Continued on next page

Table B.3 – *Continued from previous page*

Spot #	Internal Structure	Pb (ppm)	Th (ppm)	U (ppm)	Th/U	$^{207}Pb/^{235}U$ $\pm 2\sigma$	$^{206}Pb/^{238}U$ $\pm 2\sigma$	ρ	$\frac{^{207}Pb}{^{206}Pb}$ ^{206}Pb	Ages (Ma)$\pm 2\sigma$ $\frac{^{206}Pb}{^{238}U}$	Ages (Ma)$\pm 2\sigma$ $\frac{^{207}Pb}{^{206}Pb}$	Conc %
B13	Sector zoned	78	201	101	1.99	13.3712 ± 0.3548	0.5179 ± 0.0129	0.94	0.187	2690 ± 55	2718 ± 52	99
B14	Sector zoned core	57	66	91	0.72	13.6898 ± 0.3641	0.5260 ± 0.0131	0.94	0.189	2724 ± 56	2731 ± 52	100
B15	Sector zoned	64	162	84	1.93	13.3791 ± 0.3555	0.5187 ± 0.0130	0.94	0.187	2694 ± 55	2716 ± 52	99
B16-C	Osci. zoned core	33	19	32	0.60	40.9133 ± 1.0919	0.7911 ± 0.0199	0.94	0.375	3757 ± 71	3812 ± 48	99
C1-C	Metamict core	215	11	259	0.04	32.5251 ± 0.8609	0.6893 ± 0.0172	0.94	0.342	3380 ± 66	3673 ± 48	92
C1-R	Sector zoned rim	29	58	41	1.39	13.9064 ± 0.3763	0.5263 ± 0.0132	0.93	0.192	2726 ± 56	2756 ± 52	99
C2	Sector zoned	41	79	60	1.32	13.1912 ± 0.3540	0.5161 ± 0.0129	0.93	0.185	2682 ± 55	2701 ± 52	99
C3	Osci. zoned core	230	156	218	0.72	40.6302 ± 1.0757	0.7831 ± 0.0195	0.94	0.376	3729 ± 71	3817 ± 47	98
C4	Sector zoned core	21	25	34	0.74	13.7134 ± 0.3732	0.5159 ± 0.0130	0.93	0.193	2682 ± 55	2766 ± 53	97
C5	Sector zoned	46	158	63	2.53	13.0021 ± 0.3497	0.5054 ± 0.0126	0.93	0.187	2637 ± 54	2712 ± 52	97
C6	Sector zoned	54	180	70	2.56	13.0295 ± 0.3497	0.5143 ± 0.0128	0.93	0.184	2675 ± 55	2687 ± 52	100
C7	Sector zoned	35	89	52	1.72	12.6281 ± 0.3408	0.5067 ± 0.0127	0.93	0.181	2642 ± 54	2660 ± 53	99
C8-C	Black core	76	254	100	2.55	13.2943 ± 0.3566	0.5173 ± 0.0129	0.93	0.186	2688 ± 55	2710 ± 52	99
C9	Sector zoned core	39	136	52	2.63	13.0611 ± 0.3614	0.5115 ± 0.0129	0.91	0.185	2663 ± 55	2700 ± 54	99
C10	Sector zoned	73	293	107	2.75	10.6682 ± 0.2911	0.4535 ± 0.0113	0.91	0.171	2411 ± 50	2563 ± 54	94
C11-R	Sector zoned rim	38	103	55	1.87	13.3689 ± 0.3634	0.5159 ± 0.0129	0.92	0.188	2682 ± 55	2724 ± 53	98
C12	Sector zoned	42	87	58	1.50	13.8276 ± 0.3763	0.5187 ± 0.0130	0.92	0.193	2694 ± 55	2771 ± 53	97
C13-C	Osci. zoned core	33	24	42	0.57	26.8956 ± 0.7338	0.6393 ± 0.0161	0.92	0.305	3186 ± 63	3496 ± 50	91
C13-R	Osci. zoned rim	56	4	65	0.06	33.8028 ± 0.8600	0.7268 ± 0.0180	0.97	0.337	3521 ± 67	3651 ± 47	96
C14	Sector zoned	117	34	209	0.16	13.6428 ± 0.3400	0.5154 ± 0.0126	0.98	0.192	2680 ± 54	2759 ± 50	97
C15	Black rim	591	22	723	0.03	32.7592 ± 0.8149	0.7303 ± 0.0179	0.99	0.325	3535 ± 67	3595 ± 46	98
D1-C	Convoluted core	268	56	319	0.17	32.2059 ± 0.8022	0.7073 ± 0.0173	0.98	0.330	3448 ± 65	3618 ± 46	95
D1-R	Osci. zoned rim	373	20	492	0.04	29.4979 ± 0.7346	0.6579 ± 0.0161	0.98	0.325	3259 ± 63	3594 ± 46	91
D2	Convo. black core	728	31	901	0.03	31.5142 ± 0.7843	0.7017 ± 0.0172	0.98	0.326	3427 ± 65	3597 ± 46	95
D3-R	Osci. zoned rim	1023	227	1146	0.20	35.5130 ± 0.8853	0.7458 ± 0.0183	0.98	0.345	3592 ± 68	3686 ± 46	97
D4-C	Metamict core	1085	57	1942	0.03	15.0256 ± 0.3758	0.5342 ± 0.0131	0.98	0.204	2759 ± 55	2858 ± 49	97
D4-R	Sector zoned rim	46	103	66	1.55	13.4874 ± 0.3410	0.5100 ± 0.0125	0.97	0.192	2657 ± 54	2758 ± 50	96
D5	Metamict core	325	53	992	0.05	7.0715 ± 0.1773	0.3186 ± 0.0078	0.98	0.161	1783 ± 38	2465 ± 51	72
D6	Osci. zoned core	31	15	34	0.43	34.2813 ± 0.8710	0.7251 ± 0.0179	0.97	0.343	3515 ± 67	3676 ± 47	96
D7-C	Osci. zoned core	217	170	197	0.86	41.3423 ± 1.0292	0.7928 ± 0.0194	0.98	0.378	3763 ± 70	3824 ± 46	98

Continued on next page

Table B.3 – *Continued from previous page*

Spot #	Internal Structure	Pb (ppm)	Th (ppm)	U (ppm)	Th/U	$^{207}Pb/^{235}U$ $\pm 2\sigma$	$^{206}Pb/^{238}U$ $\pm 2\sigma$	ρ	$\frac{^{207}Pb}{^{206}Pb}$ ^{206}Pb	Ages (Ma)$\pm 2\sigma$ $\frac{^{206}Pb}{^{238}U}$	Ages (Ma)$\pm 2\sigma$ $\frac{^{207}Pb}{^{206}Pb}$	Conc %
D7-R	Osci. zoned rim	538	40	925	0.05	21.0205 ± 0.5300	0.5911 ± 0.0146	0.98	0.258	2994 ± 59	3234 ± 48	93
D8	Metamict	154	3	264	0.01	18.2350 ± 0.4583	0.5425 ± 0.0133	0.98	0.244	2794 ± 56	3145 ± 48	89
D9-R	Metamict core	781	56	904	0.06	35.5336 ± 0.8859	0.7333 ± 0.0180	0.98	0.351	3546 ± 67	3713 ± 46	96
D10	Metamict	587	22	1551	0.01	8.2258 ± 0.2057	0.3600 ± 0.0088	0.98	0.166	1982 ± 42	2515 ± 51	79
D11-C	Inh. black core	531	47	542	0.09	42.3907 ± 1.0572	0.8069 ± 0.0198	0.98	0.381	3814 ± 71	3836 ± 46	99
D11-R	Osci. zoned rim	350	50	631	0.08	14.2911 ± 0.3581	0.5247 ± 0.0129	0.98	0.198	2719 ± 54	2806 ± 50	97
D12	Metamict	811	67	1892	0.04	9.3521 ± 0.2337	0.4238 ± 0.0104	0.98	0.160	2278 ± 47	2456 ± 51	93
D13-C	Convo. zoned core	79	69	88	0.78	28.7322 ± 0.7213	0.6729 ± 0.0165	0.98	0.310	3317 ± 64	3519 ± 47	94
D13-R	Osci. zoned rim	451	16	515	0.03	34.1654 ± 0.8525	0.7209 ± 0.0177	0.98	0.344	3499 ± 66	3679 ± 46	95
D14	Metamict core	693	101	875	0.12	29.1518 ± 0.7263	0.6874 ± 0.0168	0.98	0.308	3373 ± 64	3509 ± 47	96
D15	Metamict core	634	85	1269	0.07	11.5463 ± 0.2878	0.4861 ± 0.0119	0.98	0.172	2554 ± 52	2580 ± 51	99
D16-C	Black core	938	19	1210	0.02	27.4508 ± 0.6846	0.6962 ± 0.0170	0.98	0.286	3406 ± 65	3396 ± 47	100
D16-R	Black rim	265	26	478	0.05	14.5833 ± 0.3644	0.5266 ± 0.0129	0.98	0.201	2727 ± 54	2833 ± 49	96
D17-C	Black core	293	66	433	0.15	22.5740 ± 0.5646	0.5973 ± 0.0146	0.98	0.274	3019 ± 59	3329 ± 47	91
D17-R	Black rim	314	50	560	0.09	14.8123 ± 0.3700	0.5304 ± 0.0130	0.98	0.203	2743 ± 55	2847 ± 49	96
E1-C1	Black core	452	230	469	0.49	36.1233 ± 0.9028	0.7573 ± 0.0186	0.98	0.346	3634 ± 68	3689 ± 46	99
E1-C2	Black core	678	13	929	0.01	25.4113 ± 0.6354	0.6573 ± 0.0161	0.98	0.280	3257 ± 63	3365 ± 47	97
E2	Metamict	402	27	750	0.04	13.5847 ± 0.3394	0.5179 ± 0.0127	0.98	0.190	2690 ± 54	2744 ± 50	98
E3-C1	Metamict core	427	34	512	0.07	33.2329 ± 0.8302	0.7136 ± 0.0175	0.98	0.338	3472 ± 66	3652 ± 46	95
E3-C2	Metamict core	417	45	501	0.09	32.8704 ± 0.8213	0.7123 ± 0.0175	0.98	0.335	3467 ± 66	3638 ± 46	95
E4	Osci. zoned core	644	297	810	0.37	27.4364 ± 0.6860	0.6611 ± 0.0162	0.98	0.301	3272 ± 63	3475 ± 47	94
E5-C	Black core	609	32	802	0.04	27.7358 ± 0.6945	0.6668 ± 0.0164	0.98	0.302	3293 ± 63	3479 ± 47	95
E5-R	Black rim	160	11	283	0.04	14.7531 ± 0.3698	0.5343 ± 0.0131	0.98	0.200	2760 ± 55	2828 ± 50	98
E6	Metamict	566	68	818	0.08	22.6254 ± 0.5664	0.6148 ± 0.0151	0.98	0.267	3089 ± 60	3288 ± 48	94
E7-C	Black core	63	33	110	0.30	13.8592 ± 0.3517	0.5224 ± 0.0128	0.97	0.192	2710 ± 54	2763 ± 50	98
E7-R	White rim	21	22	34	0.66	13.5869 ± 0.3504	0.5170 ± 0.0128	0.96	0.191	2686 ± 54	2747 ± 51	98
E8	Black	587	14	739	0.02	29.6042 ± 0.7424	0.6957 ± 0.0171	0.98	0.309	3404 ± 65	3514 ± 47	97
E9-C	Osci. zoned core	214	34	368	0.09	15.0285 ± 0.3772	0.5473 ± 0.0134	0.98	0.199	2814 ± 56	2819 ± 50	100
E10-C	Osci. zoned core	726	23	899	0.03	31.2531 ± 0.7837	0.7002 ± 0.0172	0.98	0.324	3422 ± 65	3587 ± 47	95
E12-C	Osci. zoned core	102	33	123	0.27	30.3737 ± 0.7654	0.6904 ± 0.0170	0.98	0.319	3384 ± 65	3565 ± 47	95

Continued on next page

Table B.3 – *Continued from previous page*

Spot #	**Internal Structure**	**Pb** (ppm)	**Th** (ppm)	**U** (ppm)	**Th/U**	^{207}**Pb**/^{235}**U** $\pm 2\sigma$	^{206}**Pb**/^{238}**U** $\pm 2\sigma$	ρ	$\frac{^{207}Pb}{^{206}Pb}$ ^{206}Pb	**Ages (Ma)**$\pm 2\sigma$ $\frac{^{206}Pb}{^{238}U}$	$\frac{^{207}Pb}{^{206}Pb}$	**Conc** %
E12-R	Osci. zoned rim	456	28	548	0.05	33.6995 ± 0.8467	0.7000 ± 0.0172	0.98	0.349	3421 ± 65	3703 ± 46	92
E13	Metamict	324	42	570	0.07	14.9181 ± 0.3759	0.5373 ± 0.0132	0.97	0.201	2772 ± 55	2837 ± 50	98
E14-C	Convo. zoned core	632	122	671	0.18	38.6803 ± 0.9716	0.7681 ± 0.0188	0.97	0.365	3674 ± 69	3772 ± 46	97
E14-R	Osci. zoned rim	597	76	796	0.10	26.5126 ± 0.6661	0.6518 ± 0.0160	0.98	0.295	3235 ± 62	3444 ± 47	94
E15	Metamict core	748	23	1318	0.02	16.3492 ± 0.4114	0.5250 ± 0.0129	0.98	0.226	2720 ± 54	3023 ± 49	90
E16	Sector zoned	39	91	55	1.66	13.0658 ± 0.3373	0.5075 ± 0.0125	0.95	0.187	2646 ± 54	2713 ± 51	98
E17	Osci. zoned core	86	76	97	0.78	28.8658 ± 0.7299	0.6813 ± 0.0167	0.97	0.307	3349 ± 64	3507 ± 47	96
E18-C	Inh. zoned core	464	130	500	0.26	37.1564 ± 0.9348	0.7430 ± 0.0182	0.97	0.363	3582 ± 67	3761 ± 46	95
E18-R	Osci. zoned rim	362	20	413	0.05	36.2342 ± 0.9128	0.7434 ± 0.0182	0.97	0.353	3583 ± 67	3722 ± 46	96
F1-C	Osci. zoned core	68	34	72	0.47	35.9444 ± 0.9217	0.7482 ± 0.0185	0.96	0.348	3601 ± 68	3700 ± 47	97
F1-R	Black rim	119	8	159	0.05	27.2405 ± 0.6935	0.6601 ± 0.0163	0.97	0.299	3268 ± 63	3466 ± 48	94
F2-C	Osci. zoned core	95	34	178	0.19	12.6023 ± 0.3200	0.4990 ± 0.0123	0.97	0.183	2609 ± 53	2682 ± 51	97
F2-R	Osci. zoned rim	20	23	35	0.66	12.4249 ± 0.3257	0.4959 ± 0.0123	0.95	0.182	2596 ± 53	2668 ± 52	97
F3-C	Osci. zoned core	210	221	209	1.06	37.0368 ± 0.9388	0.7422 ± 0.0183	0.97	0.362	3579 ± 68	3758 ± 46	95
F3-R	Osci. zoned rim	513	17	625	0.03	31.5520 ± 0.7968	0.7135 ± 0.0175	0.97	0.321	3471 ± 66	3573 ± 47	97
F4-C	Black core	89	55	157	0.35	13.4317 ± 0.3434	0.5181 ± 0.0128	0.97	0.188	2691 ± 54	2725 ± 51	99
F4-R	Sector zoned rim	55	196	70	2.78	13.1463 ± 0.3374	0.5112 ± 0.0126	0.96	0.186	2662 ± 54	2711 ± 51	98
F5	Sector zoned	35	91	49	1.85	13.4964 ± 0.3490	0.5242 ± 0.0130	0.96	0.187	2717 ± 55	2713 ± 51	100
F6-C	Osci. zoned core	68	90	67	1.34	34.5884 ± 0.8895	0.7282 ± 0.0180	0.96	0.345	3527 ± 67	3683 ± 47	96
F6-R	Osci. zoned rim	198	36	344	0.11	14.7484 ± 0.3761	0.5468 ± 0.0134	0.96	0.196	2812 ± 56	2790 ± 50	101
F7-C	Black core	75	117	136	0.86	12.0177 ± 0.3107	0.4672 ± 0.0116	0.96	0.187	2471 ± 51	2712 ± 51	91
F7-R	Sector zoned rim	43	92	62	1.49	13.2828 ± 0.3435	0.5116 ± 0.0126	0.95	0.188	2664 ± 54	2727 ± 51	98
F8-C	Convo. zoned core	87	48	85	0.56	40.4064 ± 1.0299	0.7750 ± 0.0191	0.97	0.378	3699 ± 69	3824 ± 46	97
F8-R	Osci. zoned rim	31	16	29	0.54	43.5559 ± 1.1184	0.8083 ± 0.0200	0.96	0.391	3819 ± 71	3874 ± 47	99
F9-C	Convo. black core	97	86	162	0.53	13.7733 ± 0.3518	0.5177 ± 0.0128	0.97	0.193	2689 ± 54	2767 ± 50	97
F10-C	Black core	79	29	144	0.20	13.3818 ± 0.3426	0.5148 ± 0.0127	0.96	0.188	2677 ± 54	2729 ± 51	98
F10-R	Osci. zoned rim	24	36	38	0.95	13.1208 ± 0.3474	0.5087 ± 0.0127	0.94	0.187	2651 ± 54	2716 ± 52	98
F11	Inh. black core	363	28	482	0.06	27.3189 ± 0.6954	0.6638 ± 0.0163	0.96	0.298	3282 ± 63	3462 ± 48	95
F12	Sector zoned	35	39	58	0.68	13.5848 ± 0.3534	0.5151 ± 0.0128	0.96	0.191	2678 ± 54	2753 ± 51	97
F14	Metamict	398	62	747	0.08	13.3997 ± 0.3412	0.5048 ± 0.0124	0.96	0.193	2634 ± 53	2764 ± 50	95

Continued on next page

Table B.3 – *Continued from previous page*

Spot #	Internal Structure	Pb (ppm)	Th (ppm)	U (ppm)	Th/U	$^{207}Pb/^{235}U$ $\pm 2\sigma$	$^{206}Pb/^{238}U$ $\pm 2\sigma$	ρ	$\frac{^{207}Pb}{^{206}Pb}$ ^{206}Pb	Ages (Ma)$\pm 2\sigma$ $\frac{^{206}Pb}{^{238}U}$	Ages (Ma)$\pm 2\sigma$ $\frac{^{207}Pb}{^{206}Pb}$	Conc %
F15	Metamict	372	22	464	0.05	30.9592 ± 0.7884	0.6947 ± 0.0171	0.97	0.323	3401 ± 65	3585 ± 47	95
F16-C	Convoluted core	126	137	133	1.04	31.0287 ± 0.7932	0.6905 ± 0.0170	0.96	0.326	3385 ± 65	3598 ± 47	94
F16-R	Black rim	211	25	396	0.06	13.7821 ± 0.3559	0.5075 ± 0.0125	0.95	0.197	2646 ± 54	2801 ± 51	94
F17-C	Osci. zoned core	25	17	30	0.56	27.6561 ± 0.7173	0.6646 ± 0.0165	0.96	0.302	3285 ± 64	3479 ± 48	94
F17-R	Rim	72	30	98	0.30	23.5817 ± 0.6094	0.6183 ± 0.0153	0.96	0.277	3103 ± 61	3344 ± 49	93
F18	Sector zoned	46	103	66	1.57	12.8841 ± 0.3353	0.5037 ± 0.0125	0.95	0.185	2630 ± 53	2702 ± 51	97
SG-025 trondhjemite												
A1	Black core	353	86	623	0.14	14.1253 ± 0.3635	0.5332 ± 0.0134	0.98	0.192	2755 ± 56	2760 ± 50	100
A2	Black core	333	279	536	0.52	14.2971 ± 0.3681	0.5394 ± 0.0135	0.97	0.192	2781 ± 57	2761 ± 50	101
A3	Convo. black core	372	87	637	0.14	14.9678 ± 0.3857	0.5460 ± 0.0137	0.97	0.199	2809 ± 57	2816 ± 50	100
A4	Sector zoned	114	50	198	0.25	13.9106 ± 0.3600	0.5271 ± 0.0132	0.97	0.191	2729 ± 56	2754 ± 50	99
A5	Black core	105	99	173	0.58	13.6141 ± 0.3527	0.5251 ± 0.0132	0.97	0.188	2721 ± 56	2725 ± 50	100
A6	Sector zoned	137	176	215	0.82	13.6188 ± 0.3522	0.5231 ± 0.0131	0.97	0.189	2712 ± 56	2732 ± 50	99
A7	Sector zoned	130	167	210	0.80	13.6709 ± 0.3538	0.5224 ± 0.0131	0.97	0.190	2709 ± 56	2740 ± 50	99
A8	Black core	247	125	420	0.30	14.2220 ± 0.3671	0.5344 ± 0.0134	0.97	0.193	2760 ± 56	2768 ± 50	100
A9-C	Metamict core	188	7	220	0.03	33.6750 ± 0.8697	0.7367 ± 0.0185	0.97	0.331	3558 ± 69	3624 ± 47	98
A9-R	Grey rim	48	104	70	1.48	13.3482 ± 0.3505	0.5152 ± 0.0130	0.96	0.188	2679 ± 55	2724 ± 51	98
A10	Osci. zoned core	137	155	223	0.70	13.5818 ± 0.3521	0.5229 ± 0.0131	0.97	0.188	2711 ± 56	2728 ± 51	99
A11	Black core	335	217	559	0.39	14.2466 ± 0.3679	0.5381 ± 0.0135	0.97	0.192	2775 ± 56	2759 ± 50	101
A12	Osci. zoned core	218	128	376	0.34	13.8297 ± 0.3576	0.5256 ± 0.0132	0.97	0.191	2723 ± 56	2749 ± 50	99
A13	Black core	263	79	462	0.17	14.1569 ± 0.3661	0.5291 ± 0.0133	0.97	0.194	2738 ± 56	2777 ± 50	99
A14	Osci. zoned core	538	45	707	0.06	27.8443 ± 0.7199	0.6700 ± 0.0168	0.97	0.301	3306 ± 65	3477 ± 47	95
A15	Sector zoned	76	89	125	0.71	13.6154 ± 0.3579	0.5235 ± 0.0132	0.96	0.189	2714 ± 56	2730 ± 51	99
A16-C	Black core	276	198	471	0.42	14.0231 ± 0.3627	0.5285 ± 0.0132	0.97	0.192	2735 ± 56	2763 ± 50	99
A16-R	Grey rim	73	65	125	0.52	13.5676 ± 0.3535	0.5204 ± 0.0131	0.97	0.189	2701 ± 55	2734 ± 51	99
B1	Sector zoned	110	173	178	0.97	13.1026 ± 0.3421	0.5127 ± 0.0129	0.96	0.185	2668 ± 55	2701 ± 51	99
B2-C	Black core	263	189	444	0.43	14.1130 ± 0.3655	0.5340 ± 0.0134	0.97	0.192	2758 ± 56	2756 ± 50	100
B3-C	Black core	368	301	613	0.49	14.1501 ± 0.3663	0.5353 ± 0.0134	0.97	0.192	2764 ± 56	2757 ± 50	100
B3-R	Sector zoned rim	79	51	147	0.34	12.2357 ± 0.3234	0.4909 ± 0.0124	0.96	0.181	2574 ± 53	2660 ± 52	97
B4	Black core	277	85	486	0.17	14.0335 ± 0.3638	0.5328 ± 0.0133	0.96	0.191	2753 ± 56	2751 ± 51	100

Continued on next page

Table B.3 – *Continued from previous page*

Spot #	Internal Structure	Pb (ppm)	Th (ppm)	U (ppm)	Th/U	$^{207}Pb/^{235}U$ $\pm 2\sigma$	$^{206}Pb/^{238}U$ $\pm 2\sigma$	ρ	$\frac{^{207}Pb}{^{206}Pb}$ ^{206}Pb	Ages (Ma)$\pm 2\sigma$ $\frac{^{206}Pb}{^{238}U}$	Ages (Ma)$\pm 2\sigma$ $\frac{^{207}Pb}{^{206}Pb}$	Conc %
B5	Black core	176	92	304	0.30	13.8420 ± 0.3594	0.5260 ± 0.0132	0.97	0.191	2725 ± 56	2749 ± 51	99
B6-C	Black core	330	89	585	0.15	13.9412 ± 0.3614	0.5285 ± 0.0132	0.96	0.191	2735 ± 56	2753 ± 51	99
B6-R	Grey rim	87	53	148	0.36	13.6549 ± 0.3565	0.5265 ± 0.0132	0.96	0.188	2727 ± 56	2725 ± 51	100
B7	Black core	311	131	534	0.25	14.1908 ± 0.3684	0.5348 ± 0.0134	0.97	0.192	2762 ± 56	2763 ± 51	100
B8	Black core	316	226	529	0.43	14.0470 ± 0.3648	0.5300 ± 0.0133	0.97	0.192	2741 ± 56	2761 ± 51	99
B9	Sector zoned	108	58	182	0.32	14.1383 ± 0.3689	0.5344 ± 0.0134	0.96	0.192	2760 ± 56	2758 ± 51	100
B10	Black core	258	11	309	0.04	30.7600 ± 0.7994	0.7041 ± 0.0176	0.96	0.317	3436 ± 67	3554 ± 47	97
B11-C	Sector zoned	132	138	215	0.64	13.6271 ± 0.3556	0.5217 ± 0.0131	0.96	0.189	2706 ± 55	2737 ± 51	99
B11-R	White zoned rim	32	52	48	1.07	13.6776 ± 0.3653	0.5202 ± 0.0131	0.94	0.191	2700 ± 56	2748 ± 52	98
B12	Black core	246	133	416	0.32	14.0161 ± 0.3649	0.5348 ± 0.0134	0.96	0.190	2762 ± 56	2743 ± 51	101
B13-C	Metamict core	801	38	868	0.04	37.6801 ± 0.9791	0.7825 ± 0.0196	0.96	0.349	3726 ± 71	3703 ± 47	101
B13-R	Metamict core	231	133	392	0.34	14.1540 ± 0.3692	0.5288 ± 0.0132	0.96	0.194	2736 ± 56	2777 ± 51	99
B14-R	Black core	117	120	188	0.64	13.8802 ± 0.3637	0.5314 ± 0.0133	0.96	0.189	2748 ± 56	2737 ± 51	100
B15-C2	Sector zoned core	120	155	195	0.80	13.8035 ± 0.3614	0.5289 ± 0.0132	0.95	0.189	2737 ± 56	2736 ± 51	100
B15-R	Sector zoned rim	68	100	109	0.92	13.7113 ± 0.3608	0.5259 ± 0.0132	0.95	0.189	2724 ± 56	2734 ± 51	100
B16-C	Metamict core	925	1552	3268	0.47	4.8565 ± 0.1322	0.2555 ± 0.0069	0.99	0.138	1467 ± 35	2200 ± 52	67
B16-R	Sector zoned core	60	46	110	0.42	12.5634 ± 0.3503	0.4835 ± 0.0131	0.97	0.188	2543 ± 57	2728 ± 51	93
C1-C	Inherited core	471	101	514	0.20	36.3342 ± 0.9884	0.7525 ± 0.0203	0.99	0.350	3617 ± 75	3708 ± 46	98
C1-R	Black rim	145	104	241	0.43	14.0628 ± 0.3836	0.5305 ± 0.0143	0.99	0.192	2744 ± 60	2761 ± 50	99
C2	Black rim	157	73	271	0.27	14.2855 ± 0.3896	0.5262 ± 0.0142	0.99	0.197	2725 ± 60	2800 ± 49	97
C3	Black core	1126	49	1877	0.03	18.4672 ± 0.5019	0.5551 ± 0.0149	0.99	0.241	2846 ± 62	3128 ± 48	91
C4-C	Black core	339	36	436	0.08	31.4007 ± 0.8568	0.6543 ± 0.0176	0.99	0.348	3245 ± 69	3698 ± 46	88
C4-R	Osci. zoned rim	213	131	363	0.36	13.8884 ± 0.3782	0.5254 ± 0.0141	0.99	0.192	2722 ± 60	2757 ± 50	99
C5	Sector zoned core	219	177	361	0.49	13.9881 ± 0.3809	0.5322 ± 0.0143	0.99	0.191	2751 ± 60	2747 ± 50	100
C6	White zoned core	183	13	206	0.06	34.3554 ± 0.9344	0.7350 ± 0.0198	0.99	0.339	3552 ± 73	3658 ± 46	97
C7	Metamict	285	37	500	0.07	14.8882 ± 0.4046	0.5425 ± 0.0146	0.99	0.199	2794 ± 61	2818 ± 49	99
C8-C	Osci. zoned core	269	245	448	0.55	13.8583 ± 0.3766	0.5331 ± 0.0143	0.99	0.188	2755 ± 60	2729 ± 50	101
C8-R	Grey rim	166	101	289	0.35	13.7170 ± 0.3733	0.5241 ± 0.0141	0.99	0.190	2716 ± 60	2741 ± 50	99
C9-C	Inherited core	1390	835	1882	0.44	25.5359 ± 0.6929	0.6156 ± 0.0165	0.99	0.301	3092 ± 66	3474 ± 47	89
C9-R	Osci. zoned rim	187	123	314	0.39	14.3843 ± 0.3909	0.5371 ± 0.0144	0.99	0.194	2771 ± 60	2778 ± 50	100

Continued on next page

Table B.3 – *Continued from previous page*

Spot #	**Internal Structure**	**Pb** (ppm)	**Th** (ppm)	**U** (ppm)	**Th/U**	^{207}**Pb**/^{235}**U** $\pm 2\sigma$	^{206}**Pb**/^{238}**U** $\pm 2\sigma$	ρ	$\frac{^{207}Pb}{^{206}Pb}$ ^{206}Pb	**Ages (Ma)**$\pm 2\sigma$ $\frac{^{206}Pb}{^{238}U}$	$\frac{^{207}Pb}{^{206}Pb}$	**Conc** %
C10-C	Black core	640	92	1216	0.08	14.9201 ± 0.4053	0.4900 ± 0.0131	0.98	0.221	2571 ± 57	2987 ± 49	86
C10-R	Sector zoned rim	76	95	122	0.78	13.8805 ± 0.3789	0.5346 ± 0.0143	0.98	0.188	2761 ± 60	2727 ± 50	101
C11	Black core	169	117	287	0.41	13.9218 ± 0.3785	0.5321 ± 0.0143	0.99	0.190	2750 ± 60	2740 ± 50	100
C12-R	Black rim	414	174	731	0.24	13.9374 ± 0.3780	0.5174 ± 0.0139	0.99	0.195	2688 ± 59	2788 ± 49	96
C14	Metamict	721	50	886	0.06	29.5570 ± 0.8006	0.7141 ± 0.0191	0.99	0.300	3474 ± 72	3471 ± 47	100
C15-C	inh. zoned core	127	59	217	0.27	14.1567 ± 0.3847	0.5338 ± 0.0143	0.99	0.192	2757 ± 60	2762 ± 50	100
C15-R	Black rim	118	122	191	0.64	13.6250 ± 0.3707	0.5268 ± 0.0141	0.98	0.188	2728 ± 60	2721 ± 50	100
C16	Convoluted core	319	23	557	0.04	15.0369 ± 0.4076	0.5474 ± 0.0146	0.98	0.199	2815 ± 61	2820 ± 49	100
D2-C	White zoned	56	24	57	0.42	39.1080 ± 1.0652	0.7851 ± 0.0210	0.98	0.361	3736 ± 76	3755 ± 46	99
D2-R	Black half	289	92	512	0.18	13.9819 ± 0.3789	0.5317 ± 0.0142	0.99	0.191	2749 ± 60	2748 ± 50	100
D3	Black core	97	129	157	0.83	13.5836 ± 0.3698	0.5269 ± 0.0141	0.98	0.187	2728 ± 59	2716 ± 50	100
D4	Black core	111	73	191	0.38	13.6611 ± 0.3719	0.5252 ± 0.0140	0.98	0.189	2721 ± 59	2730 ± 50	100
D5-C	Black core	293	213	500	0.42	13.8963 ± 0.3771	0.5306 ± 0.0142	0.99	0.190	2744 ± 60	2741 ± 50	100
D5-R	Sector zoned rim	88	111	143	0.78	13.7636 ± 0.3749	0.5289 ± 0.0141	0.98	0.189	2737 ± 60	2731 ± 50	100
D6-C2	Inherited core	542	61	630	0.10	31.9126 ± 0.8642	0.7340 ± 0.0196	0.99	0.315	3548 ± 73	3547 ± 47	100
D6-R	Sector zoned	105	127	173	0.74	13.7004 ± 0.3726	0.5245 ± 0.0140	0.98	0.189	2718 ± 59	2737 ± 50	99
D7	Sector zoned rim	84	99	136	0.73	13.7729 ± 0.3746	0.5289 ± 0.0141	0.98	0.189	2737 ± 60	2732 ± 50	100
D8	Metamict	163	28	282	0.10	15.1758 ± 0.4123	0.5335 ± 0.0142	0.98	0.206	2756 ± 60	2877 ± 49	96
D9	Black core	166	175	266	0.66	13.8939 ± 0.3768	0.5322 ± 0.0142	0.98	0.189	2751 ± 60	2736 ± 50	101
D10	Black core	273	158	471	0.33	13.8634 ± 0.3755	0.5253 ± 0.0140	0.98	0.191	2721 ± 59	2754 ± 50	99
D11-C	Inh. zoned core	397	306	379	0.81	39.1068 ± 1.0580	0.7827 ± 0.0209	0.99	0.362	3727 ± 75	3760 ± 46	99
D11-R	Sector zoned	74	73	121	0.61	13.6382 ± 0.3717	0.5248 ± 0.0140	0.98	0.188	2720 ± 59	2729 ± 50	100
D12	Black core	326	91	584	0.16	13.8552 ± 0.3753	0.5250 ± 0.0140	0.98	0.191	2720 ± 59	2754 ± 50	99
D13	Sector zoned	126	176	197	0.89	13.6418 ± 0.3704	0.5243 ± 0.0140	0.98	0.189	2717 ± 59	2731 ± 50	100
D14	Metamict	544	340	969	0.35	12.5866 ± 0.3403	0.5112 ± 0.0136	0.98	0.179	2662 ± 58	2640 ± 50	101
D15	Black core	349	130	609	0.21	14.0284 ± 0.3795	0.5306 ± 0.0141	0.98	0.192	2744 ± 59	2757 ± 50	100
D16	Black core	379	97	680	0.14	13.7386 ± 0.3716	0.5249 ± 0.0140	0.99	0.190	2720 ± 59	2740 ± 50	99
D17-C	Inherited core	1071	272	1100	0.25	39.8710 ± 1.0772	0.7901 ± 0.0210	0.98	0.366	3754 ± 76	3775 ± 46	99
D17-R	Black rim	61	65	97	0.67	13.9400 ± 0.3815	0.5236 ± 0.0140	0.98	0.193	2714 ± 59	2768 ± 50	98
D18	Sector zoned	148	192	233	0.82	13.4535 ± 0.3653	0.5237 ± 0.0139	0.98	0.186	2715 ± 59	2710 ± 50	100

Continued on next page

Table B.3 – *Continued from previous page*

Spot #	Internal Structure	Pb (ppm)	Th (ppm)	U (ppm)	Th/U	$^{207}Pb/^{235}U$ $\pm 2\sigma$	$^{206}Pb/^{238}U$ $\pm 2\sigma$	ρ	$\frac{^{207}Pb}{^{206}Pb}$ ^{206}Pb	Ages (Ma)$\pm 2\sigma$ $\frac{^{206}Pb}{^{238}U}$	Ages (Ma)$\pm 2\sigma$ $\frac{^{207}Pb}{^{206}Pb}$	Conc %
E1	Black	381	137	664	0.21	13.9668 ± 0.3778	0.5329 ± 0.0141	0.98	0.190	2754 ± 59	2743 ± 50	100
E2	Sector zoned	151	197	236	0.83	13.4897 ± 0.3661	0.5228 ± 0.0139	0.98	0.187	2711 ± 59	2717 ± 50	100
E3-C	Core	861	61	1172	0.05	27.3963 ± 0.7420	0.6429 ± 0.0171	0.98	0.309	3200 ± 67	3516 ± 47	91
E3-R	Sector zoned rim	104	130	170	0.77	13.8188 ± 0.3753	0.5276 ± 0.0140	0.98	0.190	2731 ± 59	2742 ± 50	100
E4	Sector zoned	87	110	141	0.78	13.8713 ± 0.3774	0.5304 ± 0.0141	0.98	0.190	2743 ± 59	2739 ± 50	100
E5	Black core	165	135	280	0.48	13.8457 ± 0.3753	0.5282 ± 0.0140	0.98	0.190	2734 ± 59	2743 ± 50	100
E6	Black core	368	139	646	0.22	14.0523 ± 0.3800	0.5320 ± 0.0141	0.98	0.191	2750 ± 59	2755 ± 50	100
E7	Sector zoned core	95	83	158	0.52	13.9544 ± 0.3801	0.5308 ± 0.0141	0.98	0.191	2745 ± 59	2748 ± 50	100
E8-C1	Black core	209	198	400	0.50	12.3163 ± 0.3364	0.4659 ± 0.0124	0.97	0.192	2466 ± 54	2757 ± 50	89
E8-C2	White core	191	23	193	0.12	42.1184 ± 1.1398	0.8001 ± 0.0212	0.98	0.382	3790 ± 76	3839 ± 46	99
E10	Black core	328	116	579	0.20	13.9527 ± 0.3774	0.5304 ± 0.0140	0.98	0.191	2743 ± 59	2749 ± 50	100
E11-C	Metamict core	899	122	1253	0.10	23.7370 ± 0.6413	0.6445 ± 0.0170	0.98	0.267	3207 ± 67	3289 ± 48	97
E11-R	Black rim	282	92	490	0.19	14.3619 ± 0.3887	0.5351 ± 0.0142	0.98	0.195	2763 ± 59	2782 ± 50	99
E12	Black core	199	138	337	0.41	14.1348 ± 0.3836	0.5290 ± 0.0140	0.98	0.194	2737 ± 59	2774 ± 50	99
E13-C	Metamict	1262	152	2285	0.07	16.2868 ± 0.4400	0.5093 ± 0.0134	0.97	0.232	2654 ± 57	3065 ± 49	87
E13-R	Black rim	121	51	213	0.24	13.8088 ± 0.3750	0.5194 ± 0.0137	0.97	0.193	2697 ± 58	2766 ± 50	97
E14	Black rim	382	49	674	0.07	14.7338 ± 0.3990	0.5364 ± 0.0142	0.98	0.199	2768 ± 59	2819 ± 50	98
E15	Black core	103	52	183	0.28	13.2363 ± 0.3596	0.5210 ± 0.0138	0.97	0.184	2703 ± 58	2691 ± 51	100
E16-C	White core	144	87	243	0.36	14.0864 ± 0.3820	0.5383 ± 0.0142	0.97	0.190	2776 ± 60	2740 ± 50	101
E17	Osci. zoned core	227	136	386	0.35	14.2221 ± 0.3852	0.5287 ± 0.0140	0.98	0.195	2736 ± 59	2785 ± 50	98
F1	Black core	156	140	261	0.54	13.8139 ± 0.3752	0.5291 ± 0.0140	0.97	0.189	2738 ± 59	2736 ± 50	100
F2	Black core	345	200	587	0.34	18.0704 ± 0.4924	0.5132 ± 0.0136	0.97	0.255	2670 ± 58	3218 ± 49	83
F3	Black core	229	131	394	0.33	13.9344 ± 0.3776	0.5312 ± 0.0140	0.97	0.190	2747 ± 59	2744 ± 50	100
F4-C	Black core	400	379	655	0.58	14.0338 ± 0.3799	0.5315 ± 0.0140	0.97	0.191	2748 ± 59	2755 ± 50	100
F4-R	Osci. zoned rim	96	53	174	0.31	12.7355 ± 0.3464	0.5143 ± 0.0136	0.97	0.180	2675 ± 58	2649 ± 51	101
F5	Metamict	253	198	419	0.47	14.2620 ± 0.3864	0.5411 ± 0.0143	0.98	0.191	2788 ± 60	2752 ± 50	101
F6	Metamict	243	78	427	0.18	14.1086 ± 0.3823	0.5304 ± 0.0140	0.97	0.193	2743 ± 59	2767 ± 50	99
F7	Black core	243	188	412	0.46	14.0247 ± 0.3803	0.5312 ± 0.0140	0.97	0.191	2747 ± 59	2755 ± 50	100
F8	Black core	384	386	638	0.61	13.9621 ± 0.3783	0.5289 ± 0.0139	0.97	0.191	2737 ± 59	2754 ± 50	99
F9	Sector zoned	151	244	237	1.03	13.7326 ± 0.3734	0.5272 ± 0.0139	0.97	0.189	2730 ± 59	2733 ± 51	100

Continued on next page

Table B.3 – *Continued from previous page*

Spot #	Internal Structure	Pb (ppm)	Th (ppm)	U (ppm)	Th/U	$^{207}Pb/^{235}U$ $\pm 2\sigma$	$^{206}Pb/^{238}U$ $\pm 2\sigma$	ρ	$\frac{^{207}Pb}{^{206}Pb}$ ^{206}Pb	Ages (Ma)$\pm 2\sigma$ $\frac{^{206}Pb}{^{238}U}$	Ages (Ma)$\pm 2\sigma$ $\frac{^{207}Pb}{^{206}Pb}$	Conc %
F10	Black core	240	154	412	0.37	13.9821 ± 0.3791	0.5312 ± 0.0140	0.97	0.191	2746 ± 59	2750 ± 50	100
F11	Black core	267	218	449	0.48	13.9588 ± 0.3784	0.5316 ± 0.0140	0.97	0.190	2748 ± 59	2746 ± 50	100
F12-C	Osci. zoned core	339	21	398	0.05	32.3751 ± 0.8770	0.7201 ± 0.0189	0.97	0.326	3496 ± 71	3599 ± 47	97
F12-R	Grey rim	70	49	119	0.41	13.9388 ± 0.3813	0.5281 ± 0.0139	0.96	0.191	2734 ± 59	2754 ± 51	99
F13-I	White core	48	45	77	0.58	13.9349 ± 0.3930	0.5320 ± 0.0141	0.94	0.190	2750 ± 59	2742 ± 52	100
F13-R	Sector zoned rim	124	153	198	0.77	13.7935 ± 0.3758	0.5294 ± 0.0139	0.96	0.189	2739 ± 59	2733 ± 51	100
F13-C	Osci. zoned core	185	59	322	0.18	14.0222 ± 0.3810	0.5345 ± 0.0140	0.96	0.190	2760 ± 59	2744 ± 51	101
F14	Black rim	147	64	242	0.27	15.2819 ± 0.4165	0.5242 ± 0.0138	0.97	0.211	2717 ± 58	2916 ± 50	93
F15-R	Metamict	1116	135	2609	0.05	8.5288 ± 0.2311	0.4254 ± 0.0112	0.97	0.145	2285 ± 50	2292 ± 53	100
F16	Metamict	228	48	347	0.14	18.9170 ± 0.5136	0.5894 ± 0.0155	0.97	0.233	2987 ± 63	3071 ± 49	97
F17-C	Metamict core	558	38	630	0.06	34.7790 ± 0.9429	0.7582 ± 0.0199	0.97	0.333	3638 ± 73	3629 ± 47	100
F17-R	Black rim	278	106	487	0.22	14.0112 ± 0.3805	0.5328 ± 0.0140	0.97	0.191	2753 ± 59	2748 ± 51	100
SG-026 Mg-tonalite												
A2-C	Grey core	53	72	51	1.43	33.3278 ± 0.8910	0.7190 ± 0.0185	0.96	0.336	3492 ± 69	3645 ± 48	96
A3	Sector zoned core	45	43	42	1.02	37.6256 ± 0.9953	0.7695 ± 0.0197	0.97	0.355	3679 ± 72	3727 ± 47	99
A4-C	Sector zoned core	48	53	44	1.20	37.5514 ± 0.9934	0.7692 ± 0.0197	0.97	0.354	3678 ± 72	3725 ± 47	99
A4-R	Black rim	430	52	501	0.10	33.4570 ± 0.8683	0.7250 ± 0.0184	0.98	0.335	3515 ± 69	3639 ± 47	97
A5	Grey core	74	81	86	0.95	27.4897 ± 0.7293	0.6442 ± 0.0165	0.97	0.309	3205 ± 65	3518 ± 48	91
A6	Sector zoned core	35	40	35	1.15	32.4965 ± 0.8655	0.7116 ± 0.0182	0.96	0.331	3464 ± 69	3623 ± 48	96
A7-C	Sector zoned core	50	62	44	1.40	38.0597 ± 1.0065	0.7689 ± 0.0197	0.97	0.359	3677 ± 72	3746 ± 47	98
A8	Sector zoned core	47	66	45	1.46	31.8266 ± 0.8434	0.7064 ± 0.0181	0.97	0.327	3445 ± 68	3602 ± 48	96
A9-C	Sector zoned core	32	38	30	1.29	35.8290 ± 0.9626	0.7503 ± 0.0193	0.96	0.346	3609 ± 71	3691 ± 48	98
A9-R	Black rim	265	86	309	0.28	32.1244 ± 0.8382	0.7079 ± 0.0179	0.97	0.329	3451 ± 68	3613 ± 47	96
A10	Sector zoned core	57	70	57	1.23	31.0210 ± 0.8210	0.6964 ± 0.0178	0.97	0.323	3407 ± 68	3584 ± 48	95
A11	Black core	126	13	150	0.08	32.9162 ± 0.8645	0.7170 ± 0.0182	0.97	0.333	3485 ± 68	3631 ± 47	96
A12-C	White core	55	60	51	1.19	37.2869 ± 0.9861	0.7575 ± 0.0194	0.97	0.357	3635 ± 71	3737 ± 47	97
A12-R	Osci. zoned rim	176	32	210	0.15	32.3081 ± 0.8463	0.7105 ± 0.0180	0.97	0.330	3460 ± 68	3616 ± 47	96
A13	Sector zoned core	71	58	70	0.82	36.0059 ± 0.9514	0.7522 ± 0.0192	0.97	0.347	3616 ± 71	3694 ± 47	98
A14-C	Sector zoned core	43	45	42	1.05	34.7670 ± 0.9264	0.7350 ± 0.0188	0.96	0.343	3552 ± 70	3676 ± 47	97
A14-R	Black rim	333	36	423	0.08	29.2225 ± 0.7623	0.6835 ± 0.0173	0.97	0.310	3358 ± 66	3521 ± 47	95

Continued on next page

Table B.3 – *Continued from previous page*

Spot #	Internal Structure	Pb (ppm)	Th (ppm)	U (ppm)	Th/U	$^{207}Pb/^{235}U$ $\pm 2\sigma$	$^{206}Pb/^{238}U$ $\pm 2\sigma$	ρ	$\frac{^{207}Pb}{^{206}Pb}$ ^{206}Pb	Ages (Ma)$\pm 2\sigma$ $\frac{^{206}Pb}{^{238}U}$	Ages (Ma)$\pm 2\sigma$ $\frac{^{207}Pb}{^{206}Pb}$	Conc %
A15	Sector zoned core	27	24	27	0.88	35.8471 ± 0.9726	0.7461 ± 0.0193	0.95	0.348	3593 ± 71	3700 ± 48	97
B1-C	Black core	114	125	124	1.00	29.2689 ± 0.7700	0.6752 ± 0.0172	0.97	0.314	3326 ± 66	3543 ± 47	94
B1-R	Black rim	339	38	402	0.10	33.2811 ± 0.8689	0.7186 ± 0.0182	0.97	0.336	3491 ± 68	3644 ± 47	96
B2-C	Convoluted core	57	40	99	0.40	15.2307 ± 0.4060	0.5015 ± 0.0128	0.96	0.220	2620 ± 55	2983 ± 50	88
B3	Sector zoned core	79	104	75	1.39	33.1559 ± 0.8752	0.7187 ± 0.0183	0.96	0.335	3491 ± 69	3638 ± 47	96
B4	Sector zoned core	55	71	50	1.42	36.2237 ± 0.9617	0.7458 ± 0.0191	0.96	0.352	3592 ± 70	3717 ± 47	97
B5	Black	631	266	721	0.37	32.1138 ± 0.8395	0.7152 ± 0.0181	0.97	0.326	3478 ± 68	3597 ± 47	97
B6-C	inh. black core	103	12	208	0.06	13.8338 ± 0.3785	0.4657 ± 0.0120	0.94	0.215	2465 ± 53	2947 ± 51	84
B7	Metamict	59	20	73	0.28	28.6859 ± 0.7770	0.6751 ± 0.0174	0.95	0.308	3325 ± 67	3512 ± 49	95
B9	Metamict	261	28	327	0.09	30.9695 ± 0.8116	0.6871 ± 0.0174	0.97	0.327	3372 ± 67	3602 ± 47	94
B10-C	Osci. zoned core	40	54	44	1.21	27.4349 ± 0.7449	0.6370 ± 0.0164	0.95	0.312	3177 ± 65	3533 ± 49	90
B10-R	Black rim	316	66	374	0.18	32.5354 ± 0.8545	0.7107 ± 0.0180	0.96	0.332	3461 ± 68	3626 ± 47	95
B11	Metamict	355	27	441	0.06	31.2355 ± 0.8215	0.6965 ± 0.0177	0.97	0.325	3407 ± 67	3595 ± 47	95
B12	Osci. zoned core	24	22	25	0.88	32.0325 ± 0.8722	0.7025 ± 0.0182	0.95	0.331	3430 ± 69	3620 ± 48	95
B13	Inherited core	112	36	122	0.29	36.0174 ± 0.9540	0.7505 ± 0.0191	0.96	0.348	3610 ± 70	3698 ± 47	98
B14-C	Sector zoned core	34	35	33	1.07	36.2225 ± 0.9791	0.7496 ± 0.0193	0.95	0.350	3606 ± 71	3709 ± 48	97
B15-C	Sector zoned core	28	23	29	0.80	33.7895 ± 0.9119	0.7239 ± 0.0186	0.95	0.338	3511 ± 70	3656 ± 48	96
B15-R	Black rim	262	72	307	0.23	32.4105 ± 0.8553	0.7079 ± 0.0180	0.96	0.332	3450 ± 68	3627 ± 47	95
B16	Osci. zoned core	37	36	33	1.08	40.5463 ± 1.0899	0.7935 ± 0.0204	0.96	0.371	3766 ± 73	3794 ± 47	99
C1-C	Sector zoned core	261	34	305	0.11	33.8768 ± 0.8956	0.7202 ± 0.0183	0.96	0.341	3497 ± 69	3668 ± 47	95
C1-R	Black rim	143	22	171	0.13	32.4788 ± 0.8636	0.7057 ± 0.0180	0.96	0.334	3442 ± 68	3635 ± 48	95
C2	Black core	499	127	585	0.22	32.4196 ± 0.8556	0.7091 ± 0.0180	0.96	0.331	3455 ± 68	3624 ± 47	95
C3	Sector zoned core	41	50	49	1.02	25.1856 ± 0.6871	0.6260 ± 0.0161	0.94	0.292	3134 ± 64	3427 ± 49	91
C5	Sector zoned core	69	63	66	0.95	36.8569 ± 0.9840	0.7538 ± 0.0192	0.95	0.355	3621 ± 71	3727 ± 47	97
C6	Sector zoned core	47	57	56	1.02	24.4223 ± 0.6603	0.6164 ± 0.0158	0.95	0.287	3095 ± 63	3403 ± 49	91
C7	Black	797	70	999	0.07	30.5977 ± 0.8084	0.6867 ± 0.0174	0.96	0.323	3370 ± 67	3585 ± 47	94
C8-C	Sector zoned core	52	67	48	1.40	35.1840 ± 0.9487	0.7391 ± 0.0189	0.95	0.345	3567 ± 70	3686 ± 48	97
C8-R	Black rim	241	87	349	0.25	21.9148 ± 0.5817	0.6001 ± 0.0152	0.95	0.265	3030 ± 61	3276 ± 49	93
C9-C	Metamict core	382	281	413	0.68	32.1693 ± 0.8531	0.7089 ± 0.0180	0.96	0.329	3454 ± 68	3613 ± 47	96
C9-R	White rim	10	0	20	0.01	12.1632 ± 0.3861	0.4772 ± 0.0128	0.85	0.185	2515 ± 56	2697 ± 59	93

Continued on next page

Table B.3 – *Continued from previous page*

Spot #	Internal Structure	Pb (ppm)	Th (ppm)	U (ppm)	Th/U	$^{207}Pb/^{235}U$ $\pm 2\sigma$	$^{206}Pb/^{238}U$ $\pm 2\sigma$	ρ	$\frac{^{207}Pb}{^{206}Pb}$ ^{206}Pb	Ages (Ma)$\pm 2\sigma$ $\frac{^{206}Pb}{^{238}U}$	Ages (Ma)$\pm 2\sigma$ $\frac{^{207}Pb}{^{206}Pb}$	Conc %
C10	Sector zoned core	50	77	52	1.46	28.0104 ± 0.7583	0.6579 ± 0.0168	0.94	0.309	3259 ± 65	3515 ± 49	93
C11	Sector zoned core	31	33	31	1.07	33.5983 ± 0.9268	0.7211 ± 0.0187	0.94	0.338	3500 ± 70	3653 ± 49	96
C12	Sector zoned core	79	76	74	1.03	38.3146 ± 1.0283	0.7766 ± 0.0198	0.95	0.358	3705 ± 72	3741 ± 48	99
C13-C	Sector zoned core	37	42	34	1.24	36.7970 ± 1.0051	0.7518 ± 0.0194	0.94	0.355	3614 ± 71	3728 ± 48	97
C13-R	Metamict rim	374	26	569	0.05	21.7110 ± 0.5774	0.5988 ± 0.0152	0.95	0.263	3025 ± 61	3265 ± 49	93
C14	Grey core	64	44	76	0.57	30.3407 ± 0.8303	0.6540 ± 0.0168	0.94	0.337	3244 ± 66	3647 ± 49	89
C15	Sector zoned	37	38	38	1.02	34.7259 ± 0.9644	0.7220 ± 0.0187	0.93	0.349	3503 ± 70	3702 ± 49	95
C16	Sector zoned core	40	45	38	1.17	35.8631 ± 0.9783	0.7466 ± 0.0192	0.94	0.348	3595 ± 71	3700 ± 48	97
C17	Sector zoned core	48	54	47	1.14	35.1248 ± 0.9533	0.7267 ± 0.0186	0.94	0.350	3521 ± 69	3709 ± 48	95
D1	Sector zoned core	41	41	41	1.01	35.3869 ± 0.9624	0.7369 ± 0.0189	0.94	0.348	3559 ± 70	3699 ± 48	96
D2	White core	40	31	47	0.66	29.2149 ± 0.8003	0.6703 ± 0.0172	0.94	0.316	3307 ± 66	3551 ± 49	93
D4-C	Sector zoned core	46	48	44	1.10	36.2601 ± 0.9890	0.7488 ± 0.0192	0.94	0.351	3603 ± 71	3712 ± 48	97
D4-R	Black rim	424	159	502	0.32	31.4638 ± 0.8458	0.6927 ± 0.0176	0.95	0.329	3393 ± 67	3614 ± 48	94
D5	Black core	88	162	121	1.34	17.3886 ± 0.4831	0.5301 ± 0.0136	0.92	0.238	2742 ± 57	3106 ± 51	88
D6	Sector zoned core	31	33	31	1.07	32.7261 ± 0.9071	0.7111 ± 0.0184	0.93	0.334	3463 ± 69	3634 ± 49	95
D7	Sector zoned	49	52	49	1.04	33.0449 ± 0.9070	0.7113 ± 0.0183	0.94	0.337	3463 ± 69	3649 ± 49	95
D8	Sector zoned	40	38	44	0.87	31.7004 ± 0.8717	0.6958 ± 0.0179	0.94	0.330	3405 ± 68	3619 ± 49	94
D9	Sector zoned core	44	60	39	1.51	36.8366 ± 1.0102	0.7519 ± 0.0193	0.94	0.355	3614 ± 71	3730 ± 48	97
D10	Sector zoned	46	55	43	1.28	37.2889 ± 1.0246	0.7591 ± 0.0195	0.93	0.356	3641 ± 71	3734 ± 48	98
D11	Black	157	72	180	0.40	32.2350 ± 0.8716	0.7112 ± 0.0181	0.94	0.329	3463 ± 68	3611 ± 48	96
D12	Sector zoned core	85	79	81	0.97	38.8555 ± 1.0239	0.7809 ± 0.0200	0.97	0.361	3720 ± 72	3753 ± 47	99
D13	Sector zoned core	62	94	60	1.58	33.9548 ± 0.8989	0.7198 ± 0.0184	0.97	0.342	3495 ± 69	3672 ± 47	95
D14	Black	444	215	510	0.42	32.2196 ± 0.8444	0.6995 ± 0.0178	0.97	0.334	3419 ± 68	3636 ± 47	94
D15	Sector zoned core	58	60	55	1.11	37.6108 ± 0.9966	0.7575 ± 0.0194	0.97	0.360	3635 ± 71	3750 ± 47	97
D16-C	Grey core	43	40	47	0.86	31.6185 ± 0.8533	0.6831 ± 0.0176	0.95	0.336	3356 ± 68	3643 ± 48	92
D16-R	Black rim	384	38	457	0.08	33.2841 ± 0.8737	0.7173 ± 0.0183	0.97	0.337	3486 ± 69	3647 ± 47	96
D17-C	Sector zoned core	91	123	80	1.54	37.8025 ± 0.9966	0.7674 ± 0.0196	0.97	0.357	3671 ± 71	3738 ± 47	98
D17-R	Black rim	513	101	632	0.16	31.3697 ± 0.8205	0.6807 ± 0.0173	0.97	0.334	3347 ± 66	3636 ± 47	92
E1	Metamict	652	43	810	0.05	31.2702 ± 0.8194	0.6945 ± 0.0177	0.97	0.327	3400 ± 67	3601 ± 47	94
E2	Sector zoned	55	63	52	1.20	36.4212 ± 0.9711	0.7448 ± 0.0191	0.96	0.355	3588 ± 71	3727 ± 47	96

Continued on next page

Table B.3 – *Continued from previous page*

Spot #	Internal Structure	Pb (ppm)	Th (ppm)	U (ppm)	Th/U	$^{207}Pb/^{235}U$ $\pm 2\sigma$	$^{206}Pb/^{238}U$ $\pm 2\sigma$	ρ	$\frac{^{207}Pb}{^{206}Pb}$ ^{206}Pb	Ages (Ma)$\pm 2\sigma$ $\frac{^{206}Pb}{^{238}U}$	Ages (Ma)$\pm 2\sigma$ $\frac{^{207}Pb}{^{206}Pb}$	Conc %
E3	Sector zoned	44	57	38	1.49	37.9453 ± 1.0138	0.7671 ± 0.0197	0.96	0.359	3670 ± 72	3744 ± 47	98
E4	Sector zoned	43	41	39	1.05	39.6112 ± 1.0606	0.7848 ± 0.0202	0.96	0.366	3734 ± 73	3775 ± 47	99
E5-C	Sector zoned core	39	41	37	1.10	36.3234 ± 0.9730	0.7472 ± 0.0192	0.96	0.353	3597 ± 71	3718 ± 47	97
E5-R	Black rim	126	3	144	0.02	35.9694 ± 0.9570	0.7444 ± 0.0191	0.96	0.350	3587 ± 71	3709 ± 47	97
E6	Sector zoned core	73	30	79	0.38	35.8302 ± 0.9484	0.7385 ± 0.0189	0.97	0.352	3565 ± 70	3715 ± 47	96
E7	Sector zoned	34	49	33	1.48	31.5721 ± 0.8486	0.6934 ± 0.0179	0.96	0.330	3396 ± 68	3618 ± 48	94
E8	Sector zoned	38	46	40	1.15	29.9389 ± 0.8090	0.6778 ± 0.0175	0.96	0.320	3336 ± 67	3571 ± 48	93
E9	Sector zoned	20	20	22	0.93	31.2221 ± 0.8636	0.6910 ± 0.0181	0.95	0.328	3387 ± 69	3606 ± 49	94
E10-C	Sector zoned core	73	96	70	1.37	34.7321 ± 0.9286	0.7248 ± 0.0186	0.96	0.347	3514 ± 70	3696 ± 47	95
E10-R	Black rim	446	50	575	0.09	29.3926 ± 0.7712	0.6696 ± 0.0170	0.97	0.318	3304 ± 66	3562 ± 47	93
E11	Sector zoned core	41	45	39	1.16	36.4973 ± 0.9811	0.7473 ± 0.0193	0.96	0.354	3598 ± 71	3725 ± 47	97
E12-C	Sector zoned	50	50	45	1.10	40.1410 ± 1.0801	0.7873 ± 0.0203	0.96	0.370	3743 ± 73	3790 ± 47	99
E13-C	Sector zoned	43	47	39	1.20	38.8825 ± 1.0577	0.7740 ± 0.0201	0.95	0.364	3695 ± 73	3768 ± 48	98
E12-R	Black rim	188	51	224	0.23	32.1048 ± 0.8513	0.7003 ± 0.0179	0.96	0.332	3422 ± 68	3628 ± 47	94
E14-C	Sector zoned	55	54	51	1.06	37.9912 ± 1.0159	0.7618 ± 0.0196	0.96	0.362	3651 ± 72	3757 ± 47	97
E15	Sector zoned	43	41	42	0.98	36.4475 ± 0.9783	0.7428 ± 0.0191	0.96	0.356	3581 ± 71	3732 ± 47	96
E16	Sector zoned	60	81	56	1.46	35.1490 ± 0.9461	0.7310 ± 0.0188	0.96	0.349	3537 ± 70	3701 ± 48	96
E17	Sector zoned	38	38	38	1.00	34.3249 ± 0.9275	0.7261 ± 0.0188	0.96	0.343	3519 ± 70	3675 ± 48	96
F1	Sector zoned	53	71	62	1.14	25.1350 ± 0.6749	0.6221 ± 0.0160	0.96	0.293	3118 ± 64	3434 ± 48	91
F2	Sector zoned	50	61	46	1.35	37.3235 ± 1.0000	0.7586 ± 0.0195	0.96	0.357	3639 ± 72	3736 ± 47	97
F3	Sector zoned	37	38	35	1.08	36.8303 ± 0.9936	0.7526 ± 0.0194	0.96	0.355	3617 ± 71	3728 ± 48	97
F4	Sector zoned	37	36	37	0.98	34.3684 ± 0.9321	0.7258 ± 0.0188	0.96	0.343	3518 ± 70	3678 ± 48	96
F5-C	Black core	248	6	295	0.02	34.1766 ± 0.9039	0.7241 ± 0.0185	0.97	0.342	3512 ± 69	3673 ± 47	96
F5-R	Sector zoned	44	39	42	0.94	37.5876 ± 1.0112	0.7601 ± 0.0196	0.96	0.359	3644 ± 72	3744 ± 47	97
F6	Sector zoned	34	35	32	1.09	37.6508 ± 1.0249	0.7568 ± 0.0196	0.95	0.361	3633 ± 72	3753 ± 48	97
F7	Sector zoned	30	30	33	0.89	29.7421 ± 0.8107	0.6723 ± 0.0174	0.95	0.321	3315 ± 67	3574 ± 48	93
F8	Black core	53	93	67	1.39	20.8971 ± 0.5768	0.5581 ± 0.0145	0.94	0.272	2859 ± 60	3315 ± 50	86
F9-C	Sector zoned core	57	68	52	1.31	37.5610 ± 1.0094	0.7592 ± 0.0195	0.96	0.359	3641 ± 72	3745 ± 47	97
F9-R	Black rim	198	37	246	0.15	30.8363 ± 0.8231	0.6861 ± 0.0176	0.96	0.326	3368 ± 67	3598 ± 48	94
F10	Sector zoned	28	43	41	1.06	15.7225 ± 0.4343	0.5318 ± 0.0138	0.94	0.214	2749 ± 58	2939 ± 51	94

Continued on next page

Table B.3 – *Continued from previous page*

Spot #	Internal Structure	Pb (ppm)	Th (ppm)	U (ppm)	Th/U	$^{207}Pb/^{235}U$ $\pm 2\sigma$	$^{206}Pb/^{238}U$ $\pm 2\sigma$	ρ	$\frac{^{207}Pb}{^{206}Pb}$ ^{206}Pb	Ages (Ma)$\pm 2\sigma$ $\frac{^{206}Pb}{^{238}U}$	Ages (Ma)$\pm 2\sigma$ $\frac{^{207}Pb}{^{206}Pb}$	Conc %
F11	Sector zoned	42	43	39	1.09	37.2790 ± 1.0109	0.7563 ± 0.0196	0.96	0.357	3631 ± 72	3739 ± 48	97
F12	Sector zoned	38	44	36	1.22	35.7264 ± 0.9665	0.7406 ± 0.0191	0.95	0.350	3573 ± 71	3706 ± 48	96
F13	Sector zoned	47	49	45	1.10	36.9511 ± 0.9980	0.7484 ± 0.0193	0.95	0.358	3602 ± 71	3742 ± 48	96
F14	Sector zoned	39	41	41	1.01	31.7121 ± 0.8616	0.6968 ± 0.0180	0.95	0.330	3409 ± 68	3617 ± 48	94
F15	Sector zoned	37	37	34	1.10	38.1522 ± 1.0366	0.7662 ± 0.0198	0.95	0.361	3667 ± 72	3755 ± 48	98
F16	Sector zoned	32	27	33	0.81	35.1496 ± 0.9600	0.7333 ± 0.0190	0.95	0.348	3546 ± 71	3697 ± 48	96
F17	Sector zoned	44	45	43	1.05	36.2359 ± 0.9826	0.7457 ± 0.0193	0.95	0.352	3592 ± 71	3717 ± 48	97
F18	Sector zoned	39	41	37	1.12	36.9713 ± 1.0088	0.7538 ± 0.0195	0.95	0.356	3622 ± 72	3732 ± 48	97
SG-027 Mg-tonalite												
A1	Metamict	364	164	658	0.25	13.3657 ± 0.3548	0.5067 ± 0.0132	0.98	0.191	2643 ± 57	2753 ± 50	96
A2-C	Osci. zoned core	33	0	64	0.00	13.7645 ± 0.3713	0.4978 ± 0.0131	0.98	0.200	2604 ± 56	2830 ± 50	92
A2-R	Osci. zoned rim	288	61	521	0.12	14.0205 ± 0.3722	0.5203 ± 0.0136	0.98	0.195	2700 ± 58	2788 ± 50	97
A3	Black core	463	144	608	0.24	25.9488 ± 0.6882	0.6485 ± 0.0170	0.99	0.290	3222 ± 66	3418 ± 47	94
A4	Sector zoned	188	78	226	0.35	29.4212 ± 0.7821	0.6857 ± 0.0179	0.98	0.311	3366 ± 69	3527 ± 47	95
A5-C	Black core	121	179	223	0.80	10.5987 ± 0.2832	0.4487 ± 0.0118	0.98	0.171	2390 ± 52	2570 ± 51	93
A6-C	White core	76	1	139	0.01	14.1776 ± 0.3795	0.5230 ± 0.0137	0.98	0.197	2712 ± 58	2798 ± 50	97
A6-R	Rim	81	65	150	0.43	11.7543 ± 0.3146	0.4790 ± 0.0126	0.98	0.178	2523 ± 55	2634 ± 50	96
A7	Sector zoned	460	125	529	0.24	32.3729 ± 0.8609	0.7259 ± 0.0190	0.98	0.323	3518 ± 71	3586 ± 46	98
A8-C	Black core	380	126	430	0.29	32.1304 ± 0.8552	0.7288 ± 0.0191	0.98	0.320	3529 ± 71	3568 ± 47	99
A8-R	Black rim	258	26	474	0.06	13.9143 ± 0.3707	0.5179 ± 0.0136	0.99	0.195	2690 ± 58	2783 ± 50	97
A9	Sector zoned	579	200	669	0.30	31.2077 ± 0.8305	0.7153 ± 0.0188	0.99	0.316	3478 ± 70	3552 ± 47	98
A10-C	White core	20	4	38	0.10	14.0134 ± 0.3866	0.5187 ± 0.0137	0.96	0.196	2694 ± 58	2792 ± 51	96
A10-R	Black rim	427	202	744	0.27	13.8752 ± 0.3702	0.5207 ± 0.0137	0.99	0.193	2702 ± 58	2770 ± 50	98
A11	Sector zoned	448	124	517	0.24	31.9227 ± 0.8514	0.7216 ± 0.0189	0.98	0.321	3502 ± 71	3574 ± 47	98
A12-C	Black core	863	137	2534	0.05	8.6292 ± 0.2303	0.3238 ± 0.0085	0.98	0.193	1808 ± 41	2770 ± 50	65
A12-R	Black rim	248	34	460	0.07	13.6573 ± 0.3652	0.5149 ± 0.0135	0.98	0.192	2678 ± 58	2762 ± 50	97
A13	Black core	571	157	646	0.24	32.3335 ± 0.8634	0.7376 ± 0.0194	0.98	0.318	3562 ± 72	3560 ± 47	100
A14-C	Metamict core	1372	145	1944	0.07	24.3921 ± 0.6514	0.6269 ± 0.0165	0.99	0.282	3137 ± 65	3375 ± 47	93
A14-R	Black rim	466	8	844	0.01	14.4713 ± 0.3868	0.5334 ± 0.0140	0.98	0.197	2756 ± 59	2799 ± 50	98
A15	Sector zoned	477	134	534	0.25	33.3340 ± 0.8914	0.7394 ± 0.0194	0.98	0.327	3568 ± 72	3603 ± 47	99

Continued on next page

Table B.3 – *Continued from previous page*

Spot #	**Internal Structure**	**Pb (ppm)**	**Th (ppm)**	**U (ppm)**	**Th/U**	^{207}**Pb**/^{235}**U** $\pm 2\sigma$	^{206}**Pb**/^{238}**U** $\pm 2\sigma$	ρ	$\frac{^{207}Pb}{^{206}Pb}$ ^{206}Pb	**Ages (Ma)**$\pm 2\sigma$ $\frac{^{206}Pb}{^{238}U}$	$\frac{^{207}Pb}{^{206}Pb}$	**Conc** %
A16-C	Sector zoned core	538	73	671	0.11	29.8778 ± 0.7999	0.6903 ± 0.0182	0.98	0.314	3384 ± 69	3540 ± 47	96
A16-R	Black rim	514	101	921	0.11	14.3728 ± 0.3850	0.5252 ± 0.0138	0.98	0.198	2721 ± 58	2813 ± 50	97
A17-C	Black core	362	218	609	0.36	14.0426 ± 0.3766	0.5271 ± 0.0139	0.98	0.193	2729 ± 59	2770 ± 50	99
A17-R	Black rim	260	285	463	0.62	11.4244 ± 0.3068	0.4777 ± 0.0126	0.98	0.173	2517 ± 55	2591 ± 51	97
A18	Sector zoned core	779	408	955	0.43	28.0323 ± 0.7525	0.6648 ± 0.0175	0.98	0.306	3286 ± 68	3500 ± 47	94
B1	Osci. zoned core	415	148	467	0.32	32.2722 ± 0.8663	0.7299 ± 0.0192	0.98	0.321	3533 ± 72	3573 ± 47	99
B2	Sector zoned core	402	142	448	0.32	33.0752 ± 0.8882	0.7372 ± 0.0194	0.98	0.325	3560 ± 72	3595 ± 47	99
B3-C	Black core	492	175	551	0.32	32.5778 ± 0.8751	0.7342 ± 0.0193	0.98	0.322	3549 ± 72	3578 ± 47	99
B3-R	White zoned rim	45	2	86	0.02	13.8799 ± 0.3809	0.5014 ± 0.0133	0.97	0.201	2620 ± 57	2832 ± 50	92
B4-C	Sector zoned core	457	155	514	0.30	32.5657 ± 0.8768	0.7333 ± 0.0193	0.98	0.322	3546 ± 72	3580 ± 47	99
B4-R	Black rim	371	106	659	0.16	14.0891 ± 0.3797	0.5259 ± 0.0139	0.98	0.194	2724 ± 59	2779 ± 50	98
B5-C	Sector zoned core	418	143	465	0.31	33.0422 ± 0.8906	0.7380 ± 0.0194	0.98	0.325	3563 ± 72	3592 ± 47	99
B5-R	Osci. zoned rim	129	115	235	0.49	11.6575 ± 0.3157	0.4828 ± 0.0128	0.98	0.175	2539 ± 55	2607 ± 51	97
B6	Black core	454	138	512	0.27	32.7212 ± 0.8829	0.7332 ± 0.0193	0.98	0.324	3545 ± 72	3587 ± 47	99
B7-C	Black core	384	107	457	0.23	30.9159 ± 0.8351	0.7038 ± 0.0186	0.98	0.319	3435 ± 70	3563 ± 47	96
B7-R	Black rim	232	24	419	0.06	14.2404 ± 0.3853	0.5278 ± 0.0139	0.97	0.196	2732 ± 59	2790 ± 50	98
B8-C	Black core	456	77	533	0.14	32.1132 ± 0.8690	0.7284 ± 0.0192	0.97	0.320	3528 ± 72	3568 ± 47	99
B8-R	Black rim	200	49	349	0.14	14.3253 ± 0.3886	0.5396 ± 0.0143	0.98	0.193	2782 ± 60	2764 ± 50	101
B9	Sector zoned core	506	161	577	0.28	31.9187 ± 0.8647	0.7287 ± 0.0192	0.97	0.318	3529 ± 72	3558 ± 47	99
B10	Sector zoned core	476	149	540	0.28	32.3426 ± 0.8768	0.7316 ± 0.0193	0.97	0.321	3540 ± 72	3573 ± 47	99
B11-C	Osci. zoned core	546	160	629	0.25	31.6795 ± 0.8593	0.7222 ± 0.0191	0.98	0.318	3504 ± 71	3561 ± 47	98
B11-R	Osci. zoned rim	192	46	342	0.13	14.1130 ± 0.3838	0.5255 ± 0.0139	0.97	0.195	2723 ± 59	2783 ± 50	98
B12-C	Sector zoned core	723	313	857	0.37	29.3490 ± 0.7973	0.6925 ± 0.0183	0.97	0.307	3392 ± 70	3508 ± 47	97
B12-R	Osci. zoned rim	319	152	560	0.27	13.6874 ± 0.3724	0.5163 ± 0.0137	0.98	0.192	2684 ± 58	2761 ± 50	97
B13	Sector zoned core	331	91	386	0.23	31.3954 ± 0.8553	0.7170 ± 0.0190	0.97	0.318	3485 ± 71	3558 ± 47	98
B14-C	Sector zoned core	364	106	416	0.25	32.2510 ± 0.8792	0.7248 ± 0.0192	0.97	0.323	3514 ± 72	3583 ± 47	98
B14-R	Black rim	555	227	983	0.23	13.3167 ± 0.3632	0.5203 ± 0.0138	0.97	0.186	2700 ± 58	2704 ± 51	100
B15	Sector zoned	481	182	556	0.33	30.5394 ± 0.8334	0.7133 ± 0.0189	0.97	0.310	3471 ± 71	3523 ± 47	99
B16	Sector zoned core	308	4	359	0.01	34.0225 ± 0.9294	0.7402 ± 0.0196	0.97	0.333	3571 ± 73	3632 ± 47	98
C1	Sector zoned core	484	156	542	0.29	32.9181 ± 0.8995	0.7380 ± 0.0196	0.97	0.323	3563 ± 73	3586 ± 47	99

Continued on next page

Table B.3 – *Continued from previous page*

Spot #	Internal Structure	Pb (ppm)	Th (ppm)	U (ppm)	Th/U	$^{207}Pb/^{235}U$ $\pm 2\sigma$	$^{206}Pb/^{238}U$ $\pm 2\sigma$	ρ	$\frac{^{207}Pb}{^{206}Pb}$ ^{206}Pb	Ages (Ma)$\pm 2\sigma$ $\frac{^{206}Pb}{^{238}U}$	Ages (Ma)$\pm 2\sigma$ $\frac{^{207}Pb}{^{206}Pb}$	Conc %
C2-C	Sector zoned core	411	149	486	0.31	30.3411 ± 0.8299	0.7009 ± 0.0186	0.97	0.314	3424 ± 70	3540 ± 47	97
C2-R	Osci. zoned rim	214	23	374	0.06	14.8663 ± 0.4075	0.5449 ± 0.0145	0.97	0.198	2804 ± 60	2809 ± 50	100
C3-C	Osci. zoned core	352	111	392	0.28	33.2351 ± 0.9118	0.7402 ± 0.0197	0.97	0.325	3572 ± 73	3596 ± 47	99
C3-R	Osci. zoned rim	621	25	1395	0.02	9.6956 ± 0.2661	0.4420 ± 0.0117	0.96	0.159	2360 ± 52	2446 ± 52	96
C4	Sector zoned	529	193	605	0.32	31.4181 ± 0.8629	0.7252 ± 0.0192	0.96	0.314	3516 ± 72	3541 ± 47	99
C5	Osci. zoned core	368	15	435	0.03	32.6556 ± 0.8978	0.7360 ± 0.0195	0.96	0.322	3556 ± 73	3578 ± 47	99
C6	Sector zoned core	424	137	487	0.28	32.0251 ± 0.8811	0.7210 ± 0.0191	0.96	0.322	3500 ± 72	3580 ± 47	98
C7	Sector zoned core	473	144	578	0.25	29.1250 ± 0.8018	0.6893 ± 0.0183	0.96	0.306	3380 ± 70	3503 ± 48	96
C8	Black core	669	215	829	0.26	28.5349 ± 0.7865	0.6803 ± 0.0181	0.97	0.304	3345 ± 69	3492 ± 48	96
C9-C	Osci. zoned core	734	295	1034	0.29	23.0899 ± 0.6365	0.6086 ± 0.0162	0.97	0.275	3065 ± 65	3335 ± 48	92
C9-R	Grey rim	233	34	427	0.08	13.8056 ± 0.3821	0.5188 ± 0.0138	0.96	0.193	2694 ± 59	2768 ± 51	97
C10	Sector zoned core	606	50	772	0.06	28.8313 ± 0.7979	0.6888 ± 0.0183	0.96	0.303	3378 ± 70	3488 ± 48	97
C11-R	Sector zoned rim	167	156	298	0.52	11.7570 ± 0.3268	0.4886 ± 0.0130	0.96	0.174	2565 ± 56	2601 ± 52	99
C12	Convoluted core	595	169	690	0.25	31.3929 ± 0.8704	0.7202 ± 0.0192	0.96	0.316	3497 ± 72	3551 ± 48	98
C13	Sector zoned core	626	172	716	0.24	32.0946 ± 0.8905	0.7279 ± 0.0194	0.96	0.320	3526 ± 72	3569 ± 48	99
C14-C	Osci. zoned core	1047	2	1689	0.00	19.5589 ± 0.5436	0.5738 ± 0.0153	0.96	0.247	2923 ± 63	3167 ± 49	92
C14-R	Black rim	298	12	541	0.02	14.1368 ± 0.3935	0.5294 ± 0.0141	0.96	0.194	2739 ± 59	2773 ± 51	99
C15-C	Osci. zoned core	474	159	540	0.29	32.1431 ± 0.8742	0.7307 ± 0.0197	0.99	0.319	3536 ± 73	3565 ± 46	99
C15-R	Osci. zoned rim	274	15	486	0.03	14.5901 ± 0.3977	0.5423 ± 0.0146	0.99	0.195	2793 ± 61	2786 ± 50	100
D1	White core	65	0	115	0.00	14.9643 ± 0.4097	0.5454 ± 0.0147	0.98	0.199	2806 ± 61	2818 ± 50	100
D2-C	Black core	849	50	1083	0.05	28.5386 ± 0.7765	0.6932 ± 0.0186	0.99	0.299	3395 ± 71	3463 ± 47	98
D2-R	Black rim	225	12	397	0.03	14.9390 ± 0.4070	0.5430 ± 0.0146	0.99	0.199	2796 ± 61	2822 ± 49	99
D3-C	White core	322	178	549	0.33	14.1486 ± 0.3857	0.5291 ± 0.0142	0.98	0.194	2738 ± 60	2776 ± 50	99
D3-R	Black rim	376	194	644	0.30	14.1888 ± 0.3864	0.5320 ± 0.0143	0.99	0.193	2750 ± 60	2771 ± 50	99
D4	Sector zoned core	679	248	798	0.31	30.3756 ± 0.8269	0.7117 ± 0.0191	0.99	0.310	3465 ± 72	3519 ± 47	98
D5	Black core	418	137	470	0.29	32.8892 ± 0.8953	0.7383 ± 0.0199	0.99	0.323	3564 ± 74	3584 ± 46	99
D6-C	Black core	419	205	461	0.44	32.5583 ± 0.8864	0.7349 ± 0.0198	0.99	0.321	3552 ± 73	3576 ± 46	99
D6-R	Osci. zoned rim	446	195	776	0.25	13.9889 ± 0.3810	0.5295 ± 0.0143	0.99	0.192	2739 ± 60	2756 ± 50	99
D7-C	Black core	534	229	593	0.39	32.2808 ± 0.8789	0.7378 ± 0.0199	0.99	0.317	3563 ± 74	3557 ± 46	100
D7-R	Black rim	278	34	503	0.07	14.2601 ± 0.3891	0.5298 ± 0.0143	0.99	0.195	2741 ± 60	2786 ± 50	98

Continued on next page

Table B.3 – *Continued from previous page*

Spot #	Internal Structure	Pb (ppm)	Th (ppm)	U (ppm)	Th/U	$^{207}Pb/^{235}U$ $\pm 2\sigma$	$^{206}Pb/^{238}U$ $\pm 2\sigma$	ρ	$\frac{^{207}Pb}{^{206}Pb}$ ^{206}Pb	Ages (Ma)$\pm 2\sigma$ $\frac{^{206}Pb}{^{238}U}$	Ages (Ma)$\pm 2\sigma$ $\frac{^{207}Pb}{^{206}Pb}$	Conc %
D8	Black core	482	203	540	0.38	32.3288 ± 0.8804	0.7311 ± 0.0197	0.99	0.321	3538 ± 73	3573 ± 46	99
D9	Black core	403	124	451	0.28	33.2528 ± 0.9059	0.7433 ± 0.0200	0.99	0.324	3583 ± 74	3591 ± 46	100
D10	Black core	404	117	463	0.25	32.2019 ± 0.8775	0.7309 ± 0.0197	0.99	0.319	3537 ± 73	3567 ± 46	99
D11-C	Black core	463	171	529	0.32	31.3953 ± 0.8555	0.7273 ± 0.0196	0.99	0.313	3524 ± 73	3536 ± 47	100
D11-R	Osci. zoned rim	108	7	191	0.04	14.8807 ± 0.4073	0.5446 ± 0.0147	0.99	0.198	2803 ± 61	2811 ± 50	100
D12	Cracked core	1133	105	1429	0.07	28.4129 ± 0.7742	0.6973 ± 0.0188	0.99	0.296	3411 ± 71	3447 ± 47	99
D13	Sector zoned	509	151	576	0.26	32.4470 ± 0.8845	0.7358 ± 0.0198	0.99	0.320	3555 ± 74	3569 ± 46	100
D14	Sector zoned core	463	140	526	0.27	32.1814 ± 0.8774	0.7322 ± 0.0197	0.99	0.319	3542 ± 73	3564 ± 46	99
D15-C	Osci. zoned core	459	139	523	0.26	32.1429 ± 0.8765	0.7308 ± 0.0197	0.99	0.319	3536 ± 73	3565 ± 46	99
D15-R	Cracked rim	202	82	350	0.23	14.0226 ± 0.3832	0.5317 ± 0.0143	0.98	0.191	2749 ± 60	2753 ± 50	100
D16	Sector zoned core	406	133	481	0.28	30.0837 ± 0.8209	0.7049 ± 0.0190	0.99	0.309	3439 ± 72	3518 ± 47	98
D17	Sector zoned core	700	234	815	0.29	30.4623 ± 0.8313	0.7200 ± 0.0194	0.99	0.307	3496 ± 73	3505 ± 47	100
E1	Oscillatory zoned	474	154	532	0.29	32.2792 ± 0.8811	0.7363 ± 0.0198	0.99	0.318	3557 ± 74	3560 ± 47	100
E2-C	Metamict core	422	211	715	0.30	13.9322 ± 0.3807	0.5337 ± 0.0144	0.99	0.189	2757 ± 60	2736 ± 50	101
E2-R	Black rim	150	162	269	0.60	11.3686 ± 0.3128	0.4816 ± 0.0130	0.98	0.171	2534 ± 57	2569 ± 51	99
E3	Black core	387	82	432	0.19	33.6171 ± 0.9180	0.7498 ± 0.0202	0.99	0.325	3607 ± 74	3594 ± 46	100
E4	Osci. zoned core	390	164	429	0.38	32.3900 ± 0.8847	0.7377 ± 0.0199	0.99	0.318	3562 ± 74	3562 ± 47	100
E5	Black	545	164	605	0.27	32.9138 ± 0.8995	0.7459 ± 0.0201	0.99	0.320	3593 ± 74	3570 ± 47	101
E6-C	Black core	385	118	436	0.27	31.9422 ± 0.8733	0.7350 ± 0.0198	0.99	0.315	3552 ± 74	3546 ± 47	100
E6-R	White inner rim	41	1	75	0.01	14.2728 ± 0.3947	0.5299 ± 0.0143	0.98	0.195	2741 ± 60	2788 ± 50	98
E7	Black core	727	222	837	0.27	30.7176 ± 0.8396	0.7283 ± 0.0196	0.98	0.306	3527 ± 73	3500 ± 47	101
E8	Black core	354	142	397	0.36	32.0430 ± 0.8764	0.7266 ± 0.0196	0.99	0.320	3521 ± 73	3569 ± 47	99
E9	Black core	285	110	380	0.29	23.7894 ± 0.6511	0.6401 ± 0.0173	0.99	0.269	3189 ± 68	3303 ± 47	97
E10-C	Osci. zoned core	415	9	491	0.02	32.6501 ± 0.8931	0.7383 ± 0.0199	0.99	0.321	3564 ± 74	3573 ± 47	100
E10-R	Osci. zoned rim	322	5	570	0.01	15.0846 ± 0.4130	0.5426 ± 0.0146	0.98	0.202	2794 ± 61	2839 ± 49	98
E11-C	Metamict core	1199	138	1704	0.08	22.6689 ± 0.6202	0.6365 ± 0.0172	0.99	0.258	3175 ± 68	3236 ± 48	98
E11-R	Black rim	202	8	373	0.02	13.7593 ± 0.3778	0.5225 ± 0.0141	0.98	0.191	2710 ± 60	2750 ± 50	99
E12-R	Black rim	108	3	189	0.02	14.8604 ± 0.4085	0.5485 ± 0.0148	0.98	0.196	2819 ± 62	2797 ± 50	101
E13	Black core	404	131	464	0.28	31.2188 ± 0.8553	0.7267 ± 0.0196	0.98	0.312	3521 ± 73	3529 ± 47	100
E14	Osci. zoned core	303	120	339	0.35	32.7471 ± 0.8978	0.7395 ± 0.0200	0.99	0.321	3569 ± 74	3575 ± 47	100

Continued on next page

Table B.3 – *Continued from previous page*

Spot #	Internal Structure	Pb (ppm)	Th (ppm)	U (ppm)	Th/U	$^{207}Pb/^{235}U$ ±2σ	$^{206}Pb/^{238}U$ ±2σ	ρ	$\frac{^{207}Pb}{^{206}Pb}$ ^{206}Pb	Ages (Ma)±2σ $\frac{^{206}Pb}{^{238}U}$	Ages (Ma)±2σ $\frac{^{207}Pb}{^{206}Pb}$	Conc %
E15-C	Osci. zoned core	480	205	544	0.38	31.9180 ± 0.8747	0.7304 ± 0.0197	0.98	0.317	3535 ± 73	3555 ± 47	99
E15-R	Black rim	177	25	309	0.08	14.8013 ± 0.4067	0.5457 ± 0.0147	0.98	0.197	2807 ± 61	2799 ± 50	100
E16	Black core	483	203	569	0.36	30.2963 ± 0.8306	0.7092 ± 0.0191	0.98	0.310	3456 ± 72	3520 ± 47	98
E17-C	Black core	457	193	522	0.37	31.6535 ± 0.8690	0.7280 ± 0.0197	0.99	0.315	3526 ± 73	3547 ± 47	99
E17-R	Sector zoned rim	228	109	402	0.27	13.7303 ± 0.3774	0.5247 ± 0.0142	0.98	0.190	2719 ± 60	2740 ± 50	99
E18-C	Black core	555	226	617	0.37	32.9077 ± 0.9031	0.7452 ± 0.0201	0.98	0.320	3590 ± 74	3571 ± 47	101
E18-R2	White inner rim	395	68	679	0.10	15.1627 ± 0.4165	0.5493 ± 0.0148	0.98	0.200	2822 ± 62	2828 ± 49	100
E18-R1	Black rim	22	0	39	0.00	14.2386 ± 0.4012	0.5307 ± 0.0144	0.96	0.195	2744 ± 61	2781 ± 51	99
F1	Metamict core	364	147	397	0.37	33.5881 ± 0.9236	0.7493 ± 0.0203	0.99	0.325	3605 ± 75	3594 ± 47	100
F2-C	White core	71	60	72	0.83	34.3471 ± 0.9534	0.7468 ± 0.0203	0.98	0.333	3596 ± 75	3633 ± 47	99
F2-R	Osci. zoned rim	147	31	248	0.13	15.2399 ± 0.4209	0.5517 ± 0.0149	0.98	0.200	2832 ± 62	2829 ± 50	100
F3-R	Black rim	166	12	294	0.04	14.5506 ± 0.4013	0.5395 ± 0.0146	0.98	0.196	2781 ± 61	2790 ± 50	100
F4	Black core	495	155	572	0.27	31.4009 ± 0.8640	0.7240 ± 0.0196	0.98	0.314	3511 ± 73	3543 ± 47	99
F5	Sector zoned core	465	148	522	0.28	33.0057 ± 0.9085	0.7398 ± 0.0200	0.98	0.324	3570 ± 74	3587 ± 47	100
F6	Osci. zoned core	612	205	700	0.29	31.4533 ± 0.8657	0.7324 ± 0.0198	0.98	0.311	3542 ± 74	3528 ± 47	100
F7	Osci. zoned core	194	25	343	0.07	14.5360 ± 0.4010	0.5397 ± 0.0146	0.98	0.195	2782 ± 61	2787 ± 50	100
F8	Black core	700	273	826	0.33	29.9410 ± 0.8248	0.7070 ± 0.0191	0.98	0.307	3447 ± 72	3506 ± 47	98
F9	Black core	514	168	589	0.29	31.6515 ± 0.8726	0.7308 ± 0.0197	0.98	0.314	3536 ± 74	3541 ± 47	100
F10-C	Black core	346	10	402	0.03	33.5046 ± 0.9244	0.7450 ± 0.0201	0.98	0.326	3589 ± 74	3599 ± 47	100
F10-R	Black rim	87	2	155	0.02	14.8389 ± 0.4115	0.5426 ± 0.0147	0.98	0.198	2794 ± 61	2812 ± 50	99
F11-C	Black core	511	176	581	0.30	31.8976 ± 0.8801	0.7328 ± 0.0198	0.98	0.316	3544 ± 74	3549 ± 47	100
F11-R	Grey rim	173	118	286	0.41	14.2767 ± 0.3951	0.5292 ± 0.0143	0.98	0.196	2738 ± 60	2790 ± 50	98
F12	Osci. zoned core	430	154	474	0.32	33.4752 ± 0.9243	0.7476 ± 0.0202	0.98	0.325	3599 ± 75	3592 ± 47	100
F14	Black core	570	195	643	0.30	32.3096 ± 0.8924	0.7365 ± 0.0199	0.98	0.318	3558 ± 74	3561 ± 47	100
F15	Black core	537	183	611	0.30	31.7257 ± 0.8771	0.7327 ± 0.0198	0.98	0.314	3543 ± 74	3541 ± 47	100
F16	Metamict	404	26	748	0.04	13.8720 ± 0.3843	0.5201 ± 0.0141	0.98	0.193	2700 ± 60	2771 ± 50	97
F17	Black core	478	169	534	0.32	32.8931 ± 0.9100	0.7412 ± 0.0200	0.98	0.322	3575 ± 74	3579 ± 47	100
SG-037 granite												
A1	Black core	519	145	1094	0.13	11.5017 ± 0.3027	0.4543 ± 0.0118	0.99	0.184	2414 ± 52	2686 ± 50	90
A2	Black core	577	383	1114	0.34	11.2779 ± 0.2962	0.4836 ± 0.0125	0.98	0.169	2543 ± 54	2549 ± 51	100

Continued on next page

Table B.3 – *Continued from previous page*

Spot #	Internal Structure	Pb (ppm)	Th (ppm)	U (ppm)	Th/U	$^{207}Pb/^{235}U$ $\pm 2\sigma$	$^{206}Pb/^{238}U$ $\pm 2\sigma$	ρ	$\frac{^{207}Pb}{^{206}Pb}$ ^{206}Pb	Ages (Ma)$\pm 2\sigma$ $\frac{^{206}Pb}{^{238}U}$	Ages (Ma)$\pm 2\sigma$ $\frac{^{207}Pb}{^{206}Pb}$	Conc %
A3	Black core	1357	1770	3177	0.56	7.8592 ± 0.2062	0.3985 ± 0.0103	0.99	0.143	2162 ± 47	2264 ± 52	95
A5	Metamict core	564	224	1332	0.17	9.1679 ± 0.2411	0.4104 ± 0.0106	0.98	0.162	2217 ± 49	2477 ± 51	89
A6	Black core	611	390	1486	0.26	8.2581 ± 0.2175	0.3947 ± 0.0102	0.98	0.152	2145 ± 47	2365 ± 52	91
A8	Metamict core	282	133	571	0.23	12.1236 ± 0.3203	0.4615 ± 0.0120	0.98	0.190	2446 ± 53	2746 ± 50	89
A9	Black rim	463	99	825	0.12	14.1562 ± 0.3722	0.5343 ± 0.0138	0.98	0.192	2760 ± 58	2760 ± 50	100
A10-C	Black core	269	370	431	0.86	14.3354 ± 0.3774	0.5391 ± 0.0140	0.99	0.193	2780 ± 58	2767 ± 50	100
A10-R	Black rim	144	165	232	0.71	14.1502 ± 0.3752	0.5267 ± 0.0137	0.98	0.195	2728 ± 58	2783 ± 50	98
A11	Metamict	441	719	948	0.76	8.9027 ± 0.2344	0.4065 ± 0.0105	0.98	0.159	2199 ± 48	2443 ± 51	90
A12	Black core	289	111	506	0.22	14.0332 ± 0.3695	0.5281 ± 0.0137	0.99	0.193	2733 ± 58	2765 ± 50	99
A13	Black core	1046	1846	2438	0.76	7.5837 ± 0.1997	0.3834 ± 0.0099	0.98	0.143	2092 ± 46	2269 ± 52	92
A14	Black core	232	227	364	0.62	15.0967 ± 0.4055	0.5608 ± 0.0146	0.97	0.195	2870 ± 60	2787 ± 50	103
A15	Black core	1395	2713	3610	0.75	6.8258 ± 0.1798	0.3462 ± 0.0090	0.99	0.143	1916 ± 43	2264 ± 52	85
A16	Black core	787	230	2152	0.11	7.0246 ± 0.1854	0.3628 ± 0.0094	0.98	0.140	1996 ± 44	2232 ± 52	89
A17	Metamict	358	73	647	0.11	13.6487 ± 0.3616	0.5254 ± 0.0136	0.98	0.188	2722 ± 58	2728 ± 50	100
B1	Black cracked core	1031	1706	2313	0.74	8.0800 ± 0.2130	0.4021 ± 0.0104	0.98	0.146	2179 ± 48	2296 ± 52	95
B2	Black core	541	289	1030	0.28	11.7641 ± 0.3101	0.4933 ± 0.0128	0.98	0.173	2585 ± 55	2586 ± 51	100
B3	Metamict	322	158	574	0.28	13.6151 ± 0.3592	0.5261 ± 0.0136	0.98	0.188	2725 ± 58	2722 ± 50	100
B4	Metamict	372	139	729	0.19	12.5172 ± 0.3317	0.4806 ± 0.0125	0.98	0.189	2530 ± 54	2732 ± 50	93
B5	Metamict	421	176	738	0.24	13.9752 ± 0.3690	0.5342 ± 0.0139	0.99	0.190	2759 ± 58	2740 ± 50	101
B6-R	Black rim	207	167	362	0.46	13.4766 ± 0.3570	0.5192 ± 0.0135	0.98	0.188	2696 ± 57	2727 ± 50	99
B7	Metamict	373	66	634	0.10	13.4522 ± 0.3556	0.5229 ± 0.0136	0.98	0.187	2711 ± 57	2712 ± 50	100
B8	Black core	926	1268	1938	0.65	7.8637 ± 0.2078	0.4049 ± 0.0105	0.98	0.141	2192 ± 48	2237 ± 52	98
B9	Metamict	364	76	601	0.13	14.1673 ± 0.3748	0.5329 ± 0.0138	0.98	0.193	2754 ± 58	2766 ± 50	100
B10-C	Osci. zoned core	271	110	437	0.25	14.3123 ± 0.3789	0.5307 ± 0.0138	0.98	0.196	2745 ± 58	2789 ± 50	98
B10-R	Black rim	328	65	553	0.12	13.7293 ± 0.3637	0.5247 ± 0.0136	0.98	0.190	2719 ± 58	2740 ± 50	99
B11	Metamict	530	76	1050	0.07	10.2160 ± 0.2704	0.4632 ± 0.0120	0.98	0.160	2454 ± 53	2455 ± 51	100
B12-C	Metamict core	1238	1286	2392	0.54	9.0627 ± 0.2400	0.4331 ± 0.0113	0.99	0.152	2320 ± 51	2366 ± 52	98
B12-R	Black cracked rim	366	133	598	0.22	13.9213 ± 0.3690	0.5296 ± 0.0137	0.98	0.191	2740 ± 58	2748 ± 50	100
B13-C	Black core	1069	339	2379	0.14	8.0167 ± 0.2124	0.4111 ± 0.0107	0.98	0.141	2220 ± 49	2244 ± 52	99
B14	Metamict	287	81	556	0.15	12.5689 ± 0.3349	0.4856 ± 0.0126	0.97	0.188	2552 ± 55	2722 ± 50	94

Continued on next page

Table B.3 – *Continued from previous page*

Spot #	Internal Structure	Pb (ppm)	Th (ppm)	U (ppm)	Th/U	$^{207}Pb/^{235}U$ $\pm 2\sigma$	$^{206}Pb/^{238}U$ $\pm 2\sigma$	ρ	$\frac{^{207}Pb}{^{206}Pb}$ ^{206}Pb	Ages (Ma)$\pm 2\sigma$ $\frac{^{206}Pb}{^{238}U}$	Ages (Ma)$\pm 2\sigma$ $\frac{^{207}Pb}{^{206}Pb}$	Conc %
B15-R	Black core	263	66	464	0.14	14.0532 ± 0.3735	0.5339 ± 0.0139	0.98	0.191	2758 ± 58	2750 ± 50	100
B16	Metamict	455	90	940	0.10	10.8598 ± 0.2884	0.4692 ± 0.0122	0.98	0.168	2480 ± 53	2536 ± 51	98
B17	Metamict	454	170	798	0.21	13.7455 ± 0.3656	0.5278 ± 0.0137	0.98	0.189	2732 ± 58	2732 ± 50	100
C1	Metamict	436	244	834	0.29	11.5989 ± 0.3089	0.4829 ± 0.0125	0.97	0.174	2540 ± 55	2598 ± 51	98
C2	Metamict	542	174	1209	0.14	9.4873 ± 0.2523	0.4306 ± 0.0112	0.98	0.160	2308 ± 50	2453 ± 51	94
C4	Metamict	509	118	977	0.12	12.5405 ± 0.3341	0.4957 ± 0.0129	0.98	0.183	2595 ± 56	2684 ± 50	97
C5-R	Metamict rim	303	116	535	0.22	13.9244 ± 0.3711	0.5303 ± 0.0138	0.98	0.190	2743 ± 58	2746 ± 50	100
C6	Metamict	481	100	865	0.12	13.6716 ± 0.3650	0.5297 ± 0.0138	0.98	0.187	2740 ± 58	2717 ± 50	101
C8	Metamict	378	142	716	0.20	12.5488 ± 0.3350	0.4956 ± 0.0129	0.98	0.184	2595 ± 56	2686 ± 50	97
C9	Metamict	160	70	279	0.25	14.0554 ± 0.3770	0.5325 ± 0.0139	0.97	0.191	2752 ± 58	2754 ± 50	100
C12	Metamict	269	100	482	0.21	13.5893 ± 0.3652	0.5223 ± 0.0136	0.97	0.189	2709 ± 58	2731 ± 51	99
C13	Metamict	481	153	1141	0.13	9.0155 ± 0.2421	0.4094 ± 0.0107	0.97	0.160	2212 ± 49	2452 ± 52	90
C14	Metamict core	261	104	454	0.23	14.2318 ± 0.3823	0.5331 ± 0.0139	0.97	0.194	2755 ± 58	2773 ± 50	99
C15	Metamict	468	101	992	0.10	10.7658 ± 0.2888	0.4567 ± 0.0119	0.97	0.171	2425 ± 53	2567 ± 51	94
D1	Metamict	424	118	893	0.13	10.2156 ± 0.2759	0.4611 ± 0.0120	0.96	0.161	2444 ± 53	2463 ± 52	99
D2	Metamict	569	172	1316	0.13	8.8675 ± 0.2379	0.4221 ± 0.0110	0.97	0.152	2270 ± 50	2372 ± 52	96
D3	Black core	1045	1210	2480	0.49	7.5540 ± 0.2027	0.3921 ± 0.0102	0.97	0.140	2133 ± 47	2223 ± 53	96
D4	Metamict	615	238	1405	0.17	8.9259 ± 0.2397	0.4264 ± 0.0111	0.97	0.152	2290 ± 50	2366 ± 52	97
D5	Black core	385	124	731	0.17	12.3675 ± 0.3324	0.5026 ± 0.0131	0.97	0.178	2625 ± 56	2638 ± 51	99
D6	Black core	458	118	1030	0.11	9.6054 ± 0.2583	0.4338 ± 0.0113	0.97	0.161	2323 ± 51	2461 ± 52	94
D7	Metamict	471	118	1107	0.11	8.6854 ± 0.2341	0.4190 ± 0.0109	0.97	0.150	2256 ± 50	2350 ± 53	96
D8	Metamict	439	101	839	0.12	12.3378 ± 0.3325	0.5035 ± 0.0131	0.97	0.178	2629 ± 56	2632 ± 51	100
D9-C	Osci. zoned core	202	47	276	0.17	24.0128 ± 0.6489	0.6462 ± 0.0169	0.97	0.269	3213 ± 66	3303 ± 48	97
D9-R	Black rim	460	111	1077	0.10	9.3587 ± 0.2528	0.4168 ± 0.0109	0.97	0.163	2246 ± 49	2485 ± 52	90
D10	Metamict	457	105	928	0.11	11.2051 ± 0.3024	0.4761 ± 0.0124	0.97	0.171	2510 ± 54	2564 ± 51	98
D11	Black core	351	136	730	0.19	11.6597 ± 0.3168	0.4525 ± 0.0118	0.96	0.187	2406 ± 52	2715 ± 51	89
D13	Metamict rim	475	113	884	0.13	12.9696 ± 0.3506	0.5120 ± 0.0134	0.97	0.184	2665 ± 57	2687 ± 51	99
D14-C	Osci. zoned core	268	376	436	0.86	13.9497 ± 0.3795	0.5222 ± 0.0136	0.96	0.194	2708 ± 58	2774 ± 51	98
D15	Black rim	478	126	992	0.13	10.7299 ± 0.2907	0.4659 ± 0.0122	0.97	0.167	2466 ± 53	2528 ± 52	98
D16	Metamict	425	143	787	0.18	12.7567 ± 0.3459	0.5102 ± 0.0133	0.96	0.181	2658 ± 57	2665 ± 51	100

Continued on next page

Table B.3 – *Continued from previous page*

Spot #	**Internal Structure**	**Pb** (ppm)	**Th** (ppm)	**U** (ppm)	**Th/U**	^{207}**Pb**/^{235}**U** $\pm 2\sigma$	^{206}**Pb**/^{238}**U** $\pm 2\sigma$	ρ	$\frac{^{207}Pb}{^{206}Pb}$ ^{206}Pb	**Ages (Ma)**$\pm 2\sigma$ $\frac{^{206}Pb}{^{238}U}$	$\frac{^{207}Pb}{^{206}Pb}$	**Conc** %
E1	Black core	678	753	1481	0.51	9.0128 ± 0.2454	0.4221 ± 0.0110	0.96	0.155	2270 ± 50	2400 ± 53	95
E2-R	Metamict rim	492	148	1103	0.13	9.5277 ± 0.2588	0.4337 ± 0.0113	0.96	0.159	2322 ± 51	2448 ± 52	95
E3	Black rim	354	238	599	0.40	13.6103 ± 0.3826	0.5259 ± 0.0145	0.98	0.188	2724 ± 61	2722 ± 50	100
E4-R	Metamict rim	511	140	938	0.15	13.4819 ± 0.3791	0.5085 ± 0.0140	0.98	0.192	2650 ± 60	2762 ± 50	96
E5-C	Black core	353	202	613	0.33	13.7318 ± 0.3859	0.5230 ± 0.0144	0.98	0.190	2712 ± 61	2746 ± 50	99
E5-R	Black rim	155	113	260	0.44	13.8285 ± 0.3890	0.5311 ± 0.0146	0.98	0.189	2746 ± 61	2732 ± 50	101
E6-R	Black cracked rim	470	171	842	0.20	13.6139 ± 0.3819	0.5199 ± 0.0143	0.98	0.190	2699 ± 61	2741 ± 50	98
E7	Core	533	80	993	0.08	13.5390 ± 0.3796	0.5123 ± 0.0140	0.97	0.192	2666 ± 60	2756 ± 50	97
E9	Black core	1301	1731	2826	0.61	8.4116 ± 0.2355	0.4085 ± 0.0112	0.98	0.149	2208 ± 51	2338 ± 52	94
E11-C	Osci. zoned core	536	73	1161	0.06	9.9554 ± 0.2788	0.4544 ± 0.0124	0.97	0.159	2415 ± 55	2444 ± 52	99
E11-R	Black rim	270	144	474	0.30	13.6099 ± 0.3813	0.5190 ± 0.0142	0.98	0.190	2695 ± 60	2744 ± 50	98
E12-C	Black core	320	128	570	0.22	13.6063 ± 0.3807	0.5211 ± 0.0142	0.97	0.189	2704 ± 60	2736 ± 50	99
E12-R	Black rim	158	118	268	0.44	13.7248 ± 0.3851	0.5237 ± 0.0143	0.97	0.190	2715 ± 61	2743 ± 50	99
E13-C	Metamict core	550	357	1125	0.32	10.5391 ± 0.2945	0.4506 ± 0.0123	0.98	0.170	2398 ± 55	2554 ± 51	94
E14	Black	861	535	2097	0.26	7.6743 ± 0.2146	0.3898 ± 0.0106	0.97	0.143	2122 ± 49	2261 ± 53	94
E15	Black core	469	76	995	0.08	10.6453 ± 0.2974	0.4574 ± 0.0125	0.98	0.169	2428 ± 55	2546 ± 51	95
E16-C	Metamict core	901	1233	1853	0.67	8.9173 ± 0.2490	0.4276 ± 0.0116	0.97	0.151	2295 ± 53	2360 ± 52	97
E16-R	Black rim	323	119	594	0.20	13.4274 ± 0.3768	0.5074 ± 0.0138	0.97	0.192	2645 ± 59	2759 ± 50	96
E17	Osci. zoned core	217	239	390	0.61	12.1332 ± 0.3406	0.4728 ± 0.0129	0.97	0.186	2496 ± 56	2708 ± 51	92
E18	Osci. zoned core	286	122	505	0.24	13.6746 ± 0.3827	0.5239 ± 0.0143	0.98	0.189	2716 ± 60	2736 ± 50	99
F2-C	Osci. zoned core	482	226	854	0.26	13.2087 ± 0.3689	0.5206 ± 0.0141	0.97	0.184	2702 ± 60	2689 ± 51	100
F3-R	Black rim	355	92	640	0.14	13.7037 ± 0.3832	0.5218 ± 0.0141	0.97	0.190	2707 ± 60	2746 ± 51	99
F4	Metamict	695	105	1773	0.06	7.8781 ± 0.2206	0.3896 ± 0.0106	0.97	0.147	2121 ± 49	2307 ± 53	92
F5-R	Metamict rim	380	95	691	0.14	13.5793 ± 0.3800	0.5168 ± 0.0140	0.97	0.191	2686 ± 59	2747 ± 51	98
F6	Metamict	661	152	1557	0.10	8.3177 ± 0.2325	0.4180 ± 0.0113	0.97	0.144	2252 ± 51	2279 ± 53	99
F7	Metamict	504	71	932	0.08	13.5696 ± 0.3799	0.5133 ± 0.0139	0.97	0.192	2671 ± 59	2757 ± 51	97
F8	Metamict	197	82	351	0.23	13.5612 ± 0.3809	0.5163 ± 0.0140	0.97	0.190	2684 ± 59	2746 ± 51	98
F9	Black core	606	124	1646	0.08	7.1533 ± 0.2012	0.3645 ± 0.0098	0.96	0.142	2003 ± 46	2256 ± 54	89
F10	Metamict	365	122	653	0.19	13.5850 ± 0.3809	0.5176 ± 0.0140	0.96	0.190	2689 ± 59	2745 ± 51	98
F11	Black core	874	679	1226	0.55	19.6065 ± 0.5486	0.5881 ± 0.0158	0.96	0.242	2982 ± 64	3132 ± 49	95

Continued on next page

Table B.3 – *Continued from previous page*

Spot #	Internal Structure	Pb (ppm)	Th (ppm)	U (ppm)	Th/U	$^{207}Pb/^{235}U$ $\pm 2\sigma$	$^{206}Pb/^{238}U$ $\pm 2\sigma$	ρ	$\frac{^{207}Pb}{^{206}Pb}$ ^{206}Pb	Ages (Ma)$\pm 2\sigma$ $\frac{^{206}Pb}{^{238}U}$	Ages (Ma)$\pm 2\sigma$ $\frac{^{207}Pb}{^{206}Pb}$	Conc %
F12	Metamict	504	141	1192	0.12	8.7239 ± 0.2453	0.4098 ± 0.0110	0.95	0.154	2214 ± 50	2395 ± 53	92
F13	Black	446	61	806	0.08	13.7879 ± 0.3863	0.5315 ± 0.0143	0.96	0.188	2748 ± 60	2726 ± 51	101
F14	Osci. zoned core	653	126	1610	0.08	8.3301 ± 0.2338	0.3995 ± 0.0107	0.95	0.151	2167 ± 50	2360 ± 53	92
F15	Metamict	492	74	984	0.08	11.5648 ± 0.3241	0.4846 ± 0.0130	0.96	0.173	2547 ± 57	2587 ± 52	98
F17	Metamict	721	498	1538	0.32	9.1750 ± 0.2576	0.4352 ± 0.0117	0.96	0.153	2329 ± 52	2378 ± 53	98
F18-C	Osci. zoned core	221	101	383	0.26	13.6769 ± 0.3848	0.5255 ± 0.0141	0.95	0.189	2723 ± 60	2731 ± 51	100
F18-R	Metamict rim	447	82	926	0.09	10.9983 ± 0.3091	0.4696 ± 0.0126	0.95	0.170	2482 ± 55	2556 ± 52	97
SG-080 granite												
A2	Oscillatory zoned	129	101	139	0.73	33.1236 ± 0.8726	0.7254 ± 0.0183	0.96	0.331	3516 ± 68	3622 ± 48	97
A3	Inh. Osci. Zoned	127	83	127	0.66	36.6734 ± 0.9705	0.7491 ± 0.0189	0.95	0.355	3604 ± 70	3729 ± 47	97
A6-C	Osci. zoned core	162	112	162	0.69	35.3257 ± 0.9287	0.7595 ± 0.0191	0.96	0.337	3642 ± 70	3651 ± 47	100
A7	Oscillatory zoned	124	67	139	0.48	32.2323 ± 0.8561	0.7157 ± 0.0181	0.95	0.327	3480 ± 68	3601 ± 48	97
A8	Oscillatory zoned	173	106	186	0.57	33.7631 ± 0.8901	0.7337 ± 0.0185	0.96	0.334	3547 ± 69	3634 ± 48	98
A11	Osci. zoned core	147	84	153	0.55	34.8395 ± 0.9195	0.7479 ± 0.0188	0.95	0.338	3600 ± 69	3653 ± 48	99
A14-C	Osci. zoned core	241	357	286	1.25	28.0766 ± 0.7403	0.6500 ± 0.0163	0.95	0.313	3228 ± 64	3537 ± 48	91
A15	Osci. zoned core	139	59	151	0.39	34.6580 ± 0.9188	0.7482 ± 0.0188	0.95	0.336	3601 ± 69	3644 ± 48	99
B4	Osci. zoned core	209	140	218	0.64	33.7115 ± 0.8896	0.7468 ± 0.0187	0.95	0.327	3596 ± 69	3605 ± 48	100
B8	Oscillatory zoned	121	97	130	0.74	32.5680 ± 0.8636	0.7173 ± 0.0180	0.95	0.329	3486 ± 68	3614 ± 48	96
C1-C	Oscillatory zoned	71	44	78	0.57	33.7078 ± 0.9011	0.7402 ± 0.0186	0.94	0.330	3571 ± 69	3618 ± 48	99
C1-R	Oscillatory zoned	102	56	113	0.49	32.7516 ± 0.8731	0.7358 ± 0.0185	0.94	0.323	3555 ± 69	3583 ± 48	99
C4	Oscillatory zoned	101	70	112	0.62	32.7003 ± 0.8702	0.7264 ± 0.0182	0.94	0.326	3520 ± 68	3600 ± 48	98
C5	Oscillatory zoned	74	44	80	0.55	32.0850 ± 0.8586	0.6766 ± 0.0170	0.94	0.344	3331 ± 65	3680 ± 48	91
C6	Oscillatory zoned	101	80	110	0.73	32.6280 ± 0.8690	0.7260 ± 0.0182	0.94	0.326	3519 ± 68	3598 ± 48	98
C7	Oscillatory zoned	136	96	149	0.64	32.4963 ± 0.8655	0.7294 ± 0.0183	0.94	0.323	3531 ± 68	3585 ± 48	99
C8-C	Black core	462	40	859	0.05	13.8737 ± 0.3677	0.5153 ± 0.0129	0.94	0.195	2679 ± 55	2787 ± 51	96
C8-R	Oscillatory zoned	146	114	156	0.73	33.5596 ± 0.8933	0.7341 ± 0.0184	0.94	0.331	3549 ± 68	3624 ± 48	98
C10	Oscillatory zoned	126	104	135	0.77	33.1996 ± 0.8858	0.7297 ± 0.0183	0.94	0.330	3533 ± 68	3617 ± 48	98
C11-C	Osci. zoned core	62	36	68	0.54	32.7464 ± 0.8795	0.7361 ± 0.0185	0.94	0.323	3556 ± 69	3582 ± 49	99
C11-R	Black rim	618	44	813	0.05	27.9767 ± 0.7422	0.6676 ± 0.0167	0.94	0.304	3297 ± 64	3490 ± 49	94
C12	Osci. zoned core	143	131	152	0.87	33.3923 ± 0.8911	0.7300 ± 0.0183	0.94	0.332	3533 ± 68	3625 ± 48	97

Continued on next page

Table B.3 – *Continued from previous page*

Spot #	Internal Structure	Pb (ppm)	Th (ppm)	U (ppm)	Th/U	$^{207}Pb/^{235}U$ $\pm 2\sigma$	$^{206}Pb/^{238}U$ $\pm 2\sigma$	ρ	$\frac{^{207}Pb}{^{206}Pb}$ ^{206}Pb	Ages (Ma)$\pm 2\sigma$ $\frac{^{206}Pb}{^{238}U}$	Ages (Ma)$\pm 2\sigma$ $\frac{^{207}Pb}{^{206}Pb}$	Conc %
C13	Osci. zoned core	151	85	164	0.52	33.4328 ± 0.8995	0.7429 ± 0.0187	0.94	0.326	3581 ± 69	3600 ± 49	99
C14	Oscillatory zoned	89	56	98	0.57	32.9341 ± 0.8841	0.7291 ± 0.0183	0.93	0.328	3530 ± 68	3606 ± 49	98
C15-C	Inherited core	96	58	94	0.62	40.8038 ± 1.0952	0.7913 ± 0.0198	0.93	0.374	3758 ± 71	3808 ± 48	99
C15-R	Osci. zoned rim	92	59	101	0.58	32.7597 ± 0.8792	0.7287 ± 0.0182	0.93	0.326	3529 ± 68	3598 ± 49	98
E1	Osci. zoned core	88	52	96	0.55	33.4495 ± 0.8999	0.7366 ± 0.0184	0.93	0.329	3558 ± 68	3614 ± 49	98
E3	Osci. zoned core	186	162	217	0.75	29.7757 ± 0.8052	0.6733 ± 0.0169	0.93	0.321	3319 ± 65	3573 ± 49	93
E5	Metamict	341	59	625	0.09	13.7238 ± 0.3679	0.5150 ± 0.0128	0.93	0.193	2678 ± 55	2770 ± 52	97
E6-C	Osci. zoned core	66	36	72	0.50	33.6720 ± 0.9127	0.7327 ± 0.0184	0.93	0.333	3543 ± 68	3632 ± 49	98
E7	Osci. zoned core	132	113	141	0.80	33.0400 ± 0.8953	0.7280 ± 0.0182	0.92	0.329	3526 ± 68	3613 ± 49	98
E8	Black core	175	88	202	0.44	31.9407 ± 0.8204	0.7028 ± 0.0174	0.96	0.330	3431 ± 66	3615 ± 47	95
E9	Osci. zoned core	69	32	76	0.42	32.6874 ± 0.8533	0.7350 ± 0.0184	0.96	0.323	3552 ± 68	3582 ± 48	99
E15-R	Black rim	346	87	606	0.14	14.1179 ± 0.3618	0.5383 ± 0.0133	0.96	0.190	2776 ± 56	2744 ± 50	101
F4	Inh. meta. core	310	142	529	0.27	14.1183 ± 0.3625	0.5337 ± 0.0132	0.96	0.192	2757 ± 56	2758 ± 50	100
F7	Metamict	528	45	1276	0.04	9.2176 ± 0.2379	0.4077 ± 0.0101	0.96	0.164	2204 ± 46	2497 ± 52	88
F12	Metamict	424	119	818	0.15	12.4319 ± 0.3197	0.4883 ± 0.0121	0.96	0.185	2563 ± 52	2695 ± 51	95
F13	Sector zoned	107	70	119	0.59	31.8808 ± 0.8247	0.7112 ± 0.0177	0.96	0.325	3463 ± 67	3594 ± 47	96
SG-084 granite												
A5	Osci. zoned core	83	31	93	0.33	34.2239 ± 0.9141	0.7293 ± 0.0183	0.94	0.340	3531 ± 68	3664 ± 48	96
A7	Metamict	713	20	953	0.02	28.2417 ± 0.7461	0.6605 ± 0.0165	0.95	0.310	3269 ± 64	3521 ± 48	93
A8-C	Osci. zoned core	41	20	42	0.48	37.5526 ± 1.0217	0.7639 ± 0.0194	0.93	0.356	3659 ± 71	3735 ± 49	98
A10-C	Osci. zoned core	225	140	260	0.54	32.1367 ± 0.8660	0.6733 ± 0.0170	0.94	0.346	3319 ± 65	3690 ± 48	90
A10-R	Osci. zoned rim	291	35	316	0.11	37.8122 ± 1.0029	0.7743 ± 0.0193	0.94	0.354	3696 ± 70	3725 ± 48	99
B8	Metamict	590	14	1194	0.01	13.9444 ± 0.3710	0.4689 ± 0.0117	0.94	0.216	2479 ± 51	2949 ± 51	84
B13	Osci. zoned core	66	19	73	0.26	35.0951 ± 0.9560	0.7384 ± 0.0186	0.92	0.345	3565 ± 69	3684 ± 49	97
C6	Metamict	254	36	292	0.12	32.7451 ± 0.8827	0.7359 ± 0.0184	0.93	0.323	3555 ± 68	3583 ± 49	99
C7	Metamict	296	12	836	0.01	6.9578 ± 0.1889	0.3572 ± 0.0089	0.92	0.141	1969 ± 42	2243 ± 55	88
C16	Metamict	710	26	943	0.03	27.6513 ± 0.7451	0.6662 ± 0.0166	0.92	0.301	3291 ± 64	3475 ± 49	95
D3	Metamict	59	31	77	0.40	26.1694 ± 0.7296	0.5931 ± 0.0150	0.91	0.320	3002 ± 61	3570 ± 50	84
D12	Metamict	552	65	1124	0.06	11.6962 ± 0.3194	0.4740 ± 0.0118	0.91	0.179	2501 ± 52	2643 ± 53	95
E1	Metamict	105	46	132	0.35	27.7489 ± 0.7707	0.6270 ± 0.0158	0.91	0.321	3138 ± 62	3574 ± 50	88

Continued on next page

Table B.3 – *Continued from previous page*

Spot #	Internal Structure	Pb (ppm)	Th (ppm)	U (ppm)	Th/U	$^{207}Pb/^{235}U$ $\pm 2\sigma$	$^{206}Pb/^{238}U$ $\pm 2\sigma$	ρ	$\frac{^{207}Pb}{^{206}Pb}$ ^{206}Pb	Ages (Ma)$\pm 2\sigma$ $\frac{^{206}Pb}{^{238}U}$	Ages (Ma)$\pm 2\sigma$ $\frac{^{207}Pb}{^{206}Pb}$	Conc %
E4-C	Osci. zoned core	131	13	148	0.09	36.8919 ± 1.0272	0.7359 ± 0.0185	0.90	0.364	3556 ± 69	3765 ± 50	94
E11	Osci. zoned core	207	123	222	0.55	35.1115 ± 0.8981	0.7132 ± 0.0176	0.96	0.357	3471 ± 66	3738 ± 47	93
F2	Osci. zoned core	563	470	557	0.84	35.4645 ± 0.9020	0.7409 ± 0.0182	0.97	0.347	3574 ± 68	3695 ± 47	97
F3	Metamict	599	44	1832	0.02	7.1568 ± 0.1825	0.3227 ± 0.0080	0.97	0.161	1803 ± 39	2465 ± 52	73
F4	Oscillatory zoned	139	53	154	0.34	34.5914 ± 0.8853	0.7342 ± 0.0181	0.96	0.342	3549 ± 67	3671 ± 47	97
F11	Osci. zoned core	359	233	364	0.64	37.1116 ± 0.9475	0.7563 ± 0.0186	0.96	0.356	3631 ± 68	3733 ± 47	97
SG-087 granite												
A1	Black core	691	124	1437	0.09	11.9306 ± 0.3079	0.4580 ± 0.0113	0.96	0.189	2431 ± 50	2733 ± 51	89
A2	Black core	231	101	398	0.25	14.3633 ± 0.3713	0.5326 ± 0.0132	0.96	0.196	2752 ± 56	2789 ± 51	99
A3	Black core	304	313	293	1.07	34.5656 ± 0.8921	0.7504 ± 0.0186	0.96	0.334	3609 ± 69	3636 ± 47	99
A4	Black core	180	105	275	0.38	17.5005 ± 0.4542	0.5681 ± 0.0141	0.96	0.223	2900 ± 58	3005 ± 50	96
A5	Black core	389	369	352	1.05	39.1886 ± 1.0140	0.7883 ± 0.0196	0.96	0.361	3747 ± 71	3752 ± 47	100
A7	Osci. zoned core	89	94	160	0.58	11.5899 ± 0.3047	0.4866 ± 0.0121	0.95	0.173	2556 ± 53	2584 ± 52	99
A8-R	White rim	20	75	24	3.18	12.0689 ± 0.3521	0.4967 ± 0.0128	0.88	0.176	2600 ± 55	2617 ± 56	99
A9	Black core	90	24	145	0.16	17.1027 ± 0.4513	0.5683 ± 0.0142	0.95	0.218	2901 ± 58	2968 ± 50	98
A10	Sector zoned	19	26	33	0.77	11.4152 ± 0.3199	0.4729 ± 0.0120	0.91	0.175	2496 ± 53	2606 ± 55	96
A12	Convoluted core	482	104	902	0.12	13.8266 ± 0.3619	0.4992 ± 0.0124	0.95	0.201	2611 ± 53	2833 ± 51	92
A13	Black	293	184	489	0.38	14.2464 ± 0.3728	0.5351 ± 0.0133	0.95	0.193	2763 ± 56	2769 ± 51	100
A14-C	Metamict	277	132	331	0.40	28.6840 ± 0.7505	0.6883 ± 0.0171	0.95	0.302	3376 ± 65	3482 ± 48	97
B1	Convoluted core	33	19	44	0.44	21.8662 ± 0.6062	0.6006 ± 0.0153	0.92	0.264	3032 ± 62	3271 ± 51	93
C1-C	Osci. zoned rim	48	56	109	0.51	9.9617 ± 0.2958	0.3786 ± 0.0098	0.87	0.191	2070 ± 46	2749 ± 56	75
B4	Metamict	484	12	1013	0.01	11.4016 ± 0.2998	0.4667 ± 0.0116	0.95	0.177	2469 ± 51	2627 ± 52	94
B14	Black core	185	169	307	0.55	13.6011 ± 0.3637	0.5202 ± 0.0130	0.93	0.190	2700 ± 55	2739 ± 52	99
B15-C	Inherited core	148	110	243	0.45	15.5117 ± 0.4199	0.5250 ± 0.0132	0.93	0.214	2720 ± 56	2938 ± 51	93
B15-R	Osci. zoned rim	147	232	222	1.04	13.6249 ± 0.3662	0.5191 ± 0.0130	0.93	0.190	2696 ± 55	2745 ± 52	98
C1-R	Sector zoned rim	47	58	62	0.93	18.7331 ± 0.5142	0.5836 ± 0.0147	0.92	0.233	2964 ± 60	3071 ± 51	96
C2	Sector zoned	170	315	242	1.30	13.7102 ± 0.3711	0.5234 ± 0.0131	0.92	0.190	2714 ± 56	2742 ± 52	99
C3	Sector zoned	37	34	55	0.61	16.6397 ± 0.4623	0.5589 ± 0.0141	0.91	0.216	2862 ± 59	2950 ± 52	97
C4-C	Black core	119	93	157	0.59	21.5804 ± 0.5843	0.6193 ± 0.0155	0.92	0.253	3107 ± 62	3202 ± 50	97
C5	White core	8	10	13	0.74	11.8991 ± 0.3818	0.4840 ± 0.0128	0.82	0.178	2545 ± 56	2637 ± 60	96

Continued on next page

Table B.3 – *Continued from previous page*

Spot #	Internal Structure	Pb (ppm)	Th (ppm)	U (ppm)	Th/U	$^{207}Pb/^{235}U$ $\pm 2\sigma$	$^{206}Pb/^{238}U$ $\pm 2\sigma$	ρ	$\frac{^{207}Pb}{^{206}Pb}$ ^{206}Pb	Ages (Ma)$\pm 2\sigma$ $\frac{^{206}Pb}{^{238}U}$	Ages (Ma)$\pm 2\sigma$ $\frac{^{207}Pb}{^{206}Pb}$	Conc %
C6-C	Osci. zoned core	18	13	21	0.63	28.0740 ± 0.8823	0.6361 ± 0.0173	0.87	0.320	3174 ± 68	3570 ± 55	89
C6-R	Osci. zoned rim	21	16	30	0.52	20.9521 ± 0.5985	0.5714 ± 0.0147	0.90	0.266	2913 ± 60	3282 ± 52	89
C7	Black	89	119	133	0.90	14.4752 ± 0.3977	0.5367 ± 0.0135	0.92	0.196	2770 ± 57	2790 ± 53	99
C8	Sector zoned	17	52	18	2.96	15.6768 ± 0.4678	0.5263 ± 0.0137	0.87	0.216	2726 ± 58	2951 ± 55	92
C9	Sector zoned	44	83	63	1.32	13.4474 ± 0.3816	0.5193 ± 0.0132	0.90	0.188	2696 ± 56	2723 ± 54	99
C10	Sector zoned	55	72	86	0.84	13.3805 ± 0.3732	0.5179 ± 0.0131	0.91	0.187	2690 ± 55	2719 ± 54	99
C11	Sector zoned	33	38	59	0.63	11.4434 ± 0.3337	0.4852 ± 0.0124	0.88	0.171	2550 ± 54	2568 ± 56	99
C12	Convoluted core	20	42	22	1.86	18.1106 ± 0.5393	0.5703 ± 0.0148	0.87	0.230	2909 ± 61	3054 ± 55	95
C13-C	Inherited core	458	376	578	0.65	22.1704 ± 0.6089	0.6410 ± 0.0161	0.91	0.251	3193 ± 63	3190 ± 51	100
C13-R	Sector zoned rim	54	191	63	3.03	13.3475 ± 0.3657	0.5013 ± 0.0130	0.95	0.193	2620 ± 56	2769 ± 52	95
C14	Sector zoned	28	79	42	1.87	10.8497 ± 0.3071	0.4640 ± 0.0121	0.92	0.170	2457 ± 53	2553 ± 54	96
C15	Sector zoned	109	111	108	1.02	34.9748 ± 0.9251	0.7349 ± 0.0188	0.97	0.345	3552 ± 70	3686 ± 47	96
C16	Sector zoned	53	82	80	1.02	14.1526 ± 0.3811	0.5192 ± 0.0134	0.96	0.198	2696 ± 57	2807 ± 51	96
C17	Sector zoned	58	125	80	1.56	14.1125 ± 0.3800	0.5249 ± 0.0135	0.96	0.195	2720 ± 57	2785 ± 51	98
D1	Osci. zoned core	108	57	115	0.49	35.8526 ± 0.9496	0.7492 ± 0.0192	0.97	0.347	3605 ± 71	3694 ± 47	98
D2	Metamict	27	48	40	1.20	13.3609 ± 0.3745	0.5139 ± 0.0134	0.93	0.188	2673 ± 57	2729 ± 53	98
D3	Sector zoned core	20	46	32	1.45	11.0927 ± 0.3291	0.4718 ± 0.0125	0.89	0.171	2491 ± 54	2563 ± 56	97
D4	Sector zoned	27	52	43	1.21	12.0262 ± 0.3381	0.4903 ± 0.0127	0.92	0.178	2572 ± 55	2633 ± 54	98
D5	Sector zoned	39	55	70	0.79	11.1759 ± 0.3052	0.4751 ± 0.0122	0.94	0.171	2506 ± 53	2563 ± 53	98
D7	Osci. zoned core	310	148	369	0.40	29.8349 ± 0.7851	0.6897 ± 0.0176	0.97	0.314	3381 ± 67	3539 ± 47	96
D8	Sector zoned	114	95	191	0.50	13.6192 ± 0.3622	0.5232 ± 0.0134	0.96	0.189	2713 ± 57	2732 ± 51	99
D9	Black	235	41	335	0.12	22.0899 ± 0.5827	0.6284 ± 0.0160	0.97	0.255	3143 ± 63	3216 ± 49	98
D10	Convoluted core	528	629	467	1.35	38.1453 ± 1.0034	0.7717 ± 0.0197	0.97	0.358	3687 ± 72	3743 ± 47	98
D11	Convoluted core	20	4	20	0.21	39.5130 ± 1.1072	0.7859 ± 0.0208	0.94	0.365	3739 ± 75	3769 ± 49	99
D12A	Osci. zoned core	206	0	334	0.00	18.1695 ± 0.4799	0.5817 ± 0.0148	0.96	0.227	2956 ± 60	3028 ± 49	98
D12B	Osci. zoned core	102	1	179	0.00	16.0443 ± 0.4266	0.5430 ± 0.0139	0.96	0.214	2796 ± 58	2938 ± 50	95
D13	Sector zoned	25	51	43	1.19	10.6985 ± 0.3017	0.4591 ± 0.0119	0.92	0.169	2436 ± 53	2548 ± 54	96
D14	Sector zoned	142	301	203	1.48	13.5508 ± 0.3612	0.5170 ± 0.0132	0.96	0.190	2686 ± 56	2743 ± 51	98
D15	Black	286	158	597	0.27	10.5441 ± 0.2819	0.4461 ± 0.0114	0.96	0.171	2378 ± 51	2571 ± 52	92
D16	Black	93	86	158	0.55	13.4203 ± 0.3588	0.5158 ± 0.0132	0.96	0.189	2681 ± 56	2731 ± 51	98

Continued on next page

Table B.3 – *Continued from previous page*

Spot #	Internal Structure	Pb (ppm)	Th (ppm)	U (ppm)	Th/U	$^{207}Pb/^{235}U$ $\pm 2\sigma$	$^{206}Pb/^{238}U$ $\pm 2\sigma$	ρ	$\frac{^{207}Pb}{^{206}Pb}$ ^{206}Pb	Ages (Ma)$\pm 2\sigma$ $\frac{^{206}Pb}{^{238}U}$	Ages (Ma)$\pm 2\sigma$ $\frac{^{207}Pb}{^{206}Pb}$	Conc %
D17	Sector zoned	33	45	58	0.78	11.1956 ± 0.3119	0.4722 ± 0.0122	0.93	0.172	2493 ± 53	2577 ± 54	97
E1	Oscillatory zoned	63	36	63	0.58	37.9324 ± 1.0163	0.7725 ± 0.0198	0.96	0.356	3690 ± 72	3733 ± 47	99
E2	Metamict	320	13	358	0.04	36.2487 ± 0.9575	0.7656 ± 0.0195	0.96	0.343	3665 ± 71	3678 ± 47	100
E10	Black	313	31	695	0.04	10.2630 ± 0.2729	0.4431 ± 0.0113	0.96	0.168	2365 ± 50	2537 ± 52	93
SG-122 trondhjemite												
A3	Metamict	420	63	1103	0.06	8.7215 ± 0.2265	0.3684 ± 0.0094	0.98	0.172	2022 ± 44	2574 ± 51	79
A11	Black rim	374	44	854	0.05	9.9912 ± 0.2584	0.4206 ± 0.0107	0.98	0.172	2263 ± 48	2580 ± 51	88
A15	Metamict	597	363	2059	0.18	5.9983 ± 0.1566	0.2784 ± 0.0071	0.98	0.156	1583 ± 36	2415 ± 52	66
A17-C	Black core	615	62	686	0.09	36.5544 ± 0.9436	0.7499 ± 0.0190	0.98	0.353	3607 ± 70	3722 ± 46	97
A17-R	Osci. zoned rim	43	15	57	0.25	26.3429 ± 0.7013	0.6154 ± 0.0158	0.96	0.310	3092 ± 63	3523 ± 48	88
A18	Metamict	526	26	1067	0.02	11.9391 ± 0.3093	0.4746 ± 0.0121	0.98	0.182	2504 ± 53	2675 ± 50	94
B1	Black core	599	100	669	0.15	34.5998 ± 0.8936	0.7533 ± 0.0191	0.98	0.333	3620 ± 70	3631 ± 46	100
B2-C	Osci. zoned core	54	11	61	0.18	35.7901 ± 0.9408	0.7340 ± 0.0188	0.97	0.354	3548 ± 70	3723 ± 47	95
B2-R	Black rim	274	12	346	0.04	29.8807 ± 0.7734	0.6854 ± 0.0174	0.98	0.316	3365 ± 67	3551 ± 47	95
B3-C	Osci. zoned core	52	19	63	0.31	28.6622 ± 0.7650	0.6805 ± 0.0175	0.96	0.305	3346 ± 67	3498 ± 48	96
B3-R	Black rim	120	33	210	0.16	14.5439 ± 0.3785	0.5327 ± 0.0136	0.98	0.198	2753 ± 57	2810 ± 50	98
B4-C	Osci. zoned core	64	21	69	0.30	35.0543 ± 0.9195	0.7528 ± 0.0193	0.98	0.338	3618 ± 71	3652 ± 47	99
B4-R	Black rim	320	19	461	0.04	22.7012 ± 0.5890	0.6250 ± 0.0159	0.98	0.263	3130 ± 63	3267 ± 48	96
B7	Black core	113	27	199	0.14	14.5772 ± 0.3798	0.5330 ± 0.0136	0.98	0.198	2754 ± 57	2812 ± 50	98
B8	Metamict	276	51	496	0.10	13.8317 ± 0.3589	0.5291 ± 0.0134	0.98	0.190	2738 ± 57	2738 ± 50	100
B9	Sector zoned	370	43	677	0.06	13.9081 ± 0.3604	0.5211 ± 0.0132	0.98	0.194	2704 ± 56	2773 ± 50	98
B10-C	Osci. zoned core	384	1	687	0.00	14.6033 ± 0.3787	0.5378 ± 0.0137	0.98	0.197	2774 ± 57	2801 ± 50	99
B10-R	Black rim	74	26	134	0.20	14.0201 ± 0.3675	0.5165 ± 0.0132	0.97	0.197	2684 ± 56	2800 ± 50	96
B11	Black core	197	50	344	0.14	14.7359 ± 0.3833	0.5368 ± 0.0137	0.98	0.199	2770 ± 57	2819 ± 50	98
B12-C	Black core	540	58	647	0.09	32.8441 ± 0.8512	0.7133 ± 0.0181	0.98	0.334	3471 ± 68	3635 ± 46	95
B12-R	Osci. zoned rim	55	11	56	0.19	40.1663 ± 1.0695	0.7923 ± 0.0204	0.97	0.368	3761 ± 74	3782 ± 47	99
B13-C	White core	24	2	47	0.03	13.2388 ± 0.3952	0.4806 ± 0.0128	0.89	0.200	2530 ± 56	2824 ± 55	90
B14	Metamict	443	56	978	0.06	10.8472 ± 0.2839	0.4213 ± 0.0107	0.97	0.187	2266 ± 49	2713 ± 50	84
B15	Metamict	416	4	1397	0.00	6.1336 ± 0.1594	0.2957 ± 0.0075	0.98	0.150	1670 ± 37	2351 ± 52	71
B18	Metamict	477	48	959	0.05	12.0350 ± 0.3129	0.4810 ± 0.0122	0.98	0.181	2532 ± 53	2666 ± 50	95

Continued on next page

Table B.3 – *Continued from previous page*

Spot #	Internal Structure	Pb (ppm)	Th (ppm)	U (ppm)	Th/U	$^{207}Pb/^{235}U$ $\pm 2\sigma$	$^{206}Pb/^{238}U$ $\pm 2\sigma$	ρ	$\frac{^{207}Pb}{^{206}Pb}$ ^{206}Pb	Ages (Ma)$\pm 2\sigma$ $\frac{^{206}Pb}{^{238}U}$	Ages (Ma)$\pm 2\sigma$ $\frac{^{207}Pb}{^{206}Pb}$	Conc %
C1	Black	493	38	591	0.06	32.4630 ± 0.8430	0.7207 ± 0.0183	0.98	0.327	3499 ± 69	3602 ± 47	97
C2-C	Osci. zoned core	40	11	53	0.21	27.7770 ± 0.7471	0.6358 ± 0.0164	0.96	0.317	3173 ± 65	3554 ± 48	89
C2-R	Black rim	100	32	175	0.18	14.4423 ± 0.3789	0.5311 ± 0.0135	0.97	0.197	2746 ± 57	2803 ± 50	98
C4-C	Osci. zoned core	38	9	44	0.21	34.3062 ± 0.9140	0.7130 ± 0.0184	0.97	0.349	3470 ± 69	3702 ± 47	94
C4-R	Black rim	265	51	537	0.09	12.4394 ± 0.3272	0.4684 ± 0.0119	0.97	0.193	2477 ± 52	2764 ± 50	90
C5-C	Black core	339	20	474	0.04	25.7566 ± 0.6721	0.6346 ± 0.0161	0.97	0.294	3168 ± 64	3441 ± 47	92
C6-C	Black core	171	42	300	0.14	14.6183 ± 0.3825	0.5370 ± 0.0137	0.98	0.197	2771 ± 57	2805 ± 50	99
C7-C	Osci. zoned core	98	33	106	0.31	36.3173 ± 0.9521	0.7455 ± 0.0190	0.97	0.353	3591 ± 70	3721 ± 47	96
C8-C	Black core	185	26	251	0.10	28.1068 ± 0.7393	0.6273 ± 0.0160	0.97	0.325	3139 ± 63	3593 ± 47	87
C9-C	Osci. zoned core	340	7	423	0.02	32.3221 ± 0.8487	0.6961 ± 0.0178	0.97	0.337	3406 ± 68	3648 ± 47	93
C10-C	Osci. zoned core	142	57	154	0.37	35.6314 ± 0.9338	0.7362 ± 0.0188	0.97	0.351	3557 ± 70	3711 ± 47	96
C10-R	Black rim	488	34	895	0.04	13.9225 ± 0.3634	0.5232 ± 0.0133	0.97	0.193	2713 ± 56	2768 ± 50	98
C11-C	Sector zoned core	532	203	751	0.27	24.2592 ± 0.6344	0.5991 ± 0.0152	0.97	0.294	3026 ± 61	3437 ± 47	88
C12-C	Osci. zoned core	51	12	55	0.21	36.6413 ± 0.9735	0.7567 ± 0.0194	0.96	0.351	3632 ± 71	3712 ± 47	98
C12-C	Osci. zoned core	258	28	443	0.06	17.6935 ± 0.4647	0.5360 ± 0.0137	0.97	0.239	2767 ± 57	3116 ± 49	89
C14-C	White core	56	14	67	0.22	33.4436 ± 0.8938	0.6989 ± 0.0180	0.96	0.347	3417 ± 68	3694 ± 47	92
C14-R	Black rim	301	62	517	0.12	15.0497 ± 0.3944	0.5464 ± 0.0139	0.97	0.200	2810 ± 58	2824 ± 50	100
C15-C	Osci. zoned core	84	21	89	0.24	37.3421 ± 0.9841	0.7710 ± 0.0197	0.97	0.351	3685 ± 72	3712 ± 47	99
C15-R	Black rim	635	33	942	0.04	24.1595 ± 0.6326	0.5973 ± 0.0152	0.97	0.293	3019 ± 61	3435 ± 47	88
C16	Black	390	102	713	0.14	13.5435 ± 0.3553	0.5147 ± 0.0131	0.97	0.191	2677 ± 56	2749 ± 50	97
C17-C1	Osci. zoned core	58	17	68	0.25	32.0139 ± 0.8500	0.7059 ± 0.0181	0.97	0.329	3443 ± 68	3612 ± 47	95
C17-C2	Osci. zoned core	147	75	158	0.48	34.6531 ± 0.9125	0.7442 ± 0.0190	0.97	0.338	3586 ± 70	3652 ± 47	98
C18-C	Osci. zoned core	48	10	51	0.20	37.2702 ± 1.0004	0.7745 ± 0.0200	0.96	0.349	3697 ± 73	3703 ± 47	100
C18-R1	Black rim	114	31	195	0.16	14.8436 ± 0.3959	0.5466 ± 0.0140	0.96	0.197	2811 ± 58	2801 ± 51	100
C19-C	Osci. zoned core	128	82	152	0.54	31.0869 ± 0.8205	0.6669 ± 0.0170	0.97	0.338	3294 ± 66	3654 ± 47	90
C18-R2	Black rim	294	59	506	0.12	15.0335 ± 0.3960	0.5462 ± 0.0139	0.97	0.200	2809 ± 58	2823 ± 50	100
C20	Osci. zoned core	65	24	86	0.28	28.0910 ± 0.7517	0.6312 ± 0.0162	0.96	0.323	3154 ± 64	3583 ± 48	88
C21-C2	Osci. zoned core	59	20	65	0.31	34.6854 ± 0.9421	0.7477 ± 0.0194	0.96	0.337	3599 ± 71	3647 ± 48	99
C21-C1	Osci. zoned core	48	10	51	0.20	37.7757 ± 1.0082	0.7775 ± 0.0200	0.96	0.352	3708 ± 72	3717 ± 47	100
C22-C1	Black core	387	7	474	0.02	31.8943 ± 0.8414	0.7082 ± 0.0181	0.97	0.327	3452 ± 68	3601 ± 47	96

Continued on next page

Table B.3 – *Continued from previous page*

Spot #	Internal Structure	Pb (ppm)	Th (ppm)	U (ppm)	Th/U	$^{207}Pb/^{235}U$ $\pm 2\sigma$	$^{206}Pb/^{238}U$ $\pm 2\sigma$	ρ	$\frac{^{207}Pb}{^{206}Pb}$ ^{206}Pb	Ages (Ma)$\pm 2\sigma$ $\frac{^{206}Pb}{^{238}U}$	Ages (Ma)$\pm 2\sigma$ $\frac{^{207}Pb}{^{206}Pb}$	Conc %
C22-C2	Black core	251	52	480	0.11	13.1334 ± 0.3487	0.4895 ± 0.0125	0.96	0.195	2569 ± 54	2781 ± 51	92
C23	Black core	227	35	402	0.09	14.6904 ± 0.3877	0.5288 ± 0.0135	0.97	0.201	2736 ± 57	2838 ± 50	96
D1-C	Osci. zoned core	122	67	136	0.49	33.1952 ± 0.8808	0.7007 ± 0.0179	0.96	0.344	3424 ± 68	3679 ± 47	93
D1-R	Black rim	252	35	453	0.08	14.5435 ± 0.3840	0.5264 ± 0.0134	0.96	0.200	2726 ± 57	2829 ± 50	96
D2-C	Osci. zoned core	41	8	44	0.17	36.3056 ± 0.9744	0.7466 ± 0.0192	0.96	0.353	3595 ± 71	3719 ± 47	97
D3-C	Osci. zoned core	150	35	203	0.17	26.1449 ± 0.6971	0.6375 ± 0.0163	0.96	0.297	3179 ± 64	3457 ± 48	92
D6-C2	White core	17	3	20	0.16	33.4211 ± 0.9233	0.7380 ± 0.0193	0.95	0.328	3563 ± 71	3610 ± 49	99
D6-C1	Osci. zoned core	49	11	61	0.17	31.5389 ± 0.8592	0.6553 ± 0.0170	0.95	0.349	3249 ± 66	3703 ± 48	88
D7	Metamict core	790	181	1466	0.12	16.2663 ± 0.4301	0.4873 ± 0.0124	0.96	0.242	2559 ± 54	3134 ± 49	82
D8-C	Metamict core	1004	194	1312	0.15	27.8569 ± 0.7372	0.6566 ± 0.0167	0.96	0.308	3254 ± 65	3509 ± 48	93
D10-C	Osci. zoned core	111	42	123	0.34	35.4193 ± 0.9508	0.7206 ± 0.0185	0.96	0.356	3498 ± 69	3735 ± 47	94
D10-R	Black rim	302	40	519	0.08	15.1049 ± 0.4007	0.5496 ± 0.0140	0.96	0.199	2823 ± 58	2821 ± 50	100
D11-C	White core	63	17	75	0.23	31.9553 ± 0.8878	0.6980 ± 0.0182	0.94	0.332	3413 ± 69	3626 ± 49	94
D11-R	Sector zoned rim	146	43	250	0.17	14.8574 ± 0.3965	0.5419 ± 0.0138	0.95	0.199	2791 ± 58	2817 ± 51	99
D15-C	Osci. zoned core	101	13	169	0.08	22.6862 ± 0.6123	0.5113 ± 0.0131	0.95	0.322	2662 ± 56	3578 ± 48	74
D16-C	Osci. zoned core	142	98	156	0.63	34.1826 ± 0.9150	0.7149 ± 0.0183	0.96	0.347	3477 ± 69	3693 ± 47	94
D17-C	Osci. zoned core	146	138	161	0.85	34.1851 ± 0.9123	0.6858 ± 0.0175	0.96	0.361	3367 ± 67	3756 ± 47	90
D18-C	Osci. zoned core	44	10	51	0.19	35.2376 ± 0.9776	0.7107 ± 0.0186	0.94	0.360	3461 ± 70	3748 ± 49	92
D18-R	Black rim	315	48	553	0.09	14.8776 ± 0.3964	0.5393 ± 0.0138	0.96	0.200	2781 ± 58	2827 ± 51	98
D19	Black core	116	18	148	0.12	30.0713 ± 0.8143	0.6699 ± 0.0172	0.95	0.325	3305 ± 67	3596 ± 48	92
D20	Black core	455	70	620	0.11	27.1502 ± 0.7241	0.6359 ± 0.0162	0.96	0.310	3173 ± 64	3519 ± 48	90
D22	Osci. zoned core	37	11	54	0.21	23.5501 ± 0.6655	0.5893 ± 0.0155	0.93	0.290	2987 ± 63	3417 ± 50	87
D23	Black core	225	31	275	0.11	30.3694 ± 0.8122	0.7057 ± 0.0180	0.95	0.312	3442 ± 68	3531 ± 48	97
E1	Osci. zoned core	57	19	65	0.29	33.5804 ± 0.9242	0.7242 ± 0.0188	0.94	0.336	3512 ± 70	3646 ± 49	96
E2-C	White core	79	38	97	0.39	31.4353 ± 0.8656	0.6902 ± 0.0179	0.94	0.330	3383 ± 68	3619 ± 49	94
E2-R1	Black inner rim	253	39	294	0.13	34.7055 ± 0.9304	0.7372 ± 0.0188	0.95	0.341	3560 ± 70	3669 ± 47	97
E2-R2	Sector zoned rim	133	43	232	0.19	14.6042 ± 0.3937	0.5378 ± 0.0137	0.94	0.197	2774 ± 58	2801 ± 51	99
E5-C	Osci. zoned core	32	6	39	0.16	32.9394 ± 0.9504	0.6856 ± 0.0182	0.92	0.348	3366 ± 70	3700 ± 50	91
E5-R1	Osci. zoned core	50	1	55	0.02	37.4578 ± 1.0198	0.7682 ± 0.0198	0.95	0.354	3674 ± 72	3723 ± 48	99
E6-C	Osci. zoned core	93	63	102	0.62	35.7077 ± 0.9704	0.7209 ± 0.0185	0.94	0.359	3500 ± 69	3746 ± 48	93

Continued on next page

Table B.3 – *Continued from previous page*

Spot #	Internal Structure	Pb (ppm)	Th (ppm)	U (ppm)	Th/U	$^{207}Pb/^{235}U$ $\pm 2\sigma$	$^{206}Pb/^{238}U$ $\pm 2\sigma$	ρ	$\frac{^{207}Pb}{^{206}Pb}$ ^{206}Pb	Ages (Ma)$\pm 2\sigma$ $\frac{^{206}Pb}{^{238}U}$	Ages (Ma)$\pm 2\sigma$ $\frac{^{207}Pb}{^{206}Pb}$	Conc %
E8-C1	Osci. zoned core	51	16	56	0.28	36.4853 ± 0.9940	0.7417 ± 0.0191	0.95	0.357	3577 ± 71	3736 ± 48	96
E8-C2	Osci. zoned core	14	4	16	0.26	34.7540 ± 0.9738	0.7396 ± 0.0193	0.93	0.341	3569 ± 72	3666 ± 49	97
E10-C	Osci. zoned core	61	32	70	0.46	33.7104 ± 0.9213	0.7012 ± 0.0181	0.94	0.349	3425 ± 68	3701 ± 48	93
E10-R2	Black rim	168	38	294	0.13	14.6986 ± 0.3984	0.5378 ± 0.0138	0.95	0.198	2774 ± 58	2811 ± 51	99
E11-C	Osci. zoned core	38	9	46	0.19	31.4175 ± 0.8486	0.6760 ± 0.0175	0.96	0.337	3329 ± 67	3649 ± 48	91
E12-C	Osci. zoned core	63	18	81	0.23	29.2036 ± 0.7840	0.6413 ± 0.0165	0.96	0.330	3194 ± 65	3618 ± 48	88
E13	Metamict	549	49	1291	0.04	9.9968 ± 0.2602	0.4097 ± 0.0104	0.98	0.177	2214 ± 47	2624 ± 51	84
E14-C	Osci. zoned core	118	36	127	0.28	37.5770 ± 0.9783	0.7504 ± 0.0191	0.98	0.363	3609 ± 70	3763 ± 46	96
E14-R	Black rim	269	56	479	0.12	14.3341 ± 0.3738	0.5280 ± 0.0134	0.97	0.197	2733 ± 56	2800 ± 50	98
E15-C	Metamict	24	28	33	0.83	25.3157 ± 0.7389	0.5966 ± 0.0160	0.92	0.308	3016 ± 65	3510 ± 52	86
E17-C	Osci. zoned core	64	27	77	0.35	30.3032 ± 0.7953	0.6787 ± 0.0173	0.97	0.324	3340 ± 66	3588 ± 47	93
E18-C	Osci. zoned core	57	12	66	0.18	34.2047 ± 0.9056	0.7202 ± 0.0185	0.97	0.344	3497 ± 69	3682 ± 47	95
E18-R	Black rim	300	39	539	0.07	14.5984 ± 0.3802	0.5240 ± 0.0133	0.97	0.202	2716 ± 56	2843 ± 50	96
E20-C	Osci. zoned core	79	13	134	0.10	19.2127 ± 0.5133	0.5171 ± 0.0132	0.96	0.269	2687 ± 56	3303 ± 49	81
E22-C	Osci. zoned core	127	73	163	0.45	26.7400 ± 0.7027	0.6322 ± 0.0161	0.97	0.307	3158 ± 64	3505 ± 48	90
E23-C	Osci. zoned core	49	11	58	0.20	31.8703 ± 0.8547	0.6990 ± 0.0180	0.96	0.331	3417 ± 68	3620 ± 48	94
E23-R1	Black inner rim	362	44	650	0.07	14.3121 ± 0.3714	0.5321 ± 0.0135	0.98	0.195	2750 ± 57	2785 ± 50	99
E23-R2	Grey rim	144	30	253	0.12	14.5339 ± 0.3787	0.5377 ± 0.0136	0.97	0.196	2774 ± 57	2793 ± 50	99
E23-R3	Black outer rim	387	43	688	0.06	14.5008 ± 0.3764	0.5374 ± 0.0136	0.97	0.196	2773 ± 57	2791 ± 50	99
E24	Metamict	410	130	750	0.17	15.8352 ± 0.4119	0.4964 ± 0.0126	0.98	0.231	2598 ± 54	3061 ± 49	85
SG-127 granite												
A1-C	Osci. zoned core	110	109	176	0.62	14.5248 ± 0.3897	0.5387 ± 0.0137	0.95	0.196	2778 ± 58	2789 ± 51	100
A1-R	Black rim	953	455	2482	0.18	7.9923 ± 0.2120	0.3690 ± 0.0094	0.96	0.157	2025 ± 44	2424 ± 52	84
A2	Metamict	730	97	1807	0.05	8.4133 ± 0.2230	0.4018 ± 0.0102	0.96	0.152	2177 ± 47	2367 ± 53	92
A4	Metamict	739	119	1705	0.07	9.4651 ± 0.2515	0.4215 ± 0.0107	0.96	0.163	2267 ± 49	2486 ± 52	91
A8	Metamict	394	50	789	0.06	12.1204 ± 0.3232	0.4815 ± 0.0122	0.95	0.183	2534 ± 53	2676 ± 51	95
A10	Metamict	550	115	1117	0.10	11.5660 ± 0.3075	0.4727 ± 0.0120	0.95	0.177	2495 ± 53	2629 ± 52	95
A11-C	Osci. zoned core	44	41	47	0.88	33.3713 ± 0.9079	0.7127 ± 0.0183	0.94	0.340	3469 ± 69	3661 ± 48	95
A14	Metamict	965	387	2160	0.18	9.4014 ± 0.2510	0.4272 ± 0.0109	0.96	0.160	2293 ± 49	2451 ± 53	94
A16-C	Osci. zoned core	262	521	373	1.40	14.8611 ± 0.3983	0.5450 ± 0.0139	0.95	0.198	2804 ± 58	2808 ± 51	100

Continued on next page

Table B.3 – *Continued from previous page*

Spot #	**Internal Structure**	**Pb** (ppm)	**Th** (ppm)	**U** (ppm)	**Th/U**	^{207}**Pb**/^{235}**U** $\pm 2\sigma$	^{206}**Pb**/^{238}**U** $\pm 2\sigma$	ρ	$\frac{^{207}Pb}{^{206}Pb}$ ^{206}Pb	**Ages (Ma)**$\pm 2\sigma$ $\frac{^{206}Pb}{^{238}U}$	$\frac{^{207}Pb}{^{206}Pb}$	**Conc** %
A17	Metamict	782	223	2045	0.11	7.9508 ± 0.2126	0.3742 ± 0.0095	0.95	0.154	2049 ± 45	2392 ± 53	86
B1-C	Osci. zoned core	103	130	163	0.80	14.7146 ± 0.3978	0.5406 ± 0.0138	0.94	0.197	2786 ± 58	2805 ± 51	99
B2	Metamict	798	395	1899	0.21	9.0124 ± 0.2415	0.4041 ± 0.0103	0.95	0.162	2188 ± 47	2474 ± 53	88
B3	Metamict	450	171	772	0.22	14.8538 ± 0.4007	0.5412 ± 0.0138	0.95	0.199	2788 ± 58	2818 ± 51	99
B10	Metamict	913	203	2086	0.10	9.5309 ± 0.2573	0.4204 ± 0.0107	0.94	0.164	2262 ± 48	2501 ± 53	90
B11	Osci. zoned core	166	93	283	0.33	14.3763 ± 0.3894	0.5291 ± 0.0134	0.94	0.197	2737 ± 57	2802 ± 52	98
B16-C	Osci. zoned core	31	35	51	0.69	14.0772 ± 0.3971	0.5287 ± 0.0136	0.91	0.193	2736 ± 57	2769 ± 53	99
C3	Metamict	353	147	2576	0.06	2.2522 ± 0.0611	0.1315 ± 0.0033	0.93	0.124	796 ± 19	2018 ± 56	39
C4	Metamict	956	135	2499	0.05	7.4487 ± 0.2019	0.3819 ± 0.0097	0.94	0.141	2085 ± 45	2245 ± 55	93
C5-C	Osci. zoned core	33	35	62	0.57	12.2770 ± 0.3697	0.4501 ± 0.0118	0.87	0.198	2396 ± 53	2808 ± 56	85
C6	Metamict	528	113	1282	0.09	9.9916 ± 0.2735	0.3974 ± 0.0101	0.93	0.182	2157 ± 47	2674 ± 53	81
C12	Metamict	737	114	1941	0.06	7.9723 ± 0.2181	0.3736 ± 0.0095	0.93	0.155	2046 ± 44	2399 ± 54	85
C14	Metamict	661	206	1610	0.13	8.2802 ± 0.2262	0.4007 ± 0.0102	0.93	0.150	2172 ± 47	2344 ± 54	93
C16	Metamict	884	57	2098	0.03	9.4064 ± 0.2570	0.4150 ± 0.0105	0.93	0.164	2238 ± 48	2501 ± 53	89
C17	Metamict	715	178	1282	0.14	14.2236 ± 0.3896	0.5219 ± 0.0132	0.92	0.198	2707 ± 56	2807 ± 52	96
C18	Metamict	456	46	843	0.05	13.8085 ± 0.3792	0.5150 ± 0.0131	0.93	0.194	2678 ± 56	2780 ± 52	96
D1	Metamict	619	67	1150	0.06	13.4774 ± 0.3711	0.5153 ± 0.0131	0.92	0.190	2679 ± 56	2739 ± 53	98
D3	Metamict	668	103	1689	0.06	8.3171 ± 0.2292	0.3890 ± 0.0099	0.92	0.155	2118 ± 46	2402 ± 54	88
D3	Metamict	507	99	1102	0.09	11.0047 ± 0.3051	0.4403 ± 0.0112	0.92	0.181	2352 ± 50	2664 ± 53	88
D4-C	Osci. zoned core	46	61	70	0.87	14.5720 ± 0.4126	0.5366 ± 0.0137	0.90	0.197	2769 ± 58	2801 ± 53	99
D4-R	Metamict rim	662	121	1183	0.10	14.1870 ± 0.3909	0.5259 ± 0.0133	0.92	0.196	2724 ± 56	2790 ± 52	98
D6	Osci. zoned core	52	40	84	0.48	14.5394 ± 0.4119	0.5344 ± 0.0137	0.90	0.197	2760 ± 57	2804 ± 53	98
D8	Metamict	293	128	1737	0.07	2.3109 ± 0.0646	0.1727 ± 0.0044	0.91	0.097	1027 ± 24	1568 ± 61	66
D9	Metamict	591	88	1299	0.07	10.0059 ± 0.2774	0.4411 ± 0.0112	0.92	0.164	2356 ± 50	2502 ± 54	94
E1-C	Osci. zoned core	87	38	151	0.25	14.4556 ± 0.3825	0.5300 ± 0.0134	0.96	0.198	2742 ± 56	2808 ± 51	98
E1-R	Metamict rim	771	224	6234	0.04	1.8150 ± 0.0475	0.1278 ± 0.0032	0.96	0.103	775 ± 18	1679 ± 57	46
E2	Metamict	711	39	1619	0.02	11.0882 ± 0.2909	0.4252 ± 0.0107	0.96	0.189	2284 ± 48	2734 ± 51	84
E3	Metamict	595	94	1548	0.06	8.5257 ± 0.2239	0.3763 ± 0.0095	0.96	0.164	2059 ± 44	2500 ± 52	82
E7	Metamict	581	52	1126	0.05	12.6209 ± 0.3287	0.4992 ± 0.0125	0.96	0.183	2610 ± 54	2683 ± 51	97
E8	Metamict	597	22	1296	0.02	11.0343 ± 0.2875	0.4509 ± 0.0113	0.96	0.177	2399 ± 50	2629 ± 51	91

Continued on next page

Table B.3 – *Continued from previous page*

Spot #	Internal Structure	Pb (ppm)	Th (ppm)	U (ppm)	Th/U	$^{207}Pb/^{235}U$ $\pm 2\sigma$	$^{206}Pb/^{238}U$ $\pm 2\sigma$	ρ	$\frac{^{207}Pb}{^{206}Pb}$ ^{206}Pb	Ages (Ma)$\pm 2\sigma$ $\frac{^{206}Pb}{^{238}U}$	Ages (Ma)$\pm 2\sigma$ $\frac{^{207}Pb}{^{206}Pb}$	Conc %
E9	Metamict	820	96	1717	0.06	11.6201 ± 0.3035	0.4618 ± 0.0116	0.96	0.183	2447 ± 51	2676 ± 51	91
E10	Metamict	571	103	1064	0.10	12.8170 ± 0.3366	0.5134 ± 0.0129	0.96	0.181	2671 ± 55	2662 ± 51	100
E12	Metamict	618	176	2363	0.07	4.7121 ± 0.1236	0.2624 ± 0.0066	0.96	0.130	1502 ± 34	2101 ± 54	71
E14	Osci. zoned core	264	215	422	0.51	14.7154 ± 0.3854	0.5427 ± 0.0136	0.96	0.197	2795 ± 57	2798 ± 51	100
E15	Metamict	670	148	1781	0.08	7.5338 ± 0.1966	0.3714 ± 0.0093	0.96	0.147	2036 ± 44	2313 ± 53	88
F1	Metamict	666	81	1561	0.05	9.4256 ± 0.2463	0.4204 ± 0.0105	0.96	0.163	2262 ± 48	2483 ± 52	91
F4	Metamict	635	72	1512	0.05	9.0650 ± 0.2371	0.4153 ± 0.0104	0.96	0.158	2239 ± 47	2437 ± 52	92
F5	Metamict	992	295	2440	0.12	8.2482 ± 0.2157	0.3951 ± 0.0099	0.96	0.151	2147 ± 46	2362 ± 53	91
F6	Metamict	788	49	1580	0.03	12.8707 ± 0.3379	0.4791 ± 0.0120	0.95	0.195	2523 ± 52	2783 ± 51	91
F13	Metamict	566	102	1248	0.08	10.0064 ± 0.2632	0.4390 ± 0.0110	0.95	0.165	2346 ± 49	2510 ± 52	93
F15	Metamict	556	48	1001	0.05	14.0910 ± 0.3707	0.5297 ± 0.0132	0.95	0.193	2740 ± 56	2767 ± 51	99
SG-143 granite												
A1	Metamict	426	330	841	0.39	12.0884 ± 0.3238	0.4626 ± 0.0118	0.95	0.190	2451 ± 52	2738 ± 51	90
A3	Black	400	227	683	0.33	14.0085 ± 0.3739	0.5292 ± 0.0135	0.96	0.192	2738 ± 57	2759 ± 51	99
A7	Black	385	303	652	0.46	14.0052 ± 0.3749	0.5150 ± 0.0132	0.96	0.197	2678 ± 56	2803 ± 51	96
A8	Black	745	184	1400	0.13	12.9710 ± 0.3468	0.5043 ± 0.0129	0.96	0.187	2632 ± 55	2712 ± 51	97
A9-C	Black core	899	36	1670	0.02	13.3444 ± 0.3579	0.5223 ± 0.0134	0.96	0.185	2709 ± 57	2701 ± 51	100
A9-R	Metamict rim	526	327	886	0.37	14.2408 ± 0.3815	0.5323 ± 0.0136	0.95	0.194	2751 ± 57	2777 ± 51	99
A10	Metamict	712	43	1328	0.03	13.6844 ± 0.3665	0.5162 ± 0.0132	0.95	0.192	2683 ± 56	2762 ± 51	97
A12-R	Black rim	372	22	689	0.03	13.6515 ± 0.3668	0.5067 ± 0.0130	0.95	0.195	2642 ± 55	2788 ± 51	95
A15	Black rim	363	198	616	0.32	14.2169 ± 0.3830	0.5316 ± 0.0136	0.95	0.194	2748 ± 57	2776 ± 51	99
A17	Black	369	243	623	0.39	14.0752 ± 0.3798	0.5316 ± 0.0136	0.95	0.192	2748 ± 57	2760 ± 51	100
B2	Black	601	37	1069	0.03	14.5776 ± 0.3934	0.5378 ± 0.0138	0.95	0.197	2774 ± 58	2798 ± 51	99
B4-C	Osci. zoned core	351	116	696	0.17	12.8569 ± 0.3538	0.4668 ± 0.0120	0.93	0.200	2470 ± 53	2824 ± 52	87
B4-R	Osci. zoned rim	654	204	1150	0.18	14.4007 ± 0.3893	0.5269 ± 0.0135	0.95	0.198	2729 ± 57	2811 ± 51	97
B7	Osci. zoned core	435	151	779	0.19	13.3683 ± 0.3631	0.5181 ± 0.0133	0.95	0.187	2691 ± 56	2717 ± 52	99
B9	Metamict	252	107	442	0.24	13.9042 ± 0.3782	0.5268 ± 0.0135	0.94	0.191	2728 ± 57	2754 ± 52	99
B11-C	Osci. zoned core	66	33	120	0.27	13.4435 ± 0.3837	0.4936 ± 0.0128	0.91	0.198	2586 ± 55	2806 ± 53	92
B11-R	Metamict rim	438	40	792	0.05	14.3048 ± 0.3890	0.5298 ± 0.0136	0.94	0.196	2740 ± 57	2792 ± 51	98
B12-R	Black rim	551	73	998	0.07	14.3388 ± 0.3914	0.5272 ± 0.0135	0.94	0.197	2730 ± 57	2804 ± 51	97

Continued on next page

Table B.3 – *Continued from previous page*

Spot #	Internal Structure	Pb (ppm)	Th (ppm)	U (ppm)	Th/U	$^{207}Pb/^{235}U$ $\pm 2\sigma$	$^{206}Pb/^{238}U$ $\pm 2\sigma$	ρ	$\frac{^{207}Pb}{^{206}Pb}$ ^{206}Pb	Ages (Ma)$\pm 2\sigma$ $\frac{^{206}Pb}{^{238}U}$	Ages (Ma)$\pm 2\sigma$ $\frac{^{207}Pb}{^{206}Pb}$	Conc %
B15	Metamict	597	1049	855	1.23	14.7522 ± 0.4032	0.5332 ± 0.0137	0.94	0.201	2755 ± 57	2831 ± 51	97
B16-C	Metamict core	680	83	1534	0.05	11.0032 ± 0.3015	0.4272 ± 0.0110	0.94	0.187	2293 ± 50	2714 ± 52	84
B17	Metamict	697	106	1263	0.08	14.0614 ± 0.3844	0.5289 ± 0.0136	0.94	0.193	2737 ± 57	2766 ± 52	99
B18-C	Black core	431	188	739	0.25	14.6415 ± 0.4012	0.5398 ± 0.0139	0.94	0.197	2783 ± 58	2799 ± 52	99
B18-R	Grey rim	485	214	828	0.26	14.5287 ± 0.3984	0.5344 ± 0.0137	0.93	0.197	2760 ± 58	2803 ± 52	98
C1	Metamict	371	120	652	0.18	13.9785 ± 0.3836	0.5290 ± 0.0136	0.94	0.192	2737 ± 57	2756 ± 52	99
C2	Metamict core	247	243	474	0.51	12.8053 ± 0.3421	0.4775 ± 0.0122	0.96	0.195	2516 ± 53	2781 ± 51	90
C3	Metamict	349	184	639	0.29	13.0702 ± 0.3466	0.4943 ± 0.0126	0.96	0.192	2589 ± 54	2757 ± 51	94
C6	Metamict	290	130	521	0.25	13.4374 ± 0.3533	0.5112 ± 0.0130	0.97	0.191	2662 ± 55	2748 ± 51	97
C7-C	Metamict	771	130	1406	0.09	13.7007 ± 0.3592	0.5196 ± 0.0132	0.97	0.191	2697 ± 56	2753 ± 50	98
C8-C	Metamict	324	242	560	0.43	13.6079 ± 0.3575	0.5127 ± 0.0130	0.97	0.192	2668 ± 55	2763 ± 51	97
C10-C	Osci. zoned core	596	135	1060	0.13	14.2274 ± 0.3726	0.5263 ± 0.0133	0.96	0.196	2726 ± 56	2794 ± 50	98
C12	Metamict core	261	80	489	0.16	13.6873 ± 0.3647	0.4980 ± 0.0127	0.96	0.199	2605 ± 55	2821 ± 51	92
C14-C	Black core	295	315	488	0.64	13.8170 ± 0.3630	0.5102 ± 0.0129	0.96	0.196	2657 ± 55	2796 ± 50	95
C14-R	Osci. zoned rim	546	495	1205	0.41	10.8079 ± 0.2830	0.4016 ± 0.0102	0.97	0.195	2176 ± 47	2786 ± 50	78
D3	Metamict	550	468	912	0.51	14.0961 ± 0.3687	0.5278 ± 0.0134	0.97	0.194	2732 ± 56	2774 ± 50	99
D8	Metamict	607	34	1234	0.03	12.9224 ± 0.3385	0.4722 ± 0.0119	0.96	0.199	2493 ± 52	2814 ± 50	89
D9	Osci. zoned core	278	61	308	0.20	35.1925 ± 0.9209	0.7540 ± 0.0191	0.97	0.338	3622 ± 70	3656 ± 47	99
D12	Black	212	106	372	0.29	13.7223 ± 0.3605	0.5227 ± 0.0132	0.96	0.190	2711 ± 56	2745 ± 51	99
D13	Metamict	485	57	943	0.06	13.1281 ± 0.3441	0.4934 ± 0.0125	0.97	0.193	2586 ± 54	2767 ± 51	93
E4	Black	337	162	583	0.28	14.0515 ± 0.3680	0.5315 ± 0.0134	0.96	0.192	2748 ± 56	2757 ± 51	100
E5	Oscillatory zoned	486	408	1049	0.39	10.2129 ± 0.2688	0.4161 ± 0.0105	0.96	0.178	2243 ± 48	2634 ± 51	85
E7	Black	543	264	935	0.28	14.1685 ± 0.3706	0.5305 ± 0.0134	0.97	0.194	2744 ± 56	2774 ± 50	99
E9	Black core	455	58	810	0.07	14.3880 ± 0.3777	0.5364 ± 0.0135	0.96	0.195	2768 ± 57	2781 ± 51	100
E10	Black	218	109	377	0.29	14.1459 ± 0.3719	0.5242 ± 0.0132	0.96	0.196	2717 ± 56	2791 ± 51	97
E12	Black core	461	152	836	0.18	13.6567 ± 0.3572	0.5151 ± 0.0130	0.96	0.192	2678 ± 55	2762 ± 51	97
E16-C	Inherited core	96	59	114	0.52	30.3183 ± 0.8055	0.6667 ± 0.0169	0.95	0.330	3293 ± 65	3616 ± 48	91
E18-C	Inherited core	492	208	634	0.33	27.0127 ± 0.7072	0.6501 ± 0.0164	0.96	0.301	3229 ± 64	3477 ± 48	93
F1	Metamict	600	183	1056	0.17	14.0788 ± 0.3682	0.5327 ± 0.0134	0.96	0.192	2753 ± 56	2757 ± 51	100
F2	Metamict	369	296	621	0.48	13.8799 ± 0.3638	0.5221 ± 0.0131	0.96	0.193	2708 ± 56	2766 ± 51	98

Continued on next page

Table B.3 – *Continued from previous page*

Spot #	Internal Structure	Pb (ppm)	Th (ppm)	U (ppm)	Th/U	$^{207}Pb/^{235}U$ $\pm 2\sigma$	$^{206}Pb/^{238}U$ $\pm 2\sigma$	ρ	$\frac{^{207}Pb}{^{206}Pb}$ ^{206}Pb	Ages (Ma)$\pm 2\sigma$ $\frac{^{206}Pb}{^{238}U}$	Ages (Ma)$\pm 2\sigma$ $\frac{^{207}Pb}{^{206}Pb}$	Conc %
F5	Metamict	407	159	966	0.16	10.5332 ± 0.2782	0.3932 ± 0.0099	0.95	0.194	2138 ± 46	2779 ± 51	77
F9	Metamict	399	188	684	0.27	14.2046 ± 0.3721	0.5333 ± 0.0134	0.96	0.193	2755 ± 56	2769 ± 51	99
F10	Metamict	555	336	1141	0.29	11.7908 ± 0.3106	0.4397 ± 0.0111	0.96	0.194	2349 ± 50	2780 ± 51	84
F13	Metamict	697	94	1477	0.06	11.7468 ± 0.3087	0.4526 ± 0.0114	0.96	0.188	2407 ± 51	2727 ± 51	88
F15	Metamict	468	112	828	0.13	14.0245 ± 0.3674	0.5326 ± 0.0134	0.96	0.191	2753 ± 56	2750 ± 51	100
SG-203 granodiorite												
A01	Osci. zoned rim	76	40	91	0.43	26.1824 ± 0.7746	0.6903 ± 0.0198	0.97	0.275	3384 ± 75	3335 ± 48	101
A02	Black ext rim	54	32	66	0.49	25.2961 ± 0.7534	0.6734 ± 0.0194	0.97	0.272	3319 ± 75	3320 ± 49	100
A02	Osci. zoned core	98	27	122	0.22	26.2808 ± 0.7757	0.6837 ± 0.0196	0.97	0.279	3359 ± 75	3356 ± 48	100
A03	Osci. zoned core	63	47	74	0.64	25.2184 ± 0.7487	0.6714 ± 0.0193	0.97	0.272	3311 ± 74	3320 ± 49	100
A03	Convoluted rim	42	10	57	0.18	23.2515 ± 0.7089	0.6390 ± 0.0185	0.95	0.264	3185 ± 73	3270 ± 50	97
A04	Osci. zoned core	36	31	41	0.76	25.9984 ± 0.7831	0.6838 ± 0.0197	0.96	0.276	3359 ± 76	3339 ± 49	101
A04	Osci. zoned rim	50	25	61	0.41	25.8708 ± 0.7715	0.6793 ± 0.0195	0.96	0.276	3342 ± 75	3342 ± 49	100
A05	Osci. zoned rim	113	51	138	0.37	25.6727 ± 0.7578	0.6836 ± 0.0196	0.97	0.272	3358 ± 75	3320 ± 48	101
A06	Osci. zoned core	44	34	51	0.67	25.5810 ± 0.7655	0.6835 ± 0.0197	0.96	0.271	3358 ± 75	3314 ± 49	101
A07	Osci. zoned core	47	29	56	0.51	26.0059 ± 0.7786	0.6832 ± 0.0197	0.96	0.276	3357 ± 75	3341 ± 49	100
A08	Osci. zoned core	279	190	333	0.57	25.1045 ± 0.7379	0.6716 ± 0.0192	0.97	0.271	3312 ± 74	3312 ± 48	100
A10	Osci. zoned core	176	96	210	0.46	26.0303 ± 0.7666	0.6836 ± 0.0196	0.97	0.276	3358 ± 75	3341 ± 48	101
A11	Osci. zoned rim	286	142	363	0.39	24.5719 ± 0.7250	0.6580 ± 0.0188	0.97	0.271	3260 ± 73	3311 ± 48	98
A12	Osci. zoned core	34	18	43	0.41	24.5143 ± 0.7541	0.6597 ± 0.0192	0.95	0.269	3266 ± 75	3303 ± 50	99
A13	Osci. zoned rim	52	29	62	0.47	26.3252 ± 0.7883	0.6854 ± 0.0197	0.96	0.279	3365 ± 76	3355 ± 49	100
A14	Osci. zoned rim	27	14	35	0.41	23.5229 ± 0.7331	0.6400 ± 0.0188	0.94	0.267	3189 ± 74	3286 ± 51	97
A15	Osci. zoned rim	31	17	40	0.44	24.0441 ± 0.7372	0.6498 ± 0.0189	0.95	0.268	3228 ± 74	3296 ± 50	98
A16	Osci. zoned core	35	25	41	0.63	25.5212 ± 0.7713	0.6758 ± 0.0196	0.96	0.274	3328 ± 75	3328 ± 49	100
A17	Osci. zoned rim	110	15	200	0.08	13.6526 ± 0.4089	0.5263 ± 0.0151	0.96	0.188	2726 ± 64	2726 ± 51	100
B01	Osci. zoned rim	85	42	107	0.39	24.7550 ± 0.7443	0.6653 ± 0.0192	0.96	0.270	3288 ± 74	3305 ± 49	99
B02	Osci. zoned rim	130	59	163	0.36	25.1804 ± 0.7511	0.6683 ± 0.0192	0.96	0.273	3300 ± 74	3325 ± 49	99
B04	Osci. zoned rim	75	3	121	0.03	17.8266 ± 0.5325	0.5849 ± 0.0168	0.96	0.221	2969 ± 68	2988 ± 50	99
B05	Osci. zoned core	48	31	58	0.53	24.8129 ± 0.7728	0.6643 ± 0.0195	0.94	0.271	3284 ± 75	3311 ± 51	99
B05	Osci. Z. Int. rim	41	22	51	0.42	25.0943 ± 0.7641	0.6675 ± 0.0194	0.95	0.273	3296 ± 75	3321 ± 50	99

Continued on next page

Table B.3 – *Continued from previous page*

Spot #	Internal Structure	Pb (ppm)	Th (ppm)	U (ppm)	Th/U	$^{207}Pb/^{235}U$ $\pm 2\sigma$	$^{206}Pb/^{238}U$ $\pm 2\sigma$	ρ	$\frac{^{207}Pb}{^{206}Pb}$ ^{206}Pb	Ages (Ma)$\pm 2\sigma$ $\frac{^{206}Pb}{^{238}U}$	Ages (Ma)$\pm 2\sigma$ $\frac{^{207}Pb}{^{206}Pb}$	Conc %
B05	Black Outer rim	185	70	234	0.30	25.4671 ± 0.7572	0.6765 ± 0.0194	0.96	0.273	3331 ± 75	3323 ± 49	100
B06	Osci. zoned core	37	20	46	0.44	24.7045 ± 0.7629	0.6617 ± 0.0193	0.94	0.271	3274 ± 75	3310 ± 50	99
B08	Black core	188	10	350	0.03	13.3045 ± 0.3971	0.5209 ± 0.0150	0.96	0.185	2703 ± 63	2700 ± 51	100
B09	Osci. zoned core	46	29	60	0.49	22.3843 ± 0.6836	0.6206 ± 0.0180	0.95	0.262	3112 ± 72	3256 ± 50	96
B10	Osci. zoned core	92	53	111	0.48	25.5388 ± 0.7676	0.6769 ± 0.0195	0.96	0.274	3333 ± 75	3327 ± 49	100
B11	Osci. zoned core	23	12	30	0.39	24.0710 ± 0.7515	0.6506 ± 0.0191	0.94	0.268	3231 ± 74	3296 ± 51	98
B12	Osci. zoned core	20	16	23	0.70	25.5178 ± 0.7939	0.6765 ± 0.0198	0.94	0.274	3331 ± 76	3327 ± 51	100
B13	Osci. zoned core	45	20	62	0.32	22.2878 ± 0.6970	0.6190 ± 0.0182	0.94	0.261	3106 ± 72	3253 ± 51	95
B14	Osci. zoned core	28	18	39	0.46	20.7309 ± 0.6546	0.5970 ± 0.0176	0.93	0.252	3018 ± 71	3196 ± 52	94
B16	Osci. zoned core	54	43	63	0.68	25.4166 ± 0.7727	0.6735 ± 0.0195	0.95	0.274	3320 ± 75	3327 ± 49	100
B17	Black core	354	172	468	0.37	22.9208 ± 0.6874	0.6338 ± 0.0182	0.96	0.262	3165 ± 72	3260 ± 49	97
B18	Osci. zoned core	39	17	55	0.32	20.1682 ± 0.6239	0.6121 ± 0.0178	0.94	0.239	3078 ± 71	3113 ± 51	99
B18	Osci. zoned rim	70	37	84	0.44	25.5577 ± 0.7741	0.6756 ± 0.0195	0.95	0.274	3328 ± 75	3331 ± 49	100
C02	Osci. zoned core	22	14	26	0.55	25.6743 ± 0.8131	0.6783 ± 0.0200	0.93	0.275	3338 ± 77	3332 ± 51	100
C03	Osci. zoned core	38	21	46	0.45	24.9424 ± 0.7734	0.6646 ± 0.0194	0.94	0.272	3285 ± 75	3319 ± 50	99
C04	Black core	72	57	83	0.69	25.4528 ± 0.7772	0.6732 ± 0.0195	0.95	0.274	3318 ± 75	3330 ± 50	100
C04	Black Outer rim	88	45	109	0.41	25.1061 ± 0.7643	0.6693 ± 0.0194	0.95	0.272	3303 ± 75	3318 ± 50	100
C05	Osci. zoned core	53	45	67	0.68	22.6207 ± 0.6959	0.6269 ± 0.0182	0.94	0.262	3138 ± 72	3257 ± 50	96
C06	Black core	605	6	978	0.01	17.4870 ± 0.5262	0.5899 ± 0.0170	0.96	0.215	2989 ± 69	2944 ± 50	102
C07	Unzoned core	52	41	66	0.61	22.8253 ± 0.7041	0.6270 ± 0.0182	0.94	0.264	3138 ± 72	3271 ± 50	96
C08	Osci. zoned core	106	93	131	0.71	22.9443 ± 0.6967	0.6311 ± 0.0182	0.95	0.264	3154 ± 72	3269 ± 50	96
C09	Black rim	96	50	118	0.42	25.4755 ± 0.7742	0.6750 ± 0.0195	0.95	0.274	3325 ± 75	3327 ± 49	100
C10	Osci. zoned core	88	38	125	0.31	21.7008 ± 0.6807	0.6071 ± 0.0178	0.93	0.259	3059 ± 71	3242 ± 51	94
C10	Black rim	402	8	682	0.01	15.9637 ± 0.4820	0.5616 ± 0.0162	0.96	0.206	2873 ± 67	2875 ± 51	100
C11	Osci. zoned core	58	35	69	0.51	25.8213 ± 0.7893	0.6795 ± 0.0197	0.95	0.276	3343 ± 76	3338 ± 50	100
C12	Osci. zoned core	27	21	33	0.64	23.7665 ± 0.7583	0.6452 ± 0.0191	0.93	0.267	3210 ± 75	3289 ± 52	98
C12	Osci. zoned rim	45	25	54	0.46	25.8658 ± 0.7963	0.6815 ± 0.0198	0.94	0.275	3350 ± 76	3336 ± 50	100
C12	Black rim	75	1	120	0.01	18.1226 ± 0.5556	0.5885 ± 0.0170	0.94	0.223	2983 ± 69	3005 ± 51	99
C13	Osci. zoned core	16	11	20	0.55	24.2062 ± 0.7781	0.6543 ± 0.0194	0.92	0.268	3245 ± 75	3296 ± 52	98
C14	Black core	429	4	682	0.01	17.9545 ± 0.5451	0.5933 ± 0.0171	0.95	0.219	3003 ± 69	2977 ± 51	101

Continued on next page

Table B.3 – *Continued from previous page*

Spot #	Internal Structure	Pb (ppm)	Th (ppm)	U (ppm)	Th/U	$^{207}Pb/^{235}U$ $\pm 2\sigma$	$^{206}Pb/^{238}U$ $\pm 2\sigma$	ρ	$\frac{^{207}Pb}{^{206}Pb}$ ^{206}Pb	Ages (Ma)$\pm 2\sigma$ $\frac{^{206}Pb}{^{238}U}$	Ages (Ma)$\pm 2\sigma$ $\frac{^{207}Pb}{^{206}Pb}$	Conc %
C15	Black core	474	4	753	0.01	17.9053 ± 0.5416	0.5945 ± 0.0171	0.95	0.218	3008 ± 69	2969 ± 51	101
C16	Black rim	261	2	421	0.00	17.9439 ± 0.5453	0.5886 ± 0.0170	0.95	0.221	2984 ± 69	2989 ± 51	100
C17	Convo. core	28	14	36	0.38	24.6495 ± 0.7806	0.6607 ± 0.0194	0.93	0.271	3270 ± 75	3309 ± 51	99
D01	Osci. zoned core	27	17	34	0.50	24.5848 ± 0.8068	0.6633 ± 0.0198	0.91	0.269	3280 ± 77	3299 ± 53	99
D01	Black rim	363	9	678	0.01	13.2035 ± 0.4030	0.5224 ± 0.0151	0.95	0.183	2709 ± 64	2683 ± 52	101
D02	Osci. zoned core	81	65	95	0.68	24.9939 ± 0.7731	0.6689 ± 0.0194	0.94	0.271	3302 ± 75	3312 ± 50	100
D03	Osci. zoned core	59	37	70	0.53	25.5169 ± 0.7893	0.6740 ± 0.0196	0.94	0.275	3321 ± 75	3332 ± 50	100
D04	Osci. zoned core	48	29	63	0.46	22.9235 ± 0.7268	0.6328 ± 0.0186	0.93	0.263	3161 ± 73	3263 ± 52	97
D04	Black rim	511	76	1070	0.07	10.3404 ± 0.3173	0.4699 ± 0.0136	0.94	0.160	2483 ± 60	2451 ± 54	101
D05	Osci. zoned core	208	117	255	0.46	25.1675 ± 0.7707	0.6724 ± 0.0195	0.95	0.271	3315 ± 75	3314 ± 50	100
D06	Osci. zoned core	60	38	77	0.49	23.5728 ± 0.7483	0.6406 ± 0.0188	0.92	0.267	3191 ± 74	3288 ± 52	97
D07	Osci. zoned core	67	46	82	0.56	24.5772 ± 0.7826	0.6599 ± 0.0194	0.92	0.270	3267 ± 75	3307 ± 52	99
D08	Osci. zoned core	28	15	36	0.41	24.0311 ± 0.7838	0.6473 ± 0.0192	0.91	0.269	3218 ± 75	3302 ± 53	97
D09	Convo. core	32	15	41	0.37	24.5298 ± 0.7814	0.6563 ± 0.0193	0.92	0.271	3253 ± 75	3312 ± 52	98
D10	Osci. zoned rim	37	22	46	0.48	24.8086 ± 0.7861	0.6637 ± 0.0195	0.93	0.271	3281 ± 75	3312 ± 51	99
D11	Osci. zoned core	25	22	29	0.76	25.1350 ± 0.7978	0.6695 ± 0.0197	0.93	0.272	3304 ± 76	3319 ± 51	100
D12	Osci. zoned core	45	26	54	0.48	25.4999 ± 0.8049	0.6763 ± 0.0198	0.93	0.273	3330 ± 76	3326 ± 51	100
D13	Osci. zoned rim	91	45	111	0.41	25.8244 ± 0.8042	0.6817 ± 0.0198	0.93	0.275	3351 ± 76	3333 ± 50	101
C04	Osci. zoned core	35	18	44	0.41	24.2465 ± 0.7168	0.6623 ± 0.0186	0.95	0.266	3276 ± 72	3280 ± 50	100
C04	Osci. Z. int. rim	41	23	52	0.44	24.0468 ± 0.7157	0.6563 ± 0.0185	0.95	0.266	3253 ± 72	3281 ± 50	99
C04	Black core	28	16	34	0.49	25.0868 ± 0.7504	0.6604 ± 0.0187	0.95	0.276	3269 ± 73	3338 ± 50	98
D14	Osci. zoned core	37	25	46	0.54	23.6963 ± 0.7007	0.6419 ± 0.0181	0.95	0.268	3196 ± 71	3293 ± 50	97
D15	Osci. zoned core	42	25	50	0.51	25.7231 ± 0.7585	0.6783 ± 0.0191	0.95	0.275	3338 ± 73	3335 ± 49	100
D16	Osci. zoned core	19	12	23	0.52	25.2965 ± 0.7837	0.6629 ± 0.0191	0.93	0.277	3278 ± 74	3345 ± 52	98
D17	Osci. zoned core	46	45	52	0.85	25.4036 ± 0.7479	0.6721 ± 0.0189	0.96	0.274	3314 ± 73	3330 ± 49	100
D17	Osci. zoned rim	46	26	56	0.47	25.5086 ± 0.7536	0.6770 ± 0.0191	0.95	0.273	3333 ± 73	3325 ± 49	100
D17	Black rim	203	2	326	0.01	17.8283 ± 0.5154	0.5917 ± 0.0165	0.96	0.219	2996 ± 67	2970 ± 50	101
E02	Osci. zoned rim	60	33	73	0.46	25.4933 ± 0.7516	0.6764 ± 0.0191	0.96	0.273	3331 ± 73	3325 ± 49	100
E03	Osci. zoned core	46	39	53	0.73	24.7788 ± 0.7369	0.6691 ± 0.0189	0.95	0.269	3302 ± 73	3298 ± 50	100
E03	Osci. zoned rim	36	20	44	0.46	25.5422 ± 0.7680	0.6776 ± 0.0192	0.94	0.273	3335 ± 74	3325 ± 50	100

Continued on next page

Table B.3 – *Continued from previous page*

Spot #	Internal Structure	Pb (ppm)	Th (ppm)	U (ppm)	Th/U	$^{207}Pb/^{235}U$ $\pm 2\sigma$	$^{206}Pb/^{238}U$ $\pm 2\sigma$	ρ	$\frac{^{207}Pb}{^{206}Pb}$ ^{206}Pb	Ages (Ma)$\pm 2\sigma$ $\frac{^{206}Pb}{^{238}U}$	Ages (Ma)$\pm 2\sigma$ $\frac{^{207}Pb}{^{206}Pb}$	Conc %
E04	Osci. zoned rim	107	47	137	0.34	24.2238 ± 0.7127	0.6646 ± 0.0187	0.96	0.264	3285 ± 72	3273 ± 49	100
E05	Convo. core	34	21	43	0.49	23.2745 ± 0.7048	0.6559 ± 0.0187	0.94	0.257	3251 ± 73	3230 ± 51	101
E06	Osci. zoned core	53	44	60	0.74	25.4436 ± 0.7612	0.6774 ± 0.0192	0.95	0.272	3334 ± 74	3320 ± 50	100
E06	Osci. zoned rim	181	83	236	0.35	23.8079 ± 0.7005	0.6453 ± 0.0181	0.95	0.268	3210 ± 71	3292 ± 49	98
E07	Osci. zoned core	34	18	43	0.43	23.5078 ± 0.7061	0.6544 ± 0.0185	0.94	0.261	3245 ± 72	3250 ± 50	100
E07	Osci. zoned rim	221	88	298	0.30	23.4547 ± 0.6905	0.6316 ± 0.0177	0.95	0.269	3156 ± 70	3302 ± 49	96
E08	Osci. zoned rim	79	42	96	0.43	25.5775 ± 0.7582	0.6790 ± 0.0191	0.95	0.273	3341 ± 73	3324 ± 49	100
E09	Osci. zoned core	81	52	97	0.53	25.3497 ± 0.7502	0.6748 ± 0.0190	0.95	0.272	3324 ± 73	3320 ± 49	100
E09	Black rim	687	10	1147	0.01	16.8012 ± 0.4939	0.5712 ± 0.0160	0.95	0.213	2913 ± 66	2931 ± 51	99
E10	Osci. zoned rim	66	33	82	0.40	25.4888 ± 0.7622	0.6780 ± 0.0192	0.95	0.273	3337 ± 74	3321 ± 50	100
E11	Osci. zoned core	58	30	75	0.39	22.6452 ± 0.6817	0.6325 ± 0.0179	0.94	0.260	3160 ± 71	3244 ± 50	97
E11	Black rim	374	117	745	0.16	10.8177 ± 0.3218	0.4777 ± 0.0134	0.94	0.164	2517 ± 59	2499 ± 53	101
E12	Osci. zoned core	113	65	137	0.48	25.1110 ± 0.7458	0.6755 ± 0.0190	0.95	0.269	3327 ± 73	3303 ± 49	101
E13	Osci. zoned core	68	50	87	0.57	22.2536 ± 0.6746	0.6198 ± 0.0176	0.94	0.260	3109 ± 70	3249 ± 51	96
E13	Black rim	114	54	144	0.37	23.5250 ± 0.7009	0.6589 ± 0.0186	0.95	0.259	3263 ± 72	3240 ± 50	101
E14	Osci. zoned core	29	17	36	0.47	24.3510 ± 0.7516	0.6528 ± 0.0187	0.93	0.271	3239 ± 73	3309 ± 51	98
E15	Osci. zoned core	25	14	30	0.49	25.6471 ± 0.7944	0.6789 ± 0.0194	0.92	0.274	3340 ± 75	3329 ± 51	100
F01	Osci. zoned core	41	29	48	0.59	24.8491 ± 0.7695	0.6721 ± 0.0192	0.92	0.268	3314 ± 74	3295 ± 51	101
F01	Black rim	165	42	230	0.18	21.7077 ± 0.6534	0.6368 ± 0.0180	0.94	0.247	3177 ± 71	3167 ± 51	100
F02	Osci. zoned core	95	58	117	0.49	24.1438 ± 0.7298	0.6638 ± 0.0188	0.94	0.264	3282 ± 73	3269 ± 50	100
F02	Osci. zoned rim	97	51	120	0.43	25.0687 ± 0.7609	0.6724 ± 0.0191	0.94	0.270	3315 ± 73	3308 ± 50	100
F03	Osci. zoned core	165	139	189	0.73	25.2936 ± 0.7602	0.6750 ± 0.0191	0.94	0.272	3325 ± 73	3316 ± 50	100
F04	Osci. zoned core	221	156	261	0.60	25.0770 ± 0.7555	0.6750 ± 0.0191	0.94	0.269	3325 ± 73	3303 ± 50	101
F05	Osci. zoned core	24	10	30	0.35	25.4211 ± 0.8069	0.6762 ± 0.0195	0.91	0.273	3330 ± 75	3321 ± 52	100
F06	Osci. zoned core	29	20	36	0.55	24.7117 ± 0.7911	0.6482 ± 0.0188	0.91	0.276	3221 ± 74	3343 ± 53	96
F07	Osci. zoned rim	49	30	63	0.47	23.0575 ± 0.7253	0.6400 ± 0.0184	0.91	0.261	3189 ± 72	3254 ± 52	98
F08	Osci. zoned core	43	27	51	0.52	25.3993 ± 0.7928	0.6755 ± 0.0193	0.92	0.273	3327 ± 74	3321 ± 52	100
F09	Osci. zoned rim	89	43	111	0.39	24.7894 ± 0.7619	0.6709 ± 0.0191	0.93	0.268	3309 ± 74	3294 ± 51	100
F10	Osci. zoned rim	89	42	111	0.38	24.9184 ± 0.7678	0.6721 ± 0.0191	0.92	0.269	3314 ± 74	3299 ± 51	100
F11	Osci. zoned core	37	30	43	0.68	25.1228 ± 0.7815	0.6712 ± 0.0194	0.93	0.271	3311 ± 75	3314 ± 51	100

Continued on next page

Table B.3 – *Continued from previous page*

Spot #	Internal Structure	Pb (ppm)	Th (ppm)	U (ppm)	Th/U	$^{207}Pb/^{235}U$ $\pm 2\sigma$	$^{206}Pb/^{238}U$ $\pm 2\sigma$	ρ	$\frac{^{207}Pb}{^{206}Pb}$ ^{206}Pb	Ages (Ma)$\pm 2\sigma$ $\frac{^{206}Pb}{^{238}U}$	Ages (Ma)$\pm 2\sigma$ $\frac{^{207}Pb}{^{206}Pb}$	Conc %
F12	Osci. zoned rim	45	21	59	0.35	23.0861 ± 0.6970	0.6521 ± 0.0185	0.94	0.257	3236 ± 72	3227 ± 50	100
F14	Osci. zoned core	48	38	56	0.68	25.4318 ± 0.7755	0.6771 ± 0.0193	0.93	0.272	3333 ± 74	3320 ± 50	100
F14	Osci. zoned rim	99	38	124	0.31	25.5379 ± 0.7700	0.6790 ± 0.0193	0.94	0.273	3341 ± 74	3322 ± 50	101
F15	Osci. zoned rim	63	15	96	0.16	18.1214 ± 0.5525	0.5876 ± 0.0167	0.93	0.224	2980 ± 68	3007 ± 52	99
F16	Osci. zoned rim	27	13	34	0.38	25.1498 ± 0.8028	0.6737 ± 0.0195	0.91	0.271	3320 ± 75	3310 ± 53	100
F17	Osci. zoned core	62	47	75	0.62	24.1294 ± 0.7569	0.6580 ± 0.0189	0.92	0.266	3260 ± 73	3282 ± 52	99
F17	Black rim	264	13	365	0.04	23.9920 ± 0.7380	0.6571 ± 0.0187	0.93	0.265	3256 ± 73	3275 ± 51	99
SG-208 granite												
A01	Osci. zoned core	57	31	68	0.45	24.7424 ± 0.7650	0.6650 ± 0.0194	0.94	0.270	3287 ± 75	3305 ± 50	99
A01	Black rim	704	65	1330	0.05	13.0549 ± 0.3938	0.5107 ± 0.0147	0.95	0.185	2660 ± 63	2702 ± 52	98
A02	Osci. zoned core	82	54	103	0.52	21.5632 ± 0.6638	0.5974 ± 0.0174	0.95	0.262	3019 ± 70	3257 ± 50	93
A02	Osci. zoned rim	61	24	78	0.30	22.9747 ± 0.7074	0.6454 ± 0.0188	0.95	0.258	3210 ± 74	3236 ± 50	99
A03	Osci. zoned core	29	12	40	0.30	21.6232 ± 0.6862	0.6176 ± 0.0182	0.93	0.254	3100 ± 72	3209 ± 52	97
A04	Osci. zoned core	54	35	62	0.56	25.5421 ± 0.7918	0.6747 ± 0.0197	0.94	0.275	3324 ± 76	3332 ± 50	100
A05	Osci. zoned core	73	42	95	0.44	21.0806 ± 0.6516	0.5943 ± 0.0173	0.94	0.257	3007 ± 70	3230 ± 51	93
A07	Osci. zoned core	55	30	67	0.45	24.7169 ± 0.7667	0.6580 ± 0.0192	0.94	0.272	3259 ± 75	3320 ± 50	98
A07	Osci. zoned rim	698	50	1474	0.03	10.5359 ± 0.3203	0.4680 ± 0.0135	0.95	0.163	2475 ± 59	2490 ± 53	99
A09	Osci. zoned core	40	20	49	0.40	24.4277 ± 0.7832	0.6474 ± 0.0191	0.92	0.274	3218 ± 75	3327 ± 52	97
A10	Black rim	657	8	1103	0.01	16.6752 ± 0.5093	0.5672 ± 0.0163	0.94	0.213	2896 ± 67	2930 ± 51	99
A11	Black core	157	80	194	0.41	23.6134 ± 0.7292	0.6288 ± 0.0182	0.94	0.272	3145 ± 72	3320 ± 50	95
A12	Osci. zoned core	53	29	66	0.44	23.9448 ± 0.7467	0.6401 ± 0.0186	0.93	0.271	3189 ± 73	3314 ± 51	96
A15	Osci. zoned core	132	83	175	0.47	21.4468 ± 0.6790	0.5918 ± 0.0172	0.92	0.263	2997 ± 70	3264 ± 52	92
A16	Osci. zoned rim	81	35	99	0.35	24.9834 ± 0.7749	0.6617 ± 0.0191	0.93	0.274	3274 ± 74	3328 ± 51	98
A17	Osci. zoned core	59	37	75	0.49	23.1625 ± 0.7586	0.6228 ± 0.0184	0.90	0.270	3121 ± 73	3304 ± 53	94
A18	Osci. zoned rim	58	29	70	0.41	25.8819 ± 0.8101	0.6769 ± 0.0196	0.93	0.277	3333 ± 75	3348 ± 51	100
A19	Black core	56	31	74	0.42	22.7055 ± 0.7302	0.6148 ± 0.0180	0.91	0.268	3089 ± 72	3293 ± 53	94
C01	Osci. zoned rim	70	31	86	0.37	25.3392 ± 0.7936	0.6695 ± 0.0194	0.93	0.275	3304 ± 75	3332 ± 51	99
C02	Osci. zoned core	28	31	41	0.74	19.1553 ± 0.6683	0.5495 ± 0.0166	0.87	0.253	2823 ± 69	3202 ± 58	88
C03	Osci. zoned core	26	13	33	0.39	23.2606 ± 0.7549	0.6441 ± 0.0189	0.90	0.262	3205 ± 74	3258 ± 53	98
C04	Osci. zoned rim	47	23	57	0.41	25.0100 ± 0.7957	0.6617 ± 0.0192	0.91	0.274	3274 ± 74	3330 ± 52	98

Continued on next page

Table B.3 – *Continued from previous page*

Spot #	Internal Structure	Pb (ppm)	Th (ppm)	U (ppm)	Th/U	$^{207}Pb/^{235}U$ $\pm 2\sigma$	$^{206}Pb/^{238}U$ $\pm 2\sigma$	ρ	$\frac{^{207}Pb}{^{206}Pb}$ ^{206}Pb	Ages (Ma)$\pm 2\sigma$ $\frac{^{206}Pb}{^{238}U}$	Ages (Ma)$\pm 2\sigma$ $\frac{^{207}Pb}{^{206}Pb}$	Conc %
C05	Osci. zoned rim	34	17	52	0.33	18.1784 ± 0.6289	0.5458 ± 0.0164	0.87	0.242	2808 ± 68	3130 ± 57	90
C06	Osci. zoned core	65	27	83	0.33	24.4250 ± 0.7917	0.6512 ± 0.0190	0.90	0.272	3233 ± 74	3318 ± 53	97
C07	Osci. zoned core	212	123	268	0.46	23.7652 ± 0.7431	0.6344 ± 0.0182	0.92	0.272	3167 ± 72	3316 ± 51	96
C08	Osci. zoned core	155	76	186	0.41	25.6098 ± 0.8014	0.6761 ± 0.0194	0.92	0.275	3329 ± 75	3333 ± 51	100
C09	Black core	210	105	264	0.40	23.5967 ± 0.7397	0.6520 ± 0.0187	0.91	0.263	3236 ± 73	3262 ± 52	99
C10	Osci. zoned core	157	62	197	0.31	24.9601 ± 0.7850	0.6606 ± 0.0189	0.91	0.274	3270 ± 74	3329 ± 52	98
C11	Osci. zoned core	39	28	49	0.57	22.6414 ± 0.7550	0.6115 ± 0.0180	0.88	0.268	3076 ± 72	3297 ± 55	93
C12	Osci. zoned core	34	17	42	0.41	22.7947 ± 0.7495	0.6473 ± 0.0189	0.89	0.255	3218 ± 74	3218 ± 54	100
C13	Osci. zoned core	225	126	285	0.44	23.8706 ± 0.7546	0.6352 ± 0.0182	0.91	0.273	3170 ± 72	3321 ± 52	95
C14	Grey	75	45	137	0.32	14.5196 ± 0.4326	0.4742 ± 0.0134	0.95	0.222	2502 ± 59	2995 ± 51	84
C16	Ext. zoned rim	69	35	84	0.42	25.2690 ± 0.7749	0.6690 ± 0.0192	0.94	0.274	3302 ± 74	3328 ± 51	99
C17	Osci. zoned core	79	52	94	0.55	24.2537 ± 0.7185	0.6504 ± 0.0184	0.95	0.270	3230 ± 72	3308 ± 49	98
C18	Convo. core	38	28	50	0.56	21.0090 ± 0.6373	0.5897 ± 0.0168	0.94	0.258	2988 ± 68	3237 ± 51	92
D01	Ext. zoned rim	67	33	80	0.42	25.8204 ± 0.7722	0.6814 ± 0.0193	0.95	0.275	3350 ± 74	3334 ± 50	100
D02	Grey core	111	48	134	0.36	25.4521 ± 0.7496	0.6791 ± 0.0191	0.95	0.272	3341 ± 73	3316 ± 49	101
D02	Osci. zoned rim	40	18	56	0.32	21.2267 ± 0.6493	0.5963 ± 0.0170	0.93	0.258	3015 ± 69	3236 ± 51	93
D03	Black core	961	470	1426	0.33	18.2978 ± 0.5304	0.5799 ± 0.0162	0.96	0.229	2948 ± 66	3044 ± 50	97
D04	Osci. zoned core	36	23	48	0.47	21.0004 ± 0.6651	0.5930 ± 0.0172	0.92	0.257	3002 ± 70	3227 ± 53	93
D05	Grey core	38	21	46	0.46	24.5885 ± 0.7473	0.6586 ± 0.0188	0.94	0.271	3262 ± 73	3310 ± 51	99
D06	Osci. zoned core	32	15	38	0.39	25.9183 ± 0.7870	0.6812 ± 0.0194	0.94	0.276	3349 ± 74	3340 ± 50	100
D07	Osci. zoned core	71	43	95	0.45	21.4106 ± 0.6425	0.5999 ± 0.0170	0.94	0.259	3030 ± 68	3240 ± 50	94
D08	Osci. zoned core	176	77	226	0.34	23.9274 ± 0.7026	0.6459 ± 0.0181	0.95	0.269	3212 ± 71	3298 ± 49	97
D09	Osci. zoned core	36	21	42	0.50	25.7187 ± 0.7843	0.6796 ± 0.0194	0.94	0.275	3343 ± 74	3332 ± 51	100
D10	Osci. zoned rim	26	14	31	0.45	26.3687 ± 0.8576	0.6843 ± 0.0201	0.90	0.279	3361 ± 77	3360 ± 54	100
D11	Osci. zoned core	67	47	78	0.60	24.7397 ± 0.7357	0.6593 ± 0.0186	0.95	0.272	3265 ± 72	3318 ± 50	98
D12	Osci. zoned core	45	26	61	0.43	21.5115 ± 0.6755	0.6042 ± 0.0174	0.92	0.258	3047 ± 70	3236 ± 53	94
D13	Black core	151	55	211	0.26	22.1095 ± 0.6542	0.6089 ± 0.0171	0.95	0.263	3066 ± 69	3267 ± 50	94
D15	Osci. zoned core	50	33	61	0.54	22.9387 ± 0.7029	0.6273 ± 0.0179	0.93	0.265	3139 ± 71	3278 ± 51	96
D16	Osci. zoned core	43	26	52	0.50	24.2875 ± 0.7396	0.6483 ± 0.0185	0.94	0.272	3222 ± 72	3316 ± 51	97
D17	Convo. core	54	35	62	0.56	25.4828 ± 0.7685	0.6758 ± 0.0191	0.94	0.273	3328 ± 74	3326 ± 50	100

Continued on next page

Table B.3 – *Continued from previous page*

Spot #	Internal Structure	Pb (ppm)	Th (ppm)	U (ppm)	Th/U	$^{207}Pb/^{235}U$ $\pm 2\sigma$	$^{206}Pb/^{238}U$ $\pm 2\sigma$	ρ	$\frac{^{207}Pb}{^{206}Pb}$ ^{206}Pb	Ages (Ma)$\pm 2\sigma$ $\frac{^{206}Pb}{^{238}U}$	Ages (Ma)$\pm 2\sigma$ $\frac{^{207}Pb}{^{206}Pb}$	Conc %
E01	Osci. zoned core	318	161	435	0.37	21.5745 ± 0.6391	0.6046 ± 0.0170	0.95	0.259	3048 ± 68	3239 ± 50	94
E02	Osci. zoned core	59	74	80	0.92	20.3637 ± 0.6423	0.5857 ± 0.0169	0.91	0.252	2972 ± 69	3198 ± 53	93
E03	Black rim	754	8	1336	0.01	15.7028 ± 0.4625	0.5387 ± 0.0151	0.95	0.211	2778 ± 63	2916 ± 51	95
E04	Osci. zoned core	39	23	49	0.47	23.7125 ± 0.7371	0.6391 ± 0.0183	0.92	0.269	3186 ± 72	3301 ± 52	97
E05	Osci. zoned core	33	22	38	0.58	25.1526 ± 0.7761	0.6689 ± 0.0191	0.93	0.273	3302 ± 74	3322 ± 51	99
E06	Black core	414	246	559	0.44	21.6980 ± 0.6447	0.5995 ± 0.0168	0.94	0.263	3028 ± 68	3262 ± 50	93
E07	Osci. zoned core	351	202	431	0.47	24.2078 ± 0.7176	0.6515 ± 0.0182	0.94	0.269	3234 ± 71	3303 ± 50	98
E08	Osci. zoned core	58	29	72	0.40	24.8466 ± 0.7529	0.6581 ± 0.0186	0.93	0.274	3260 ± 72	3328 ± 50	98
E09	Osci. zoned rim	155	71	194	0.36	24.5309 ± 0.7344	0.6544 ± 0.0184	0.94	0.272	3245 ± 72	3317 ± 50	98
E10	Osci. zoned rim	131	70	155	0.45	25.5389 ± 0.7669	0.6758 ± 0.0190	0.94	0.274	3328 ± 73	3329 ± 50	100
E11	Osci. zoned rim	158	76	192	0.40	25.4031 ± 0.7584	0.6738 ± 0.0189	0.94	0.273	3321 ± 73	3326 ± 50	100
E12	Osci. zoned core	836	436	1667	0.26	12.3512 ± 0.3672	0.4455 ± 0.0125	0.94	0.201	2375 ± 56	2835 ± 52	84
E13	Osci. zoned core	113	91	132	0.69	24.3063 ± 0.7341	0.6488 ± 0.0183	0.93	0.272	3223 ± 71	3316 ± 50	97
E13	Osci. zoned rim	50	24	59	0.41	25.8952 ± 0.7919	0.6794 ± 0.0192	0.92	0.276	3342 ± 74	3343 ± 51	100
E13	Black rim	530	4	887	0.00	16.8663 ± 0.5042	0.5698 ± 0.0159	0.93	0.215	2907 ± 65	2941 ± 51	99
E14	Osci. zoned core	37	22	50	0.44	21.3010 ± 0.7088	0.5992 ± 0.0176	0.88	0.258	3027 ± 71	3233 ± 56	94
E15	Black rim	205	104	250	0.42	24.8297 ± 0.7486	0.6605 ± 0.0185	0.93	0.273	3269 ± 72	3321 ± 50	98
E17	Black rim	43	22	51	0.43	25.9686 ± 0.8072	0.6796 ± 0.0193	0.91	0.277	3343 ± 74	3347 ± 52	100
F04	Osci. zoned core	55	29	66	0.43	25.4865 ± 0.7878	0.6756 ± 0.0191	0.91	0.274	3327 ± 74	3327 ± 51	100
F08	Osci. zoned rim	50	23	66	0.35	23.3869 ± 0.7422	0.6345 ± 0.0182	0.90	0.267	3167 ± 72	3290 ± 53	96
F09	Black core	581	17	1051	0.02	15.1718 ± 0.4626	0.5274 ± 0.0148	0.92	0.209	2731 ± 62	2895 ± 53	94
F14	Osci. zoned core	72	33	102	0.32	20.8206 ± 0.6644	0.5871 ± 0.0167	0.89	0.257	2978 ± 68	3230 ± 53	92
F16	Osci. zoned core	60	44	76	0.58	22.6440 ± 0.7224	0.6217 ± 0.0177	0.89	0.264	3117 ± 70	3272 ± 53	95
F17	Osci. zoned core	39	20	54	0.38	21.6268 ± 0.7052	0.6018 ± 0.0173	0.88	0.261	3037 ± 70	3250 ± 54	93
F19	Osci. zoned core	34	18	52	0.34	18.3345 ± 0.6251	0.5466 ± 0.0160	0.86	0.243	2811 ± 67	3142 ± 57	89
SG-210c Mg-tonalite												
A01	Osci. zoned core	208	97	184	0.53	44.0414 ± 1.2717	0.8262 ± 0.0228	0.96	0.387	3882 ± 80	3858 ± 47	101
A01	Osci. zoned rim	277	81	279	0.29	39.6014 ± 1.1428	0.7813 ± 0.0215	0.95	0.367	3722 ± 78	3781 ± 47	98
A01	Black rim	623	4	740	0.01	32.4754 ± 0.9357	0.7384 ± 0.0203	0.95	0.319	3565 ± 75	3565 ± 48	100
A02	Black core	502	47	654	0.07	28.9144 ± 0.8375	0.6565 ± 0.0181	0.95	0.319	3254 ± 70	3567 ± 48	91

Continued on next page

Table B.3 – *Continued from previous page*

Spot #	**Internal Structure**	**Pb** (ppm)	**Th** (ppm)	**U** (ppm)	**Th/U**	^{207}**Pb**/^{235}**U** $\pm 2\sigma$	^{206}**Pb**/^{238}**U** $\pm 2\sigma$	ρ	$\frac{^{207}Pb}{^{206}Pb}$ ^{206}Pb	**Ages (Ma)**$\pm 2\sigma$ $\frac{^{206}Pb}{^{238}U}$	$\frac{^{207}Pb}{^{206}Pb}$	**Conc** %
A03	Black core	640	5	961	0.01	23.7073 ± 0.6866	0.5965 ± 0.0164	0.95	0.288	3016 ± 66	3408 ± 49	88
A03	Black rim	681	3	814	0.00	31.6853 ± 0.9166	0.7356 ± 0.0203	0.95	0.312	3554 ± 75	3533 ± 48	101
A04	Osci. zoned core	533	12	677	0.02	31.5834 ± 0.9167	0.6767 ± 0.0187	0.95	0.338	3332 ± 72	3656 ± 48	91
A05	Osci. zoned core	40	15	37	0.41	43.9208 ± 1.3081	0.8165 ± 0.0229	0.94	0.390	3848 ± 81	3871 ± 48	99
A06	Osci. zoned core	61	28	58	0.48	41.4325 ± 1.2222	0.7814 ± 0.0218	0.95	0.385	3722 ± 79	3850 ± 48	97
A06	Osci. zoned rim	73	22	68	0.32	44.2873 ± 1.3033	0.8204 ± 0.0228	0.94	0.392	3862 ± 81	3877 ± 48	100
A07	Black core	436	32	579	0.05	28.2341 ± 0.8322	0.6510 ± 0.0181	0.94	0.314	3232 ± 71	3543 ± 49	91
A08	Osci. zoned core	80	38	81	0.48	38.2760 ± 1.1292	0.7394 ± 0.0206	0.94	0.375	3568 ± 76	3813 ± 48	94
A08	Osci. zoned rim	129	60	137	0.44	36.0093 ± 1.0681	0.7089 ± 0.0197	0.94	0.368	3454 ± 74	3785 ± 48	91
A09	Convo. core	56	1	67	0.01	35.3594 ± 1.0698	0.7111 ± 0.0200	0.93	0.361	3463 ± 75	3752 ± 49	92
A10	Black core	175	4	207	0.02	32.7888 ± 0.9707	0.7416 ± 0.0206	0.94	0.321	3577 ± 76	3573 ± 49	100
A11	Black core	484	2	680	0.00	27.1228 ± 0.8034	0.6255 ± 0.0173	0.93	0.314	3132 ± 69	3543 ± 49	88
A12	Black core	393	3	467	0.01	32.3905 ± 0.9599	0.7411 ± 0.0206	0.94	0.317	3575 ± 76	3555 ± 49	101
A13	Black core	308	3	364	0.01	33.0518 ± 0.9821	0.7422 ± 0.0206	0.93	0.323	3579 ± 76	3584 ± 49	100
A14	Osci. zoned core	14	1	19	0.03	29.4411 ± 0.9291	0.6522 ± 0.0187	0.91	0.327	3237 ± 73	3605 ± 52	90
A14	Black rim	278	1	402	0.00	22.8052 ± 0.6810	0.6324 ± 0.0176	0.93	0.262	3159 ± 69	3256 ± 50	97
A15	Osci. zoned core	55	25	49	0.51	44.1051 ± 1.3398	0.8246 ± 0.0231	0.92	0.388	3876 ± 82	3863 ± 49	100
A15	Osci. zoned rim	219	47	209	0.22	43.7383 ± 1.3134	0.8258 ± 0.0230	0.93	0.384	3881 ± 81	3848 ± 49	101
A16	Osci. zoned core	76	23	76	0.30	40.1324 ± 1.2270	0.7648 ± 0.0215	0.92	0.381	3662 ± 78	3834 ± 49	96
A16	Osci. zoned rim	162	49	183	0.27	34.2321 ± 1.0425	0.7029 ± 0.0196	0.92	0.353	3432 ± 74	3721 ± 50	92
A17	Black core	296	3	357	0.01	31.5447 ± 0.9590	0.7264 ± 0.0203	0.92	0.315	3520 ± 76	3545 ± 50	99
B01	Black core	499	5	594	0.01	32.1843 ± 0.9804	0.7382 ± 0.0206	0.92	0.316	3564 ± 76	3551 ± 50	100
B02	Osci. zoned core	153	74	134	0.55	44.1443 ± 1.3550	0.8140 ± 0.0228	0.91	0.393	3839 ± 81	3884 ± 49	99
B03	Osci. zoned core	109	54	103	0.52	40.9005 ± 1.2661	0.7756 ± 0.0218	0.91	0.382	3701 ± 79	3841 ± 50	96
B05	Osci. zoned core	435	4	491	0.01	36.5509 ± 1.1282	0.7610 ± 0.0213	0.91	0.348	3648 ± 78	3700 ± 50	99
B06	Osci. zoned core	290	196	262	0.75	40.8000 ± 1.2748	0.7710 ± 0.0216	0.90	0.384	3684 ± 79	3847 ± 50	96
B07	Osci. zoned core	315	184	319	0.58	37.0370 ± 1.1629	0.7212 ± 0.0203	0.90	0.372	3501 ± 76	3801 ± 50	92
B08	Osci. zoned core	69	21	67	0.31	42.2956 ± 1.2545	0.8001 ± 0.0229	0.96	0.383	3789 ± 82	3845 ± 47	99
B08	Osci. Z. ext. rim	77	25	72	0.35	43.8078 ± 1.2956	0.8167 ± 0.0233	0.96	0.389	3849 ± 83	3867 ± 47	100
B08	Osci. Z. int. rim	61	19	60	0.32	41.4171 ± 1.2533	0.7881 ± 0.0228	0.96	0.381	3747 ± 82	3836 ± 48	98

Continued on next page

Table B.3 – *Continued from previous page*

Spot #	Internal Structure	Pb (ppm)	Th (ppm)	U (ppm)	Th/U	$^{207}Pb/^{235}U$ $\pm 2\sigma$	$^{206}Pb/^{238}U$ $\pm 2\sigma$	ρ	$\frac{^{207}Pb}{^{206}Pb}$ ^{206}Pb	Ages (Ma)$\pm 2\sigma$ $\frac{^{206}Pb}{^{238}U}$	Ages (Ma)$\pm 2\sigma$ $\frac{^{207}Pb}{^{206}Pb}$	Conc %
B09	Black core	279	28	298	0.09	39.8410 ± 1.1700	0.7667 ± 0.0218	0.97	0.377	3669 ± 80	3819 ± 47	96
B10	Osci. zoned core	87	39	80	0.49	42.6017 ± 1.2609	0.8052 ± 0.0230	0.97	0.384	3808 ± 82	3846 ± 47	99
B11	Osci. zoned core	90	42	84	0.51	41.8499 ± 1.2484	0.7983 ± 0.0229	0.96	0.380	3783 ± 82	3832 ± 47	99
B12	Osci. zoned core	56	15	53	0.29	43.8744 ± 1.3049	0.8213 ± 0.0235	0.96	0.387	3865 ± 83	3861 ± 47	100
B13	Osci. zoned core	45	16	42	0.37	43.6406 ± 1.3072	0.8205 ± 0.0236	0.96	0.386	3862 ± 84	3854 ± 47	100
B14	Osci. zoned core	75	30	95	0.32	25.8141 ± 0.7676	0.6257 ± 0.0179	0.96	0.299	3133 ± 71	3466 ± 48	90
B15	Osci. zoned core	76	28	69	0.41	44.6324 ± 1.3256	0.8259 ± 0.0236	0.96	0.392	3881 ± 83	3878 ± 47	100
B16	Osci. zoned core	108	23	103	0.22	43.4910 ± 1.2835	0.8139 ± 0.0232	0.97	0.387	3839 ± 82	3861 ± 47	99
B17	Osci. zoned core	54	24	48	0.49	44.4225 ± 1.3278	0.8221 ± 0.0236	0.96	0.392	3868 ± 84	3878 ± 47	100
B18	Osci. zoned core	186	81	186	0.44	39.6175 ± 1.1911	0.7488 ± 0.0216	0.96	0.384	3603 ± 79	3846 ± 48	94
C01	Osci. zoned core	124	55	114	0.48	43.2721 ± 1.2774	0.8061 ± 0.0230	0.97	0.389	3811 ± 82	3868 ± 47	99
C01	Osci. zoned rim	70	26	75	0.34	35.7933 ± 1.0830	0.7081 ± 0.0204	0.95	0.366	3451 ± 77	3777 ± 48	91
C02	Osci. zoned core	76	29	71	0.40	42.7701 ± 1.2721	0.8083 ± 0.0231	0.96	0.384	3819 ± 82	3846 ± 47	99
C03	Osci. zoned core	109	54	101	0.53	41.3568 ± 1.2279	0.7859 ± 0.0224	0.96	0.382	3739 ± 81	3838 ± 47	97
C04	Osci. zoned core	168	21	207	0.10	32.5355 ± 0.9637	0.6836 ± 0.0195	0.96	0.345	3358 ± 75	3686 ± 48	91
C05	Osci. zoned core	221	49	208	0.23	44.7230 ± 1.3195	0.8289 ± 0.0236	0.97	0.391	3892 ± 83	3876 ± 47	100
C06	Osci. zoned core	93	43	83	0.51	44.0643 ± 1.3067	0.8204 ± 0.0234	0.96	0.389	3862 ± 83	3869 ± 47	100
C07	Osci. zoned core	124	53	140	0.38	33.6613 ± 1.0082	0.6847 ± 0.0196	0.96	0.356	3362 ± 75	3735 ± 48	90
C08	Osci. zoned core	32	10	30	0.35	45.2559 ± 1.3845	0.8267 ± 0.0240	0.95	0.397	3884 ± 85	3898 ± 48	100
C10	Osci. zoned core	117	4	139	0.03	32.4653 ± 0.9634	0.7334 ± 0.0209	0.96	0.321	3546 ± 78	3575 ± 48	99
C11	Osci. zoned core	200	96	193	0.49	40.2459 ± 1.1929	0.7642 ± 0.0218	0.96	0.382	3660 ± 79	3839 ± 47	95
C12	Osci. zoned core	120	53	114	0.47	40.9820 ± 1.2185	0.7836 ± 0.0223	0.96	0.379	3730 ± 81	3829 ± 47	97
C13	Osci. zoned core	95	31	96	0.32	39.1837 ± 1.1694	0.7710 ± 0.0220	0.96	0.368	3685 ± 80	3785 ± 48	97
C14	Osci. zoned core	283	132	255	0.52	43.4460 ± 1.2868	0.8153 ± 0.0232	0.96	0.386	3844 ± 82	3857 ± 47	100
C15	Convo. core	60	17	55	0.31	43.3057 ± 1.3031	0.8131 ± 0.0233	0.95	0.386	3836 ± 83	3856 ± 48	99
C16	Convo. core	39	14	39	0.35	39.4965 ± 1.2010	0.7619 ± 0.0220	0.95	0.376	3651 ± 80	3815 ± 48	96
C17	Black core	361	42	389	0.11	37.3417 ± 1.1076	0.7756 ± 0.0220	0.96	0.349	3701 ± 80	3703 ± 48	100
C18	Convo. core	181	17	196	0.09	38.3972 ± 1.1444	0.7724 ± 0.0220	0.96	0.361	3690 ± 80	3752 ± 48	98
C19	Black rim	329	3	390	0.01	32.4316 ± 0.9641	0.7431 ± 0.0211	0.96	0.317	3582 ± 78	3553 ± 48	101
D01	Osci. zoned core	54	18	50	0.37	44.1880 ± 1.3367	0.8232 ± 0.0236	0.95	0.389	3872 ± 84	3868 ± 48	100

Continued on next page

Table B.3 – *Continued from previous page*

Spot #	Internal Structure	Pb (ppm)	Th (ppm)	U (ppm)	Th/U	$^{207}Pb/^{235}U$ $\pm 2\sigma$	$^{206}Pb/^{238}U$ $\pm 2\sigma$	ρ	$\frac{^{207}Pb}{^{206}Pb}$ ^{206}Pb	Ages (Ma)$\pm 2\sigma$ $\frac{^{206}Pb}{^{238}U}$	Ages (Ma)$\pm 2\sigma$ $\frac{^{207}Pb}{^{206}Pb}$	Conc %
D02	Osci. zoned core	75	32	74	0.43	39.9682 ± 1.2091	0.7656 ± 0.0220	0.95	0.379	3665 ± 80	3826 ± 48	96
D03	Black core	481	2	572	0.00	32.8271 ± 0.9778	0.7382 ± 0.0210	0.96	0.323	3564 ± 78	3582 ± 48	100
D04	Black core	172	29	194	0.15	33.8339 ± 1.0112	0.7386 ± 0.0210	0.95	0.332	3565 ± 78	3627 ± 48	98
D05	Osci. zoned core	269	168	235	0.71	42.5413 ± 1.2732	0.8041 ± 0.0229	0.95	0.384	3804 ± 82	3846 ± 48	99
D06	Osci. zoned rim	52	17	57	0.29	33.9329 ± 1.0161	0.6954 ± 0.0199	0.96	0.354	3403 ± 76	3724 ± 48	91
D06	Black core	61	9	64	0.14	38.1226 ± 1.1720	0.7709 ± 0.0224	0.95	0.359	3684 ± 81	3744 ± 49	98
D07	Black core	524	15	624	0.02	32.6680 ± 0.9760	0.7360 ± 0.0209	0.95	0.322	3556 ± 78	3579 ± 48	99
D08	Osci. zoned core	129	66	113	0.59	44.3705 ± 1.3354	0.8219 ± 0.0234	0.95	0.392	3867 ± 83	3877 ± 48	100
D09	Osci. zoned core	133	69	117	0.59	43.1228 ± 1.2990	0.8123 ± 0.0232	0.95	0.385	3833 ± 82	3851 ± 48	100
D09	Black rim	379	4	415	0.01	38.4824 ± 1.1532	0.7766 ± 0.0221	0.95	0.359	3705 ± 80	3747 ± 48	99
D10	Osci. zoned core	82	31	75	0.42	44.0829 ± 1.3382	0.8191 ± 0.0234	0.94	0.390	3857 ± 83	3872 ± 48	100
D11	Osci. zoned core	57	16	53	0.29	44.8386 ± 1.3663	0.8296 ± 0.0238	0.94	0.392	3894 ± 84	3879 ± 48	100
D12	Osci. zoned core	176	31	190	0.16	38.7443 ± 1.1784	0.7472 ± 0.0214	0.94	0.376	3597 ± 79	3816 ± 48	94
D13	Black rim	837	62	917	0.07	38.2767 ± 1.1521	0.7630 ± 0.0217	0.94	0.364	3655 ± 79	3766 ± 48	97
D14	Osci. zoned core	77	34	73	0.47	40.2132 ± 1.2389	0.7672 ± 0.0221	0.94	0.380	3671 ± 81	3832 ± 49	96
D14	Osci. zoned rim	156	40	147	0.27	43.9737 ± 1.3324	0.8223 ± 0.0234	0.94	0.388	3868 ± 83	3862 ± 48	100
D15	Core	187	11	199	0.06	40.7296 ± 1.2334	0.7795 ± 0.0222	0.94	0.379	3715 ± 80	3827 ± 48	97
D15	Osci. zoned rim	149	40	146	0.28	42.0058 ± 1.2783	0.7973 ± 0.0227	0.94	0.382	3780 ± 82	3840 ± 48	98
D15	Black outer rim	673	8	817	0.01	31.4160 ± 0.9496	0.7267 ± 0.0206	0.94	0.313	3521 ± 77	3538 ± 49	100
D16	Osci. zoned core	57	15	55	0.28	43.3057 ± 1.3322	0.8109 ± 0.0233	0.93	0.387	3828 ± 83	3860 ± 49	99
D17	Osci. zoned core	73	22	69	0.32	43.5122 ± 1.3361	0.8167 ± 0.0234	0.93	0.386	3849 ± 83	3857 ± 49	100
D18	Osci. zoned core	91	11	102	0.10	37.4059 ± 1.2344	0.7234 ± 0.0216	0.90	0.375	3509 ± 81	3812 ± 52	92
D19	Osci. zoned core	151	76	132	0.58	44.1468 ± 1.3488	0.8245 ± 0.0235	0.93	0.388	3876 ± 83	3864 ± 48	100
D19	Osci. zoned rim	87	24	82	0.29	43.9179 ± 1.3508	0.8199 ± 0.0234	0.93	0.388	3860 ± 83	3865 ± 49	100
D21	Black core	317	3	379	0.01	32.7197 ± 0.9995	0.7345 ± 0.0209	0.93	0.323	3550 ± 78	3584 ± 49	99
E02	Osci. zoned core	186	11	232	0.05	30.0246 ± 0.9218	0.6942 ± 0.0198	0.93	0.314	3399 ± 75	3539 ± 50	96
E03	Osci. zoned core	105	47	121	0.39	28.7545 ± 0.8896	0.6822 ± 0.0195	0.92	0.306	3353 ± 75	3499 ± 50	96
E04	Osci. zoned core	259	134	226	0.59	44.0331 ± 1.3570	0.8217 ± 0.0234	0.92	0.389	3866 ± 83	3866 ± 49	100
E05	Black core	509	3	611	0.01	31.5586 ± 0.9717	0.7139 ± 0.0203	0.92	0.321	3473 ± 76	3573 ± 50	97
E07	Black core	345	2	429	0.01	30.8681 ± 0.9520	0.7054 ± 0.0200	0.92	0.317	3441 ± 76	3557 ± 50	97

Continued on next page

Table B.3 – *Continued from previous page*

Spot #	Internal Structure	Pb (ppm)	Th (ppm)	U (ppm)	Th/U	$^{207}Pb/^{235}U$ $\pm 2\sigma$	$^{206}Pb/^{238}U$ $\pm 2\sigma$	ρ	$\frac{^{207}Pb}{^{206}Pb}$ ^{206}Pb	Ages (Ma)$\pm 2\sigma$ $\frac{^{206}Pb}{^{238}U}$	Ages (Ma)$\pm 2\sigma$ $\frac{^{207}Pb}{^{206}Pb}$	Conc %
E08	Osci. zoned core	117	63	116	0.55	37.8736 ± 1.1930	0.7313 ± 0.0211	0.92	0.376	3538 ± 78	3814 ± 50	93
E09	Black core	135	76	138	0.55	34.6246 ± 1.0772	0.7168 ± 0.0205	0.92	0.350	3484 ± 77	3708 ± 50	94
D06	Osci. zoned rim	173	102	151	0.67	43.7250 ± 1.2892	0.8135 ± 0.0231	0.96	0.390	3837 ± 82	3870 ± 47	99
E11	Core	205	55	223	0.25	37.1950 ± 1.1033	0.7307 ± 0.0208	0.96	0.369	3536 ± 77	3788 ± 47	93
E12	Osci. zoned core	415	21	482	0.04	35.2527 ± 1.0372	0.7286 ± 0.0206	0.96	0.351	3528 ± 77	3711 ± 47	95
E15	Black core	415	5	514	0.01	30.7009 ± 0.9068	0.7099 ± 0.0201	0.96	0.314	3458 ± 76	3539 ± 48	98
E16	Osci. zoned core	212	115	199	0.58	39.7393 ± 1.1747	0.7712 ± 0.0218	0.96	0.374	3685 ± 79	3806 ± 47	97
E17	Osci. zoned core	151	18	159	0.11	40.1975 ± 1.1911	0.7800 ± 0.0221	0.96	0.374	3717 ± 80	3807 ± 47	98
E18	Osci. zoned core	81	21	83	0.25	35.9924 ± 1.0748	0.7090 ± 0.0202	0.95	0.368	3455 ± 76	3784 ± 48	91
F01	Osci. zoned core	117	36	109	0.33	44.3159 ± 1.3223	0.8235 ± 0.0233	0.95	0.390	3873 ± 83	3872 ± 48	100
F01	Osci. zoned rim	261	67	264	0.26	40.8061 ± 1.2131	0.7799 ± 0.0221	0.95	0.380	3717 ± 80	3830 ± 48	97
F02	Black core	197	70	347	0.20	13.4694 ± 0.4021	0.5207 ± 0.0147	0.95	0.188	2702 ± 62	2721 ± 52	99
F03	Osci. zoned core	64	19	59	0.31	44.5738 ± 1.3448	0.8251 ± 0.0235	0.94	0.392	3879 ± 83	3878 ± 48	100
F04	Black rim	61	0	71	0.01	34.7256 ± 1.0543	0.7541 ± 0.0215	0.94	0.334	3623 ± 79	3635 ± 49	100
F05	Osci. zoned rim	155	40	150	0.26	42.4935 ± 1.2707	0.8055 ± 0.0228	0.95	0.383	3809 ± 81	3842 ± 48	99
F06	Osci. zoned core	82	33	79	0.42	39.3328 ± 1.1832	0.7849 ± 0.0223	0.94	0.363	3735 ± 80	3764 ± 48	99
F08	Osci. zoned core	153	73	143	0.51	41.3612 ± 1.2444	0.7940 ± 0.0225	0.94	0.378	3768 ± 81	3823 ± 48	99
F09	Osci. zoned core	107	56	94	0.59	44.1058 ± 1.3323	0.8180 ± 0.0232	0.94	0.391	3853 ± 82	3875 ± 48	99
F10	Osci. zoned core	78	27	72	0.38	44.1801 ± 1.3403	0.8154 ± 0.0232	0.94	0.393	3844 ± 82	3882 ± 48	99
F11	Osci. zoned core	88	40	82	0.49	41.5080 ± 1.2656	0.7899 ± 0.0225	0.93	0.381	3753 ± 81	3836 ± 49	98
F11	Osci. zoned rim	252	67	253	0.26	41.1561 ± 1.2417	0.7856 ± 0.0222	0.94	0.380	3737 ± 80	3831 ± 48	98
F12	Osci. zoned core	54	18	56	0.32	38.8770 ± 1.2004	0.7573 ± 0.0217	0.93	0.372	3634 ± 79	3801 ± 49	96
F13	Osci. zoned core	98	29	92	0.32	44.8209 ± 1.3607	0.8275 ± 0.0234	0.93	0.393	3887 ± 83	3882 ± 48	100
F13	Osci. zoned rim	102	32	107	0.30	38.4260 ± 1.1806	0.7422 ± 0.0212	0.93	0.375	3579 ± 78	3813 ± 49	94
F14	Osci. zoned core	95	33	91	0.36	41.9945 ± 1.2845	0.7938 ± 0.0225	0.93	0.384	3767 ± 81	3846 ± 49	98
F15	Core	98	49	97	0.50	37.7356 ± 1.1562	0.7587 ± 0.0215	0.92	0.361	3640 ± 79	3753 ± 49	97
SG-265 Mg-tonalite												
A01	Osci. zoned core	151	81	208	0.39	21.0594 ± 0.6465	0.6114 ± 0.0173	0.92	0.250	3076 ± 69	3183 ± 51	97
A01	Osci. zoned rim	64	21	86	0.25	22.8649 ± 0.7093	0.6476 ± 0.0184	0.92	0.256	3219 ± 72	3222 ± 52	100
A02	Osci. zoned rim	116	43	158	0.27	22.0409 ± 0.6791	0.6288 ± 0.0178	0.92	0.254	3145 ± 70	3211 ± 52	98

Continued on next page

Table B.3 – *Continued from previous page*

Spot #	Internal Structure	Pb (ppm)	Th (ppm)	U (ppm)	Th/U	$^{207}Pb/^{235}U$ $\pm 2\sigma$	$^{206}Pb/^{238}U$ $\pm 2\sigma$	ρ	$\frac{^{207}Pb}{^{206}Pb}$ ^{206}Pb	Ages (Ma)$\pm 2\sigma$ $\frac{^{206}Pb}{^{238}U}$	Ages (Ma)$\pm 2\sigma$ $\frac{^{207}Pb}{^{206}Pb}$	Conc %
A03	Osci. zoned core	102	42	151	0.28	19.9880 ± 0.6285	0.5835 ± 0.0166	0.90	0.248	2963 ± 68	3175 ± 53	93
A04	Osci. zoned rim	126	47	168	0.28	22.4875 ± 0.6943	0.6408 ± 0.0181	0.91	0.255	3192 ± 71	3213 ± 52	99
A05	Osci. zoned core	987	513	149	3.45	16.5345 ± 0.5171	0.4992 ± 0.0142	0.91	0.240	2611 ± 61	3121 ± 53	84
A06	Osci. zoned core	146	57	200	0.29	21.9471 ± 0.6869	0.6259 ± 0.0177	0.90	0.254	3133 ± 70	3212 ± 52	98
A07	Osci. zoned core	86	47	117	0.40	21.1494 ± 0.6641	0.6088 ± 0.0173	0.90	0.252	3065 ± 69	3197 ± 53	96
A07	Osci. zoned rim	45	14	61	0.23	22.6474 ± 0.7193	0.6396 ± 0.0182	0.90	0.257	3187 ± 72	3227 ± 53	99
A08	Osci. zoned core	109	28	150	0.19	22.1602 ± 0.6953	0.6348 ± 0.0179	0.90	0.253	3168 ± 71	3205 ± 53	99
A09	Osci. zoned core	149	66	215	0.31	20.2283 ± 0.6342	0.5893 ± 0.0167	0.90	0.249	2987 ± 67	3178 ± 53	94
A11	Osci. zoned core	44	14	63	0.22	20.7022 ± 0.6884	0.6027 ± 0.0174	0.87	0.249	3041 ± 70	3179 ± 56	96
A12	Osci. zoned core	116	10	170	0.06	21.7803 ± 0.6370	0.6217 ± 0.0175	0.96	0.254	3117 ± 70	3210 ± 49	97
A13	Osci. zoned core	102	25	165	0.15	18.2916 ± 0.5435	0.5507 ± 0.0156	0.95	0.241	2828 ± 65	3126 ± 50	90
A13	Osci. zoned rim	56	22	94	0.23	16.3452 ± 0.5275	0.5158 ± 0.0151	0.91	0.230	2681 ± 64	3051 ± 55	88
A14	Osci. zoned core	89	31	121	0.25	22.3357 ± 0.6675	0.6327 ± 0.0180	0.95	0.256	3160 ± 71	3222 ± 50	98
A15	Osci. zoned core	296	38	500	0.08	17.8377 ± 0.5214	0.5450 ± 0.0154	0.97	0.237	2804 ± 64	3102 ± 49	90
A16	Osci. zoned core	214	55	323	0.17	19.9392 ± 0.5923	0.5856 ± 0.0166	0.95	0.247	2972 ± 68	3165 ± 50	94
A17	Convo. core	21	5	28	0.17	23.1019 ± 0.7048	0.6497 ± 0.0186	0.94	0.258	3227 ± 73	3234 ± 51	100
A18	Convo. core	84	50	147	0.34	15.1123 ± 0.4535	0.4895 ± 0.0139	0.95	0.224	2569 ± 60	3009 ± 51	85
B01	Osci. zoned core	97	43	157	0.28	17.5157 ± 0.5306	0.5309 ± 0.0152	0.95	0.239	2745 ± 64	3115 ± 51	88
B02	Osci. zoned core	155	63	215	0.29	21.5074 ± 0.6318	0.6077 ± 0.0172	0.96	0.257	3061 ± 69	3226 ± 49	95
B03	Osci. zoned core	324	177	474	0.37	19.4520 ± 0.5714	0.5671 ± 0.0160	0.96	0.249	2896 ± 66	3177 ± 49	91
B04	Osci. zoned core	69	27	97	0.28	20.9014 ± 0.6167	0.5997 ± 0.0170	0.96	0.253	3029 ± 68	3202 ± 50	95
B05	Osci. zoned core	129	38	176	0.22	22.4810 ± 0.6593	0.6373 ± 0.0180	0.96	0.256	3178 ± 71	3221 ± 49	99
B06	Osci. zoned core	76	30	101	0.30	22.4506 ± 0.6644	0.6394 ± 0.0181	0.96	0.255	3187 ± 71	3214 ± 50	99
B08	Osci. zoned core	67	26	96	0.27	20.7663 ± 0.6191	0.6012 ± 0.0170	0.95	0.251	3035 ± 69	3188 ± 50	95
B09	Osci. zoned rim	54	19	88	0.22	17.6456 ± 0.5369	0.5360 ± 0.0153	0.94	0.239	2767 ± 64	3112 ± 51	89
B10	Osci. zoned rim	344	91	498	0.18	20.9250 ± 0.6127	0.6045 ± 0.0170	0.96	0.251	3048 ± 68	3191 ± 49	96
B11	Osci. zoned rim	43	23	63	0.37	19.7143 ± 0.6192	0.5756 ± 0.0167	0.92	0.248	2931 ± 68	3175 ± 53	92
B12	Osci. zoned rim	66	26	86	0.31	22.8655 ± 0.6776	0.6467 ± 0.0183	0.95	0.256	3215 ± 72	3225 ± 50	100
B13	Osci. zoned core	344	98	556	0.18	18.1838 ± 0.5339	0.5440 ± 0.0153	0.96	0.242	2800 ± 64	3136 ± 50	89
B15	Osci. zoned rim	46	23	60	0.38	22.2738 ± 0.6679	0.6314 ± 0.0179	0.95	0.256	3155 ± 71	3221 ± 50	98

Continued on next page

Table B.3 – *Continued from previous page*

Spot #	Internal Structure	Pb (ppm)	Th (ppm)	U (ppm)	Th/U	$^{207}Pb/^{235}U$ $\pm 2\sigma$	$^{206}Pb/^{238}U$ $\pm 2\sigma$	ρ	$\frac{^{207}Pb}{^{206}Pb}$ ^{206}Pb	Ages (Ma)$\pm 2\sigma$ $\frac{^{206}Pb}{^{238}U}$	Ages (Ma)$\pm 2\sigma$ $\frac{^{207}Pb}{^{206}Pb}$	Conc %
B16	Osci. zoned rim	118	54	152	0.35	22.7762 ± 0.6718	0.6458 ± 0.0182	0.96	0.256	3212 ± 71	3221 ± 49	100
B17	Osci. zoned core	109	37	158	0.24	20.5548 ± 0.6109	0.5917 ± 0.0167	0.95	0.252	2996 ± 68	3197 ± 50	94
B18	Osci. zoned core	151	68	229	0.30	19.1113 ± 0.5666	0.5601 ± 0.0158	0.95	0.247	2867 ± 65	3168 ± 50	90
B19	Osci. zoned rim	65	25	85	0.30	22.8744 ± 0.6894	0.6466 ± 0.0184	0.94	0.257	3215 ± 72	3226 ± 50	100
B20	Osci. zoned rim	53	18	70	0.26	22.8451 ± 0.6839	0.6469 ± 0.0183	0.94	0.256	3216 ± 72	3223 ± 50	100
C01	Osci. zoned core	62	23	86	0.27	20.9816 ± 0.6418	0.6009 ± 0.0172	0.94	0.253	3034 ± 69	3205 ± 51	95
C02	Osci. zoned rim	60	21	80	0.26	22.9878 ± 0.6928	0.6491 ± 0.0184	0.94	0.257	3225 ± 72	3227 ± 50	100
C03	Osci. zoned rim	54	19	78	0.24	21.0340 ± 0.6420	0.6026 ± 0.0172	0.94	0.253	3040 ± 69	3204 ± 51	95
C04	Osci. zoned core	269	62	440	0.14	18.2725 ± 0.5431	0.5474 ± 0.0155	0.95	0.242	2814 ± 64	3134 ± 50	90
C05	Osci. zoned rim	93	27	123	0.22	22.9553 ± 0.6847	0.6499 ± 0.0184	0.95	0.256	3228 ± 72	3223 ± 50	100
C06	Osci. zoned core	80	42	115	0.36	19.7852 ± 0.5944	0.5763 ± 0.0163	0.94	0.249	2934 ± 67	3178 ± 50	92
C07	Osci. zoned core	72	25	96	0.26	22.8509 ± 0.6831	0.6466 ± 0.0183	0.95	0.256	3215 ± 72	3224 ± 50	100
C08	Osci. zoned core	393	315	664	0.48	15.0776 ± 0.4475	0.4853 ± 0.0137	0.95	0.225	2550 ± 59	3019 ± 51	84
C10	Osci. zoned rim	260	135	351	0.38	21.5166 ± 0.6384	0.6141 ± 0.0173	0.95	0.254	3087 ± 69	3210 ± 50	96
C11	Osci. zoned rim	119	51	159	0.32	22.1269 ± 0.6599	0.6215 ± 0.0175	0.94	0.258	3116 ± 70	3236 ± 50	96
C12	Osci. zoned core	177	48	259	0.19	20.9560 ± 0.6301	0.6005 ± 0.0170	0.94	0.253	3032 ± 68	3204 ± 50	95
C13	Osci. zoned rim	72	30	94	0.31	22.7882 ± 0.6870	0.6462 ± 0.0183	0.94	0.256	3214 ± 72	3221 ± 50	100
C14	Osci. zoned rim	126	42	169	0.25	22.5761 ± 0.6864	0.6372 ± 0.0181	0.93	0.257	3178 ± 71	3228 ± 51	98
C15	Osci. zoned rim	73	28	101	0.28	21.5504 ± 0.6600	0.6136 ± 0.0175	0.93	0.255	3085 ± 70	3214 ± 51	96
C16	Osci. zoned core	64	26	107	0.24	16.7090 ± 0.5105	0.5156 ± 0.0146	0.93	0.235	2681 ± 62	3086 ± 52	87
C17	Osci. zoned core	88	24	130	0.18	20.6393 ± 0.6328	0.5954 ± 0.0169	0.93	0.251	3011 ± 68	3193 ± 51	94
C18	Osci. zoned core	212	87	311	0.28	20.2657 ± 0.6056	0.5837 ± 0.0164	0.94	0.252	2964 ± 67	3196 ± 50	93
D01	Osci. zoned core	82	43	134	0.32	16.5189 ± 0.5304	0.5126 ± 0.0148	0.90	0.234	2668 ± 63	3078 ± 54	87
D02	Osci. zoned core	75	34	107	0.32	20.2464 ± 0.6335	0.5842 ± 0.0167	0.91	0.251	2966 ± 68	3193 ± 52	93
D03	Osci. zoned core	163	82	233	0.35	20.2289 ± 0.6151	0.5809 ± 0.0164	0.93	0.253	2953 ± 67	3201 ± 51	92
D04	Osci. zoned core	115	57	166	0.34	19.9256 ± 0.6117	0.5788 ± 0.0164	0.92	0.250	2944 ± 67	3183 ± 52	92
D05	Osci. zoned core	44	19	63	0.30	20.3282 ± 0.6629	0.5916 ± 0.0172	0.89	0.249	2996 ± 70	3180 ± 55	94
D06	Osci. zoned core	98	37	148	0.25	19.3847 ± 0.6045	0.5645 ± 0.0161	0.91	0.249	2885 ± 66	3179 ± 52	91
D07	Osci. zoned core	56	23	78	0.30	21.2053 ± 0.6568	0.6061 ± 0.0173	0.92	0.254	3054 ± 69	3208 ± 52	95
D08	Osci. zoned core	442	593	631	0.94	16.6083 ± 0.5028	0.5120 ± 0.0144	0.93	0.235	2665 ± 61	3088 ± 51	86

Continued on next page

Table B.3 – *Continued from previous page*

Spot #	**Internal Structure**	**Pb** (ppm)	**Th** (ppm)	**U** (ppm)	**Th/U**	^{207}**Pb**/^{235}**U** $\pm 2\sigma$	^{206}**Pb**/^{238}**U** $\pm 2\sigma$	ρ	$\frac{^{207}Pb}{^{206}Pb}$ ^{206}Pb	**Ages (Ma)**$\pm 2\sigma$ $\frac{^{206}Pb}{^{238}U}$	$\frac{^{207}Pb}{^{206}Pb}$	**Conc** %
D09	Osci. zoned core	127	88	191	0.46	18.4010 ± 0.5636	0.5435 ± 0.0154	0.93	0.246	2798 ± 64	3156 ± 52	89
D10	Osci. zoned core	99	31	142	0.22	20.8620 ± 0.6400	0.6010 ± 0.0170	0.92	0.252	3034 ± 68	3196 ± 51	95
D11	Osci. zoned rim	63	33	90	0.37	20.1865 ± 0.6335	0.5852 ± 0.0167	0.91	0.250	2970 ± 68	3186 ± 53	93
D12	Osci. zoned core	49	17	64	0.26	23.1384 ± 0.7168	0.6520 ± 0.0185	0.92	0.257	3236 ± 72	3231 ± 52	100
D13	Osci. zoned rim	117	48	167	0.29	20.7719 ± 0.6404	0.5954 ± 0.0169	0.92	0.253	3011 ± 68	3204 ± 52	94
D14	Osci. zoned core	71	30	91	0.33	22.9487 ± 0.7076	0.6498 ± 0.0184	0.92	0.256	3227 ± 72	3223 ± 52	100
D15	Osci. zoned rim	160	47	228	0.21	21.2786 ± 0.6536	0.6096 ± 0.0172	0.92	0.253	3068 ± 69	3205 ± 51	96
D16	Osci. zoned rim	42	12	56	0.21	23.0926 ± 0.7243	0.6505 ± 0.0185	0.91	0.257	3230 ± 72	3231 ± 52	100
D17	Osci. zoned rim	46	17	74	0.24	17.7856 ± 0.5790	0.5391 ± 0.0156	0.89	0.239	2780 ± 65	3115 ± 55	89
D18	Osci. zoned core	59	33	82	0.41	20.5716 ± 0.6634	0.5919 ± 0.0170	0.89	0.252	2997 ± 69	3198 ± 54	94
D19	Osci. zoned core	44	15	62	0.24	21.4519 ± 0.6779	0.6100 ± 0.0174	0.90	0.255	3070 ± 70	3216 ± 53	95
E01	Osci. zoned core	96	34	135	0.25	21.4399 ± 0.6730	0.6085 ± 0.0173	0.91	0.255	3064 ± 69	3219 ± 52	95
E02	Osci. zoned core	33	13	49	0.26	20.1982 ± 0.7014	0.5854 ± 0.0174	0.86	0.250	2971 ± 71	3186 ± 58	93
E03	Osci. zoned core	205	76	300	0.25	20.3769 ± 0.6331	0.5858 ± 0.0166	0.91	0.252	2972 ± 67	3199 ± 52	93
E04	Osci. zoned core	231	152	317	0.48	20.3359 ± 0.6320	0.5852 ± 0.0165	0.91	0.252	2970 ± 67	3197 ± 52	93
E06	Osci. zoned core	48	18	67	0.27	21.6707 ± 0.6724	0.6169 ± 0.0181	0.95	0.255	3097 ± 72	3215 ± 50	96
E06	Osci. zoned rim	210	69	316	0.22	20.3922 ± 0.6210	0.5768 ± 0.0168	0.96	0.256	2936 ± 69	3225 ± 50	91
E08	Osci. zoned core	267	184	359	0.51	20.7452 ± 0.6283	0.5906 ± 0.0172	0.96	0.255	2992 ± 70	3214 ± 49	93
E10	Osci. zoned rim	88	24	130	0.18	20.5374 ± 0.6311	0.5935 ± 0.0173	0.95	0.251	3004 ± 70	3191 ± 50	94
E11	Osci. zoned core	86	47	113	0.42	21.6609 ± 0.6659	0.6136 ± 0.0179	0.95	0.256	3084 ± 72	3222 ± 50	96
E12	Osci. zoned rim	48	14	63	0.23	22.9556 ± 0.7094	0.6431 ± 0.0188	0.95	0.259	3201 ± 74	3240 ± 50	99
E15	Osci. zoned core	119	46	171	0.27	20.8302 ± 0.6427	0.5906 ± 0.0173	0.95	0.256	2992 ± 70	3221 ± 50	93
E16	Osci. zoned core	93	51	147	0.35	17.4772 ± 0.5448	0.5324 ± 0.0156	0.94	0.238	2751 ± 66	3107 ± 51	89

Table B.4

Full data set of the in-situ Lu-Hf composition analysis.

Zircon number	Texture	$^{176}Hf/^{177}Hf$ $\pm 2\sigma$	$^{178}Hf/^{177}Hf$ $\pm 2\sigma$	$^{176}Lu/^{177}Hf$ $\pm 2\sigma$	$^{176}Yb/^{177}Hf$ $\pm 2\sigma$	$\frac{^{207}Pb}{^{206}Pb}$ $\pm 2\sigma$ Age (Ma)	Conc %	$\varepsilon Hf_{(i)}$ $\pm 2\sigma$ Single grain	$\varepsilon Hf_{(i)}$ $\pm 2\sigma$ Rock age
	SG-007								
	2769 Ma cluster metamorphic zircons								
E7	metamict	0.28045 ± 2	1.46728 ± 4	0.000424 ± 10	0.01088 ± 18	2374 ± 52	99	-29.7 ± 0.7	-20.6 ± 0.7
D15r	zoned rim	0.28041 ± 2	1.46724 ± 4	0.000501 ± 1	0.01299 ± 21	2459 ± 52	100	-29.3 ± 0.7	-22.2 ± 0.7
C4r	metamict rim	0.28040 ± 2	1.46723 ± 3	0.000266 ± 3	0.00692 ± 20	2626 ± 50	99	-25.2 ± 0.6	-21.9 ± 0.6
F2	metamict	0.28038 ± 2	1.46725 ± 4	0.000271 ± 3	0.00700 ± 5	2651 ± 50	100	-25.4 ± 0.8	-22.6 ± 0.8
D5r	metamict core	0.28041 ± 2	1.46725 ± 5	0.000323 ± 3	0.00813 ± 3	2726 ± 50	100	-22.8 ± 0.6	-21.8 ± 0.6
A9r	metamict rim	0.28043 ± 2	1.46726 ± 3	0.000546 ± 76	0.01351 ± 182	2781 ± 50	100	-21.0 ± 0.7	-21.3 ± 0.7
A11r	metamict rim	0.28041 ± 2	1.46725 ± 4	0.000229 ± 2	0.00586 ± 11	2826 ± 50	100	-20.2 ± 0.7	-21.6 ± 0.7
	3529 Ma recrystallyzed zircons								
A4	metamict	0.28041 ± 2	1.46728 ± 3	0.000803 ± 23	0.02249 ± 93	3308 ± 48	100	-10.3 ± 0.6	-5.1 ± 0.6
D14r	black rim	0.28038 ± 2	1.46727 ± 3	0.000382 ± 13	0.01015 ± 14	3488 ± 47	100	-6.0 ± 0.6	-5.0 ± 0.6
C14c	black core	0.28039 ± 2	1.46724 ± 4	0.000567 ± 15	0.01421 ± 41	3499 ± 47	102	-5.9 ± 0.9	-5.2 ± 0.9
E5	black rim	0.28038 ± 2	1.46722 ± 3	0.000600 ± 2	0.01517 ± 15	3499 ± 47	100	-6.1 ± 0.6	-5.4 ± 0.6
H8c	zoned core	0.28036 ± 2	1.46722 ± 4	0.000755 ± 7	0.01685 ± 14	3504 ± 47	98	-7.2 ± 0.8	-6.6 ± 0.8
F7	metamict	0.28041 ± 1	1.46727 ± 3	0.000306 ± 11	0.00681 ± 24	3535 ± 47	101	-3.7 ± 0.5	-3.9 ± 0.5
B7c	metamict core	0.28039 ± 2	1.46724 ± 4	0.000522 ± 18	0.01466 ± 65	3570 ± 47	100	-4.1 ± 0.8	-5.1 ± 0.8
F13r	black rim	0.28040 ± 2	1.46726 ± 3	0.000536 ± 1	0.01411 ± 17	3615 ± 46	101	-2.8 ± 0.9	-4.8 ± 0.9
D3	metamict core	0.28041 ± 2	1.46726 ± 4	0.000293 ± 5	0.00857 ± 25	3617 ± 47	100	-1.7 ± 0.7	-3.8 ± 0.7
	3883 Ma Igneous Zircons								
F13c1	zoned core	0.28037 ± 2	1.46728 ± 4	0.000667 ± 50	0.02063 ± 148	3734 ± 46	100	-1.2 ± 0.6	2.3 ± 0.6
D14c	zoned core	0.28033 ± 2	1.46727 ± 4	0.000412 ± 5	0.01298 ± 9	3765 ± 46	99	-1.4 ± 0.8	1.4 ± 0.8

Continued on next page

Table B.4 – *Continued from previous page*

Zircon Number	Texture	$^{176}Hf/^{177}Hf$ $\pm 2\sigma$	$^{178}Hf/^{177}Hf$ $\pm 2\sigma$	$^{176}Lu/^{177}Hf$ $\pm 2\sigma$	$^{176}Yb/^{177}Hf$ $\pm 2\sigma$	$\frac{^{207}Pb}{^{206}Pb}$ $\pm 2\sigma$ Age (Ma)	Conc %	$\varepsilon Hf_{(i)}$ $\pm 2\sigma$ Single grain	$\varepsilon Hf_{(i)}$ $\pm 2\sigma$ Rock age
A8c	zoned core	0.28039 ± 3	1.46727 ± 4	0.001182 ± 33	0.03109 ± 60	3785 ± 46	98	-0.8 ± 0.9	1.5 ± 0.9
A14	zoned core	0.28034 ± 3	1.46722 ± 5	0.000687 ± 7	0.01604 ± 27	3810 ± 47	97	-0.7 ± 1.0	1.0 ± 1.0
A10r	zoned rim	0.28032 ± 2	1.46725 ± 4	0.000226 ± 4	0.00604 ± 11	3815 ± 46	99	-0.2 ± 0.7	1.5 ± 0.7
A13	zoned core	0.28037 ± 2	1.46725 ± 4	0.000428 ± 9	0.01382 ± 41	3824 ± 46	99	1.4 ± 0.8	2.8 ± 0.8
E10c	zoned core	0.28040 ± 2	1.46726 ± 4	0.001203 ± 5	0.03804 ± 36	3854 ± 46	99	1.2 ± 0.7	1.9 ± 0.7
E15c	zoned core	0.28042 ± 2	1.46726 ± 4	0.001361 ± 49	0.03656 ± 175	3867 ± 46	99	1.7 ± 0.9	2.1 ± 0.9
C5	zoned core	0.28041 ± 3	1.46722 ± 3	0.001141 ± 43	0.02932 ± 126	3883 ± 46	99	2.4 ± 1.1	2.4 ± 1.1
C5bis	zoned core	0.28031 ± 2	1.46726 ± 3	0.000532 ± 2	0.01291 ± 21	3883 ± 46	99	0.5 ± 0.8	0.5 ± 0.8
	SG-017								
	Metamict zircons								
C2	white core	0.28064 ± 2	1.46722 ± 4	0.000043 ± 0	0.00111 ± 2	2695 ± 56	99	-14.8 ± 0.8	- ± -
A7	black core	0.28064 ± 2	1.46726 ± 3	0.000665 ± 78	0.02062 ± 257	2719 ± 52	96	-15.1 ± 0.8	- ± -
	2802 Ma old zircons cluster								
F3	black core	0.28063 ± 2	1.46725 ± 4	0.000296 ± 7	0.00788 ± 31	2764 ± 53	99	-13.8 ± 0.8	-12.9 ± 0.8
F6	black core	0.28064 ± 2	1.46730 ± 4	0.000347 ± 19	0.01022 ± 65	2785 ± 53	101	-13.0 ± 0.6	-12.6 ± 0.6
C9	black core	0.28062 ± 2	1.46725 ± 5	0.000292 ± 15	0.00762 ± 34	2788 ± 52	98	-13.8 ± 0.8	-13.5 ± 0.8
D3	zoned core	0.28062 ± 1	1.46729 ± 5	0.000125 ± 1	0.00386 ± 8	2791 ± 54	99	-13.3 ± 0.5	-13.1 ± 0.5
C16	black core	0.28063 ± 2	1.46726 ± 2	0.000061 ± 0	0.00148 ± 2	2806 ± 52	100	-12.6 ± 0.8	-12.7 ± 0.8
D2	black core	0.28066 ± 2	1.46729 ± 4	0.000467 ± 35	0.01395 ± 96	2809 ± 52	96	-12.1 ± 0.7	-12.3 ± 0.7
A11	black core	0.28064 ± 2	1.46726 ± 4	0.000332 ± 1	0.00999 ± 7	2830 ± 51	97	-12.1 ± 0.6	-12.8 ± 0.6
	Inherited age								
A15	black core	0.28036 ± 1	1.46728 ± 3	0.000477 ± 9	0.01235 ± 12	3575 ± 48	100	-4.9 ± 0.5	-4.8 ± 0.5
	SG-019								
	2574 Ma zircon cluster								

Continued on next page

Table B.4 – *Continued from previous page*

Zircon Number	Texture	$^{176}Hf/^{177}Hf$ $\pm 2\sigma$	$^{178}Hf/^{177}Hf$ $\pm 2\sigma$	$^{176}Lu/^{177}Hf$ $\pm 2\sigma$	$^{176}Yb/^{177}Hf$ $\pm 2\sigma$	$\frac{^{207}Pb}{^{206}Pb}$ $\pm 2\sigma$ Age (Ma)	Conc %	$\varepsilon Hf_{(i)}$ $\pm 2\sigma$ Single grain	$\varepsilon Hf_{(i)}$ $\pm 2\sigma$ Rock age
C10	metamict	0.28080 ± 2	1.46729 ± 4	0.000278 ± 0	0.00819 ± 9	2569 ± 52	93	-12.6 ± 0.6	-12.4 ± 0.6
D13	black	0.28073 ± 3	1.46724 ± 4	0.000677 ± 1	0.01950 ± 15	2570 ± 53	101	-15.6 ± 1.0	-15.6 ± 1.0
D19	black	0.28072 ± 3	1.46727 ± 4	0.000527 ± 5	0.01451 ± 10	2570 ± 54	101	-15.6 ± 1.0	-15.5 ± 1.0
A8	black core	0.28072 ± 3	1.46724 ± 3	0.000418 ± 2	0.01167 ± 19	2572 ± 52	97	-15.2 ± 0.9	-15.2 ± 0.9
C9	metamict	0.28083 ± 2	1.46728 ± 3	0.000169 ± 2	0.00544 ± 6	2573 ± 52	90	-11.1 ± 0.6	-11.1 ± 0.6
D9	black core	0.28073 ± 3	1.46725 ± 4	0.000662 ± 2	0.01912 ± 18	2581 ± 53	99	-15.1 ± 0.9	-15.3 ± 0.9
D11	black core	0.28076 ± 3	1.46729 ± 4	0.000690 ± 3	0.02014 ± 10	2584 ± 53	98	-14.1 ± 0.9	-14.3 ± 0.9
F7	black core	0.28082 ± 2	1.46725 ± 3	0.000348 ± 11	0.01051 ± 20	2604 ± 54	94	-10.9 ± 0.7	-11.6 ± 0.7
	2732 Ma igneous zircon								
E14	zoned core	0.28073 ± 2	1.46727 ± 4	0.000199 ± 3	0.00536 ± 9	2668 ± 55	99	-12.4 ± 0.7	-10.9 ± 0.7
D2c	metamict	0.28044 ± 2	1.46733 ± 4	0.000517 ± 1	0.01355 ± 8	2715 ± 58	98	-22.3 ± 0.7	-22.0 ± 0.7
B7c	metamict core	0.28077 ± 2	1.46731 ± 4	0.000244 ± 4	0.00664 ± 5	2722 ± 51	101	-9.8 ± 0.8	-9.6 ± 0.8
B7r	zoned rim	0.28063 ± 2	1.46726 ± 4	0.000228 ± 1	0.00600 ± 9	2723 ± 51	99	-14.7 ± 0.6	-14.5 ± 0.6
D10	zoned core	0.28070 ± 2	1.46725 ± 4	0.000256 ± 5	0.00663 ± 6	2728 ± 53	99	-12.3 ± 0.7	-12.2 ± 0.7
D15	zoned core	0.28069 ± 2	1.46729 ± 4	0.000342 ± 1	0.00925 ± 15	2730 ± 53	100	-12.7 ± 0.7	-12.7 ± 0.7
C7r	zoned rim	0.28075 ± 2	1.46725 ± 3	0.000160 ± 1	0.00405 ± 6	2738 ± 52	99	-10.0 ± 0.8	-10.2 ± 0.8
C1	black cristal	0.28073 ± 3	1.46721 ± 4	0.000498 ± 2	0.01290 ± 14	2739 ± 51	98	-11.3 ± 0.9	-11.5 ± 0.9
B4	metamict	0.28085 ± 2	1.46731 ± 3	0.000123 ± 10	0.00395 ± 28	2748 ± 51	96	-6.0 ± 0.6	-6.4 ± 0.6
D8	metamict	0.28067 ± 2	1.46728 ± 4	0.000338 ± 4	0.00853 ± 14	2803 ± 52	99	-11.6 ± 0.8	-13.3 ± 0.8
	Inherited ages								
D3c	black core	0.28046 ± 3	1.46726 ± 4	0.000355 ± 11	0.01002 ± 42	3481 ± 51	99	-3.5 ± 0.9	-1.8 ± 0.9
D2r	grey	0.28068 ± 2	1.46722 ± 4	0.000098 ± 5	0.00235 ± 12	3555 ± 48	99	6.8 ± 0.8	6.8 ± 0.8
	SG-024								
	2731 Ma metamorphic zircons								

Continued on next page

Table B.4 – *Continued from previous page*

Zircon Number	Texture	$^{176}Hf/^{177}Hf$ $\pm 2\sigma$	$^{178}Hf/^{177}Hf$ $\pm 2\sigma$	$^{176}Lu/^{177}Hf$ $\pm 2\sigma$	$^{176}Yb/^{177}Hf$ $\pm 2\sigma$	$\frac{^{207}Pb}{^{206}Pb}$ $\pm 2\sigma$ Age (Ma)	Conc %	$\varepsilon Hf_{(i)}$ $\pm 2\sigma$ Single grain	$\varepsilon Hf_{(i)}$ $\pm 2\sigma$ Rock age
C7	Metamict	0.28060 ± 2	1.46722 ± 3	0.000548 ± 2	0.01595 ± 28	2660 ± 53	99	-17.8 ± 0.7	-16.2 ± 0.7
F2r	Sector zoned	0.28043 ± 2	1.46730 ± 3	0.000217 ± 1	0.00686 ± 2	2668 ± 52	97	-23.2 ± 0.8	-21.7 ± 0.8
B5	Sector zoned	0.28042 ± 2	1.46724 ± 4	0.000154 ± 14	0.00517 ± 55	2695 ± 52	98	-22.7 ± 0.6	-21.9 ± 0.6
C8c	Metamict	0.28061 ± 2	1.46724 ± 3	0.000712 ± 3	0.02086 ± 31	2710 ± 52	99	-16.6 ± 0.7	-16.1 ± 0.7
F5	Metamict	0.28056 ± 3	1.46725 ± 5	0.000509 ± 22	0.01494 ± 84	2713 ± 51	100	-18.2 ± 1.1	-17.7 ± 1.1
B15	Metamict	0.28064 ± 3	1.46722 ± 4	0.000589 ± 15	0.01745 ± 73	2716 ± 52	99	-15.3 ± 1.0	-15.0 ± 1.0
B3	Metamict	0.28059 ± 2	1.46720 ± 5	0.000351 ± 1	0.01003 ± 9	2725 ± 52	100	-16.3 ± 0.8	-16.1 ± 0.8
B14	Sector zoned	0.28046 ± 2	1.46728 ± 3	0.000416 ± 6	0.01368 ± 21	2731 ± 52	100	-21.1 ± 0.7	-21.1 ± 0.7
F6r	Sector zoned	0.28050 ± 2	1.46723 ± 4	0.000094 ± 1	0.00288 ± 2	2790 ± 50	101	-17.7 ± 0.8	-19.0 ± 0.8
E9	Sector zoned	0.28047 ± 2	1.46719 ± 5	0.000295 ± 32	0.00872 ± 102	2819 ± 50	100	-18.2 ± 0.8	-20.2 ± 0.8
	3869 Ma cluster and Lu-Hf undisturbed re-crystallized zircons								
D16c	Metamict	0.28044 ± 2	1.46726 ± 5	0.000773 ± 8	0.02249 ± 33	3396 ± 47	100	-7.1 ± 0.7	4.0 ± 0.7
F1r	Metamict	0.28042 ± 2	1.46724 ± 3	0.000565 ± 24	0.01575 ± 70	3466 ± 48	94	-5.4 ± 0.8	4.1 ± 0.8
F3r	Metamict	0.28047 ± 2	1.46722 ± 3	0.000519 ± 5	0.01519 ± 16	3573 ± 47	97	-1.1 ± 0.6	5.9 ± 0.6
D6c	zoned core	0.28041 ± 2	1.46724 ± 5	0.000351 ± 1	0.00999 ± 12	3676 ± 47	96	-0.4 ± 0.8	4.2 ± 0.8
F6c	zoned core	0.28039 ± 3	1.46726 ± 6	0.000346 ± 10	0.01088 ± 50	3683 ± 47	96	-0.9 ± 1.1	3.6 ± 1.1
D3r	Rim	0.28038 ± 2	1.46723 ± 4	0.000178 ± 7	0.00601 ± 32	3686 ± 46	97	-0.8 ± 0.6	3.6 ± 0.6
E1c	Black core	0.28045 ± 2	1.46727 ± 4	0.000917 ± 8	0.02948 ± 36	3689 ± 46	99	0.0 ± 0.7	4.2 ± 0.7
F1c	zoned core	0.28041 ± 2	1.46720 ± 4	0.000382 ± 2	0.01112 ± 5	3700 ± 47	97	-0.1 ± 0.8	3.9 ± 0.8
E14c	Osci. zoned	0.28035 ± 2	1.46725 ± 4	0.000696 ± 22	0.02029 ± 89	3772 ± 46	97	-1.2 ± 0.5	1.0 ± 0.5
A17c	Osci. Zoned	0.28059 ± 2	1.46724 ± 4	0.003271 ± 22	0.10485 ± 114	3792 ± 47	98	1.0 ± 0.8	2.7 ± 0.8
B16c	Osci. Zoned	0.28044 ± 3	1.46720 ± 4	0.001245 ± 61	0.03831 ± 227	3812 ± 48	99	1.4 ± 1.1	2.7 ± 1.1
F8c	black core	0.28048 ± 3	1.46727 ± 4	0.001623 ± 2	0.05211 ± 68	3824 ± 46	97	2.0 ± 1.0	3.0 ± 1.0
D7c	black core	0.28040 ± 3	1.46726 ± 3	0.001137 ± 9	0.03417 ± 63	3824 ± 46	98	0.6 ± 1.0	1.6 ± 1.0

Continued on next page

Table B.4 – *Continued from previous page*

Zircon Number	Texture	$^{176}Hf/^{177}Hf$ $\pm 2\sigma$	$^{178}Hf/^{177}Hf$ $\pm 2\sigma$	$^{176}Lu/^{177}Hf$ $\pm 2\sigma$	$^{176}Yb/^{177}Hf$ $\pm 2\sigma$	$\frac{^{207}Pb}{^{206}Pb}$ $\pm 2\sigma$ Age (Ma)	Conc %	$\varepsilon Hf_{(i)}$ $\pm 2\sigma$ Single grain	$\varepsilon Hf_{(i)}$ $\pm 2\sigma$ Rock age
D11c	core	0.28038 ± 1	1.46720 ± 3	0.000068 ± 1	0.00250 ± 4	3836 ± 46	99	2.9 ± 0.4	3.7 ± 0.4
A17r	Osci.zoned	0.28040 ± 3	1.46725 ± 4	0.001060 ± 4	0.03193 ± 51	3867 ± 47	99	1.9 ± 1.0	1.9 ± 1.0
F8r	Osci. zoned	0.28037 ± 2	1.46728 ± 4	0.001060 ± 3	0.03207 ± 29	3874 ± 47	99	0.9 ± 0.8	0.8 ± 0.8
	SG-025								
	2747 Ma Recrystallized zircons								
F4r	zoned rim	0.28056 ± 2	1.46720 ± 4	0.000061 ± 1	0.00195 ± 4	2649 ± 51	101	-18.8 ± 0.8	-16.5 ± 0.8
E15	zoned rim	0.28055 ± 2	1.46724 ± 4	0.000165 ± 3	0.00527 ± 3	2691 ± 51	100	-18.4 ± 0.6	-17.1 ± 0.6
A9r	metamict	0.28059 ± 2	1.46728 ± 4	0.000364 ± 2	0.01099 ± 5	2724 ± 51	98	-16.5 ± 0.7	-16.0 ± 0.7
D11r	metamict	0.28057 ± 2	1.46730 ± 5	0.000382 ± 2	0.01072 ± 17	2729 ± 50	100	-17.2 ± 0.8	-16.8 ± 0.8
E4	metamict	0.28059 ± 3	1.46728 ± 3	0.000393 ± 1	0.01093 ± 12	2739 ± 50	100	-16.1 ± 0.9	-15.9 ± 0.9
D5c	black core	0.28057 ± 2	1.46726 ± 4	0.000324 ± 6	0.00912 ± 18	2741 ± 50	100	-16.8 ± 0.7	-16.7 ± 0.7
F17r	black core	0.28059 ± 2	1.46724 ± 3	0.000183 ± 1	0.00576 ± 3	2748 ± 51	100	-15.6 ± 0.6	-15.6 ± 0.6
B4	black core	0.28060 ± 2	1.46725 ± 3	0.000150 ± 1	0.00523 ± 8	2751 ± 51	100	-14.9 ± 0.5	-15.0 ± 0.5
B2c	black core	0.28057 ± 2	1.46727 ± 4	0.000301 ± 8	0.00921 ± 40	2756 ± 50	100	-16.1 ± 0.7	-16.3 ± 0.7
B9	zoned rim	0.28053 ± 2	1.46723 ± 4	0.000103 ± 1	0.00316 ± 3	2758 ± 51	100	-17.1 ± 0.8	-17.4 ± 0.8
F6	black core	0.28062 ± 3	1.46723 ± 3	0.000131 ± 2	0.00430 ± 13	2767 ± 50	99	-13.9 ± 0.9	-14.4 ± 0.9
C7	black core	0.28060 ± 3	1.46726 ± 5	0.000447 ± 5	0.01401 ± 45	2818 ± 49	99	-13.8 ± 1.0	-15.5 ± 1.0
	3838 Ma igneous and Lu-Hf undisturbed zircons								
F16	Metamict core	0.28042 ± 2	1.46724 ± 4	0.000395 ± 12	0.01286 ± 48	3071 ± 49	97	-14.5 ± 0.6	3.5 ± 0.6
E11c	Metamict core	0.28035 ± 2	1.46721 ± 4	0.000296 ± 8	0.00960 ± 10	3289 ± 48	97	-11.5 ± 0.7	1.5 ± 0.7
C14	Metamict core	0.28036 ± 2	1.46725 ± 3	0.000388 ± 8	0.01229 ± 44	3471 ± 47	100	-7.1 ± 0.8	1.6 ± 0.8
A9c	Metamict core	0.28040 ± 1	1.46724 ± 3	0.000256 ± 2	0.00802 ± 11	3624 ± 47	98	-1.8 ± 0.5	3.3 ± 0.5
F17c	Metamict core	0.28047 ± 2	1.46722 ± 4	0.001267 ± 84	0.04385 ± 365	3629 ± 47	100	-1.6 ± 0.7	3.3 ± 0.7
C1c	zoned core	0.28035 ± 2	1.46723 ± 3	0.000461 ± 12	0.01416 ± 39	3708 ± 46	98	-2.0 ± 0.7	1.1 ± 0.7

Continued on next page

Table B.4 – *Continued from previous page*

Zircon Number	Texture	$^{176}Hf/^{177}Hf$ $\pm 2\sigma$	$^{178}Hf/^{177}Hf$ $\pm 2\sigma$	$^{176}Lu/^{177}Hf$ $\pm 2\sigma$	$^{176}Yb/^{177}Hf$ $\pm 2\sigma$	$\frac{^{207}Pb}{^{206}Pb}$ $\pm 2\sigma$ Age (Ma)	Conc %	$\varepsilon Hf_{(i)}$ $\pm 2\sigma$ Single grain	$\varepsilon Hf_{(i)}$ $\pm 2\sigma$ Rock age
D2c	zoned core	0.28039 ± 3	1.46726 ± 4	0.000463 ± 4	0.01376 ± 11	3755 ± 46	99	0.2 ± 0.9	2.2 ± 0.9
D11c	zoned core	0.28036 ± 2	1.46728 ± 4	0.000344 ± 11	0.01063 ± 43	3760 ± 46	99	-0.2 ± 0.5	1.7 ± 0.5
D17c	zoned core	0.28037 ± 2	1.46723 ± 3	0.000863 ± 10	0.02683 ± 38	3775 ± 46	99	-0.9 ± 0.7	0.6 ± 0.7
E8c2	inherited core	0.28042 ± 3	1.46729 ± 4	0.000202 ± 16	0.00611 ± 54	3839 ± 46	99	4.1 ± 1.1	4.1 ± 1.1
	SG-026								
	3820 Ma crystallization								
F14	zoned core	0.28042 ± 3	1.46729 ± 5	0.000298 ± 1	0.00884 ± 4	3617 ± 48	94	-1.3 ± 1.0	3.6 ± 1.0
B12	zoned core	0.28042 ± 2	1.46724 ± 5	0.000390 ± 8	0.01143 ± 16	3620 ± 48	95	-1.6 ± 0.8	3.1 ± 0.8
A9c	Sector zoned	0.28040 ± 3	1.46727 ± 5	0.000416 ± 6	0.01274 ± 37	3691 ± 48	98	-0.6 ± 1.2	2.5 ± 1.2
A13	Sector zoned	0.28040 ± 2	1.46728 ± 5	0.000380 ± 1	0.01171 ± 13	3694 ± 47	98	-0.4 ± 0.7	2.6 ± 0.7
C15	Sector zoned	0.28038 ± 2	1.46731 ± 5	0.000228 ± 1	0.00690 ± 10	3702 ± 49	95	-0.7 ± 0.9	2.2 ± 0.9
B14	Sector zoned	0.28042 ± 3	1.46727 ± 4	0.000380 ± 10	0.01209 ± 41	3709 ± 48	97	0.5 ± 1.0	3.2 ± 1.0
C17	Sector zoned	0.28042 ± 3	1.46728 ± 3	0.000357 ± 6	0.01096 ± 27	3709 ± 48	95	0.7 ± 1.2	3.3 ± 1.2
A4c	Sector zoned	0.28045 ± 2	1.46726 ± 4	0.000525 ± 13	0.01603 ± 37	3725 ± 47	99	1.6 ± 0.9	3.9 ± 0.9
A3	Sector zoned	0.28042 ± 2	1.46724 ± 7	0.000469 ± 6	0.01431 ± 3	3727 ± 47	99	0.8 ± 0.9	3.0 ± 0.9
D17c	Sector zoned	0.28045 ± 2	1.46725 ± 5	0.000584 ± 3	0.01898 ± 4	3738 ± 47	98	1.7 ± 0.7	3.6 ± 0.7
F11	Sector zoned	0.28043 ± 3	1.46725 ± 6	0.000421 ± 17	0.01307 ± 44	3739 ± 48	97	1.5 ± 1.1	3.4 ± 1.1
C12	Sector zoned	0.28043 ± 2	1.46725 ± 5	0.000349 ± 4	0.01112 ± 20	3741 ± 48	99	1.9 ± 0.7	3.8 ± 0.7
E3	Sector zoned	0.28045 ± 3	1.46724 ± 5	0.000609 ± 7	0.02030 ± 19	3744 ± 47	98	1.7 ± 1.1	3.5 ± 1.1
A7c	Sector zoned	0.28040 ± 3	1.46723 ± 5	0.000330 ± 2	0.01036 ± 10	3746 ± 47	98	0.8 ± 1.1	2.5 ± 1.1
D12	Sector zoned	0.28040 ± 2	1.46725 ± 5	0.000382 ± 1	0.01204 ± 17	3753 ± 47	99	0.8 ± 0.9	2.4 ± 0.9
F15	Sector zoned	0.28046 ± 3	1.46729 ± 5	0.000437 ± 2	0.01310 ± 5	3755 ± 48	98	2.8 ± 0.9	4.4 ± 0.9
E13	Sector zoned	0.28046 ± 3	1.46724 ± 4	0.000458 ± 9	0.01348 ± 21	3768 ± 48	98	3.1 ± 1.0	4.4 ± 1.0
E4	Sector zoned	0.28043 ± 3	1.46724 ± 4	0.000433 ± 1	0.01303 ± 8	3775 ± 47	99	2.3 ± 1.1	3.4 ± 1.1

Continued on next page

Table B.4 – *Continued from previous page*

Zircon Number	Texture	$^{176}Hf/^{177}Hf$ $\pm 2\sigma$	$^{178}Hf/^{177}Hf$ $\pm 2\sigma$	$^{176}Lu/^{177}Hf$ $\pm 2\sigma$	$^{176}Yb/^{177}Hf$ $\pm 2\sigma$	$\frac{^{207}Pb}{^{206}Pb}$ $\pm 2\sigma$ Age (Ma)	Conc %	$\varepsilon Hf_{(i)}$ $\pm 2\sigma$ Single grain	$\varepsilon Hf_{(i)}$ $\pm 2\sigma$ Rock age
E12	Sector zoned	0.28041 ± 2	1.46728 ± 5	0.000340 ± 3	0.00999 ± 3	3790 ± 47	99	2.1 ± 0.7	2.8 ± 0.7
B16	Sector zoned	0.28040 ± 2	1.46721 ± 6	0.000364 ± 3	0.01142 ± 11	3794 ± 47	99	2.0 ± 0.9	2.7 ± 0.9
	SG-027								
	Late 2595 Ma Re-crystallization age								
E2r	Metamict rim	0.28060 ± 2	1.46726 ± 4	0.000433 ± 2	0.01110 ± 16	2569 ± 51	99	-19.7 ± 0.9	-19.1 ± 0.9
A17r	Metamict rim	0.28062 ± 2	1.46725 ± 4	0.000491 ± 10	0.01386 ± 9	2591 ± 51	97	-18.7 ± 0.8	-18.6 ± 0.8
C11r	Metamict rim	0.28061 ± 2	1.46722 ± 3	0.000288 ± 4	0.00802 ± 3	2601 ± 52	99	-18.6 ± 0.7	-18.7 ± 0.7
B5r	Metamict rim	0.28059 ± 3	1.46724 ± 4	0.000229 ± 2	0.00539 ± 5	2607 ± 51	97	-19.0 ± 1.1	-19.3 ± 1.1
	2785 Ma re-crystallization age								
B14r	Black rim	0.28054 ± 3	1.46727 ± 4	0.000262 ± 1	0.00625 ± 3	2704 ± 51	100	-18.6 ± 1.0	-16.7 ± 1.0
E2c	Black core	0.28057 ± 3	1.46728 ± 4	0.000401 ± 18	0.00972 ± 54	2736 ± 50	101	-16.7 ± 1.1	-15.6 ± 1.1
E11r	zoned rim	0.28062 ± 3	1.46726 ± 5	0.000267 ± 3	0.00581 ± 11	2750 ± 50	99	-14.4 ± 0.9	-13.6 ± 0.9
D15r	zoned rim	0.28057 ± 2	1.46720 ± 4	0.000217 ± 3	0.00552 ± 5	2753 ± 50	100	-16.2 ± 0.6	-15.5 ± 0.6
A17c	black core	0.28056 ± 3	1.46724 ± 4	0.000354 ± 1	0.00850 ± 10	2770 ± 50	99	-16.5 ± 1.0	-16.2 ± 1.0
C15r	zoned rim	0.28057 ± 1	1.46724 ± 2	0.000139 ± 2	0.00332 ± 7	2786 ± 50	100	-15.3 ± 0.5	-15.3 ± 0.5
F7	zoned	0.28065 ± 3	1.46725 ± 5	0.000359 ± 4	0.00820 ± 21	2787 ± 50	100	-12.9 ± 1.2	-13.0 ± 1.2
F3r	zoned rim	0.28060 ± 3	1.46722 ± 4	0.000182 ± 1	0.00414 ± 7	2790 ± 50	100	-14.2 ± 1.1	-14.3 ± 1.1
C2r	zoned rim	0.28059 ± 2	1.46726 ± 4	0.000162 ± 3	0.00381 ± 6	2809 ± 50	100	-14.2 ± 0.9	-14.7 ± 0.9
	3632 Ma igneous crystallization age								
E11c	mtamict core	0.28045 ± 3	1.46727 ± 4	0.000454 ± 3	0.01013 ± 8	3236 ± 48	98	-9.8 ± 0.9	-0.5 ± 0.9
D17	black core	0.28040 ± 3	1.46727 ± 5	0.000598 ± 2	0.01497 ± 14	3505 ± 47	100	-5.3 ± 1.1	-2.3 ± 1.1
E13	zoned core	0.28045 ± 3	1.46729 ± 5	0.000751 ± 4	0.01807 ± 13	3529 ± 47	100	-3.7 ± 1.0	-1.2 ± 1.0
F15	zoned core	0.28044 ± 3	1.46725 ± 3	0.000733 ± 2	0.01813 ± 39	3541 ± 47	100	-3.7 ± 1.1	-1.6 ± 1.1
F9	zoned core	0.28045 ± 3	1.46727 ± 5	0.000723 ± 10	0.01769 ± 8	3541 ± 47	100	-3.2 ± 0.9	-1.0 ± 0.9

Continued on next page

Table B.4 – *Continued from previous page*

Zircon Number	Texture	$^{176}Hf/^{177}Hf$ $\pm 2\sigma$	$^{178}Hf/^{177}Hf$ $\pm 2\sigma$	$^{176}Lu/^{177}Hf$ $\pm 2\sigma$	$^{176}Yb/^{177}Hf$ $\pm 2\sigma$	$\frac{^{207}Pb}{^{206}Pb}$ $\pm 2\sigma$ Age (Ma)	Conc %	$\varepsilon Hf_{(i)}$ $\pm 2\sigma$ Single grain	$\varepsilon Hf_{(i)}$ $\pm 2\sigma$ Rock age
D7c	zoned core	0.28041 ± 2	1.46725 ± 5	0.000704 ± 28	0.01779 ± 69	3557 ± 46	100	-4.2 ± 0.8	-2.5 ± 0.8
E4	zoned core	0.28042 ± 3	1.46724 ± 6	0.000649 ± 18	0.01646 ± 23	3562 ± 47	100	-3.4 ± 0.9	-1.8 ± 0.9
C15c	zoned core	0.28046 ± 2	1.46723 ± 3	0.000852 ± 17	0.02133 ± 21	3565 ± 46	99	-2.7 ± 0.6	-1.1 ± 0.6
D13	zoned core	0.28043 ± 2	1.46727 ± 4	0.000583 ± 3	0.01422 ± 16	3569 ± 46	100	-2.7 ± 0.9	-1.2 ± 0.9
B2	black core	0.28048 ± 2	1.46729 ± 4	0.000676 ± 6	0.01604 ± 34	3578 ± 47	99	-1.1 ± 0.9	0.1 ± 0.9
B14c	black core	0.28042 ± 2	1.46729 ± 6	0.000552 ± 8	0.01347 ± 13	3583 ± 47	98	-2.9 ± 0.8	-1.7 ± 0.8
F10c	zoned core	0.28043 ± 3	1.46727 ± 4	0.000296 ± 12	0.00586 ± 28	3599 ± 47	100	-1.3 ± 0.9	-0.5 ± 0.9
	SG-037								
	2744 Ma cristallisation age								
B8	black core	0.28066 ± 2	1.46726 ± 3	0.001150 ± 88	0.03135 ± 191	2237 ± 52	98	-26.3 ± 0.6	-14.9 ± 0.6
E16c	black core	0.28068 ± 2	1.46726 ± 3	0.000847 ± 20	0.02563 ± 42	2360 ± 52	97	-22.4 ± 0.8	-13.6 ± 0.8
B12c	black core	0.28069 ± 3	1.46721 ± 6	0.000708 ± 30	0.02224 ± 86	2366 ± 52	98	-21.7 ± 0.9	-13.0 ± 0.9
F17	black	0.28066 ± 2	1.46725 ± 4	0.000496 ± 16	0.01486 ± 59	2378 ± 53	98	-22.0 ± 0.7	-13.6 ± 0.7
B11	black cristal	0.28065 ± 2	1.46723 ± 3	0.000041 ± 3	0.00141 ± 12	2455 ± 51	100	-20.1 ± 0.6	-13.3 ± 0.6
D1	metamict	0.28063 ± 1	1.46726 ± 4	0.000142 ± 23	0.00417 ± 57	2463 ± 52	99	-20.5 ± 0.5	-13.9 ± 0.5
F18r	black rim	0.28062 ± 1	1.46722 ± 3	0.000014 ± 2	0.00043 ± 7	2556 ± 52	97	-18.5 ± 0.5	-14.1 ± 0.5
F15	black	0.28065 ± 2	1.46726 ± 3	0.000133 ± 19	0.00406 ± 47	2587 ± 52	98	-17.1 ± 0.6	-13.5 ± 0.6
F2	black core	0.28065 ± 2	1.46724 ± 4	0.000313 ± 6	0.00968 ± 12	2689 ± 51	100	-15.0 ± 0.7	-13.7 ± 0.7
F13	metaminct	0.28064 ± 2	1.46725 ± 3	0.000021 ± 2	0.00070 ± 5	2726 ± 51	101	-13.9 ± 0.6	-13.5 ± 0.6
F18c	zoned core	0.28069 ± 2	1.46723 ± 4	0.001404 ± 23	0.04024 ± 88	2731 ± 51	100	-14.7 ± 0.6	-14.4 ± 0.6
B12r	black rim	0.28064 ± 2	1.46726 ± 3	0.000019 ± 0	0.00066 ± 2	2748 ± 50	100	-13.6 ± 0.6	-13.7 ± 0.6
B15r	black rim	0.28065 ± 2	1.46723 ± 4	0.000050 ± 0	0.00154 ± 2	2750 ± 50	100	-13.3 ± 0.6	-13.4 ± 0.6
A12	black core	0.28065 ± 2	1.46724 ± 3	0.000019 ± 1	0.00064 ± 2	2765 ± 50	99	-12.8 ± 0.8	-13.3 ± 0.8
B9	black core	0.28064 ± 1	1.46722 ± 4	0.000243 ± 1	0.00758 ± 10	2766 ± 50	100	-13.4 ± 0.5	-13.9 ± 0.5

Continued on next page

Table B.4 – *Continued from previous page*

Zircon Number	Texture	$^{176}Hf/^{177}Hf$ $\pm 2\sigma$	$^{178}Hf/^{177}Hf$ $\pm 2\sigma$	$^{176}Lu/^{177}Hf$ $\pm 2\sigma$	$^{176}Yb/^{177}Hf$ $\pm 2\sigma$	$\frac{^{207}Pb}{^{206}Pb}$ $\pm 2\sigma$ Age (Ma)	Conc %	$\varepsilon Hf_{(i)}$ $\pm 2\sigma$ Single grain	$\varepsilon Hf_{(i)}$ $\pm 2\sigma$ Rock age
A10c	zoned core	0.28063 ± 3	1.46724 ± 4	0.000823 ± 14	0.02389 ± 71	2767 ± 50	100	-15.0 ± 0.9	-15.5 ± 0.9
C14	zoned core	0.28065 ± 2	1.46726 ± 4	0.001005 ± 44	0.03008 ± 198	2773 ± 50	99	-14.3 ± 0.7	-14.9 ± 0.7
B10c	zoned core	0.28063 ± 2	1.46731 ± 4	0.000533 ± 46	0.01409 ± 131	2789 ± 50	98	-13.6 ± 0.8	-14.7 ± 0.8
	Inherited core								
D9c	zoned core	0.28044 ± 2	1.46724 ± 3	0.000281 ± 7	0.00812 ± 20	3303 ± 48	97	-8.0 ± 0.7	-8.0 ± 0.7
	SG-080								
	2752 Re-crystallization age								
E15	black rim	0.28061 ± 2	1.46725 ± 5	0.000518 ± 1	0.01447 ± 18	2744 ± 50	101	-15.4 ± 0.8	-15.2 ± 0.8
F4	black core	0.28055 ± 3	1.46731 ± 4	0.000485 ± 6	0.01419 ± 26	2758 ± 50	100	-17.3 ± 0.9	-17.4 ± 0.9
	3647 Crystallization igneous zircons								
C8r	zoned rim	0.28045 ± 3	1.46723 ± 4	0.000457 ± 16	0.01338 ± 54	3624 ± 48	98	-0.5 ± 1.0	0.1 ± 1.0
E9	zoned core	0.28039 ± 2	1.46729 ± 5	0.000159 ± 5	0.00437 ± 18	3582 ± 48	99	-2.8 ± 0.9	-1.2 ± 0.9
C11c	zoned core	0.28040 ± 3	1.46728 ± 5	0.000281 ± 15	0.00788 ± 33	3582 ± 49	99	-2.7 ± 1.0	-1.2 ± 1.0
C1r	zoned core	0.28036 ± 3	1.46728 ± 5	0.000248 ± 15	0.00694 ± 45	3583 ± 48	99	-4.2 ± 1.0	-2.7 ± 1.0
C7	zoned core	0.28043 ± 4	1.46723 ± 6	0.000345 ± 4	0.01017 ± 9	3585 ± 48	99	-2.1 ± 1.5	-0.6 ± 1.5
C6	zoned core	0.28044 ± 3	1.46729 ± 5	0.000365 ± 5	0.01093 ± 8	3598 ± 48	98	-1.4 ± 1.0	-0.2 ± 1.0
C15r	zoned rim	0.28038 ± 3	1.46730 ± 5	0.000343 ± 4	0.00903 ± 18	3598 ± 49	98	-3.3 ± 1.2	-2.1 ± 1.2
C13	zoned core	0.28041 ± 3	1.46726 ± 5	0.000586 ± 13	0.01684 ± 49	3600 ± 49	99	-2.7 ± 1.1	-1.6 ± 1.1
C4	zoned core	0.28041 ± 3	1.46724 ± 6	0.000361 ± 1	0.01001 ± 7	3600 ± 48	98	-2.3 ± 1.1	-1.1 ± 1.1
B4	zoned core	0.28043 ± 3	1.46731 ± 5	0.000475 ± 4	0.01347 ± 12	3605 ± 48	100	-1.7 ± 1.2	-0.7 ± 1.2
C14	zoned core	0.28037 ± 3	1.46725 ± 6	0.000368 ± 2	0.01032 ± 5	3606 ± 49	98	-3.6 ± 0.9	-2.6 ± 0.9
C10	zoned core	0.28039 ± 3	1.46725 ± 5	0.000315 ± 3	0.00896 ± 5	3617 ± 48	98	-2.4 ± 1.1	-1.7 ± 1.1
E6	zoned core	0.28039 ± 3	1.46728 ± 4	0.000295 ± 14	0.00790 ± 25	3632 ± 49	98	-1.9 ± 0.9	-1.6 ± 0.9
A8	zoned core	0.28042 ± 3	1.46728 ± 5	0.000422 ± 6	0.01207 ± 28	3634 ± 48	98	-1.1 ± 0.9	-0.8 ± 0.9

Continued on next page

Table B.4 – *Continued from previous page*

Zircon Number	Texture	$^{176}Hf/^{177}Hf$ $\pm 2\sigma$	$^{178}Hf/^{177}Hf$ $\pm 2\sigma$	$^{176}Lu/^{177}Hf$ $\pm 2\sigma$	$^{176}Yb/^{177}Hf$ $\pm 2\sigma$	$\frac{^{207}Pb}{^{206}Pb}$ $\pm 2\sigma$ Age (Ma)	Conc %	$\varepsilon Hf_{(i)}$ $\pm 2\sigma$ Single grain	$\varepsilon Hf_{(i)}$ $\pm 2\sigma$ Rock age
A15	zoned core	0.28042 ± 2	1.46726 ± 6	0.000273 ± 8	0.00797 ± 29	3644 ± 48	99	-0.5 ± 0.8	-0.5 ± 0.8
A6c	zoned core	0.28045 ± 3	1.46732 ± 4	0.000482 ± 4	0.01402 ± 25	3651 ± 47	100	-0.1 ± 0.9	-0.1 ± 0.9
A11	zoned core	0.28040 ± 2	1.46732 ± 5	0.000356 ± 3	0.01000 ± 10	3653 ± 48	99	-1.5 ± 0.6	-1.7 ± 0.6
	3805 Inherited grain								
C15c	Inherited core	0.28044 ± 4	1.46722 ± 5	0.001573 ± 22	0.04704 ± 90	3805 ± 15	99	0.4 ± 1.3	0.4 ± 1.3
	SG-084								
	Late recrystallized zircon								
D12	Metamict	0.28059 ± 3	1.46727 ± 5	0.001519 ± 2	0.04964 ± 57	2643 ± 53	95	-20.4 ± 0.9	- ± -
	3710 Igneous crystallization age								
C16	Metamict	0.28039 ± 1	1.46731 ± 4	0.000332 ± 13	0.01048 ± 32	3475 ± 49	95	-5.7 ± 0.4	-0.2 ± 0.4
A7	Metamict	0.28044 ± 2	1.46732 ± 2	0.000494 ± 17	0.01562 ± 44	3521 ± 48	93	-3.5 ± 0.7	1.0 ± 0.7
C6	black core	0.28058 ± 2	1.46732 ± 4	0.001361 ± 29	0.03791 ± 107	3583 ± 49	99	0.8 ± 0.9	3.8 ± 0.9
C12	zoned core	0.28054 ± 2	1.46729 ± 6	0.000882 ± 26	0.02881 ± 101	±		-79.5 ± 0.9	3.5 ± 0.9
A5	zoned core	0.28035 ± 2	1.46731 ± 4	0.000240 ± 4	0.00670 ± 5	3664 ± 48	96	-2.4 ± 0.8	-1.4 ± 0.8
F4	zoned core	0.28042 ± 3	1.46722 ± 3	0.000541 ± 10	0.01488 ± 38	3671 ± 47	97	-0.8 ± 0.9	0.2 ± 0.9
B13	zoned core	0.28038 ± 2	1.46726 ± 4	0.000163 ± 4	0.00457 ± 22	3684 ± 49	97	-0.8 ± 0.8	-0.2 ± 0.8
A10c	zoned core	0.28045 ± 3	1.46728 ± 4	0.001484 ± 17	0.04288 ± 25	3690 ± 48	90	-1.6 ± 1.0	-1.2 ± 1.0
F2	zoned core	0.28039 ± 2	1.46722 ± 3	0.000601 ± 11	0.01731 ± 25	3695 ± 47	97	-1.3 ± 0.8	-0.9 ± 0.8
A10r	zoned rim	0.28037 ± 2	1.46728 ± 3	0.000323 ± 1	0.00939 ± 8	3725 ± 48	99	-0.7 ± 0.6	-1.0 ± 0.6
F11	zoned core	0.28044 ± 3	1.46736 ± 5	0.001151 ± 8	0.03275 ± 9	3733 ± 47	97	0.1 ± 1.2	-0.5 ± 1.2
A8	zoned core	0.28046 ± 3	1.46724 ± 6	0.000724 ± 1	0.01986 ± 25	3735 ± 49	98	1.7 ± 1.2	1.1 ± 1.2
E11	cracked core	0.28042 ± 4	1.46732 ± 4	0.000837 ± 29	0.02391 ± 107	3738 ± 47	93	0.2 ± 1.3	-0.5 ± 1.3
E4	zoned core	0.28041 ± 3	1.46725 ± 5	0.000685 ± 5	0.01941 ± 20	3765 ± 50	94	0.9 ± 1.0	-0.3 ± 1.0

Continued on next page

Table B.4 – *Continued from previous page*

Zircon Number	Texture	$^{176}Hf/^{177}Hf$ $\pm 2\sigma$	$^{178}Hf/^{177}Hf$ $\pm 2\sigma$	$^{176}Lu/^{177}Hf$ $\pm 2\sigma$	$^{176}Yb/^{177}Hf$ $\pm 2\sigma$	$\frac{^{207}Pb}{^{206}Pb}$ $\pm 2\sigma$ Age (Ma)	Conc %	$\varepsilon Hf_{(i)}$ $\pm 2\sigma$ Single grain	$\varepsilon Hf_{(i)}$ $\pm 2\sigma$ Rock age
	SG-087								
	2996 Ma igneous crystallization								
D5	black zoned	0.28075 ± 2	1.46731 ± 4	0.000208 ± 0	0.00644 ± 11	2563 ± 53	98	-14.1 ± 0.8	-4.0 ± 0.8
A7	zoned core	0.28072 ± 3	1.46726 ± 5	0.000379 ± 4	0.01201 ± 28	2584 ± 52	99	-15.0 ± 1.0	-5.4 ± 1.0
A8r	white rim	0.28077 ± 2	1.46726 ± 4	0.000252 ± 7	0.00681 ± 19	2617 ± 56	99	-12.1 ± 0.7	-3.3 ± 0.7
C9	sector zoned	0.28078 ± 2	1.46725 ± 5	0.000165 ± 2	0.00525 ± 13	2723 ± 54	99	-9.4 ± 0.8	-3.0 ± 0.8
C7	sector zoned	0.28089 ± 2	1.46727 ± 3	0.000682 ± 2	0.01861 ± 22	2790 ± 53	99	-4.8 ± 0.9	0.0 ± 0.9
D12B	zoned core	0.28083 ± 2	1.46727 ± 3	0.000300 ± 11	0.00965 ± 56	2938 ± 50	95	-2.9 ± 0.5	-1.5 ± 0.5
C8	sector zoned	0.28082 ± 2	1.46726 ± 6	0.000202 ± 6	0.00524 ± 22	2951 ± 55	92	-2.6 ± 0.9	-1.6 ± 0.9
A9	black zoned	0.28079 ± 2	1.46730 ± 4	0.000197 ± 8	0.00554 ± 26	2968 ± 50	98	-3.4 ± 0.8	-2.7 ± 0.8
D12A	zoned core	0.28089 ± 2	1.46726 ± 3	0.000804 ± 12	0.02576 ± 53	3028 ± 49	98	0.3 ± 0.6	-0.4 ± 0.6
	3200 Ma disturbed zircons								
C13c	Inherited core	0.28074 ± 2	1.46728 ± 4	0.000850 ± 4	0.02427 ± 29	3190 ± 51	100	-1.1 ± 0.7	-0.8 ± 0.7
C4c	Zoned core	0.28073 ± 2	1.46727 ± 4	0.000787 ± 3	0.02258 ± 28	3202 ± 50	97	-1.3 ± 0.8	-1.2 ± 0.8
	Inherited zircons								
A3	black core	0.28049 ± 3	1.46729 ± 5	0.000945 ± 38	0.03152 ± 157	3636 ± 47	99	0.1 ± 0.9	2.6 ± 0.9
E1	Osci. zoned	0.28040 ± 2	1.46724 ± 4	0.000409 ± 9	0.01103 ± 18	3733 ± 47	99	0.3 ± 0.7	0.6 ± 0.7
D10	convo. core	0.28054 ± 3	1.46728 ± 4	0.002424 ± 104	0.06795 ± 297	3743 ± 47	98	0.3 ± 1.1	0.3 ± 1.1
A5	black core	0.28062 ± 3	1.46728 ± 5	0.002713 ± 193	0.07795 ± 680	3752 ± 47	100	2.7 ± 1.0	2.5 ± 1.0
D11	convo. core	0.28038 ± 2	1.46724 ± 4	0.000224 ± 16	0.00481 ± 39	3769 ± 49	99	1.0 ± 0.7	0.4 ± 0.7
	SG-122								
	2804 Ma recrystallized zircons								
B10c	black core	0.28067 ± 1	1.46726 ± 2	0.000465 ± 45	0.01368 ± 146	2801 ± 50	99	-12.0 ± 0.4	-11.9 ± 0.4
E2r2	Sector zoned	0.28069 ± 2	1.46722 ± 3	0.000152 ± 0	0.00460 ± 4	2801 ± 51	99	-10.7 ± 0.8	-10.6 ± 0.8

Continued on next page

Table B.4 – *Continued from previous page*

Zircon Number	**Texture**	^{176}**Hf**/^{177}**Hf** ±2σ	^{178}**Hf**/^{177}**Hf** ±2σ	^{176}**Lu**/^{177}**Hf** ±2σ	^{176}**Yb**/^{177}**Hf** ±2σ	$\frac{^{207}Pb}{^{206}Pb}$ ±2σ **Age (Ma)**	**Conc %**	ε**Hf**$_{(i)}$ ±2σ **Single grain**	ε**Hf**$_{(i)}$ ±2σ **Rock age**
C18r1	Sector zoned	0.28063 ± 2	1.46728 ± 3	0.000444 ± 5	0.01324 ± 24	2801 ± 51	100	-13.5 ± 0.9	-13.4 ± 0.9
E10r2	Sector zoned	0.28067 ± 2	1.46726 ± 4	0.000122 ± 1	0.00380 ± 2	2811 ± 51	99	-10.9 ± 0.6	-11.1 ± 0.6
D11r	Sector zoned	0.28068 ± 2	1.46728 ± 4	0.000173 ± 1	0.00550 ± 5	2817 ± 51	99	-10.9 ± 0.7	-11.1 ± 0.7
D10r	Sector zoned	0.28060 ± 2	1.46724 ± 4	0.000336 ± 16	0.00956 ± 29	2821 ± 50	100	-13.8 ± 0.6	-14.2 ± 0.6
C18r2	Black rim	0.28066 ± 2	1.46727 ± 5	0.000197 ± 4	0.00537 ± 13	2823 ± 50	100	-11.3 ± 0.6	-11.7 ± 0.6
C14r	Black rim	0.28066 ± 1	1.46726 ± 3	0.000266 ± 1	0.00833 ± 6	2824 ± 50	100	-11.2 ± 0.5	-11.7 ± 0.5
	3781 Ma igneous zircon with Lu-Hf undisturbed								
C1	black core	0.28041 ± 2	1.46727 ± 3	0.000391 ± 10	0.01182 ± 41	3602 ± 47	97	-2.4 ± 0.9	1.9 ± 0.9
D6r1	white rim	0.28034 ± 2	1.46721 ± 3	0.000127 ± 3	0.00364 ± 13	3610 ± 49	99	-4.1 ± 0.6	0.0 ± 0.6
B1	Black core	0.28054 ± 2	1.46722 ± 4	0.001824 ± 16	0.05477 ± 25	3631 ± 46	100	-0.6 ± 0.8	2.8 ± 0.8
E1	zoned core	0.28039 ± 2	1.46725 ± 3	0.000226 ± 3	0.00648 ± 4	3646 ± 49	96	-1.7 ± 0.6	1.5 ± 0.6
C21r1	zoned core	0.28040 ± 2	1.46729 ± 2	0.000240 ± 4	0.00746 ± 14	3647 ± 48	99	-1.2 ± 0.6	2.0 ± 0.6
B4c	zoned core	0.28039 ± 2	1.46725 ± 4	0.000311 ± 8	0.00914 ± 36	3652 ± 47	99	-1.6 ± 0.7	1.5 ± 0.7
C17r1	zoned core	0.28041 ± 2	1.46727 ± 3	0.000623 ± 9	0.02056 ± 13	3652 ± 47	98	-1.7 ± 0.6	1.3 ± 0.6
E2r1	black rim	0.28044 ± 2	1.46724 ± 3	0.000356 ± 2	0.00976 ± 19	3669 ± 47	97	0.5 ± 0.7	3.1 ± 0.7
C18c	zoned core	0.28036 ± 2	1.46722 ± 3	0.000294 ± 5	0.00861 ± 25	3703 ± 47	100	-1.3 ± 0.8	0.5 ± 0.8
C12c	zoned core	0.28041 ± 2	1.46727 ± 4	0.000310 ± 7	0.00863 ± 11	3712 ± 47	98	0.4 ± 0.6	2.0 ± 0.6
C15c	zoned core	0.28039 ± 2	1.46725 ± 4	0.000250 ± 9	0.00745 ± 21	3712 ± 47	99	-0.1 ± 0.6	1.5 ± 0.6
C21c	zoned core	0.28037 ± 2	1.46721 ± 3	0.000199 ± 7	0.00563 ± 23	3717 ± 47	100	-0.5 ± 0.6	1.0 ± 0.6
D2c	zoned core	0.28038 ± 2	1.46724 ± 4	0.000253 ± 7	0.00669 ± 8	3719 ± 47	97	-0.3 ± 0.6	1.2 ± 0.6
A17c	Black core	0.28037 ± 2	1.46727 ± 2	0.000607 ± 4	0.01627 ± 18	3722 ± 46	97	-1.3 ± 0.7	0.1 ± 0.7
B2c	zoned core	0.28038 ± 2	1.46724 ± 3	0.000340 ± 1	0.01009 ± 6	3723 ± 47	95	-0.3 ± 0.7	1.1 ± 0.7
E5r1	zoned core	0.28042 ± 2	1.46724 ± 3	0.000242 ± 4	0.00614 ± 9	3723 ± 48	99	1.1 ± 0.6	2.5 ± 0.6
E14c	zoned core	0.28038 ± 2	1.46723 ± 4	0.000228 ± 6	0.00679 ± 13	3763 ± 46	96	0.9 ± 0.8	1.3 ± 0.8

Continued on next page

Table B.4 – *Continued from previous page*

Zircon Number	Texture	$^{176}Hf/^{177}Hf$ $\pm 2\sigma$	$^{178}Hf/^{177}Hf$ $\pm 2\sigma$	$^{176}Lu/^{177}Hf$ $\pm 2\sigma$	$^{176}Yb/^{177}Hf$ $\pm 2\sigma$	$\frac{^{207}Pb}{^{206}Pb}$ $\pm 2\sigma$ Age (Ma)	Conc %	$\varepsilon Hf_{(i)}$ $\pm 2\sigma$ Single grain	$\varepsilon Hf_{(i)}$ $\pm 2\sigma$ Rock age
B12r	zoned rim	0.28035 ± 2	1.46723 ± 3	0.000162 ± 3	0.00466 ± 2	3782 ± 47	99	0.5 ± 0.8	0.5 ± 0.8
	SG-127								
	Igneous 2789 Ma old zircons								
D9	Metamict	0.28060 ± 2	1.46725 ± 4	0.000005 ± 0	0.00014 ± 2	2502 ± 54	94	-20.7 ± 0.7	-17.0 ± 0.7
E10	Metamict	0.28075 ± 2	1.46725 ± 4	0.001002 ± 201	0.02952 ± 635	2662 ± 51	100	-13.1 ± 0.9	-13.1 ± 0.9
E7	Black core	0.28063 ± 2	1.46729 ± 4	0.000006 ± 0	0.00015 ± 1	2683 ± 51	97	-15.1 ± 0.6	-15.6 ± 0.6
D1	Metamict	0.28065 ± 2	1.46731 ± 4	0.000814 ± 39	0.02318 ± 146	2739 ± 53	98	-14.6 ± 0.8	-13.5 ± 0.8
F15	Metamict	0.28083 ± 3	1.46725 ± 4	0.001982 ± 24	0.06025 ± 93	2767 ± 51	99	-9.9 ± 1.0	-9.4 ± 1.0
B16c	zoned core	0.28065 ± 3	1.46721 ± 5	0.000073 ± 2	0.00213 ± 6	2769 ± 53	99	-12.8 ± 1.2	-12.3 ± 1.2
C18	metamict	0.28066 ± 2	1.46730 ± 5	0.000221 ± 4	0.00583 ± 17	2780 ± 52	96	-12.2 ± 0.8	-12.0 ± 0.8
A1c	zoned core	0.28067 ± 2	1.46724 ± 5	0.000530 ± 3	0.01649 ± 20	2789 ± 51	100	-12.4 ± 0.9	-12.4 ± 0.9
E14	black core	0.28067 ± 3	1.46726 ± 5	0.000993 ± 3	0.02979 ± 38	2798 ± 51	100	-13.0 ± 0.9	-13.2 ± 0.9
D4c	zoned core	0.28059 ± 2	1.46726 ± 4	0.000271 ± 9	0.00826 ± 24	2801 ± 53	99	-14.5 ± 0.9	-14.8 ± 0.9
B11	zoned core	0.28064 ± 3	1.46724 ± 3	0.000603 ± 26	0.01753 ± 59	2802 ± 52	98	-13.3 ± 0.9	-13.6 ± 0.9
D6	zoned core	0.28060 ± 4	1.46722 ± 6	0.000274 ± 5	0.00801 ± 26	2804 ± 53	98	-13.9 ± 1.4	-14.2 ± 1.4
B1c	zoned core	0.28067 ± 3	1.46728 ± 5	0.000625 ± 7	0.01834 ± 17	2805 ± 51	99	-12.3 ± 1.2	-12.6 ± 1.2
C17	Black core	0.28073 ± 2	1.46729 ± 5	0.000640 ± 41	0.01752 ± 108	2807 ± 52	96	-10.1 ± 0.8	-10.5 ± 0.8
A16	zoned core	0.28071 ± 2	1.46727 ± 6	0.001024 ± 20	0.03119 ± 52	2808 ± 51	100	-11.5 ± 0.8	-11.9 ± 0.8
E1	zoned core	0.28069 ± 3	1.46725 ± 6	0.000046 ± 0	0.00148 ± 2	2808 ± 51	98	-10.3 ± 1.1	-10.7 ± 1.1
B3	metamict	0.28070 ± 3	1.46728 ± 5	0.000609 ± 9	0.01708 ± 34	2818 ± 51	99	-10.9 ± 0.9	-11.6 ± 0.9
	Inherited cores								
A11	zoned core	0.28039 ± 3	1.46725 ± 4	0.000468 ± 9	0.01272 ± 41	3661 ± 48	95	-2.0 ± 1.0	-2.0 ± 1.0
	SG-143								
	Igneous 2780 Ma old zircon								

Continued on next page

Table B.4 – *Continued from previous page*

Zircon Number	**Texture**	^{176}**Hf**/^{177}**Hf** $\pm 2\sigma$	^{178}**Hf**/^{177}**Hf** $\pm 2\sigma$	^{176}**Lu**/^{177}**Hf** $\pm 2\sigma$	^{176}**Yb**/^{177}**Hf** $\pm 2\sigma$	$\frac{^{207}Pb}{^{206}Pb}$ $\pm 2\sigma$ **Age (Ma)**	**Conc %**	ε**Hf**$_{(i)}$ $\pm 2\sigma$ **Single grain**	ε**Hf**$_{(i)}$ $\pm 2\sigma$ **Rock age**
A9c	black core	0.28071 ± 2	1.46728 ± 4	0.000522 ± 15	0.01363 ± 45	2701 ± 51	100	-12.8 ± 0.6	-11.0 ± 0.6
B7	zoned core	0.28080 ± 2	1.46729 ± 4	0.000636 ± 23	0.01419 ± 57	2717 ± 52	99	-9.6 ± 0.8	-8.1 ± 0.8
D12	black core	0.28064 ± 2	1.46728 ± 4	0.000098 ± 1	0.00318 ± 7	2745 ± 51	99	-13.6 ± 0.6	-12.8 ± 0.6
F15	black core	0.28070 ± 2	1.46731 ± 4	0.000118 ± 1	0.00386 ± 4	2750 ± 51	100	-11.5 ± 0.6	-10.8 ± 0.6
C7	black core	0.28069 ± 2	1.46723 ± 4	0.000308 ± 45	0.00773 ± 92	2753 ± 50	98	-11.9 ± 0.6	-11.3 ± 0.6
C1	metamict	0.28070 ± 2	1.46726 ± 4	0.000112 ± 0	0.00345 ± 4	2756 ± 52	99	-11.4 ± 0.7	-10.8 ± 0.7
E4	black core	0.28065 ± 2	1.46727 ± 3	0.000048 ± 1	0.00197 ± 2	2757 ± 51	100	-12.9 ± 0.5	-12.4 ± 0.5
C3	zoned core	0.28069 ± 2	1.46729 ± 3	0.000778 ± 19	0.02385 ± 51	2757 ± 51	94	-12.7 ± 0.8	-12.2 ± 0.8
A3	black core	0.28066 ± 2	1.46728 ± 4	0.000077 ± 3	0.00306 ± 15	2759 ± 51	99	-12.7 ± 0.9	-12.2 ± 0.9
A17	black core	0.28068 ± 2	1.46728 ± 4	0.000098 ± 1	0.00373 ± 3	2760 ± 51	100	-12.0 ± 0.8	-11.5 ± 0.8
F2	black core	0.28069 ± 2	1.46727 ± 4	0.000168 ± 0	0.00479 ± 3	2766 ± 51	98	-11.4 ± 0.6	-11.1 ± 0.6
D13	black core	0.28071 ± 2	1.46724 ± 3	0.000516 ± 39	0.01333 ± 74	2767 ± 51	93	-11.6 ± 0.6	-11.3 ± 0.6
F9	black core	0.28071 ± 2	1.46724 ± 3	0.000273 ± 2	0.00957 ± 16	2769 ± 51	99	-10.8 ± 0.8	-10.5 ± 0.8
A9r	metamict rim	0.28068 ± 2	1.46725 ± 3	0.000120 ± 1	0.00373 ± 3	2777 ± 51	99	-11.4 ± 0.6	-11.4 ± 0.6
C2	black core	0.28072 ± 3	1.46730 ± 4	0.000831 ± 97	0.02732 ± 323	2781 ± 51	90	-11.4 ± 1.1	-11.4 ± 1.1
E9	black core	0.28068 ± 2	1.46720 ± 5	0.000212 ± 12	0.00661 ± 36	2781 ± 51	100	-11.5 ± 0.9	-11.6 ± 0.9
B11r	zoned rim	0.28067 ± 2	1.46726 ± 4	0.000286 ± 11	0.00743 ± 18	2792 ± 51	98	-11.8 ± 0.7	-12.0 ± 0.7
B18c	black core	0.28064 ± 2	1.46727 ± 3	0.000702 ± 12	0.01857 ± 18	2799 ± 52	99	-13.6 ± 0.9	-14.0 ± 0.9
B11c	zoned core	0.28079 ± 3	1.46727 ± 4	0.000237 ± 18	0.00598 ± 44	2806 ± 53	92	-7.1 ± 1.0	-7.7 ± 1.0
	Inherited cores								
D9	zoned core	0.28040 ± 2	1.46728 ± 4	0.000352 ± 16	0.01019 ± 45	3656 ± 47	99	-1.2 ± 0.7	-1.3 ± 0.7
D9bis	zoned core	0.28045 ± 2	1.46730 ± 3	0.000334 ± 24	0.00939 ± 67	3656 ± 47	99	0.5 ± 0.6	0.5 ± 0.6
	SG-203								
	3330 Ma old zircons (not disturbed by the 3200 Metamorphic recrystallzation)								

Continued on next page

Table B.4 – *Continued from previous page*

Zircon Number	Texture	$^{176}Hf/^{177}Hf$ $\pm 2\sigma$	$^{178}Hf/^{177}Hf$ $\pm 2\sigma$	$^{176}Lu/^{177}Hf$ $\pm 2\sigma$	$^{176}Yb/^{177}Hf$ $\pm 2\sigma$	$\frac{^{207}Pb}{^{206}Pb}$ $\pm 2\sigma$ Age (Ma)	Conc %	$\varepsilon Hf_{(i)}$ $\pm 2\sigma$ Single grain	$\varepsilon Hf_{(i)}$ $\pm 2\sigma$ Rock age
A02c	Zoned core	0.28047 ± 3	1.46724 ± 4	0.000658 ± 20	0.01877 ± 59	3356 ± 48	100	-6.5 ± 1.0	-7.1 ± 1.0
A03c	Zoned core	0.28047 ± 2	1.46719 ± 4	0.000441 ± 6	0.01278 ± 26	3320 ± 49	100	-7.1 ± 0.8	-6.9 ± 0.8
A04c	Zoned core	0.28049 ± 2	1.46719 ± 3	0.000716 ± 18	0.02113 ± 42	3339 ± 49	101	-6.5 ± 0.7	-6.7 ± 0.7
A06c	Zoned core	0.28049 ± 2	1.46722 ± 3	0.000768 ± 6	0.02310 ± 36	3314 ± 49	101	-7.0 ± 0.6	-6.6 ± 0.6
A07c	Zoned core	0.28046 ± 2	1.46722 ± 2	0.000432 ± 1	0.01250 ± 12	3341 ± 49	100	-6.8 ± 0.7	-7.0 ± 0.7
A08c	Zoned core	0.28049 ± 3	1.46718 ± 4	0.000590 ± 10	0.01656 ± 14	3312 ± 48	100	-6.7 ± 0.9	-6.3 ± 0.9
A10c	Zoned core	0.28051 ± 2	1.46718 ± 3	0.000794 ± 8	0.02187 ± 39	3341 ± 48	101	-5.7 ± 0.6	-6.0 ± 0.6
A12c	Zoned core	0.28045 ± 2	1.46715 ± 5	0.000457 ± 2	0.01279 ± 13	3303 ± 50	99	-8.0 ± 0.8	-7.4 ± 0.8
A13R	Zoned core	0.28044 ± 2	1.46719 ± 4	0.000354 ± 2	0.01025 ± 7	3355 ± 49	100	-7.1 ± 0.8	-7.7 ± 0.8
A16c	Zoned core	0.28053 ± 2	1.46725 ± 5	0.000309 ± 3	0.00764 ± 23	3328 ± 49	100	-4.2 ± 0.9	-4.2 ± 0.9
B05c	Zoned core	0.28055 ± 2	1.46719 ± 3	0.001088 ± 26	0.03299 ± 65	3311 ± 51	99	-5.9 ± 0.8	-5.4 ± 0.8
B06c	Zoned core	0.28048 ± 3	1.46719 ± 4	0.000617 ± 8	0.01748 ± 9	3310 ± 50	99	-7.1 ± 0.9	-6.7 ± 0.9
B10c	Zoned core	0.28047 ± 2	1.46726 ± 4	0.000589 ± 24	0.01692 ± 82	3327 ± 49	100	-7.1 ± 0.7	-7.0 ± 0.7
B11c	Zoned core	0.28046 ± 2	1.46722 ± 4	0.000505 ± 4	0.01411 ± 14	3296 ± 51	98	-7.9 ± 0.7	-7.1 ± 0.7
B12c	Zoned core	0.28049 ± 3	1.46721 ± 5	0.000392 ± 3	0.01149 ± 21	3327 ± 51	100	-6.1 ± 1.2	-6.0 ± 1.2
B18c	Zoned core	0.28054 ± 2	1.46719 ± 5	0.000591 ± 11	0.01587 ± 26	3113 ± 51	100	-9.6 ± 0.9	-4.6 ± 0.9
B18R	Zoned core	0.28048 ± 3	1.46721 ± 3	0.000452 ± 1	0.01345 ± 10	3331 ± 49	100	-6.5 ± 1.0	-6.5 ± 1.0
C17c	Convo.centre	0.28050 ± 2	1.46719 ± 4	0.000445 ± 5	0.01330 ± 21	3309 ± 51	99	-6.2 ± 0.8	-5.8 ± 0.8
D01c	Zoned core	0.28048 ± 3	1.46721 ± 6	0.000601 ± 14	0.01836 ± 39	3299 ± 53	99	-7.4 ± 1.1	-6.7 ± 1.1
D02c	Zoned core	0.28046 ± 3	1.46720 ± 3	0.000466 ± 6	0.01350 ± 18	3312 ± 50	100	-7.6 ± 1.0	-7.2 ± 1.0
D07c	Zoned core	0.28050 ± 2	1.46722 ± 3	0.000703 ± 22	0.02103 ± 77	3307 ± 52	99	-6.8 ± 0.7	-6.3 ± 0.7
D11c	Zoned core	0.28049 ± 2	1.46722 ± 3	0.000473 ± 9	0.01323 ± 33	3319 ± 51	100	-6.2 ± 0.7	-5.9 ± 0.7
D12c	Zoned core	0.28047 ± 2	1.46721 ± 3	0.000343 ± 13	0.00963 ± 37	3326 ± 51	100	-6.5 ± 0.7	-6.4 ± 0.7
D15c	Zoned core	0.28051 ± 3	1.46718 ± 4	0.000680 ± 8	0.01966 ± 38	3335 ± 49	100	-5.9 ± 1.2	-6.0 ± 1.2

Continued on next page

Table B.4 – *Continued from previous page*

Zircon Number	Texture	$^{176}Hf/^{177}Hf$ $\pm 2\sigma$	$^{178}Hf/^{177}Hf$ $\pm 2\sigma$	$^{176}Lu/^{177}Hf$ $\pm 2\sigma$	$^{176}Yb/^{177}Hf$ $\pm 2\sigma$	$\frac{^{207}Pb}{^{206}Pb}$ $\pm 2\sigma$ Age (Ma)	Conc %	$\varepsilon Hf_{(i)}$ $\pm 2\sigma$ Single grain	$\varepsilon Hf_{(i)}$ $\pm 2\sigma$ Rock age
D17c	Zoned core	0.28055 ± 3	1.46718 ± 3	0.001095 ± 156	0.03348 ± 509	3330 ± 49	100	-5.4 ± 1.1	-5.4 ± 1.1
E03c	Zoned core	0.28047 ± 1	1.46717 ± 4	0.000411 ± 5	0.01163 ± 16	3325 ± 50	100	-6.8 ± 0.4	-6.7 ± 0.4
E05c	Convo. core	0.28048 ± 2	1.46724 ± 4	0.000502 ± 26	0.01426 ± 82	3230 ± 51	101	-8.9 ± 0.8	-6.6 ± 0.8
E15c	Zoned core	0.28049 ± 3	1.46721 ± 4	0.000464 ± 15	0.01377 ± 39	3329 ± 51	100	-6.1 ± 0.9	-6.1 ± 0.9
F05c	Zoned core	0.28048 ± 3	1.46718 ± 7	0.000399 ± 3	0.01179 ± 2	3321 ± 52	100	-6.5 ± 1.0	-6.3 ± 1.0
F08c	Zoned core	0.28044 ± 2	1.46725 ± 4	0.000569 ± 4	0.01639 ± 19	3321 ± 52	100	-8.2 ± 0.8	-8.0 ± 0.8
F17c	Zoned core	0.28050 ± 3	1.46718 ± 4	0.000412 ± 7	0.01096 ± 18	3282 ± 52	99	-6.6 ± 1.0	-5.5 ± 1.0
F17c2	black rim	0.28044 ± 2	1.46725 ± 4	0.000569 ± 4	0.01639 ± 19	3275 ± 51	99	-9.3 ± 0.8	-8.0 ± 0.8
	Late recrystallization								
B08c	Black core	0.28074 ± 2	1.46719 ± 4	0.000278 ± 1	0.00669 ± 2	2701 ± 51	100	-11.5 ± 0.7	-11.4 ± 0.7
	SG-208								
	3330 Ma old zircons (not disturbed by the 3200 Metamorphic recrystallzation)								
A01c	Zoned core	0.28050 ± 3	1.46722 ± 4	0.000660 ± 25	0.01846 ± 67	3305 ± 50	99	-6.6 ± 0.9	-6.1 ± 0.9
A02c	Zoned core	0.28052 ± 3	1.46721 ± 4	0.000811 ± 8	0.02480 ± 23	3257 ± 50	99	-7.6 ± 0.9	-5.9 ± 0.9
A04c	Zoned core	0.28050 ± 3	1.46721 ± 3	0.000835 ± 7	0.02499 ± 22	3332 ± 50	100	-6.4 ± 1.0	-6.4 ± 1.0
A07c	Zoned core	0.28052 ± 3	1.46719 ± 5	0.000599 ± 3	0.01728 ± 9	3320 ± 50	98	-5.5 ± 1.0	-5.3 ± 1.0
A16c	Zoned rim	0.28049 ± 3	1.46720 ± 5	0.000584 ± 10	0.01631 ± 29	3328 ± 51	98	± 0.9	-6.2 ± 0.9
A18R	Zoned rim	0.28047 ± 3	1.46718 ± 5	0.000510 ± 3	0.01494 ± 17	3348 ± 51	100	-6.3 ± 0.9	-6.7 ± 0.9
C03c	Zoned core	0.28044 ± 3	1.46723 ± 4	0.000432 ± 5	0.01264 ± 12	3258 ± 53	98	-9.5 ± 0.9	-7.8 ± 0.9
C04R	Zoned rim	0.28050 ± 3	1.46717 ± 5	0.000592 ± 6	0.01619 ± 26	3330 ± 52	98	-5.8 ± 0.9	-5.8 ± 0.9
C08c	Zoned core	0.28055 ± 3	1.46720 ± 3	0.000717 ± 19	0.02128 ± 77	3333 ± 51	100	-4.3 ± 1.0	-4.4 ± 1.0
C09b	black core	0.28048 ± 2	1.46721 ± 2	0.000714 ± 21	0.02075 ± 43	3262 ± 52	99	-8.7 ± 0.9	-7.1 ± 0.9
C10c	Zoned core	0.28047 ± 3	1.46720 ± 4	0.000505 ± 18	0.01486 ± 64	3329 ± 52	98	-7.0 ± 1.0	-7.0 ± 1.0
C12c	Zoned core	0.28049 ± 2	1.46722 ± 4	0.000676 ± 24	0.01906 ± 81	3218 ± 54	100	-9.2 ± 0.8	-6.6 ± 0.8

Continued on next page

Table B.4 – *Continued from previous page*

Zircon Number	Texture	$^{176}Hf/^{177}Hf$ $\pm 2\sigma$	$^{178}Hf/^{177}Hf$ $\pm 2\sigma$	$^{176}Lu/^{177}Hf$ $\pm 2\sigma$	$^{176}Yb/^{177}Hf$ $\pm 2\sigma$	$\frac{^{207}Pb}{^{206}Pb}$ $\pm 2\sigma$ Age (Ma)	Conc %	$\varepsilon Hf_{(i)}$ $\pm 2\sigma$ Single grain	$\varepsilon Hf_{(i)}$ $\pm 2\sigma$ Rock age
C16R	Ext zoned rim	0.28049 ± 3	1.46720 ± 4	0.000626 ± 22	0.01874 ± 68	3328 ± 51	99	-6.4 ± 0.9	-6.4 ± 0.9
C17c	zoned centre	0.28053 ± 2	1.46722 ± 3	0.000872 ± 27	0.02582 ± 72	3308 ± 49	98	-6.0 ± 0.8	-5.5 ± 0.8
D02c	grey	0.28051 ± 2	1.46723 ± 4	0.001027 ± 18	0.02494 ± 66	3316 ± 49	101	-7.0 ± 0.7	-6.7 ± 0.7
D03c	grey rim	0.28056 ± 4	1.46718 ± 5	0.001646 ± 33	0.04870 ± 72	3044 ± 50	93	-12.5 ± 1.3	-6.1 ± 1.3
D05c	grey	0.28051 ± 2	1.46720 ± 4	0.000637 ± 11	0.01866 ± 38	3310 ± 51	99	-6.3 ± 0.9	-5.8 ± 0.9
D06c	Zoned core	0.28051 ± 4	1.46726 ± 6	0.000889 ± 53	0.02519 ± 125	3340 ± 50	100	-6.0 ± 1.3	-6.3 ± 1.3
D09c	Zoned core	0.28051 ± 2	1.46724 ± 4	0.000503 ± 20	0.01451 ± 74	3332 ± 51	100	-5.3 ± 0.7	-5.3 ± 0.7
D10R	Zoned rim	0.28051 ± 2	1.46724 ± 3	0.000455 ± 6	0.01156 ± 3	3360 ± 54	100	-4.4 ± 0.8	-5.1 ± 0.8
D17B	Convo. centre	0.28054 ± 2	1.46721 ± 4	0.000564 ± 25	0.01423 ± 43	3326 ± 50	100	-4.7 ± 0.6	-4.7 ± 0.6
E05c	Zoned core	0.28051 ± 2	1.46719 ± 3	0.000886 ± 8	0.02742 ± 21	3322 ± 51	99	-6.4 ± 0.8	-6.2 ± 0.8
E08c	Zoned core	0.28046 ± 2	1.46724 ± 4	0.000501 ± 2	0.01459 ± 8	3328 ± 50	98	-7.1 ± 0.7	-7.1 ± 0.7
E10c	Zoned rim	0.28048 ± 2	1.46721 ± 5	0.000765 ± 33	0.02220 ± 100	3329 ± 50	100	-7.2 ± 0.7	-7.2 ± 0.7
E11R	Zoned rim	0.28049 ± 2	1.46724 ± 3	0.000719 ± 23	0.02013 ± 70	3326 ± 50	100	-6.9 ± 0.7	-6.8 ± 0.7
E13R	Zoned rim	0.28046 ± 3	1.46723 ± 4	0.000494 ± 11	0.01478 ± 43	3316 ± 50	100	-7.5 ± 0.9	-7.2 ± 0.9
F04c	Zoned core	0.28052 ± 2	1.46723 ± 4	0.000652 ± 7	0.01737 ± 11	3327 ± 51	100	-5.5 ± 0.6	-5.5 ± 0.6
	3330 Ma Old zircon that exhibit an original Lu-Hf compoition relative to the others								
C01R	Zoned rim	0.28067 ± 2	1.46717 ± 5	0.000579 ± 12	0.01412 ± 38	3332 ± 51	99	0.0 ± 0.6	-0.1 ± 0.6
	SG-210c								
	2720 Ma Disturbed zircon								
F02c	black centre	0.28058 ± 2	1.46726 ± 4	0.000179 ± 4	0.00494 ± 9	2721 ± 52	99	-16.5 ± 0.7	-16.5 ± 0.7
	3558 Ma Re-Crystallyzed zircons								
A01R1	zoned rim	0.28053 ± 2	1.46720 ± 2	0.000690 ± 2	0.01584 ± 2	3781 ± 47	98	5.3 ± 0.8	0.1 ± 0.8
A01R2	black rim	0.28039 ± 1	1.46721 ± 3	0.000582 ± 3	0.01286 ± 9	3565 ± 48	100	-4.5 ± 0.5	-4.7 ± 0.5
A03R	black rim	0.28042 ± 2	1.46721 ± 4	0.000396 ± 2	0.00902 ± 5	3533 ± 48	101	-3.6 ± 0.7	-3.0 ± 0.7

Continued on next page

Table B.4 – *Continued from previous page*

Zircon Number	Texture	$^{176}Hf/^{177}Hf$ $\pm 2\sigma$	$^{178}Hf/^{177}Hf$ $\pm 2\sigma$	$^{176}Lu/^{177}Hf$ $\pm 2\sigma$	$^{176}Yb/^{177}Hf$ $\pm 2\sigma$	$\frac{^{207}Pb}{^{206}Pb}$ $\pm 2\sigma$ Age (Ma)	Conc %	$\varepsilon Hf_{(i)}$ $\pm 2\sigma$ Single grain	$\varepsilon Hf_{(i)}$ $\pm 2\sigma$ Rock age
A10c	black centre	0.28049 ± 3	1.46724 ± 4	0.001484 ± 79	0.03403 ± 172	3573 ± 49	100	-2.7 ± 1.2	-3.0 ± 1.2
A13c	black centre	0.28045 ± 3	1.46723 ± 4	0.001564 ± 2	0.03728 ± 33	3584 ± 49	100	-4.3 ± 1.0	-4.9 ± 1.0
B01c	black centre	0.28052 ± 2	1.46721 ± 3	0.001549 ± 28	0.03519 ± 80	3551 ± 50	100	-2.4 ± 0.5	-2.2 ± 0.5
B05c	zoned core	0.28037 ± 2	1.46720 ± 3	0.000793 ± 42	0.01989 ± 151	3700 ± 50	99	-2.5 ± 0.6	-5.8 ± 0.6
C14c	zoned centre	0.28051 ± 3	1.46723 ± 4	0.001381 ± 55	0.03695 ± 153	3857 ± 47	100	4.7 ± 1.2	-2.1 ± 1.2
C17c	black core	0.28043 ± 2	1.46719 ± 4	0.001114 ± 23	0.02607 ± 101	3703 ± 48	100	-1.0 ± 0.6	-4.3 ± 0.6
D07c	black centre	0.28052 ± 2	1.46721 ± 3	0.001383 ± 9	0.03234 ± 18	3579 ± 48	99	-1.4 ± 0.8	-1.9 ± 0.8
E15c	black centre	0.28045 ± 2	1.46721 ± 3	0.000654 ± 15	0.01370 ± 36	3539 ± 48	98	-3.1 ± 0.8	-2.7 ± 0.8
	3869 Ma Old igneous zircons								
A01c	zoned core	0.28043 ± 3	1.46723 ± 5	0.001788 ± 54	0.05033 ± 159	3858 ± 47	101	0.8 ± 0.9	1.0 ± 0.9
A05c	zoned core	0.28034 ± 2	1.46724 ± 4	0.000882 ± 55	0.02361 ± 160	3871 ± 48	99	0.2 ± 0.8	0.2 ± 0.8
A06R	zoned rim	0.28032 ± 2	1.46725 ± 4	0.000675 ± 9	0.01762 ± 18	3877 ± 48	100	0.1 ± 0.7	0.0 ± 0.7
A15c	zoned core	0.28037 ± 3	1.46720 ± 4	0.001233 ± 50	0.03450 ± 149	3863 ± 49	100	0.2 ± 1.0	0.3 ± 1.0
B02c	zoned core	0.28042 ± 3	1.46722 ± 4	0.001687 ± 111	0.04713 ± 348	3884 ± 49	99	1.4 ± 1.0	1.1 ± 1.0
B08c	zoned core	0.28039 ± 2	1.46716 ± 4	0.000959 ± 8	0.02515 ± 13	3845 ± 47	99	1.1 ± 0.7	1.6 ± 0.7
B12c	zoned core	0.28039 ± 3	1.46719 ± 5	0.001175 ± 8	0.03061 ± 18	3861 ± 47	100	0.8 ± 0.9	1.0 ± 0.9
B15c	zoned core	0.28043 ± 2	1.46718 ± 4	0.001452 ± 31	0.03716 ± 109	3878 ± 47	100	2.0 ± 0.9	1.8 ± 0.9
B17c	zoned core	0.28040 ± 3	1.46715 ± 5	0.000920 ± 55	0.02638 ± 202	3878 ± 47	100	2.6 ± 1.0	2.4 ± 1.0
C01c	zoned core	0.28042 ± 3	1.46718 ± 5	0.001183 ± 64	0.02909 ± 184	3868 ± 47	99	2.2 ± 1.1	2.2 ± 1.1
C02c	zoned core	0.28038 ± 2	1.46713 ± 5	0.000487 ± 19	0.01133 ± 60	3846 ± 47	99	2.1 ± 0.7	2.7 ± 0.7
C05c	zoned core	0.28047 ± 2	1.46716 ± 3	0.001519 ± 20	0.03994 ± 47	3876 ± 47	100	3.5 ± 0.8	3.3 ± 0.8
C06c	zoned core	0.28051 ± 3	1.46721 ± 4	0.001434 ± 24	0.03961 ± 89	3869 ± 47	100	4.7 ± 0.9	4.7 ± 0.9
C08c	zoned centre	0.28044 ± 3	1.46716 ± 5	0.001034 ± 68	0.02912 ± 181	3898 ± 48	100	4.1 ± 1.2	3.5 ± 1.2
C10c	zoned core	0.28057 ± 2	1.46725 ± 3	0.001010 ± 17	0.02253 ± 38	3575 ± 48	99	1.1 ± 0.5	7.9 ± 0.5

Continued on next page

Table B.4 – *Continued from previous page*

Zircon Number	Texture	$^{176}Hf/^{177}Hf$ $\pm 2\sigma$	$^{178}Hf/^{177}Hf$ $\pm 2\sigma$	$^{176}Lu/^{177}Hf$ $\pm 2\sigma$	$^{176}Yb/^{177}Hf$ $\pm 2\sigma$	$\frac{^{207}Pb}{^{206}Pb}$ $\pm 2\sigma$ Age (Ma)	Conc %	$\varepsilon Hf_{(i)}$ $\pm 2\sigma$ Single grain	$\varepsilon Hf_{(i)}$ $\pm 2\sigma$ Rock age
D01c	zoned core	0.28040 ± 3	1.46720 ± 4	0.000906 ± 16	0.02334 ± 50	3868 ± 48	100	2.3 ± 1.0	2.3 ± 1.0
D05c	zoned core	0.28036 ± 2	1.46720 ± 4	0.000771 ± 8	0.01906 ± 15	3846 ± 48	99	0.7 ± 0.8	1.2 ± 0.8
D08c	zoned core	0.28037 ± 3	1.46717 ± 4	0.001269 ± 11	0.03079 ± 37	3877 ± 48	100	0.2 ± 1.1	0.1 ± 1.1
D10c	zoned core	0.28041 ± 2	1.46720 ± 4	0.001252 ± 16	0.03397 ± 36	3872 ± 48	100	2.0 ± 0.8	1.9 ± 0.8
D11c	zoned core	0.28040 ± 4	1.46723 ± 5	0.000877 ± 53	0.02239 ± 134	3879 ± 48	100	2.6 ± 1.5	2.4 ± 1.5
D17c	zoned core	0.28038 ± 3	1.46720 ± 5	0.001152 ± 13	0.02920 ± 29	3857 ± 49	100	0.8 ± 1.2	1.1 ± 1.2
E04c	zoned core	0.28052 ± 3	1.46719 ± 3	0.002934 ± 106	0.07902 ± 360	3866 ± 49	100	1.2 ± 1.0	1.2 ± 1.0
E17c	zoned core	0.28036 ± 2	1.46721 ± 4	0.000663 ± 41	0.01515 ± 113	3807 ± 47	98	0.2 ± 0.7	1.7 ± 0.7
F01c	zoned core	0.28036 ± 3	1.46720 ± 4	0.000742 ± 16	0.01900 ± 47	3872 ± 48	100	1.5 ± 0.9	1.4 ± 0.9
F03c	zoned core	0.28032 ± 3	1.46720 ± 5	0.000545 ± 2	0.01394 ± 5	3878 ± 48	100	0.5 ± 0.9	0.2 ± 0.9
F05c	zoned rim	0.28037 ± 2	1.46719 ± 4	0.000978 ± 35	0.02239 ± 93	3842 ± 48	99	0.5 ± 0.8	1.2 ± 0.8
F09c	zoned core	0.28036 ± 2	1.46719 ± 5	0.000845 ± 14	0.01991 ± 32	3875 ± 48	99	1.3 ± 0.7	1.2 ± 0.7
F10c	zoned core	0.28041 ± 2	1.46721 ± 5	0.001224 ± 30	0.03133 ± 71	3882 ± 48	99	2.0 ± 0.7	1.6 ± 0.7
F13c	zoned core	0.28040 ± 3	1.46720 ± 6	0.001739 ± 45	0.04442 ± 115	3882 ± 48	100	0.2 ± 1.1	-0.1 ± 1.1
F14c	zoned core	0.28034 ± 4	1.46720 ± 6	0.000643 ± 7	0.01641 ± 16	3846 ± 49	98	0.5 ± 1.5	1.0 ± 1.5
	SG-265								
	3224 Lister igneous zircons								
A02R	zoned rim	0.28079 ± 2	1.46719 ± 6	0.000545 ± 18	0.01346 ± 56	3211 ± 52	98	1.5 ± 0.9	1.8 ± 0.9
A04R	zoned rim	0.28075 ± 2	1.46723 ± 4	0.000091 ± 2	0.00310 ± 5	3213 ± 52	99	1.4 ± 0.8	1.6 ± 0.8
A06c	zoned core	0.28078 ± 2	1.46722 ± 4	0.000627 ± 11	0.01699 ± 25	3212 ± 52	88	1.3 ± 0.7	1.6 ± 0.7
A07c	zoned core	0.28076 ± 3	1.46722 ± 4	0.000561 ± 19	0.01323 ± 55	3197 ± 53	96	0.2 ± 1.0	0.8 ± 1.0
A07R	zoned rim	0.28069 ± 4	1.46721 ± 5	0.000216 ± 2	0.00525 ± 7	3227 ± 53	99	-0.8 ± 1.4	-0.9 ± 1.4
A08c	zoned core	0.28074 ± 2	1.46722 ± 3	0.000784 ± 7	0.02102 ± 16	3205 ± 53	99	-0.6 ± 0.7	-0.2 ± 0.7
A14c	zoned core	0.28076 ± 3	1.46717 ± 4	0.000593 ± 5	0.01432 ± 14	3222 ± 50	98	0.7 ± 1.0	0.8 ± 1.0

Continued on next page

Table B.4 – *Continued from previous page*

Zircon Number	**Texture**	^{176}**Hf**/^{177}**Hf** $\pm 2\sigma$	^{178}**Hf**/^{177}**Hf** $\pm 2\sigma$	^{176}**Lu**/^{177}**Hf** $\pm 2\sigma$	^{176}**Yb**/^{177}**Hf** $\pm 2\sigma$	$\frac{^{207}Pb}{^{206}Pb}$ $\pm 2\sigma$ **Age (Ma)**	**Conc %**	ε**Hf**$_{(i)}$ $\pm 2\sigma$ **Single grain**	ε**Hf**$_{(i)}$ $\pm 2\sigma$ **Rock age**
A17c	convol. centre	0.28074 ± 2	1.46722 ± 4	0.000089 ± 4	0.00209 ± 8	3234 ± 51	100	1.5 ± 0.8	1.2 ± 0.8
	Standard 91500								
#01	-	0.28230 ± 3	1.46725 ± 5	0.000440 ± 1	0.01295 ± 15				
#02	-	0.28236 ± 3	1.46726 ± 5	0.000440 ± 1	0.01287 ± 13				
#03	-	0.28229 ± 3	1.46726 ± 6	0.000439 ± 1	0.01283 ± 12				
#04	-	0.28232 ± 4	1.46724 ± 6	0.000433 ± 2	0.01266 ± 11				
#05	-	0.28228 ± 3	1.46729 ± 4	0.000432 ± 1	0.01260 ± 12				
#06	-	0.28231 ± 4	1.46726 ± 5	0.000401 ± 2	0.01177 ± 10				
#07	-	0.28229 ± 3	1.46724 ± 6	0.000389 ± 2	0.01108 ± 8				
#08	-	0.28232 ± 4	1.46725 ± 6	0.000397 ± 1	0.01131 ± 11				
#09	-	0.28229 ± 3	1.46733 ± 7	0.000380 ± 2	0.01060 ± 6				
#10	-	0.28232 ± 4	1.46725 ± 5	0.000374 ± 0	0.01039 ± 12				
#11	-	0.28230 ± 3	1.46726 ± 7	0.000379 ± 1	0.01051 ± 10				
#12	-	0.28227 ± 3	1.46727 ± 6	0.000391 ± 1	0.01115 ± 10				
#13	-	0.28226 ± 5	1.46722 ± 5	0.000372 ± 1	0.01037 ± 8				
#14	-	0.28226 ± 4	1.46726 ± 7	0.000376 ± 1	0.01050 ± 13				
#15	-	0.28227 ± 5	1.46726 ± 6	0.000370 ± 1	0.01018 ± 10				
#16	-	0.28232 ± 4	1.46722 ± 6	0.000377 ± 1	0.01050 ± 9				
#17	-	0.28230 ± 5	1.46738 ± 6	0.000377 ± 1	0.01030 ± 10				
#18	-	0.28232 ± 3	1.46726 ± 5	0.000386 ± 0	0.01066 ± 12				
#19	-	0.28234 ± 4	1.46724 ± 8	0.000371 ± 1	0.01009 ± 7				
#20	-	0.28228 ± 4	1.46731 ± 6	0.000367 ± 0	0.00996 ± 10				
#21	-	0.28228 ± 4	1.46731 ± 6	0.000367 ± 0	0.00996 ± 10				

Continued on next page

Table B.4 – *Continued from previous page*

Zircon Number	Texture	$^{176}Hf/^{177}Hf$ $\pm 2\sigma$	$^{178}Hf/^{177}Hf$ $\pm 2\sigma$	$^{176}Lu/^{177}Hf$ $\pm 2\sigma$	$^{176}Yb/^{177}Hf$ $\pm 2\sigma$	$\frac{^{207}Pb}{^{206}Pb}$ $\pm 2\sigma$ Age (Ma)	Conc %	$\varepsilon Hf_{(i)}$ $\pm 2\sigma$ Single grain	$\varepsilon Hf_{(i)}$ $\pm 2\sigma$ Rock age
#22	-	0.28225 ± 4	1.46722 ± 6	0.000372 ± 2	0.01014 ± 7				
#23	-	0.28230 ± 4	1.46725 ± 6	0.000374 ± 1	0.01011 ± 8				
#24	-	0.28229 ± 4	1.46734 ± 5	0.000374 ± 1	0.01042 ± 11				
#25	-	0.28233 ± 4	1.46723 ± 7	0.000360 ± 1	0.00996 ± 12				
#26	-	0.28228 ± 5	1.46726 ± 5	0.000365 ± 1	0.00993 ± 9				
#27	-	0.28230 ± 4	1.46735 ± 6	0.000363 ± 1	0.00979 ± 10				
Mean	-	0.28230 ± 3	1.46727 ± 4	0.000388 ± 26	0.01087 ± 103				
	Plesovice								
#01	-	0.28248 ± 2	1.46728 ± 3	0.000104 ± 2	0.00463 ± 3				
#02	-	0.28252 ± 2	1.46727 ± 5	0.000144 ± 1	0.00638 ± 6				
#03	-	0.28249 ± 3	1.46727 ± 3	0.000164 ± 1	0.00718 ± 11				
#04	-	0.28250 ± 3	1.46722 ± 4	0.000155 ± 0	0.00673 ± 8				
#05	-	0.28251 ± 2	1.46725 ± 3	0.000116 ± 0	0.00491 ± 6				
#06	-	0.28251 ± 3	1.46728 ± 3	0.000128 ± 0	0.00575 ± 10				
#07	-	0.28247 ± 2	1.46723 ± 4	0.000085 ± 0	0.00361 ± 6				
#08	-	0.28247 ± 2	1.46725 ± 4	0.000134 ± 2	0.00576 ± 3				
#09	-	0.28247 ± 2	1.46729 ± 5	0.000117 ± 0	0.00501 ± 5				
#10	-	0.28250 ± 2	1.46722 ± 5	0.000146 ± 1	0.00621 ± 12				
#11	-	0.28245 ± 3	1.46727 ± 5	0.000108 ± 4	0.00447 ± 8				
#12	-	0.28246 ± 2	1.46724 ± 4	0.000150 ± 1	0.00626 ± 4				
#13	-	0.28246 ± 2	1.46728 ± 4	0.000150 ± 0	0.00629 ± 9				
#14	-	0.28249 ± 2	1.46727 ± 4	0.000116 ± 1	0.00495 ± 5				
#15	-	0.28244 ± 2	1.46731 ± 4	0.000114 ± 1	0.00487 ± 9				
#16	-	0.28247 ± 3	1.46723 ± 4	0.000086 ± 1	0.00353 ± 2				

Continued on next page

Table B.4 – *Continued from previous page*

Zircon Number	**Texture**	^{176}**Hf**/^{177}**Hf** $\pm 2\sigma$	^{178}**Hf**/^{177}**Hf** $\pm 2\sigma$	^{176}**Lu**/^{177}**Hf** $\pm 2\sigma$	^{176}**Yb**/^{177}**Hf** $\pm 2\sigma$	$\frac{^{207}Pb}{^{206}Pb}$ $\pm 2\sigma$ **Age (Ma)**	**Conc %**	ε**Hf**$_{(i)}$ $\pm 2\sigma$ **Single grain**	ε**Hf**$_{(i)}$ $\pm 2\sigma$ **Rock age**
#17	-	0.28248 ± 2	1.46728 ± 4	0.000111 ± 0	0.00464 ± 4				
#18	-	0.28245 ± 2	1.46723 ± 4	0.000135 ± 0	0.00566 ± 7				
#19	-	0.28246 ± 2	1.46726 ± 4	0.000108 ± 0	0.00456 ± 7				
#20	-	0.28246 ± 2	1.46719 ± 4	0.000122 ± 1	0.00507 ± 3				
#21	-	0.28247 ± 3	1.46724 ± 5	0.000119 ± 0	0.00495 ± 7				
#22	-	0.28249 ± 3	1.46723 ± 5	0.000138 ± 1	0.00572 ± 9				
#23	-	0.28246 ± 3	1.46727 ± 5	0.000109 ± 1	0.00456 ± 6				
#24	-	0.28251 ± 2	1.46719 ± 5	0.000117 ± 0	0.00494 ± 6				
#25	-	0.28245 ± 3	1.46726 ± 5	0.000121 ± 1	0.00501 ± 2				
#26	-	0.28248 ± 3	1.46731 ± 5	0.000088 ± 1	0.00353 ± 4				
#27	-	0.28248 ± 2	1.46725 ± 4	0.000125 ± 0	0.00519 ± 7				
Mean	-	0.28248 ± 2	1.46725 ± 3	0.000123 ± 21	0.00520 ± 93				

Appendix C

Supplementary materials for the "Chapter 3"

This appendix contains all Supplementary Figures and Tables referenced in Chapter 1: "Combined long- and short-lived Sm-Nd systematics of the Saglek-Hebron Complex felsic crust and implications for its early evolution"

Table C.1

Summary of the major (wt. %; anhydrous composition) and trace (ppm) element composition associated to the age and εHf initial values for the SHC granitoids used in this studies. Data are from the Chapter 2. Coordinates are in UTM NAD 27 Zone 20

	Trondhjemite				**Mg-tonalite**			
Sample	**SG-024**	**SG-025**	**SG-122**	**SG-267**	**SG-026**	**SG-027**	**SG-210C**	**SG-265**
Age (Ma)	3869	3838	3781	3229	3820	3632	3869	3229
$\pm 2\sigma$	±10	±10	±12	±8	±20	±9	±6	±8
Easting	522423	522390	513518	522648	522479	522296	512166	522500
Northing	6460895	6460922	6482946	6474107	6461234	6461349	6478307	6474060
$\varepsilon Hf_{(i)}$	2.19	2.23	1.44	n.a.	3.42	-1.35	1.60	0.97
$\pm 2\sigma$	±0.3	±0.3	±0.2		±0.2	±0.3	±0.2	±0.3
SiO_2	67.26	74.13	70.94	70.87	66.98	59.76	67.94	60.58
Al_2O_3	18.75	15.25	16.83	16.04	15.54	17.12	16.29	18.90
FeO_t	1.41	1.01	1.17	2.21	3.73	4.90	3.97	5.07
MnO	0.02	0.01	0.02	0.04	0.07	0.09	0.07	0.06
MgO	0.51	0.34	0.59	0.86	2.53	3.99	1.45	2.25
CaO	3.16	3.08	3.22	3.08	4.04	6.60	3.48	5.87
Na_2O	5.00	4.73	5.21	5.20	4.29	4.76	4.50	5.13
K_2O	3.58	1.30	1.84	1.44	2.17	2.04	1.71	1.42
TiO_2	0.28	0.12	0.13	0.26	0.47	0.58	0.50	0.63
P_2O_5	0.03	0.02	0.05	0.00	0.18	0.15	0.08	0.09
LOI	0.91	0.70	0.70	0.78	0.65	0.74	1.63	1.82
Sc	0	0	1	-	8	11	-	-
V	17	11	10	27	62	99	47	82
Cr	20	0	0	-	90	100	-	30
Co	4	2	2	6	13	18	9	15
Ni	0	0	0	-	60	80	-	-
Zn	0	30	40	50	80	110	50	70
Ga	24	18	22	20	20	22	24	22
Ge	0.8	0.9	1.00	0.90	1.00	1.00	1.00	0.70
Rb	92	33	67	107	93	80	105	75
Sr	676	400	390	308	508	381	252	493
Y	0.6	0.8	1.2	3.80	8.7	10.6	7.30	7.40
Zr	173	59	58	89	168	104	156	159
Nb	2.3	0.8	2.8	2.70	2.00	2.8	4.50	2.70
Ba	1065	319	304	400	569	269	213	314
La	17.00	9.82	7.92	19.10	32.7	18.7	17.80	7.60
Ce	26.2	15.9	12.8	32.20	65.9	41.3	41.60	18.30
Pr	2.35	1.47	1.41	3.49	7.81	5.52	4.33	2.54
Nd	6.83	4.67	5.03	11.30	30.3	23.00	15.90	11.10
Sm	0.65	0.59	0.85	1.87	5.33	4.64	3.02	2.63
Eu	0.941	0.765	0.387	0.46	1.24	1.08	0.65	0.80
Gd	0.32	0.36	0.58	1.26	3.32	3.39	2.21	2.03
Tb	0.03	0.04	0.06	0.17	0.4	0.42	0.30	0.29
Dy	0.12	0.14	0.24	0.80	1.97	2.26	1.55	1.50
Ho	0.02	0.02	0.04	0.13	0.33	0.4	0.27	0.25
Er	0.07	0.07	0.09	0.30	0.8	1.15	0.72	0.64
Tm	0.01	0.009	0.013	0.04	0.104	0.158	0.09	0.09
Yb	0.08	0.06	0.08	0.20	0.63	0.93	0.54	0.50
Lu	0.017	0.009	0.013	0.03	0.104	0.156	0.08	0.07
Hf	5.00	1.3	1.6	2.00	3.5	2.8	4.30	3.40
Ta	0.05	0.06	0.31	0.48	0.1	0.13	0.31	0.21
Pb	17	13	20	15	11	9	16	8
Th	0.74	0.14	3.78	5.77	3.93	0.78	3.82	0.98
U	0.24	0.10	0.57	0.29	0.10	0.15	0.47	0.65

Continued on next page

Sample	Granodiorite SG-203	Granite SG-080	SG-143	SG-037	SG-084	SG-127	SG-208
Age (Ma)	3330	3612	2780	2744	3710	2789	3330
$\pm 2\sigma$	±15	±9	±8	±8	±24	±12	±7
Easting	522581	513607	506844	491059	512529	502065	522737
Northing	6463604	6477781	6477239	6470294	6478890	6483594	6463758
$\varepsilon Hf_{(i)}$	-6.48	-1.20	-11.26	-14.73	-0.11	-12.34	-6.19
$\pm 2\sigma$	±0.2	±0.2	±0.2	±0.2	±0.3	±0.2	±0.2
SiO_2	68.91	76.16	74.12	74.44	75.08	75.09	75.00
Al_2O_3	13.79	13.56	14.31	14.02	14.12	13.81	13.03
FeO_t	5.33	0.69	1.35	1.43	0.99	1.13	2.02
MnO	0.09	0.01	0.02	0.02	0.02	0.03	0.03
MgO	1.11	0.19	0.29	0.34	0.47	0.17	0.44
CaO	2.94	1.23	1.74	1.51	1.17	1.43	0.93
Na_2O	3.31	3.28	3.76	3.27	3.67	3.66	3.02
K_2O	3.60	4.77	4.14	4.76	4.36	4.57	5.28
TiO_2	0.77	0.10	0.16	0.15	0.10	0.07	0.24
P_2O_5	0.14	0.01	0.09	0.05	0.02	0.02	0.00
LOI	1.10	0.76	0.33	0.52	0.62	0.62	0.69
Sc	-	0	2	3	2	2	-
V	48	6	11	13	0	6	11
Cr	30	0	0	30	0	20	-
Co	9	0	2	3	1	1	3
Ni	0	0	0	0	0	0	-
Zn	110	40	50	40	40	30	-
Ga	20	16	20	20	20	21	19
Ge	2.30	1.1	1.2	1.6	0.9	1.3	2.20
Rb	117	162	169	230	155	163	269
Sr	262	188	181	128	202	120	94
Y	33.20	0.9	6.2	5.2	4.5	5.00	20.40
Zr	324	114	134	114	65	74	153
Nb	6.40	0.7	2.8	3.9	2.8	3.1	4.50
Ba	1010	571	811	659	383	595	437
La	69.30	21.1	27.3	23.7	12.6	22.8	63.20
Ce	145.00	36.2	51.5	46.6	22.00	41.5	125.00
Pr	16.40	3.6	5.6	4.46	2.34	4.39	12.60
Nd	57.80	11.3	19.3	14.9	8.14	14.9	39.80
Sm	9.85	1.51	3.17	2.37	1.39	2.5	5.74
Eu	1.51	0.526	0.67	0.489	0.4	0.403	0.57
Gd	6.89	0.7	2.3	1.53	1.07	1.85	3.60
Tb	1.03	0.07	0.29	0.22	0.14	0.21	0.56
Dy	5.83	0.26	1.3	1.07	0.78	0.98	3.18
Ho	1.09	0.04	0.24	0.19	0.14	0.18	0.65
Er	3.00	0.11	0.6	0.5	0.41	0.52	1.94
Tm	0.42	0.015	0.075	0.068	0.062	0.071	0.30
Yb	2.67	0.09	0.44	0.41	0.42	0.44	1.92
Lu	0.39	0.014	0.071	0.066	0.076	0.069	0.27
Hf	6.80	2.9	3.5	3.7	2.00	2.9	4.70
Ta	0.66	0.05	0.14	0.03	0.11	0.08	0.67
Pb	19	24	22	25	32	31	22
Th	7.63	9.01	9.43	11.5	4.08	18.9	18.70
U	0.86	0.52	0.55	0.66	0.69	1.86	0.97

Continued on next page

Table C.2
Detail summary of the analytic conditions for the Nd isotopic analyses

.

Analytical Procedure	
Laboratory and Sample Preparation	
Laboratory name	Advanced Research Complex Laboratory, University of Ottawa, CANADA
Sample type/mineral	Powdered granitoid
Blank	Total Nd blank =84 pg. ^{142}Nd
Running condition for ^{147}Sm-^{143}Nd isotopic measurement	
Laboratory	Isotope Geochemistry and Geochronology Research Centre (IGGRC) of Carleton University in Ottawa GEOTOP laboratory of Université du Québec à Montréal
Make, Model & type	Thermo-Fisher Triton TIMS
Filament	double Re filaments
Sample size	1 to 2 μL in HCl droplet containing between 200 and 400 ng of Sm-Nd for Sm-Nd analysis
Source Vacuum	$\sim$9e^{-8} Pa using cryogenic trap
Forward Vacuum	$\sim$4.3e^{-3} Pa
Ion Getting Vacuum	$\sim$2e^{-9} Pa
type of collection	Multycollection (Faraday cup)
Number of block run	10 to 14 per sample
Measurement Cycles	10 per block
Integration time	8.39 s per peak
Baseline	30 s each block
Peak center & Lenses focus	every 2 blocks
Amplifier	$10^{11}\Omega$ Amplifiers in rotation each block
Masses measured	see table C.3
Running Intensity	$\sim$1-2 Volts
Analitic mode	Static analyses
Mass bias and interferences	The instrumental mass bias fractionation on Mass 148, 149, 150, and 154 was corrected using the exponential law to ^{147}Sm/^{152}Sm =0.56081 for Sm and ^{146}Nd/^{144}Nd =0.7219 for Nd. Measurement of ^{147}Sm for isobaric interference corrections on Nd isotopic compositions and monitoring ^{146}Nd and ^{155}Gd isobaric interference corrections on Sm isotopic compositions

Analytical Procedure Sm-Nd & ^{142}Nd *(continued)*	
Running condition for ^{142}Nd isotopic measurement	
Laboratory	Isotope Geochemistry and Geochronology Research Centre (IGGRC) of Carleton University in Ottawa
Make, Model & type	Thermo-Fisher Triton TIMS
Filament	zone refined double Re filaments
Sample size	1 to 2 μL in HCl droplet containing between 700 and 1100 ng of Nd
Source Vacuum	$\sim 9e^{-8}$ Pa using cryogenic trap
Forward Vacuum	$\sim 4.3e^{-3}$ Pa
Ion Getting Vacuum	$\sim 2e^{-9}$ Pa
type of collection	Multicollection (Faraday cup)
Number of block run	24 per sample
Measurement Cycles	25 per block
Integration time	8.39 s
Baseline	30 s each block
Peak center & Lenses focus	every 2 blocks
Amplifier	$10^{11}\Omega$ Amplifiers in rotation each block
Masses measured	see table C.3
Running Intensity	$\sim$3-4 Volts
Analitic mode	Dynamic analyses
Mass bias and interferences	The instrumental mass fractionation on the mass 143,145,147,148, and 150 was corrected using exponential law to $^{146}Nd/^{144}Nd = 0.7219$. Interferences of Ce on mass 142 and the Sm on mass 144 have been corrected by measuring Mass 140 (Ce) and 147 (Sm). Mass 148 and 150 were also corrected for Sm.
Additional Resources	SEM Uottawa TIMS IGGRC TIMS Geotope

Table C.3

Cup configurations for 142 and Sm-Nd analysis

.

Analysis	L4	L3	L2	L1	C	H1	H2	H3	H4
Nd Isotopes	^{142}Nd	^{143}Nd	^{144}Nd	^{145}Nd	^{146}Nd	^{147}Sm	^{148}Nd	^{149}Sm	^{150}Nd
Sm Isotopes	^{146}Nd	^{147}Sm	^{148}Sm	^{149}Sm	^{150}Sm	^{152}Sm	^{154}Sm	^{155}Gd	N.A.
^{142}Nd 1^{st}line	^{140}Ce	^{141}Pr	^{142}Nd	^{143}Nd	^{144}Nd	^{145}Nd	^{146}Nd	^{148}Nd	N.A.
^{142}Nd 2^{nd}line	^{142}Nd	^{143}Nd	^{144}Nd	^{145}Nd	^{146}Nd	^{147}Sm	^{148}Nd	^{150}Nd	N.A.

Table C.4

Full results of the dynamic analysis of ^{142}Nd/^{144}Nd isotopic composition for each analytic session. Label *"a"*, *"b"* refer to duplicate run of the sample filament for a single samples. The compilation of both a and b duplicate analysis is label as *"tot"*

Sample	Line	$\frac{^{140}Ce}{^{144}Nd}$	$\frac{^{141}Pr}{^{144}Nd}$	$\frac{^{147}Sm}{^{144}Nd}$	$\frac{^{146}Nd}{^{144}Nd}$	$\frac{^{142}Nd}{^{144}Nd}$ $\pm 2\sigma$	$\frac{^{143}Nd}{^{144}Nd}$ $\pm 2\sigma$	$\frac{^{145}Nd}{^{144}Nd}$ $\pm 2\sigma$	$\frac{^{148}Nd}{^{144}Nd}$ $\pm 2\sigma$	$\frac{^{150}Nd}{^{144}Nd}$ $\pm 2\sigma$	$\mu^{142}Nd$ $\pm 2\sigma$
		Samples									
		Analytic session 06-2018									
SG-024-a	1	0.000024	1.957047	-0.000003	0.7207	1.141865 ± 5	0.509515 ± 2	0.348406 ± 1	0.241578 ± 2		
	2				0.7207	1.141846 ± 6	0.509501 ± 2	0.348404 ± 1	0.241583 ± 2	0.236458 ± 2	
	Dyn					1.141847 ± 4					8.4 ± 3.9
SG-024-a	1	0.000001	1.323392	-0.000003	0.7215	1.141865 ± 6	0.509513 ± 2	0.348404 ± 1	0.241578 ± 2		
	2				0.7215	1.141849 ± 5	0.509504 ± 2	0.348403 ± 1	0.241584 ± 1	0.236458 ± 2	
	Dyn					1.141842 ± 5					3.4 ± 4.0
SG-024 tot	1	0.000013	1.640220	-0.000003	0.7211	1.141865 ± 4	0.509514 ± 2	0.348405 ± 1	0.241578 ± 1		
	2				0.7211	1.141848 ± 4	0.509503 ± 2	0.348404 ± 1	0.241583 ± 1	0.236458 ± 1	
	Dyn					1.141845 ± 3					6.4 ± 2.8
SG-027-a	1	0.000014	0.582628	-0.000002	0.7208	1.141863 ± 6	0.510859 ± 2	0.348407 ± 1	0.241577 ± 2		
	2				0.7208	1.141843 ± 6	0.510852 ± 2	0.348404 ± 1	0.241581 ± 2	0.236458 ± 2	
	Dyn					1.141844 ± 5					5.7 ± 4.2
SG-027-b	1	0.000000	0.405541	-0.000003	0.7223	1.141872 ± 5	0.510859 ± 2	0.348406 ± 1	0.241579 ± 1		
	2				0.7223	1.141850 ± 5	0.510855 ± 2	0.348403 ± 1	0.241583 ± 2	0.236461 ± 2	
	Dyn					1.141851 ± 4					11.3 ± 3.8
SG-027 tot	1	0.000007	0.494085	-0.000003	0.7215	1.141868 ± 4	0.510859 ± 2	0.348407 ± 1	0.241578 ± 1		
	2				0.7215	1.141846 ± 4	0.510854 ± 1	0.348404 ± 1	0.241582 ± 1	0.236460 ± 1	
	Dyn					1.141848 ± 3					8.8 ± 2.8
SG-080	1	0.000015	1.526541	-0.000004	0.7217	1.141869 ± 6	0.510064 ± 2	0.348405 ± 1	0.241579 ± 1		
	2				0.7217	1.141854 ± 6	0.510052 ± 2	0.348405 ± 1	0.241583 ± 2	0.236462 ± 2	
	Dyn					1.141851 ± 4					11.3 ± 3.9
SG-122	1	0.000008	0.588204	-0.000003	0.7214	1.141868 ± 5	0.510509 ± 2	0.348408 ± 1	0.241577 ± 1		
	2				0.7214	1.141848 ± 5	0.510500 ± 2	0.348402 ± 1	0.241583 ± 2	0.236460 ± 2	
	Dyn					1.141846 ± 4					7.4 ± 3.7

Continued on next page

Table C.4 – *Continued from previous page*

Sample	Line	$\frac{^{140}Ce}{^{144}Nd}$	$\frac{^{141}Pr}{^{144}Nd}$	$\frac{^{147}Sm}{^{144}Nd}$	$\frac{^{146}Nd}{^{144}Nd}$	$\frac{^{142}Nd}{^{144}Nd}$ $\pm 2\sigma$	$\frac{^{143}Nd}{^{144}Nd}$ $\pm 2\sigma$	$\frac{^{145}Nd}{^{144}Nd}$ $\pm 2\sigma$	$\frac{^{148}Nd}{^{144}Nd}$ $\pm 2\sigma$	$\frac{^{150}Nd}{^{144}Nd}$ $\pm 2\sigma$	$\mu^{142}Nd$ $\pm 2\sigma$
SG-143	1	0.000016	1.411787	-0.000004	0.7219	1.141868 ± 6	0.510494 ± 2	0.348405 ± 1	0.241580 ± 2		
	2				0.7219	1.141853 ± 5	0.510483 ± 2	0.348403 ± 1	0.241584 ± 2	0.236459 ± 2	
	Dyn					1.141854 ± 4					14.1 ± 3.8
SG-203-a	1	0.000000	1.532321	-0.000003	0.7211	1.141867 ± 5	0.510408 ± 2	0.348406 ± 1	0.241577 ± 2		
	2				0.7211	1.141852 ± 5	0.510395 ± 2	0.348403 ± 1	0.241583 ± 2	0.236457 ± 2	
	Dyn					1.141846 ± 4					7.5 ± 3.9
SG-203-b	1	-0.000003	1.145207	-0.000003	0.7220	1.141869 ± 5	0.510409 ± 2	0.348404 ± 1	0.241576 ± 2		
	2				0.7219	1.141845 ± 6	0.510396 ± 2	0.348404 ± 1	0.241585 ± 2	0.236459 ± 2	
	Dyn					1.141843 ± 5					4.3 ± 4.0
SG-203 tot	1	-0.000002	1.338764	-0.000003	0.7216	1.141868 ± 4	0.510409 ± 2	0.348405 ± 1	0.241576 ± 1		
	2				0.7215	1.141848 ± 4	0.510396 ± 1	0.348404 ± 1	0.241584 ± 1	0.236458 ± 1	
	Dyn					1.141844 ± 3					5.9 ± 2.8
SG-210c	1	-0.000005	1.217467	-0.000003	0.7215	1.141869 ± 5	0.510594 ± 2	0.348406 ± 1	0.241579 ± 1		
	2				0.7215	1.141853 ± 5	0.510582 ± 2	0.348403 ± 1	0.241583 ± 2	0.236460 ± 2	
	Dyn					1.141855 ± 4					14.9 ± 3.8
SG-265	1	0.000001	1.175729	-0.000003	0.7213	1.141857 ± 5	0.511308 ± 2	0.348407 ± 1	0.241579 ± 2		
	2				0.7213	1.141841 ± 6	0.511298 ± 2	0.348404 ± 1	0.241581 ± 1	0.236458 ± 2	
	Dyn					1.141840 ± 5					2.3 ± 4.0
		Analytic session 10-2018									
SG-025	1	0.000211	0.707170	-0.000003	0.7213	1.141859 ± 5	0.510046 ± 2	0.348404 ± 1	0.241579 ± 2		
	2				0.7213	1.141863 ± 5	0.510042 ± 2	0.348403 ± 1	0.241582 ± 1	0.236538 ± 2	
	Dyn					1.141846 ± 4					10.7 ± 3.8
SG-026	1	-0.000008	0.322982	-0.000002	0.7223	1.141859 ± 6	0.510415 ± 2	0.348405 ± 1	0.241579 ± 2		
	2				0.7223	1.141868 ± 6	0.510418 ± 2	0.348405 ± 1	0.241583 ± 2	0.236460 ± 2	
	Dyn					1.141843 ± 5					8.1 ± 4.1
SG-037	1	0.000027	1.190687	0.000000	0.7213	1.141858 ± 5	0.510292 ± 2	0.348406 ± 1	0.241579 ± 2		
	2				0.7213	1.141851 ± 6	0.510285 ± 2	0.348406 ± 1	0.241586 ± 1	0.236463 ± 2	
	Dyn					1.141835 ± 4					1.6 ± 3.9

Continued on next page

Table C.4 – *Continued from previous page*

Sample	Line	$\frac{^{140}Ce}{^{144}Nd}$	$\frac{^{141}Pr}{^{144}Nd}$	$\frac{^{147}Sm}{^{144}Nd}$	$\frac{^{146}Nd}{^{144}Nd}$	$\frac{^{142}Nd}{^{144}Nd}$ $\pm 2\sigma$	$\frac{^{143}Nd}{^{144}Nd}$ $\pm 2\sigma$	$\frac{^{145}Nd}{^{144}Nd}$ $\pm 2\sigma$	$\frac{^{148}Nd}{^{144}Nd}$ $\pm 2\sigma$	$\frac{^{150}Nd}{^{144}Nd}$ $\pm 2\sigma$	$\mu^{142}Nd$ $\pm 2\sigma$
SG-084	1	-0.000005	0.764008	-0.000003	0.7216	1.141860 ± 5	0.510560 ± 2	0.348406 ± 1	0.241578 ± 2		
	2				0.7216	1.141867 ± 6	0.510560 ± 2	0.348405 ± 1	0.241582 ± 2	0.236478 ± 2	
	Dyn					1.141847 ± 4					12.0 ± 3.7
SG-127	1	-0.000003	1.232692	-0.000003	0.7217	1.141857 ± 6	0.510555 ± 2	0.348407 ± 1	0.241579 ± 2		
	2				0.7216	1.141861 ± 6	0.510549 ± 2	0.348403 ± 1	0.241582 ± 2	0.236457 ± 2	
	Dyn					1.141845 ± 5					10.1 ± 4.0
SG-208	1	0.000013	0.601643	-0.000003	0.7216	1.141860 ± 5	0.510087 ± 2	0.348405 ± 1	0.241577 ± 2		
	2				0.7216	1.141865 ± 5	0.510085 ± 2	0.348405 ± 1	0.241582 ± 2	0.236458 ± 2	
	Dyn					1.141848 ± 4					12.4 ± 3.8
		Analytic session 11-2018									
SG-267	1	-0.000002	1.214171	-0.000003	0.7218	1.141857 ± 5	0.510648 ± 2	0.348406 ± 1	0.241580 ± 2		
	2				0.7218	1.141850 ± 5	0.510641 ± 2	0.348403 ± 1	0.241583 ± 2	0.236459 ± 2	
	Dyn					1.141839 ± 5					1.8 ± 4.1
			STANDARDS								
		Analytic session 06-2018									
JNdi-1	1	-0.000003	0.000049	-0.000001	0.7213	1.141861 ± 3	0.512107 ± 1	0.348406 ± 1	0.241578 ± 1		
	2				0.7213	1.141838 ± 3	0.512105 ± 1	0.348403 ± 1	0.241584 ± 1	0.236461 ± 1	
	Dyn					1.141836 ± 3					-1.4 ± 2.3
JNdi-1	1	-0.000002	0.000044	-0.000001	0.7216	1.141859 ± 3	0.512108 ± 1	0.348406 ± 1	0.241578 ± 1		
	2				0.7215	1.141840 ± 3	0.512104 ± 1	0.348404 ± 1	0.241583 ± 1	0.236459 ± 1	
	Dyn					1.141838 ± 3					0.4 ± 2.3
JNdi-1	1	0.000001	0.000046	-0.000001	0.7218	1.141860 ± 4	0.512107 ± 2	0.348406 ± 1	0.241580 ± 1		
	2				0.7218	1.141842 ± 4	0.512106 ± 2	0.348403 ± 1	0.241583 ± 1	0.236460 ± 1	
	Dyn					1.141841 ± 3					2.9 ± 2.8
JNdi-1	1	-0.000004	0.000035	-0.000001	0.7221	1.141858 ± 3	0.512107 ± 1	0.348405 ± 1	0.241578 ± 1		
	2				0.7221	1.141838 ± 3	0.512105 ± 1	0.348403 ± 1	0.241583 ± 1	0.236460 ± 1	
	Dyn					1.141835 ± 3					-1.9 ± 2.3
Mean		-0.000002	0.000043	-0.000001	0.721687	1.141838 ± 5	0.512106 ± 3	0.348405 ± 3	0.241581 ± 5	0.236460 ± 2	**0.0 ± 4.3**

Continued on next page

Table C.4 – *Continued from previous page*

Sample	Line	$\frac{^{140}Ce}{^{144}Nd}$	$\frac{^{141}Pr}{^{144}Nd}$	$\frac{^{147}Sm}{^{144}Nd}$	$\frac{^{146}Nd}{^{144}Nd}$	$\frac{^{142}Nd}{^{144}Nd}$ $\pm 2\sigma$	$\frac{^{143}Nd}{^{144}Nd}$ $\pm 2\sigma$	$\frac{^{145}Nd}{^{144}Nd}$ $\pm 2\sigma$	$\frac{^{148}Nd}{^{144}Nd}$ $\pm 2\sigma$	$\frac{^{150}Nd}{^{144}Nd}$ $\pm 2\sigma$	$\mu^{142}Nd$ $\pm 2\sigma$
		Analytic session 10-2018									
JNdi-1	1	0.000000	0.000045	-0.000001	0.7213	1.141857 ± 6	0.512108 ± 2	0.348407 ± 1	0.241578 ± 2		
	2				0.7213	1.141860 ± 5	0.512111 ± 2	0.348405 ± 1	0.241583 ± 2	0.236460 ± 2	
	Dyn					1.141834 ± 5					0.3 ± 4.0
JNdi-1	1	-0.000001	0.000044	-0.000001	0.7212	1.141856 ± 6	0.512108 ± 2	0.348406 ± 1	0.241578 ± 2		
	2				0.7212	1.141856 ± 6	0.512110 ± 2	0.348405 ± 1	0.241583 ± 2	0.236458 ± 2	
	Dyn					1.141835 ± 5					0.9 ± 4.2
JNdi-1	1	-0.000005	0.000026	-0.000002	0.7232	1.141848 ± 8	0.512104 ± 4	0.348406 ± 2	0.241580 ± 2		
	2				0.7232	1.141854 ± 8	0.512110 ± 3	0.348404 ± 2	0.241585 ± 2	0.236460 ± 3	
	Dyn					1.141835 ± 6					0.9 ± 5.6
JNdi-1	1	0.000002	0.000061	-0.000001	0.7204	1.141853 ± 5	0.512105 ± 2	0.348407 ± 1	0.241580 ± 2		
	2				0.7204	1.141840 ± 5	0.512106 ± 2	0.348404 ± 1	0.241583 ± 2	0.236460 ± 2	
	Dyn					1.141830 ± 4					-3.2 ± 3.9
JNdi-1	1	-0.000001	0.000042	0.000000	0.7214	1.141854 ± 5	0.512107 ± 2	0.348407 ± 1	0.241578 ± 1		
	2				0.7214	1.141844 ± 5	0.512108 ± 2	0.348405 ± 1	0.241584 ± 2	0.236461 ± 2	
	Dyn					1.141835 ± 4					1.2 ± 3.9
Mean		-0.000001	0.000044	-0.000001	0.721506	1.141834 ± 4	0.512108 ± 4	0.348406 ± 2	0.241581 ± 5	0.236460 ± 2	**0.0 ± 3.7**
		Analytic session 11-2018									
JNdi-1	1	-0.000005	0.000028	0.000000	0.7226	1.141859 ± 7	0.512108 ± 3	0.348407 ± 1	0.241577 ± 2		
	2				0.7225	1.141842 ± 7	0.512107 ± 2	0.348403 ± 1	0.241583 ± 2	0.236459 ± 3	
	Dyn					1.141837 ± 6					0.6 ± 5.0
JNdi-1	1	0.000001	0.000045	0.000001	0.7214	1.141855 ± 6	0.512107 ± 2	0.348406 ± 1	0.241578 ± 2		
	2				0.7214	1.141845 ± 6	0.512109 ± 2	0.348405 ± 1	0.241582 ± 2	0.236458 ± 2	
	Dyn					1.141838 ± 5					1.3 ± 4.0
JNdi-1	1	-0.000003	0.000037	0.000000	0.7218	1.141862 ± 5	0.512108 ± 2	0.348406 ± 1	0.241577 ± 2		
	2				0.7218	1.141841 ± 5	0.512104 ± 2	0.348402 ± 1	0.241584 ± 2	0.236461 ± 2	
	Dyn					1.141837 ± 5					0.4 ± 4.0

Continued on next page

Table C.4 – *Continued from previous page*

Sample	Line	$\frac{^{140}Ce}{^{144}Nd}$	$\frac{^{141}Pr}{^{144}Nd}$	$\frac{^{147}Sm}{^{144}Nd}$	$\frac{^{146}Nd}{^{144}Nd}$	$\frac{^{142}Nd}{^{144}Nd}$ $\pm 2\sigma$	$\frac{^{143}Nd}{^{144}Nd}$ $\pm 2\sigma$	$\frac{^{145}Nd}{^{144}Nd}$ $\pm 2\sigma$	$\frac{^{148}Nd}{^{144}Nd}$ $\pm 2\sigma$	$\frac{^{150}Nd}{^{144}Nd}$ $\pm 2\sigma$	$\mu^{142}Nd$ $\pm 2\sigma$
JNdi-1	1	-0.000007	0.000026	0.000000	0.7226	1.141861 ± 7	0.512106 ± 3	0.348407 ± 2	0.241576 ± 2		
	2				0.7226	1.141843 ± 7	0.512106 ± 3	0.348405 ± 2	0.241581 ± 2	0.236458 ± 3	
	Dyn					1.141835 ± 6					-1.9 ± 5.0
JNdi-1	1	0.000000	0.000041	-0.000003	0.7216	1.141851 ± 6	0.512107 ± 3	0.348405 ± 1	0.241581 ± 2		
	2				0.7216	1.141843 ± 6	0.512108 ± 2	0.348405 ± 1	0.241583 ± 2	0.236460 ± 2	
	Dyn					1.141836 ± 5					-0.4 ± 4.2
Mean		-0.000003	0.000035	0.000000	0.721977	1.141837 ± 3	0.512107 ± 3	0.348405 ± 3	0.241580 ± 6	0.236459 ± 3	**0.0 ± 2.5**

Appendix D

Scientific contributions

Precambrian Research 328 (2019) 129–150

Contents lists available at ScienceDirect

Precambrian Research

journal homepage: www.elsevier.com/locate/precamres

Geochemistry and petrogenesis of the early Archean mafic crust from the Saglek-Hebron Complex (Northern Labrador)

Benjamin Wasilewski [a,], Jonathan O'Neil [a], Hanika Rizo [b]

[a] Ottawa-Carleton Geoscience Centre [redacted]

[b] Ottawa-Carleton Geoscience Centre [redacted]

ARTICLE INFO

Keywords:
Saglek-Hebron Complex
Eoarchean crust
Geochemistry
Petrology
Tholeiitic magmas
Komatiitic basalts

ABSTRACT

The Saglek-Hebron Complex located in Northern Labrador, Canada, is one of the oldest granite-greenstone terrains on Earth. It is dominated by granitoids as old as 3.9 Ga and several enclaves of supracrustal rocks. We present here the largest whole-rock major and trace element geochemical dataset (over 100 samples) on the mantle-derived rocks from the Saglek-Hebron Complex to constrain their petrogenesis. The mafic amphibolites are metavolcanic rocks basaltic in composition, have tholeiitic affinities, and exhibit relatively homogeneous compositions with flat rare-earth element profiles. They include incompatible element enriched and depleted compositions, both which appear to be related by fractional crystallization of a gabbroic assemblage within volcanic flows. The enriched mafic rocks exhibit higher Ti contents compared to the more depleted mafic rocks, representing, respectively, evolved liquids and pyroxene-rich cumulate-liquid mixtures. Previous work has suggested the occurrence of two distinct supracrustal units in the Saglek-Hebron Complex, the Eoarchean Nulliak assemblage and the Mesoarchean Upernavik assemblage. Here we report that the petrological and geochemical composition of both assemblages is indistinguishable. This suggests either that the Nulliak and Upernavik metavolcanic rocks represent a single unit, or that they were formed by identical processes in a comparable context, despite an age difference of 400 Ma. Contrary to some other early metavolcanic belts, such as the Isua supracrustal belt and Nuvvuagittuq greenstone belt, none of the metavolcanic rocks from the Saglek-Hebron Complex studied here exhibit geochemical compositions that could be reminiscent of suprasubduction environments. The Saglek-Hebron Complex also includes two compositionally distinct groups of ultramafic rocks characterized by different Al/Ti ratios, Fe contents and controlled by olivine fractionation with different Fo contents. Ultramafic rocks from both groups appear to be cumulates derived from distinct parental magmas with a komatiitic basalt composition. One of these parental magmas may be genetically linked through fractional crystallization with the mafic metavolcanic rocks, whereas the other group is more difficult, at least geochemically, to relate to the Saglek-Hebron basaltic rocks.

Conference abstracts

Abstract YNHN 2019

Geochronology and crustal evolution of the Eoarchean Saglek-Hebron Complex (Northern Labrador)

Wasilewski B., O'Neil J., Rizo H.

The Saglek-Hebron Complex (SHC) located in Northern Labrador (Canada) is part of the North Atlantic Craton. It is amongst the oldest terrains in the world and closely associated to the Itsaq Gneiss Complex (southwest Greenland). The SHC rocks are dominated by trondhjemite-tonalite-granodiorites (TTG) and recorded over one billion years of magmatic history, between ~3900 Ma and ~2700 Ma. Such ancient and protracted magmatic history is ideal to further our understanding on the evolution of the early crust. We used in-situ U-Pb and Lu-Hf isotopes in zircons and whole-rock $^{147-146}$Sm-$^{143-142}$Nd isotopes to constrain the timing of crustal growth and the precursor sources of the SHC oldest crust. Uranium-Pb geochronology showed that 6 major magmatic episodes occurred in the SHC between 3869 Ma (Eoarchean) and 2770 Ma (Neoarchean). Most Eoarchean TTG yielded juvenile initial isotopic signatures in Hf suggesting derivation from contemporaneous mantle-derived mafic crust. They also exhibit excesses in ^{142}Nd with ^{143}Nd/^{144}Nd higher than the normal depleted mantle, implying that their mafic precursor was produced from a mantle source formed during the Hadean (>4000 Ma). In contrast, the Mesoarchean (~3330 Ma) magmatic pulse yielded Hf and Nd isotopic signatures requiring the participation of an older mafic source, potentially Hadean. Combining the geochemistry, geochronology and isotopic data from the SHC and Itsaq granitoids, we propose a common Eoarchean formation and evolution involving subcression-type tectonic setting. However, after the Mesoarchean, both terrains seem to record different history. The SHC experienced crustal reworking while the Itsaq Gneiss Complex continued to produce juvenile crust.

Geophysical Research Abstracts
Vol. 20, EGU2018-10284-1, 2018
EGU General Assembly 2018

From early juvenile source to late crustal reworking: The evolution of the Saglek-Hebron crust

Benjamin Wasilewski (1), Jonathan O'Neil (1), Hanika Rizo (2), Jean-Louis Paquette (3), and Maud Boyet (3)
(1) University of Ottawa, Earth and Evironmental Sciences, Canada, (2) Carleton University, Departement of Earth Sciences, Ottawa, Canada, (3) Université Clermont Auvergne, Laboratoire Magmas et Volcans, Clermont-Ferrand, France

The Saglek-Hebron Complex (SHC) in Northern Labrador includes some of the oldest crustal rocks on Earth. This granite-greenstone terrain recorded over one billion years of early magmatic history spanning between ∼3900 Ma and ∼2700 Ma. The SHC is dominated by rocks from the trondhjemite-tonalite-granodiorite suite (TTG) and granites with Eoarchean to Neoarchean crystallization ages. Our results suggest that the earliest Eoarchean felsic crust is derived from a relatively juvenile source, whereas later Neoarchean crust appears to be mainly produced by crustal reworking. The SHC TTG are generally older than the granites and can be separated into multiple generations based on their zircon ages. Zircons from the oldest Iqualuk gneiss yielded a U-Pb age of 3870 ± 8 Ma for the oldest concordant grains. This age is slightly younger, but overlap within uncertainties with the U-Pb age of 3920 ± 49 Ma recently obtained by Shimojo et al. (2016) for zircons of the same lithology. The main TTG unit, the Uivak gneiss, exhibits crystallization ages ranging over an extended period of time between 3794 ± 7 Ma and 3633 ± 8 Ma. Uivak gneisses are mostly tonalitic in composition but comprise distinct Mg-rich tonalites exhibiting clinopyroxene and hornblende. The Uivak gneisses are consistent with derivation from mafic crustal precursors, possibly the Eoarchean mafic supracrustal lithologies comprised within the SHC. Most analysed granites from the SHC are Neoarchean with zircon ages between 2774 ± 9 Ma and 2805 ± 10 Ma with one older sample that appears to have been emplaced at 3606 ± 9 Ma. In-situ Hf isotopic data on zircons from the Eoarchean Iqualuk and Uivak samples yield chondritic to slightly suprachondritic initial εHf values (up to +3), consistent with derivation from an early juvenile Eoarchean component. The later Paleoarchean and Neoarchean felsic rocks yield low initial εHf values, from ∼-2 at 3600 Ma to ∼-15 at 2750 Ma. The Itsaq Gneiss Complex of SW Greenland is commonly correlated to the SHC. Both complexes appear to show similar Eoarchean crustal evolution, but contrary to what is observed in SW Greenland, no juvenile input has been recorded by the youngest Archean granitoids from the SHC. Considering a common crustal evolution for all SHC granitoids, the zircon εHf vs time trend corresponds to a 176Lu/177Hf ratio of ∼0.01, suggesting that the post-3700 Ma felsic crust from the SHC may be mainly produced by crustal reworking of the oldest TTG. The geochemical composition of the high-Mg Paleoarchean Uivak tonalitic gneiss is however inconsistent with reworking of felsic crust, but rather suggests derivation from a mafic precursor. Assuming a 176Lu/177Hf ratio of ∼0.02 for such mafic source would imply the involvement of a Hadean component to produce the Hf isotopic composition measured in the zircons from the ∼3600 Ma Uivak gneiss.

Goldschmidt2017 Abstract

Over one billion years of crustal evolution recorded in the Saglek-Hebron Complex (Northern Labrador)

B. WASILEWSKI[1], J. O'NEIL[1], H. RIZO[2], J-L. PAQUETTE[3] AND M. BOYET[3]

[1] Depart. of Earth and Env Science, University of Ottawa, Ottawa, ON, Canada
[2] GEOTOP, Départ. des sciences de la Terre et de l'atmosphère, Université du Québec à Montréal, Montréal, QC, Canada
[3] Laboratoire Magmas et Volcans, Université Clermont Auvergne, Clermont-Ferrand, France

The Saglek-Hebron complex (SHC) in Northern Labrador represents one of the oldest terrains on Earth. It is a granite-greenstone terrain that recorded over one billion years of magmatism history between ~3900 Ma and ~2700 Ma. It is dominated by trondhjemite-tonalite-granodiorite suite (TTG) called the Iqualuk tonalites and the Uivak gneisses. Uivak are subdivided into the most extensive Uivak I consisting of Qtz +Pl +Bio ±Kfs tonalite gneisses and the subordinate porphyritic Uivak II granodioritic and Iqualuk tonalitic gneisses consisting of Qtz +Pl +Hbd +Cpx +Ttn ±Kfs. Zircons from the Iqualuk yield a U-Pb upper intercept age of 3888± 28 Ma and zircon U-Pb ages of Uivak I&II are 3838± 8 and 3631± 10 Ma respectively. The Eoarchean gneisses are intruded by younger 2775±7 Ma (mean $^{206}Pb/^{207}Pb$ age) granites consisting of Qtz +Kfs +Pl ±Ap. In-situ Hf isotopic data on zircons from the Eoarchean Iqualuk and Uivak samples yield chondritic to slightly suprachondritic initial εHf values (-2 to +2) suggesting a relatively juvenile source with limited contribution, if any, of much older crust. Zircons from the Neoarchean granites yield low initial εHf values (-13) consistent with reworking of the Eoarchean Uivak gneisses evolving with a $^{176}Lu/^{177}Hf$=0.01, without significant contribution of a juvenile source. The SHC is often correlated to the Itsaq gneiss complex of SW Greenland and our zircon εHf data suggest that both gneissic complexes share a similar Eoarchean crustal history however the SHC younger granitoids do not appear to have recorded a more juvenile source within the Meso-Neoarchean unlike the SW Greenland granitoids (Næraa et *al.* Nature 2012).

AGU international conference San Francisco 2016

Crustal evolution of the Eoarchean Saglek-Hebron Complex, Northern Labrador

Benjamin Wasilewski[1], Jonathan O'Neil[1], Hanika L Rizo Garza[2], Paquette Jean-Louis[3], Abdelmouhcine Gannoun[4] and Maud Boyet[5], (1)University of Ottawa, Ottawa, ON, Canada, (2)GEOTOP, Université du Québec à Montréal, Département des sciences de la Terre et de l'atmosphère, Montréal, QC, Canada, (3)Laboratoire Magmas et Volcans, Clermont-Ferrand Cedex, France, (4)University Blaise Pascal Clermont-Ferrand II, Clermont-Ferrand, France, (5)CNRS, Clermont-Ferrand, Paris Cedex 16, France

Abstract #166598 text:

The scarcity of Hadean and Eoarchean rocks worldwide limits our understanding of early crust formation. The Saglek-Hebron complex (SHC) in Northern Labrador is a granite-greenstone terrain comprising rocks as old as ~3800 Ma. The SHC thus represents one of the oldest terrains on Earth and could shed light on the formation and evolution of the early crust. The oldest suite of supracrustal rocks in the SHC is known as the Nulliak assemblage and is interpreted to be ~3800 Ma. It has been recently proposed that the Nulliak metavolcanic rocks were emplaced through an accretionary complex within an active plate tectonics environment [1]. Their geochemical compositions however are tholeiitic with relatively flat trace element patterns (La/Yb_Nranging from 0.54 to 2) with no evidence of calc-alkaline or boninitic compositions typically found in subduction-zone related rocks. The oldest and most common granitoids in the SHC are Trondhjemite-Tonalite-Granodiorite (TTG) referred as the Uivak. The oldest Uivak sample that we have analyzed yields a zircon U-Pb upper intercept age of 3834 ± 30 Ma (oldest concordant zircon at 3883 ± 7 Ma). The Uivak TTG are subdivided in Uivak I orthogneisses consisting of Qtz+Pl+Bio±Kfs and porphyritic Uivak II gneisses composed of Qtz+Pl+Hbd+Cpx+Ttn±Kfs. The Uivak II unit share geochemical compositions with sanukitoids believed to be felsic melts that have interacted with the mantle. However, sanukitoids are generally restricted to the late Archean [2]. Sanukitoid-like Uivak gneisses yield zircon U-Pb ages between 3870 Ma and 3631 Ma suggesting that the processes responsible for the formation of sanukitoids may have also operated in the Eoarchean. Preliminary in-situ Hf isotopic data on zircons from the oldest Uivak samples yield chondritic to slightly suprachondritic initial εHf values (ranging from -1.5 to +2) suggesting limited contribution of much older crust. The ~3600 Ma granitoids yield zircons with lower initial εHf values (down to -4.5) that may reflect remelting of the Eoarchean Uivak gneisses or the contribution of an older mafic component.

[1] Komiya et al. 2015

[2] Laurent et al. 2014

Advances in Earth Science Research Conference (AESRC 2016)

GEOCHEMICAL INVESTIGATION OF THE SAGLEK-HEBRON COMPLEX, NORTHERN LABRADOR: IMPLICATIONS FOR THE FORMATION OF THE EARLY CRUST.

WASILEWSKI, Benjamin, O'NEIL, Jonathan (Department of Earth and Environmental Sciences, University of Ottawa, Ottawa, Canada), RIZO, Hanika (GEOTOP, Département des sciences de la Terre et de l'atmosphère, Université du Québec à Montréal, Montréal, Canada)

The Saglek-Hebron Complex (SHC), located in northern Labrador, is an Archean terrain in the Nain province of the North Atlantic Craton. The SHC includes two volcano-sedimentary supracrustal assemblages referred as the Nulliak and the Upernavik. These assemblages are intruded by three generations of tonalitic to granitic complexes from the 3.7 Ga to 2.7 Ga. Metasedimentary rocks from the Nulliak assemblage include ~3.8 Ga detrital zircons [1] and Sm-Nd whole rock ages on metavolcanic rocks suggest an age as old as 4.0 Ga [2]. Therefore, the Nulliak assemblage represents one of the oldest suites of mantle-derived rocks on Earth and could shed light on the formation of the early crust. Recent work proposed, based on structural evidence, a subduction tectonic setting for the emplacement of the SHC rocks [3]. Here, we focus on the geochemistry and petrology of the SHC mafic and felsic rocks. The mafic supracrustal rocks of both the 3.8 Ga Nulliak and 3.2 Ga Upernavik supracrustal assemblages are composed of hornblende, plagioclase, and pyroxene ± garnet. They exhibit flat REE patterns and Ti, Fe, Mg and Al concentrations consistent with tholeiitic compositions. Metavolcanic rocks with compositions associated with subduction settings such as calc-alkaline or boninitic lavas are therefore missing, which contrasts with the previously proposed model for the tectonic environment of the SHC [3]. The mafic rocks from both the Nulliak and Upernavik transition from high-Ti to low-Ti concentrations. The low-Ti mafic rocks are pyroxene-rich and are generally poorer in REE and other incompatible trace element concentrations compared to the high-Ti rocks. This suggests that similar fractional crystallization processes played a role in the compositional variations of the mafic rocks of both assemblages independently of their age, suggesting a similar petrogenesis despite more than 500 Ma between both sequences. Our preliminary geochemical work on granitoids suggests the presence of rocks from the tonalite-trondhjemite-granodiorite series, potassic granites and rocks with chemical affinities to Archean sanukitoids. Sanukitoids are produced by interaction of felsic melts with the mantle and seem to be restricted to late Archean magmatic activity in other cratons [4]. The SHC sanukutoids however yielded U-Pb zircon ages of 3.6 Ga suggesting that the processes responsible for the formation of sanukutoids started earlier in the SHC compared to other Archean complexes.

1. Schiotte et al. 1989 Can.J.Earth.Sci
2. Collerson et al. 1991, Nature
3. Komiya et al. 2015, Tectonophysics
4. Laurent et al. 2014, Lithos

GAC-MAC conferences, Montréal 2015

grains and within gneiss samples and require isotopically distinct components.

Our data are generally consistent with published Hf data from the Acasta Gneiss Complex[4-7] and demonstrate involvement of 4.0 Ga or older crust in younger generations of crust. There are no rocks with zircon Hf isotopic signatures consistent with derivation from a LREE-depleted source; instead, the measured compositions may reflect mixing between a compositionally evolved and relatively unradiogenic reservoir with a reservoir bearing a more radiogenic signature. The simplest interpretation is that these rocks formed in an environment that allowed crustal melting, assimilation and rapid recycling.

[1]Bowring and Williams (1999). *CoMP*, 134(1), 3-16. [2]Iizuka, T. et al. (2006) *Geology*, *34*(4), 245-248.[3]Iizuka et al (2007). *Precambrian Res*, 153(3), 179-208. [4]Amelin et al (2000). *GCA*, 644, 205-4225. [5]Guitreau, M., et al. (2012). *EPSL*, 337, 211-223 [6]Iizuka, T. et al. (2009). *Chemical Geology*, *259*(3), 230-239. [7]Guitreau, M., et al. (2014). *GCA* 135, 251-269. [8]Pietranik et al (2008). *Geology* 36(11), 875-878.

Abstract ID: 34524

Final Number: PG34A-0272

Title: Petrological and geochemical investigation of the Eoarchean crust from the Saglek-Hebron Complex, Northern Labrador

Presenter/First Author: Benjamin Wasilewski, University of Ottawa, Gatineau,

Presenter/First Author Email: bwasi082@uottawa.ca

Co-authors: Jonathan O'Neil, University of Ottawa, Ottawa, ON, Canada; Hanika Rizo, Carnegie Institution for Science, Washington, DC

Abstract Body: The Saglek-Hebron Complex is located in Northern Labrador and is part of the Nain Province. The Eoarchean rocks include two suites of supracrustal assemblages, both composed of metavolcanic and metasedimentary lithologies. The oldest suite consists of the Nulliak assemblage which is estimated to be ~3.8 Ga, with Sm-Nd systematics suggesting an older age of ~4.0 Ga [1] for the mantle-derived rocks. Therefore, the Nulliak assemblage represents one of the oldest suites of mantle-derived rocks at the surface of the Earth and could shed light on the formation of the primitive crust and early mantle evolution. The Nulliak unit is intruded by the ~ 3.6 Ga Uivak gneisses, which could be derived from an older mafic component. Supracrustal rocks from the Upernavik assemblage are consistent with a younger emplacement age of ~3.5 Ga. In order to constrain the formation and evolution of the early crust, here we present a preliminary petrological and geochemical study of well-preserved supracrustal rocks from the Nulliak assemblage (Pangertok and Aupaluttok areas) as well as rocks from the younger Upernavik assemblage. These mafic metavolcanic rocks are mainly composed of hornblende + plagioclase ± garnet of variable grain size. Identification of deformed pillow lavas in both supracrustal assemblages and alternation of the mafic metavolcanic rocks with quartz-biotite-garnet schists is consistent with volcano-sedimentary environments of deposition. Preliminary trace and major element data will also help constraining the composition and formation setting of these ancient volcanic rocks. It has been suggested that the Saglek-Hebron Complex may have been related to the well-studied Eoarchean Itsaq Gneiss Complex in Southwest Greenland [2].

[1] Collerson et al. (1991), *Nature.* [2] Bridgwater and Schiotte (1991), *DGF*.

Abstract ID: 36213

Final Number: PG34A-0273

Title: A Provenance and Metamorphic History of the Sedimentary Rocks in the Eastern Part of the North Caribou Greenstone Belt, Host of the Musselwhite Gold Deposit

Presenter/First Author: Octavia E Bath, University of Ottawa, Ottawa,

Presenter/First Author Email: octaviabath88@live.ca

Co-authors: Keiko Hattori, University of Ottawa, Ottawa, ON, Canada; John Biczok, Goldcorp, Thunder Bay, ON, Canada

Published Material: Some data was presented in at GAC-MAC 2014Bath, O., Hattori, K., Biczok, J., 2014. Young un-metamorphosed sedimentary rock in the North Caribou greenstone belt. *Joint Annual meeting of the Geological Association of Canada and Mineralogical Association of Canada, Fredericton, NB. Abstract*

Abstract Body: This study characterizes the sedimentary rocks in the eastern portion of the North Caribou Greenstone Belt, which hosts the Musselwhite Au deposit. The center of the belt is comprised of siliciclastic rocks of the Eyapamikama Lake Assemblage (ELS) and Zeemal Heaton Lake Assemblage (ZHL). The ZHL is close to the terrane boundary with the Island Lake Domain and the Totogon shear zone. Quartz-rich wackes of the ZHL contain detrital zircon grains of igneous origin (Th/U ~ 0.6) with fine oscillatory zoning. They show a wide range of morphologies and yielded three age populations; 2698-2750, 2844-2903 and 2970-2985 Ma. These rocks show elevated MgO (>1%), Ni (>104 ppm), Cr (>180 ppm) and low REE (>88 ppm) and a relatively undifferentiated signature (Th/Sc: 0.67-0.83, $[Ce]_N/[Yb]_N$: 8.1-19, Cr/Zr: 1.3-2.1). They display εNd(2.7 Ga) of -0.97 to +0.50 and DM model ages of ~2.88 Ga. The data indicates a provenance of surrounding batholiths as well as mafic and 2.7 Ga igneous rocks. These sediments contain X_{sp} (0.246-0.414), X_{alm}(0.378-0.548) garnet and ferro-tschermakite, indicating the peak metamorphism under lower amphibolite facies conditions followed by greenschist retrogression chlorite, epidote and actinolite. Quartz-rich wackes of the ZHL show a gradual decrease in metamorphic grade to the east where garnet composition (X_{sp} ~0.381) indicates peak greenschist facies conditions. The arkosic sediments in the central portion of the belt show one population of detrital zircon ages between 2800-2850 Ma. Zircons display similar morphology and lower Th/U (~0.44). Bulk rocks contain low Mg (<1%), Ni (<24 ppm), and Cr (<50 ppm), relatively high REE (104-166 ppm) and an evolved signature (Th/Sc: 0.8-2.1, $[Ce]_N/[Yb]_N$: 14-21, Cr/Zr: 0.07-0.27). εNd(2.85Ga) of -0.14 to +0.77 and DM model ages of 2.92-2.95 Ga, suggesting a provenance primarily derived from the surrounding batholiths (~2.85Ga). They garnet (X_{grs}0.136-0.196, X_{alm}0.606-0.678, X_{pyr}0.038-0.053). These amphibolite facies sediments show varied compositional zoning of garnet, suggesting protracted history of metamorphism.

Abstract ID: 35807

Final Number: PG34A-0274

Title: Characterizing the Archean rocks of eastern Hall Peninsula, Baffin Island, Nunavut, Canada: An integrated approach using U-Pb and Lu-Hf isotopes

Presenter/First Author: Richard Eric From, University of Manitoba, Winnipeg, MB

Presenter/First Author Email: fromr@myumanitoba.ca

Co-authors: Nicole Rayner, , , ; Qiao Shu, University of Alberta, Edmonton, AB, Canada; Alfredo Camacho, University of Manitoba, Winnipeg, MB, Canada; Graham D Pearson, University of Alberta, Edmonton, AB, Canada

"It is just as if we were to refit the torn pieces of a newspaper
by matching their edges and then check whether the lines of print ran smoothly across.
If they do,
there is nothing left but to conclude that the pieces were in fact joined in this way."

"Alfred.L , Wegner *1922"*

"La vie c'est comme une randonnée..."
-
"Tu as une montagne immence devant toi
Ta vie est un flanc de cette montagne
Et il te faut la franchir"

"Tuumasi Itua Annanack*, 2014"*

Abstract

The Saglek-Hebron Complex (SHC) in Northern Labrador represents one of the oldest terrains on Earth and it is closely related to the Archean Itsaq Gneiss Complex (IGC). The SHC is a typical granite-greenstone terrain that recorded over one billion years of magmatic history between ∼3900 Ma and ∼2700 Ma. Our geochronological and geochemical study shows that the SHC includes five generations of trondhjemite-tonalite-granodiorite suites (TTG): the ∼3870 Ma Iqaluk gneiss, the ∼3750 Ma Uivak I gneiss, the ∼3600 Ma Uivak II gneiss, the newly described ∼3300 Ma Iluilik gneiss, and the ∼3220 Ma Lister gneiss. These granitoid units are mostly consist of trondhjemite and tonalite with only rare granodiorites that appear to define a distinct unit formed at ∼3330 Ma and newly defined as the *Iluilik* gneiss. The Iluilik granodiorite appears to be derived from a Hadean mafic crust as supported by its combined whole-rock geochemical composition, its positive μ^{142}Nd value of +6, and its low ε^{176}Hf = −6 and ε^{143}Nd = −3, at 3300 Ma. SHC granites were throughout the Archean, from 3800 to 2700 Ma, but are predominant in the Neoarchean. They appear to have been mainly formed from the reworking of the SHC TTG, as supported by their low ε^{176}Hf and ε^{143}Nd initial values of respectively −16 and −11 at 2700 Ma. The granitoid include numerous enclaves of supracrustal rocks from various size, up to a few kilometers in scale, consisting of metavolcanic metasedimentary rocks. Previous work has suggested that they have been formed at two different ages with the younger Upernavik supracrustal unit deposited around 3400 Ma, and the older Nulliak supracrustal assemblage deposited at around 3750 Ma. We showed that both units are relatively geochemically homogeneous with no distinction between the mafic and ultramafic rocks from both supracrustal assemblages. They mainly consist of mafic metavolcanic amphibolites with tholeiitic affinities and consistent with more depleted mafic and more enriched compositions produced by magmatic differentiation. Their complementary Eu anomaly and whole-rock geochemistry suggest that they formed from fractional crystallization of gabbroic assemblage that derived from similar if not the same parental magma. The mafic metavolcanic rocks are also often associated with ultramafic rocks that we divided into two distinct units, respectively referred as the high-Fe and the Low Fe ultramafic rocks, characterized by different FeO contents and Al/Ti ratio. They both represent olivine-rich cumulative rocks derived from distinct parental komatiitic basalt magmas. Our interpretation contrasts with previous work suggesting that the SHC ultramafic rocks were komatiites and slivers of residual lithospheric mantle. Most SHC TTG exhibit a positive ^{142}Nd anomaly, as high as μ^{142}Nd = +15, suggesting a source formed by differentiation in the Hadean. This ^{142}Nd isotopic composition is similar to the Nulliak supracrustal rocks that exhibit on average a μ^{142}Nd of +10. TTG is generally considered to derive from a mafic precursor. This study therefore shows that mafic crustal source of the SHC Eoarchean TTG, potentially the Nulliak metabasalts, derives from an ancient highly depleted mantle, described as the Saglek mantle, sharing a similar early history as the mantle reservoir involved in the formation of the ancient Itsaq terrane of southwest Greenland. The Saglek depleted mantle interpreted to have formed at ∼4400 Ma, exhibit highly depleted signature with a ^{147}Sm/^{144}Nd ratio up to $0.221 - 0.240$.